IDENTIFYING VIRULENCE FACTORS AND REGULATORS CONTRIBUTING TO PATHOGENESIS BY THE SELECT-AGENT BACTERIUM *BURKHOLDERIA PSEUDOMALLEI*

A DISSERTATION SUBMITTED TO THE GRADUATE DIVISION OF THE UNIVERSITY OF HAWAI‘I AT MĀNOA IN PARTIAL FULFILLMENT OF THE REQUIREMENTS FOR THE DEGREE OF

DOCTOR OF PHILOSOPHY

IN

MOLECULAR BIOSCIENCES AND BIOENGINEERING

AUGUST 2014

By

Michael H. Norris

Dissertation Committee:

Tung Hoang, Chairperson
Dulal Borthakur
Yuanan Lu
Gernot Presting
Richard Yanagihara

Keywords: Michael Norris, Burkholderia pseudomallei, melioidosis, pathogenesis

This doctoral dissertation is dedicated to my loving wife, Malia, without whose support I could not have completed this work; to my son, Henry, for the many years of affection to come; and to my parents for a lifetime of patience.

Acknowledgements: I would like to acknowledge the time and resources Dr. Tung Hoang has dedicated to my professional development over the years. I also greatly appreciate the financial support from the NSF Integrative Graduate Education and Research Traineeship (IGERT)(0549514) and the NIH Centers of Biomedical Research Excellence (COBRE) program (P20GM103516).

ABSTRACT

Many virulence factors contribute to the molecular pathogenesis of *Bp*, such as type III and VI secretion systems, flagella, toxins, and capsule. A large subset of *Bp* proteins, particularly those annotated as hypothetical and putative (~35.5% of the genome), are avoided in experiments. Some of these proteins probably contribute to pathogenesis and its' regulation. Whether for a lack of tools or techniques, many questions about the molecular pathogenesis of *Bp* remain unanswered.

Engineered K96243, 1026b, and MSHR487 Δ*asd* mutants could not grow without the essential cell-wall component diaminopimelic acid (DAP) and were unable to replicate in mice. All strains were excluded from select-agent regulations, providing the research community with helpful BSL-2 surrogates. Intracellular replication and time-lapse movies of fluorescent two-color cell-fusion assays demonstrated that B0011 behaved similarly to WT. B0011's utility in virulence factor investigations was demonstrated by testing in the nematode *Caenorhabditis elegans*. B0011 was also found to kill *Tenebrio molitor* (yellow mealworm) in a novel feeding assay indicating the biosafe B0011 would be a good surrogate for research of virulence factors. The CDC and Los Alamos have obtained the strains for diagnostics and JCVI for persister cell research.

To identify essential virulence factors**,** a transposon mutant library was constructed in *Bp* K96243 Δ*asd* and passaged through macrophages 3 times. gDNA from the passaged pool and the un-passaged pool was isolated and the transposon/genome junctions were enriched using TN-seq. Bacterial genes that were not present in the

samples after passaging through macrophages were considered putative virulence factors. 113 genes underwent greater than 1,000-fold negative selection. Of those, many were deficient in some part of the infectious process. 20 were used to infect mice in an intranasal melioidosis model. 10 mutants demonstrated attenuation and represent new virulence factors.

40 hypothetical regulatory genes were deleted and mutants tested for a decreased plaque forming ability in cell monolayers. Nine regulatory mutants were unable to form plaques, indicating a role in virulence regulation and were complemented with ChIP-seq vectors. Nine regulators were characterized by growth and infection *in vitro*. Of nine, six regulators were used to infect mice and showed attenuation *in vivo.*

TABLE OF CONTENTS

LIST OF TABLES

LIST OF FIGURES

Chapter 2

Chapter 3

Chapter 4

CURRICULUM VITAE

CONTACT:

NAME: Michael H. Norris
ADDRESS: 2802 Koaniani Way Apt. A
Honolulu, Hawaii, U.S.A. 96822
PHONE: Home: (808)-599-0645
Lab: (808)-956-5075
e-mail: [mhnorris@hawaii.edu]
Website: http://www.hawaii.edu/microbiology/Hoang/index.html

PERSONAL INFORMATION:

DATE AND PLACE OF BIRTH: March 25, 1982, Houston, Texas

CITIZENSHIP/RESIDENCY: US citizen and resident

EDUCATION:

B.Sc. (Microbiology, 2004) School of Biological Sciences, University of Texas at Austin, Austin, Texas.

Ph.D. (Molecular Biosciences and Bioengineering, 2007-present) College of Tropical Agriculture and Human Resources, University of Hawaii at Manoa, Honolulu, Hawaii.

EMPLOYMENT HISTORY:

Teaching Assistant, Department of Biology, University of Hawaii at Manoa (08/07 to 12/07)

Research Assistant, Department of Microbiology, University of Hawaii at Manoa (01/08 to 08/08)

NSF Fellow, Department of Molecular Biology and Bioengineering, University of Hawaii at Manoa (08/08 to 03/11)

Research Assistant, Department of Molecular Biology and Bioengineering, University of Hawaii at Manoa (03/11 to present)

AWARDS:

Predoctoral

National Science Foundation Interdisciplinary Graduate Education Research Traineeship (IGERT) pre-doctoral fellowship, awarded by the National Science Foundation (Bethesda, Maryland) on August 30, 2008, re-awarded on August 30, 2009, and a continuing award from August 30, 2010 until March 1, 2011.

4/20/2013-1st place for outstanding oral presentation entitled "Select-agent excluded *Burkholderia pseudomallei* and cell infection model systems for research in BSL-2 laboratories" PhD division, Hawaii Branch of the American Society for Microbiology, 2013 annual spring meeting

9/18/2013-Award for best poster presentation-Pathogenesis division for poster entitled "Select-agent excluded *Burkholderia pseudomallei* and cell infection model systems for research in BSL-2 laboratories", 7th World Melioidosis Congress 2013, Bangkok, Thailand

10/08/2013-Awarded best oral presentation in the session on Infectious Diseases-bacteria and fungi for talk entitled "Identification of virulence factors in the bacterium *Burkholderia pseudomallei"*, 3rd Biennial Western Regional IDeA Conference, Honolulu, HI

04/25/2014-1st place for outstanding oral presentation entitled "Characterization of the intramacrophagic virulome of the bacterium *Burkholderia pseudomallei* " PhD division, Hawaii Branch of the American Society for Microbiology, 2014 annual spring meeting

REFEREED PAPERS PUBLISHED

1. Kang, Y., **Norris, M.H.**, Barrett, A.R., Wilcox, B.A. and Hoang, T.T. 2009. Engineering of tellurite-resistant genetic tools for single-copy chromosomal analysis of *Burkholderia* spp. and characterization of the *B. thailandensis betBA*-operon. ***Applied and Environmental Microbiology*** 75(12):4015-4027.
2. **Norris, M.H.**, Kang, Y., Lu, D., Wilcox, B.A. and Hoang, T.T. 2009. Glyphosate Resistance as a Novel Select-Agent-Compliant, Non-Antibiotic-Selectable Marker in Chromosomal Mutagenesis of the Essential Genes *asd* and *dapB* of *Burkholderia pseudomallei*. ***Applied and Environmental Microbiology*** 75(19):6062-6075.
3. **Norris, M.H.**, Kang, Y., Wilcox, B.A. and Hoang, T.T. 2010. Stable, site-specific fluorescent tagging constructs optimized for *Burkholderia* species. ***Applied and Environmental Microbiology*** 76(22):7635-7640.
4. Kang, Y., Zarzycki-Siek, J., Walton, C. B., **Norris, M. H.**, Videau P., Son, M., and Hoang, T.T. 2010. Multiple FadD acyl-CoA synthetases contribute to differential fatty acid degradation and virulence in *Pseudomonas aeruginosa*. ***PLoS ONE*** 5(10):e13557.
5. Kang, Y., **Norris**, **M.H.**, Zarzycki-Siek, J., Nierman, W.C., Donachie S.P., and Hoang, T.T. 2011. Transcript amplification from single bacterium for transcriptome analysis. ***Genome Research*** 21(6):925-935.
6. Kang, Y., **Norris, M.H.**, Wilcox, B.A., Tuanyok, A., Keim, P.S., and Hoang, T.T. 2011. Knock-out and pull-out recombineering protocols for naturally transformable *Burkholderia thailandensis* and *Burkholderia pseudomallei*. ***Nature Protocols*** 6(8):1085-1104.
7. **Norris, M.H.,** Propst K.L., Kang Y., Dow S.W., Schweizer H.P., and Hoang, T.T. 2011. The *Burkholderia pseudomallei* Δ*asd* mutant exhibits attenuated intracellular infectivity and imparts protection against acute inhalation melioidosis in mice. ***Infection and Immunity*** 79(10):4010-4018.

8. Zarzycki-Siek, J., **Norris, M.H.**, Kang, Y., Sun, Z., Bluhm, A.P., McMillan, I.A., Hoang, T.T. 2013. Elucidating the Pseudomonas aeruginosa Fatty Acid Degradation Pathway: Identification of Additional Fatty Acyl-CoA Synthetase Homologues. ***PLoS ONE*** 8(5):e64554.

9. Sun, Z., Kang, Y., Norris, M.H., Troyer, R.M., Son, M.S., Schweizer, H.P., Dow, S.W., and Hoang, T.T. Blocking phosphatidylcholine utilization in *Pseudomonas aeruginosa*, via mutagenesis of fatty acid, glycerol and choline degradation pathways, confirms the importance of this nutrient source *in vivo*. ***PLoS ONE*** 9(7):e103778.

Manuscripts in Review:

1. Kang, Y., McMillan, I., Norris, M.H., Hoang, T.T. Single prokaryotic cell isolation and total transcript amplification protocol for transcriptomic analysis. (in review at ***Nature Protocols***)

Manuscripts in Preparation (will submit within a couple of months)**:**

1. Kang, Y., **Norris**, **M.H.**, McMillan, I.A., Zarzycki-Siek, J., and Hoang, T.T. Single cell analysis of the transitome of *Burkholderia pseudomallei.* (submittal to ***Nature***).
2. Kang, Y., **Norris**, **M.H.**, McMillan, I.A., Sun, Z., Zarzycki-Siek, J., and Hoang, T.T. Spatial analysis of the global transcriptome in *Pseudomonas aeruginosa* biofilm. (submittal to ***Science***)
3. **Norris, M.H.**, Zarzycki-Siek, J., Kang, Y., Sun, Z., Bluhm, A.P., McMillan, I.A., Hoang, T.T. Select-Agent Excluded *Burkholderia pseudomallei* Strains and Cell Infection Model Systems for Research in BSL-2 Laboratories. (submittal to ***PLoS Pathogens***)
4. **Norris, M.H.**, Zarzycki-Siek, J., Sun, Z., Bluhm, A.P., McMillan, I.A., Kang, Y., Hoang, T.T. Identification of novel *Burkholderia pseudomallei* virulence factors using TNSeq. (submittal to ***PNAS)***

PATENT

A provisional patent application (# 61383699; submitted 16 September 2010) has been filed for a single bacterium total transcript amplification method. T.T. Hoang, Y.Kang, and **M.H. Norris** are named as the inventors on this patent.

ABSTRACTS PRESENTED at MEETINGS (presenter underlined**):**

1. **Norris, M.H.**, Kang, Y., Lu, D., Wilcox, B.A. and Hoang, T.T. Glyphosate Resistance as a Novel Select-Agent-Compliant, Non-Antibiotic-Selectable Marker in Chromosomal Mutagenesis of the Essential Genes *asd* and *dapB* of *Burkholderia pseudomallei*. Poster presented 09/11/2009 at the European Melioidosis Network Meeting, London, England, United Kingdom.

2. Kang, Y., **Norris, M.H.**, Zarzycki-Siek, J., and Hoang T.T. Lambda red recombineering system for naturally transformable *Burkholderia thailandensis* and *Burkholderia pseudomallei.* Poster

number F-27, presented 05/28/2010 at the Banff Conference on Infectious Diseases, Banff, Alberta, Canada.

3. Kang, Y., Zarzycki-Siek, J., Walton, C.B., **Norris, M.H.,** and Hoang, T.T. Multiple FadD acyl-CoA synthetases contribute to differential fatty acid degradation and virulence in *Pseudomonas aeruginosa*. Poster number R-20, presented 05/27/2010 at the Banff Conference on Infectious Diseases, Banff, Alberta, Canada.

4. **Norris, M.H.**, Yun Kang, Katie Propst, Steven Dow, Herbert Schweizer, and Tung T. Hoang. The *Burkholderia pseudomallei* Δ*asd* mutant exhibits attenuated intracellular infectivity and imparts protection against acute inhalation melioidosis. Poster number F-18, presented 05/28/2010 at the Banff Conference on Infectious Diseases, Banff, Alberta, Canada.

5. **Norris, M.H.**, Kang, Y., Zarzycki-Siek, J., Khan, A.G., and T.T. Hoang. Efforts in identification of *Burkholderia* genes contributing to natural competency and DNA degradation. Poster number P67, presented 12/01/2010 at the 6th World Melioidosis Congress, Townsville, Australia.

6. Kang Y., **Norris,M.H.**, Sun Z., Neirman W.C., and T.T. Hoang. Single-cell microarray reveals spatial gene expression of *Bukholderia pseudomallei* during macrophage infection. Poster number P100, presented 12/01/2010 at the 6th World Melioidosis Congress, Townsville, Australia.

7. **Norris M.H.**, Kang Y., Bluhm A.P., Zarzycki-Siek J., Sun Z., and Hoang T.T. Select-agent excluded *Burkholderia pseudomallei* strains and cell infection model systems for research in BSL-2 laboratories. American Society for Microbiology General Meeting. June 16-19, 2012. San Francisco, CA. Poster 1263.

8. Zarzycki-Siek J., **Norris M.H.**, Kang Y., Sun Z., Bluhm A.P., and Hoang T. Elucidating the Pseudomonas aeruginosa fatty acid degradation pathway: Identification of additional FadD fatty acyl-CoA synthetases. American Society for Microbiology General Meeting. June 16-19, 2012. San Francisco, CA. Poster 671.

10. **Norris M.H.**, Kang Y., Bluhm A.P., Zarzycki-Siek J., Sun Z., and Hoang T. Select-agent excluded *Burkholderia pseudomallei* strains and cell infection model systems for research in BSL-2 laboratories. 8th Pacific Southwest RCE meeting. Squaw Valley, CA July 29-31, 2012.

11. **Norris M.H.**, Kang Y., McMillan I., and Hoang T. Select-agent excluded *Burkholderia pseudomallei* and cell infection model systems for research in BSL-2 laboratories. 7th World Melioidosis Congress. Bangkok, Thailand September 19-20, 2013. Poster PPII-19.

12. McMillan, I., **Norris, M.,** Kang Y., Zarzycki-Siek J., Bluhm A., Sun Z., and Hoang T. Autophagy evasion by *Burkholderia pseudomallei*. 7th World Melioidosis Congress. Bangkok, Thailand September 19-20, 2013. Poster PPII-03.

13. **Norris M.H.**, Belcaid M, and Hoang T.T. Identification of virulence factors in the bacterium *Burkholderia pseudomallei"*, 3rd Biennial Western Regional IDeA Conference, Honolulu, HI October 6-8, 2013. Oral presentation in Infectious Disease-bacteria and fungi session.

OTHER ATTENDED MEETINGS

1. The 5th World Melioidosis Congress November 21st-23rd, 2007, Khon Kaen Thailand. Attended soil sampling and bacterial isolation workshop.

2. The American Society for Microbiology 109th general meeting, Philadelphia, PA, USA. May 17-21 2009.

3. The 13th International Conference on Pseudomonas, Sydney, Australia. September 4-7, 2011.

ACADEMIC MEMBERSHIPS/ACTIVITIES:

- National American Society for Microbiology Jan/04-present
- Hawaiian American Society for Microbiology Jan/08-present

SERVICES:

Courses taught (whole semester at 100% effort for each course):

- Taught a section of BIO375 lab (Genetics), Fall 2007

Other Teaching Experiences:

- Former High School Students supervised in the laboratory:

Diana Lu (May-Aug/09) Currently in medical school

- Former Undergraduate supervised in the laboratory:

Mr. Ken Inamasu (Sept/07-July/08)- Currently in medical school

Services to the Department and the University:

- Developed protocols and manuals to initiate the Select Agent program at the University of Hawaii at Manoa, the first of its kind in an educational institution in the state of Hawaii.
- Developed protocols and manuals to initiate the Select Agent animal research program at the University of Hawaii at Manoa, the first of its kind in an educational institution in the state of Hawaii.

Continual development and streamlining of the program occurs on a regular basis.

Chapter 1. Introduction: *Burkholderia pseudomallei*, the etiological agent of melioidosis, a potentially life-threatening tropical infectious disease

The melioid bacillus, *Burkholderia pseudomallei (Bp)*, is typically found in soil and water environments between the latitudes of 20°N and 20°S and so is primarily a tropical organism [1]. Originally described as causing a glanders-like disease by Alfred Whitmore in 1912, it was named Whitmore's disease [2]. In 1932, the disease was renamed melioidosis; taken from "melis" Greek for the disease affecting asses (glanders) and "eidos" meaning of the same [3]. The affliction was also called "the Vietnamese time bomb" because soldiers returning to the U.S. from the Vietnam War would become ill many years after exposure [4]. At the beginning of the 19th century, the bacterium itself was known as *Bacillus whitmorii,* but more recently was called *Pseudomonas pseudomallei*. In 1992, based on 16S rRNA sequence homology and cellular profiles it was proposed that many bacteria in the genus *Pseudomonas* be moved to a new genus called *Burkholderia*, changing *Pseudomonas pseudomallei* to *Burkholderia pseudomallei* (*Bp*) [5].

Bp can be found in soils at pH 2-9 but optimally at 5-8 [6] preferring to grow in wet environments where survival times greatly increase with increased water content (70 days at 10% wc compared to >726 days at 40% wc) [6,7]. Sample sites in northeastern and central Thailand, near Bangkok, are consistently positive for *Bp* and the soil can contain upwards of 17,000 CFU/mL [8]. In endemic areas such as Thailand very high levels of the bacterium are found in the pooled surface waters of rice paddies [9] coinciding with high disease and exposure rates in among rice farmers [10]. There are currently between 3,000 and 4,000 cases of melioidosis in Thailand each year [11]. The season for greatest infection risk is the beginning of the wet season, May to June, when fields are plowed for rice planting [8]. Typically there is a regional hospital far from the individual's home and by the time they arrive, the disease has progressed to an acute form leading to a high mortality rate of 40.5% in Northeastern Thailand

[12]. Nearly 80% of individuals diagnosed with melioidosis are farmers and nearly 70% of these patients have poorly controlled or undiagnosed Type 2 diabetes mellitus [13]. Interestingly, children rarely get sick, but in endemic regions ~80% are seropositive by age 4 [14]. It is believed the organism in contaminated waters gains entry into the host through breaks in the skin or via inhalation of aerosolized particulates. Recently, consuming contaminated drinking water has been implicated as a common route of infection [15] and studies have shown *Bp* is able to colonize gastric epithelium [16]. Human-to-human transmission of *Bp* is very rare and has only been documented a handful of times. In two well-documented cases from the 1970's, prostatic abscesses in male U.S. serviceman were believed to be the infectious source when sexually transmitted to a wife and a neonatal baby [17-19].

Not only does the melioid bacillus pose a public health challenge in Northeastern Thailand but the US Centers for Disease Control has listed *B. pseudomallei* (causing melioidosis) and the closely related *Burkholderia mallei* (causing glanders) as Tier-1 Select Agents. Tier 1 organisms have the potential of posing a severe threat to US public health and safety and the U.S. Congress passed laws to develop vaccines and therapeutics for their associated disease including melioidosis and glanders [20]. Research on these bacteria is a high priority because the historical usage of *B. mallei* in biological warfare by Germany on horses during World War I and on humans by Japan in World War II, and weaponization by the U.S.S.R. [21] and high pathogenicity when aerosolized. An important step in combating a disease is to understand the fundamental basis. In this case, only by understanding the molecular pathogenesis of *Bp* infection will an effective vaccine come to fruition. Additionally, a highly secure Bio-Safety Level 3 (BSL-3) laboratory is required for all live bacteria manipulations.

The disease melioidosis is known as the 'great mimicker' due to the wide variety of symptoms and clinical presentations, which resemble other diseases [22]. Melioidosis can present as an acute, chronic, or latent infection. Studies from Northern Australia indicate that 88% of melioidosis cases were acute while 12% were chronic [23]. Overall, bacteremia during melioidosis occurs in ~50% of cases [24]. Pneumonia and respiratory infection is found in half of patients but severity can range from severe septicemia to mild pneumonia with few symptoms [24]. Other presentations include skin and soft-tissue infection, bone and joint infection, visceral abscesses, infection of the parotid gland and urinary tract, and infections of the nervous system, including the brain. *Bp* has been known to infect every tissue and organ of the body, with the exception that endocarditis has never been observed [25]. *Bp* strains found in Thailand differ genetically to those found in Australia (to be discussed later). In Thailand, melioidosis often presents with parotid gland infections but only a single event has been observed in Australia while prostatic abscesses and neurological melioidosis are more common in Australia than Thailand [24]. When symptoms persist beyond two months, the infection is considered as chronic melioidosis [23]. Chronic melioidosis accounts for ~10% of cases in Thailand and Australia but most cases identified in non-endemic regions are chronic infections. Patients with chronic lung infections typically present with chest pain and bloody sputum. Visible as cavitation and infiltration in X-ray radiography, the lungs appear very similar to tuberculosis-infected lungs. Often times misdiagnosed as tuberculosis, the name great mimicker is certainly appropriate. Unfortunately, drugs used to treat tuberculosis are ineffective for melioidosis, so doctors in endemic regions must be wary about making the correct diagnosis. With education there is less misdiagnosis, resulting in increasing reports of melioidosis cases. Latent *Bp* infections are considered initially asymptomatic that are eventually diagnosed as melioidosis.

The longest latent infection described was in a U.S. serviceman taken prisoner during World War II [26], who, presented with an ulcerated wound on his thumb 62 years later. Bacteria isolated from the wound were identified as *Bp*. It can be considered a unique case considering serological studies indicate 3% of the three million military personnel were seropositive for *Bp* exposure after returning from the Vietnam War, compared to the low number of verified cases of melioidosis [27].

Melioidosis is a serious disease that demands immediate treatment. Once *Bp* is verified by culture or if melioidosis is suspected in endemic regions, treatment begins with parenteral therapy. The discovery that ceftazadime, a ß-lactam third-generation cephalosporin antibiotic, decreased mortality by ~50% was a milestone in the treatment of melioidosis and is the gold standard for initial parenteral treatment of acute melioidosis in Thailand [28]. The recommended dose for curing melioidosis is 120 mg/kg/day of ceftazidime at 2 g every 8 hours via IV for at least 10-14 days or until improvement. Carbapenems, such as imipenem and meropenem, are considered just as effective during parenteral therapy and are the standard treatment antibiotics in North Australian hospitals. The carbapenems are more effective at inhibiting bacterial growth during *in vitro* testing but the verdict is still out as to their superiority over ceftazidime. Dosages for the carbapenems are in the 70 mg/kg/day range at 1g every 8 hours [29]. If clinical improvement is observed after 10-14 days, parenteral treatment can be ended and the eradication phase begun.

Bp is a facultative intracellular bacterium, similar to *Mycobacterium tuberculosis*, so antibiotics must be taken for a long period to prevent relapse. The prescribed first-line treatment during the eradication phase is trimethoprim-sulfomethoxazole (TMP-SMX) with or without doxycycline for 3-6 months depending on the health of the patient [1]. Relapse of infection is

very common if the therapeutic regimen is not followed. *Bp* has high strain-to-strain genetic variability so *in vitro* antibiotic susceptibility testing is recommended as soon as a strain is isolated because some strains can be resistant to ceftazidime [30] or TMP-SMX [31].

As stated above, much of the population in endemic areas is seropositive but only a small fraction becomes ill. How does the body react and respond to *Bp* infection? Once inhaled into the respiratory tract, *Bp* is exposed to anti-bacterial compounds such as lysozyme, complement, and defensins. *Bp* is known to be resistant to all these molecules allowing for cellular contact between bacteria and cells of the host. The upper airway surfaces can then be colonized, providing for rapid access to the nervous system via the olfactory epithelium and the nerves therein [32]. In recognizing *Bp*, the toll-like receptors (TLRs) and other pathogen recognition receptors (PRR) are the first to detect the pathogen-associated molecular patterns (PAMPs). Many of the TLRs (TLR1-5, 8 and 10) are upregulated in melioidosis patients [33]. When MyD88 (the essential TLR adaptor for NF-κB activation) is knocked out, mice died 50% quicker and pulmonary neutrophil infiltration was repressed while normal phagocytosis was not changed [34]. Initial recognition and activation of innate immunity can have a large effect on disease prognosis. Indeed, certain polymorphisms in TLR4, the canonical TLR for lipopolysaccharide (LPS) detection, have been associated with increased susceptibility to melioidosis [35]. *Bp* is known to invade and replicate within macrophages and polymorphonuclear cells (PMNs) [36]. These cells are believed to be very important for bacterial containment as it has been shown that PMNs from diabetic patients have a reduced ability to migrate and phagocytize *Bp in vitro* [37] and that BALB/c mice, which are very sensitive to *Bp* infection, recruit less monocytes to infection sites than resistant mouse strains like C57BL/6 [38]. Additionally, *in vivo* macrophage depletion experiments showed C57BL6 mice infected with *Bp* via the intranasal route were much

more sensitive to *Bp* mediated killing and had higher levels of internal *Bp* CFUs following infection than untreated controls [39]. It has also been shown that both TNF-α and IFN-γ, which work to activate macrophages, are essential in extending survival during early-stage experimental melioidosis. Administration of IFN-γ directed antibodies into *Bp* infected mice lowered the lethal doses by 50%, emphasizing the essential role for IFN-γ in activating cells of the immune system during initial infection with *Bp* [40]. IL-18, probably due to its ability to initiate IFN-γ release that subsequently activates macrophages, also plays a role [41]. Following the initial stages of infection, host-defense is reliant on a T_H1 cell response to propagate macrophage activation and bactericidal activities along with clonal expansion of *Bp* antigen-specific T cells [42,43]. Dendritic cells have been shown to serve an important role in activating CD4+ T-cells and to some extent CD8+ T-cells during melioidosis. Monocytic dendritic cells were pulsed with bulk antigen as well as purified antigens and caused memory T-cell expansion in T cells isolated from seropositive donors, further substantiating the importance of a T_H1 response to *Bp* infection [44]. One caveat is that HIV has not been implicated as a risk factor in studies, which would be counterintuitive to the hypothesis that cell-mediated immunity is required for host defense [45]. Perhaps HIV patients do not come into contact with the bacterium in its natural environment. Although cell-mediated immunity is the major player in host resistance to *Bp* infection, a humoral response is still mounted. Many of the antibodies identified are against the LPS and capsular polysaccharide (CPS) surrounding the bacterium. Virtually all antibodies are IgG of the subclass IgG1 (~65%) that is consistent with a tendency towards a cell-mediated response [46]. Melioidosis survivors usually have very high anti-*Bp* antibody titers but they are not protective as relapse is high [47] and seem to be useful only for opsonizing extracellular bacteria. Antibodies have proven useful in positive identification of *Bp* where the

latex agglutination test was used for colony identification [48] and in the new dipstick assay for identifying *Bp* in clinical specimens [49] but passive immunizations have failed to protect mice during infection; again lending credence that cell-mediated immunity is paramount to fighting the infection.

Currently there is no vaccine licensed for melioidosis but interest in developing one has increased following the realization that the organism could be weaponized. *Bp* is a facultative intracellular pathogen that will enter host cells and replicate, necessitating a powerful cell-mediated immune response to counter the infection. Many types of auxotrophic strains have been developed and immunization with these strains can create protection from acute melioidosis [50,51]. Live attenuated mutants auxotrophic for purine metabolism and amino acid metabolism have shown the most significant protection from lethal challenge doses but sterile immunity is never achieved and death is merely delayed in animal models [51,52]. Data generated in our lab (delineated in Chapter 5 of this dissertation) found that mice immunized intranasally with a live-attenuated *Bp* prior to intranasal high lethal dose challenge of wildtype were protected from acute melioidosis. Survival was increased from 4 days post-infection to between 20 and 60 days post-infection. Protection was conveyed at the site of initial infection but failed to protect secondary infections in the spleens. Mice then succumbed to a chronic infection at the secondary sites of infection. Survival data like this is typical for live-attenuated studies and future work will address the prevention of chronic infection by boosting the cell-mediated immune response. Heat-killed whole-cell vaccines have been produced with *Bp* and closely related species but the only details gleaned from such a confusing combination of site immunizations and site challenges, is that the heat-killed vaccines convey some protection but that it is dependent on where the immunization is given and what route the challenge dose is given [53]. Species similar

to *Bp*, *B. mallei* and *B. thailandensis*, can produce cross-reactive immunity to *Bp* but in all cases sterile immunity is elusive and more work must be done on optimizing route and dosage of a heat-killed whole-cell vaccine. Several sub-unit vaccines have been tested including the CPS and LPS. LPS has been shown to increase the mean time to death, but again sterile immunity is not occurring [54]. In the previous study the LPS vaccine can only protect against intraperitoneal challenge and not the more relevant respiratory challenge. Subcutaneous challenge was not attempted. A major problem with *Bp* LPS as a subunit vaccine, is that the structure can vary depending on the strain. Three types of LPS have been identified [55] and LPS sub-unit vaccines are type specific. It has not been investigated weather or not cross-protective immunity can be achieved for LPS variant strains without using all LPS types in the vaccine. Mechanisms that could improve the activity of the vaccines include the production of glycoconjugate vaccines. Glycoconjugate vaccines consist of either LPS, CPS, or both conjugated to a known *Bp* immunogenic protein to stimulate both the cell-mediated (protein) and humoral (polysaccharide) immunity. Currently, there have only been conjugations of non-specific immunogens, such as BSA, but still result in higher IgG production against the T-cell independent CPS antigen than either component alone [56]. Mouse survival was not tested. The search for a melioidosis vaccine is ongoing and with increased research on *Bp* virulence factors and how they contribute to host infection, a more effective vaccine will be realized.

When *Bp* cells come into contact with host cells a plethora of host modifications occur in response to bacterial infiltration and virulence factor expression leading to a diseased state. Within-host, *Bp* can infect most tissues and invades, then replicate inside the cytoplasm of many cell types [51,57-61]. To accomplish this feat *Bp* attaches to the host cell via an unknown mechanism, causing actin rearrangement and inducing bacterial phagocytosis [62]. Once,

internalized *Bp* utilizes the *Burkholderia secretion apparatus* (Bsa, one of three genomically encoded type 3 secretion systems, T3SS) to secrete the effector BopE through the membrane of the phagocytic vesicle [63,64]. BopE is a guanine nucleotide exchange factor (GEF) for host-cell Rho GTPases that undermines the surrounding cytoskeletal framework, damaging the membrane and allowing vesicular escape before phagosomal degradation of *Bp* occurs [65]. The T3SS effector BopA is believed to play a role in host-cell autophagy evasion [66] but data from our lab indicates another protein may have a more significant effect on the process. The action and impact of both effectors to mammalian infections has been demonstrated *in vitro* but BopA and BopE mutants do not make a significant impact on mouse survival [67,68]. Once inside the cytoplasm the well characterized *Bp*-intracellular motility protein A, BimA, polymerizes host-cell actin [69]. The polar actin "tail" allows intracellular movement and eventually leads to formation of membrane protrusions [70]. The membrane protrusions allow *Bp* to seek out uninfected cells and begin the cycle anew without transitioning into the extracellular milieu. Intracellular motility quickly oscillates between actin-mediated movement and use of flagella, where *Bp* swims within the host-cell cytoplasm [71]. During the infectious process an infected cell may fuse with healthy neighboring host cells and is attributed to the main *Bp* type 6 secretion system (T6SS-1) of which *Bp* has 6. [72]. The formation of multi-nucleated giant cells (MNGCs) has been observed *in vitro* and *in vivo* and is a major hallmark of *Bp* infection [70,73]. As discussed earlier, *Bp* produces CPS and LPS. Mutants of both are attenuated in mice [74,75]. *Bp* encodes genes to make up to seven quorum-sensing (QS) molecules that allow bacterial communication and concerted gene expression. The genes that are activated by quorum sensing in *Bp* are still unknown but deletion of the *luxR* homologues (a transcriptional activator of QS) results in decreased virulence in hamsters [76]. Recently, the QS molecules have been shown to

negatively affect macrophage MNCG formation *in vitro* [77]. The list of virulence factors goes on with flagella and pili contributing to efficient adherence to and invasion of host-cells [78,79]. The bacteria replicate concurrently with the production of several known and unknown virulence factors causing death of the host-cell. However, questions remain; how does *Bp* sense when to fuse, where to travel, what nutrients to use, how are mediators (e.g. autophagy) of innate immunity avoided, and what causes the observed cytoskeletal rearrangements (Fig. 1)? These questions are indicative of the knowledge *gap* present in fully understanding the molecular pathogenesis of *Bp.*

A major hurdle in understanding more about how *Bp* causes disease is the lack of adequate tools. Tools in the sense of genetic methodologies (Chapters 3 and 4 of this work) and disease models (Chapter 5). *Bp* is highly resistant to antibiotics and it's listing as a select agent prohibits the use of many antibiotic markers; making classic genetic analysis difficult. The candidate's initial projects included the development of non-antibiotic selectable markers for use in *Bp* and *Bm.* Two non-antibiotic markers commonly used in plants were adapted and customized for use in *Burkholderia* sp. The glyphosate acetyl-transferase (*gat*) and bi-aliphos resistance (*bar*) genes, conferring resistance to the herbicides glyphosate and glufosinate respectively, were used for various genetic manipulations in *Bp* strains [80]. In the previously published study, the *gat* marker was used to delete the aspartate semialdehyde dehydrogenase (*asd*)-encoding gene in two *Bp* type strains, 1026b and K96243. Asd is essential for creating diaminopimelic acid (DAP), which is the amino acid cross-linking neighboring strand of peptidoglycan in the gram-negative cell wall. Without Asd or exogenous DAP, bacteria swell and lyse [81]. The publication accomplished two goals: 1) providing the research community with non-antibiotic selectable markers for safe genetic manipulation of select-agent

Burkholderia; and 2) creation of two biosafe strains with live-attenuated vaccine potential that can conditionally grow only in the presence of exogenous DAP. Attenuation of both strains has since been verified by high-dose intranasal challenge in BALB/c mice [51]. The data in Chapter 4 of this work was summarized and the CDC approved an application for exclusion of these two strains from the select agent regulations (SAR). These strains can now be used as bio-safe surrogates outside of the SAR. Several other *asd* mutants have been made in different *Bp* strain backgrounds and verified for attenuation in BALB/c mice (unpublished data). Current research with this pathogen is highly regulated, requiring SAR, approved personnel, and BSL-3 biocontainment facilities. Time investment and research costs can skyrocket under project requirements. BSL-2-trained personnel and research space far outnumber those available for BSL-3 and represent underutilized resources in research of select agents. Bio-safe strains can be moved to the BSL-2 and utilized as surrogates for many parts of the research project. **The first aim of my dissertation is to demonstrate the utility of our bio-safe strain in infection models for use at BSL-2.** Many models have been used to study *Bp* infection including *in vitro* cell infection models. Numerous cell lines have been infected by *Bp* including epithelial, hepatic, macrophage, and polymorphonuclear leukocyte cell-lines among others [57-59,61]. Monolayers infected with *Bp* form multi-nucleated giant cells (MNGCs) and eventually plaques. Plaque formation can be used to identify important virulence factors by studying plaque-forming ability of virulence-factor mutants [71,82]. Monolayers can also be used to study invasion efficiency and intracellular replication of *Bp* [83]. A cell-fusion assay has also been developed utilizing two HEK293T cell lines; one expresses GFP cytoplasmically and the other RFP [71]. When seeded together in one monolayer followed by infection with *Bp*; intracellular bacteria induce fusion of neighboring cells mixing the cytoplasms creating a yellow color. Live-cell imaging is also a very

important tool in investigating bacteria/host-cell interactions and tracking infectious stages. Besides cell lines, *Bp* infection models used to investigate virulence include invertebrate animal models such as the nematode, *Caenorhabditis elegans* [84-86], and wax moth larvae, *Galleria mellonella* [87,88]. Chapter 5 of this work encompasses the utility testing of our bio-safe *Bp* strain in various infection models.

While many *Bp* virulence factors lead to attenuation in mouse models of infections, mutational *in vitro* cell infection studies indicate a delay of the cellular infectious events rather than abolishment [67,72,89] and as described above. *Bp* has nearly 6,000 genes and an open genome [90,91]. Many genes (approximately 35.5% in *Bp* strain K96243) are hypothetical or putative with no proven function [90]. It stands to reason that there are *Bp*-specific virulence factors contributing to disease that remain to be discovered and that mutating these factors may produce a live-attenuated strain that is capable of protecting from inhalation melioidosis. To identify all the *Bp* genes contributing to infection, known and unknown, we screened a large random transposon library pool through RAW264.7 macrophages. The resulting output transposon pool was compared to the input pool using Tn-seq analysis [92]. Before the advent of Next Generation Sequencing (NGS) microarray technology was used to reduce the amount of screening used in high-throughput signature-tagged mutagenesis (STM) experiments targeting bacterial virulence factors [93]. The technique is based on the principle that if the transposon inactivates a gene important for intracellular survival (i.e., a virulence factor) that particular mutant is unable to survive in the host–cell and the gene will not be detected in the output pool. Tn-seq enriches the genome/transposon junctions then Illumina sequencing is used to sequence the enriched DNA. Tn-seq is a variation on a theme but was used to identify all the genes contributing to antibiotic resistance in *Pseudomonas aeruginosa* [92]. With all high throughput

screens it is critical to verify contributions by mutational analysis. Several genes were positively identified as aiding in antibiotic resistance. The development of a vaccine remains elusive, placing urgency on elucidating the functional contributions of hypothetical/putative genes to the molecular pathogenesis model. In total, we consider the effort of this work in identification and characterization of novel virulence factors to be innovative and of significance to the field. The details of the Tn-seq experiment are summarized in Chapter 6 of this dissertation.

Bp commands an arsenal of virulence factors that are put into use during host-cell infection. To organize and time the use of these virulence factors for full effect, a complex regulatory cascade must be fine tuned and maintained. Identifying the transcriptional regulators that are responsible for such fine-tuning would give insight to the virulence network of *Bp* and provide targets for novel therapeutic development.

Transcriptional regulation of virulence genes has been well studied in *Vibrio cholerae*, as well as in *P. aeruginosa.* In these pathogens external compounds and sensors are known to turn on a suite of transcriptional regulators that then mediate toxin, pili, flagella, phospholipases and proteases production among others. *V. cholerae* responds to temperature, osmolarity, bile, and pH to up regulate cholera toxin synthesis [94]. Moreover, studies have uncovered several regulons of virulence factors that control the ability of *V. cholerae* to attach and adhere to intestinal mucosa (ToxR regulon and the toxin coregulated pilus), but that all need to be coordinated for successful colonization. Secretion of mucinases, lipases, and proteases must also be coordinated to digest the mucous surrounding the membranes. The model pathogen, *P. aeruginosa*, is known to coordinate a complex and intricate web of regulation that allows the bacterium to infect a wide variety of hosts and survive in a wide variety of environments [95].

A few *Bp* transcriptional regulators have been investigated. The AraC-type regulator, HrpB, and its role in regulating the plant-pathogen like T3SS has been elucidated [96]. BsaN has been identified as a direct regulator of the T6SS-5, a major virulence factor [97] and BspR has been identified as a regulator of the major virulence factor T3SS [98]. These regulators are located proximal to these virulence factors and were obvious candidates for direct regulation of these two loci. Our goal was to identify additional regulators including global regulators that affect virulence factor expression during host infection and aide in coordinating the process of host-cell infection. Previous data generated in the lab by Dr. Yun Kang using single-cell transcriptomics [99] of the *Bp* transitome (in preparation) identified the global transcriptional profile of *Bp* as it transits through the host-cell during infection. Many genes were differentially regulated as *Bp* invaded host cells, replicated in the cytoplasm, and formed protrusions. Within this data set, 40 transcriptional regulators were identified that showed differential gene expression during host-cell infectious stages. The targets of these regulators are unknown and we hypothesized that at least some of them would be contributing to the coordinated expression of virulence factors during infection.

1 REFERENCES

1. Cheng AC, Currie BJ (2005) Melioidosis: epidemiology, pathophysiology, and management. Clin Microbiol Rev 18: 383-416.
2. Whitmore A, Krishnaswami CS (1912) An account of the discovery of a hitherto undescribed infective disease occuring among the population of Rangoon. Ind Med Gaz 1912: 262-267.
3. Stanton AT, Fletcher W (1921) Melioidosis, a new disease of the tropics. Trans Fourth Congr Far East Assoc Trop Med 2: 196-198.
4. Stone R (2007) Infectious Diseases: Racing to diffuse a bacterial time bomb. Science 317: 1022-1024.
5. Yabuuchi E, Kosako Y, Oyaizu H, Yano I, Hotta H, Hashimoto Y, Ezaki T, Arakawa M. Proposal of *Burkholderia* gen. nov. and transfer of seven species of the genus *Pseudomonas* homology group II to the new genus, with the type species *Burkholderia cepacia* (Palleroni and Holmes 1981) comb. nov.
6. Limmathurotsakul D, Wuthiekanun V, Tuanyok A, Peacock SJ (2012) Presence and sampling of *Burkholderia pseudomallei* in soil. In: Ketheesan N, editor. Melioidosis- A Century of Observation and Research. San Diego: Elsevier. pp. 349-357.
7. Inglis TJJ, Sagripanti J-L (2006) Environmental factors that affect the survival and persistence of *Burkholderia pseudomallei*. Applied and Environmental Microbiology 72: 6865-6875.
8. Smith MD, Wuthiekanun V, Walsh AL, White NJ (1995) Quantitative recovery of *Burkholderia pseudomallei* from soil in Thailand. Trans R Soc Trop Med Hyg 89: 488-490.

9. Finkelstein RA, Atthasampunna P, Chulasamaya M (2000) Pseudomonas (Burkholderia) pseudomallei in Thailand, 1964-1967: geographic distribution of the organism, attempts to identify cases of active infection, and presence of antibody in representative sera. The American Journal of Tropical Medicine and Hygiene 62: 232-239.

10. Nachiangmai N, Patamasucon P, Tipayamonthein B, Kongpon A, Nakaviroj S (1985) *Pseudomonas pseudomallei* in southern Thailand. Southeast Asian J Trop Med Public Health 16: 83-87.

11. Wongratanacheewin S, Sirisinha S (2012) Epidemiology of melioidosis in Thailand. In: Ketheesan N, editor. Melioidosis - A Century of Observation and Research. San Diego: Elsevier. pp. 37-42.

12. Limmathurotsakul D, Wongratanacheewin S, Teerawattanasook N, Wongsuvan G, Chaisuksant S, et al. (2010) Increasing incidence of human melioidosis in Northeast Thailand. The American Journal of Tropical Medicine and Hygiene 82: 1113-1117.

13. Tiyawisutsri R, Peacock SJ, Langa S, Limmathurotsakul D, Cheng AC, et al. (2005) Antibodies from patients with melioidosis recognize *Burkholderia mallei* but not *Burkholderia thailandensis* antigens in the indirect hemagglutination assay. Journal of Clinical Microbiology 43: 4872-4874.

14. Kanaphun P, Thirawattanasuk N, Suputtamongkol Y, Naigowit P, Dance DA, et al. (1993) Serology and carriage of *Pseudomonas pseudomallei*: a prospective study in 1000 hospitalized children in northeast Thailand. J Infect Dis 167: 230-233.

15. Limmathurotsakul D, Wongsuvan G, Aanensen D, Ngamwilai S, Saiprom N, et al. (2014) Melioidosis caused by *Burkholderia pseudomallei* in drinking water, Thailand, 2012. Emerg Infect Dis 20: 265-268.

16. Goodyear A, Bielefeldt-Ohmann H, Schweizer H, Dow S (2012) Persistent gastric colonization with *Burkholderia pseudomallei* and dissemination from the gastrointestinal tract following mucosal inoculation of mice. PLoS ONE 7: e37324.

17. McCormick JB, Sexton DJ, McMurray JG, Carey E, Hayes P, et al. (1975) Human-to-human transmission of *Pseudomonas pseudomallei*. Annals of Internal Medicine 83: 512.

18. Sanford JP (1977) Melioidosis: Forgotten but not gone. Trans Am Clin Climatol Assoc 89: 201-205.

19. Osteraas GR, Hardman JR, Bass JW, Wilson C (1971) Neonatal Melioidosis. Am J Dis Chl 122: 446-448.

20. (2002) Public Health Security and Bioterrorism Preparedness and Response Act 107th ed.

21. Dance DA (2005) Melioidosis and glanders as possible biological weapons. In: Alibek Fa, editor. Bioterrorism and Infectious Agents. New York: Springer Science+Business Media Inc. pp. 99-145.

22. Yee KC, Lee MK, Chua CT, Puthucheary SD (1988) Melioidosis, the great mimicker: a report of 10 cases from Malaysia. J Trop Med Hyg 91: 249-254.

23. Currie BJ, Fisher DA, Anstey NM, Jacups SP (2000) Melioidosis: acute and chronic disease, relapse and re-activation. Trans R Soc Trop Med Hyg 94: 301-304.

24. Currie BJ, Chaowagul W, Cheng AC (2012) Clinical features of acute melioidosis. In: Ketheesan N, editor. Melioidosis- A Century of Observation and Research. San Diego: Elsevier. pp. 113-119.

25. White NJ (2003) Melioidosis. Lancet 361: 1715-1722.

26. Ngauy V, Lemeshev Y, Sadowski L, Crawford C (2005) Cutaneous melioidosis in a man who was taken as prisoner of war by the Japanese during World War II. J Clin Microbiol 43: 970-972.

27. Kishimoto RAM, Brown GLL, Blair EBC, Wenkheimer D (1971) Melioidosis: Serological studies on US Army personnel returning from Southeast Asia. Military Medicine 136: 694-698.

28. White NJ, Chaowagul W, Wuthiekanun V, Dance DAB, Wattanagoon Y, et al. (1989) Halving of severe melioidosis by ceftazidime. The Lancet 334: 697-701.

29. Chierakul W, Chetchotisakd P (2012) Parenteral antimicrobial therapy for melioidosis. In: Ketheesan N, editor. Melioidosis: A Century of Observation and Research. San Diego: Elsevier. pp. 185-196.

30. Chantratita N, Rholl DA, Sim B, Wuthiekanun V, Limmathurotsakul D, et al. (2011) Antimicrobial resistance to ceftazidime involving loss of penicillin-binding protein 3 in *Burkholderia pseudomallei*. Proc Natl Acad Sci U S A 108: 17165-17170.

31. Wuthiekanun V, Cheng AC, Chierakul W, Amornchai P, Limmathurotsakul D, et al. (2005) Trimethoprim/sulfamethoxazole resistance in clinical isolates of Burkholderia pseudomallei. J Antimicrob Chemother 55: 1029-1031.

32. St. John JA, Ekberg JAK, Dando SJ, Meedeniya ACB, Horton RE, et al. (2014) *Burkholderia pseudomallei* penetrates the brain via destruction of the olfactory and trigeminal nerves: implications for the pathogenesis of neurological melioidosis. mBio 5.

33. Wiersinga WJ, Wieland CW, Dessing MC, Chantratita N, Cheng AC, et al. (2007) Toll-like receptor 2 impairs host defense in gram-negative sepsis caused by *Burkholderia pseudomallei* (Melioidosis). PLoS Med 4: e248.

34. Wiersinga WJ, Wieland CW, Roelofs JJTH, van der Poll T (2008) MyD88 dependent signaling contributes to protective host defense against *Burkholderia pseudomallei*. PLoS ONE 3: e3494.

35. West TE, Chierakul W, Chantratita N, Limmathurotsakul D, Wuthiekanun V, et al. (2012) Toll-like receptor 4 region genetic variants are associated with susceptibility to melioidosis. Genes Immun 13: 38-46.

36. Stevens MP, Galyov EE (2004) Exploitation of host cells by *Burkholderia pseudomallei*. Int J Med Microbiol 293: 549-555.

37. Chanchamroen S, Kewcharoenwong C, Susaengrat W, Ato M, Lertmemongkolchai G (2009) Human polymorphonuclear neutrophil responses to *Burkholderia pseudomallei* in healthy and diabetic subjects. Infect Immun 77: 456-463.

38. Tan GY, Liu Y, Sivalingam SP, Sim SH, Wang D, et al. (2008) *Burkholderia pseudomallei* aerosol infection results in differential inflammatory responses in BALB/c and C57Bl/6 mice. J Med Microbiol 57: 508-515.

39. Barnes JL, Williams NL, Ketheesan N (2008) Susceptibility to *Burkholderia pseudomallei* is associated with host immune responses involving tumor necrosis factor receptor-1 (TNFR1) and TNF receptor-2 (TNFR2). FEMS Immunol Med Microbiol 52: 379-388.

40. Santanirand P, Harley VS, Dance DAB, Drasar BS, Bancroft GJ (1999) Obligatory role of gamma interferon for host survival in a murine model of infection with *Burkholderia pseudomallei*. Infection and Immunity 67: 3593-3600.

41. Wiersinga WJ, Wieland CW, van der Windt GJW, de Boer A, Florquin S, et al. (2007) Endogenous interleukin-18 improves the early antimicrobial host response in mevere melioidosis. Infection and Immunity 75: 3739-3746.

42. Haque A, Chu K, Easton A, Stevens MP, Galyov EE, et al. (2006) A live experimental vaccine against *Burkholderia pseudomallei* elicits CD4+ T cell-mediated immunity, priming T cells specific for 2 type III secretion system proteins. J Infect Dis 194: 1241-1248.

43. Rowland CA, Lertmemongkolchai G, Bancroft A, Haque A, Lever MS, et al. (2006) Critical role of type 1 cytokines in controlling initial infection with *Burkholderia mallei*. Infection and Immunity 74: 5333-5340.

44. Tippayawat P, Pinsiri M, Rinchai D, Riyapa D, Romphruk A, et al. (2011) *Burkholderia pseudomallei* proteins presented by monocyte-derived dendritic cells stimulate human memory T cells in vitro. Infect Immun 79: 305-313.

45. Chierakul W, Rajanuwong A, Wuthiekanun V, Teerawattanasook N, Gasiprong M, et al. (2004) The changing pattern of bloodstream infections associated with the rise in HIV prevalence in northeastern Thailand. Trans R Soc Trop Med Hyg 98: 678-686.

46. Chenthamarakshan V, Kumutha MV, Vadivelu J, Puthucheary SD (2001) Distribution of immunoglobulin classes and IgG subclasses against a culture filtrate antigen of *Burkholderia pseudomallei* in melioidosis patients. J Med Microbiol 50: 55-61.

47. Vasu C, Vadivelu J, Puthucheary SD (2003) The humoral immune response in melioidosis patients during therapy. Infection 31: 24-30.

48. Steinmetz I, Reganzerowski A, Brenneke B, Haussler S, Simpson A, et al. (1999) Rapid identification of *Burkholderia pseudomallei* by latex agglutination based on an exopolysaccharide-specific monoclonal antibody. J Clin Microbiol 37: 225-228.

49. Houghton RL, Reed DE, Hubbard MA, Dillon MJ, Chen H, et al. (2014) Development of a prototype lateral flow immunoassay (LFI) for the rapid diagnosis of melioidosis. PLoS Negl Trop Dis 8: e2727.

50. Silva EB, Dow SW (2013) Development of *Burkholderia mallei* and *pseudomallei* vaccines. Front Cell Infect Microbiol 3: 10.

51. Norris MH, Propst KL, Kang Y, Dow SW, Schweizer HP, et al. (2011) The *Burkholderia pseudomallei* {delta} *asd* mutant exhibits attenuated intracellular infectivity and imparts protection against acute inhalation melioidosis in mice. Infection and Immunity 79: 4010-4018.

52. Propst KL, Mima T, Choi K-H, Dow SW, Schweizer HP (2010) A *Burkholderia pseudomallei* {Delta}*purM* mutant is avirulent in immunocompetent and immunodeficient animals: candidate strain for exclusion from select-agent lists. Infect Immun 78: 3136-3143.

53. Sarkar-Tyson M, Smither SJ, Harding SV, Atkins TP, Titball RW (2009) Protective efficacy of heat-inactivated *B. thailandensis*, *B. mallei* or *B. pseudomallei* against experimental melioidosis and glanders. Vaccine 27: 4447-4451.

54. Nelson M, Prior JL, Lever MS, Jones HE, Atkins TP, et al. (2004) Evaluation of lipopolysaccharide and capsular polysaccharide as subunit vaccines against experimental melioidosis. Journal of Medical Microbiology 53: 1177-1182.

55. Tuanyok A, Stone JK, Mayo M, Kaestli M, Gruendike J, et al. (2012) The genetic and molecular basis of O-antigenic diversity in *Burkholderia pseudomallei* lipopolysaccharide. PLoS Negl Trop Dis 6: e1453.

56. Burtnick MN, Heiss C, Roberts RA, Schweizer HP, Azadi P, et al. (2012) Development of capsular polysaccharide-based glycoconjugates for immunization against melioidosis and glanders. Front Cell Infect Microbiol 2: 108.

57. Ahmed K, Enciso HD, Masaki H, Tao M, Omori A, et al. (1999) Attachment of *Burkholderia pseudomallei* to pharyngeal epithelial cells: a highly pathogenic bacteria with low attachment ability. The American Journal of Tropical Medicine and Hygiene 60: 90-93.

58. Harley VS, Dance DA, Drasar BS, Tovey G (1998) Effects of *Burkholderia pseudomallei* and other *Burkholderia* species on eukaryotic cells in tissue culture. Microbios 96: 71-93.

59. Jones AL, Beveridge TJ, Woods DE (1996) Intracellular survival of *Burkholderia pseudomallei*. Infection and Immunity 64: 782-790.

60. Pruksachartvuthi S, Aswapokee N, Thankerngpol K (1990) Survival of *Pseudomonas pseudomallei* in human phagocytes. Journal of Medical Microbiology 31: 109-114.

61. Razak N, Ismail G (1982) Interaction of human polymorphonuclear leukocytes with *Pseudomonas pseudomallei*. The Journal of General and Applied Microbiology 28: 509-518.

62. Harley VS, Dance DA, Tovey G, McCrossan MV, Drasar BS (1998) An ultrastructural study of the phagocytosis of *Burkholderia pseudomallei*. Microbios 94: 35-45.

63. Warawa J, Woods DE (2005) Type III secretion system cluster 3 is required for maximal virulence of *Burkholderia pseudomallei* in hamster infection model. FEMS Microbiol Lett 242: 101-108.

64. Stevens MP, Wood MW, Taylor LA, Monaghan P, Hawes P, et al. (2002) An Inv/Mxi-Spa-like type III protein secretion system in *Burkholderia pseudomallei* modulates intracellular behavior of the pathogen. Mol Microbiol 46: 649-659.

65. Stevens MP, Friebel A, Taylor LA, Wood MW, Brown PJ, et al. (2003) A *Burkholderia pseudomallei* type III secreted protein, BopE, facilitates bacterial invasion of epithelial cells and exhibits guanine nucleotide exchange factor activity. J Bacteriol 185: 4992-4996.

66. Cullinane M, Gong L, Li X, Lazar-Adler N, Tra T, et al. (2008) Stimulation of autophagy suppresses the intracellular survival of *Burkholderia pseudomallei* in mammalian cell lines. Autophagy 4: 744-753.

67. Stevens MP, Haque A, Atkins T, Hill J, Wood MW, et al. (2004) Attenuated virulence and protective efficacy of a *Burkholderia pseudomallei* bsa type III secretion mutant in murine models of melioidosis. Microbiology 150: 2669-2676.

68. Whitlock GC, Valbuena GA, Popov VL, Judy BM, Estes DM, et al. (2009) *Burkholderia mallei* cellular interactions in a respiratory cell model. Journal of Medical Microbiology 58: 554-562.

69. Stevens MP, Stevens JM, Jeng RL, Taylor LA, Wood MW, et al. (2005) Identification of a bacterial factor required for actin-based motility of *Burkholderia pseudomallei*. Mol Microbiol 56: 40-53.

70. Kespichayawattana W, Rattanachetkul S, Wanun T, Utaisincharoen P, Sirisinha S (2000) *Burkholderia pseudomallei* induces cell fusion and actin-associated membrane protrusion: a possible mechanism for cell-to-cell spreading. Infect Immun 68: 5377-5384.

71. French CT, Toesca IJ, Wu T-H, Teslaa T, Beaty SM, et al. (2011) Dissection of the *Burkholderia* intracellular life cycle using a photothermal nanoblade. Proceedings of the National Academy of Sciences 108: 12095-12100.

72. Burtnick MN, Brett PJ, Harding SV, Ngugi SA, Ribot WJ, et al. (2011) The cluster 1 type VI secretion system is a major virulence determinant in *Burkholderia pseudomallei*. Infection and Immunity 79: 1512-1525.

73. Wong KT, Puthucheary SD, Vadivelu J (1995) The histopathology of human melioidosis. Histopathology 26: 51-55.

74. Atkins T, Prior R, Mack K, Russell P, Nelson M, et al. (2002) Characterisation of an acapsular mutant of *Burkholderia pseudomallei* identified by signature tagged mutagenesis. J Med Microbiol 51: 539-553.

75. Wikraiphat C, Charoensap J, Utaisincharoen P, Wongratanacheewin S, Taweechaisupapong S, et al. (2009) Comparative in vivo and in vitro analyses of putative virulence factors of *Burkholderia pseudomallei* using lipopolysaccharide, capsule and flagellin mutants. FEMS Immunol Med Microbiol 56: 253-259.

76. Ulrich RL, Deshazer D, Brueggemann EE, Hines HB, Oyston PC, et al. (2004) Role of Quorum sensing in the pathogenicity of *Burkholderia pseudomallei*. J Med Microbiol 53: 1053-1064.

77. Horton RE, Grant GD, Matthews B, Batzloff M, Owen SJ, et al. (2013) Quorum sensing negatively regulates multinucleate cell formation during intracellular growth of *Burkholderia pseudomallei* in macrophage-like cells. PLoS ONE 8: e63394.

78. Chuaygud T, Tungpradabkul S, Sirisinha S, Chua KL, Utaisincharoen P (2008) A role of *Burkholderia pseudomallei* flagella as a virulent factor. Transactions of the Royal Society of Tropical Medicine and Hygiene 102: S140-S144.

79. Essex-Lopresti AE, Boddey JA, Thomas R, Smith MP, Hartley MG, et al. (2005) A type IV pilin, PilA, contributes to adherence of *Burkholderia pseudomallei* and virulence in vivo. Infect Immun 73: 1260-1264.

80. Norris MH, Kang Y, Lu D, Wilcox BA, Hoang TT (2009) Glyphosate resistance as a novel select-agent-compliant, non-antibiotic selectable-marker in chromosomal mutagenesis of the essential genes *asd* and *dapB* of *Burkholderia pseudomallei*. Appl Environ Microbiol 75: 6062-6075.

81. Galan JE, Nakayama K, Curtiss R (1990) Cloning and characterization of the *asd* gene of *Salmonella typhimurium*: use in stable maintenance of recombinant plasmids in *Salmonella* vaccine strains. Gene 94: 29-35.

82. Pilatz S, Breitbach K, Hein N, Fehlhaber B, Schulze J, et al. (2006) Identification of *Burkholderia pseudomallei* genes required for the intracellular life cycle and *in vivo* virulence. Infect Immun 74: 3576-3586.

83. Kespichayawattana W, Intachote P, Utaisincharoen P, Sirisinha S (2004) Virulent *Burkholderia pseudomallei* is more efficient than avirulent *Burkholderia thailandensis* in invasion of and adherence to cultured human epithelial cells. Microbial Pathogenesis 36: 287-292.

84. Gan Y-H, Chua KL, Chua HH, Liu B, Hii CS, et al. (2002) Characterization of *Burkholderia pseudomallei* infection and identification of novel virulence factors using a *Caenorhabditis elegans* host system. Molecular Microbiology 44: 1185-1197.

85. Lee S-H, Ooi S-K, Mahadi NM, Tan M-W, Nathan S (2011) Complete killing of *Caenorhabditis elegans* by *Burkholderia pseudomallei* is dependent on prolonged direct association with the viable pathogen. PLoS ONE 6: e16707.

86. O'Quinn AL, Wiegand EM, Jeddeloh JA (2001) *Burkholderia pseudomallei* kills the nematode *Caenorhabditis elegans* using an endotoxin-mediated paralysis. Cellular Microbiology 3: 381-393.

87. Wand M, Muller C, Titball R, Michell S (2011) Macrophage and *Galleria mellonella* infection models reflect the virulence of naturally occurring isolates of *B. pseudomallei*, *B. thailandensis* and *B. oklahomensis*. BMC Microbiology 11: 11.

88. Müller CM, Conejero L, Spink N, Wand ME, Bancroft GJ, et al. (2012) Role of RelA and SpoT in *Burkholderia pseudomallei* virulence and immunity. Infection and Immunity 80: 3247-3255.

89. Burtnick MN, Brett PJ, Nair V, Warawa JM, Woods DE, et al. (2008) *Burkholderia pseudomallei* type III secretion system mutants exhibit delayed vacuolar escape phenotypes in RAW 264.7 murine macrophages. Infect Immun 76: 2991-3000.

90. Holden MTG, Titball RW, Peacock SJ, Cerdeno-Tarraga AM, Atkins T, et al. (2004) Genomic plasticity of the causative agent of melioidosis, *Burkholderia pseudomallei*. Proc Natl Acad Sci USA 101: 14240-14245.

91. Tuanyok A, Leadem B, Auerbach R, Beckstrom-Sternberg S, Beckstrom-Sternberg J, et al. (2008) Genomic islands from five strains of *Burkholderia pseudomallei*. BMC Genomics 9: 566.

92. Gallagher LA, Shendure J, Manoil C (2011) Genome-Scale Identification of Resistance Functions in *Pseudomonas aeruginosa* Using Tn-seq. mBio 2.

93. Chan K, Kim CC, Falkow S (2005) Microarray-based detection of *Salmonella enterica* serovar typhimurium transposon mutants that cannot survive in macrophages and mice. Infection and Immunity 73: 5438-5449.

94. Peterson KM (2002) Expression of *Vibrio cholerae* virulence genes in response to environmental signals. Curr Issues Intest Microbiol 3: 29-38.

95. Balasubramanian D, Schneper L, Kumari H, Mathee K (2013) A dynamic and intricate regulatory network determines *Pseudomonas aeruginosa* virulence. Nucleic Acids Research 41: 1-20.

96. Lipscomb L, Schell MA (2011) Elucidation of the regulon and cis-acting regulatory element of HrpB, the AraC-type regulator of a plant pathogen-like type III secretion system in *Burkholderia pseudomallei*. J Bacteriol 193: 1991-2001.

97. Chen Y, Wong J, Sun GW, Liu Y, Tan GY, et al. (2011) Regulation of type VI secretion system during *Burkholderia pseudomallei* infection. Infect Immun 79: 3064-3073.

98. Sun GW, Chen Y Fau - Liu Y, Liu Y Fau - Tan G-YG, Tan Gy Fau - Ong C, Ong C Fau - Tan P, et al. Identification of a regulatory cascade controlling Type III Secretion System 3 gene expression in *Burkholderia pseudomallei*.

99. Kang Y, Norris MH, Zarzycki-Siek J, Nierman WC, Donachie SP, et al. (2011) Transcript amplification from single bacterium for transcriptome analysis. Genome Research 21: 925-935.

Chapter 2. Non-antibiotic selectable markers and production of the *Burkholderia pseudomallei* Δ*asd* and Δ*dapB* mutants

Published as:

Glyphosate Resistance as a Novel Select-Agent-Compliant Non-antibiotic Selectable-Marker: Chromosomal Mutagenesis of the Essential *Burkholderia pseudomallei asd* and *dapB* Genes in Applied and Environmental Microbiology 2009 Oct;75(19):6062-6075.

Michael H. Norris,[2] Yun Kang,[2] Diana Lu,[1] Bruce A.Wilcox,[3] and Tung T. Hoang[1,2]*

Department of Microbiology[1], Department of Molecular Biosciences and Bioengineering[2], Department of Ecology and Health[3], University of Hawaii at Manoa, Honolulu, HI 96822, USA

* Corresponding author. Tel: +1 808 956 3522; Fax: +1 808 956 5339; e-mail: tongh@hawaii.edu

Journal Section: Genetics and Molecular Biology

2.1 ABSTRACT

Genetic manipulation in the category B select agents *Burkholderia pseudomallei* and *Burkholderia mallei* has been stifled, due to the lack of compliant selectable-markers. Hence, there is a need for additional select-agent-compliant selectable-markers. We engineered a selectable-marker based upon the *gat* gene (encoding glyphosate-acetyl-transferase), which confers resistance to the common herbicide glyphosate (GS). To show the ability of GS to inhibit bacterial growth, we determined the effective GS concentrations for *Escherichia coli* and several *Burkholderia* species. Plasmids based on *gat*, flanked by unique flip-recombination-target (*FRT*) sequences, were constructed for allelic-replacement. Both allelic-replacement approaches, using i) the counter-selectable marker *pheS* and the *gat-FRT* cassette or ii) the DNA incubation method with the *gat-FRT* cassette, were successfully utilized to create deletions in the *asd* and *dapB* genes of wildtype *B. pseudomallei* strains. The *asd* and *dapB* genes encode for an aspartate-semialdehyde-dehydrogenase (BPSS1704, chromosome 2) and dihydrodipicolinate reductase (BPSL2941, chromosome 1), respectively. Mutants unable to grow on media without diaminopimelate (DAP) and other amino acids of this pathway were PCR verified. These mutants displayed cellular morphology consistent with the inability to cross-link peptidoglycan in the absence of DAP. The *B. pseudomallei* 1026b D*asd*::*gat-FRT* mutant was complemented with the asd_{Bp} gene on a site-specific transposon, mini-Tn7-*bar*, by selecting with phosphinothricin for the *bar* gene (encoding bialaphos/phosphinothricin resistance). We conclude that the *gat* gene is one of very few appropriate, effective, and beneficial compliant markers available for *Burkholderia* select-agent species. Together with the *bar* gene, the *gat*-cassette will aid various genetic manipulations in *Burkholderia* select-agent species.

2.2 INTRODUCTION

Members of the genus *Burkholderia*, comprised of over 40 different species, are extremely diverse Gram-negative non-spore-forming facultative bacilli. Many exist as innocuous soil saprophytes or plant pathogens (53), while other *Burkholderia* species cause human and animal diseases. Among these human and animal pathogens are the etiological agents of melioidosis (*Burkholderia pseudomallei*) and glanders (*Burkholderia mallei*) (10, 56, 57). Melioidosis is an emerging infectious disease generally considered endemic to Southeast Asia and Northern Australia (14). Positive diagnoses in many tropical countries around the world have expanded the global awareness of melioidosis (4, 17, 29, 30, 33, 40, 44, 47, 58). In contrast to the ubiquitous nature of *B. pseudomallei*, *B. mallei* is also a highly infectious agent causing glanders, a predominantly equine disease (39, 56). *B. mallei*, a clone derived from genomic downsizing of *B. pseudomallei,* has been used in biowarfare (20). This historical significance, along with the low infectious dose and route of infection, has contributed to the decision by the Centers for Disease Control and Prevention to classify these two microbes as category B select agents (48).

Classification of *B. pseudomallei* as a select agent has stimulated interest and research into the pathogenesis of melioidosis, necessitating the development of appropriate tools for genetic manipulation. In the struggle to elucidate the molecular mechanisms of pathogenesis, selectable markers are indispensable genetic tools (51). Current regulations prohibit the cloning of clinically important antibiotic resistance genes into human, animal, or plant select-agent pathogens, if the transfer could compromise the ability to treat or control the disease. The only antibiotic markers currently approved for use in *B. pseudomallei* are based on aminoglycoside resistance (gentamycin, kanamycin, and zeocin) (51). However, the efficacy of these markers is

limited due to i) high levels of aminoglycoside resistance inherent within the *Burkholderia* genus and ii) spontaneous resistance in *B. pseudomallei* (11, 24, 46). In addition, the use of aminoglycosides for selection (e.g. gentamycin) may require aminoglycoside efflux-pump mutants (11, 38). Utilization of aminoglycoside selection in efflux-pump mutants may be counter-intuitive as aminoglycosides, although not routinely used for treatment, could be used effectively against efflux-pump mutants in case of accidental exposure by aminoglycoside-sensitive strains (22, 50). With the advent of improved selective media containing gentamycin by Ashdown in 1979 (1), isolation of gentamycin sensitive *B. pseudomallei* strains is rare. However, prior to this, many gentamycin and kanamycin sensitive *B. pseudomallei* strains were isolated (19, 23) and successful treatment with aminoglycosides has been documented (13, 62). Another potential drawback is that efflux-pumps play a major role in bacterial physiology and mutating them may change the pathogenic traits under investigation (8, 45). A more logical approach employs alternative non-antibiotic selectable-markers conferring resistance to compounds that are not potentially important in clinical treatment.

There have been very few non-antibiotic resistance markers utilized successfully in *Burkholderia* species. The non-antibiotic selectable-marker, based on Tel^r, has been successfully developed and used in *Pseudomonas putida*, *Pseudomonas fluorescens*, and *Burkholderia thailandensis* (3, 32, 49). The engineering of Tel^r-*FRT* cassettes, coupled to flip-recombination-target (*FRT*) sequences, could be used to generate unmarked mutations and allow recycling of the Tel^r selectable-marker (3). In addition, utilization of Flp-*FRT* resistant-cassettes to generate mutants allows downstream modification and manipulation, such as fusion integration (34). However, the disadvantage of the Tel^r-cassette is the number of genes required (*kilA-telA-telB*)

and the large size (>3 kb), making it less likely to obtain PCR product for allelic-replacement by natural transformation (52). Another potentially useful non-antibiotic selectable marker is based on the *bar* gene encoding for resistance to bialaphos or its degradation product phosphinothricin (PPT) (55). PPT inhibits glutamine synthetase in plants (54), starving the cell for glutamine, and the *bar* gene has been used successfully in Gram-negatives as a selection marker (26). In select-agent *Burkholderia* species, however, the PPT MIC was found to be greater than 1024 mg/ml (M. Frazier, K. Choi, A. Kumar, C. Lopez, R. R. Karkhoff-Schweizer, and H. P. Schweizer, 2007 American Society for Microbiology, Biodefense and Emerging Diseases Research Meeting, Washington, DC). We have found that the effective PPT concentration for *B. pseudomallei* and *B. mallei* to be ~2.5% (25,000 mg/ml; data not shown). The high concentration of PPT required for selection in these species may be costly, considering purified PPT costs ~$380 per gram. Therefore, further development of non-antibiotic makers and search for a more economical source of herbicide to use in restricted select-agent species are required.

Work by Castle *et al*. (6) generated a highly active GAT (glyphosate *N*-acetyltransferase) enzyme for plant engineering, making it possible to utilize the *gat* gene as an effective non-antibiotic marker for bacterial selection with glyphosate. The commonly used herbicide, glyphosate (GS), inhibits the 5-enolpyruvylshikimate-3-phospate synthase (EPSPS) of plants through competition with phosphoenolpyruvate (PEP) for overlapping binding sites on EPSPS (16), depriving plants of the three aromatic amino acids (Fig. 1). Since humans and animals obtain tryptophan and phenylalanine (giving rise to tyrosine) through dietary intake, GS is relatively non-toxic. Similar to plants, bacteria must make these amino acids, when lacking, from basic precursors. GS has been found to be inhibitory to a variety of different bacteria including

Pseudomonas aeruginosa, *Escherichia coli*, *Bacillus subtilis*, and *Bradyrhizobium japonicum* (18, 61), while other bacterial strains are able to metabolize low concentrations of GS (31, 36). Although *B. pseudomallei* has been reported to have two genes (*glpA* and *glpB*) for GS degradation and metabolism (43), our searches of all available genomes of *Burkholderia* species in the GenBank yielded no *glpA* or *glpB* genes within this genus. GS resistance by bacteria has been documented through the EPSPS target mutations or GS detoxification mechanisms (41). However, these mechanisms did not give resistance to relatively high GS concentrations. More recently, directed-evolution of the *gat*-gene, based on various bacterial *gat* sequences and selection in *E. coli*, yielded a very active GAT protein sequence with an efficiency increase of nearly four orders of magnitude (6), holding promise as an appropriate non-antibiotic marker for select-agent species.

Here, we engineered and tested a novel non-antibiotic selectable-marker (*gat*) for use in the select-agent *B. pseudomallei*. GS is the active ingredient in RoundUp®, which was used for selection (Fig. 1). The effective compound GS is readily available, inexpensive, relatively non-toxic, very soluble, not clinically important, and yields tight selection. The engineered *gat* marker (~500 bp) was optimized for *Burkholderia* codon-usage and adapted (with a *Burkholderia rpsL* promoter) for use in the select agent *B. pseudomallei*. Effective concentrations of GS in several species of *Burkholderia*, including the select agents *B. pseudomallei* and *B. mallei*, were determined. Using the *gat* gene, we created deletional mutants of the essential asd_{Bp} and $dapB_{Bp}$ genes (encoding aspartate-semialdehyde dehydrogenase and dihydrodipicolinate reductase) in two wildtype *B. pseudomallei* strains. The Dasd_{Bp} mutant of *B. pseudomallei* showed a phenotypic defect consistent with the lack of diaminopimelate for cell-

wall cross-linking. Complementation of the *B. pseudomallei* Dasd_{Bp} mutant with the asd_{Bp} located on a site-specific transposon, mini-Tn7-*bar*, was successful by using an inexpensive source of phosphinothricin for selection.

2.3 MATERIALS AND METHODS:

Bacterial strains, media, and culturing conditions. All strains and plasmids used in this study are located in Tables 1 and 2. All manipulations with *B. pseudomallei* and *B. mallei* were conducted in a CDC/USDA approved and registered BSL3 facility at UHM, and experiments with these select-agents were performed with BSL3 practices by following the recommendations of the *Biosafety in Microbiological and Biomedical Laboratories* (BMBL) 5th edition.

Luria-Bertani (LB) medium (Difco) was used to culture all *E. coli* strains. *Burkholderia* strains (*B. pseudomallei, B. mallei, B. thailandensis*, *B. cenocepacia*, and *B. dolosa*) were cultured in LB or 1x M9 minimal medium + 20 mM glucose (MG). Diaminopimelate (DAP) was prepared in 1 M NaOH as a 100 mg/ml stock and used when necessary as described previously (3). A ~1 L bottle of the 'super-concentrated' herbicide RoundUp® (50% w/v GS) was purchased at a City Mill® hardware store as a source of GS for approximately $50 and used in this study. Purified GS was purchased from Sigma. We also purchased the herbicide Finale (9.5 L with 11.33% w/v phosphinothricin) for $125 at a local farm supply store (Pacific Agricultural Sales and Services), and it was used as a source of phosphinothricin (PPT) in this study. MG medium plus GS or PPT was utilized for *gat* or *bar* selection, respectively. Since GS blocks the biosynthesis of aromatic amino acids (Fig. 1), it is necessary to use minimal media without Phe, Trp, and Tyr. We observed that minimal media provided with any two aromatic amino acids abolished the selective potential of GS. Likewise, minimal media lacking glutamine is required for selection of *bar* with PPT. Antibiotics and non-antibiotic antibacterial compounds in solid media were utilized as follows: For *E. coli*, ampicillin (Ap) 110 μg/ml, GS 0.3%, kanamycin (Km) 35 μg/ml, and PPT 0.3% were used; for *B. mallei*, GS 0.2% effective concentration was

determined; for *B. pseudomallei*, GS 0.3% and PPT 2.5% were used; and for *B. thailandensis*, Km 500 µg/ml, GS 0.04%, and PPT 1.5% were used.

Two derivatives of *E. coli* EPmax10B (BioRad), one containing *lacI*^{q} and *pir* (E1869) and the other containing *lacI*^{q}, *pir*, and *leu*$^{+}$ (E1889), were routinely used as cloning strains in rich and minimal media, respectively. The *E. coli* conjugal and suicidal strain, EPMax10B-*pir116*-D*asd*-*mob*-Km-D*trp*::Gm (E1354), was used for plasmid mobilization into *B. pseudomallei* and *B. thailandensis*. Growth of *E. coli* Δ*asd* strains was carried out as previously described (3). *E. coli* strain EPMax10B-*pir116*-D*asd*::Gm (E1345) was used for cloning of *asd*-complementing vectors (e.g. pBAKA; *asd* gene encodes for aspartate-semialdehyde dehydrogenase). Briefly, selection of E1345 complemented with various *asd*- and *gat*-containing constructs (e.g. pBAKA-D*asd*$_{Bp}$::*gat-FRT* or pBAKA-D*dapB*$_{Bp}$::*gat-FRT*) was performed on MG + GS media supplemented with leucine (Leu). To simplify selection and replace strain E1345, EPMax10B-*lacI*^{q}/*pir*/*leu*$^{+}$/Δ*asd*::Gm (E1951) was later created to select for *asd*-, *bar*-, and *gat*-containing plasmids on MG + GS or PPT media, so that leucine can be omitted from the minimal media. Selection of *asd*-, *bar*-, and *gat*-containing plasmids in the conjugation proficient strain E1354 was carried out with MG + Leu, Trp, and GS or PPT; in the absence of a complementing *asd* gene (e.g. pBBR1MCS-2-PC$_{S12}$-*gat*), an additional 1 mM each of lysine (Lys), methionine (Met), threonine (Thr) and 100 µg/ml of DAP were added. For selection against E1354 following conjugation, Leu and Trp were omitted from the growth media. Counter-selection of *pheS* was carried out on MG media containing 0.1% *p*-chlorophenylalanine (cPhe; DL-4-chlorophenylalanine from Acros Organics) as described previously (3). *B. pseudomallei* Δ*asd*$_{Bp}$::*gat-FRT* and Δ*dapB*$_{Bp}$::*gat-FRT* mutants were grown on rich LB media + 200 µg/ml DAP. For Δ*dapB*$_{Bp}$::*gat-FRT* mutants grown in minimal media, MG medium + 200 µg/ml DAP +

1 mM Lys was used; this minimal medium was also supplemented with 1 mM of both Met and Thr for growing Δ*asd*$_{Bp}$::*gat-FRT* mutants.

Molecular methods and reagents. Oligonucleotides used in this study are shown in Table 3. All molecular methods and reagents used were as described previously (3).

Conjugation into *Burkholderia* spp. Conjugation between the *E. coli* strain E1354 and *Burkholderia* strains was routinely carried out by growing both donor and recipient to log-phase prior to conjugation. Equal volumes of the donor and recipient (500 ml each) were mixed and centrifuged at 8,000x *g* for 1 minute. The supernatant was removed leaving approximately 30 μl of the conjugation mix which was spotted directly onto the surface of an LB plate with 100 μg/ml of DAP and incubated overnight at 37°C. Cells were scraped off using a disposable loop, resuspended and washed twice in 1 ml of 1x M9 buffer (to remove trace amino acids), and then resuspended in a final 1 ml of the same buffer. Aliquots of 100 μl and 200 μl of the cell suspensions were plated on the appropriate media. Conjugation using this method usually resulted in 50-100 colonies for recombination of non-replicating vectors when 100 μl of a conjugation recovery was plated, and 500-700 colonies for replicating plasmids when 100 μl of a 10x dilution was plated.

Determination of GS minimal inhibitory concentrations (MIC) and effective concentrations. To determine the liquid MIC for GS, we first grew all strains overnight in LB. One ml of culture was harvested by centrifugation, washed twice in 1x M9 buffer to remove trace amounts of amino acids, resuspended in 1x M9 buffer, and diluted 100x in the same buffer.

GS gradients in MG medium with a starting concentration of 0.8% GS and decreasing by 2x dilutions to 0.00625% GS were inoculated with the 100x dilutions (~10^5 cfu/ml) of each strain listed in Table 4. The liquid MIC was then determined after 2 days of incubation, with shaking, at 37°C. To establish the MIC of GS on solid media, we used MG + GS + 1.5 % agar (w/v). LB cultures of all species were grown to an OD_{600} of ~ 0.8. One ml of each culture was harvested by centrifugation, washed twice in 1x M9 buffer to remove trace amounts of amino acids, and resuspended in 1x M9 buffer. One hundred µl of the high-cell-density cultures were then plated on MG plates containing different concentrations of GS (ranging from 0-0.5%). The concentration where no growth was observed after 2 weeks was identified as the plate MIC. The GS concentration for each species was increased by ~30% above the MIC, and complete growth inhibition after 4 days in liquid and 3 weeks on solid media was taken as the effective concentration ($[GS]_{EC}$) (Table 4).

Engineering of pUC57-P_{S12}-*gat*, pwFRT-PC_{S12}-*gat*, and pBBR1MCS-2-PC_{S12}-*gat*. Driven by the *B. pseudomallei rpsL* promoter (P_{S12}) (60), the *gat* gene sequence was optimized to the codon-usage of *B. pseudomallei*. The *gat*-gene sequence was synthesized by GenScript Corporation, which was cloned into pUC57 as an EcoRV-XhoI fragment yielding pUC57-P_{S12}-*gat*. pUC57-P_{S12}-*gat* was digested with EcoRV + XhoI and inserted into the EcoRV + XhoI digested pwFRT-Tp^r, replacing the Tp^r-cassette and yielding pwFRT-P_{S12}-*gat*. We overlooked a SacI restriction site, which was removed by site-directed mutagenesis using oligonucleotide #894 to yield pwFRT-P_{S12}-*gat*-SDM. Additionally, the *gat* gene was initially engineered to be driven by the P_{S12}-promoter on pUC57-P_{S12}-*gat*. However, homologous recombination may occur with the P_{S12}-promoter region at the native locus on the chromosome or an additional P_{S12}-promoter

located on pBAKA. To prevent this possibility, the *gat* gene from pwFRT-P$_{S12}$-*gat*-SDM was removed using NcoI + XhoI and ligated into pwFRT-Tel^r cut with the same enzymes, replacing the Tel^r-cassette with the *gat* gene, yielding pwFRT-PC$_{S12}$-*gat* (Fig. 4A). Unique enzyme sites are present on the *gat* cassette to allow for ease of manipulation (Fig. 4A).

pBBR1MCS-2-PC$_{S12}$-*gat* was constructed to first test the effectiveness of GS selection in *E. coli* and *B. thailandensis* by comparing colony numbers on LB + Km and MG + GS media. pBBR1MCS-2 was digested with KpnI, blunt ended, and then digested with XhoI. The resultant fragment was ligated to the 533-bp EcoRV-XhoI PC$_{S12}$-*gat* fragment from pwFRT-PC$_{S12}$-*gat*, yielding pBBR1MCS-2-PC$_{S12}$-*gat*. When introduced into *E. coli* and *B. thailandensis*, this plasmid yielded the same number of colonies on kanamycin-containing media when compared to GS-containing media with RoundUp® as a source of GS (data not shown). This indicates that no other ingredients in RoundUp® have adverse effects on the selection of *gat*-containing constructs and that this source of GS is appropriate for selective media.

Testing the inhibitory action of glyphosate on *Burkholderia* select agent species after 24 hours. We wanted to determine if GS was a bacteriostatic or bactericidal compound by exposing *B. pseudomallei* strains 1026b and K96243 and *B. mallei* ATCC23344 to increasing concentrations of GS for 24 hours. First, *B. mallei* and the two *B. pseudomallei* strains (1026b and K96243) were grown overnight in LB. The cultures were then washed twice in 1 ml of 1x M9 buffer and resuspended in 1 ml of the same buffer, which were inoculated (1:100 dilution) into 3 ml of MG + 0.25%, 0.5%, 1.0%, 1.5%, 2.0%, 2.5%, 3.0%, 3.5%, or 4.0% GS with 30µl of the washed cultures. Immediately, 100 µl of serial dilutions of each culture were plated to determine initial bacterial cfu for each strain. After 24 hours, 100 µl of serial dilutions from each

culture were plated and bacterial cfu were again calculated. We used the ratio of bacterial cfu at 24 hrs to bacterial cfu at initial exposure to determine the percent of survival after 24 hours of exposure to GS (Fig. 2).

Determination of the effective concentration of phosphinothricin and construction of pBBR1MCS-2-PC$_{S12}$-*bar*. The effective concentration of PPT ([PPT]$_{EC}$) from the herbicide Finale was determined in the same manner as for the GS effective concentration. We first determined whether *bar* would be an efficient selectable marker in *E. coli* and *B. thailandensis* by constructing pBBR1MCS-2-PC$_{S12}$-*bar*. The *bar* gene was amplified from pCAMBIA-1301-*bar* using oligonucleotides #881 and #882. The product was then used as a template for a second PCR using oligonucleotides #837 and #882 to introduce the PC$_{S12}$-promoter. The 800 bp PCR product was then digested with XhoI and ligated into the EcoRV + XhoI digested pBBR1MCS-2 to yield pBBR1MCS-2-PC$_{S12}$-*bar*. This construct was then introduced into *E. coli* and, subsequently, into *B. thailandensis* via electroporation. The [PPT]$_{EC}$ was determined to be 0.3% and 1.5% for *E. coli* and *B. thailandensis*, respectively. Introduction of pBBR1MCS-2-PC$_{S12}$-*bar* into *E. coli* and *B. thailandensis* yielded the same number of colonies on kanamycin media as PPT containing media (data not shown), indicating that this source of PPT contains no other ingredients that could adversely affect selection of *bar*-containing constructs. The [PPT]$_{EC}$ for *B. pseudomallei* 1026b, *B. pseudomallei* K96243, and *B. mallei* was found to be 2.5% by the same methods described above for the [GS]$_{EC}$.

Construction of *gat-FRT* and *bar-FRT* vectors. Using pwFRT-PC$_{S12}$-*gat* with TCTAGAAA as the wildtype spacer of the flanking *FRT* sequences, we also constructed four

other plasmids based on four other unique *FRT* sequences: pmFRT-PC_{S12}-*gat* with flanking *FRT*-spacer TGTAGATA; pFRT1-PC_{S12}-*gat* with TCTTGAAA spacer; pFRT2-PC_{S12}-*gat* with TCTAGGAA spacer; and pFRT3-PC_{S12}-*gat* with TCTCGAAA spacer. The differences in the spacer sequence yield unique *FRT*s. The unique *FRT*s in these 5 plasmids (pwFRT-PC_{S12}-*gat*, pmFRT-PC_{S12}-*gat*, pFRT1-PC_{S12}-*gat*, pFRT2-PC_{S12}-*gat*, pFRT3-PC_{S12}-*gat*) allow for multiple rounds of allelic-replacement by recycling the same marker with Flp-*FRT* excision, reducing the risk of chromosomal deletions and rearrangements as observed previously (2). To construct these four plasmids, laboratory vectors pmFRT-Gm^r, pFRT1-Gm^r, pFRT2-Gm^r, and pFRT3-Gm^r were PCR amplified with oligos #715 and #716 to obtain plasmid backbones without the Gm^r-marker. Each plasmid backbone was digested with EcoRV + XhoI and ligated with the PC_{S12}-*gat* fragment obtained from pwFRT-PC_{S12}-*gat* by EcoRV + XhoI digestion. Essentially, the sequences of all four new pFRT-PC_{S12}-*gat-FRT* plasmids are the same as pwFRT-PC_{S12}-*gat*, with the exception of the *FRT*-spacer sequences flanking the *gat* cassette. The *FRT*-flanked *bar* cassette on pwFRT-PC_{S12}-*bar* was constructed by first amplifying the *bar* gene from pCAMBIA-1301-*bar*, via a two-step PCR, as described above for the construction of pBBRMCS1-2-PC_{S12}-*bar*. The 800 bp *bar* fragment was digested with XhoI and ligated into the EcoRV + XhoI digested pwFRT-PC_{S12}-Tel^r, replacing the Tel^r-cassette with the *bar* gene to produce pwFRT-PC_{S12}-*bar*.

Construction of pBAKA-Δasd_{Bp}::*gat-FRT* and pBAKA-Δ$dapB_{Bp}$::*gat-FRT*. The *B. pseudomallei* K96243 asd_{Bp} gene was amplified from chromosomal DNA using oligonucleotides #892 and #893. This asd_{Bp} gene sequence is essentially identical for both K96243 and 1026b. The 1.4 kb fragment was digested with EcoRI + HindIII and cloned into pUC18 digested with

the same enzymes. After cloning, the purified plasmid, pUC18-asd_{Bp}, was then electroporated into the *dam*$^-$ strain GM33. Plasmids were isolated, digested with BclI (*dam* methylation sensitive) + EcoRV, and blunt ended. The plasmid backbone was then ligated to the 0.7 kb fragment from SmaI digested pwFRT-PC_{S12}-*gat,* resulting in a 250 bp deletion in the asd_{Bp} gene. pUC18-Δasd_{Bp}::*gat-FRT* was then digested with EcoRI + HindIII and the 1.9 kb fragment was cloned into pBAKA, cut with the same enzymes, to produce pBAKA-Δasd_{Bp}::*gat-FRT*. The *gat* gene is in the same orientation as the asd_{Bp} gene (Fig. 5A).

To construct pBAKA-Δ$dapB_{Bp}$::*gat-FRT*, the *B. pseudomallei* K96243 *dapB* gene was amplified from chromosomal DNA using oligonucleotides #1048 and #1050. The 1.9 kb fragment was digested with HindIII + XbaI and ligated into pBAKA cut with the same enzymes. pBAKA-$dapB_{Bp}$ was then digested with SalI and ligated with the 0.7 kb fragment from the SalI digestion of pwFRT-PC_{S12}-*gat*, producing pBAKA-Δ$dapB_{Bp}$::*gat-FRT*. The *gat* gene is in the opposite orientation as the $dapB_{Bp}$ gene.

Engineering of *B. pseudomallei* Δasd_{Bp}::*gat-FRT* and Δ$dapB_{Bp}$::*gat-FRT* mutants. E1354 was utilized as the conjugal donor to introduce the allelic-replacement vectors, pBAKA-Δasd_{Bp}::*FRT-gat* and pBAKA-Δ$dapB_{Bp}$::*gat-FRT*, into *B. pseudomallei* strain K96243. Conjugations were carried out as described above, and 100 µl and 200 µl of the conjugation mixures were plated on MG medium + 200 µg/ml DAP + 0.3% GS + 1 mM each of Lys, Met, and Thr; these last 3 amino acids (3AA) are required for the specific D*asd* mutation (Fig. 5B). Colonies appearing after 3 to 4 days were streaked-out on the same medium supplemented with 0.1% cPhe to counter-select against *pheS*. It is critical that the media, in the presence of cPhe, contain no competing phenylalanine for clean counter-selection as previously described (3). GS

resistant mutants were screened by patching with toothpicks onto plates with and without DAP (MG + 0.3% GS + 0.1% cPhe + 1 mM 3AA ± 200 mg/ml DAP). Mutants unable to grow without DAP were purified once on LB + DAP, and patched again on MG + 0.3% GS + 0.1% cPhe + 1 mM 3AA ± 200 mg/ml DAP to confirm. Purification from potential background on LB + DAP is recommended and is very important because GS is static, rather than cidal, at this effective concentration. Further screening and confirmation of DAP requiring mutants were performed by PCR, using oligonucleotides #1062 and #1063 which annealed to the chromosome outside of the region cloned for allelic-replacement (Fig. 5A and 5C).

To engineer the *B. pseudomallei* K96243 Δ$dapB_{Bp}$::*gat-FRT* mutant, methodologies were essentially the same as for the engineering of Δasd_{Bp}::*gat-FRT*, except only 1 mM Lys was supplemented in the media with DAP rather than all 3AA (Fig. 5B). DAP requiring colonies were further purified as above on LB + DAP because GS is a static agent. Screening of D$dapB_{Bp}$ mutants was carried out by PCR using oligonucleotides #1070 and #1071, which anneal outside of the oligonucleotides used for cloning (Fig. 5C).

For *B. pseudomallei* strain 1026b, we engineered and confirmed the Dasd_{Bp} mutant essentially as above for strain K96243 via counter selection with cPhe/*pheS*. To demonstrate that the DNA incubation approach also works using *gat* for selection with GS in strain 1026b, we used the published DNA incubation and natural transformation approach to delete the $dapB_{Bp}$ gene in strain 1026b (52). pBAKA-Δ$dapB_{Bp}$::*gat-FRT* was used as a template along with oligos #1049 + #1051 in a PCR to obtain a linear 2.7 kb Δ$dapB_{Bp}$::*gat-FRT* fragment. Allelic-replacement was performed as previously published (3), but selection was carried-out on MG medium + 0.3% GS + 200 μg/ml DAP + 1 mM Lys. GS resistant colonies that were DAP requiring were purified and further confirmed by PCR with oligos #1070 and #1071 as above.

Phenotypic lysis of Δ*asd* and Δ*dapB* mutants without DAP. The *B. pseudomallei* wildtype K96243, K96243-Dasd_{Bp}::*gat-FRT* mutant, and K96243-D$dapB_{Bp}$::*gat-FRT* mutant were first grown overnight in LB (wildtype strain) or LB + DAP (Dasd_{Bp}::*gat-FRT* and D$dapB_{Bp}$::*gat-FRT* strains). One ml of each culture was centrifuged, the cell pellets were washed twice with LS (LB no salt) medium, and resuspended in 20 ml of LS. Ten ml of each concentrated cell resuspension was spotted on LS and LS + DAP plates and incubated at 37^{o}C. After 18 hours, cells were resuspended in sterile saline (0.85% NaCl) and smeared on glass slides. The slides were then air dried and fixed with 1% paraformalydehyde (in PBS) for 1 hour. This fixing method was initially tested on wildtype K96243 and the slide was incubated in rich LB media for 3 weeks to ensure no growth was observed, indicating complete killing. Finally, the cells were stained with safranin for 10 minutes, gently rinsed with water, and examined under 100x oil immersion (Fig. 6).

Construction of mini-Tn7-*bar* and mini-Tn7-*bar-asd*$_{Bp}$. To construct the site-specific mini-Tn7-*bar* transposon, mini-Tn7-Tel^{r} was digested with XbaI (cut in the flanking *FRT*-spacer regions) and the *bar*-cassette from pwFRT-PC_{S12}-*bar* (also digested with XbaI in the *FRT*-spacer regions) was ligated to replace the Tel^{r} cassette. Recovery of the *FRT* sequences was verified by confirming the orientation of the cloned PC_{S12}-*bar* fragment and recovery of the XbaI sites via restriction enzyme digestions. To construct mini-Tn7-*bar*-asd_{Bp}, the asd_{Bp} gene with 600 bp of upstream sequence was amplified from the *B. pseudomallei* K96243 chromosome to include the putative promoter. The 1.8 kb asd_{Bp} gene was PCR amplified from K96243 chromosomal DNA using oligos #893 and #1117, and the product was digestd with EcoRI + HindIII. mini-Tn7-*bar* was digested with the same enzymes and ligated to this 1.8 kb asd_{Bp} gene resulting in mini-Tn7-*bar*-asd_{Bp}. The asd_{Bp} gene was cloned in the same orientation as the *bar*-cassette. Functionality

of the asd_{Bp} was verified by transformation into a D*asd E.coli* strain (E1345) and growth was observed on LB in the absence of DAP.

Complementation of the *B. pseudomallei* Δasd_{Bp}::*gat-FRT* mutant. The *B. pseudomallei* 1026b Δasd_{Bp}::*gat-FRT* mutant was complemented using the mini-Tn7-*bar*-asd_{Bp} vector. The mini-Tn7-*bar*-asd_{Bp} vector and its helper plasmid (pTNS3-asd_{Ec}) were transformed individually into *E. coli* E1354 (a conjugation proficient tryptophan auxotroph) and conjugated into *B. pseudomallei* Δasd_{Bp}::*gat-FRT* in a tri-parental mating experiment. Conjugation mixtures were scraped from the plate using a disposable loop and resuspended in 1 ml of 1x M9 minimal media. Then 100 µl of a 1:10 dilution was plated on MG medium + 200 µg/ml DAP + 2.5% PPT + 1 mM of each Lys, Met, and Thr. This medium prevents the *E. coli* donor (Trp auxotroph) from growing and selects for PPT resistant *B. pseudomallei*. Of seventy colonies initially patched onto 1x M9 + 1% casamino acids ± DAP, forty-five separate isolates grew in the absence of DAP, indicating a complementation frequency of ~64%. Ten isolates were screened for positive integration using oligonucleotides #876, which anneals in the Tn7L region of the mini-Tn7-*bar* site-specific transposon, and one of the oligos #1079, #1080, or #1081, specific for each of the three possible integration sites on the chromosome (11). Of the ten isolates screened, two had Tn7-*bar*-asd_{Bp} integrated downstream of *glmS1*, while the remaining 8 isolates had Tn7-*bar*-asd_{Bp} integrated downstream of *glmS2*. Neither integration at *glmS3* nor multiple integrations at different *glmS* integration sites were observed. Two positive isolates with insertion at *glmS1* and three isolates with insertion at *glmS2* were chosen for further characterization below.

Growth of wildtype *B. pseudomallei* strain 1026b, its Δ*asd*$_{Bp}$::*gat-FRT* mutant, and Δ*asd*$_{Bp}$::*gat-FRT/attTn7-bar-asd*$_{Bp}$ complements. To further characterize the D*asd* mutation, we first grew strain 1026b, the D*asd*$_{Bp}$ mutant strain, and several complements overnight in LB + DAP, at 37°C with shaking at 250 rpm. One ml of each culture was harvested by centrifugation at 8,000x *g* for 2 minutes. The pellet was washed twice with 1x M9 buffer to remove any residual nutrients and resuspended in 1 ml of 1x M9 buffer. To determine the amino acid auxotrophic properties of these strains, the cell suspensions were diluted 20x in 1x M9 buffer. Five µl of each culture was spotted onto plates with MG medium + 200 µg/ml DAP + 1 mM each of Ile + Lys + Met + Thr; the same amount of the diluted cultures was spotted onto 5 other plates, each missing one of the four amino acids or DAP. Growth on the plates was observed after 24 hrs and 7 days (Fig. 8).

GenBank Accession Numbers. The sequences for all constructs in figure 4 were submitted to GenBank. The accession numbers are: pwFRT-PC$_{S12}$-*gat*, **FJ384986**; pwFRT-PC$_{S12}$-*bar*, **FJ858786**; mini-Tn7-*gat*, **FJ858785**; and mini-Tn7-*bar*, **FJ826509**.

2.4 RESULTS AND DISCUSSION

Effectiveness of glyphosate (GS) against *Burkholderia* species. Although studies have measured the GS inhibitory concentrations for *P. aeruginosa*, *E. coli*, *B. subtilis*, and *B. japonicum* (18, 61), no studies have determined the GS inhibitory concentration for *Burkholderia* species. It was previously shown that growth inhibition of *B. japonicum* was observed at lower GS concentrations (5 mM or 0.085%), and rapid death occurred at a higher GS concentration (10 mM or 0.17%) (61). Thus, GS could be bacteriostatic depending on the concentration used. We initially determined the inhibitory or killing action of GS for three *Burkholderia* select-agent strains (Fig. 2). When exposed to different concentrations of GS for 24 hours, *B. mallei* was found to be more sensitive to GS than *B. pseudomallei* and over 60% death was observed when exposed to a concentration as low as 0.25%. Both *B. pseudomallei* strains replicated slightly less than double at 0.25% GS and were killed at higher concentrations of GS (Fig. 2). Clearly, no significant replication was observed at concentrations as low as 0.25% GS. Although to be determined in future studies, the mechanism of GS inhibition on *Burkholderia* species is likely similar to the mechanism of EPSPS inhibition in plants, having been confirmed for *P. aeruginosa*, *E. coli*, *B. subtilis*, and *B. japonicum* (18, 61).

We next wanted to determine the minimal inhibitory concentration of GS for members of the *Burkholderia* genus, then identify the effective GS concentration ($[GS]_{EC}$) in liquid and on solid media (see Materials and Methods). Significantly high cell densities typical in genetic manipulations (e.g. 10^5 cfu in liquid media and 100 ml of ~10^9 cfu/ml was plated on solid media containing different concentrations of GS) were inoculated to determine the $[GS]_{MIC}$ where no spontaneous resistance to GS was observed after 2 days (liquid media) or 2 weeks (solid media). The $[GS]_{EC}$ above the $[GS]_{MIC}$ was defined and utilized to ensure no growth of high inocula in

liquid media after 4 days or no growth for 3 weeks on solid media (Table 4). We determined the $[GS]_{EC}$ within this time frame for liquid and solid media, because this time period is sufficient to observe most mutants that will arise during allelic-replacement and also allows most *Burkholderia* species to grow on minimal media during selection. The $[GS]_{EC}$ for *E. coli* and *B. pseudomallei*, *B. mallei*, and *B. cenocepacia* K56-2 are higher than other *Burkholderia* (Table 4). We have utilized the $[GS]_{EC}$ on Table 4 to select for the *gat* gene (below) successfully in *E. coli*, *B. thailandensis*, and the two wildtype *B. pseudomallei* strains. Thus, we are confident that the $[GS]_{EC}$ in Table 4 for other species are appropriate.

Roundup® is an appropriate source of GS for selection. We have not encountered any problem with the solubility of GS at high concentration (10% was the highest concentration tested using purified GS). Indeed, the 'super-concentrated' Roundup® purchased contained 50% GS in aqueous solution. In addition to this advantage, GS is readily available, inexpensive, relatively non-toxic, not in clinical use, and gives tight selection (below). Although purified GS could be purchased from Sigma and other distributors, we do not have concerns with using Roundup® for selection, since purified GS gave the same $[GS]_{EC}$. One bottle of 'super-concentrated' Roundup® purchased from a local garden supply store has lasted through the duration of this study. Roundup® with lower concentrations of GS are also available, although we recommend the 'super-concentrated' Roundup® as it is potent enough for >150 liters of cultures when used at 0.3% final concentration. The other evidence that Roundup® is appropriate for selection, with no observed adverse affects on bacteria from other ingredients, is that selection of pBBR1MCS-2-PC_{S12}-*gat* (kanamycin and GS resistant) in *E. coli* and *B. thailandensis* on kanamycin or GS from Roundup® yielded the same number of colonies (data not shown).

Engineering of a *gat*-cassette and effective selection with glyphosate. We engineered the *gat*-gene through GenScript Corporation, based on the previously described GAT protein sequences (6), using an approach similar to the synthesis of the *pheS* gene (3). We utilized this approach to optimize the codon-usage for efficient expression in *Burkholderia* species, while eliminating many restrictions sites within the gene and strategically placing others at certain locations for future manipulation. The engineered *gat*-cassette, including the *B. cenocepacia* PC_{S12} promoter of the *rpsL* gene, is only 533 bp (Fig. 3). The small size of the *gat*-cassette makes it easy to manipulate, clone, and perform PCR for use in the DNA incubation method of allelic-replacement in naturally competent *Burkholderia* species (52). As proof-of-concept, we utilized this cassette in the DNA incubation approach to delete the asd_{Bt} gene of *B. thailandensis* at its $[GS]_{EC}$ (data not shown). This confirmed that the $[GS]_{EC}$ on Table 4 are sufficient for selection.

Deletional mutagenesis of the essential *B. pseudomallei* asd_{Bp} and $dapB_{Bp}$ genes using GS and *gat*. The reliability of any marker for mutagenesis would best be demonstrated by the successful mutagenesis of essential genes. Therefore, we chose two essential genes, *asd* and *dapB*, that are absolutely required for diaminopimelate (DAP) synthesis and cell-wall cross-linking in most Gram-negative bacteria (Fig. 5B) (9, 12, 25, 27, 42). Mutation of the *asd* gene makes Gram-negative bacteria auxothrophic for three amino acids (Thr, Met, DAP), while *dapB* mutants only require DAP. Although Lys and Ile are also made from the same pathway, the provided DAP and Thr should act as precursors for Lys and Ile biosynthesis, respectively (Fig. 5B). The asd_{Bp} and $dapB_{Bp}$ genes encode for aspartate-semialdehyde-dehydrogenase (BPSS1704 on chromosome 2) and a dihydrodipicolinate reductase (BPSL2941 on chromosome 1), respectively.

To knock-out the asd_{Bp} and $dapB_{Bp}$ genes in *B. pseudomallei*, we engineered *gat-FRT* cassettes for allelic-replacement (Fig. 4A). As mentioned above, utilization of a *gat-FRT* cassette was successfully tested in *B. thailandensis* to delete the asd_{Bt} gene using the DNA incubation and natural transformation method (52), where the selection with 0.04% GS yielded ~80% *B. thailandensis* Dasd_{Bt} mutation frequencies (data not shown). We then utilized pBAKA and the *pheS* counter-selection approach as previously described (3), with the *gat-FRT* cassette from pwFRT-PC_{S12}-*gat*, to inactivate the asd_{Bp} and $dapB_{Bp}$ genes in *B. pseudomallei* (Fig. 4A and 5A). Independent merodiploids resulting from the first recombination in strain K96243 were obtained with 0.3% GS after three days of growth (see Materials and Methods). Streaking of merodiploids on media containing 0.1% cPhe and 0.3% GS for counter-selection to resolve the mutations yielded DAP-requiring colonies at frequencies of ~25% and ~80% for the *B. pseudomallei* K96243 Dasd_{Bp} and D$dapB_{Bp}$ mutants, respectively. To demonstrate this principle of allelic-replacement in another *B. pseudomallei* strain, we utilized this same approach with cPhe/*pheS* counter-selection to create a 1026b Dasd_{Bp} mutant, which yielded a lower mutation frequency of ~10% in this essential gene. Since strain 1026b is also naturally competent, we wanted to utilize the published DNA incubation method for allelic-replacement (52) by engineering a D$dapB_{Bp}$ mutant, yielding 1026b D$dapB_{Bp}$ mutants at a frequency of ~25%. We confirmed these mutations by PCR with oligos annealing to chromosomal regions outside of the initial oligos used for cloning (Fig. 5A and 5C). Because GS is bacteriostatic at the concentration used (Table 4 and Fig. 2), it is critical to purify all mutants from the potential background contamination before reconfirming the phenotype, PCR confirmation, and growth for long-term storage at -80^{o}C. Phenotypically, *B. pseudomallei* D$dapB_{Bp}$ mutants required DAP for growth (data not shown), while Dasd_{Bp} mutants required DAP, Thr, and Met (Fig. 8). Using wildtype and mutants of strain

K96243 as examples, we further characterized the phenotype of D*asd*$_{Bp}$ and D*dapB*$_{Bp}$ mutants. In the presence of DAP, both D*asd*$_{Bp}$ and D*dapB*$_{Bp}$ mutants displayed normal rod-shape celllular morphology (Fig. 6). However, in the absence of DAP, these two mutants lack DAP for cell-wall biosynthesis and cross-linking, demonstrating 'cell-rounding' characteristics and evidence of lysis (Fig. 6).

***B. pseudomallei* D*asd*$_{Bp}$ mutant complementation with a site-specific mini-Tn7-*bar-asd*$_{Bp}$ transposon.** We engineered a site-specific transposon based on mini-Tn7, which has previously been demonstrated to integrate at three possible *glmS* sites in the *B. pseudomallei* chromosome (11) (Fig. 4D and 7A). Our construct, mini-Tn7-*bar*, is based on the non-antibiotic *bar* gene that encodes for resistance to bialaphos and phosphinothricin (a bialaphos degradation product also known as glufosinate). Since bialaphos can be very expensive, a cheaper alternative, phosphinothricin (PPT), can be used. We determined the effective concentration of PPT ($[PPT]_{EC}$) for *B. mallei* and *B. pseudomallei* to be ~2.5%. Many herbicide brands (e.g. Basta, Buster, Dash, Finale, Hayabusa, Ignite, Conquest, Liberty, Rely, Shield, Harvest, Sweep, Arise, and others) contain PPT as the active ingredient. Since the $[PPT]_{EC}$ was quite high, we picked the herbicide Finale because it contains the highest PPT concentration (11.33% w/v) we could find, although other brands not available on our island (e.g. Liberty and Ignite) can contain 20-25% PPT. In this study, we utilized the 11.33% PPT in Finale as the working stock to make media at the 2.5% $[PPT]_{EC}$. As proof-of-concept, we introduced the constructed mini-Tn7-*bar-asd*$_{Bp}$ into the *B. pseudomallei* 1026b D*asd*$_{Bp}$ strain to complement the D*asd*$_{Bp}$ mutation. The suicidal helper plasmid pTNS3-*asd*$_{Ec}$, harboring the *E. coli asd*$_{Ec}$ gene for maintenance in an *E. coli* D*asd*$_{Ec}$ strain, aids the transposition of the Tn7-*bar-asd*$_{Bp}$ transposon to one of three possible

glmS chromosomal targets (Fig. 7A). We selected PPT resistant colonies in the presence of DAP, Lys, Met, and Thr to prevent bias in immediately selecting for complements. After patching on media ± DAP, it was found that ~64% of PPT resistant colonies tested (45 out of 70) were complements of the D*asd*$_{Bp}$ mutation and did not require DAP. It was further confirmed that the majority of the complements (8 out of 10 tested) had the mini-Tn7-*bar*-*asd*$_{Bp}$ transposed to the region downstream of the *glmS2* target, while 2 out of 10 recombined at the *glmS1* target (Fig. 7B). No transposition at the *glmS3* target was observed. These data indicated that PPT in Finale© was appropriate for selection of the *bar* gene and yielded a fairly high frequency of transposition.

To further characterize five complements along with the wildtype 1026b and the D*asd*$_{Bp}$ mutant, we spotted these strains on various media lacking one of the five amino acids (DAP, Lys, Met, Thr, and Ile) in the aspartate family of amino acid biosynthetic pathways. Media lacking Met, Thr, or DAP yielded no growth of the D*asd*$_{Bp}$ mutant compared to the wildtype 1026b and the five complements, confirming that the Asd reaction gives rise to these amino acids (Fig. 5B and 8). Ile and Lys were not required in the D*asd*$_{Bp}$ mutant, as Thr and DAP will yield Ile and Lys, respectively (Fig 8E and 8H). In summary, the D*asd*$_{Bp}$ mutant of *B. pseudomallei* displayed a similar phenotype to *asd* mutants of other Gram-negatives, and the successful complementation of this mutant suggests that our allelic-replacement approach did not introduce any undesirable mutations during selection with Roundup® and Finale®.

Conclusions. (i) We engineered and successfully demonstrated the use of a novel non-antibiotic *gat*-marker, based on resistance to glyphosate in *Burkholderia* species. This cassette was demonstrated to be useful for allelic-replacement of essential genes in *B. pseudomallei*, adding valuably to the limited number of select-agent approved markers. The advantages of

using GS-containing herbicides to select for the *gat*-cassette in recombinant work include cost effectiveness, availability, low toxicity, non-clinical use, high solubility, relatively tight selection, and the small size of the *gat*-marker. The *gat*-cassette was used successfully in more than one allelic-replacement strategy to delete two essential genes confirming its value, the usefulness of *pheS* as a counter-selectable marker, and the compatibility with the DNA incubation method for naturally competent *Burkholderia* species (52). (ii) We initiated the successful utilization of a second non-antibiotic resistance marker, based on the better characterized *bar* gene (55), encoding for bialaphos and phosphinothricin (glufosinate) resistance. This will hopefully also expand its future use in select-agent species. One minor disadvantage of using *gat* and *bar* is the requirement for minimal media lacking two of the three aromatic amino acids (Phe, Tyr, or Trp) and glutamine, respectively. However, for most mutations, using 1x M9 + 20 mM glucose should suffice for *B. pseudomallei*, *B. mallei*, and *B. thailandensis*. Note that we added DAP, Lys, Met, and Thr to the media in this study because of the mutant-specific amino acid requirements (e.g. Dasd_{Bp} and D$dapB_{Bp}$). (iii) We created two mutants in two wildtype *B. pseudomallei* strains, which may be promising as future attenuated vaccine candidates, since DAP is a bacterial specific product not available in mammalian hosts. (iv) Finally, it is important to point out that all genetic tools used in this study are completely devoid of antibiotic resistance during introduction and selection. The potential use of *gat* and *bar* may be expanded to other select agent species (e.g. *Brucella* and *Francisella*), since minimal media lacking Phe, Tyr, Trp, and Gln has been defined for some of these species (7, 21). These compounds (GS and PPT), originally designed to kill plant weeds, may prove quite useful for the future selection of recombinants in bacterial select-agent species

2.5 ACKNOWLEDGEMENTS

This work was supported by a National Institute of Health grant R21-AI074608 to T.T. H. Graduate stipend to M.H.N. was supported by an NSF IGERT Award 0549514 to B.A.W.

2.6 FIGURE LEGENDS

FIG. 1. (A) A 946 ml bottle of the 'super concentrated' herbicide Roundup® used in this study, available for ~$50 from most local hardware stores and garden or farm supply centers. Indicated are the 50% glyphosate active ingredient and the chemical structure of glyphosate. The glyphosate *N*-acetyl-transferase (Gat), encoded by the *gat* gene, catalyzes the inactivation of glyphosate via *N*-acetylation. (B) Pathways of aromatic amino acids biosyntheses. Glyphosate inhibits the enzyme 5-enolpyruvylshikimate-3-phosphate synthase (EPSPS) required for aromatic amino acid biosyntheses, starving bacteria for tyrosine, phenylalanine, and tryptophan.

FIG. 2. Bacterial survival after incubation with different concentrations of GS for 24 hours. *B. mallei* was more sensitive to GS than both *B. pseudomallei* strains and killing of *B. mallei* by GS was observed at 0.25% GS. *B. pseudomallei* strain 1026b is significantly more resistant to GS than strain K96243. Insignificant replication of both *B. pseudomallei* strains (less than double) after 24 hours was observed at 0.25% GS. Killing was observed at 2% GS for strain K96243 and 3% GS for strain 1026b.

FIG. 3. A schematic diagram of the engineered 533-bp *gat*-gene on pwFRT-PC$_{S12}$-*gat*. The *B. cenocepacia rpsL* promoter (PC$_{S12}$) and ribosomal-binding-site (*rbs*) are shown in relation to the *gat* gene. Below the schematic are the corresponding nucleotide and protein sequences. Codons were optimized according to codon preference within the *B. pseudomallei* K96243 *asd* gene. Also indicated are the -35 and -10 regions of the PC$_{S12}$-promoter. Restriction sites were positioned strategically (in bold) for subsequent cloning and manipulation.

FIG. 4. Maps of the pwFRT-PC$_{S12}$-*gat* (A), pwFRT-PC$_{S12}$-*bar* (B), mini-Tn7-*gat* (C), and mini-Tn7-*bar* (D). (A) pwFRT-PC$_{S12}$-*gat* is flanked with symmetrical restriction-sites (HindIII to SacI) that will cut to remove the *gat*-cassette flanked with identical wildtype *FRT* sequences. Not shown are four other *FRT*-*gat* cassettes with flanking unique *FRT*-sequences (pmFRT-*gat*, pFRT1-*gat*, pFRT2-*gat*, and pFRT3-*gat*), where the *gat* marker is flanked by identical *FRT*s with unique spacer sequences. The DNA sequences and restriction sites for all five *gat*-*FRT* are identical with the exception of the spacers. (B) pwFRT-PC$_{S12}$-*bar* with *bar* flanked by wildtype *FRT* sequences and symmetrical restriction enzyme sites. (C) mini-Tn7-*gat* and (D) mini-Tn7-*bar* were engineered to allow site-specific integration of cloned gene(s), using the non-antibiotic *bar* or *gat* selectable marker, with the assistance of a helper-plasmid (pTNS3-*asd*$_{Ec}$). Abbreviations: *bar*, gene encoding bialaphos/phosphinothricin resistance; *bla*, beta-lactamase encoding gene; *ori,* ColE1 origin of replication; *FRT,* flippase recognition target sequences; *oriT,* conjugal origin of transfer; PC$_{S12}$, promoter of the *B. cenocepacia rpsL* gene; R6K*γori*, π protein dependent R6K origin of replication; *Tn7L/Tn7R,* left and right transposase recognition sequences; T_1T_o, transcriptional terminator.

FIG. 5. (A) Gene replacement strategy using a *gat*-*FRT* cassette to inactivate the *B. pseudomallei* strain K96243 and 1026b *asd*$_{Bp}$ gene. Oligoss #892 and #893 were used in the initial cloning of the *asd*$_{Bp}$ gene into the allelic-replacement vector pBAKA, and the *asd*$_{Bp}$ gene was inactivated with the *gat*-*FRT* cassette. Deletion of the chromosomal *asd*$_{Bp}$ gene with pBAKA-D*asd*$_{Bp}$::*gat* was performed as shown. PCR verification of the Δ*asd*$_{Bp}$ mutant was done using outside oligoss #1062 and #1063. The *asd*$_{Bp}$ gene of both K96243 and 1026b strains were inactivated using pBAKA and *pheS* for counter-selection. Similarly, the *dapB*$_{Bp}$ gene of strain

K96243 was also inactivated using pBAKA and *pheS* for counter-selection (not shown, see Materials and Methods). Oligos #1049 and #1051 were used to amplify the D*dapB*$_{Bp}$::*gat* cassette from plasmid pBAKA-D*dapB*$_{Bp}$::*gat* to inactivate the *dapB*$_{Bp}$ gene from strain 1026b using the DNA incubation method (52) (Materials and Methods). (B) Bacterial amino acid biosynthetic pathway of the aspartate family, where asparate is used to synthesize DAP, Lys, Met, Thr, and Ile. The indicated reactions catalyzed by Asd and DapB are central to this pathway and mutants of these genes cannot cross-link their cell-walls due to the lack of DAP. (C) PCR verification of the D*asd*$_{Bp}$ and D*dapB*$_{Bp}$ mutants. In each case as expected, the PCR products indicated that the chromosomal fragment of the mutant is larger than the wt, and the no template negative control (nc) showed no PCR product. Abbreviations: *asd*$_{Bp}$, *B. pseudomallei asd* gene encoding aspartate-semialdehyde-dehydrogenase; *asd*$_{Pa}$, *P. aeruginosa asd* gene; *dapB*$_{Bp}$, *B. pseudomallei* gene encoding dihydrodipicolinate reductase; *gat*, glyphosate resistance gene encoding glyphosate acetyl transferase; GS, glyphosate; M, 1-kb ladder (New England Biolabs); P*lac*, *lac*-promoter; *pheS*, mutant *B. pseudomallei* gene encoding the a-subunit of phenylalanyl tRNA synthase.

FIG. 6. Phenotypic characterization of *B. pseudomallei* K96243 D*asd*$_{Bp}$ and D*dapB*$_{Bp}$ mutants. Wildtype K96243 was rod-shape when grown in the absence or presence of DAP (left top and bottom panels). The mutant D*asd*$_{Bp}$ (middle panels) and D*dapB*$_{Bp}$ (right panels) strains grow, but 'pop-and-die' without the ability to cross-link their cell-walls in the absence of DAP. The majority of the bacteria are in the process of forming protoplasts. Some protoplast cells could be observed (black arrows) as well as cell debris (white arrows) due to bacterial lysis, which were absent when these mutants were grown in the presence of DAP (bottom panels).

FIG. 7. Single-copy complementation of the *B. pseudomallei* 1026b D*asd*$_{Bp}$ mutant using mini-Tn7-*bar-asd*$_{Bp}$. (A) The suicidal plasmid mini-Tn7-*bar-asd*$_{Bp}$ and its suicidal helper plasmid, pTNS3-*asd*$_{Ec}$, were introduced into *B. pseudomallei* 1026b D*asd*$_{Bp}$ mutant by conjugation. Tn7 has three possible integration sites on different chromosomes (denoted by red triangles), which can result in complementation of the D*asd*$_{Bp}$ mutation from three different chromosomal loci as depicted according to the annotation of *B. pseudomallei* K96243. Screening of ten random complements was done using oligonucleotide Tn7L (#876) and an oligonucleotide specific for each potential integration site (#1079, #1080, or #1081) as indicated by arrows. (B) For each isolate, PCR verification of ten random complements was performed for all three *glmS* sites (lanes 1, 2, and 3). Insertion downstream of *glmS1* would result in a 218 bp PCR product, downstream of *glmS2* would result in a 263 bp fragment, and downstream of *glmS3* would result in a 309 bp PCR product. Isolates #1, 2, 3, 4, 5, 6, 8, and 10 had Tn7 inserted downstream of *glmS2*. Isolates #7 and #9 showed a PCR product near 200 bp indicating Tn7 integration downstream of *glmS1*. Abbreviations: *asd*$_{Ec}$, *E. coli* aspartate-semialdehyde-dehydrogenase gene; M, 100-bp ladder (New England Biolabs); P1, P1 integron promoter; *glmS1*, *glmS2*, and *glmS3* encode for three different *B. pseudomallei* glucosamine 6-phosphate synthetases; *tnsABCD*, Tn7-transposase genes.

FIG. 8. Growth characteristics of the *B. pseudomallei* K96243 D*asd*$_{Bp}$ mutant and five complements, relative to wildtype (wt), on media lacking amino acids (AA) of the aspartate family. (A) On 1x M9 minimal glucose (MG) medium, the D*asd*$_{Bp}$ mutant did not grow compared to wt, whereas five complements (numbered 1-5) using mini-Tn7-*bar-asd*$_{Bp}$ transposon

all grew as well as wt. Spots 1 and 2 are Tn7-*bar-asd*$_{Bp}$ complements transposed at the *glmS1* site, while spots 3-5 are complements transposed at the *glmS2* site. (B) The D*asd*$_{Bp}$ mutant grew similarly to the wt on MG media when provided with all five AA of the aspartate family (DAP, Lys, Met, Thr, and Ile). The D*asd*$_{Bp}$ mutant cannot grow when provided with four of the five AA when one aa such as Met (C), Thr (D), or DAP (F) was omitted from MG medium; whereas the wt and all complements grew well on these media. (E) The D*asd*$_{Bp}$ mutant still grew when Ile was omitted from MG medium containing the other 4 AA, because Thr in the medium could be converted to Ile in this pathway. (G) Surprisingly, no growth was observed when Lys was omitted from the MG medium + 4 AA (Met, Thr, DAP, and Ile). We suspect that the amount of DAP provided was shuffled for use in cell-wall biosynthesis and very little gets converted to Lys for growth and the D*asd*$_{Bp}$ mutant grows slowly on this media. When the plate in panel (G) was incubated for another six days, growth was observed for the D*asd*$_{Bp}$ mutant (H), indicating that some DAP does get converted to Lys. All other plates, where the D*asd*$_{Bp}$ mutant did not grow after one day, did not show growth of this mutant after seven days (data not shown).

TABLE 1. Bacterial strains used in this study[a]

Strains	Lab ID[b]	Relevant properties	Sources
E. coli			
K-12	E0577	Wildtype F^+	Coli Genetic Stock Center
EPMax10B-*pir116*/D*asd*::Gm^r	E1345	Gm^r; F^- *l*$^-$ *mcrA* D(*mrr-hsdRMS-mcrBC*) *f80dlacZDM15* D*lacX74 deoR recA1 endA1 araD139* D*(ara, leu)7697 galU galK rpsL nupG Tn-pir116-FRT2* □*asd*::Gm^r-*wFRT*	–[c]
EPMax10B-*lacI*^{q}/*pir*/*leu*$^+$/Δ*asd*::Gm^r	E1951	Gm^r; F^- λ$^-$ *mcrA* Δ(*mrr-hsdRMS-mcrBC*) *f*80*dlacZ*Δ*M15* Δ*lacX74 deoR recA1 endA1 araD139 galU galK rpsL nupG lacI*^{q}*-FRT8 pir*::*FRT4* Δ*asd*::Gm^r-*wFRT*	–[c]
EPMax10B-*pir116*/D*asd*/D*trp*::Gm^r/ *mob*-Km^r	E1354	Gm^r, Km^r; F^- *l*$^-$ *mcrA* D(*mrr-hsdRMS-mcrBC*) *f80dlacZDM15* D*lacX74 deoR recA1 endA1 araD139* D*(ara, leu)7697 galU galK rpsL nupG Tn-pir116-FRT2* □*asd*::*wFRT* □*trp*::Gm^r-*FRT5 mob*[*recA*::*RP4-2 Tc*::*Mu*-Km^r]	–[c]
EPMax10B-*lacI*^{q}/*pir*	E1869	F^- *l*$^-$ *mcrA* □(*mrr-hsdRMS-mcrBC*) *f*80*dlacZDM15* D*lacX74 deoR recA1 endA1 araD139* □(*ara, leu*)7697 *galU galK rpsL nupG lacI*^{q}*-FRT8 pir-FRT4*	–[c]
EPMax10B-*lacI*^{q}/*pir*/*leu*$^+$	E1889	F^- *l*$^-$ *mcrA* □(*mrr-hsdRMS-mcrBC*) *f*80*dlacZDM15* D*lacX74 deoR recA1 endA1 galU galK rpsL nupG lacI*^{q}*-FRT8 pir-FRT4*	–[c]
GM33	E0021	F^- *l*$^-$ *IN*(*rrnD-rrnE*)*1 dam-3 sup-85*	(37)
***Burkholderia* spp.**			
B. dolosa AU0158	E1551	Prototroph	J. Goldberg
B. cenocepacia Bc7	E1552	Prototroph	J. Goldberg
B. cenocepacia K56-2	E1554	Prototroph; cystic fibrosis isolate	P. Sokol
B. mallei ATCC23344	B0002	Wildtype strain; post-mortem isolate	(39)
B. pseudomallei			
1026b	B0004	Wildtype strain; clinical melioidosis isolate	(15)
1026b-Δasd_{Bp}::*gat-FRT*	B0011	GS^r; 1026b with *gat-FRT* cassette inserted in the asd_{Bp} gene	This study
1026b-Δasd_{Bp}::*gat-FRT*/ *att*Tn7-*bar*-asd_{Bp}	B0015	GS^r, PPT^r; 1026b Δasd_{Bp}::*gat-FRT* mutant with mini-Tn7-*bar*-asd_{Bp} inserted	This study
1026b-Δ$dapB_{Bp}$::*gat-FRT*	B0013	GS^r; 1026b with *gat* cassette inserted in the $dapB_{Bp}$ gene	This study
K96243	B0002	Wildtype strain; clinical melioidosis isolate	(28)
K96243-Δasd_{Bp}::*gat-FRT*	B0007	GS^r; K96243 with *gat* cassette inserted in the asd_{Bp} gene	This study
K96243-Δ$dapB_{Bp}$::*gat-FRT*	B0010	GS^r; K96243 with *gat* cassette inserted in the chromosomal $dapB_{Bp}$ gene	This study
B. thailandensis E264	E1298	Prototroph; environmental isolate	(5)

[a] Abbreviations: *bar,* gene encoding bialaphos (phosphinothricin) resistance; *gat*, gene encoding glyphosate acetyltransferase; Gm^r, gentamycin resistant; GS^r, glyphosate resistant; Km^r, kanamycin resistant; PPT^r, phosphinothricin resistant.

[b] Please use laboratory identification number (Lab ID) when requesting strains.

[c] Details on the engineering of these strains are to be published elsewhere.

TABLE 2. Plasmids used in this study[a]

	Lab ID[c]	Relevant properties	Sources
mini-Tn7-Tel^r	E1825	Tel^r; mini-Tn7 integration vector based on Tel^r	(34)
mini-Tn7-*bar*	E2218	PPT^r; mini-Tn7 integration vector based on *bar*	This study
mini-Tn7-*gat*	E1981	GS^r; mini-Tn7 integration vector based on *gat*	This study
mini-Tn7-*bar*-asd_{Bp}	E2226	PPT^r; *B. pseudomallei* K96243 asd_{Bp} gene cloned into mini-Tn7-*bar*	This study
pBAKA	E1624	Select-agent-compliant allelic-replacement vector based on asd_{Pa}	(3)
pBAKA-Δasd_{Bp}::*gat-FRT*	E2062	GS^r; *gat-FRT* cassette inserted into asd_{Bp}	This study
pBAKA-$dapB_{Bp}$	E2075	*B. pseudomallei* K96243 *dapB* gene cloned into pBAKA	This study
pBAKA-Δ$dapB_{Bp}$::*gat-FRT*	E2083	GS^r; *gat-FRT* cassette inserted into $dapB_{Bp}$	This study
pBBR1MCS-2	E1277	Km^r; broad-host-range cloning vector	(35)
pBBR1MCS-2-PC_{S12}-*bar*	E1773	Km^r, PPT^r; broad-host-range cloning vector harboring *bar*	This study
pBBR1MCS-2-PC_{S12}-*gat*	E1794	GS^r, Km^r; broad-host-range cloning vector harboring *gat*	This study
pCAMBIA-1301-*bar*	E1775	PPT^r; plant transformation vector harboring *bar*	CAMBIA
pTNS3-asd_{Ec}	E1831	helper plasmid containing asd_{Ec} for Tn7 site-specific transposition system	(34)
pUC18	E0135	Ap^r; cloning vector	(59)
pUC18-asd_{Bp}	E1819	Ap^r; cloning vector pUC18 containing asd_{Bp}	This study
pUC18-Δasd_{Bp}::*gat-FRT*	E1867	Ap^r, GS^r; cloning vector pUC18 containing asd_{Bp} inactivated by *gat-FRT*	This study
pUC57-P_{S12}-*gat*	E1763	Ap^r, GS^r; cloning vector pUC57 containing *B. pseudomallei* codon optimized *gat*	This study
pwFRT-P_{S12}-*gat*	E1798	Ap^r, GS^r; *gat*-cassette flanked by wild-type *FRT*	This study
pwFRT-P_{S12}-*gat*-SDM	E1812	Ap^r, GS^r; *gat*-cassette flanked by wild-type *FRT* after SDM removing internal SacI site	This study
pwFRT-PC_{S12}-*gat*$^{-b}$	E1929	Ap^r, GS^r; *gat*-cassette flanked by wild-type *FRT* with the P_{S12} replaced by the PC_{S12}	This study
pwFRT-PC_{S12}-*bar*	E2209	Ap^r, PPT^r; *bar*-cassette flanked by wild-type *FRT*	This study
pwFRT-Tp^r	E1659	Tp^r; Tp^r-cassette flanked by wild-type *FRT*	(3)
pwFRT-Tel^r	E1584	Telr; Tel^r-cassette flanked by wild-type *FRT*	(3)

[a] Other abbreviations: Ap^r, ampicillin resistance; P_{S12}, *rpsL* promoter from *B. pseudomallei*; PC_{S12}, *rpsL* promoter of *B. cenocepacia*;SDM, site-directed mutagenesis; Tel^r, tellurite resistant.

[b] Four other *FRT* mutants exist for this plasmid, where the only sequence difference in the mutated plasmids is within the spacer sequence of each *FRT* (see Materials and Methods for detail).

[c] Please use laboratory identification number (Lab ID) when requesting plasmids.

TABLE 3. Oligonucleotide primers used in this study

Oligos number and name	Sequences*
557; M13-RP	5'-AGCGGATAACAATTTCACACAGGA-3'
558; M13-FP	5'-CGCCAGGGTTTTCCCAGTCACGAC-3'
715; pPS854-XhoI	5’-AAGCTCGAGCTAATTCC-3’
716; pPS854-Cla-EcoRV	5’-CAATATCGATATCCATTGCTGTTGACAAAG-3’
837; PS12(cenocepacia)	5’-ATCAGCCGTTGACTTAGTTGGTATTTCCGGAATATCATGCTGGTTC CGAATAATTTTGTTTAACTTTAAGAAGGAGATATACC-3’
849; Tel-term-BamHI	5'-TCGAGGATCCAGAAAGTCAAAAGCCTCCG-3'
876; Tn7L	5’-ATTAGCTTACGACGCTACACCC-3’
881; bar-start	5’CTTTAAGAAGGAGATATACCATGAGCCCAGAACGACGCC-3’
882; bar-XhoI	5’-GAAACTCGAGTCAAATCTCGGTGCCGGGCA-3'
892; Bpasdup-HindIII	5'-CGTCAAGCTTTCCCGGCCGTTGTG-3'
893; Bpasddown-EcoRI	5'-GTTGTGAATTCGTCGTAATCGCGTAG-3'
894; gat-SacSDM	5'-GCACTCGGAGCTTCAGGGGAAGAAGC-3'
1048; dapB-up-XbaI	5'-CGGCTCTAGAAGCCATGCAGGCGG-3'
1049; dapB-up-nest	5’-GAGCAGAACGACGCGAAC-3’
1050; dapB-down-HindIII	5'-CGAGAAGCTTGTACGCGAGCACCG-3'
1051; dapB-down-nest	5’-GAACGCGGTCATGATGAG -3’
1062; 1026b-asd-up	5’-CCCGAAAACGGGGTCCGT-3’
1063; 1026b-asd-dn	5’-CGACGCTTTCGGGTTGTGTA-3’
1070; dapB-dn-out	5’-CAGACGAACACGTGCAGATC-3’
1071; dapBK9-upout-2	5’-AGCTCGATCTGCTCGCCGACAT-3’
1079; glmS1-K9	5’-GAGGAGTGGGCGTCGATCAAC-3’
1080; glmS2-K9	5’-ACACGACGCAAGAGCGGAATC-3’
1081; glmS3-K9	5’-CGGACAGGTTCGCGCCATGC-3’
1117; BpK9asd-upstrm-HindIII	5’-GCGCGAAGCTTTCGACACGATG-3’

*Restriction enzyme sites used in this study are underlined

TABLE 4. Glyphosate effective concentrations ($[GS]_{EC}$) for *Burkholderia* species and *E. coli*

Strain	Effective Concentrations (EC)	
	[GS] (%) Liquid[a]	**[GS] (%) Solid**[b]
B. cenocepacia K56-2	0.32%	0.5%
B. cenocepacia Bc7	<0.005%	<0.005%
B. dolosa AUO158	<0.005%	<0.005%
B. mallei ATCC23344	0.1%	0.2%
B. pseudomallei K96243	0.1%	0.3%
B. pseudomallei 1026b	0.1%	0.3%
B. thailandensis E264	0.01%	0.04%
E. coli K12	0.1%	0.3%

[a] Effective concentration in liquid media determined by absence of growth after 4 days.
[b] Effective concentration on solid media by absence of growth or spontaneous resistant colonies after 3 weeks.

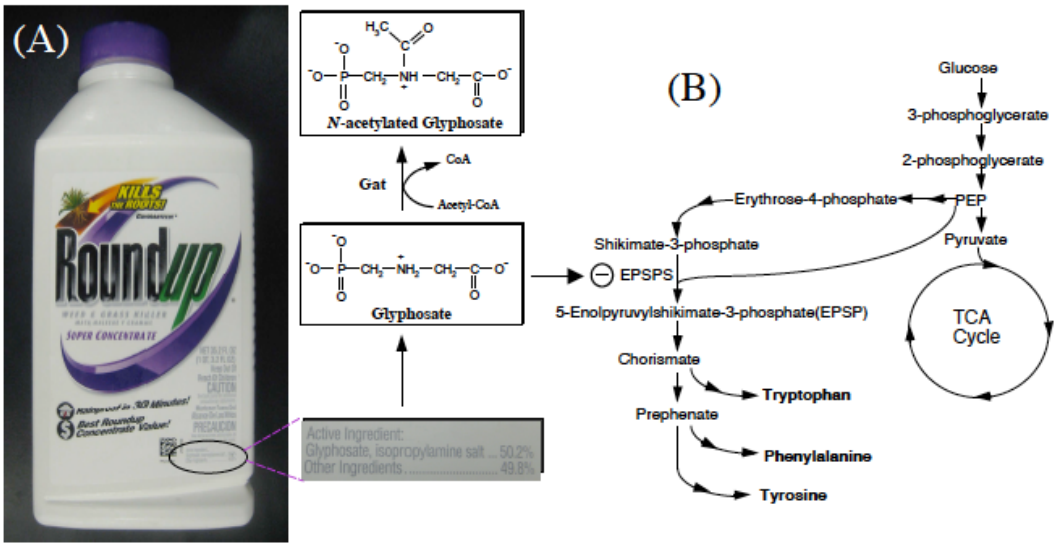
(A)
Roundup
SUPER CONCENTRATE
Active Ingredient:
Glyphosate, isopropylamine salt ... 50.2%
Other Ingredients ... 49.8%
N-acetylated Glyphosate
Gat
CoA
Acetyl-CoA
Glyphosate
(B)
Glucose
3-phosphoglycerate
2-phosphoglycerate
Erythrose-4-phosphate
PEP
Pyruvate
Shikimate-3-phosphate
EPSPS
5-Enolpyruvylshikimate-3-phosphate(EPSP)
TCA Cycle
Chorismate
Tryptophan
Prephenate
Phenylalanine
Tyrosine

Figure 1

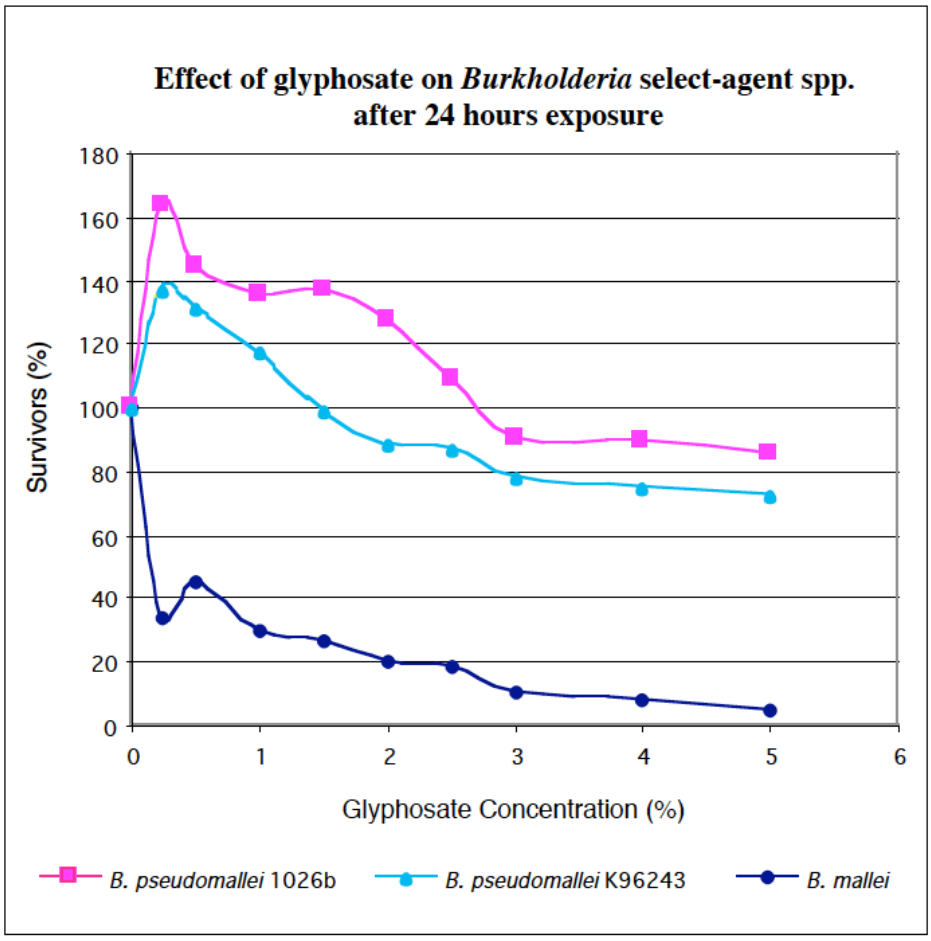
Effect of glyphosate on *Burkholderia* select-agent spp. after 24 hours exposure
Survivors (%)
180
160
140
120
100
80
60
40
20
0
0
1
2
3
4
5
6
Glyphosate Concentration (%)
B. pseudomallei 1026b
B. pseudomallei K96243
B. mallei

Figure 2


EcoRV
NcoI
NdeI
XhoI
PC$_{S12}$
rbs
gat
(563 bp)
EcoRV
GATATCAGCCGTTGACTTAGTTGGTATTTCCGGAATATCATGCTGGGTTCCGAATAATTTTGTTT
-35
NcoI
-10
NdeI
AACTTTAAGAAGGAGATATACCATGGGATCGAGCTTCGAAAGGACAAGCATATGATCGAGGTCAA
rbs
M I E V K
GCCCATCAACGCCGAGGACACCTACGACCTGCGGCATCGGGTCCTCCGGCCCAACCAGCCGATCGA
P I N A E D T Y D L R H R V L R P N Q P I E
GGCGTGCATGTTCGAAAGCGATCTCACGCGGAGCGCCTTCCACCTGGGCGGGTTCTACGGGGGCAA
A C M F E S D L T R S A F H L G G F Y G G K
GCTGATTTCGGTCGCTTCGTTCCACCAGGCCGAGCACTCGGAGCTTCAGGGGAAGAAGCAGTACCA
L I S V A S F H Q A E H S E L Q G K K Q Y Q
GCTGCGCGGTGTGGCCACCCTGGAGGGCTACCGGGAGCAGAAGGCCGGGTCGTCGCTGGTCAAGCA
L R G V A T L E G Y R E Q K A G S S L V K H
CGCCGAAGAGATCCTGCGGAAGCGGGGGGCCGACATGATCTGGTGCAACGCCCGGACCTCGGCCTC
A E E I L R K R G A D M I W C N A R T S A S
GGGGTACTACCGGAAGCTGGGGTTCAGCGAGCAGGGGGAGGTCTTCGACACCCCGCCCGTGGGGCC
G Y Y R K L G F S E Q G E V F D T P P V G P
XhoI
CCACATCCTGATGTACAAGCGGATCACCTAACTCGAG
H I L M Y K R I T •

Figure 3

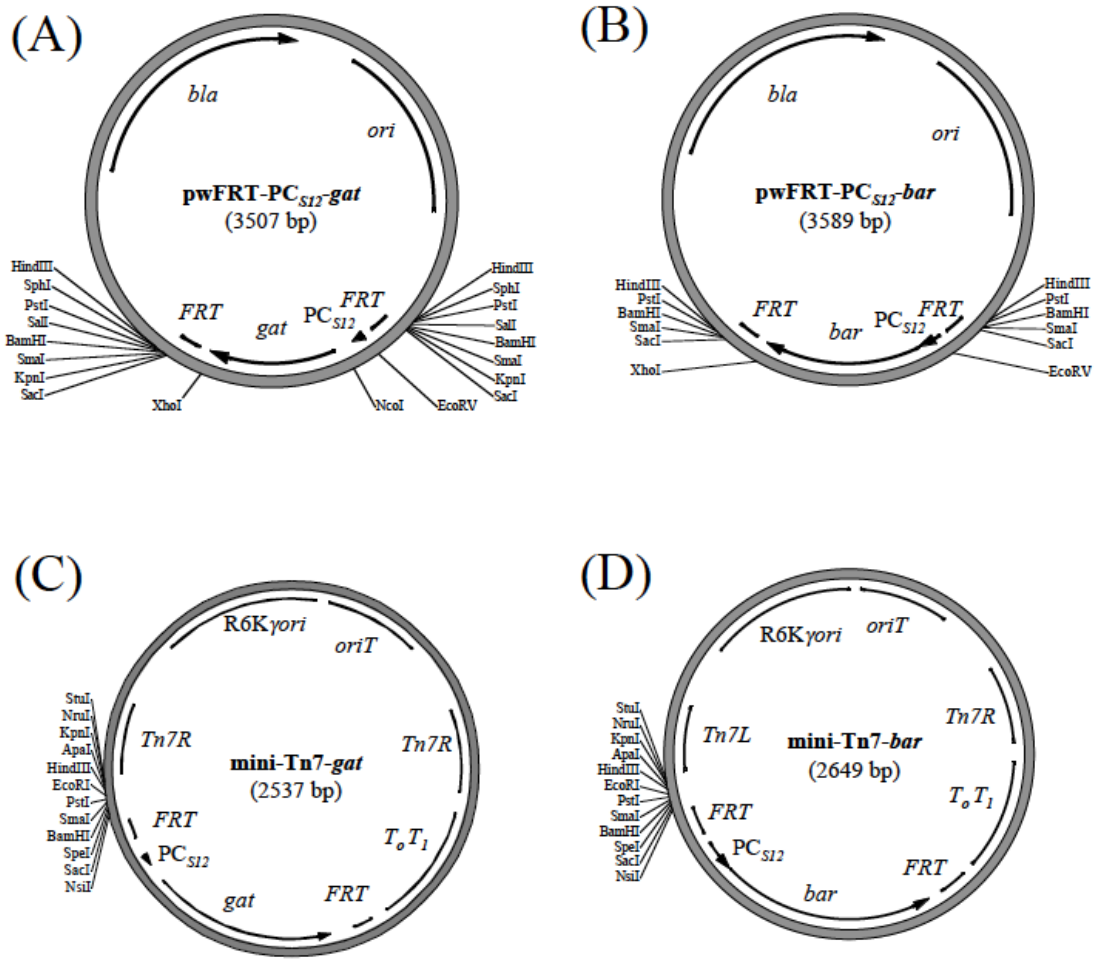
(A)
bla
ori
pwFRT-PC$_{S12}$-gat
(3507 bp)
FRT
gat
PC$_{S12}$
FRT
HindIII
SphI
PstI
SalI
BamHI
SmaI
KpnI
SacI
XhoI
NcoI
EcoRV
(B)
bla
ori
pwFRT-PC$_{S12}$-bar
(3589 bp)
FRT
bar
PC$_{S12}$
FRT
HindIII
PstI
BamHI
SmaI
SacI
XhoI
EcoRV
(C)
R6Kγori
oriT
Tn7R
mini-Tn7-gat
(2537 bp)
Tn7R
FRT
PC$_{S12}$
T$_o$T$_1$
gat
FRT
StuI
NruI
KpnI
ApaI
HindIII
EcoRI
PstI
SmaI
BamHI
SpeI
SacI
NsiI
(D)
R6Kγori
oriT
Tn7L
mini-Tn7-bar
(2649 bp)
Tn7R
T$_o$T$_1$
FRT
PC$_{S12}$
FRT
bar

Figure 4

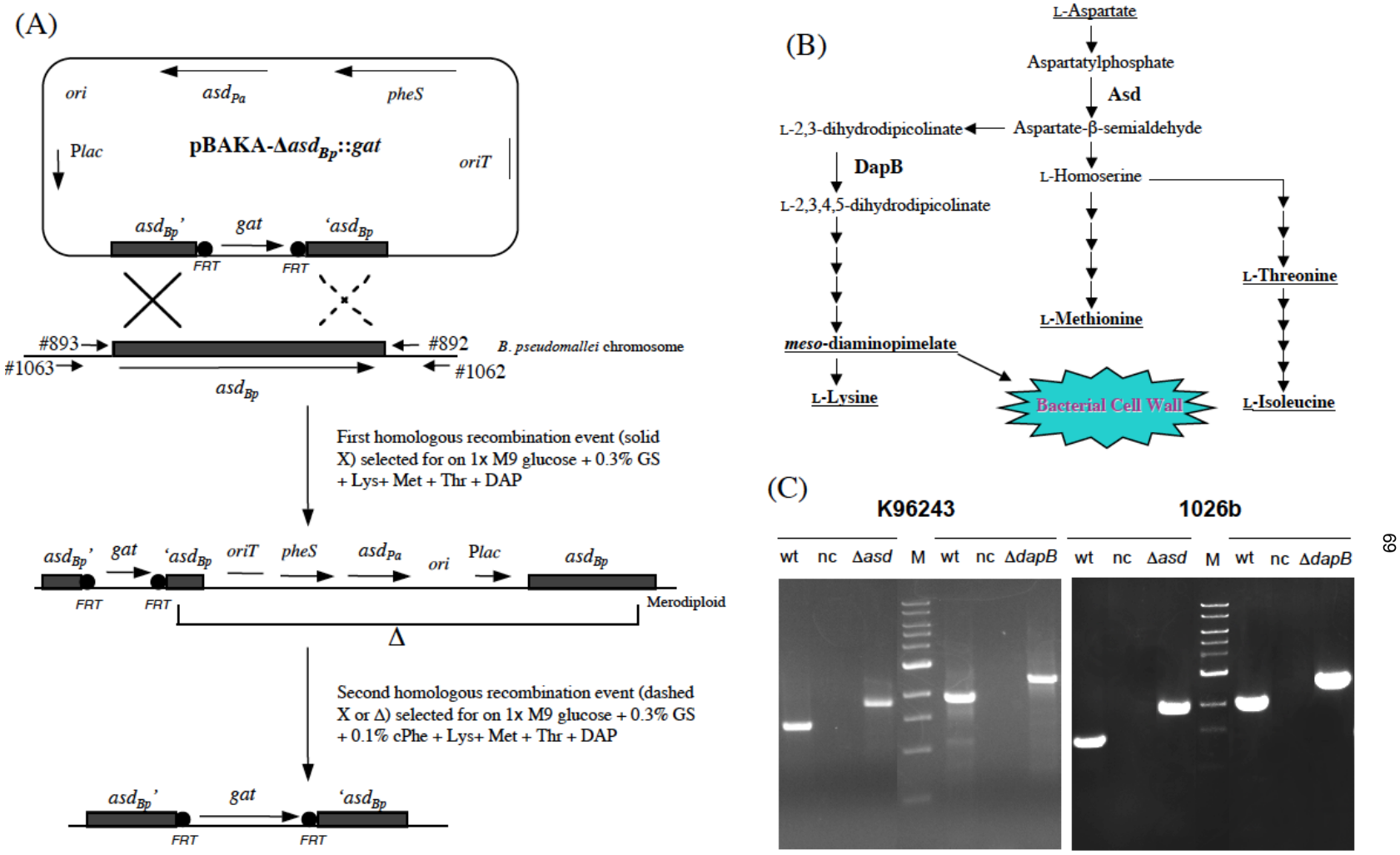
(A)
ori
asdPa
pheS
Plac
pBAKA-ΔasdBp::gat
oriT
asdBp'
gat
'asdBp
FRT
FRT
#893
#892
B. pseudomallei chromosome
#1063
#1062
asdBp
First homologous recombination event (solid X) selected for on 1x M9 glucose + 0.3% GS + Lys+ Met + Thr + DAP
asdBp'
gat
'asdBp
oriT
pheS
asdPa
ori
Plac
asdBp
FRT
FRT
Merodiploid
Δ
Second homologous recombination event (dashed X or Δ) selected for on 1x M9 glucose + 0.3% GS + 0.1% cPhe + Lys+ Met + Thr + DAP
asdBp'
gat
'asdBp
FRT
FRT
(B)
L-Aspartate
Aspartatylphosphate
Asd
L-2,3-dihydrodipicolinate
Aspartate-β-semialdehyde
DapB
L-Homoserine
L-2,3,4,5-dihydrodipicolinate
L-Threonine
L-Methionine
meso-diaminopimelate
L-Lysine
Bacterial Cell Wall
L-Isoleucine
(C)
K96243
1026b
wt
nc
Δasd
M
wt
nc
ΔdapB
wt
nc
Δasd
M
wt
nc
ΔdapB

Figure 5

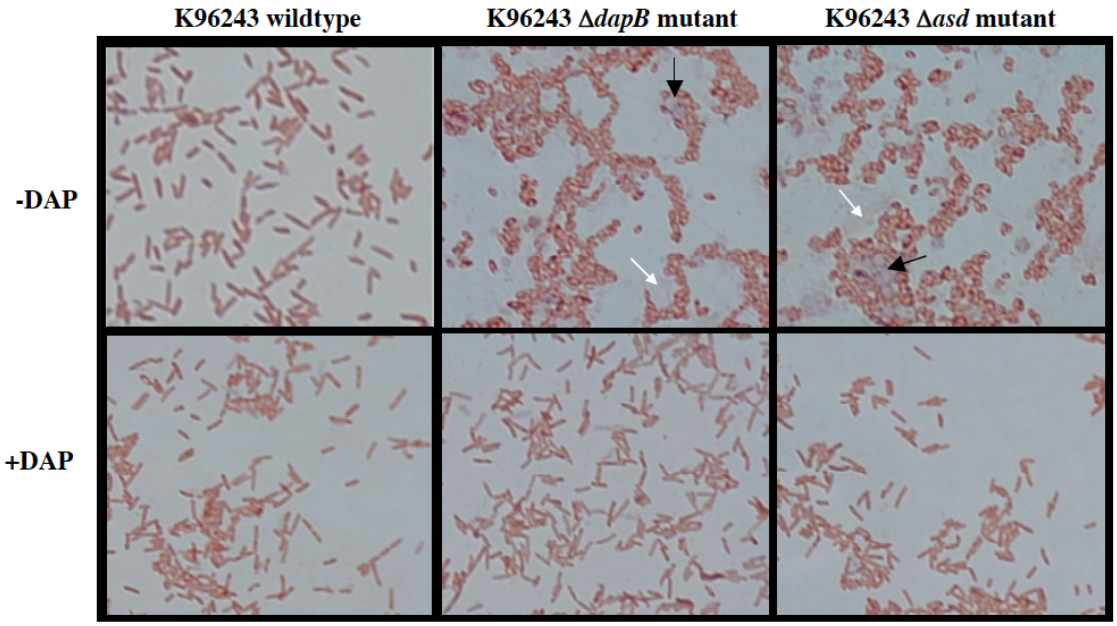
K96243 wildtype
K96243 Δ*dapB* mutant
K96243 Δ*asd* mutant
-DAP
+DAP

Figure 6

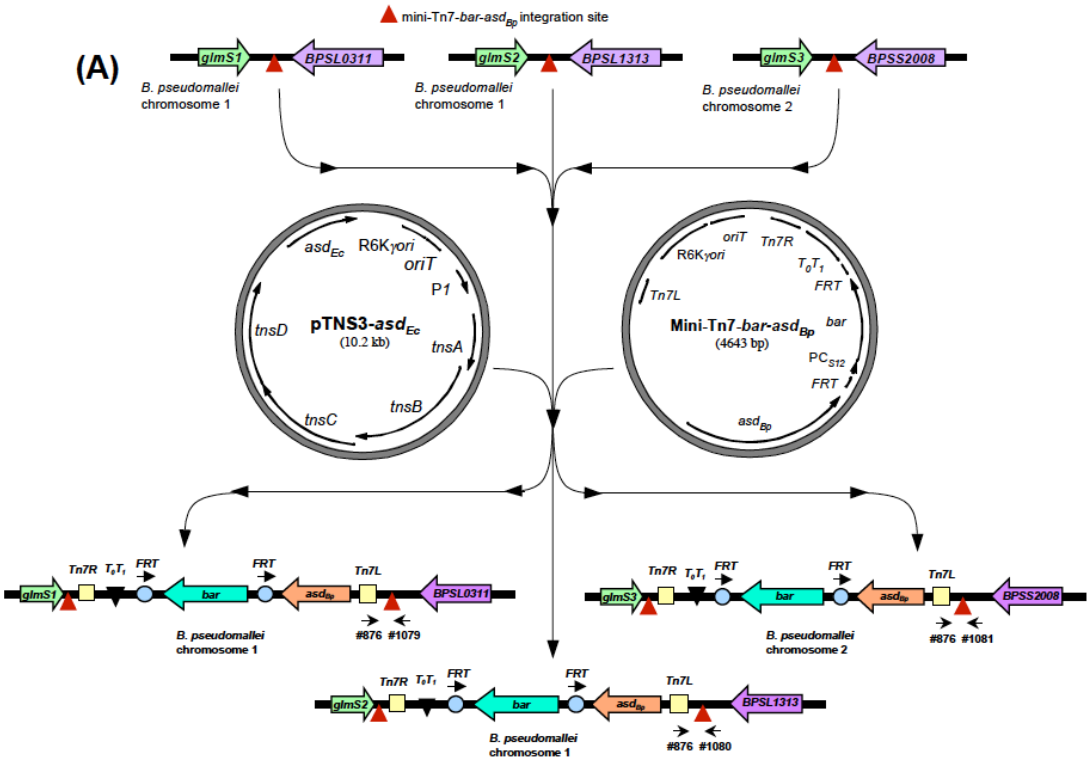

PCR Product Sizes: Lane 1 = *glmS1* = 218 bp Lane 2 = *glmS2* = 263 bp Lane 3 = *glmS3* = 309 bp

Figure 7

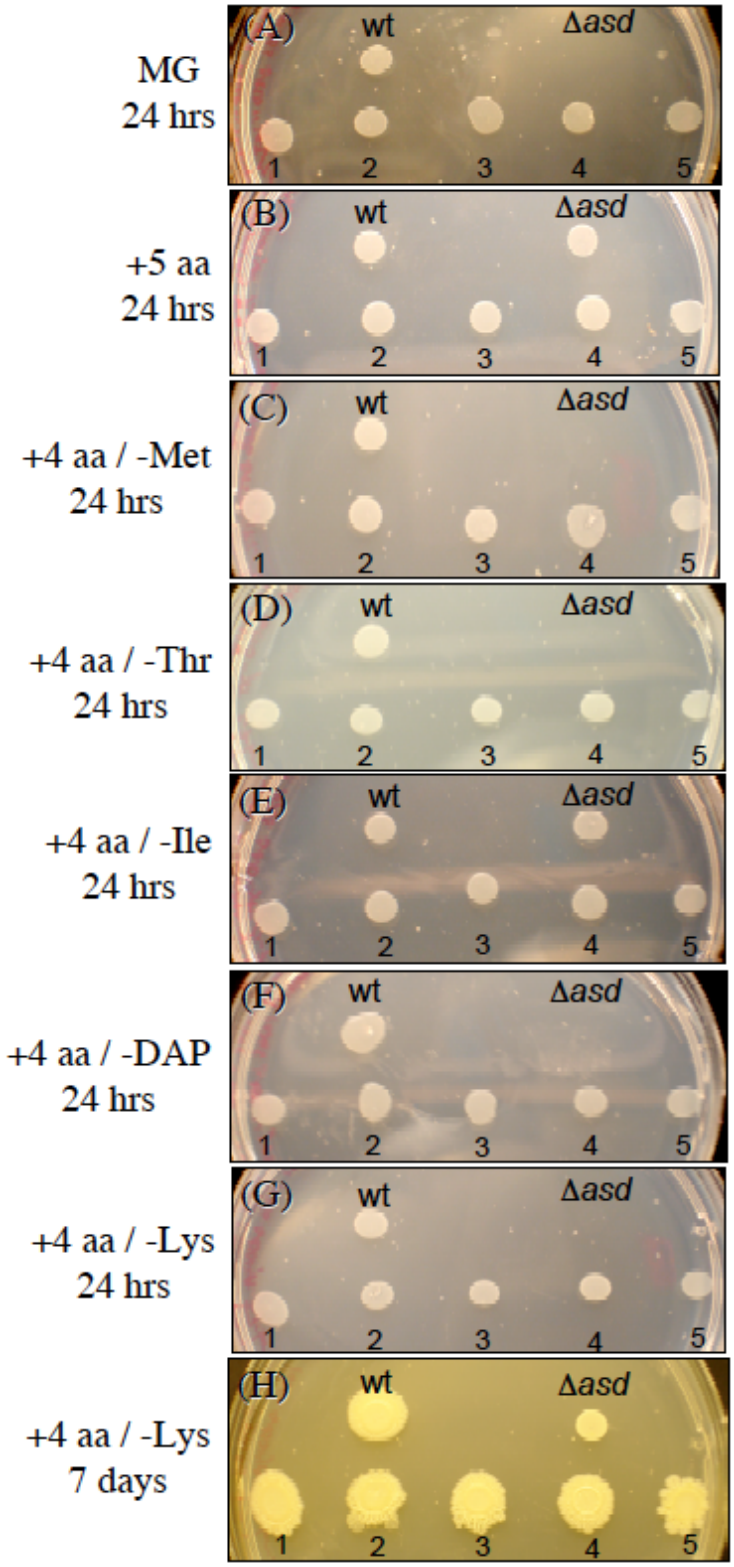
MG
24 hrs
(A)
wt
Δasd
1
2
3
4
5
+5 aa
24 hrs
(B)
wt
Δasd
1
2
3
4
5
+4 aa / -Met
24 hrs
(C)
wt
Δasd
1
2
3
4
5
+4 aa / -Thr
24 hrs
(D)
wt
Δasd
1
2
3
4
5
+4 aa / -Ile
24 hrs
(E)
wt
Δasd
1
2
3
4
5
+4 aa / -DAP
24 hrs
(F)
wt
Δasd
1
2
3
4
5
+4 aa / -Lys
24 hrs
(G)
wt
Δasd
1
2
3
4
5
+4 aa / -Lys
7 days
(H)
wt
Δasd
1
2
3
4
5

Figure 8

2.7 REFERENCES

1. Ashdown, L. R. 1979. An improved screening technique for isolation of *Pseudomonas pseudomallei* from clinical specimens. Pathology. 11:293-297.
2. Barekzi, N., K. L. Beinlich, T. T. Hoang, X.-Q. Pham, R. R. Karkhoff-Schweizer, and H. P. Schweizer. 2000. The *oriC*-containing region of the *Pseudomonas aeruginosa* chromosome undergoes large inversions at high frequency. J. Bacteriol. 182:7070-7074.
3. Barrett, A. R., Y. Kang, K. S. Inamasu, M. S. Son, J. M. Vukovich, and T. T. Hoang. 2008. Genetic tools for allelic replacement in *Burkholderia* species. Appl. Environ. Microbiol. 74(14):4498-4508.
4. Borgherini, G., P. Poubeau, F. Paganin, S. Picot, A. Michault, F. Thibault, and C. A. Berod. 2006. Melioidosis: an imported case from Madagascar. J. Travel. Med. 13(5):318-320.
5. Brett, P. J., D. DeShazer, and D. E. Woods. 1998. *Burkholderia thailandensis* sp. nov., description of *Burkholderia pseudomallei*-like species. Int. J. Syst. Bacteriol. 48:317-320.
6. Castle, L. A., D. L. Siehl, R. Gorton, P. A. Patten, Y. H. Chen, S. Bertain, H.-J. Cho, N. Duck, J. Wong, D. Liu, and M. W. Lassner. 2004. Discovery and directed evolution of a glyphosate tolerance gene. Science. 304:1151-1154.
7. Chamberlain, R. E. 1965. Evaluation of Live Tularemia Vaccine Prepared in a Chemically Defined Medium. Appl. Microbiol. 13(2):232-235.
8. Chan, Y. Y., and K. L. Chua. 2005. The *Burkholderia pseudomallei* BpeAB-OprB efflux pump: expression and impact on quorum sensing and virulence. J. Bacteriol. 187(14):4707-4719.
9. Chen, N. Y., S. Q. Jiang, D. A. Klein, and H. Paulus. 1993. Organization and nucleotide sequence of the *Bacillus subtilis* diaminopimelate operon, a cluster of genes encoding the

first three enzymes of diaminopimelate synthesis and dipicinolate synthase. J. Biol. Chem. 268:9448-9465.

10. Cheng, A. C., and B. J. Currie. 2005. Melioidosis: Epidemiology, Pathophysiology, and Management. Clinical Microbiological Reviews. 18(2):383-416.
11. Choi, K. H., T. Mima, Y. Casart, D. Rholl, A. Kumar, I. R. Beacham, and H. P. Schweizer. 2008. Genetic tools for select-agent-compliant manipulation of *Burkholderia pseudomallei*. Appl. Environ. Microbiol. 74(4):1064-1075.
12. Cirillo, J. D., T. R. Weisbrod, L. Pascopella, B. R. Bloom, and W. R. Jacob Jr. 1994. Isolation and characterization of the aspartokinase and aspartate seminaldehyde dehydrogenase operon from mycobacteria. Mol. Microbiol. 11(4):629-639.
13. Cooper, E. B. 1967. Melioidosis. JAMA. 200(6):452-453.
14. Dance, D. A. B. 1991. Melioidosis: the tip of the iceberg? Clin. Microbiol. Rev. 4:52-60.
15. DeShazer, D., P. J. Brett, R. Carlyon, and D. E. Woods. 1997. Mutagenesis of *Burkholderia pseudomallei* with Tn5-OT182: isolation of motility mutant and molecular characterization of the flagellin structural gene. J. Bacteriol. 179(7):2116-2125.
16. Dill, G. M. 2005. Glyphosate-resistance crops: history, status, and future. Pest Manage. Sci. 61:219-224.
17. Dorman, S. E., V. J. Gill, J. I. Gallin, and S. M. Holland. 1998. *Burkholderia pseudomallei* infection in a Puerto Rican patient with chronic granulomatous disease: case report and review of occurrences in the Americas. Clin. Infect. Dis. 26(4):889-894.
18. Fischer, R., A. Berry, C. G. Gaines, and R. A. Jensen. 1986. Comparative action of glyphosate as a trigger of energy drain in eubacteria. J. Bacteriol. 168(3):1147-1154.

19. Franklin, M. 1971. Effect of gentamycin on *Pseudomonas pseudomallei*. J. Infect. Dis. 124:S30-S32.

20. Frischknecht, F. 2003. The history of biological warfare. Eur. Mol. Biol. Org. 4:S47-S52.

21. Gerhardt, P., and J. B. Wilson. 1948. The Nutrition of Brucellae: Growth in Simple Chemically Defined Media. J. Bacteriol. 56:17-24.

22. Green, R. N., and P. G. Tuffnell. 1968. Laboratory acquired melioidosis. Am. J. Med. 44:599-605.

23. Hall, W. H., and R. E. Manion. 1973. Antibiotic suseptibility of *Pseudomonas pseudomallei*. Antimicrob. Agents Chemother. 4(2):193-195.

24. Hamad, M. A., S. L. Zajdowicz, R. K. Holmes, and M. I. Voskuil. 2008. An allelic exchange system for compliant genetic manipulation of the selet agents *Burkholderia pseudomallei* and *Burkholderia mallei*. Gene. doi: 10.1016/j.gene.2008.10.011.

25. Hatten, L.-A., H. P. Schweizer, N. Averill, L. Wang, and A. B. Schryvers. 1993. Cloning and characterization of the *Neisseria meningitidis asd* gene. Gene. 129:123-128.

26. Herrero, M., V. De Lorenzo, and K. N. Timmis. 1990. Transposon vectors containing non-antibiotic resistance selection markers for cloning and stable chromosomal insertion of foreign genes in Gram-negative bacteria. J. Bacteriol. 172:6557-6567.

27. Hoang, T., S. Williams, H. P. Schweizer, and J. S. Lam. 1997. Molecular genetic analysis of the region containing the essential *Pseudomonas aeruginosa asd* gene encoding aspartate-b-semialdehyde dehydrogenase. Microbiology. 143:899-907.

28. Holden, M. T. G., R. W. Titball, S. J. Peacock, A. M. Cerdeño-Tárraga, T. Atkins, L. C. Crossman, T. Pitt, C. Churcher, K. Mungall, S. D. Bentley, M. Sebaihia, N. R. Thomson, N. Bason, I. R. Beacham, K. Brooks, K. A. Brown, N. F. Brown, G. L. Challis, I. Cherevach, T.

Chillingworth, A. Cronin, B. Crossett, P. Davis, D. DeShazer, T. Feltwell, A. Fraser, Z. Hance, H. Hauser, S. Holroyd, K. Jagels, K. E. Keith, M. Maddison, S. Moule, C. Price, M. A. Quail, E. Rabbinowitsch, K. Rutherford, M. Sanders, M. Simmonds, S. Songsivilai, K. Stevens, S. Tumapa, M. Vesaratchavest, S. Whitehead, C. Yeats, B. G. Barrell, P. C. F. Oyston, and J. Parkhillal. 2004. Genomic plasticity of the causative agent of melioidosis, *Burkholderia pseudomallei*. Proc. Natl. Acad. Sci. U.S.A. 101(39):14240-14245.

29. How, H. S., K. H. Ng, H. P. Tee, and A. Shah. 2005. Pediatric melioidosis in Pahang, Malaysia. J. Microbiol. Immunol. Infect. 38(5):314-319.
30. Issack, M. I., C. D. Bundhun, and H. Gokhool. 2005. Melioidosis in Mauritius. Emerg. Infect. Dis. 11(1):139-140.
31. Jacob, G. S., J. R. Garbow, L. E. Hallas, N. M. Kimack, G. M. Kinshore, and J. Schaefer. 1988. Metabolism of glyphosate in *Pseudomonas* strain LBr. Appl. Environ. Microbiol. 54:2953-2958.
32. Jaderlund, L., M. Hellman, I. Sundh, M. J. Bailey, and J. K. Jansson. 2008. Use of a novel nonantibiotic triple marker gene cassette to monitor high survival of *Pseudomonas fluorescens* SBW25 on winter wheat in the field. FEMS Microbiol. Ecol. 63(2):156-168.
33. Jesudason, M. V., A. Anbarasu, and T. J. John. 2003. Septicaemic melioidosis in a tertiary care hospital in south India. Indian J. Med. Res. 117:119-121.
34. Kang, Y., M. H. Norris, A. R. Barrett, B. A. Wilcox, and T. T. Hoang. 2009. Development of tellurite resistant genetic elements for single copy analysis in *Burkholderia* spp. Appl. Environ. Microbiol. (submitted).

35. Kovach, M. E., P. H. Elzer, D. S. Hill, G. T. Robertson, M. A. Farris, R. M. Roop II, and K. M. Peterson. 1995. Four new derivatives of the broad-host-range cloning vector pBBR1MCS, carrying different anitbiotic-resistance cassettes. Gene. 166:175-176.

36. Liu, C.-M., P. A. McLean, C. C. Sookdeo, and F. C. Cannon. 1991. Degradation of the herbicide glyphosate by members of the family *Rhizobiaceae*. Appl. Environ. Microbiol. 57:1799-1804.

37. Marinus, M. G., and N. R. Morris. 1974. Biological function for 6-methyladenine residues in the DNA of *Escherichia coli* K-12. J. Mol. Biol. 85:309-322.

38. Moore, R. A., D. DeShazer, S. Reckseidler, A. Weissman, and D. E. Woods. 1999. Efflux-mediated aminoglycoside and macrolide resistance in *Burkholderia pseudomallei*. Antimicrob. Agents Chemother. 43:465-470.

39. Nierman, W. C., D. DeShazer, H. S. Kim, H. Tettelin, K. E. Nelson, T. Feldblyum, R. L. Ulrich, C. M. Ronning, L. M. Brinkac, S. C. Daugherty, T. D. Davidsen, R. T. Deboy, G. Dimitrov, R. J. Dodson, A. S. Durkin, M. L. Gwinn, D. H. Haft, H. Khouri, J. F. Kolonay, R. Madupu, Y. Mohammoud, W. C. Nelson, D. Radune, C. M. Romero, S. Sarria, J. Selengut, C. Shamblin, S. A. Sullivan, O. White, Y. Yu, N. Zafar, L. Zhou, and C. M. Fraser. 2004. Structural flexibility in the *Burkholderia mallei* genome. Proc. Natl. Acad. Sci. U.S.A. 101(39):14246-14251.

40. Orellana, C. 2004. Melioidosis strikes Singapore. Lancet Infect. Dis. 4(11):655.

41. Padgete, S. R., D. B. Re, G. F. Barry, D. E. Eichholtz, X. Delannay, R. L. Fuchs, G. M. Kinshore, and R. T. Fraley. 1996. New weed control opportunities: development of soybeans with a Roundup Ready‰ gene., p. 53-84. *In* S. O. Duke (ed.), Herbicide resistant crops. CRC Press, Boca Raton, Fla.

42. Pavelka Jr., M. S. 2007. Another brick in the wall. Trends Microbiol. 15(4):147-149.

43. Penaloza-Vazquez, A., G. L. Mena, L. Herrera-Estrella, and A. M. Bailey. 1995. Cloning and sequencing of the genes involved in glyphosate utilization by *Pseudomonas pseudomallei*. Appl. Environ. Microbiol. 61(2):538-543.

44. Phetsouvanh, R., S. Phongmany, P. Newton, M. Mayxay, A. Ramsay, V. Wuthiekanun, and N. J. White. 2001. Melioidosis and pandora's box in the Lao People's Democratic Republic. Clin. Infect. Dis. 32:653-654.

45. Poole, K. 2008. Bacterial multidrug efflux-pumps serve other functions. ASM Microbe. 3(4):179-185.

46. Rholl, D. A., L. A. Trunck, and H. P. Schweizer. 2008. Himar1 in vivo Transposon Mutagenesis of *Burkholderia pseudomallei*. Appl. Environ. Microbiol. doi:10.1128/AEM.01973-08.

47. Rolim, D. B. 2005. Melioidosis, northeastern Brazil. Emerg. Infect. Dis. 11(9):1458-1460.

48. Rotz, L. D., A. S. Khan, S. R. Lillibridge, S. M. Ostroff, and J. M. Hughes. 2002. Public health assessment of potential biological terrorism agents. Emerg. Infect. Dis. 8:225-230.

49. Sanchez-Romero, J. M., R. Diaz-Orejas, and V. De Lorenzo. 1998. Resistance to tellurite as a selection marker for genetic manipulations of *Pseudomonas* strains. Appl. Environ. Microbiol. 64(10):4040-4046.

50. Schlech, W. F., J. B. Turchick, R. E. Westlake, G. C. Klein, J. D. Band, and R. E. Weaver. 1981. Laboratory-acquired infection with Pseduomonas pseudomallei (melioidosis). N. Engl. J. Med. 305:1133-1135.

51. Schweizer, H. P., and S. J. Peacock. 2008. Antimicrobial drug-selection markers for *Burkholderia pseudomallei* and *B. mallei*. Emerg. Infect. Dis. 14(11):1689-1692.

52. Thongdee, M., L. A. Gallagher, M. Schell, T. Dharakul, S. Songsivilai, and C. Manoil. 2008. Targetted mutagenesis of *Burkholderia pseudomallei* and *Burkholderia thailandensis* through natural transformation of PCR fragments. Appl. Environ. Microbiol. 74(10):2985-2989.

53. Vandamme, P., J. Govan, and J. LiPuma. 2007. Diversity and role of *Burkholderia* spp., p. 1-28. *In* T. Coenye and P. Vandamme (ed.), Burkholderia: Molecular Microbiology and Genomics. Horizon Scientific, Wymondham.

54. Vasil, I. K. 1996. Phosphinithricin-Resistant Crops., p. 85-91. *In* S. O. Duke (ed.), Herbicide-Resistant Crops. CRC Press, Boca Raton.

55. Wehrmann, A., A. V. Vliet, C. Opsomer, J. Botterman, and A. Schulz. 1996. The similarities of *bar* and *pat* gene products make them equally applicable for plant engineering. Nat. Biotechnol. 14:1274-1278.

56. Whitlock, G. C., D. M. Estes, and A. G. Torres. 2007. Glanders: off to the race with *Burkholderia mallei*. FEMS Microbiol. Lett. 277(2):115-122.

57. Wiersinga, W. J., T. van der Poll, N. J. White, N. P. Day, and S. J. Peacock. 2006. Melioidosis: insight into the pathogenicity of *Burkholderia pseudomallei*. Nature Rev. Microbiol. 4:272-282.

58. Wuthiekanun, V., N. Pheaktra, H. Putchhat, L. Sin, B. Sen, V. Kumar, S. Langla, S. J. Peacock, and N. P. Day. 2008. *Burkholderia pseudomallei* antibodies in children, Cambiodia. Emerg. Infect. Dis. 14(2):301-303.

59. Yanisch-Perron, C., J. Vieira, and J. Messing. 1985. Improved M13 cloning vectors and host strains: nucleotide sequences of the M13mp18 and pUC19 vectors. Gene. 33:103-119.

60. Yu, M., and J. S. H. Tsang. 2006. Use of ribosomal promoters from *Burkholderia cenocepacia* and *Burkholderia cepacia* for improved expression of transporter protein in *Escherichia coli*. Protein Expr. Purif. 49:219-227.

61. Zablotowicz, R. M., and K. N. Reddy. 2004. Impact of glyphosate on the *Bradyrhizobium japonicum* symbiosis with glyphosate-resistant transgenic soybean: a minireview. J. Environ. Qual. 33:825-831.

62. Zimmerman, J. E. 1970. Acute septicemic melioidosis. Successful treatment with gentamycin. JAMA. 213:2266-2267.

Chapter 3. Stable site-specific fluorescent tagging constructs optimized for *Burkholderia* species

Published as:

Stable site-specific fluorescent tagging constructs optimized for *Burkholderia* species in Applied and Environmental Microbiology 2010 Nov;76(22):7635-7640.

Michael H. Norris[2], Yun Kang[2], Bruce Wilcox[3] and Tung T. Hoang[1,2*]

Department of Microbiology[1], Department of Molecular Biosciences and Bioengineering[2], Department of Ecology and Health[3], University of Hawaii at Manoa, HI 96822, USA

*Corresponding author. Tel +1 808 956 3522; Fax +1 808 956 5339; e-mail: tongh@hawaii.edu

3.1 ABSTRACT

Several vectors were constructed that facilitate stable fluorescent labeling of *Burkholderia pseudomallei* and *Burkholderia thailandensis*. These vectors combined the effectiveness of the miniTn7 site-specific transposition system with fluorescent proteins optimized for *Burkholderia* spp., enabling bacterial tracking during cellular infection.

3.2 INTRODUCTION

Burkholderia pseudomallei is a highly infectious Gram-negative bacterium and is a facultative intracellular pathogen. The ability to observe infectious processes of this bacterium at various stages is critical in understanding pathogenesis. Fluorescent proteins facilitate bacterial tagging and have been powerful investigative tools in deciphering biological processes [100-105]. However, the lack of optimized fluorescent constructs used to label *B. pseudomallei* for visualization necessitate further development. Although there are many fluorescent tools available besides the green fluorescent protein, they are not optimized for use in *B. pseudomallei* and the less pathogenic model species, *B. thailandensis*. Commercially available fluorescent proteins are optimized for eukaryotic expression or, at the very best, for bacteria with low G/C genomes and hence codon preference may cause problems [106,107] during protein expression in *Burkholderia* spp. Also, there is usually an ineffective promoter driving transcription in *Burkholderia* spp., and available constructs are usually replicating plasmids that require selective maintenance. The restricted use of antibiotic markers in select agents (e.g. *B. pseudomallei*) adds another level of complexity to the genetic manipulation of these species [108]. Hence, these obstacles have limited the applications of fluorescent proteins in pathogenesis studies of *Burkholderia* spp.

3.3 RESULTS and DISCUSSION

The well-established miniTn7 system [109-111] inserts itself at a unique neutral site(s) in the bacterial genome with the aid of a non-replicating helper plasmid encoding the transposase [112]. The *B. pseudomallei* chromosome contains three insertion sites downstream of three *glmS* genes, whereas *B. thailandensis* contains two insertion sites downstream of two *glmS* genes [113]. Insertion of miniTn7 is quite stable in the bacterial genome [110,114] without the need for selective maintenance. Here, we constructed and demonstrated the use of fluorescent proteins encoded on miniTn7-based site-specific transposition vectors for fluorescent tagging of *B. pseudomallei* and *B. thailandensis.* We optimized the fluorescent protein genes (cyan, red, and yellow) for *B. pseudomallei*, which were synthesized through Genscript Corporation based on the amino acid sequences from Evrogen (http://www.evrogen.com/), by driving their transcription with a P_{S12} promoter [115] and changing the codons to those preferred by *B. pseudomallei*. Since the eGFP is sufficiently bright in *Burkholderia spp.*, we utilized the *gfp* gene driven by the P_{S12} promoter (Table 1). The four new fluorescent proteins were combined with two miniTn7 backbones to produce eight fluorescent tagging vectors (Fig. 1 and Table 1). The first series of four vectors encode the non-antibiotic selectable marker *gat* (resistance to glyphosate) [80,116] and the other series of vectors encode kanamycin resistance (Kan^r) (Fig. 1). Both are currently approved selectable markers in *B. pseudomallei* [80,113]. Nevertheless, prior CDC/USDA approval for each laboratory to use these markers is necessary and must be sought. All manipulations of *B. pseudomallei* were carried out in a CDC/USDA approved biosafety level 3 laboratory, following the guidelines presented in the Biosafety in Microbiological and Biomedical Laboratories (BMBL) 5^{th} edition [117].

The four vectors based on *gat* were used to tag *B. pseudomallei* 1026b (Fig. 1). To introduce the fluorescent tags, tri-parental matings were conducted using an *E. coli* donor (E1354, Table 1) carrying a helper plasmid (pTNS3-asd_{Ec}), *B. pseudomallei* 1026b, and one of the four fluorescent vectors shown in Fig. 1, as previously described [80]. *B. pseudomallei* containing the inserted transposon were selected for on 1x M9 minimal glucose media containing 0.3% (v/v) glyphosate, as previously described [80]. Colonies appeared ~2 days later and were purified on the same media. Insertion at one of the three *glmS* sites in the chromosome was verified by PCR as described previously [80,113,118]. *B. pseudomallei* could be labeled and all four colors could be observed as shown in Fig. 2. To visualize fluorescently labeled bacteria, all samples were fixed in 1% paraformaldehyde based on previously published protocols for 30 min [37,119]. Fluorescent microscopy was carried out using the suggested filter cube sets as shown in Table 2. As our laboratory has not applied for approval to introduce Kan^r genes into *B. pseudomallei*, we used the *gat*-based constructs to tag *B. pseudomallei* for the rest of our experiments. Regardless, the other four fluorescent vectors based on Kan^r (Fig.1) were constructed for use in *B. pseudomallei* by those laboratories with appropriate USDA/CDC approval, and we have validated proper transposition and fluorescence in *B. thailandensis*, as well as in *Burkholderia cenocepacia* strain K56-2 and *Pseudomonas aeruginosa* strain PAO1 (data not shown).

The ability to tag *Burkholderia* spp. with different colors could facilitate studies where one or more strains expressing different colors could be located or tracked. To demonstrate this, we took advantage of the intracellular replication of *B. pseudomallei* by using two of the fluorescent strains engineered above (e.g. green and red) to infect the murine macrophage cell-line, RAW264.7, in a modified aminoglycoside protection assay [120]. Briefly, the respective *B.*

pseudomallei cultures were grown overnight and used to infect the RAW 264.7 monolayers at an MOI of 10:1 for 1 h [89,121-124]. Afterwards, the extracellular bacteria were removed and the monolayers were washed twice with 1x PBS. Fresh DMEM containing 750 μg/ml amikacin and 750 μg/ml kanamycin was then added to inhibit extracellular bacterial replication. At 7 h post-infection, the monolayers were fixed with 1% (w/v) paraformaldehyde for 30 min and visualized using fluorescent microscopy [37,119]. As Figure 3 indicates, *B. pseudomallei* tagged with different colors were easily distinguishable within the murine macrophage cell-monolayers and can be seen inside host cells as the bacteria replicate. When both green and red fluorescent *B. pseudomallei* are mixed together and used to infect a murine macrophage cell monolayer at a total MOI of 10:1, differently colored bacteria can be distinguished and neighboring bacteria of either color can be differentiated from one another (Fig. 4). To observe the different infectious stages with fluorescently tagged *B. pseudomallei*, RAW 264.7 macrophages were infected at an MOI of 1:5 (1 bacteria per 5 host cells). In Figure 5A and 5B, the host-cells were infected with RFP-tagged *B. pseudomallei*, fixed, permeabilized, then stained with the far-red lipophilic styryl dye FM 4-64-FX (Molecular Probes). This stains all lipid bilayers far-red, including vacuoles, leaving the slightly orange color of the RFP-tagged *B. pseudomallei* visible i) in the macrophage vesicle (Fig. 5A) and ii) during vesicular escape (Fig. 5B). Alternatively, *B. pseudomallei* could be labeled with GFP for visualization (Fig. 5C and 5D). By infecting the macrophages at an MOI of 1:5 with GFP-tagged *B. pseudomallei*, then staining host-cell actin far-red, one can visualize bacterial replication in the cytoplasm (Fig. 5C) and the formation of actin tails during protrusion from the host cell (Fig. 5D).

In summary, we have constructed and demonstrated the use of transposon vectors for site-specific stable fluorescent tagging of *B. pseudomallei* with four unique colors. These tools

will be beneficial for microbiological studies involving the tracking or microscopy of *B. pseudomallei* during cellular infection. There are real needs for these vectors in the field and several applications can be envisioned. Infection studies that require tracking more than one strain through the infectious process would benefit from these tagging vectors, which do not require plasmid maintenance. Although bioluminescent tools have been of value in *in vivo* and non-invasive imaging of *B. pseudomallei* animal infections [125], our fluorescent constructs are of similar value [126,127]. Fluorescence activated cell sorting could also be used to enumerate host cells infected with a particular strain or strains of fluorescent *B. pseudomallei* or to monitor gene expression when using engineered constructs [102,128]. We believe these constructs will be beneficial to colleagues in this field and can be obtained upon request (Table 1).

This work was supported by National Institutes of Health grant R21-AI074608 to T.T.H. A graduate stipend for M.H.N. was provided by an NSF IGERT award (0549514) to Bruce A. Wilcox.

3.4 FIGURE LEGENDS

FIG. 1. Maps of miniTn7-*gat-cfp* and miniTn7-*kan-cfp* (A), miniTn7-*gat-gfp* and miniTn7-*kan-gfp* (B), miniTn7-*gat-rfp* and miniTn7-*kan-rfp* (C), and miniTn7-*gat-yfp* and miniTn7-*kan-yfp* (D). These constructs allow for site-specific transposition of fluorescent protein genes (*cfp, gfp, rfp,* and *yfp*), using the non-antibiotic resistance marker *gat* or the kanamycin resistance marker *kan* assisted by the helper plasmid pTNS3-asd_{Ec}. Differences in plasmid size are denoted in parenthesis. The P_{S12} promoter drives all fluorescent proteins. The *gat* or *kan* cassette is driven by the PC_{S12} on all constructs. These selectable markers are flanked by *FRT* sequences for Flp protein excision. Abbreviations: *oriT*, RP4 conjugal origin of transfer; PC_{S12}, *rpsL* promoter of *B. cenocepacia*; P_{S12}, *rpsL* promoter of *B. pseudomallei*; $R6K_{\gamma ori}$, π protein-dependent R6K origin of replication; *Tn7L* and *Tn7R*, left and right transposase recognition sequences; T_0T_1, transcriptional terminator.

FIG. 2. Fluorescent microscopy of *B. pseudomallei* labeled at the *att*Tn7 site with *gat-cfp* (A), *gat-gfp* (B), *gat-rfp* (C), and *gat-yfp* (D). Fluorescent signals were obtained using the respective filter cube sets on a Zeiss AxioObserver D1 microscope and AxioCam MRc 5 monochrome camera. Pseudo-color was applied to the signal intensity at the time of capture using Zeiss AxioVision software. The middle row is comprised of differential interference contrast (DIC) images from the respective samples. At the time of capture, Zeiss AxioVision software was used to superimpose the fluorescent signal and DIC images displayed in the bottom row. When comparing the overlay in the bottom row to the DIC image in the middle, it can be seen that almost all bacteria are fluorescing at one exposure time or at a set fluorescent intensity. Differing expression of fluorescent protein genes and extended fixation can result in slightly

different fluorescent intensities among a population of bacteria, since extended paraformaldehyde fixation could damage the fluorescent proteins [129]. Total magnification is 630x and scale bars equal 10μm.

FIG. 3. Fluorescent microscopy of *B. pseudomallei* labeled at the *att*Tn7 site with *gat-cfp* (A), *gat-gfp* (B), *gat-rfp* (C), and *gat-yfp* (D) to infect murine macrophage-like cell line RAW264.7. Cell monolayers were seeded overnight onto poly-L-lysine coated coverslips at the bottom of a 6-well plate. The respective *B. pseudomallei* cultures were grown overnight and used to infect the RAW 264.7 monolayers at an MOI of 10:1 for 1 h. Afterwards, the extracellular bacteria were removed and the monolayers were washed twice with 1x PBS. Fresh DMEM containing 750μg/ml amikacin and 750 μg/ml kanamycin was then added to inhibit extracellular bacterial replication. The infection was allowed to proceed for 6 hrs after which the DMEM was removed; the monolayers were washed with 1x PBS and fixed with fresh 1% (w/v) paraformaldehyde for 30 min. Images were obtained as in Fig. 2. Total magnification is 630x and scale bars equal 10μm.

FIG. 4. Dual infection of RAW264.7 macrophages by differentially labeled (green and red) *B. pseudomallei*. Infections were carried out identically to those in Fig. 3. (A) The green fluorescent signal was obtained indicating where *gfp*-tagged *B. pseudomallei* are replicating inside macrophages. (B) The red fluorescent signal was obtained from the same field indicating where *rfp*-tagged *B. pseudomallei* are replicating within macrophages. A DIC image was then captured and is presented in (C). Overlay of images captured sequentially in (A), (B), and (C). Images were superimposed at the time of capture using Zeiss AxioVision software. (E) and (F)

are close-ups of the two macrophages indicated by arrows in (D), where the two differently fluorescing *B. pseudomallei* strains are clearly visible and distinguishable within the macrophages and even within the same host cell. Total magnification in (A), (B), (C), and (D) is 630x and all scale bars equal 10μm.

FIG. 5. Tracking of *B. pseudomallei* infectious stages. Infections were carried out as in Fig. 3 except *B. pseudomallei* were used to infect macrophages at an MOI of 1:5 to enable isolated bacterial infection. (A) RAW 264.7 monolayers were infected with RFP-tagged *B. pseudomallei.* The infection was allowed to progress for 1 h and then vesicles were stained far-red with the lipophilic styryl dye, FM-4-64-FX (Molecular Probes). Phase contrast microscopy in the red fluorescent channel captured an image of two RFP-tagged *B. pseudomallei* in a phagocytic vesicle. The image in (B) was obtained similarly except that a single RFP-tagged *B. pseudomallei* is possibly escaping the far-red stained phagocytic vesicle. (C) RAW 264.7 macrophages were infected with GFP-tagged *B. pseudomallei* for 2 hrs after which the monolayers were then fixed, permeabilized, and host-cell actin was stained far-red with phalloidin. GFP-tagged *B. pseudomallei* can be seen polymerizing host-cell actin enabling observation of actin-based intracellular motility. (D) GFP-tagged *B. pseudomallei* were used to infect RAW 264.7 monolayers for 6 hrs. The bacteria are polymerizing host-cell actin to infect neighboring host cells via membrane protrusions. The arrows indicate GFP-tagged *B. pseudomallei* at the tip of polymerized actin tails. Total magnification in (A), (B), (C), and (D) is 1,000x.

TABLE 1. Bacterial strains and plasmids used in this study[a]

Strains	Lab ID[b], (Addgene ID[c])	GenBank ID No.	Relevant properties	Sources
E. coli				
EPMax10B-*pir116*/Δ*asd*/Δ*trp*::Gm^r/*mob*-Kan^r	E1354		Gm^r, Kan^r; F$^-$ λ$^-$ *mcrA*Δ(*mrr-hsdRMS-mcrBC*) ϕ*80dlacZ*Δ*M15* Δ*lacX74 deoR recA1 endA1 araD139* Δ*(ara, leu)7697 galU galK rpsL nupG Tn-pir116-FRT2* Δ*asd*::*wFRT* Δ*trp*::Gm^r-*FRT5 mob*[*recA*::*RP4-2 Tc*::*Mu*-Kan^r]	_[d]
EPMax10B-*lacI^q*/*pir*	E1869		F$^-$ λ$^-$ *mcrA* Δ(*mrr-hsdRMS-mcrBC*) ϕ80*dlacZ*Δ*M15* Δ*lacX74 deoR recA1 endA1 araD139* Δ(*ara, leu*)7697 *galU galK rpsL nupG lacI^q-FRT8 pir-FRT4*	_[d]
***Burkholderia* spp.**				
B. pseudomallei				
1026b	B0004		Type-strain; clinical melioidosis isolate	[130]
1026b/*att*Tn7-*gat-cfp*	B0036		GS^r, 1026b with miniTn7-*gat-cfp* inserted	This study
1026b/*att*Tn7-*gat-gfp*	B0037		GS^r, 1026b with miniTn7-*gat-gfp* inserted	This study
1026b/*att*Tn7-*gat-rfp*	B0038		GS^r, 1026b with miniTn7-*gat-rfp* inserted	This study
1026b/*att*Tn7-*gat-yfp*	B0039		GS^r, 1026b with miniTn7-*gat-yfp* inserted	This study
B. thailandensis				
E264	E1298		Prototroph; environmental isolate	[131]
E264/*att*Tn7-*kan-cfp*	E2552		Kan^r, E264 with miniTn7-*kan-cfp* inserted	This study
E264/*att*Tn7-*kan-gfp*	E2491		Kan^r, E264 with miniTn7-*kan-gfp* inserted	This study
E264/*att*Tn7-*kan-rfp*	E2553		Kan^r, E264 with miniTn7-*kan-rfp* inserted	This study
E264/*att*Tn7-*kan-yfp*	E2554		Kan^r, E264 with miniTn7-*kan-yfp* inserted	This study
Plasmids				
miniTn7-*gat*	E1981		GS^r, miniTn7 integration vector based on *gat*	[80]
miniTn7-*gat-cfp*	E2460 (24274)	HM150704	GS^r, miniTn7-*gat* harboring *cfp*	This study
miniTn7-*gat-gfp*	E2462 (24275)	HM150705	GS^r, miniTn7-*gat* harboring *gfp*	This study
miniTn7-*gat-rfp*	E2326 (24276)	HM150706	GS^r, miniTn7-*gat* harboring *rfp*	This study
miniTn7-*gat-yfp*	E2468 (24277)	HM150707	GS^r, miniTn7-*gat* harboring *yfp*	This study
miniTn7-*kan-cfp*	E2480 (24278)	HM150708	Kan^r, miniTn7-*kan* harboring *cfp*	This study
miniTn7-*kan-gfp*	E2482 (24279)	HM150709	Kan^r, miniTn7-*kan* harboring *gfp*	This study
miniTn7-*kan-rfp*	E2486 (24280)	HM150710	Kan^r, miniTn7-*kan* harboring *rfp*	This study
miniTn7-*kan-yfp*	E2488 (24281)	HM150711	Kan^r, miniTn7-*kan* harboring *yfp*	This study
pPS747	E0042		Ap^r; plasmid harboring eGFP from pUCP20-GFPmut2	[128]
pRK2013	E1358		Kan^r; Helper plasmid encoding conjugative proteins.	[132]
pTNS3-asd_{Ec}	E1831		Suicidal helper plasmid containing asd_{Ec} and transposase for the Tn7 site-specific transposition system	[118]
pUC57-P_{S12}-*cfp*	E1739 (24912)	HM150701	Ap^r; plasmid harboring *B. pseudomallei* codon optimized *cfp* driven by P_{S12}	This study
pUC57-P_{S12}-*rfp*	E1735 (24913)	HM150702	Ap^r; plasmid harboring *B. pseudomallei* codon optimized *rfp* driven by P_{S12}	This study
pUC57-P_{S12}-*yfp*	E1738 (24914)	HM150703	Ap^r; plasmid harboring *B. pseudomallei* codon optimized *yfp* driven by P_{S12}	This study

[a] Abbreviations: *gat*, gene encoding glyphosate acetyltransferase; Gm^r, gentamycin resistant; GS^r, glyphosate resistant; *kan,* gene encoding kanamycin resistance; Kan^r, kanamycin resistant; P_{S12}, *rpsL* promoter from *B. pseudomallei*.

[b] Please use laboratory identification number (Lab ID) when requesting strains and plasmids.

[c] Plasmids denoted with an Addgene number should be obtained from Addgene.

[d] Details on the engineering of these strains are to be published elsewhere.

TABLE 2. Fluorescent Protein Characteristics[a]

Fluorescent protein (original source)	Excitation max. (nm)	Emission max. (nm)	Recommended fluorescence microscopy filter set	Maturation at 37˚C
Tag CFP (*Aequorea macrodactyla*)	458	480	Omega Optical sets XF114-2 or XF130-2	fast
eGFP (*Aequorea victoria*)	488	509	Omega Optical set XF116-2 or Chroma Technology set 41017	fast
Turbo YFP (*Phialidium* sp.)	525	538	Omega Optica set XF104-3 or Chroma Technology set 42003	superfast
Turbo RFP (*Entacmaea quadricolor*)	553	574	Omega Optical sets QMAX-Yellow, XF108-2, XF101-2, and XF111-2	superfast

[a] These characteristics were found on the Evrogen website (http://www.evrogen.com/).

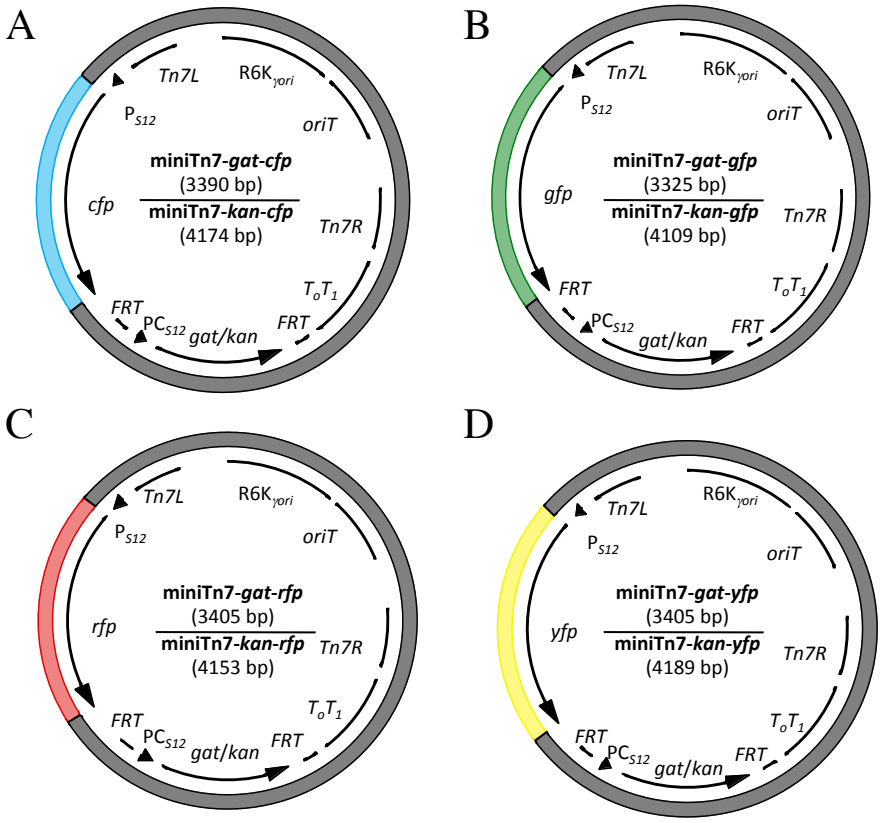
A
Tn7L
R6K$_{\gamma ori}$
P$_{S12}$
oriT
miniTn7-gat-cfp
(3390 bp)
cfp
miniTn7-kan-cfp
(4174 bp)
Tn7R
T$_o$T$_1$
FRT
PC$_{S12}$
gat/kan
FRT
B
Tn7L
R6K$_{\gamma ori}$
P$_{S12}$
oriT
miniTn7-gat-gfp
(3325 bp)
gfp
miniTn7-kan-gfp
(4109 bp)
Tn7R
FRT
T$_o$T$_1$
PC$_{S12}$
gat/kan
FRT
C
Tn7L
R6K$_{\gamma ori}$
P$_{S12}$
oriT
miniTn7-gat-rfp
(3405 bp)
rfp
miniTn7-kan-rfp
(4153 bp)
Tn7R
T$_o$T$_1$
FRT
PC$_{S12}$
gat/kan
FRT
D
Tn7L
R6K$_{\gamma ori}$
P$_{S12}$
oriT
miniTn7-gat-yfp
(3405 bp)
yfp
miniTn7-kan-yfp
(4189 bp)
Tn7R
T$_o$T$_1$
FRT
PC$_{S12}$
gat/kan
FRT

Figure 1

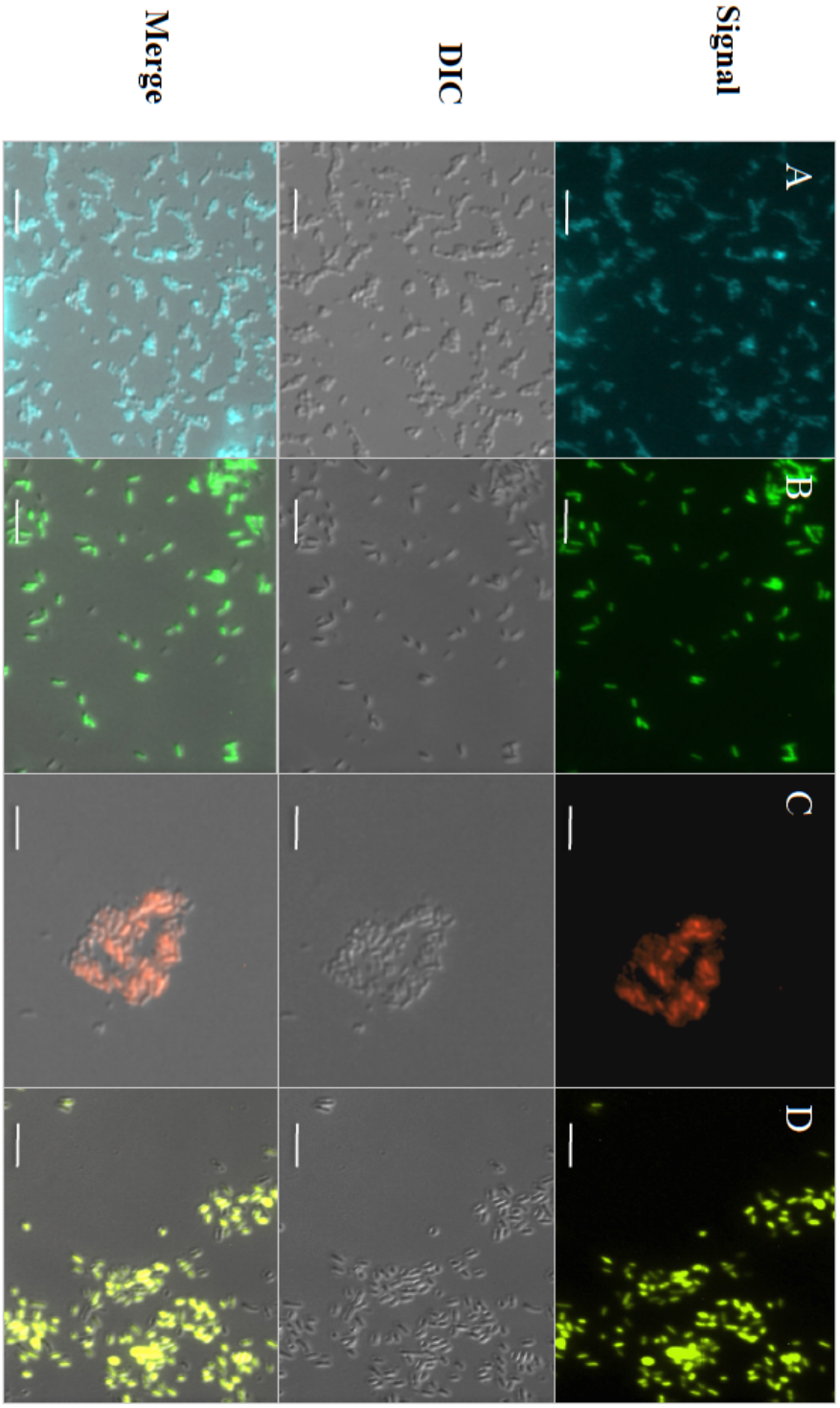

Figure 2

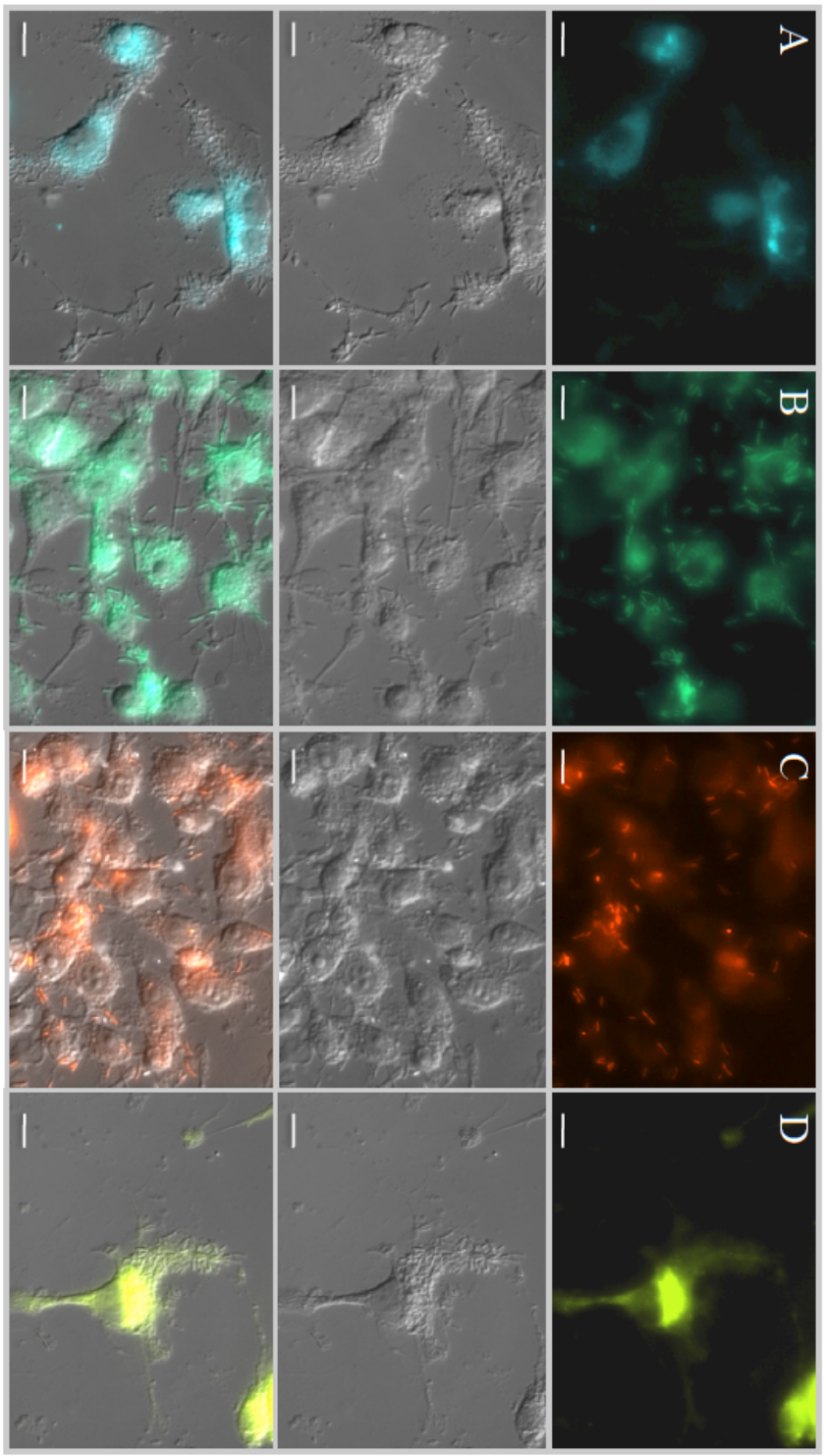

Figure 3

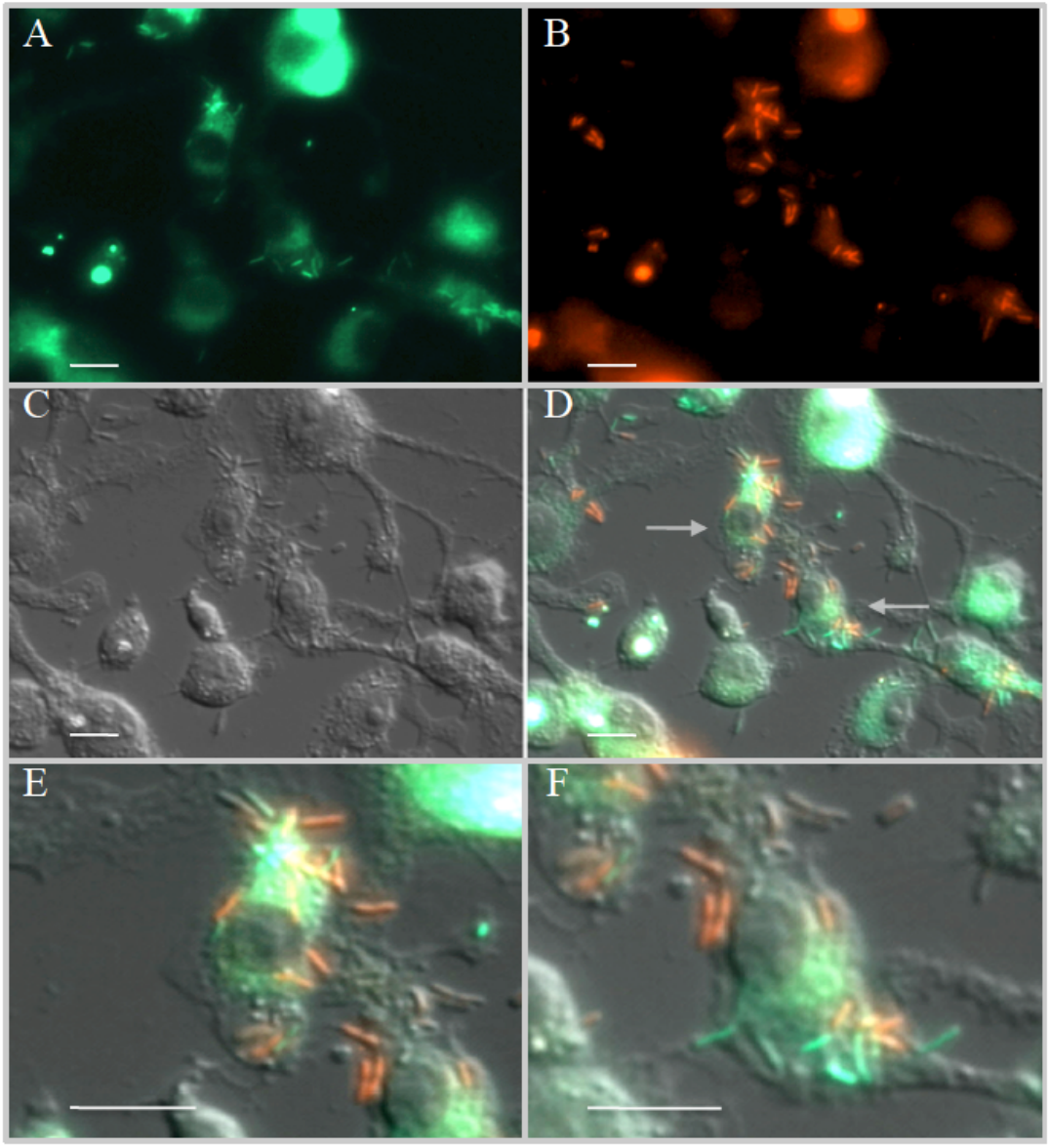

Figure 4

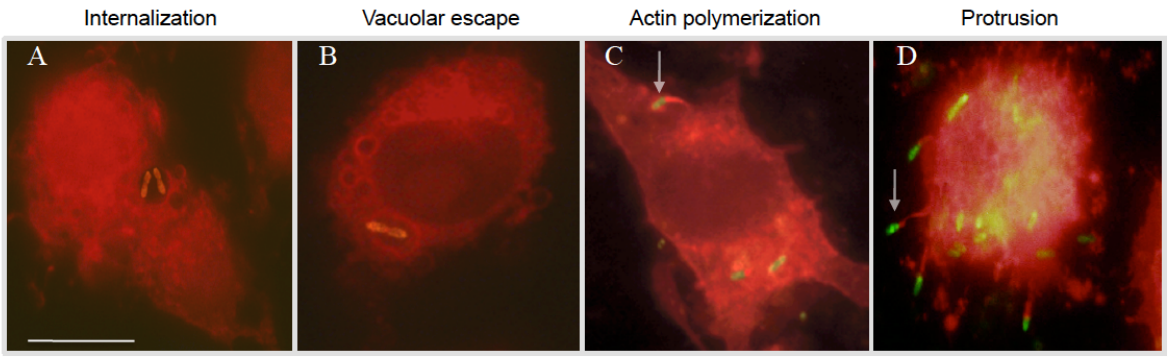
Internalization
Vacuolar escape
Actin polymerization
Protrusion
A
B
C
D

Figure 5

3.5 REFERENCES

1. Biery, M. C., M. Lopata, and N. L. Craig. 2000. A minimal system for Tn7 transposition: the transposon-encoded proteins TnsA and TnsB can execute DNA breakage and joining reactions that generate circularized Tn7 species. J. Mol. Biol. 297:25-37.
2. Brett, P. J., D. DeShazer, and D. E. Woods. 1998. *Burkholderia thailandensis* sp. nov., description of *Burkholderia pseudomallei*-like species. Int. J. Syst. Bacteriol. 48:317-320.
3. Bumann, D. 2001. *In vivo* visualization of bacterial colonization, antigen expression, and specific T-cell induction following oral administration of live recombinant *Salmonella enterica* serovar Typhimurium. Infect. Immun. 69:4618-4626.
4. Burtnick, M. N., P. J. Brett, V. Nair, J. M. Warawa, D. E. Woods, and F. C. Gherardini. 2008. *Burkholderia pseudomallei* type III secretion system mutants exhibit delayed vacuolar escape phenotypes in RAW 264.7 murine macrophages. Infect. Immun. 76:2991-3000.
5. Castle, L. A., D. L. Siehl, R. Gorton, P. A. Patten, Y. H. Chen, S. Bertain, H. Cho, N. Duck, J. Wong, D. Liu, and M. W. Lassner. 2004. Discovery and directed evolution of a glyphosate tolerance gene. Science 304:1151-1154.
6. Chanchamroen, S., C. Kewcharoenwong, W. Susaengrat, M. Ato, and G. Lertmemongkolchai. 2009. Human polymorphonuclear neutrophil responses to *Burkholderia pseudomallei* in healthy and diabetic subjects. Infect. Immun. 77:456-463.
7. Choi, K.-H., J. B. Gaynor, K. G. White, C. Lopez, C. M. Bosio, R. R. Karkhoff-Schweizer, and H. P. Schweizer. 2005. A Tn7-based broad-range bacterial cloning and expression system. Nat. Meth. 2:443-448.

8. Choi, K.-H., T. Mima, Y. Casart, D. Rholl, A. Kumar, I. R. Beacham, and H. P. Schweizer. 2008. Genetic tools for select-agent-compliant manipulation of *Burkholderia pseudomallei*. Appl. Environ. Microbiol. 74:1064-1075.

9. Cormack, B., R. Valdivia, and S. Falkow. 1996. FACS-optimized mutants of the green fluorescent protein (GFP). Gene. 173:33-38.

10. DeShazer, D., P. J. Brett, R. Carlyon, and D. E. Woods. 1997. Mutagenesis of *Burkholderia pseudomallei* with Tn5-OT182: isolation of motility mutant and molecular characterization of the flagellin structural gene. J. Bacteriol. 179:2116-2125.

11. Figurski, D. H., and D. R. Helinski. 1979. Replication of an origin-containing derivative of plasmid RK2 dependent on a plasmid function provided in *trans*. Proc. Natl. Acad. Sci. USA 76:1648-1652.

12. Fischer, A. H., K. A. Jacobson, J. Rose, and R. Zeller. 2006. Basic methods in microscopy: preparation of cells and tissues for fluorescence microscopy. Cold Springs Harbor Laboratory Press, Cold Springs Harbor, NY.

13. Gustafsson, C., S. Govindarajan, and J. Minshull. 2004. Codon bias and heterologous protein expression. Trends in Biotech. 22:346-353.

14. Hagemann, A. T., and N. L. Craig. 1993. Tn7 transposition creates a hotspot for homologous recombination at the transposon donor site. Genetics 133:9-16.

15. Hoang, T. T., R. R. Karkhoff-Schweizer, A. J. Kutchma, and H. P. Schweizer. 1998. A broad-host-range Flp-*FRT* recombination system for site-specific excision of chromosomally-located DNA sequences: application for isolation of unmarked *Pseudomonas aeruginosa* mutants. Gene 212:77-86.

16. Jones, A. L., T. J. Beveridge, and D. E. Woods. 1996. Intracellular survival of *Burkholderia pseudomallei*. J. Bacteriol. 64:782-790.

17. Kang, Y., M. H. Norris, A. R. Barrett, B. A. Wilcox, and T. T. Hoang. 2009. Engineering of tellurite-resistant genetic tools for single-copy chromosomal analysis of *Burkholderia* spp. and characterization of the *Burkholderia thailandensis betBA* operon. Appl. Environ. Microbiol. 75:4015-4027.

18. Koch, B., L. E. Jensen, and O. Nybroe. 2001. A panel of Tn7-based vectors for insertion of the gfp marker gene or for delivery of cloned DNA into Gram-negative bacteria at a neutral chromosomal site. J. Microbiol. Meth. 45:187-195.

19. Kurland, C. G. 1991. Codon bias and gene expression. FEBS Lett. 285:165-169.

20. LoVullo, E. D., C. R. Molins-Schneekloth, H. P. Schweizer, and M. S. Pavelka, Jr. 2009. Single-copy chromosomal integration systems for *Francisella tularensis*. Microbiology 155:1152-1163.

21. Norris, M. H., Y. Kang, D. Lu, B. A. Wilcox, and T. T. Hoang. 2009. Glyphosate resistance as a novel select-agent-compliant, non-antibiotic selectable-marker in chromosomal mutagenesis of the essential genes *asd* and *dapB* of *Burkholderia pseudomallei*. Appl. Environ. Microbiol. 75:6062-6075.

22. Owen, S., M. Batzloff, F. Chehrehasa, A. Meedeniya, Y. Casart, C. A. Logue, R. Hirst, I. R. Peak, A. Mackay,Sim, and I. R. Beacham. 2009. Nasal associated lymphoid tissue and olfactory epithelium as portals of entry for *Burkholderia pseudomallei* in murine melioidosis. The Journal of Infectious Diseases 199:1761-1770.

23. Parker, A. E., and L. E. Bermudez. 1997. Expression of the green fluorescent protein (GFP) in *Mycobacterium aviumas* a tool to study the interaction between mycobacteria and host cells. Microb. Path. 22:193-198.

24. Poschet, J. F., J. C. Boucher, L. Tatterson, J. Skidmore, R. W. Van Dyke, and V. Deretic. 2001. Molecular basis for defective glycosylation and *Pseudomonas* pathogenesis in cystic fibrosis lung. Proc. Natl. Acad. Sci. U.S.A. 98:13972-13977.

25. Reckseidler, S. L., D. DeShazer, P. A. Sokol, and D. E. Woods. 2001. Detection of bacterial virulence genes by subtractive hybridization: identification of capsular polysaccharide of *Burkholderia pseudomallei* as a major virulence determinant. Infect. Immun. 69:34-44.

26. Ribot, W. J., and R. L. Ulrich. 2006. The animal pathogen-like type III secretion system is required for the intracellular survival of *Burkholderia mallei* within J774.2 macrophages. Infect. Immun. 74:4349-4353.

27. Schweizer, H. P., and S. J. Peacock. 2008. Antimicrobial drug–selection markers for *Burkholderia pseudomallei* and *B. mallei*. Emerg. Infect. Dis. 14
:1689-1692.

28. Stevens, J. M., R. L. Ulrich, L. A. Taylor, M. W. Wood, D. Deshazer, M. P. Stevens, and E. E. Galyov. 2005. Actin-binding proteins from *Burkholderia mallei* and *Burkholderia thailandensis* can functionally compensate for the actin-based motility defect of a *Burkholderia pseudomallei bimA* mutant. J. Bacteriol. 187:7857-7862.

29. Tan, M.-W., S. Mahajan-Miklos, and F. M. Ausubel. 1999. Killing of *Caenorhabditis elegans* by *Pseudomonas aeruginosa* used to model mammalian bacterial pathogenesis. Proc. Natl. Acad. Sci. U.S.A. 96:715-720.

30. Utaisincharoen, P., S. Arjcharoen, I. Lengwehasatit, K. Limposuwan, and S. Sirisinha. 2005. *Burkholderia pseudomallei* invasion and activation of epithelial cells requires activation of p38 mitogen-activated protein kinase. Microb. Path. 38:107-112.

31. Valdivia, R. H., and S. Falkow. 1998. Flow cytometry and bacterial pathogenesis. Curr. Opin. Microbiol. 1:359-363.

32. Valdivia, R. H., and S. Falkow. 1997. Fluorescence-based isolation of bacterial genes expressed within host cells. Science. 277:2007-2011.

33. van Schaik, E. J., M. Tom, and D. E. Woods. 2009. *Burkholderia pseudomallei* isocitrate lyase is a persistence factor in pulmonary melioidosis: implications for the development of isocitrate lyase inhibitors as novel antimicrobials. Infect. Immun. 77:4275-4283.

34. Wilson, D. E., and L. C. Chosewood (ed.). 2007. Biosafety in microbiological and biomedical laboratories, 5th ed., Atlanta, GA.

35. Yang, M., E. Baranov, A. R. Moossa, S. Penman, and R. M. Hoffman. 2000. Visualizing gene expression by whole-body fluorescence imaging. Proc. Natl. Acad. Sci. U.S.A. 97:12278-12282.

36. Yu, M., and J. S. H. Tsang. 2006. Use of ribosomal promoters from *Burkholderia cenocepacia* and *Burkholderia cepacia* for improved expression of transporter protein in *Escherichia coli*. Protein Expr. Purif. 49:219-227.

37. Zhao, M., M. Yang, E. Baranov, X. Wang, S. Penman, A. R. Moossa, and R. M. Hoffman. 2001. Spatial-temporal imaging of bacterial infection and antibiotic response in intact animals. Proc. Natl. Acad. Sci. U.S.A. 98:9814-9818.

Chapter 4. The *Burkholderia pseudomallei* Δ*asd* mutant exhibits attenuated intracellular infectivity and imparts protection against acute inhalation melioidosis in mice

Published as:

The *Burkholderia pseudomallei* Δ*asd* mutant exhibits attenuated intracellular infectivity and imparts protection against acute inhalation melioidosis in mice

in Infection and Immunity 2011 Oct;79(10):4010-4018.

Michael H. Norris[b], Katie L. Propst[c], Yun Kang[a], Steven W. Dow[c], Herbert P. Schweizer[c], and Tung T. Hoang[a,b*]

[a]*Department of Microbiology,* [b]*Department of Molecular Biosciences and Bioengineering, University of Hawaii at Manoa, HI 96822, USA*

[c]*Department of Microbiology, Immunology, and Pathology, Colorado State University, Fort Collins, CO 80523, USA*

*Corresponding author. Tel +1 808 956 3522; Fax +1 808 956 5339; e-mail: tongh@hawaii.edu

4.1 ABSTRACT

Burkholderia pseudomallei, the cause of serious and life threatening diseases in humans, is of national biodefense concern because of its potential use as a bioterrorism agent. This microbe is listed as a select agent by the CDC, therefore, development of vaccines is of significant importance. Here, we further investigated the growth characteristics of a recently created *B. pseudomallei* 1026b Δ*asd* mutant *in vitro,* in a cell model, and in an animal model of infection. The mutant was typified by an inability to grow in the absence of exogenous diaminopimelate (DAP) and, upon single-copy complementation with a wildtype copy of the *asd* gene, growth was restored to wildtype levels. Further characterization of the *B. pseudomallei* Δ*asd* mutant revealed a marked decrease in RAW264.7 murine macrophage cytotoxicity when compared to the wildtype and the complemented Δ*asd* mutant. RAW264.7 cells infected by the Δ*asd* mutant did not exhibit signs of cytopathology or multi-nucleated giant cell (MNGC) formation observed in wildtype *B. pseudomallei* cell infections. The Δ*asd* mutant was found to be avirulent in BALB/c mice and mice vaccinated with the mutant were protected against acute inhalation melioidosis. Thus, the *B. pseudomallei* Δ*asd* mutant may be a promising live-attenuated vaccine strain and a biosafe strain to be considered for exclusion from the select agent list.

4.2 INTRODUCTION

Burkholderia pseudomallei, a gram-negative saprophyte and facultative intracellular pathogen, is a common cause of environmentally acquired septicemia in Southeast Asia and Northern Australia [1,133,134]. It is the etiological agent of the disease, melioidosis, and is listed as a category B select agent by the U.S. Centers for Disease Control and Prevention. Bacterial select agent research is currently focused on basic research into virulence and pathogenesis to fulfill the five main points of the United States Public Health Security and Bioterrorism Preparedness and Response Act of 2002 [20]. One of the goals is to develop and maintain medical countermeasures (such as drugs, vaccines and other biological products, medical devices, and other supplies) against biological agents and toxins in a bioterrorism event. To combat potential foul play associated with intentional release of select agents, a focus on vaccine development for first responders, such as military and health service professionals, is of the utmost importance [135]. Currently, there are no vaccines against *B. pseudomallei* and treatment entails prolonged regimens of intravenous and orally administered antibiotic therapy [136].

In a recent publication, we engineered a *B. pseudomallei* strain with a deletional mutation in the aspartate-β-semialdehyde dehydrogenase (*asd*) gene that is auxotrophic for diaminopimelate (DAP) in rich media and auxotrophic for DAP, lysine, methionine, and threonine in minimal media [80], which is consistent with similar mutations in many other bacterial species [81,137-139]. DAP is a diamino acid that crosslinks to D-alanine in neighboring peptidoglycan strands, and the Δ*asd* mutant exhibited the "pop-and-die" phenotype associated with an inability to synthesize DAP for cell-wall biosynthesis. Previous works have created *asd* mutants in *Salmonella typhimurium* [81] and *Legionella pneumophila* [140] and demonstrated a growth requirement for DAP. In addition, the *S. typhimurium* Δ*asd* strain has been extensively

used in clinical studies with human subjects as a vaccine delivery strain [141,142]. The pathway for synthesizing DAP from aspartate is absent in mammals, therefore no DAP is present in mammalian hosts, including humans [81,143]. The other amino acids (lysine, methionine, and threonine) made from aspartate via Asd are essential amino acids in humans, affording another possible level of nutrient limitation *in vivo*. Without a considerable exogenous concentration of DAP, the Δ*asd* mutant is unable to crosslink its cell wall and cannot replicate. Even when supplied with high levels of DAP, intracellularly replicating *L. pneumophila* Δ*asd* could not recover to wildtype levels of pathogenicity in both macrophage and protozoan infection models [140].

Live-attenuated vaccines are particularly effective vaccines because live bacteria may replicate modestly in the host, similar to situations encountered during an actual infection. In addition, live-attenuated vaccines contain complex epitopes not found in subunit or heat-inactivated vaccines, thus stimulating parts of the immune system that could otherwise be neglected (*e.g.* a strong Th1 response) [144]. Previous studies testing the efficacy of auxotrophic *B. pseudomallei* and *B. mallei* strains as live-attenuated vaccines have resulted in varying degrees of success [145,146]. In order to determine if the Δ*asd* strain may be appropriate as a future vaccine candidate, we evaluated the growth and attenuation of the *B. pseudomallei* 1026b Δ*asd* mutant *in vitro* and in cell culture. Animal studies were carried out to determine virulence levels and attenuation of the Δ*asd* strain. Efficacy of the *B. pseudomallei* 1026b Δ*asd* strain as a live-attenuated vaccine against inhalation melioidosis was then ascertained in a BALB/c mouse model.

4.3 MATERIALS and METHODS

Bacterial strains, media, and culture conditions. All manipulations of *B. pseudomallei* were conducted in CDC/USDA approved and registered BSL3 facilities at the University of Hawaii at Manoa and Colorado State University, and experiments with select agents were performed in accordance with the recommended BSL3 practices [147]. Derivatives of *Escherichia coli* strain EPMax10B (BioRad), E1345, E1354, E1869, and E1889 (Table 1) were routinely used for cloning or plasmid mobilization into *B. pseudomallei* as described previously [80,118]. Luria-Bertani (LB) medium (Difco) was used to culture *E. coli* strains. *B. pseudomallei* strains were cultured in LB or 1x M9 minimal medium supplemented with 20 mM glucose (MG). Antibiotics and non-antibiotic anitbacterials in solid media were utilized as follows: for *E. coli*, glyphosate (GS) 0.3% (w/v) and phosphinothricin (PPT) 0.3% (w/v) were used; for *B. pseudomallei*, GS 0.3% (w/v) and PPT 2.5% (w/v) were used. Growth of *E. coli* Δ*asd* strains and preparation of DAP were carried out as previously described [148]. Selection for *bar* or *gat* genes in *E. coli* and *B. pseudomallei* strains was performed as previously described [80]. *B. pseudomallei* Δ*asd*::*gat* strains were grown on LB containing 200 mg/ml DAP or on MG containing, 1 mM Lys, 1 mM Met, 1 mM Thr, and 200 mg/ml meso-DAP, as described previously [80].

Molecular methods and reagents. Molecular methods, PCR conditions, and conjugation into select agents were conducted as described previously [80,148,149].

Engineering of *B. pseudomallei* Δasd_{Bp}::*gat-FRT*. *B. pseudomallei* Δasd_{Bp}::*gat-FRT* was engineered as described previously [80] but briefly, the allelic-replacement vector, pBAKA-

Δ*asd*$_{Bp}$::*FRT-gat* was conjugally introduced into *B. pseudomallei* strain 1026b and selection of the mutation was carried out on MG medium + 200 µg/ml DAP + 0.3% GS + 1 mM each of Lys, Met, and Thr; these last 3 amino acids (3AA) are required for the specific Δ*asd* mutation. Colonies were streaked-out on the same medium supplemented with 0.1% cPhe to counter-select against *pheS*. GS resistant mutants were DAP were purified once on LB + DAP, and patched again on MG + 0.3% GS + 0.1% cPhe + 1 mM 3AA ± 200 mg/ml DAP to confirm.

Construction of single-copy *rfp*-containing vectors. The red fluorescent protein gene (*rfp*) was optimized for the codon preference of *B. pseudomallei* and the constitutive *B. pseudomallei rpsL* promoter (P$_{S12}$) was incorporated upstream of the gene [150]. Constructed as previously described [150], *rfp* was cloned from pUC57-P$_{S12}$-*rfp* into mini-Tn7-PC$_{S12}$-*bar* to yield mini-Tn7-*bar*-*rfp* (Fig. 1). The mini-Tn7-PC$_{S12}$-*bar* [80] construct was digested with PstI + SpeI and ligated to the *rfp* fragment obtained from pUC57-P$_{S12}$-*rfp* digested with PstI + XbaI, producing mini-Tn7-*bar*-*rfp*. Next, the complementation and fluorescent tagging transposon was constructed by digesting mini-Tn7-*bar*-*asd*$_{Bp}$ [80] with PstI + SpeI and ligating it to the *rfp* fragment from PstI + XbaI digested pUC57-P$_{S12}$-*rfp*, yielding the single copy complementation/fluorescent tagging vector, mini-Tn7-*bar*-*asd*$_{Bp}$-*rfp*. In addition to the *bar* based vector, the fluorescent tagging vector mini-Tn7-*gat*-*rfp* based on *gat,* constructed as previously described [150], was also utilized below.

Engineering of *rfp*-tagged *B. pseudomallei* strains and complemented mutants. E1354 was utilized as the conjugal donor to introduce the single copy vector mini-Tn7-*bar*-*rfp* into the *B. pseudomallei* Δ*asd* mutant for fluorescent tagging, producing *B. pseudomallei*

Δ*asd*::*gat-FRT*/*att*Tn7-*bar-rfp* (Δ*asd*/*rfp*). The mini-Tn7-*bar-asd*$_{Bp}$-*rfp* construct was introduced into the Δ*asd* mutant for complementation and fluorescent tagging, yielding *B. pseudomallei* Δ*asd*::*gat-FRT*/*att*Tn7-*bar-asd*$_{Bp}$-*rfp* (Δ*asd*/complement/*rfp*). The mini-Tn7-*gat-rfp* construct was introduced into wildtype *B. pseudomallei* strain 1026b for fluorescent tagging of the wildtype, resulting in *B. pseudomallei att*Tn7-*gat-rfp* (wt/*rfp*). These strains were obtained from a tri-parental mating experiment using the pTNS3-*asd*$_{Ec}$ helper plasmid and bacteria containing the integrated transposon were selected and screened via PCR as described previously [80,118,151]. The mini-Tn7 system allows site-specific insertion of the transposon at a neutral site in the chromosome, downstream of any *glmS* gene, of which *B. pseudomallei* has three [113]. In all cases the transposon had inserted at the highly favored *glmS2* site. Fluorescence was verified by fixing the bacteria with fresh 1% paraformaldehyde in phosphate buffered saline (PBS) for 30 min followed by imaging with a Zeiss Axio Observer D.1 fluorescent microscope and accompanying AxioVision release 4.7 software.

Construction of fluorescent strains, including selection for glyphosate or phosphinothricin resistant colonies, and transposon integration and screening were performed as previously described [80,113,118,150]. Sample preparation and fluorescent imaging were also carried out as previously described [150].

Growth analysis of the *rfp*-tagged *B. pseudomallei* Δ*asd* mutant, complemented Δ*asd* mutant, and wildtype strain. Growth curve experiments were performed on the three RFP-labeled *B. pseudomallei* strains engineered above (wt/*rfp*, Δ*asd*/*rfp*, and Δ*asd*/complement/*rfp*). These strains were grown overnight at 37°C in LB medium, where the Δ*asd* mutant was supplemented with 200 mg/ml of DAP. Overnight cultures were then washed twice with 1x M9 medium to remove trace amounts of DAP and resuspended in an equal volume of 1x M9

medium. Resuspended cultures were diluted 100-fold into fresh LB medium, without DAP, and shaken at 225 rpm at 37°C. At each time point, 300 µl aliquots were removed, diluted two-fold in LB medium, and their optical densities were measured at 600 nm using an Eppendorf Biophotometer.

DAP dependency of *B. pseudomallei* Δ*asd*/*rfp*. A growth curve experiment was performed on the *B. pseudomallei* Δ*asd*/*rfp* and *B. pseudomallei* wt/*rfp* strains. The strains were grown overnight and washed with 1x M9 and inoculated into LB media as described above, supplemented with different concentrations of DAP (0, 50, 100, 200, and 500 mg/ml). At each indicated time point, 300 µl aliquots were removed and the optical densities at 600nm were determined.

Intracellular replication assays. Both murine macrophage RAW264.7 and human cervical carcinoma HeLa cell lines were grown in a 5% CO_2 environment at 37°C in Dulbecco's Modified Eagles Medium (DMEM) with 10% (v/v) fetal bovine serum (FBS). Gibco 100x anti-biotic/anti-mycotic was added at a 1x working concentration (containing 100 U/ml of penicillin, 100 mg/ml of streptomycin, and 250 ng/ml of amphotericin B) to the cell culture media during cell culture growth but was omitted during the infection assay. Intracellular replication assays were performed using a modified kanamycin protection assay as previously described [120]. Briefly, cells (HeLa and RAW264.7 lines) were cultured in DMEM to confluency, scraped from cell-culture flasks, and seeded at $1x10^5$ cells per well into 24-well Corning CellBIND culture plates. To prepare cells for infection study, cells were allowed to attach overnight and were washed twice with 1x PBS in the morning.

The three bacterial strains used in this experiment were the same as used above for the complementation growth study. To investigate whether exogenous DAP allowed intracellular infection, two series of infection were carried out with the Δ*asd*/*rfp* strain. One series was allowed to infect during the entire course of the study in the presence of DAP and the other had DAP omitted from the media after 1 h of infection (T=1). During the first hour of infection, both series of the *B. pseudomallei* Δ*asd*/*rfp* strain were supplemented with 200 mg/ml of DAP in the cell culture media, so as not to bias invasion ability during attachment and internalization. Assays with the wildtype and complemented Δ*asd*/*rfp* mutant strains were carried out essentially the same as those with the Δ*asd*/*rfp* mutant, except that no DAP was added. Briefly, *B. pseudomallei* strains were grown to high-cell-density, washed twice with 1x PBS, then diluted to ~1x10^6 CFU/ml. At time zero, 1 ml of DMEM containing diluted bacteria was added to the macrophage monolayers (MOI 10:1). After allowing the infection to progress for one hour, the media was removed and the monolayers were washed twice with 1x PBS to remove any unattached bacteria. Next, fresh DMEM with 700 mg/ml each of amikacin and kanamycin was added to the monolayers to kill any non-internalized bacteria and inhibit extracellular bacterial replication. During the assay, medium was removed from the wells at three time points (2, 6, and 24 h post-infection) and the infected cell monolayers were washed twice with 1x PBS, and then lysed with 0.1% Triton X-100. Serial dilutions of the lysates were plated on Brucella agar (Difco) plus 4% (v/v) glycerol (BAG) media at 37^{o}C, as described previously [89,152]. BAG medium was supplemented with 200 mg/ml of DAP when enumerating *B. pseudomallei* Δ*asd*/*rfp* colonies. Colonies were counted within 48 h. Experiments with both HeLa and RAW264.7 cell lines, in combination with all bacterial strains, were performed in triplicate and the standard error of the mean (SEM) was calculated for each.

RAW264.7 macrophage cytotoxicity assay. Macrophages were cultured as described above and seeded into a 96-well CellBIND plate at ~$5x10^4$ cells per well. A kanamycin protection and infection assay was carried out, as described above for the intracellular replication assay, with bacteria infected at an MOI of 10:1. At 2, 6, 12, and 24 h post-infection, the cellular supernatant was removed and lactate dehydrogenase (LDH) levels were determined using the CytoTox 96 Non-radioactive Cytotoxicity Assay (Promega). LDH levels of infected monolayers were compared and normalized to maximal LDH levels (after complete monolayer lysis using 0.1% Triton X-100) to determine percent cytotoxicity. The cytotoxicity assay was carried out in triplicate and the standard error of the mean (SEM) was calculated.

Light microscopy and time course of *B. pseudomallei wt*/*rfp*, Δ*asd*/*rfp*, and Δ*asd*/complement/*rfp* infection of RAW264.7 murine macrophages. Light microscopy of infected cell monolayers was carried out as described [150], except for a few modifications. Glass coverslips were sterilized in 70% (v/v) ethanol and then treated for 4 h with 150 mg/ml poly-L-lysine in sterile double distilled water (ddH_2O). The glass coverslips were washed twice with ddH_2O and allowed to air-dry within a sterile petri dish overnight. In our experience, glass coverslips treated with poly-L-lysine provided the best surface for cell attachment and microscopic imaging. The 22 x 22 mm coverslips were placed at the bottom of the wells in a 6-well Corning CellBIND plate prior to seeding. RAW264.7 macrophages were seeded at ~$8x10^5$ cells per well, allowed to attach overnight, and the infection was initiated by adding different bacterial strains at an MOI of 10:1. At 1 h post-infection, the coverslips were washed twice with 1x PBS and then fresh DMEM media containing 700 mg/ml of kanamycin was added to inhibit

extracellular bacterial replication. At 2, 6, 12, and 24 h post-infection the media was removed and the cell monolayers were washed twice with 1x PBS and fixed with 1% paraformaldehyde for 30 min. After 30 min, the paraformaldehyde was removed and the coverslips were washed twice with 1x PBS. For safe removal of fixed samples from the BSL-3 for imaging, this method must be initially tested by incubating fixed cover slips for 5 d in LB to confirm the absence of growth and viable bacteria. Coverslips were mounted with a slide-mounting buffer containing 50% glycerol in 1x PBS. Images were obtained as previously described [150].

Animal studies. BALB/c mice between 4 and 6 weeks of age were purchased from Jackson Laboratories (Bar Harbor, ME). Animals were housed in micro-isolator cages under pathogen-free conditions. The Institutional Animal Care and Use Committee at Colorado State University approved the animal experiments conducted for these studies. *B. pseudomallei* infections were done using intranasal (i.n.) inoculation [52]. Animals were anesthetized with 100 mg/kg ketamine plus 10 mg/kg xylazine. The desired challenge dose of *B. pseudomallei* was suspended in PBS and 20 µl was delivered i.n., alternating nostrils. For the challenge studies, groups of 5 mice were challenged with the wildtype and mutant strain. For the vaccination studies, mice (n=10) were administered $1x10^7$ CFU Δ*asd* mutant *B. pseudomallei* intranasally, and then boosted in the same manner 3 weeks later. Two weeks following the boost, mice were challenged intranasally with $4x10^3$ CFU wild type *B. pseudomallei* 1026b. For all *B. pseudomallei* challenge and survival studies, animals were monitored for disease symptoms twice daily and were euthanized according to pre-determined humane endpoints. Lungs, liver, and spleen were removed and homogenized using a tissue stomacher (Teledyne Tekmar, Mason OH) and homogenates were plated in serial dilutions to determine bacterial counts in the *B.*

pseudomallei challenged mice 75 d post-infection. Statistical differences in survival times were determined by Kaplan-Meier curves followed by the log-rank test (Prism5 software, GraphPad, LaJolla, CA).

4.4 RESULTS

Construction and growth analysis of the *rfp*-tagged *B. pseudomallei* Δ*asd*, Δ*asd*/complement, and wildtype strains. In the previous work [80], we developed two non-antibiotic markers, *bar* and *gat*, which are effective for the genetic manipulation of *B. pseudomallei.* In this study it became apparent that another marker besides *gat* was needed for fluorescent tagging of *B. pseudomallei* during infection studies. Therefore, we constructed a new non-antibiotic based single-copy transposon vector (mini-Tn7-*bar-rfp*; Fig. 1) for stable site-specific insertion of red fluorescent protein genes (*rfp*) without the need for plasmid maintenance. We used the *gat* select agent compliant non-antibiotic marker to fluorescently tag wildtype bacteria as previously described [150]. However, mini-Tn7-*bar-rfp* based constructs were used to fluorescently tag the *B. pseudomallei* Δ*asd*::*gat-FRT* strain, as well as to tag and complement this mutant strain.

The amino acid requirements of the *B. pseudomallei* Δ*asd*/*rfp* mutant were previously demonstrated by showing that the mutant could not grow in the absence of methionine, threonine, and DAP on minimal media plates [80]. In this study, we wanted to show that this mutant is unable to grow in rich liquid media in the absence of DAP. A growth-curve experiment was initiated to allow the comparison of growth between *B. pseudomallei* wt/*rfp, B. pseudomallei* Δ*asd*/*rfp*, and the *B. pseudomallei* Δ*asd*/complement/*rfp* strains in a rich nutrient source (LB medium). The *B. pseudomallei* Δ*asd* mutant displayed an inability to grow compared to wildtype strain (Fig 2A). This was expected, as in previously published work the *B. pseudomallei* 1026b Δ*asd* mutant began to lyse after 6 h without DAP [80]. When the *B. pseudomallei* Δ*asd*/*rfp* strain was complemented using a transposon containing a single copy of the *B. pseudomallei asd* gene, the growth defect of the mutant was abolished and normal growth

was restored. This indicated that the growth defect exhibited by the mutant was solely caused by deletion of the *asd* gene.

We next investigated the effect of different concentrations of DAP on growth of the Δ*asd/rfp* mutant in rich media (Fig. 2B). In the presence of DAP, all curves showed a significant growth lag, however, when compared to the wildtype, the OD_{600} eventually reached wildtype levels. This demonstrated that the Δ*asd* mutant can grow well when DAP is added to the media and not at all in the absence of DAP.

The *B. pseudomallei* Δ*asd* mutant is highly attenuated in intracellular replication. Assessment of the Δ*asd* mutant attenuation in HeLa and RAW264.7 cell infection models were necessary before animal vaccination. In agreement with previous work [120], our experience suggested that an MOI of 10:1 would initiate an infection that would maximally affect the cell-monolayer within 24 h. Internalization was very inefficient in HeLa cells, with only ~500 CFU out of ~$1x10^6$ CFU internalized by the monolayers (Fig. 3A). As shown in Figure 3A, the *B. pseudomallei* Δ*asd*/*rfp* strain is unable to replicate in HeLa cells. It was able to attach and become internalized as well as the wildtype indicated by similar intracellular CFUs obtained at 2 h post-infection. However, by 6 h post-infection (T=6), the Δ*asd*/*rfp* mutant alone (without DAP) was only able to replicate modestly. By 24 h post-infection, intracellular mutant bacteria were undetectable. However, when complemented with a single wildtype copy of the *asd* gene the Δ*asd* mutant strain behaved exactly as wildtype, reaching a maximum of ~$1x10^6$ CFU. Interestingly, the Δ*asd*/*rfp* strain could infect HeLa cell monolayers when the growth medium was supplemented with 200 μg/ml of DAP and only slowed down the rate of decline in RAW

264.7 macrophages. This indicates that a sufficient amount of DAP was transported into HeLa cells.

B. pseudomallei was internalized efficiently and replicated much more significantly within RAW264.7 cells (Fig. 3B). The *B. pseudomallei* Δ*asd*/*rfp* strain is not internalized efficiently or is killed more efficiently by macrophages than the wildtype, denoted by one log difference in CFU at 2 h post-infection. The Δ*asd* mutant could not sustain a wildtype level of replication even in the presence of 200 μg/ml of DAP, unlike HeLa cell infection. By the end of the assay (24 h), the Δ*asd*/complement/*rfp* and the wt/*rfp* strains replicated to a similar level (~$1x10^6$ CFU) within the RAW264.7 macrophage monolayer. This indicates that even a single copy of the asd_{Bp} gene can restore the mutant's abilities to grow within cells.

Cytotoxicity and light/fluorescent microscopy time course of the *B. pseudomallei* 1026b Δ*asd* mutant infection of RAW264.7 murine macrophages. Although the Δ*asd* mutant does not replicate to high cell numbers like the wildtype, it was of interest whether or not the Δ*asd* mutant damages the cell monolayers comparably to the wildtype. LDH assays of all strains infecting RAW264.7 monolayers at 2 and 6 h post-infection revealed little differences in cytotoxicity when compared to the non-infected control (Fig. 4A) while LDH levels of the wildtype and complement began to rise at 12 h post-infection. The wildtype and complemented Δ*asd* mutant infected monolayers had surpassed the maximum cytotoxicity at 24 h (determined by lysing the initially seeded macrophages), reaching ~100% (Fig. 4A). Independently of DAP, the Δ*asd* mutant did not damage the monolayers to the same level as the wildtype and was still comparable to the non-infected control. LDH levels of the non-infected macrophage monolayer rose at 24 h, indicating the spontaneous lysis of macrophages at high confluency, a usual

occurrence where rapid division leads to low nutrient availability, macrophage death, and LDH release.

Intracellular replication and host-cell cytotoxicity were then placed in a visual context by tracking the *rfp*-tagged bacteria via fluorescent microscopy. Visible in representative images from 24 h post-infection was a pervasive red fluorescence indicative of high numbers of intracellular bacteria (Fig. 4B). The majority of macrophages are joined together in multi-nucleated-giant-cells (MNGCs). Upon closer inspection (Fig. 5), the MNGCs were observed teaming with bacteria in both the wt/*rfp*- and Δ*asd*/complement/*rfp*-infected monolayers. The bacteria-containing protrusions are clearly visible extending from the surface of the macrophages (Fig. 5). The Δ*asd* mutant infected monolayers neither contain high numbers of replicating bacteria nor do they show any sign of MNGC formation in the monolayer at 24 h and in fact appear as healthy as the non-infected control (Fig. 4B). Although not unexpected, the data reaffirms that the mutant was internalized by the macrophages but was unable to produce cytopathology (or MNGCs), with or without DAP, consistent with the wildtype infection.

Attenuation, vaccination, and acute protection of the Δ*asd* mutant in mice. We first tested the Δ*asd* mutant for attenuation *in vivo*. The LD_{50} of *B. pseudomallei* 1026b in BALB/c mice has been determined to be approximately 900 CFU via the inhalation route [152]. An intranasal (i.n.) dose of 4,500 CFU has been experimentally determined to produce 100% mortality in BALB/c mice after 3 d [52,153]. Intranasal inoculation mimics inhalation melioidosis and produces a characteristic acute pneumonic infection to which BALB/c mice succumb within a few days. Five BALB/c mice (n=5) were challenged i.n. with 4,500 CFU of *B. pseudomallei* 1026b and another five BALB/c mice were challenged i.n. with $1x10^7$ CFU (5 logs

x LD_{50}). Survival of the mice was then monitored. After 3 d, mice challenged with wildtype *B. pseudomallei* had all been euthanized due to progressive infection (Fig. 6A). In contrast, mice infected with asd *mutant B. pseudomallei* showed no outward signs of infection and were observed for 75 d post-challenge and all remained healthy during this period (Fig. 6A). Thus, the Δ*asd* mutant was highly attenuated when compared to wildtype strain of *B. pseudomallei*. To assess possible bacterial persistence *in vivo*, mice challenged with mutant *B. pseudomallei* were euthanized on day 75 and the lungs, livers, and spleens were homogenized, diluted, and plated on LB agar. Bacteria were not detected in any organ, using assays with limits of detection of approximately 50 CFU/organ, indicating the mutant bacteria did not persist in organs typically infected during the chronic phase of infection with virulent *B. pseudomallei*. The numbers of mice used in these studies were judged to be adequate [52] to assure that the mutant bacterium was avirulent in immune competent mice.

We then considered if the Δ*asd* mutant could be used as a vaccine against inhalation melioidosis in BALB/c mice. Numerous publications support the fact that single vaccinations with attenuated live *B. pseudomallei* vaccines are generally unable to protect mice from developing chronic melioidosis [145,154,155]. Therefore, we investigated whether an i.n. prime-boost vaccination strategy could extend protection against development of chronic melioidosis. The i.n. route of infection and vaccination emulates aerosol exposure/vaccination and typically vaccination at the route of pathogen entry generally leads to more effective disease prevention [156]. Ten BALB/c mice were primed with an i.n. vaccination of 1 x 10^7 CFU of the *B. pseudomallei* 1026b Δ*asd* mutant. Three weeks later, the same mice were boosted with another i.n. vaccination of 1x10^7 CFU of the Δ*asd* mutant. The time period between the initial exposure and the boost would presumably allow for an adaptive cellular and humoral immune response to

occur. Two-weeks post-boost, the mice were challenged with 4 x 10^3 CFU of wildtype strain 1026b and survival was compared to unvaccinated mice challenged with the same amount of the wildtype. The boost was administered 2 weeks before the infection to further enhance the immune response presumably allowing time for enhanced adaptive immunity [157,158].[158] The data show that vaccinated mice survived significantly longer than the unvaccinated control mice (Fig. 6B). While the prime-boost strategy used in this study protected mice from acute infection, it failed to protect mice from development of chronic *B. pseudomallei* infection, as nearly all of the vaccinated and challenged mice developed infection of organs at secondary sites, particularly the spleen (data not shown).

4.5 DISCUSSION

The essentiality of the *asd* gene in *E. coli* has been known for some time, but its requirement for growth and infectivity of select agent species has not been thoroughly investigated. This study evaluated the growth and pathogenicity of the *B. pseudomallei* Δ*asd* mutant produced in the previous work [80] and its potential for use as a live-attenuated vaccine. By performing growth experiments, it was found that without DAP the mutant is unable to replicate and complementation, with a single copy of wildtype asd_{Bp}, is sufficient for *in vitro* and intracellular replication compared to the wildtype bacterium in both HeLa and RAW264.7 cells. These studies demonstrated that by adding DAP, the Δ*asd* strain can be easily propagated within a laboratory setting and, by complementing the *asd* gene, a markerless balanced lethal system could be used for various *B. pseudomallei* studies [159]. It is important to note that while adding DAP during *asd* mutant infection can re-establish wildtype growth levels in some cell lines (i.e. HeLa cells), it is not homologous to replication of the mutant after single copy complementation, where high levels of replication are seen within both cell lines. This may have important implications in future subcutaneous vaccine experiments due to the epithelial nature of the HeLa cell line.

In the absence of DAP, the mutant was unable to replicate in both the HeLa and RAW 264.7 cell infection models. Cytotoxicity data showed that the mutant did not cause increased death or distress to the macrophages, indicating that the mutant is unable to replicate within or cause significant damage to host cell macrophages via endotoxin or exoenzyme release. The link between cytotoxicity and inflammation has been known for some time and can be partially attributed to free radical release during cellular damage both *in vitro* and *in vivo* [160]. Although inflammatory modulators were not measured in the cytotoxicity assay, a tentative hypothesis

would place the corresponding inflammatory modulator levels in the same trend as LDH. By tagging the *B. pseudomallei* strains with RFP and tracking them *in vitro* during intracellular replication, we were able to confirm the intracellular location of the mutant and further demonstrate the utility of non-antibiotic selectable markers in pathogenesis research.

B. pseudomallei Δ*asd* mutants should be considered biosafe strains suitable for laboratory use and exclusion from the USDA/CDC select agent lists. First, the Δ*asd* mutant was constructed by deleting several hundred bases in the middle of the *asd* gene [80], producing a stable mutant unable to revert. Additionally, as DAP is not present within mammals, there is no source of exogenous DAP, affording another level of safety for this strain. On the other hand, it can be seen that the *B. pseudomallei* Δ*asd* mutant invades host-cells although, like the *B. pseudomallei purM* mutant [52], the Δ*asd* mutant is unable to replicate in the host and bacterial persistence cannot occur. These data, together with the use of Δ*asd* mutants of other species as vaccine delivery strains in humans [81,141] provides strong evidence supporting the removal of this strain from select agent lists, as was previously achieved with the 1026b D*purM* strain Bp82 (33).

Previous vaccination studies utilizing live-attenuated strains and a single vaccination were unable to prevent death from chronic infection [65,74,145,161,162]. However, we had reason to believe that the Δ*asd* mutant would be more effective than previous live attenuated strains. It has been shown that a more protective immune response can be achieved by increasing short-term vaccine persistence, which we attempted with the booster vaccine [163-165]. Unfortunately, while vaccination with the Δ*asd* mutant did indeed protect against acute melioidosis, the vaccine failed to protect against chronic melioidosis. This failure might have been because because the Δ*asd* mutant vaccine was unable to persist long enough or disseminate

and proliferate enough, even after the boost, to induce systemic protection. The route of vaccination can be important because of increased protection at the site of challenge (e.g. mucosal surfaces), however, this may not generate systemic protection [156]. This is a possible reason for why mice were protected from the initial lung infection but eventually succumbed to systemic infection at secondary sites. Even so, protection from acute pneumonic melioidosis may provide a vital increase in survival time that could allow for the administration of antibiotic therapeutics.

Future investigations should be carried out to address whether short-term persistence, proliferation, and dissemination of the Δ*asd* mutant, achieved by adding DAP to the vaccine, would provide systemic protection against chronic melioidosis. Within-host persistence of the Δ*asd* mutant would then be contingent on the amount of DAP administered with the vaccination. Addition of DAP to mutant infected HeLa cells, an epithelial cell line, did allow some intracellular replication therefore it may be highly beneficial to incorporate a subcutaneous vaccine containing DAP. Longer exposure to the cutaneous and subcutaneous dendritic cells could prolong T-cell activation at draining lymph nodes [157] and create the powerful cell-mediated immune response hypothetically necessary for sterile immunity [166]. Other means of producing systemic dissemination and, perhaps, protection would be to incorporate an intramuscular or subcutaneous vaccination along with the inhaled vaccination. This two-pronged approach may give rise to longer protection from chronic or latent infection, which is proving more difficult to combat than acute melioidosis. Seemingly, the greatest prospect for an effective vaccine against melioidosis is a live-attenuated strain. In conclusion, this initial work suggests the utility of the *B. pseudomallei* Δ*asd* mutant as a live-attenuated vaccine against acute melioidosis and further justifies its potential removal from the select agent list.

4.6 ACKNOWLEDGEMENTS

This project was supported by Award Number AI065359 from the National Institute of Allergy and Infectious Diseases and by the Center of Biomedical Research Excellence grant P20RR018727 from the National Center for Research Resources of the National Institutes of Health to TTH. SWD and HPS were supported by NIH NIAID grant AI065357. The content is solely the responsibility of the authors and does not necessarily represent the official view of the funding agencies.

4.7 FIGURE LEGENDS

FIG 1. Mini-Tn7-*bar-rfp*, single-copy tagging vector based on phosphinothricin resistance, harboring *rfp* driven by the P_{S12} promoter. After insertion aided by pTNS3-asd_{Ec} [150], the non-antibiotic resistance marker, which is flanked by identical *FRT*s, can be removed by Flp-mediated excision. Abbreviations: *bar,* gene encoding bialaphos/phosphinothricin resistance; *FRT,* Flp recombination target sequences*; oriT*, RP4 conjugal origin of transfer; PC_{S12}, promoter of the *B. cenocepacia rpsL* gene; P_{S12}, promoter of the *B. pseudomallei rpsL* gene; R6K*γori*, π protein dependent R6K origin of replication; *rfp*, red fluorescent protein encoding gene; *Tn7L*/*Tn7R*, left and right transposase recognition sequences; T_oT_1, transcriptional terminator.

FIG 2. Growth curve experiments performed with *B. pseudomallei* strains. (A) *B. pseudomallei* strains were grown in the absence of DAP. The wildtype strain and the Δ*asd* strain complemented with a single copy of the *asd* gene on a site-specific transposon exhibit the same growth rates and final optical densities, while the Δ*asd* mutant exhibited a typical DAP-dependent phenotype. (B) The *B. pseudomallei* Δ*asd* mutant was tested in different concentrations of DAP, ranging from 0 μg/ml to 500 μg/ml. When compared to wildtype, the Δ*asd* mutant exhibits absence of growth without DAP. All other concentrations of DAP afforded a partial growth rate recovery and final optical density, albeit only after a lag in growth.

FIG 3. Infection of HeLa and RAW264.7 cells by *B. pseudomallei* and the Δ*asd* strain. HeLa (A) and RAW264.7 (B) cell monolayers were infected at an MOI of 10:1. The complemented Δ*asd* strain shows no decrease in its ability to invade and replicate within either cell line.

However, the Δ*asd* mutant in the absence of DAP cannot sustain an infection in either cell line, denoted by an overall drop in bacterial numbers.

FIG 4. (A) Cytotoxicity of *B. pseudomallei* strains to the RAW264.7 murine macrophage cell line. RAW264.7 cells were infected with the Δ*asd* mutant (in the presence and absence of DAP), the complemented mutant strain, and wildtype strain. Between 2 h and 6 h post-infection there was a slight increase in cytotoxicity associated with infection by the complemented and wildtype strains when compared to the Δ*asd* mutant infected monolayers. By 12 h post-infection, cytotoxicities of the complement and wildtype infected monolayers were more obvious, while cytotoxicity caused by the Δ*asd* mutant remained similar to the non-infected control. At 24 h post-infection, the complement and wildtype infected monolayers exhibited maximal cytotoxicity. (B) Microscopy and time course of the cytopathic effects of *B. pseudomallei* Δ*asd* infection. Monolayers were infected at an MOI of 10:1 then analyzed for red fluorescence at 2 h and 24 h post-infection. Differential interference contrast (DIC) images were overlaid with the red fluorescent channel. Red fluorescence indicates the presence of *B. pseudomallei*. Note the high bacterial levels in the complement and wildtype infected monolayers at 24 h and the confluent MNGC formation. This coincides with high levels of cytotoxicity at 24 h post-infection. Abbreviations: CT, non-infected control; Δ*asd, B. pseudomallei* Δ*asd*/*rfp*; Δ*asd* + DAP, *B. pseudomallei* Δ*asd*/*rfp* in the presence of 200 μg/ml of DAP; Δ*asd* + complement, *B. pseudomallei* Δ*asd*/*complement*/*rfp*; WT, *B. pseudomallei wt*/*rfp*. Error bars represent the SEM of three experiments. Statistical significance was determined by the two-tailed unpaired T-test (***, $P < 0.0005$).

FIG 5. Intracellular replication of *B. pseudomallei*. RAW264.7 murine macrophage monolayers were visualized using a combination of differential interference contrast and red fluorescence microscopy 24 h post-infection with the *B. pseudomallei* Δ*asd/complement/ rfp*, (A) and (B), and with *B. pseudomallei wt*/*rfp*, (C) and (D), strains. All macrophages in the field of view are involved in MNGCs and are filled with intracellular bacteria about to burst into the extracellular milieu. (A) and (C) were captured at 600x magnification while (B) and (D) are zoomed in images of the regions denoted in (A) and (C), respectively. Note the large number of bacteria projecting out of the remaining macrophages in (C) and (D). There were no bacteria and an absence of protrusions as well as MNGCs at all time points in monolayers infected with the Δ*asd* mutant (data not shown).

FIG 6. (A) *B. pseudomallei* 1026b Δ*asd* mutant is avirulent to mice. Mice (n=5 animals per group) were challenged i.n. with either 4,500 CFU *B. pseudomallei* 1026b (wildtype) or $1x10^7$ CFU *B. pseudomallei* 1026b Δ*asd* mutant, and survival was monitored. Statistical differences in survival times were determined by Kaplan-Meier curves followed by log-rank test (**, $P < 0.01$ for *B. pseudomallei* 1026b *wt* vs. *B. pseudomallei* 1026b Δ*asd* mutant). (B) Intranasal vaccination with *B. pseudomallei* 1026b Δ*asd* mutant protects mice from lethal *B. pseudomallei* challenge. Mice (n=10 animals per group) were primed i.n. with $1x10^7$ CFU *B. pseudomallei* 1026b Δ*asd* and boosted in the same manner 3 weeks later. Two weeks post-boost, mice were challenged i.n. with $4x10^3$ CFU wildtype *B. pseudomallei* 1026b. Survival was monitored, and statistical differences in survival times were determined by Kaplan-Meier curves followed by log-rank test (***, $P < 0.0001$ for vaccinated vs. non-vaccinated mice). Data represents two individual pooled experiments

Table 1

Strains	Lab ID[a]	Relevant properties	Sources
E. coli			
EPMax10B-*pir116*/D*asd*::Gm^r	E1345	Gm^r; F$^-$ l$^-$ *mcrA* D(*mrr-hsdRMS-mcrBC*) f80*lacZ*DM15 D*lacX74 deoR recA1 endA1 araD139* D*(ara, leu)7697 galU galK rpsL nupG* Tn-*pir116-FRT2* □*asd*::Gm^r-*wFRT*	Available lab strain
EPMax10B-*pir116*/D*asd*/D*trp*::Gm^r/ *mob*-Km^r	E1354	Gm^r, Km^r; F$^-$ l$^-$ *mcrA* D(*mrr-hsdRMS-mcrBC*) f80*lacZ*DM15 D*lacX74 deoR recA1 endA1 araD139* D*(ara, leu)7697 galU galK rpsL nupG* Tn-*pir116-FRT2* □*asd*::*wFRT* □*trp*::Gm^r-*FRT5 mob*[*recA*::*RP4-2 Tc*::*Mu*-Km^r]	Available lab strain
EPMax10B-*lacI^q/pir*	E1869	F$^-$ l$^-$ *mcrA* □(*mrr-hsdRMS-mcrBC*) f80*lacZ*DM15 D*lacX74 deoR recA1 endA1 araD139* □(*ara, leu*)7697 *galU galK rpsL nupG lacI^q-FRT8 pir-FRT4*	Available lab strain
EPMax10B-*lacI^q/pir/leu*$^+$	E1889	F$^-$ l$^-$ *mcrA* □(*mrr-hsdRMS-mcrBC*) f80d*lacZ*DM15 D*lacX74 deoR recA1 endA1 galU galK rpsL nupG lacI^q-FRT8 pir-FRT4*	Available lab strain
***Burkholderia* spp.**			
B. pseudomallei			
1026b (*wt*)	B0004	Wildtype strain; clinical melioidosis isolate	[130]
1026b *att*Tn7-*gat-rfp* (*wt*/*rfp)*	B0015	GS^r; 1026b with mini-Tn*7-gat-rfp* inserted at *glmS2* site	[150]
1026b-Δ*asd$_{Bp}$*::*gat-FRT* (Δ*asd*)	B0011	GS^r; 1026b with *gat-FRT* cassette inserted in the *asd$_{Bp}$* gene	[80]
1026b-Δ*asd$_{Bp}$*::*gat-FRT*/ *att*Tn7-*bar-rfp* (Δ*asd*/*rfp)*	B0024	GS^r, PPT^r; 1026b Δ*asd$_{Bp}$*::*gat-FRT* mutant with mini-Tn*7-bar-rfp* inserted at *glmS2* site	This study
1026b-Δ*asd$_{Bp}$*::*gat-FRT*/ *att*Tn7-*bar-asd$_{Bp}$-rfp* (Δ*asd*/*complement*/*rfp)*	B0022	GS^r, PPT^r; 1026b Δ*asd$_{Bp}$*::*gat-FRT* mutant with mini-Tn*7-bar-asd$_{Bp}$-rfp* inserted at *glmS2* site	This study

[a] *E. coli* strains are available lab strains. Please use Lab ID number when requesting.

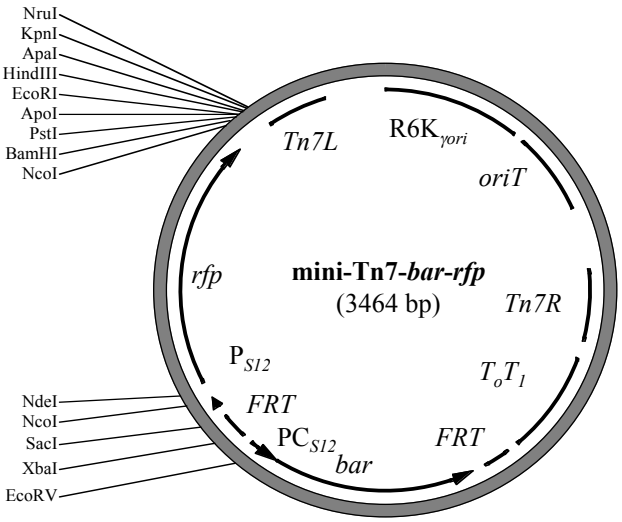
NruI
KpnI
ApaI
HindIII
EcoRI
ApoI
PstI
BamHI
NcoI
NdeI
NcoI
SacI
XbaI
EcoRV
Tn7L
R6K$_{\gamma ori}$
oriT
rfp
mini-Tn7-bar-rfp
(3464 bp)
Tn7R
P$_{S12}$
T_oT_1
FRT
PC$_{S12}$
bar
FRT

Figure 1

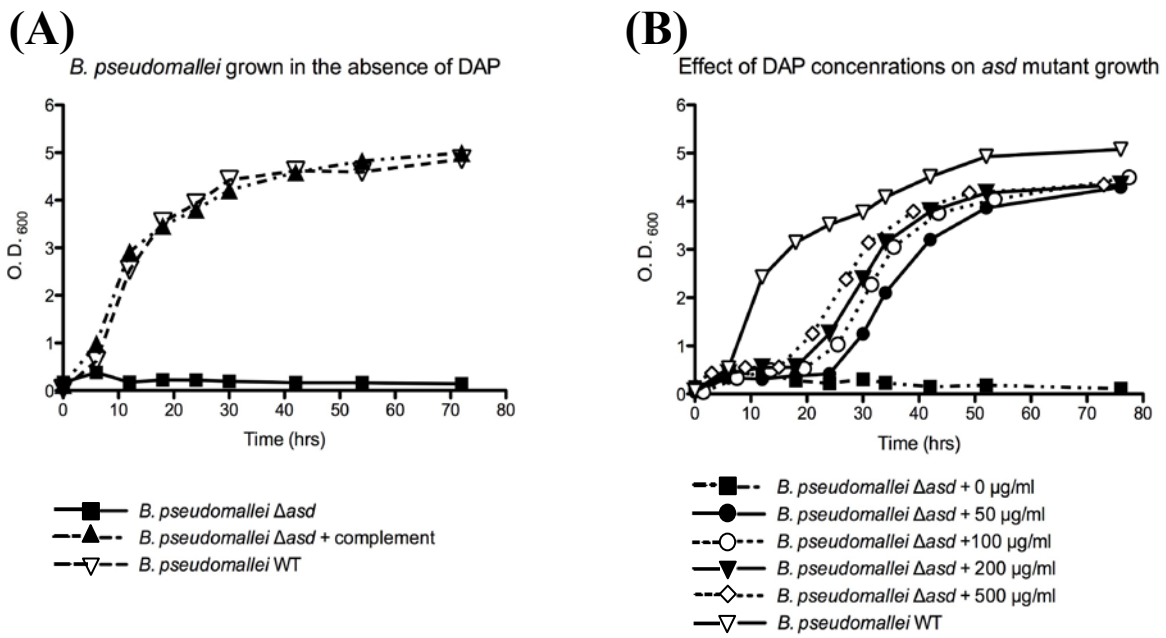

Figure 2

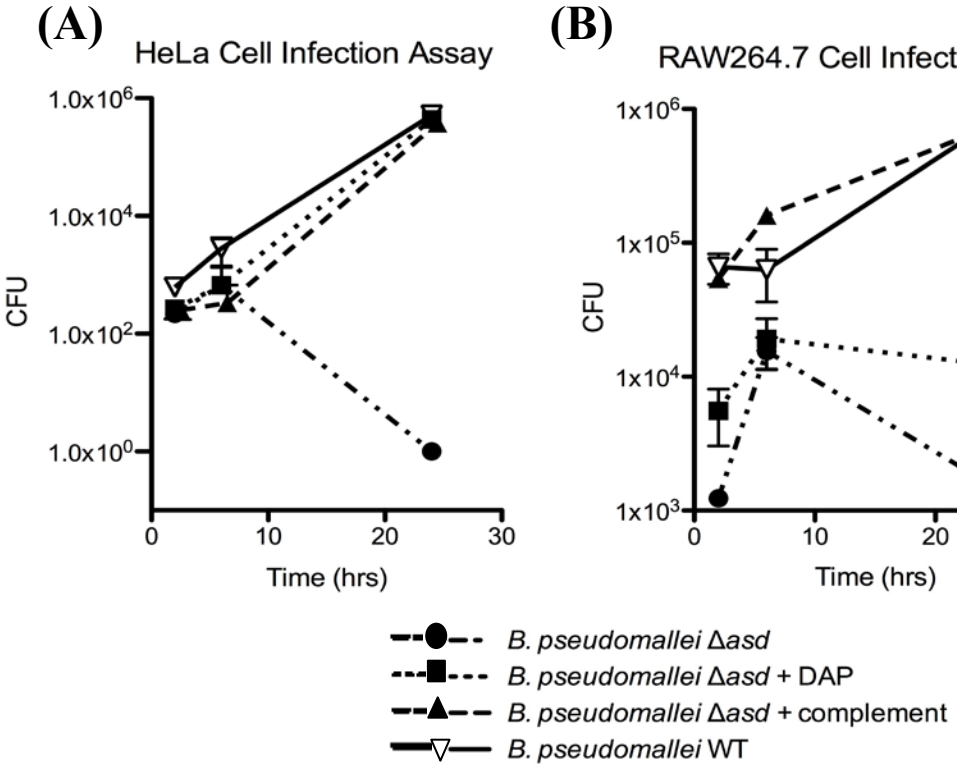

Figure 3

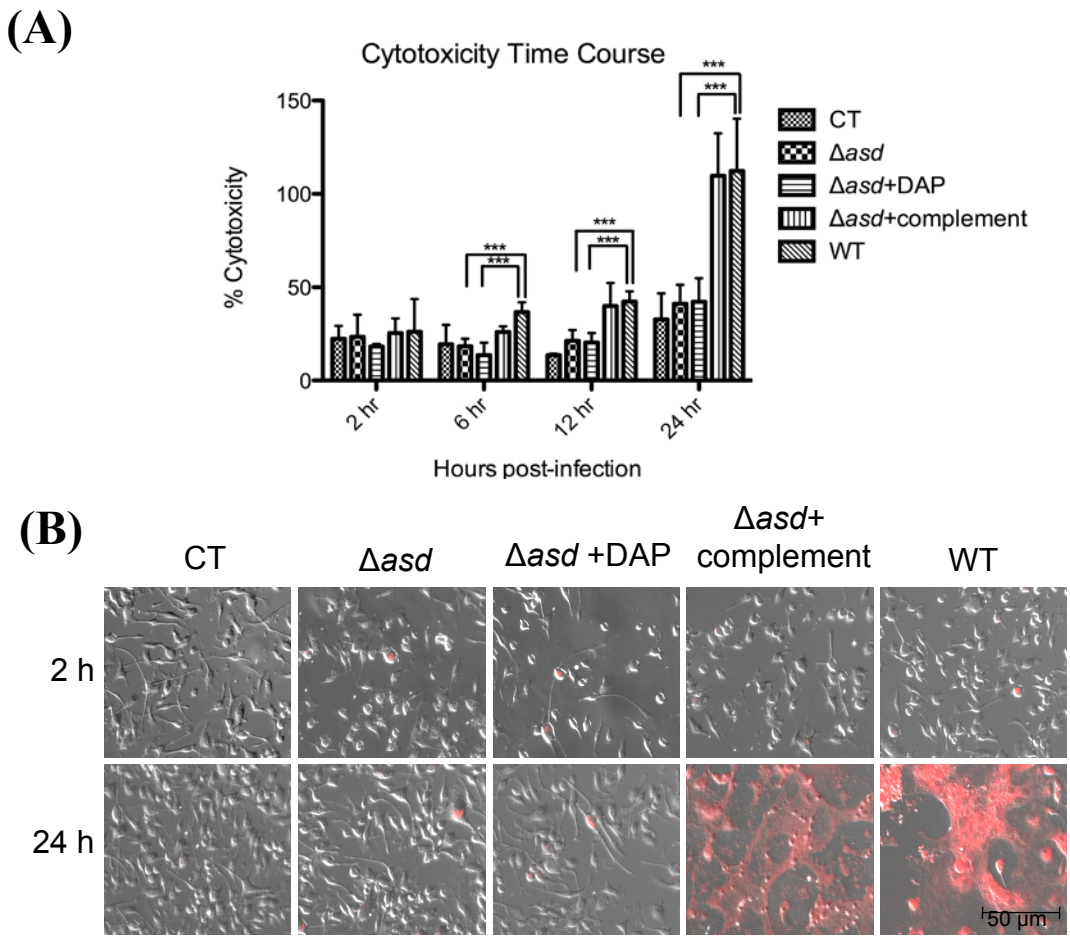
(A)
Cytotoxicity Time Course
% Cytotoxicity
150
100
50
0
2 hr
6 hr
12 hr
24 hr
Hours post-infection
***
CT
Δasd
Δasd+DAP
Δasd+complement
WT
(B)
CT
Δasd
Δasd +DAP
Δasd+ complement
WT
2 h
24 h
50 µm

Figure 4

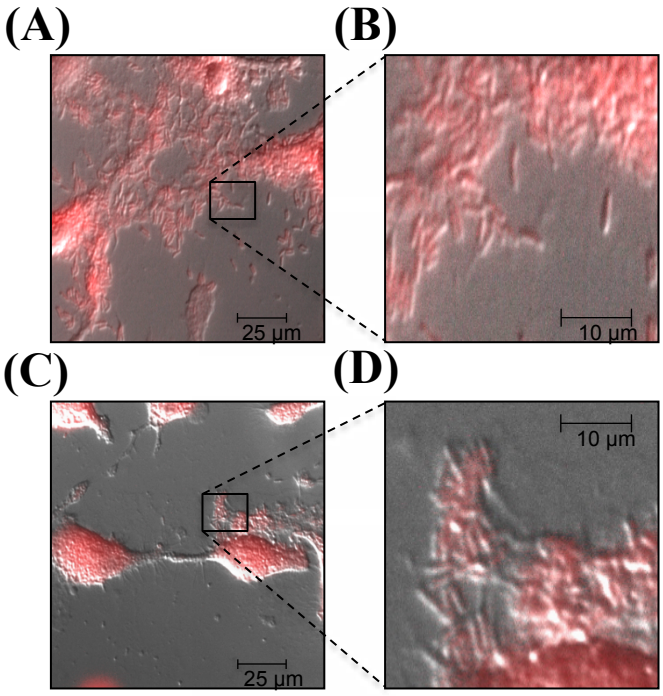

Figure 5

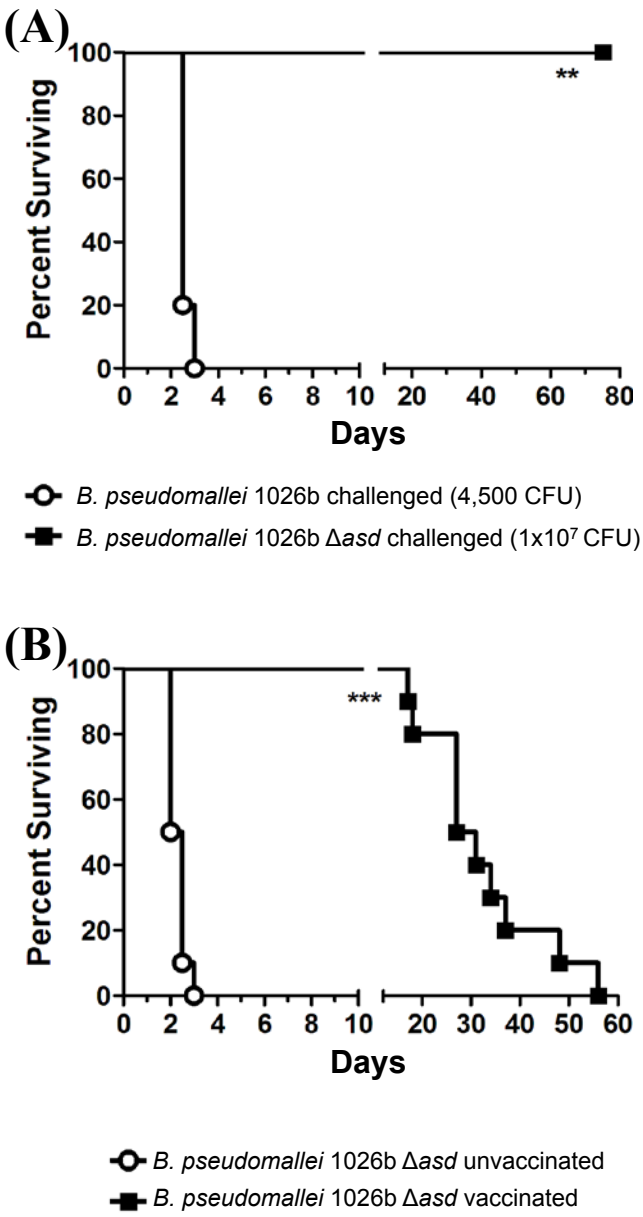
(A)
Percent Surviving
100
80
60
40
20
0
0 2 4 6 8 10 20 40 60 80
Days
**
B. pseudomallei 1026b challenged (4,500 CFU)
B. pseudomallei 1026b Δasd challenged (1x10^7 CFU)
(B)
Percent Surviving
100
80
60
40
20
0
0 2 4 6 8 10 20 30 40 50 60
Days
***
B. pseudomallei 1026b Δasd unvaccinated
B. pseudomallei 1026b Δasd vaccinated

Figure 6

4.8 REFERENCES

1. Public Health Security and Bioterrorism Preparedness and Response Act 107th ed. 2002.
2. Atkins, T., R. Prior, K. Mack, P. Russell, M. Nelson, J. Prior, J. Ellis, P. C. F. Oyston, G. Dougan, and R. W. Titball. 2002. Characterisation of an acapsular mutant of *Burkholderia pseudomallei* identified by signature tagged mutagenesis. J Med Microbiol 51:539-553.
3. Barrett, A. R., Kang, Y., Inamasu, K. S., Son, M. S., Vukovich, J. M., and Hoang, T. T. 2008. Genetics tools for allelic-replacement in *Burkholderia* species. Appl. Environm. Microbiol. 74:4498-4508.
4. Belyakov, I. M., and J. D. Ahlers. 2009. What role does the route of immunization play in the generation of protective immunity against mucosal pathogens? J. Immunol. 183:6883-6892.
5. Breitbach, K., J. Kohler, and I. Steinmetz. 2008. Induction of protective immunity against *Burkholderia pseudomallei* using attenuated mutants with defects in the intracellular life cycle. Trans. Roy. Soc. Trop. Med. Hyg. 2008:S89-S94.
6. Buckley, A. M., J. Wang, D. L. Hudson, A. J. Grant, M. A. Jones, D. J. Maskell, and M. P. Stevens. 2010. Evaluation of live-attenuated *Salmonella* vaccines expressing *Campylobacter* antigens for control of *C. jejuni* in poultry. Vaccine 28:1094-1105.
7. Burtnick, M. N., P. J. Brett, V. Nair, J. M. Warawa, D. E. Woods, and F. C. Gherardini. 2008. *Burkholderia pseudomallei* type III secretion system mutants exhibit delayed vacuolar escape phenotypes in RAW 264.7 murine macrophages. Infect. Immun. 76:2991-3000.

8. Cheng, A. C., and B. J. Currie. 2005. Melioidosis: Epidemiology, Pathophysiology, and Management. Clin. Microbiol. Rev. 18:383-416.

9. Choi, K.-H., T. Mima, Y. Casart, D. Rholl, A. Kumar, I. R. Beacham, and H. P. Schweizer. 2008. Genetic tools for select-agent-compliant manipulation of *Burkholderia pseudomallei*. Appl. Environ. Microbiol. 74:1064-1075.

10. Choi, K. H., T. Mima, Y. Casart, D. Rholl, A. Kumar, I. R. Beacham, and H. P. Schweizer. 2008. Genetic tools for select-agent-compliant manipulation of *Burkholderia pseudomallei*. Appl. Environ. Microbiol. 74:1064-1075.

11. Cuccui, J., A. Easton, K. K. Chu, G. J. Bancroft, P. C. F. Oyston, R. W. Titball, and B. W. Wren. 2007. Development of signature-tagged mutagenesis in *Burkholderia pseudomallei* to identify genes important for survival and pathogenesis. Infect. Immun. 75:1186-1195.

12. Dance, D. A. B. 1991. Melioidosis: the Tip of the Iceberg? Clin. Microbiol. Rev. 4:52-60.

13. DeShazer, D., P. J. Brett, R. Carlyon, and D. E. Woods. 1997. Mutagenesis of *Burkholderia pseudomallei* with Tn5-OT182: isolation of motility mutant and molecular characterization of the flagellin structural gene. J. Bacteriol. 179:2116-2125.

14. Drabner, B., and C. A. Guzman. 2001. Elicitation of predictable immune responses by using live bacterial vectors. Biomol. Eng. 17:75-82.

15. Galan, J. E., K. Nakayama, and R. Curtiss. 1990. Cloning and characterization of the *asd* gene of *Salmonella typhimurium*: use in stable maintenance of recombinant plasmids in *Salmonella* vaccine strains. Gene 94:29-35.

16. Goodyear, A., L. Kellihan, H. Bielefeldt-Ohmann, R. Troyer, K. Propst, and S. Dow. 2009. Protection from pneumonic infection with *Burkholderia* species by inhalational immunotherapy. Infect. Immun. 77:1579-1588.

17. Haque, A., K. Chu, A. Easton, M. P. Stevens, E. E. Galyov, T. Atkins, R. Titball, and G. J. Bancroft. 2006. A live experimental vaccine against *Burkholderia pseudomallei* elicits CD4+ T cell-mediated immunity, priming T cells specific for 2 type III secretion system proteins. J. Infect. Dis. 194:1241-1248.

18. Haque, A., A. Easton, D. Smith, A. O,ÄôGarra, N. Van Rooijen, G. Lertmemongkolchai, R. W. Titball, and G. J. Bancroft. 2006. Role of T cells in innate and adaptive immunity against murine *Burkholderia pseudomallei* infection. J. Infect. Dis. 193:370-379.

19. Harb, O. S., and Y. A. Kwaik. 1998. Identification of the Aspartate-beta-semialdehyde dehydrogenase gene of *Legionella pneumophila* and characterization of a null mutant. Infect. Immun. 66:1898-1903.

20. Hatten, L.-A., H. P. Schweizer, N. Averill, L. Wang, and A. B. Schryvers. 1993. Cloning and characterization of the *Neisseria meningitidis asd* gene. Gene 129:123-128.

21. Haziza, C., P. Stragier, and J. C. Patte. 1982. Nucleotide sequence of the *asd* gene of *Escherichia coli*: absence of a typical attenuation signal. EMBO J. 1:379-384.

22. Hoang, T., S. Williams, H. P. Schweizer, and J. S. Lam. 1997. Molecular genetic analysis of the region containing the essential *Pseudomonas aeruginosa asd* gene encoding aspartate-b-semialdehyde dehydrogenase. Microbiology 143:899-907.

23. Jeddeloh, J. A., D. L. Fritz, D. M. Waag, J. M. Hartings, and G. P. Andrews. 2003. Biodefense-driven murine model of pneumonic melioidosis. Infect. Immun. 71:584-587.

24. Jones, A. L., T. J. Beveridge, and D. E. Woods. 1996. Intracellular survival of *Burkholderia pseudomallei*. J. Bacteriol. 64:782-790.

25. Kahl-McDonagh, M. M., and T. A. Ficht. 2006. Evaluation of protection afforded by *Brucella abortus* and *Brucella melitensis* unmarked deletion mutants exhibiting different rates of clearance in BALB/c mice. Infect. Immun. 74:4048-4057.

26. Kang, Y., M. H. Norris, A. R. Barrett, B. A. Wilcox, and T. T. Hoang. 2009. Engineering of tellurite-resistant genetic tools for single-copy chromosomal analysis of *Burkholderia* spp. and characterization of the *Burkholderia thailandensis betBA* operon. Appl. Environ. Microbiol. 75:4015-4027.

27. Kong, W., S.-Y. Wanda, X. Zhang, W. Bollen, S. A. Tinge, K. L. Roland, and R. C. III. 2008. Regulated programmed lysis of recombinant *Salmonella* in host tissues to release protective antigens and confer biological containment. Proc. Natl. Acad. Sci. U.S.A 105:9361-9366.

28. Lane, H. C., J. L. Montagne, and A. S. Fauci. 2001. Bioterrorism: A clear and present danger. Nat. Med. 7:1271-1273.

29. McCord, J. M., and K. Wong. 1979. Phagocyte-produced free radicals: roles in cytotoxicity and inflammation. John Wiley & Sons, Ltd.

30. Norris, M. H., Y. Kang, D. Lu, B. A. Wilcox, and T. T. Hoang. 2009. Glyphosate resistance as a novel select-agent-compliant, non-antibiotic selectable-marker in chromosomal mutagenesis of the essential genes *asd* and *dapB* of *Burkholderia pseudomallei*. Appl. Environ. Microbiol. 75:6062-6075.

31. Norris, M. H., Y. Kang, B. Wilcox, and T. T. Hoang. 2010. Stable, site-specific fluorescent tagging constructs optimized for *Burkholderia* species. Appl. Environ. Microbiol. 76:7635-7640.

32. Peacock, S. J., H. P. Schweizer, D. A. B. Dance, T. L. Smith, J. E. Gee, and V. Wuthiekunan. 2008. Management of accidental laboratory exposure to *Burkholderia pseudomallei* and *B. mallei* Emerg Infect Dis July.

33. Propst, K. L., T. Mima, K.-H. Choi, S. W. Dow, and H. P. Schweizer. 2010. A *Burkholderia pseudomallei* {Delta}*purM* mutant is avirulent in immunocompetent and immunodeficient animals: candidate strain for exclusion from select-agent lists. Infect. Immun. 78:3136-3143.

34. Richmond, J. Y., and R.W. McKinney. 2007. Biosafety in microbiological and biomedical laboratories, 5th ed. Centers for Disease Control and Prevention, Atlanta, GA.

35. Roake, J. A., A. S. Rao, P. J. Morris, C. P. Larsen, D. F. Hankins, and J. M. Austyn. 1995. Dendritic cell loss from nonlymphoid tissues after systemic administration of lipopolysaccharide, tumor necrosis factor, and interleukin 1. J. Exp. Med. 181:2237-2247.

36. Rodrigues, F., M. Sarkar-Tyson, S. V. Harding, S. H. Sim, H. H. Chua, C. H. Lin, X. Han, R. K. M. Karuturi, K. Sung, K. Yu, W. Chen, T. P. Atkins, R. W. Titball, and P. Tan. 2006. Global map of growth-regulated gene expression in *Burkholderia pseudomallei*, the causative agent of melioidosis. J. Bacteriol. 188:8178-8188.

37. Sambrook, J., and D. W. Russell. 2001. Molecular Cloning: A Laboratory Manual, 2nd ed. Cold Spring Harbor Laboratory Press, Cold Spring Harbor, New York.

38. Schleifer, K. H., and O. Kandler. 1972. Peptidoglycan types of bacterial cell walls and their taxonomic implications. Bacteriol.Rev. 36:407-477.

39. Spreng, S., and J.-F. Viret. 2005. Plasmid maintenance systems suitable for GMO-based bacterial vaccines. Vaccine 23:2060-2065.

40. Stavnezer, J. 1996. Immunoglobulin class switching. Curr. Opin. Immunol. 8:199-205.

41. Stevens, M. P., A. Friebel, L. A. Taylor, M. W. Wood, P. J. Brown, W. D. Hardt, and E. E. Galyov. 2003. A *Burkholderia pseudomallei* type III secreted protein, BopE, facilitates bacterial invasion of epithelial cells and exhibits guanine nucleotide exchange factor activity. J. Bacteriol. 185:4992-4996.

42. Tacket, C. O., S. M. Kelly, F. Schodel, G. Losonsky, J. P. Nataro, R. Edelman, M. M. Levine, and R. C. III. 1997. Safety and immunogenicity in humans of an attenuated *Salmonella typhi* vaccine vector strain expressing plasmid-encoded hepatitis B antigens stabilized by the *asd*-balanced lethal vector system. Infect. Immun. 65:3381-3385.

43. Titball, R. W., P. Russell, J. Cuccui, A. Easton, A. Haque, T. Atkins, M. Sarkar-Tyson, V. Harley, B. Wren, and G. J. Bancroft. 2008. *Burkholderia pseudomallei*: animal models of infection. Transactions of the Royal Society of Tropical Medicine and Hygiene 102:S111-S116.

44. Ulrich, R. L., K. Amemiya, D. M. Waag, C. J. Roy, and D. DeShazer. 2005. Aerogenic vaccination with a *Burkholderia mallei* auxothroph protects against aerosol-initiated glanders in mice. Vaccine 23:1986-1992.

45. Wiersinga, W. J., T. van der Poll, N. J. White, N. P. Day, and S. J. Peacock. 2006. Melioidosis: insight into the pathogenicity of *Burkholderia pseudomallei*. Nat. Rev. Microbiol. 4:272-282.

46. Zhao, Z., Y. Xue, B. Wu, X. Tang, R. Hu, Y. Xu, A. Guo, and H. Chen. 2008. Subcutaneous vaccination with attenuated *Salmonella enterica* serovar *Choleraesuis* C500 expressing recombinant filamentous hemagglutinin and pertactin antigens protects mice against fatal infections with both *S. enterica* serovar *Choleraesuis* and *Bordetella bronchiseptica*. Infect. Immun. 76:2157-2163.

Chapter 5. Select-Agent excluded *Burkholderia pseudomallei* strains and cell infection model systems for research in BSL2 laboratories

Michael H. Norris,[2] Yun Kang,[1] Andrew Bluhm,[1] Jan Zarzycki-Siek,[1] Zhenxin Sun,[1] and Tung T. Hoang[1,2*]

Department of Microbiology[1], Department of Molecular Biosciences and Bioengineering[2], University of Hawaii at Manoa, Honolulu, HI 96822, USA

* Corresponding author. Tel: +1 808 956 3522; Fax: +1 808 956 5339; e-mail: tongh@hawaii.edu www.hawaii.edu/microbiology/Hoang/index.html

5.1 ABSTRACT

Burkholderia pseudomallei (*Bp*), causes a serious and life threatening disease in humans called melioidosis. Since this microbe is a potential bioterrorism agent, it is listed as a select-agent (SA) by the CDC, therefore requiring strict regulations and costly BSL3 laboratories to perform research, which can hamper research progress. Additionally, some experiments are nearly impossible to carry out under BSL3 practices and procedures, and the closely related BSL2 *Burkholderia thailandensis* species is not an appropriate model for *Bp* infection. To alleviate these problems for current researchers and to attract new investigators into this field, we developed SA exempt *Bp* strains and eukaryotic cell infection models that could be manipulated in BSL2 laboratories. The SA exempt *Bp* strain B0011 was also tested in a nematode infection model.

Recently, the CDC excluded the *Bp* 1026b Δ*asd* (B0011) strain from the select-agent list. Here, we investigated the cellular infection characteristics of strain B0011 in cellular models of infection, including epithelial, macrophage, and kidney cell lines, among others. The mutants could be grown in the BSL2 lab with the addition of exogenous diaminopimelate (DAP) in rich media. We investigated different concentrations of exogenous DAP added to eukaryotic cell growth media during cell infection experiments using B0011. Invasion and intracellular replication assays were then carried out in addition to capturing time-lapse microscopy of mutant bacteria during cell infection of the various cell lines. Hallmarks of a chronic infection model have also been observed in other cell lines such as human microglial and neuroblastoma cell lines. Utilizing this model, it was discovered that the mutant strain could chronically infect and grow in the nucleus of host cells, which was then verified in wildtype acute infections using electron microscopy. Here, we showed that with supplemental DAP certain eukaryotic cells and

C. elegans could be infected by strain B0011 as well as the wildtype *Bp* strain, and could serve as an appropriate model for BSL2 studies. We also demonstrated that the mealworm *Tenebrio molitor* could serve as BSL2 model for our *asd* strains. Animal studies with two newly excluded *Bp* strains K96243 Δ*asd* and MSHR487 Δ*asd* demonstrated avirulence thus providing two new strain backgrounds for BSL2 work.

In conclusion, cell infection and animal models are indispensable tools in pathogenesis studies of this intracellular pathogen, *Bp*. Our *Bp* mutants and cell infection models provide valuable, safe, and cost effective alternative resources for scientists to study *Bp* pathogenesis, which will help expedite progress in this field.

5.2 INTRODUCTION

Burkholderia pseudomallei (*Bp*), a gram-negative soil bacterium and facultative intracellular pathogen, is a common cause of environmentally acquired septicemia in Southeast Asia and Northern Australia although global prevalence is on the rise [1,133,134]. It causes the disease melioidosis in humans and animals and is listed as a Tier-1 select-agent by the Centers for Disease Control and Prevention (CDC). Research priorities regarding SA bacteria are currently centered on basic research into virulence and pathogenesis mechanisms. Fulfilling the five main goals of the Public Health Security and Bioterrorism Preparedness and Response Act of 2002 [20], including development of medical countermeasures (such as vaccines) against biological agents and toxins that may be involved in such emergencies, is the driving force behind much of the research taking place in the United States. BSL2 laboratories across the nation far outnumber BSL3 laboratories and represent significantly underutilized assets. More resources could be applied to solving these goals if basic research into the pathogenesis of *Bp* could be elucidated without the restrictive accessibility and costs of running a BSL3 laboratory.

Previously, we engineered a *Bp* 1026b strain with a deletional mutation in the aspartate-beta-semialdehyde dehydrogenase (*asd*) gene that is auxotrophic for diaminopimelate (DAP) in rich media [80] and could not crosslink the cell wall. In our more recent paper [51], we showed that the *Bp* 1026b Δ*asd* strain (B0011) is attenuated in cell infection and BALB/c mouse infection models, and furthermore, that the strain is an effective vaccine for acute melioidosis. We also determined that with the addition of exogenous DAP, strain B0011 is able to continue infecting host-cells *in vitro*. Pending select-agent exemption, this would then allow observation of the non-infectious strain in various BSL2 experiments, where adding DAP to the media would allow controlled bacterial growth yet maintain the attenuation of the strain. It was also shown

that our strain is very amiable to downstream genetic manipulation by tagging it with multiple fluorescent proteins and producing secondary chromosomal mutations.

B. thailandensis is a popular BSL1 alternative to *Bp* but the reality remains that it is a BSL1 organism and does not cause disease in healthy individuals, indicating significant differences in pathogenesis. Presently, exempt *Bp* strains have not demonstrated effectiveness in infection models with a simple chemical additive, such as DAP. Cell infection assays, including intracellular replication and invasion assays, are indispensable for investigating infectivity of *Bp*. With this in mind, CDC exemption of strain B0011 from SA regulations was requested and approved. Many labs are interested in studying pathogenesis of *Bp* but the inaccessibility of BSL3 labs may be hampering research progress. Here, we demonstrated in several models that the Δ*asd* strain may be used to investigate the pathogenesis of *Bp* at BSL2. We also demonstrated a BSL2 model using the mealworm *Tenebrio molitor*. BALB/c animal studies were carried out on two *Bp* Δ*asd* strains from the K96243 and MSHR487 backgrounds. We now have 3 *Bp* SA excluded strains for use in a variety of BSL2 assays.

5.3 MATERIALS and METHODS

Bacterial strains, media, and culture conditions. All manipulations of wildtype *Bp* were conducted in CDC/USDA approved and registered BSL3 facilities at the University of Hawaii at Manoa John A. Burns School of Medicine (JABSOM) and experiments with select agents were performed in accordance with the recommended BSL3 practices [7]. *Escherichia coli* strain EOP50 and its rifampicin resistant derivative, EOP50-rif, were used as a nutrient source for *Caenorhabditis elegans* maintenance. Luria-Bertani (LB) medium (Difco) was used to culture *E. coli* strains. Wildtype *Bp* strains were cultured in LB while Δ*asd* strains were cultured in no salt LB with 200 μg/ml diaminopimelic acid (LS+DAP200) or in minimal salts media containing 1 mM lysine, 1 mM, methionine, 1 mM threonine, and 200 μg/ml DAP (3AA+DAP). Antibiotics in solid media were utilized as follows: for *E. coli*, rifampicin (Rif) 200 μg/ml and for *Bp* Δ*asd* kanamycin (Km) 1000 μg/ml and trimethoprim (Tp) 100 μg/ml; non-antibiotics 0.3% glyphosate (GS) in minimal media. Growth on and preparation of DAP were carried out as previously described [8]. All bacterial growth was carried out at 37°C and shaken cultures were maintained at 225 rpm.

Molecular methods and reagents. Molecular methods and reagents were carried out as described previously [5,6,9,10].

Engineering of the *Bp* 1026b virulence factor mutants. The *Bp hcp*-I (BPSS1498) and was knocked out in B0011 Δ*asd*::*gat* background using lambda RED recombineering as previously described [9] but with modifications as follows. Two primers whose 3' regions anneal to the upstream or downstream M13 regions surrounding the *FRT-dhfr-pheS* cassette and

designed to contain 45 bp of homology to the upstream or downstream regions of the targeted gene, respectively, were used in the PCR to create an *FRT-dhfr-pheS* cassette bounded upstream by 45 bp homologous to the upstream region of the knock out target and downstream by 45 bp homologous to the downstream region of the knock out target (~2.3 kb). Primers were then used in amplification by PCR of the lambda RED region from pKaKa1, to include the *beta, gam,* and *exo* genes to create a second DNA fragment (~3 kb). Strain B0011 was grown in 4 ml of M9 media + 20 mM glucose + 3AA+DAP (MG+3AA+DAP) overnight to an optical density at 600 nm ($O.D._{600}$) of 1-1.4 then all 4 ml were pelleted by centrifugation and all supernatant removed. 1 µg of each of the two DNA fragments was combined in a total volume of 5 µl and resuspended with the pelleted bacteria. The suspension was incubated at room temperature for 30 min then allowed to outgrow in 3-4 ml of the same media at 37°C with shaking. The bacteria were then pelleted and plated on MG+3AA+DAP+Tp60. Colonies appeared 5-6 d later and were screened for correct insertion size using primers outside of the region used to create the knockout cassette. After Flp mediated excision of the *gat* cassette from B0011 Δ*asd*::*gat* [8], lambda RED was used to delete BPSS1818 and BPSS1860 with the *gat-pheS-FRT* cassette (instead of *dhfr-pheS*) in the GS^S strain B0011 Δ*asd*::*FRT*. The *wbiI*::*gat-sacB* insertional mutant was made in B0011 Δ*asd*::*FRT* by conventional allelic replacement methods [5,8]. All mutants were verified using PCR.

Cell lines and culture conditions. Human embryonic kidney cells (293T), human neuroblastoma cells (HTB-11 a.k.a. SK-N-SH cells [11-13]), human epithelial cells (HeLa), and human microglial cells (CHME [13,14]) were cultured in Dulbecco's modified Eagle's medium (DMEM; HyClone) containing 4500 mg/l glucose with 4.0 mM L-glutamine. Murine microglial

cell line BV-2 ([13,15]) and murine macrophage cell line RAW264.7 were also cultured in DMEM containing 4500 mg/l glucose with 4.0 mM L-glutamine. All cultures were supplemented with 10% (v/v) heat-inactivated standard fetal bovine serum (FBS; HyClone) and antibiotic/antimycotic solution (100 U/ml penicillin, 100 μg/ml streptomycin, and 250 ng/ml amphotericin B; HyClone). Cells were maintained at 37°C and 5% CO_2 in a humidified incubator. 293T, HeLa, and RAW264.7 cell lines were maintained at 50-80% confluency and were passaged by scraping the cells from the flasks using a cell scraper. BV-2, CHME, and HTB-11 cell lines were passaged by trypsinization with 0.25% trypsin (Gibco) and 1 mM EDTA in pre-warmed phosphate buffered saline (PBS) while being maintained at 50-80% confluency. Cell lines were maintained in Corning™ flasks and plates with CellBIND™ surfaces. Cell concentrations were verified with the Scepter handheld automated cell counter (Millipore).

***C. elegans* strains, media, and culture conditions.** The two *C. elegans* strains used in this study (N2 and DH26) were obtained from the *C. elegans* Genetics Center maintained at the University of Minnesota. Both strains are hermaphroditic. N2 is a wildtype strain [16] and DH26 is a temperature sensitive mutant that cannot reproduce at temperatures above 25°C [17,18]. To reduce risk of contamination during prolonged [19] *C. elegans* culturing, *E. coli* EOP50 was plated on LB+Rif 200 to obtain spontaneous rifampicin resistant mutants (EOP50-rif). EOP50-rif were then used as nematode food by spotting onto Nematode Growth Media (NGM; [18]) supplemented with 200 μg/ml rifampicin and allowed to grow at 37°C overnight. The plates were removed and allowed to cool in a 20°C incubator for several hours. Nematode cultures were passaged to fresh bacterial lawns by "chunking" whereby a cube of agar containing worms

is cut out of the plate and moved to another. Cultures were grown at 20°C and passaged every 4-6 days onto fresh *E. coli* EOP50-rif lawns.

Growth curves of B0011. Growth curves of the mutants were initiated by growing them overnight in 96-deepwell plates then diluting them 200 x into the indicated media. The 96-well plate was incubated at 37°C with shaking in the BioTek ELx808IU and measuring the O.D. 600 nm every 30 min for 48 h. Each growth curve was done in duplicate with the average and the SEM shown (Fig. 1).

Determination of ideal exogenous DAP concentrations. Previously, we found that a DAP concentration of 200 μg/ml would allow for growth of B0011 in HeLa cells and for slow killing in RAW264.7 cells after 24 h. Several different concentrations of DAP were added to the infections to see if higher DAP concentrations would allow better or prolonged growth. Briefly, cell lines (BV-2, CHME, HeLa, HTB-11, and RAW264.7) were harvested and seeded into 24 well plates at 70% maximum confluency as determined by cell counting using the Scepter and allowed to attach overnight. After attaching, the monolayers were washed twice in pre-warmed 1x PBS. Wildtype *Bp* 1026b and B0011 were grown overnight in LS+DAP200 then diluted to a multiplicity of infection (MOI) of ten bacteria per host cell (10:1) in pre-warmed DMEM containing 10% FBS and 250 μg/ml of DAP to allow cell wall cross-linking during the initial infection. The DMEM containing B0011 bacteria was added to the washed monolayers and the infection progressed for 1 h. After 1 h, the monolayers were again washed twice with pre-warmed PBS. Different concentrations of DAP were added (0 μg/ml, 250 μg/ml, 500 μg/ml, 1000 μg/ml, 2000 μg/ml) to separate aliquots of DMEM with 10% FBS containing 750 μg/ml

amikacin and 750 μg/ml of kanamycin (to kill extracellular bacteria). The infection was allowed to progress for 24 h. At 24 hours post infection (hpi) the media was removed and the monolayers were washed twice with pre-warmed PBS. 1 ml of 0.2% (v/v) Triton-X100 non-ionic detergent in PBS was added to the wells and incubated for 15 min. The mixture was pipetted repeatedly to disrupt the cell monolayers then serially diluted in PBS. 100 μl aliquots were plated on LS-DAP200 and incubated at 37°C for 48 h or until colonies were visible. Colonies were counted and CFU/well determined. Numbers shown are the averages of two independent experiments (Fig. S1).

Infection characteristics of various *Bp* strains and their cognate Δ*asd* mutants. *Bp* strains isolated from various sources were obtained from Drs. Paul Keim and Apichai Tuanyok at Northern Arizona State University, while the Δ*asd* mutants of those strains were produced in our previous work using lambda RED recombineering [9]. Wildtype *Bp* strains were grown overnight in LS while the Δ*asd* strains were grown overnight in LS+DAP200. When the optical densities of the cultures were equal, wildtype strains were diluted in DMEM + 10% FBS and Δ*asd* strains were diluted in the same media with 250 μg/ml DAP. HeLa and RAW264.7 cell monolayers were treated as in the determination of optimal exogenous DAP concentration above. The infection was allowed to progress for 1 h before the addition of antibiotics to kill the extracellular bacteria and maintain intracellular infection. Monolayers were lysed at 24 h, diluted, and plated for CFU/well as described above. The numbers indicated are the average of two independent experiments graphed with the standard error of the mean (SEM; Fig. S2).

Invasion and intracellular replication assays of *Bp* 1026b WT and the strain B0011 with and without DAP. Invasion and intracellular replication assays were carried out using a slightly modified kanamycin protection assay as previously described [6,20]. The cell lines utilized were: 293T, BV-2, CHME, HTB-11, and RAW264.7. 293T cells do not attach well so to stabilize the monolayers during washing, Corning™ 24-well plates with CellBIND™ surface were prepared by incubating the wells with a 1:40 dilution of phenol-Red free BD Matrigel Matrix with reduced growth factors in PBS for 30 min prior to seeding. Invasion assays were initiated as described above in DMEM + 10% FBS for *Bp* 1026b and with 250 μg/ml DAP for strain B0011. 1 hpi the medium was removed and the monolayers were washed twice with pre-warmed PBS and fresh DMEM containing 750 μg/ml amikacin and 750 μg/ml of kanamycin was added to kill extracellular bacteria for another hour. At this point the medium was removed again and washed twice with pre-warmed PBS. Monolayers were lysed with 0.2% Triton-X100 in PBS, diluted, plated onto LS+DAP200, and incubated at 37°C for 48 h. Colonies were enumerated and invasion efficiency was determined by dividing the number of intracellular bacteria at 2 hpi by the total number of infecting bacteria. The experiment was carried out in triplicate and the numbers are the average of all three replicates with the error bars representing the SEM (Fig. 2A). The student t-test was used to determine the significance between invasion efficiencies of the wildtype and strain B0011.

The intracellular replication assays were carried out by using the same cell lines and also set up as described above. Each cell line was infected singly with wildtype *Bp* 1026b, strain B0011 with 250 μg/ml of DAP for the whole infection, or strain B0011 without DAP. The monolayers were infected at an MOI of 10:1 for 1 h then washed and the medium was replaced with DMEM containing 750 μg/ml amikacin and 750 μg/ml kanamycin. At the indicated time

points, from 2 h until 4 days post infection (dpi), monolayers were again lysed, diluted, and intracellular bacteria enumerated after 48 h incubation on LS+DAP200. The numbers shown are the average of three experiments; SEMs are shown but were so low that they are not visible in the graphs (Fig. 2B-F).

Plaque assay of HEK 293T cells infected with strain B0011 in the presence or absence of DAP. Plaque assays were carried out as previously described [21] but with some modifications. Briefly, 293T cells were seeded in CellBIND™ coated Corning™ 6-well plates with a 35 mm diameter. The plates were incubated with a 1:40 dilution of phenol-red free BD Matrigel Matrix with reduced growth factors in PBS for 30 min prior to seeding. After a short period of drying within a bio-safety cabinet, cells were seeded at $8x10^5$ cells/well and allowed to attach overnight. In the morning the media was removed and the monolayers were washed twice with PBS. An overnight culture of B0011 was resuspended in DMEM with 250 μg/ml of DAP. The culture was diluted down in the same media to reach an MOI of 100:1 and 10:1. The suspension of bacteria was used to infect two monolayers at an MOI of 100:1 and a third at 10:1 all for 1 h. After 1 h, the bacteria-containing media was removed and the monolayers were gently washed twice with PBS to remove any extracellular bacteria. DMEM containing melted 0.5% agarose, 750 μg/ml of amikacin, and 750 μg/ml of kanamycin was cooled to near solidity then used to overlay one of the 293T monolayers infected at an MOI of 100:1. The other two monolayers were overlaid with the same media but supplemented with 250 μg/ml of DAP. At 24 hpi, 400 μl of DMEM with 0.1% (w/v) neutral red solution (Invitrogen) was added to the agarose overlay and incubated for 2 h to allow staining. Plates were inverted on a light box and images

were captured and the negative black and white image created using imageJ version 1.440 (Fig. 4C-E).

Microscopy and live-cell time lapse imaging of acute and persistently infected cell lines. Light microscopy of infected cell monolayers was carried out as described [10], except for a few modifications. Glass bottom 12-well plates were obtained from MatTek Corporation (Ashland, MA). The plates were sterile, uncoated, and contained bottoms of No. 1.5 covers lips. Glass coverslip bottoms were treated for four hours with 150 µg/ml poly-L-lysine in ddH_2O. The plates were washed twice with ddH_2O and allowed to air-dry within a biosafety cabinet overnight. For 293T cells, the wells were treated as indicated above with the BD Matrigel Matrix. Monolayers were seeded at nearly $3x10^8$ cells/well verified by the Scepter handheld automated cell counter. Cells were allowed to attach and grow for 24 h prior to initiating the infection. Cell lines were infected with an MOI of 10:1 bacteria in 200 µl of DMEM + 250 µg/ml DAP to increase the contact between the bacteria in the DMEM and the monolayers. After 1 h the medium containing bacteria was removed, the monolayers were washed 2X with PBS, and DMEM containing 250 µg/ml DAP, 750 µg/ml amikacin, and 750 µg/ml kanamycin was added for the remainder of the experiment. For fluorescent microscopy, the DMEM was removed and washed from the monolayers with PBS then replaced by Medium 199 (with Earle's Salts, L-glutamine, 2.2 g/l sodium bicarbonate, and without phenol red; gibco) + 250 µg/ml DAP. DMEM is somewhat auto-fluorescent in the green channel due to the thiamine in the media. M199 contains significantly less thiamine so the auto-fluorescence is greatly reduced.

Live-cell imaging consisted of 10 min movies taken in a pre-warmed room after the ambient equipment temperature stabilized for an hour. A Zeiss Axio-observer D1 fluorescent

microscope was utilized to capture images. The Axiovision software with the Smart Experiment Time-Lapse Module was used to capture live-cell infection by B0011. Images were captured at 1 frame/s for 10 min total. Images were compiled into videos using imageJ version 1.440.

Long term live-cell two color fluorescent time-lapse fusion assay. GFP and RFP tagged HEK293 cells were obtained from Dr. Jeff Miller's lab at UCLA [22]. These cell lines were maintained in DMEM + 10% FBS as described above with the addition of 3 μg/ml of puromycin and passaged by gently tapping the side of the culture flask. At ~80% confluence both cell lines were treated with 0.25% trypsin (Gibco) and 1 mM EDTA in pre-warmed phosphate buffered saline (PBS) for 5 minutes to break up aggregations of cells. The Millipore Scepter was used to enumerate the cell concentration and equal numbers of each cell line were mixed, resuspended thoroughly, then seeded into 12-well cover glass bottom plates that had been pre-treated with BD Matrigel as described above. After allowing attachment overnight, an infection at an MOI of 1:1 was carried out as described above, where after 1 h of infection media containing DAP + aminoglycosides was added. The plate was then placed in a stage mounted incubator chamber custom fabricated by Bioscience Tools where a 5% CO_2 atmosphere was maintained at 37°C. During the next 2 hours the monolayers were observed closely to identify infected cells. Once an infected cell was identified by visualizing intracellular bacteria or protrusions, the multi-channel live-cell time-lapse fluorescent imaging using a custom capture sequence was initiated and images in the green, red, and brightfield were captured every 2 min for 24 h. At the conclusion of the experiment, images were exported to imageJ for intensity normalization and movie production.

Transmission electron microscopy of wildtype *Bp* 1026b infected RAW264.7 macrophages. 60 mm tissue culture dishes were treated for four hours with 150 µg/ml poly-L-lysine in sterile double distilled water (ddH_2O). The dishes were washed twice with ddH_2O and allowed to air-dry within a biosafety cabinet overnight. RAW264.7 murine macrophages were scraped from flasks and allowed to attach in DMEM overnight. The next day wildtype *Bp* 1026b were resuspended in 200 µl of DMEM at a concentration adequate for an MOI of 10:1 and used to infect the monolayer for 1 h. After 1 h, the media was removed and monolayers were washed twice with PBS. Fresh DMEM containing 750 µg/ml amikacin and 750 µg/ml kanamycin was added for the remainder of the experiment to kill all uninternalized bacteria. At 18 hpi, the media was removed and the monolayers were fixed for 2 h with 2.5% glutaraldehyde in 0.1 M sodium cacodylate buffer at pH 7.4. The dishes were washed twice with 0.1 M cacodylate buffer for 20 min each. Samples were post-fixed in 1% osmium tetroxide in 0.1 M cacodylate buffer for 1 h then dehydrated in a graded ethanol series. Epoxy resin was used to infiltrate samples and allowed to polymerize at 60°C for 2 d. Samples were visualized using a 120 kV Hitachi HT7700 digital transmission electron microscope. Images were captured using an AMT XR-41 2048 x 2048 pixel bottom-mount high-resolution camera (Fig. S3).

Determination of endonuclear B0011. 293T cells were infected with strain B0011 as above for the intracellular replication assays but in 6-well CellBIND™ coated Corning™ 6-well plates with a 35 mm diameter. At 20 and 24 hpi, the culture medium was removed and the monolayers were washed with PBS then scraped off the well bottom using a cell scraper. The cells were then washed in cold PBS by centrifugation after which the supernatant was discarded. The cells were resuspended in chilled hypotonic buffer solution (20 mM Tris-HCl pH 7.4, 10

mM NaCl, and 3 mM $MgCl_2$) by pipetting and incubated on ice for 15 min. 25 µl of NP40 detergent (10% w/v) was added and the tube vortexed for 10 s at the highest setting. The homogenate was then centrifuged at 4°C and 1,850 x g for 10 min. The supernatant containing the cytoplasmic fraction was removed and saved. The pellet containing the nuclei was resuspended in 3 ml of buffer S1 (0.25 M sucrose and 10 mM $MgCl_2$) then layered carefully over a 3 ml cushion of buffer S3 (0.88 M sucrose and 0.5 mM $MgCl_2$) and centrifuged at 4°C and 2,800 x g for 10 min. This step is done twice to provide a cleaner nuclear pellet that was then resuspended in nuclear lysis buffer (0.2% Triton-X100 in PBS) and vortexed at the highest setting for 10s. The cytoplasmic and nuclear lysates were serially diluted in PBS and plated on LS+DAP200 to determine cytoplasmic and nuclear bacterial load. This experiment was performed in triplicate and the error bars represent the SEM of the CFU obtained from the different fractions.

***C. elegans* survival, prolonged killing, and intraorganism replication assay.** Survival and prolonged killing assays were carried out as previously described [23,24], but with a few modifications. We used *C. elegans* strain DH26, a temperature sensitive mutant, in both the survival and prolonged killing assays. Survival assay experiments were initiated by transferring 30 worms in the L2 stage to B0011 lawns on NGM supplemented with 3AA+DAP (when growing the B0011 strains). Animals were left on the lawns for the duration of the survival assay. The assay plates were moved to the non-permissive temperature of 28°C to prevent reproduction of the nematodes. Progeny nematodes may confound the data, so eliminating them prevents accidental counting during the assay. At the indicated time points, the number of dead worms was observed using a Zeiss SteREO Discovery V.8 stereomicroscope and prodded gently

with a platinum wire to verify death. The survival assay experiment was carried out in triplicate, where the survival curve represents the average % surviving and the error bars are the SEM (Fig. 5A). For the prolonged killing assay, the nematodes were exposed to B0011 for 30 min then removed from the lawn of bacteria, washed 3X with PBS, then transferred to a new NGM plate containing a lawn of EOP50. The prolonged killing assay is shown as survival % of three trials of independent experiments compared to a control of EOP50 (Fig. 5B).

To enumerate intracellular bacteria within *C. elegans*, an assay was adapted from the previously described method [25] with a few modifications. Nematodes were transferred to a plate containing a lawn of B0011 for 1 h, after which they were picked using a "worm hook" made from a platinum loop, and were placed ten per microcentrifuge tube for each of the three indicated time points. The nematodes were washed 3X with PBS in their separate tubes by centrifugation in a tabletop centrifuge for 5 min at 540 x g. The worms were then resuspended in M9 minimal salts media containing the 3AA, and either with or without 400 μg/ml of DAP. This media also contained 750 μg/ml of amikacin and 750 μg/ml of kanamycin to promote invasion by strain B0011 and kill off other extracellular bacteria. At the indicated time points, the nematodes were again centrifuged and washed 3X in PBS. 1 ml of modified worm lysis buffer (this buffer contains 10X Pfu buffer, 60 μg/ml Proteinase-K, and 0.2% Triton X-100 non-ionic detergent in PBS) [26] was added to each tube and incubated for up to an hour at 42°C with intermediate vortexing until the worms looked mostly digested under a stereomicroscope. The solution was serially diluted in PBS and CFU/tube determined. Time points were done in triplicate and the numbers shown are the average with the SEM (Fig. 5C).

***C. elegans* live-animal time-lapse imaging.** 200 µl of *Bp* Δ*asd*::*gat–FRT*/*att*Tn7-*kan-gfp* grown in LS+DAP200 overnight was plated on NGM plates supplemented with 3AA+DAP using a disposable spreader. The bacteria were allowed to grow for 48 h at 37°C until a thin lawn was visible. The plates were then transferred to 28°C for 2 h prior to transferring *C. elegans* nematodes from the EOP50 lawn to the lawn of *gfp*-tagged B0011 for 1 h. Live *C. elegans* were visualized with the Zeiss SteREO Discovery V.8 stereomicroscope and the KLD cold halogen light source. The attached green fluorescent LED excitation unit and emission filters were used to visualize intra-organism green fluorescence. A Retiga 2000R high precision camera was attached via binocular node and time-lapse images were captured by QCapture Pro7 software. ImageJ was used to process the images into movies and for production of montages.

Challenge of *C. elegans* with live cells, heat-killed cells, and cell-free supernatant. Strain B0011 was grown over night in LS+DAP200 media and frozen at -80°C in aliquots of 30% glycerol. A single frozen aliquot was thawed the following morning and serially diluted in S-basal media [27]. The dilutions were plated onto LS+DAP200 plates to determine the CFU/ml of the frozen aliquots thus taking into account bacterial survival percentage during freezing. For the experiments the aliquots were thawed and diluted to the desired CFU in S-basal media. *Bp* were heat inactivated by heating the diluted aliquots to 80°C for 1 h. 100 ul of the least dilute samples were spotted on LS+DAP200 plates to confirm heat inactivation of all bacteria. To confirm bacteria were intact and had not lysed, samples were visualized under 1,000X magnification. Cell-free supernatants were obtained by centrifugation of undiluted samples at 20,000 X g followed by filtration of the supernatant through a Millipore PES 0.22 µm filter. Aliquots were plated on LS+DAP200 to ensure supernatant were cell-free.

20 age matched L2 *C. elegans* strain DH26 were collected and placed 1.5 ml centrifuge tubes containing 10 ul of S-basal media. The nematodes were then exposed to the indicated CFU of strain B0011, heat-killed B0011, or corresponding dilutions of cell-free supernatant in a total of 50 µl of S-basal media containing 3AA+DAP for 30 min. The nematodes were then spun down and resuspended in S-basal media containing 3AA+DAP and heat-killed EOP50 as a food source in the wells of a 12-well plate to make sure the food source did not overgrow them. At the indicated time points survival percentages were determined by observation under a Zeiss SteREO Discovery V.8 stereomicroscope, survival was verified in unmoving worms by gentle prodding with a titanium loop. The numbers presented are the averages of two independent experiments carried out in triplicate and the error bars are the SEM of the survival percentages (Fig. 5D-F). Modified prolonged killing assays using B0011 virulence factor mutants were carried out in the same manner but exposed to only $1x10^6$ CFU of the indicated strains.

***Tenebrio molitor* (yellow mealworm) survival assay.** Fresh giant mealworms were obtained from PETCO. Worms were removed from the food source and starved for 24 h at room temperature. It is essential to purchase twice as many worms than what is needed due to mealworm die-off during starvation. 100 mm by 15 mm petri dishes were used as the feeding chambers for each replicate and were humidified by placing a 35 mm petri dish containing a folded paper towel soaked with double distilled water inside. A piece of the rim of the 35 mm dish was shaved off with scissors to allow for humidification, ensuring the opening was small enough to prevent the worms from entering the humidifier. 20 starved worms were added to each feeding chamber.

Bacterial cultures were grown to an OD_{600} of 5 in 6 ml of LS broth+200 μg/ml DAP by heavy inoculation 24 h prior to initiating the experiment. For each replicate, 1 g of oats was measured into borosilicate glass tubes and autoclaved to sterilize. 2 ml of each strain were concentrated via centrifugation and were then resuspended in 1 ml LS broth+1,000 μg/ml DAP. 1 ml of each culture was used to soak 1 g of oats for every replicate and strain. Once the oats absorbed all liquid they were added to the inside of the 100 mm petri plate (outside of the 35 mm plate humidifier), this is taken as time zero (T=0). Survival assays were carried out in triplicate with 20 worms per replicate for a total of 60 worms per strain tested.

The lids of the 100 mm petri dishes were taped shut to prevent mealworm escape and placed in a ziploc bag to maintain humidity then incubated at room temperature. Animals were checked every 12-24 h for movement, if the animals did not move they were picked up gently with forceps and observed for any movements. If the animals did not respond or showed melanization they were considered dead and marked as such. Survival curves were plotted by pooling the replicates in GraphPad Prism 6.

Engineering of *Bp* Δ*asd*::*gat–FRT*/*att*Tn7-*kan-gfp*. The *Bp* 1026b Δ*asd*::*gat –FRT* strain (B0011) was engineered as previously described [5] and was tagged with pTn7-*kan*-P_{S12}-*gfp* as previously described [10]. B0011 was grown for 36 h in 4 ml of LS+DAP200 then washed 4 times in room temperature sterile double distilled water (ddH_2O). The pellet was resuspended in 40 μl of ddH_2O and added to 2 mm electroporation cuvettes along with 250 ng of both pTn7-*kan*-P_{S12}-*gfp* and pTNS3-asd_{Ec}. Following a pulse of 250 kV, the bacteria were resuspended in 1 ml of LS+DAP200 and recovered for 1 h at 37°C with shaking. After 1 h, bacteria were pelleted and plated onto LS+DAP200+Km1000. Colonies appeared after 3-4 days and 4 isolates were

streaked for purity on the same media. Two colonies from each were PCR confirmed to contain the Tn7 element at the *glmS*3 site [28] and verified via fluorescent microscopy as being green fluorescent.

5.4 RESULTS

Determination of ideal exogenous DAP concentrations for intracellular infection models. Previously, we had established the ideal concentration of DAP for log growth of strain B0011 in rich media at 250 μg/ml of DAP [6]. Since DAP allows growth of the attenuated mutant in liquid media, we wanted to investigate whether DAP present in cell monolayer growth media would allow for intracellular replication of the attenuated B0011 strain. In addition to intracellular replication, we wanted to determine the concentration of DAP that would give us optimal infection of various cell lines. Many different cell lines were chosen, some that have been extensively utilized in cell infection models (HeLa [6,20,21] and RAW264.7 [6,29,30]) and others that may prove useful for future *Bp* pathogenesis experiments. Wildtype *Bp* 1026b was able to infect all the cell lines tested including the newly introduced murine (BV-2) and human microglial (CHME) cell lines as well as the human neuroblastoma cell line (HTB-11). The wildtype was also able to produce plaques in these cell lines (data not shown). When the culture media was not supplemented with DAP post-infection there were no B0011 bacteria detectable at 18 hpi in any of the cell lines, as expected. To determine the appropriate concentration of DAP, the amount supplemented was titrated up from 250 μg/ml of DAP, the optimal concentration used in shaken culture, to 2,000 μg/ml of DAP. There is a step-down in infection efficiency as the amount of DAP increases. Fewer bacteria are recovered at higher supplemental DAP concentrations (Fig. S1). DAP is an amino acid specific to bacterial peptidoglycan which at higher concentrations begins to activate the innate immunity of the cell lines via the NOD1 pathway [31] resulting in more efficient host-cell mediated killing. The numbers of recovered B0011 bacteria were a log or two lower than those of the wildtype. At 24 hpi, under bright-field microscopy, it was observed that mutant bacteria were infecting the cell lines with a similar

phenotype as the wildtype (Fig. 1). At 18 h the mutant can be seen polymerizing actin at a velocity of ~17.4 μm/min measured by the average distance traveled in the supplementary time-lapse videos (compared to 4.8 μm/min for *Rickettsia rickettsii* [32] and ~10 μm/min reported for *Listeria monocytogenes* [33]) and protruding from the various cell lines, indicating key infectious stages of phagosome escape, actin polymerization, and protrusion occur similarly between the wildtype *Bp* 1026b and the biosafe Δ*asd* strain, B0011.

Infection characteristics of various *Bp* strains and their cognate Δ*asd* mutants. Many experiments with *Bp* have focused on the type strains 1026b and K96243. While the importance of these virulent type strains cannot be underscored, it may be important to understand that they are isolates from acute human infections and that within-host adaptation is known to occur frequently [34]. *Bp* isolated from human chronic cases, from the soil environment, and from different geographic locations can all infect humans but subtle genomic differences may yield diverse pathogenic outcomes. To this end we tested nine naturally competent *Bp* in the two commonly used cell line models, HeLa human epithelial cells and RAW264.7 murine macrophages. All wildtype strains tested besides the chronic case isolates were able to infect intracellularly to around 10^6 CFU/well (Fig. S2) and produce plaques (data not shown). Strain Bp4141, Bp4144, and Bp6340 are clinical isolates from chronic cases occurring in Australia isolated over the course of a decade (Table 1). The number of intracellular bacteria was consistently 10 and 100 times lower than the acute and environmental isolates in the two independent experiments for one or both cell lines (Fig. S2) although there were some disparities between HeLa and RAW264.7 cell lines. Whether chronic *Bp* isolates have adapted to a slower infectious course within-host remains to be seen but it is certainly plausible given

adaptations in other chronically infecting pathogens such as those of *Pseudomonas aeruginosa* (22) and *Burkholderia dolosa* [35].

That aside, we thought it would be of use if strains from alternate sources, such as those above, could be accessible to BSL2 researchers and assist in answering some of these interesting questions. The Δ*asd* mutants of all the strains were created previously [9] and used to infect the monolayers above and the CFU/well recovered were compared to those of the wildtype. Some of the Δ*asd* strains were unable to infect while others could. Numbers were generally higher for the RAW264.7 monolayers, compared to HeLa cells, possibly because of the phagocytic nature of the cell line. Fine-tuning of the DAP concentration may be necessary for the different strains as their growth behavior in supplemental DAP has not been investigated. Interestingly, the Δ*asd* mutant of the chronic Australian isolate had nearly the same replication numbers as its cognate wildtype strain in RAW264.7 macrophages after 24 h.

B0011 growth rate in different media. Strain B0011 was grown in several different growth media to find the best one for future experiments (Fig. 1A). Low salt Lennox LB broth, no salt LB broth, and M9 minimal media supplemented with 200 μg/ml DAP were chosen along with the unsupplemented media. Growth curves in triplicate are shown for all media. Strain B0011 was unable to grow without DAP supplementation regardless of media. LB broth supplemented with DAP gave the best growth rate and eliminating the salt allowed an increased rate of exponential phase growth. We then wanted to compare the growth rate of B0011 to the wildtype 1026b strain (Fig. 1B). Again, without DAP strain B0011 could not grow. In LB broth without salt (LS) strain B0011 had the same growth rate as wildtype 1026b.

Invasion and intracellular replication assays of *Bp* 1026b WT and the B0011 Δ*asd* mutant with and without DAP. Alternate strains would be useful in studying some aspects of *Bp* pathogenesis such as innate pathogenesis or differences between acute, chronic, and latent forms of infection in BSL2 cell models. However, the type strain 1026b is still the major workhorse for investigating the molecular pathogenesis of *Bp*, so demonstrating the usefulness of strain B0011 in invasion and intracellular replication assays is paramount. A wide variety of cell lines were chosen to determine the invasion efficiencies; including HEK293T, BV-2, CHME, HTB-11, and RAW264.7 (Fig. 2A). As it can be seen, the invasion efficiencies between the wildtype 1026b and B0011 were very similar in all the cell lines and the efficiencies were found to be insignificantly different by the student *t*-test. This indicates that attachment and invasion of the Δ*asd* mutant B0011 occurs virtually identically as the widltype regardless of the cell type. Whereas *B. thailandensis* may exhibit certain cell line tropism and decreased invasion efficiencies [36], the B0011 exhibits wide tropism and wildtype invasion efficiencies irrespective of cell type.

The intracellular replication assays were carried out in the same cell lines as the invasion assays. To properly illustrate intracellular growth characteristics, the assays were carried out to 4 d (96 h; Fig. 2B-F). In all cell lines tested, the wildtype reached a peak of $1x10^6$ CFU/well at 18 hpi and rapidly declined to very low numbers by day four of the assay. Without supplemental DAP after the initial 1 h infection, B0011 was unable to replicate within any of the cell lines and no CFU were recoverable at 18 hpi. When DAP was supplemented in the cell culture media at 250 μg/ml throughout the experiment, strain B0011 was able to infect HEK293T cells the same as the wildtype, reaching $1x10^6$ CFU/well after 18 hpi then declining in numbers for the remainder of the experiment (Fig. 2B). Contrastingly, the Δ*asd* mutant B0011was unable to

"acutely" infect all other cell lines (Fig. 3C-3F). Instead the detected CFUs drop to between $1x10^4$-$1x10^5$ CFU/well then plateau to "persist" within the monolayers for the remaining 4 d of the experiment. Strain B0011 infected the cell monolayers well beyond the normal 24 h wildtype infection and we predicted that it would continue to infect past the 4 d window of the initial intracellular replication assay.

Intracellular replication of B0011 in HEK293T and HeLa cell lines. A finer scale infection assay showed that with DAP, B0011 can infect 293T (Fig. 3A) cells and Hela cells (Fig. 3B) similar to wildtype 1026b. Without DAP, B0011 cannot grow intracellulary and eventually dies. For comparison the B0011 Δ*hcpI* mutant was used and showed that in this particular model the major T6SS is contributing to intracellular replication more so in HeLa epithelia cell than the HEK293T kidney cells. In both cell lines the B0011 Δ*hcpI* mutant numbers increase like the wildtype and B0011 strains then in HeLa cells intracellular CFU drop by 12 and 24 hpi. Bright-field phase images represent well-wide MNGCs full of B0011 bacteria in the process of fusing with healthy HEK 293T cells that then completely lyse by 48 hpi (Fig. 3C, 3D, and V1). To this end, the plaque assay was attempted with B0011 in HEK293T cells. Without DAP the cell monolayers appeared healthy at 24 hpi (Fig. 3E), whereas when infected with DAP at an MOI of 10:1 and 1:1 the plaques can clearly be seen (dark areas; Fig. 3F, and 3G).

Cell lines remain persistently infected by the *Bp* 1026 Δ*asd* mutant, B0011, for up to 3 weeks. Cell monolayers were infected with B0011 at an MOI of 10:1 with DAP and monitored via light microscopy and live-cell time-lapse imaging at various dpi (Fig. S3). At five and nine

dpi Δ*asd* mutant bacteria can be seen infecting BV-2 murine microglial cells at high density (Fig. S3A). Carets indicate multiple bacteria undergoing actin-mediated protrusion and flagella-based intracellular movement. In Figure S3B, CHME human microglial cells are observed at 16 dpi where carets indicate a few of the many protruding bacteria infecting the host-cells. 48 h later at 18 dpi compact spheres packed with moving bacteria are observed. Carets at 18 dpi indicate two of the spheres, one small and one large. The phenotypic difference between these perfectly round bacteria-filled spheres and the very rough, bacteria free apoptotic cells lying between and around them indicate a unique origin. The source of these spheres was initially a mystery that will be addressed later. Infected HTB-11 human neuroblastoma cells can be seen in Figure S3C at 4 dpi. Multiple bacteria are swimming in the cell and around the nucleus, while others protrude, searching for neighboring cells to infect. Two weeks later (14 d), bacteria are still infecting some of the cells. Mutant bacteria are tightly packed at high cell density within the live cell and are observed in motion. In Figure S3D, RAW cells stay infected for many days similarly to the other cell lines. All of the images are single frames of 5-10 min time-lapse videos located online in the supplemental materials (V6-8).

***Burkholderia pseudomallei* can undergo endonucleobiosis during the course of infection.** Our new model of persistently infected cells allowed easy observation of the infectious process at BSL2. Rather than having only 24 h to observe infected monolayers, there was an average of 3 weeks available. Frequent observation during this period allowed surveillance of infection events that would normally be difficult to detect in “acute” infection models. Time-lapse movies of HTB-11 human neuroblastoma cells infected with strain B0011 revealed bacteria swimming within the nucleus of the host cell and running into the nucleolus

(data not shown). Another host-cell was found containing two daughter nuclei, one of which was highly infected with over 50 *gfp*-tagged B0011 bacteria (Fig. S4A, S4B, and S4C). Time-lapse video shows the bacteria moving around in the nucleus and possibly exiting the nuclear membrane through an unknown mechanism (V9). The presence of endonuclear *Bp* has never been described and, to the authors' knowledge, never been observed. After seeing the way the bacteria fill the nucleus, it became clear that the perfect spheres enclosing moving bacteria in other cell lines described above were actually free-floating intact nuclei of lysed cells containing bacteria at high density. The larger the nuclei the more swollen and tightly packed the bacteria, consistent with observations of endonucleobiosis in *Euglena hemichromata* [37]. It has also been observed that the nucleus remains intact after cell membrane destruction by wildtype *Bp* 1026b (Fig. S4G); whether nuclear located bacteria play a role in pathogenesis remains to be investigated.

In case this was an aberration observed solely with B0011 and to verify if wildtype *Bp* infects the nucleus, transmission electron microscopy (TEM) was carried out on fixed RAW264.7 macrophage monolayers infected with wildtype at 24 hpi. In Figure S4D-F, TEM images captured many wildtype *Bp* 1026b in the nuclei of host-cells. Figure S4D shows two nuclei of a five nuclei multi nucleated giant cell (MNGC) infected with bacteria. Figure 6E is a close up of one nucleus from a different MNGC infected with 6 bacteria in the same plane and Figure S4F is a giant free-floating nucleus full of bacteria reminiscent of the bacteria filled spheres seen earlier. This heavily infected nucleus is almost indistinguishable from nuclear *Rickettsia* infection [38] implying there are plenty of nutrients to sustain high cell density growth while remaining secluded from the host immune system components. Observation of free-

floating nuclei after destruction of the cell membrane was frequently observed in wildtype infected monolayers (Fig. S4G).

It was observed that during infections endonuclear bacteria were present more so during the later stages. At two time points, 20 and 24 hpi, cytoplasmic and endonuclear CFU of B0011 were determined. Endonuclear *Bp* increased 10 fold between the two time points and accounted for 0.4% of the total bacteria infecting the monolayers. This may not seem substantial but in an intracellular population of millions of bacteria quite a few bacteria are entering the nucleus. Endonucleobiosis of *Bp* does not seem to be an isolated event but a previously unknown intracellular niche exploited by this organism during pathogenesis, the mechanism of which remains to be elucidated.

B0011 is useful for live-cell imaging at BSL2. Utilizing the previously published GFP/RFP HEK293 cell lines [22] at BSL2 in monolayer infection studies with B0011 can be a very valuable tool. For this experiment it was possible to use time-lapse fluorescent microscopy to track strain B0011 ability to infect monolayers with monolayer fusion detectable as MNGCs at around 12 hpi (Fig. 4A and V2). By 20 hpi the entire monolayer appears fused into MNGCs and by 24 hpi the monolayer is destroyed by cascading lysis. B0011 can also be used to visualize more detailed processes of intracellular infection. In figure 4B, fusion of two HEK293T cells is visualized. B0011 bacteria can be seen producing actin tails and protruding from the surface of the host-cell as the two host-cells fuse (Fig. 4B top panel and V3). Bacteria can also be tracked as they transit through the host-cell (Fig. 4B bottom panel). The blue line tracks one bacterium through one host-cell as it transits into the next. The green line tracks a second bacterium as it alternates from protruding to cytoplasmic locations and back again.

Use of B0011 in the *C. elegans* challenge model. Another model useful for study of *Bp* pathogenesis is the *C. elegans* nematode model [23,39,40]. It is an animal model easily reproducible in the BSL2 lab and does not require IACUC oversight since *C. elegans* are invertebrates. Our *Bp* Δ*asd* mutant strain, B0011, can be used in this model at BSL2 with the addition of DAP to the NGM plates. After the worms are placed on the media they begin ingesting B0011 bacteria while moving through the thin lawn. Figure 5A shows the survival of *C. elegans* over time after they are transferred to the various bacterial lawns. Strain B0011 kills the nematodes at the same rate as *B. thailandensis* E264, which has been previously shown to kill the same as wildtype *Bp*, thus clearly agreeing with previously published observations of wildtype kill-curves [23]. A few *C. elegans* do not survive until the first time point in all replicates observed and survival percentages drop exponentially thereafter. All nematodes stopped moving by 30-40 h after assay initiation and death was verified by gentle prodding. Worms placed on negative control plates containing *E. coli* had high survival rates the entire length of the experiment.

Another effect *Bp* has on *C. elegans* survival is prolonged killing [39,40]. After a short exposure (30 min in this study) to B0011, nematodes were transferred to a fresh plate of *E. coli* and monitored for survival. Nematode survival was monitored for 4 days and Figure 5B shows the Kaplan Meier survival curves for three separate trials. The data agrees with previously published results regarding prolonged *C.elegans* killing by wildtype *Bp*. In this study, we exposed the nematodes for a shorter amount of time and observed them longer than the previous studies. By day 4 the survival rate was reduced to ~ 65%. It is apparent that even a short

exposure to *Bp* can significantly reduce the lifespan of *C. elegans* compared to the negative control that was never exposed to strain B0011 and only *E. coli*.

A modified whole organism infection model was developed with the potential to identify and characterize the effects of virulence factors required for intracellular replication at the whole-animal level. At the indicated time points post-infection, worms were enzymatically digested and intracellular bacteria were counted. In the presence of DAP, strain B0011 was able to replicate and maintain bacterial levels at ~$1x10^4$ CFU/tube and ~$1x10^3$ CFU/worm (Fig. 5C). When DAP was not present, internalized CFU plummeted by 24 hpi. The CFUs recovered without DAP were 1,000 fold less than when DAP was provided during infection. The negative *E. coli* control showed no presence of bacteria by the first time point. Survival of nematodes throughout the experiment was verified by observing continuous nematode movement throughout the assay (data not shown) indicating the intracellular bacteria levels observed were not lethal.

Time-lapse bright field imaging of *C. elegans* mock infected with *E.coli* compared to *C. elegans* fed with B0011 reveals clear phenotypic changes in the nematode (Fig. V4). They became larger and the bodies appeared distended as the intestinal and motor muscles become paralyzed during infection. The typical sinusoidal movement associated with healthy worms was replaced with disjointed spasmodic movement with no forward progress in infected worms. Visualizing internal bacteria would also be of use, so we fed the *gfp*-tagged B0011 strain to *C. elegans* and were able to visualize the fluorescent bacteria lining the intestinal lumen. This could be useful in competition experiments with two different color strains of B0011 (e.g. *gfp*- and *rfp*-tags, [10]). Tagging B0011 with *gfp* also allows time-lapse live organism stereomicroscopy. Video 5 shows the green fluorescent bacteria filling the intestinal lumen during nematode

locomotion. A pronounced intestinal bulge of bacteria seems to be giving the nematode considerable digestive difficulty.

Challenge of *C. elegans* with live cells, heat-killed cells, and cell-free supernatant. To further fine-tune the model of *C. elegans* we wanted to titer the number of bacteria the nematodes were exposed to. Expectedly, the virulent effect was dose-dependent but when the *C. elegans* were exposed to 10^6 bacteria in small liquid volumes, the prolonged killing effect was greater than when placed directly on a lawn of *Bp* (Fig. 5D). As the CFU used for the challenge was titrated down the killing effect was still present but the killing rate decreased, ranging from an exponential decline at 10^6 CFU to more of a linear decline at 10^2 CFU. This trend was also observed when using heat-killed (Fig. 5E) and cell-free supernatant (Fig. 5F). For all CFU used, the live cells killed the best followed by heat-killed bacteria, then cell-free supernatant. Secreted components present in the cell-free supernatant, i.e. proteases and heat labile and stable toxins contribute the least. Intrinsic components, such as endotoxin and heat-stable toxins, are the next greatest contributors to *C. elegans* killing. This can be analyzed by comparing the cell-free supernatant (just secreted components) to the heat-killed (secreted and intrinsic components) (Fig. 5G). Live cells presumably have secreted, intrinsic, and also cell contact dependent active virulence components (toxin secretion directly into host organisms). Even 30 min exposures of 100 bacteria are potent enough to kill all worms ~8 days post-exposure. Strain B0011 is capable of killing *C. elegans* with all the processes tested.

Challenge of *C. elegans* with B0011 virulence factor mutants. To demonstrate that *C. elegans* and B0011 can be used to screen virulence factors we used the fast-kill challenge model

and the modified prolonged killing model. In the fast-kill model the *C. elegans* were placed on lawns of the indicated strains for the duration of the experiment. Two virulence factors of known function, *hcp1* a component of the T6SS-5 [41] and *wbiI* the last gene in O-antigen biosynthesis, were mutated and tested for attenuation in the two *C. elegans* models [42,43]. In the fast-kill model the nematodes challenged with the Δ*hcpI* mutant compared to B0011 had an almost tripled median time to death from 6 h to 19 h. The survival curves were highly significantly different. The *wbiI* mutant also had a doubling of median survival time from 6 h to 12 h and a significantly different survival curve when compared to B0011 challenged *C. elegans*. In this model, *C. elegans* exposed to the B0011 putative virulence factor mutants ΔBPSS1818 and ΔBPSS1860 survived the same as those exposed to B0011 (Fig. 4H). The same mutants were used to infect *C. elegans* in the slow-killing model (Fig5I). In the slow killing model the *wbiI* mutant did not survive significantly longer than B0011 exposed worms while the Δ*hcp1*-exposed worms had a significantly different survival curve with no increase in median survival time. In contrast the nematodes exposed to ΔBPSS1818 mutant bacteria had a highly significant difference in survival compared to B0011 exposed nematodes with a median increase in survival time from 40 to 68 hpi. Nematodes exposed to the putative attachment factor mutants ΔBPSS1860 showed the largest difference in the slow killing model with survival curves similar to the EOP50 exposed control.

Studying *Bp* virulence at BSL2 with the mealworm survival assay. Mealworms have a more complicated immune system than the nematode *C. elegans.* The ability to study the virulence of *Bp* in a higher-level organism at BSL2 is an invaluable model system. Similar to *G. mellonella*, the mealworm *T. molitor* begins to melanize during an infection until completely

moribund where the entire worm turns dark in color. Of particular note, these worms appear to be paralyzed from the mid-section outwards. The paralysis first manifests itself as twitching then spreads to encompass the entire animal, leaving only the legs with the ability to move before mealworm death. Observations indicate that mealworm paralysis is followed eventually by a spreading melanization and appear to have the same focus in the animal's anatomy. Strain B0011 was fed to the worms, the region of melanization begins at the junction of the crop and the proventriculous (mid-gut). The

The practicality of the mealworm model in studying *Bp* virulence with B0011 at BSL2 was demonstrated by a survival assay with B0011 and several virulence factor mutants (fig. 6A). Feeding on B0011 spiked oats kills the mealworms much faster than the EOP50 control indicating the mealworm can be a new, cheap, fast, and effective model for studying *Bp* pathogenesis at BSL2. Survival curves of mealworms infected with *wbiI* and *hcpI* mutants were both significantly different than the B0011 with many worms surviving on average double those infected with B0011 but without an increase in median survival time (Fig. 6A). ΔBPSS1860 infected mealworms had increased median survival times from 48 h to 60 h but only slightly longer average survival times and was significant compared to the B0011 control curve (Fig. 6A). In the *T. molitor* model, bacterial dissemination can be followed from the digestive track by feeding the worm B0011 tagged with stable GFP constructs [10]. Figure 6B shows a picture of the worm and a diagram of its digestive tract anatomy. After brief feeding of mealworms with GFP-tagged B0011, the entire tract can be removed by severing the head and carefully pulling the final few segments until the tract comes free. The tract can be mounted on a microscope slide for viewing. The anatomical diagram can be compared to the DIC images of the mealworm (Fig. 6B compared to 6C top panels). The fluorescent bacteria are visible in the digestive tract and you

can see permeation of the surrounding tissues with fluorescent bacteria (Fig. 6C middle panels). Paralyzed worms that still reacted to touch but could not move were dissected. A large portion of the crop and anterior end of the midgut were liquefied and were unable to be removed intact. Under magnification the mealworm digestive tract cells appeared to be fused into the characteristic MNGCs of monolayer infections (Fig. 6C bottom panels). MNGC type formations are termed nodules in insects and are hallmarks of innate cell-mediated. Within the nodule green-fluorescent bacteria can be seen.

BALB/c attenuation studies of two new *Bp* strains. The previously constructed *Bp* K96243 Δ*asd* mutant and the newly made MSHR487 Δ*asd* mutant were tested for avirulence in the BALB/c inhalation melioidosis animal model. The LD_{100} dose for both strains is ~4,500 CFU with all animals succumbing to infection by 4 dpi. $1x10^7$ CFU were used to challenge the mice (~2,000 time the LD_{100}) and survival was followed. All mice challenged with the Δ*asd* mutants survived 60 days until the end of the experiment. Organs loads were determined to be 0 CFU in all organs tested (lungs, liver, spleen) indicating the bacteria were unable to infect the mice and were completely attenuated. The CDC has since excluded these two strains from the SA regulations.

5.5 DISCUSSION

Burkholderia pseudomallei research has been restricted to BSL3 laboratories in the United States. This limits much of the pathogenesis research to entities and institutions that have access to and can afford to run a BSL3 lab. It is no surprise that BSL2 labs far outnumber BSL3 labs in the United States, representing underutilized assets in the search for therapeutics and vaccines. Recently a bio safe vaccine strain developed by this laboratory has been excluded from the select agent list and can be used at BSL2 pending IBC approval and entity specific exclusion.

Previously, the utility of *Bp* 1026b Δ*asd* strain B0011 as a vaccine was demonstrated. In this paper, experiments were undertaken to expand the utility of this strain into standard assays used by researchers for *Bp* pathogenesis investigation. After finding that 250 μg/ml of DAP was an ideal concentration for allowing infection of multiple cell types of different lineages, images were captured of strain B0011 protruding from host cells while polymerizing actin. This shows that the mutation in the *asd* gene has no effect on the molecular pathogenesis of the mutant and that cell-type tropism seen with other model bacteria does not occur.

Several other wildtype *Bp* strains isolated from different sources (environmental and clinical) and different disease presentations (acute and chronic) were tested along with their Δ*asd* counterparts in two common cell infection models, HeLa and RAW264.7. First, this demonstrated that regardless of the source, all the strains were able to infect the cell lines and second, that there may be subtle changes in chronic isolates that predisposes them to slower growth rates during infection. That aside, the Δ*asd* mutants of the strains were still able to invade and infect the two cell lines but grew at a slower rate, similarly to what was seen with strain B0011. Future work will focus on getting the *asd* mutants of these other strains excluded from

the SA list for BSL 2 use. This would allow researchers to study the effects of source and disease presentation on pathogenesis in a BSL 2 laboratory.

Efficacy of strain B0011 in the invasion assay was tested and compared to wildtype 1026b. The mutation in the *asd* gene does not affect the ability of the mutant to enter any of the five cell lines tested, where approximately 1 in 50 cells become infected. Since there was no defect in invasion, the assumption that there is no defect in attachment is probably true. The mutant attaches, invades, and escapes the vacuole the same as the wildtype and would therefore be a good BSL2 model for studying these *Bp* infection stages in the cell types tested. Beyond invasion, the intracellular replication assay was carried out in several cell lines and found that in 293T and HeLa cells, when DAP was present, strain B0011 grew intracellularly at the same rate as the wildtype. Strain B0011 would be very useful for intracellular replication assays in 293T cells at BSL2. Microscopy revealed the presence of MNGCs followed by plaque formation. When a plaque assay was performed in 293T cells with DAP, plaques were the same size as wildtype at 24 hpi, indicating strain B0011 would be excellent for plaque assays at BSL2.

However, intracellular replication assays turned out quite different in the other cell lines tested. An initial drop then plateau of intracellular CFU and microscopic observation indicated long-term persistent infections atypical of rapid infections caused by wildtype bacteria. Previous studies of chronic animal melioidosis distinguish acute infection from chronic infections as those with lethality occurring before 7 days as acute and after 7 days as chronic [44,45]. In agreement with the previous studies, strain B0011 infects cell lines, besides 293T, chronically and up to the lifespan of the monolayer (23 days in this study). Until now there has not been a practical *in vitro* chronic cell infection model at any safety level, let alone for use at BSL2. Observation of these chronic cell infections revealed a novel intracellular niche previously unknown to be exploited

by *Bp*. Endonucleobiosis was verified in wildtype *Bp*, necessitating modification of the infection model to reflect *Bp* exploitation of the intracellular niche. The nuclear niche is exploited by pathogens of the genus *Rickettsia* as a means to escape host-cell defenses and more recently intracellular bacteria have been found to produce proteins called nucleomodulins that directly modify host cell gene expression [46,47]. Once *Bp* enters the nucleus, it escapes the defenses and enters a high nutrient environment where it can potentially modify host-cell behavior. Furthermore, interesting implications arise when direct contact between host cell genetic material and naturally competent *Bp* strains capable of DNA uptake as nutrient source occurs. As an example, *Plasmodium falcipurim* has been shown to take host cell DNA into its own nucleus [48] and genomic analysis of *Rickettsia bellii* indicates gene exchange between different bacteria while inside host amoeba nuclei [38].

Live-cell imaging is a technique that can tell us many things about bacteria host-cell interactions. B0011 can fuse neighbor cells, cause plaques, and be tracked through a host-cell during infection. When coupled with fluorescent microscopy a great many experiments can be envision such as live-cell co-localization experiments and membrane dynamics, all at BSL2 with a bio safe strain. Timing of the events can also be compared between strains in these types of experiments.

Expanding the *Bp C. elegans* infection model into BSL2 labs would allow for greater access to an animal model and allow further verification of data beyond cell infection models. We demonstrated that our *Bp* 1026b Δ*asd* mutant, B0011, can replace wildtype 1026b in the typical survival and prolonged killing assays. A whole organism intracellular replication model was also introduced so, if desired, a virulence factor's effect on intracellular replication at the animal level could be investigated. Bright-field videography of our B0011 infecting *C.elegans* in

virulence screens could be used in concert with high-throughput image analysis applications such as the recently published WormToolbox [49]. Fluorescent protein tagged B0011 can be visualized in the worm gut allowing studies such as *in vivo* observation of competition. Several virulence factor mutants were compared in their ability to kill *C. elegans*. The nature of the virulence factor under investigation will determine which *C. elegans* assay will demonstrate attenuation. It must be taken into account that during the fast-killing assay *C. elegans* are in constant contact with the bacteria that are also constantly ingested. In the slow-killing assay we saw the largest impact with a putative attachment factor mutant that our lab has been investigating. The brief exposure of the nematodes to the bacteria would necessitate efficient attachment for virulence factor-mediated damage to occur. This work has also introduced a new animal feeding model with the mealworm *Tenebrio molitor*. The mealworm-feeding model is very easy to use with mealworms being freely available at your neighborhood pet shop, such as PETCO®. The model also allows for tissue dissemination studies that can be difficult at the size of the nematode and the ease of removing the entire digestive tract quickly provides another benefit to this model. The role of LPS in invertebrate pathogenesis was verified in the various models. Previous works found no effect on pathogenesis but experimental design flaws of the initial study are believed to be the reason [23]. The T6SS-5 also contributed to invertebrate killing in the models tested, verifying its important role in animal pathogenesis.

We already demonstrated the usefulness of these models by discovering a novel intracellular niche occupied by *Bp* during acute and chronic infections that had not been observed in available models. Besides the innate costs of running a BSL3, time-lapse bright field and fluorescent microscopy equipment can be costly as well as cumbersome. Movement of these animal/cell infection models and assays to the BSL2 allows for much simpler observation and a

decrease in redundant, sometimes expensive, equipment. The ability to study *Bp* pathogenesis in BSL2 model systems should accelerate the already burgeoning field and help reduce research costs. Lastly, we also developed and tested two new Δ*asd Bp* strains. *Bp* K96243 is a very popular type strain in *Bp* infection investigations. *Bp* MSHR487 is an Australian strain from a chronic type infection. Both strains were found to be avirulent in BALB/c mice with no bacteria recovered from inside the animals. These strains have been excluded from the select agent regulations by the CDC and are available after entity specific exclusion is obtained. There are now 4 SA excluded strains of *Bp* available, 3 prodcued in our lab, and with the diversification of strain background could be used in various investigations of *Bp* pathogenesis.

5.6 ACKNOWLEDGEMENTS

This research was supported by award number AI065359 from the NIAID Pacific Southwest Regional Center of Excellence and by the NIGMS Center of Biomedical Research Excellence grant 5P20RR018727 of the National Institutes of Health to TTH. Thanks to Tina Carvalho for SEM sample preparation and training at the Biological Electron Microscope Facility the University of Hawaii at Manoa.

5.7 FIGURE LEGENDS

Figure 1. Growth curve of B0011 on various media and compared to wildtype. Growth of B0011 on LB agar was slower than on media with lower salt concentrations and a comprehensive growth curve using a Biotek plate reader was used to compare growth rates in different salted media. (A) Salt does affect the growth of B0011 and can be seen in comparing LB-Lennox broth (green line, 0.5% NaCl) to no salt LB broth (blue line, 0.0% NaCl). LB miller broth (1% NaCl) was not tested because of a long growth lag in this media. (B) When 200 μg/ml DAP is added to the media B0011 grows the same as wildtype 1026b and without DAP, B0011 cannot grow in no salt LB.

Figure 2. Invasion and replication assays of B0011 in several cell types. A) Invasion assays were carried out by infecting the indicated cell lines with B0011 and wildtype 1026b. DMEM was supplemented with 250 ug/ml DAP for the mutant. There was some variability between cell lines, but the variability in invasiveness between the WT and the Δ*asd* mutant was not significant as determined by the student t-test. Replication assays were also performed on B) HEK 293T, C) BV2 murine microglial, D) CHME, human microglial, E) HTB-11, human neuroblastoma, and F) RAW264.7 macrophage cells. Infection of 293T cells by the mutant was similar to the WT. The remaining cell lines showed a decrease at the initial time-points. Bacterial numbers plateaued and persisted for up to 2 weeks pi. Each time point is done in triplicate with the error bars showing the SEM (not visible at this scale).

Figure 3. B0011 infects 293T and HeLa cells and causes plaques similar to wildtype. B0011 was tested in many cell lines. Intracellular replication of B0011 was most comparable to

wildtype 1026b in 293T cells (A) and HeLa (B). Phase contrast microscopy indicated cell fusion, bacterial replication, and host-cell lysis were occurring similarly to virulent *Bp* 1026b in the infection model at 24 and 48 hpi (C,D). Without DAP, B0011 was unable to create plaques in 293T cell monolayers. Plaques formed in the same time frame as wildtype infections when infecting 293T cells with B0011 in the presence of DAP within agarose overlays (F,G).

Figure 4. B0011 live-cell fusion and infection events using time-lapse microscopy. B0011 was used to infect monolayers consisting of two strains of HEK293 cells, each expressing either cytoplasmic GFP or RFP. When neighboring cells fuse and cytoplasm mixes, a yellow color is produced [22]. (A) Using live-cell time-lapse fluorescent microscopy (every 5 min for 30 h, above) of cell fusion all the way to plaque formation. (B) At higher magnification the moment of cell fusion and infectious processes such as actin polymerization are observed (top), and tracking software can track individual bacteria in live cells at BSL2 (blue and green lines; every 1 min for 4 h, bottom).

Figure 5. B0011 used with the *C. elegans* infection model at BSL2. In A), 30 *C. elegans* nematodes grown on *E.coli* OP50 to the L2 stage were transferred to a plate containing either *B. thailandensis* E264, B0011*, or E. coli* OP50. Nematodes were checked for movement at the indicated time-points and verified by gentle prodding. Survival % was determined to be the number of live animals/total number of animals and is the SEM of three experiments. B) 30 animals were exposed to the 1026b Δ*asd* mutant or *E. coli* food source for 30 m then transferred onto *E. coli* lawns. Survival percentages are presented as Kaplan Meier survival curves in 3 independent experiments. C) Whole organism intracellular replication assay. Nematodes were

used in a modified intracellular invasion assay then lysed to determine intracellular bacteria. D, E, F, G, H) B0011 kills *C. elegans* in a dose dependent manner with the major contributor being live-cells and mainly the T6SS-1 surface component HcpI. I) Fast-killing assay on *Bp* mutants of known and putative virulence factor. 20 *C. elegans* were placed on plates containing the indicated *Bp* strain and survival % measured. Performed in triplicate with the SEM shown. J) Slow-killing assay on *Bp* mutants of known and putative virulence factors. 20 *C. elegans* were exposed to $1x10^6$ CFU of the indicated *Bp* strain for 30 m. Surival % is shown from an experiment done in triplicate with the SEM shown.

Figure 6. B0011 in the *Tenebrio molitor* mealworm-feeding model. B0011 is able to kill the mealworm *T. molitor* through feeding, (A). We found that the T6SS-1 *hcpI* is not important for killing of the worm in this particular feeding model. Combining numbers form three independent experiments generated the Kaplan-meir curve. B) Diagram of *T. molitor* anatomy (external, top; internal digesive tract anatomy, bottom). C) Bright field image of the *gfp*-tagged B0011 infected excised *T. molitor* digestive tract at 20X magnification (top). Green fluorescent channel of the same images (middle). Magnified images of the indicated insets at 63X in the green channel (bottom).

Figure 7. BALB/c attenuation studies using two newly excluded *Bp* Δ*asd* mutants. A) Survival curve of five BALB/c mice infected intranasally with $1x10^7$ CFU of the *Bp* K96243 Δ*asd* mutant. B) Survival curve of five BALB/c mice infected intranasally with $1x10^7$ CFU of the *Bp* MSHR487 Δ*asd* mutant. 3,000 CFU of wildtype killed all five mice by 3 dpi. All mice infected with Δ*asd* mutants survived the 60-day study. C and D) Bacterial organ loads of lung,

liver, and spleens of all Δ*asd* mutant infected mice. No bacteria were detected in either *Bp* K96243 Δ*asd* mutant or MSHR487 Δ*asd* mutant infected mice, respectively.

Figure 8. Proposed *Bp* cellular pathogenesis model including endonuclear niche. *Bp* (purple) attach and are internalized using unknown bacterial gene products and host-cell surface receptors (yellow). Once internalized the bacteria escape the endosome utilizing the $T3SS_{Bsa}$ and move within the host cell by using flagella or by polymerzing host cell actin utilizing BimA. *Bp* can then enter the host cell nucleus (green) via active penetration of the nuclear envelope or become trapped after reformation of the envelope following mitosis. Bacteria can then be passed to daughter cells during replication, or form MNGCs with neighboring cells by actin-based membrane protrusion or direct membrane fusion using T6SS.

Figure S1. Exogenous DAP can allow B0011 to infect many cell types. The indicated cell lines were first grown in various concentrations of DAP alone to control for possible DAP toxicity. Cell lines appeared healthy up to 2,000 μg/ml of DAP (data not shown). The adequate concentration was first determined in all cell lines by supplementing DMEM/ 10% FBS with 0 μg/ml to 2,000 μg/ml of DAP at the indicated increments. As expected, bacteria were not recoverable from any of the cell lines 18 hpi without DAP present. Interestingly, a trend appeared that as the exogenous DAP concentration was increased the CFU recovered at 18 hpi decreased in most cell lines. A) BV-2, murine microglial cell line. B), CHME, human microglial cell line. C), HeLa, human epithelial cell line. D), HTB-11, human neuroblastoma cell line. E) RAW264.7, murine macrophage cell line. The bottom row are phase contrast microscopy

pictures taken 24 hpi at 600X. Carets indicate B0011 bacteria protruding from host-cells at 18 hpi.

Figure S2. Differential infection by various *Bp* strains. A) HeLa and B) RAW264.7 cells were infected with 9 strains of *Bp* isolated from various sources and their cognate Δ*asd* mutants produced previously (Table 1 and [9]) by lambda RED recombination. The data shown is the average of two independent 24 h intracellular replication experiments at an MOI of 1:1 with the SEM. Strains cause differential infection, particularly WT Bp6340 from a chronic case grows less than all the other strains tested in both cell lines. Adaptation to a chronic lifestyle could allow the bacteria to reach a homeostasis with the host cell and might explain why levels of the Bp6340 Δ*asd* are similar to wildtype *Bp* 1026b in the infected RAW monolayers after 24 h.

Figure S3. *Bp* 1026b Δ*asd* persistently infects some cell lines *in vitro*. Besides 293T cells, the replication assay and initial microscopy indicated that the cell lines remain infected with B0011 far beyond the normal *in vitro* "acute" infection time of ~24 h. Monolayers were infected at an MOI of 10:1 and media containing 750 μg/ml amikacin, 750 μg/ml of kanamycin, and 250 μg/ml DAP. Every 3 days, fresh media was added to the monolayers. Pictures are representative images at different time points taken from video clips during the course of infection. Carets indicate infecting bacteria. A) BV2, murine microglial cell line at 5 d.p.i. (100X) and 9 d.p.i. (40X), B) CHME, human microglial cell line at 16 d.p.i (100X) and 18 d.p.i (100X). Spheres containing tightly packed, motile bacteria are seen predominantly at later stages in many cell types. C) HTB-11, human neuroblastoma cells at 4 d.p.i. (60X) and at 22 d.p.i. (100X) a cell full of

bacteria (boxed). D) RAW264.7, murine macrophages at 7 d.p.i. (20X) and MNGC bounding a plaque at 10 d.p.i. (20X).

Figure S4. During *in vitro* infection, both *B.pseudomallei* 1026b Δ*asd* strain (B0011) and wildtype 1026b replicate in the host-cell nucleus. The presence of near-perfect spheres containing tightly packed, motile bacteria in Fig. 5 was identified as intra-nuclear bacteria close observation of live cell time-lapse video . HTB-11 cells 8 d.p.i. containing *gfp*-tagged B0011 within a daughter nuclei of an undivided neuroblastoma cell. A) Green fluorescent channel. B) DIC bright field channel. C) Green fluorescent channel and brightfield overlay. D) TEM image of a RAW264.7 macrophage MNGC containing two nuclei with carets indicating endonuclear WT *Bp* 1026b at 1.2 kX magnification. E) TEM close-up image of a RAW264.7 nucleus containing six endonuclear bacteria at 4.0 kX magnification, two of which are indicated by carets. F) TEM image of a large nucleus without a cell membrane containing hundreds of endonuclear bacteria. G) RAW264.7 monolayer infected by WT *Bp* 1026b at 24 h. Nuclei are dyed blue with DAPI and the cell membranes are dyed red with FM 4-64X lipohilic dye. The blue, red, and DIC brightfield images are overlaid. The caret indicates two intact nuclei that have lost the cell membrane and remain floating in the media.

Figure S5. The *Bp* 1026b Δ*asd* mutant (B0011) can be used in the *C. elegans* infection model. Nematodes were used in a modified intracellular invasion assay then lysed to determine intracellular bacteria counts. D) Green fluorescent image of *gfp*-tagged B0011 within the lumen of *C. elegans.* E) Time-lapse imaging of healthy worms compared to those fed strain B0011 as nutrient source. F) *gfp*-tagged B0011 are visible in the *C. elegans* gut. G) Fluorescent time-lapse

imaging of live infected *C. elegans*. The *gfp*-tagged bacteria are visible in the gut of the moving animal.

Supplemental videos:

Video 1: 293T cells 48 hpi a large amount of protruding and intracellular B0011 bacteria can be seen in this 5 m time-lapse video of Figure 3D.

Video 2: Red and green fluorescent 293 cells being infected with B0011. Time-lapse fluorescent microscopy of Figure 4A. Bright field is on the left and fluorescent channels on the right. Each frame is 5 minutes taken for 24 hours.

Video 3: DIC time-lapse microscopy of Figure 4B. B0011 was used to infect 293T cells. A picture was captured every minute for 5 hours. The image on the left is unmodified. The image on the right tracks two bacteria through the fusion of the neighboring cells.

Video 4: A short video of a healthy *C. elegans* nematode beside a B0011 infected nematode for comparison.

Video 5: A short fluorescent video taken of *C. elegans* after being fed *gfp*-tagged B0011.

Video 6: A short time-lapse video of B0011 infected BV-2 cells in Figure 5A 9 dpi.

Video 7: A short time-lapse video of B0011 infected CHME cells 16 dpi from Figure 5B. Spheres containing packed moving bacteria are visible.

Video 8: A short time-lapse video from Figure 5C of B0011 infected HTB-11 cells 22 dpi. The host-cell is still alive and is tightly packed with bacteria.

Video 9: A short time-lapse video from Figure 6B of B0011 infecting the nucleus of HTB-11 cells 22 dpi.

TABLE 1. Bacterial strains and plasmids used in this study[a]

Strains	Lab ID[b]	Relevant properties	Sources
E. coli			
EOP50		*E. coli* B strain uracil auxotroph for *C. elegans* maintenance	[50]
EOP50-rif		Rif^r; *E. coli* B strain uracil auxotroph spontaneous rifampicin resistant mutant for *C. elegans* maintenance	This study
B. pseudomallei			
1026b	B0004	Type-strain; clinical melioidosis isolate	[51]
1026b-Δ*asd*::*gat-FRT*	B0011	GS^r; 1026b with *gat* cassette inserted in the asd_{Bp} gene	[5]
1026b-Δ*asd*::*gat-FRT*/ *att*Tn7-*kan-gfp*	X0004	GS^r, Km^r; 1026b Δ*asd*::*gat-FRT* mutant with mini-Tn7-*kan-gfp* integrated	This study
Bp0085	B0040	WT strain; clinical strain from a sepsis case (fatal) in Thailand, 2006	[9]
Bp0085-Δ*asd*::*pheS-gat*	B0079	GS^r; Bp0085 with *pheS-gat-FRT* fragment replacing the *asd* gene	[9]
Bp0091	B0042	WT strain; clinical strain from a sepsis case (fatal) in Thailand, 2006	[9]
Bp0091-Δ*asd*::*pheS-gat*	B0080	GS^r; Bp0091 with *pheS-gat-FRT* fragment replacing the *asd* gene	[9]
Bp0094	B0044	WT strain; clinical strain from a sepsis case (fatal) in Thailand, 2006	[9]
Bp0094-Δ*asd*::*pheS-gat*	B0081	GS^r; Bp0094 with *pheS-gat-FRT* fragment replacing the *asd* gene	[9]
Bp4001	B0054	WT strain; environmental isolate from soil in Australia, 1997	[9]
Bp4001-Δ*asd*::*pheS-gat*	B0082	GS^r; Bp4001 with *pheS-gat-FRT* fragment replacing the *asd* gene	[9]
Bp4003	B0058	WT strain; clinical strain from a sepsis case (fatal) in Australia, 1999	[9]
Bp4003-Δ*asd*::*pheS-gat*	B0083	GS^r; Bp4003 with *pheS-gat-FRT* fragment replacing the *asd* gene	[9]
Bp4122	B0064	WT strain; environmental isolate from soil in Australia, 2006	[9]
Bp4122-Δ*asd*::*pheS-gat*	B0084	GS^r; Bp4122 with *pheS-gat-FRT* fragment replacing the *asd* gene	[9]
Bp4141	B0066	WT strain; clinical isolate from chronic case (survived) in Australia, 1991	[9]
Bp4141-Δ*asd*::*pheS-gat*	B0085	GS^r; Bp4141 with *pheS-gat-FRT* fragment replacing the *asd* gene	[9]
Bp4144	B0068	WT strain; clinical isolate from chronic case (survived) in Australia, 1995	[9]
Bp4144-Δ*asd*::*pheS-gat*	B0086	GS^r; Bp4144 with *pheS-gat-FRT* fragment replacing the *asd* gene	[9]
Bp6340	B0078	WT strain; clinical isolate from chronic case (survived) in Australia, 2003	[9]
Bp6340-Δ*asd*::*pheS-gat*	B0087	GS^r; Bp6340 with *pheS-gat-FRT* fragment replacing the *asd* gene	[9]

[a] Abbreviations: *asd, B. pseudomallei* aspartate semi-aldehyde dehydrogenase encoding gene; *FRT*- yeast 2 μm plasmid recombination target; *gat*, gene encoding glyphosate acetyltransferase; GS^r, glyphosate resistant; *gfp,* green fluorescent protein encoding gene; Km^r, kanamycin resistant; *pheS*- engineered mutant version of the α-subunit of phenylalanyl tRNA synthase; Rif^r, rifampicin resistant.

[b] Please use laboratory identification number (Lab ID) when requesting strains and plasmids. Request of select agent bacteria requires entity specific approval and requests may not be granted

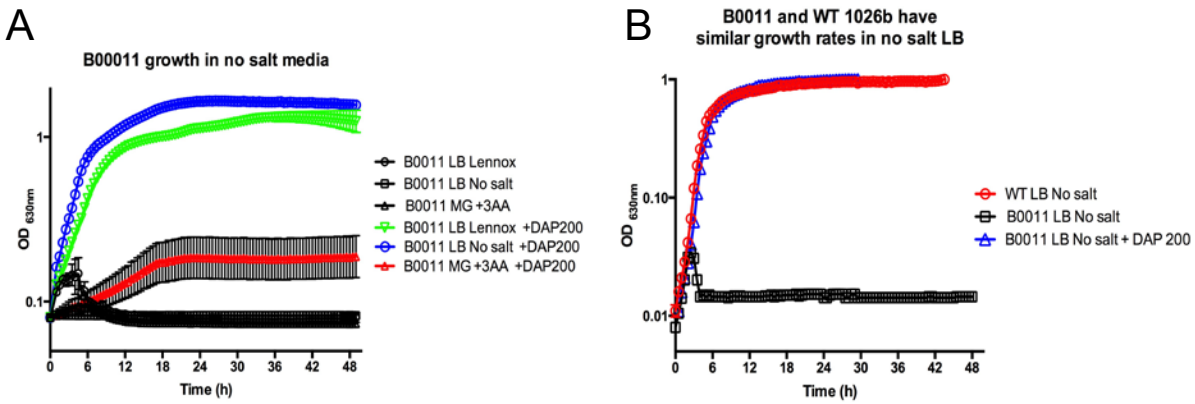
A
B00011 growth in no salt media
OD 630nm
1
0.1
0 6 12 18 24 30 36 42 48
Time (h)
B0011 LB Lennox
B0011 LB No salt
B0011 MG +3AA
B0011 LB Lennox +DAP200
B0011 LB No salt +DAP200
B0011 MG +3AA +DAP200
B
B0011 and WT 1026b have similar growth rates in no salt LB
OD 630nm
1
0.10
0.01
0 6 12 18 24 30 36 42 48
Time (h)
WT LB No salt
B0011 LB No salt
B0011 LB No salt + DAP 200

Figure 1

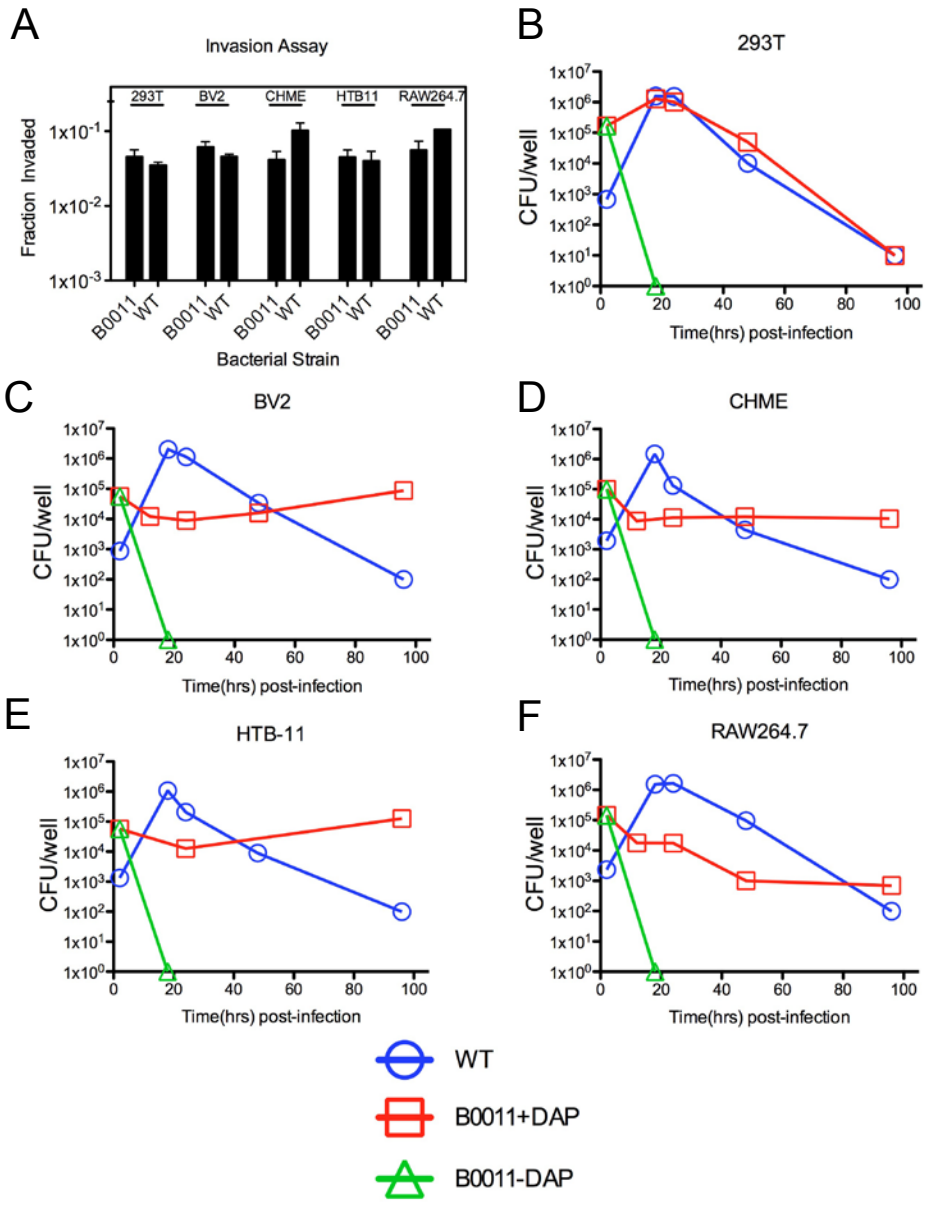
A
Invasion Assay
293T
BV2
CHME
HTB11
RAW264.7
Fraction Invaded
1x10-1
1x10-2
1x10-3
B0011
WT
Bacterial Strain
B
293T
CFU/well
Time(hrs) post-infection
C
BV2
D
CHME
E
HTB-11
F
RAW264.7
WT
B0011+DAP
B0011-DAP

Figure 2

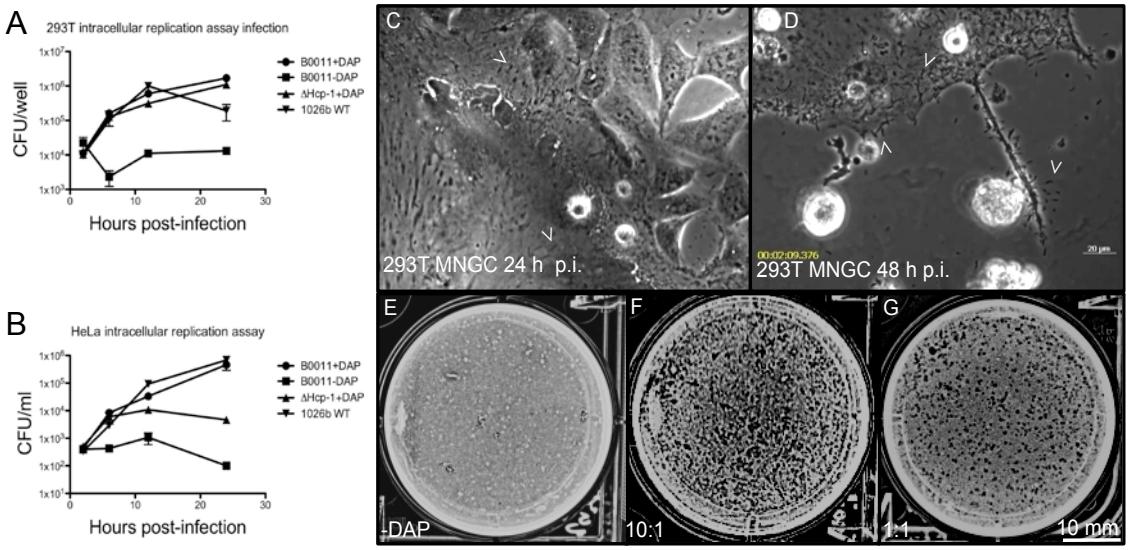

Figure 3 and Video1

A

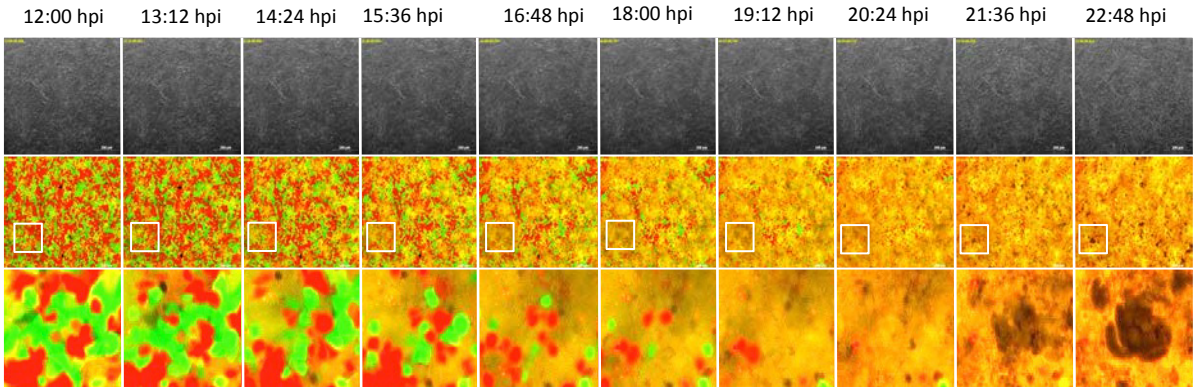

B

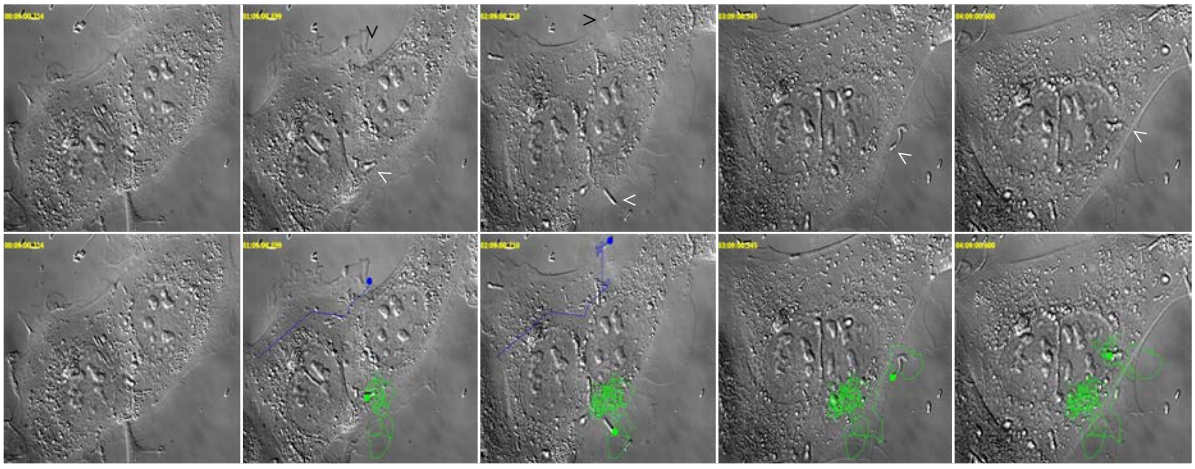

Figure 4 and Videos 2 and 3

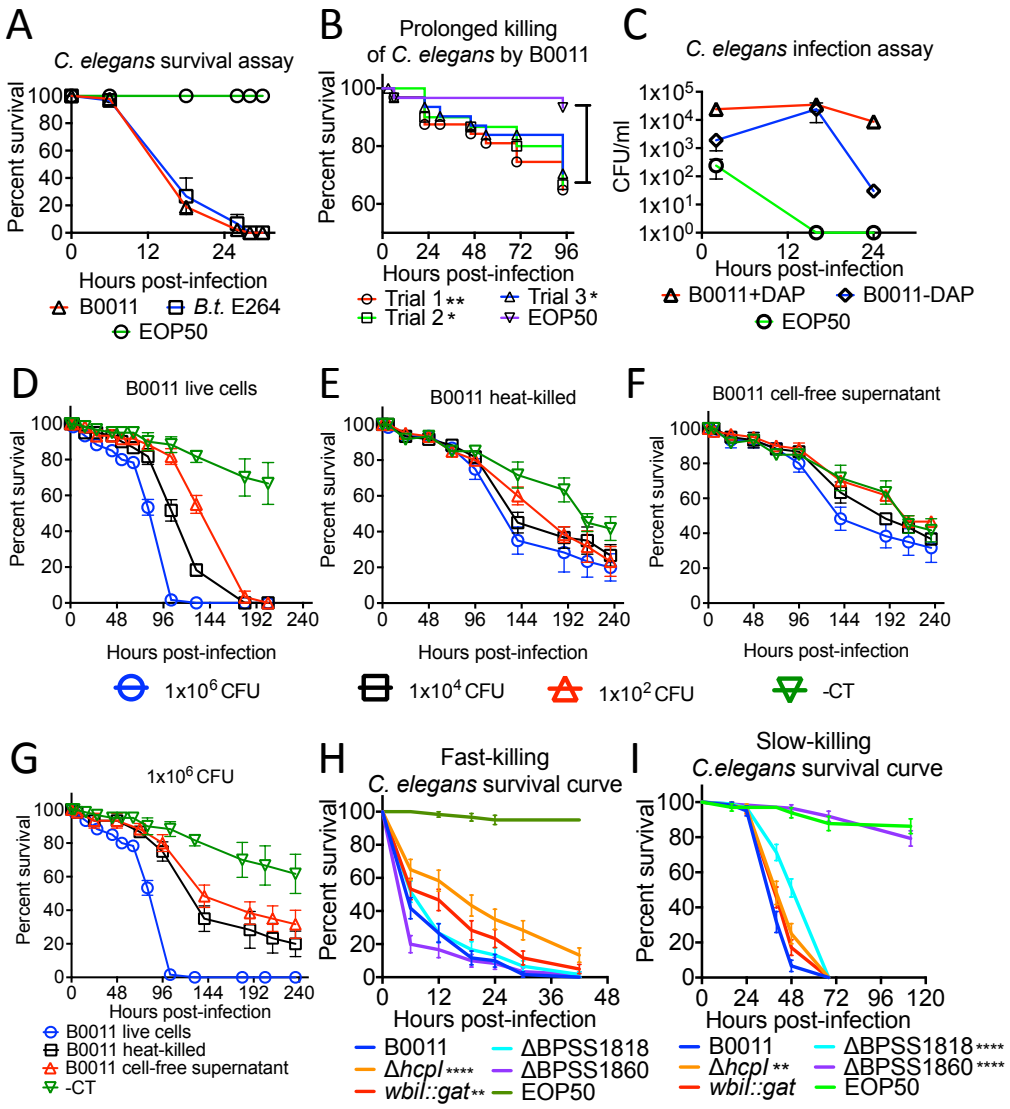

Figure 5 and Video 4

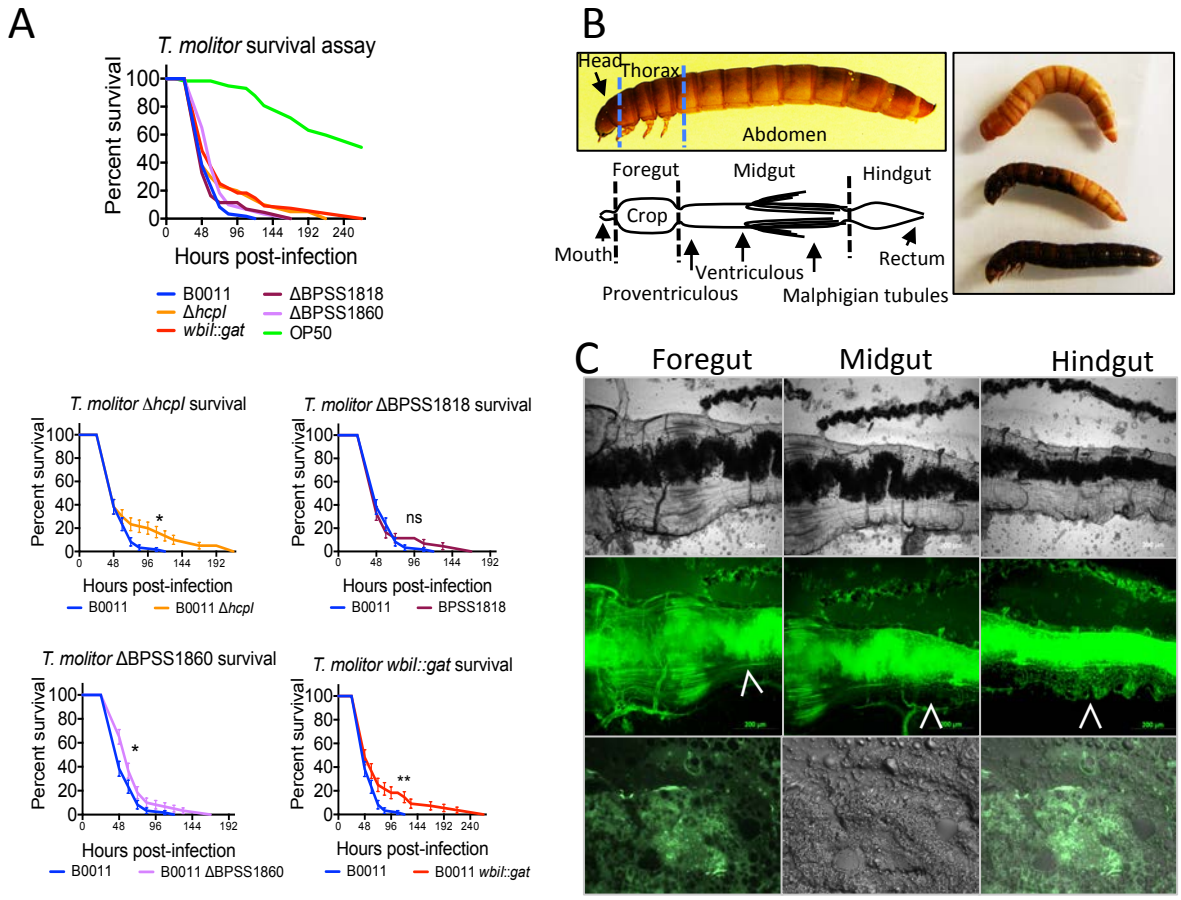
A
T. molitor survival assay
Percent survival
Hours post-infection
B0011
Δhcpl
wbil::gat
ΔBPSS1818
ΔBPSS1860
OP50
T. molitor Δhcpl survival
T. molitor ΔBPSS1818 survival
T. molitor ΔBPSS1860 survival
T. molitor wbil::gat survival
ns
B
Head
Thorax
Abdomen
Foregut
Midgut
Hindgut
Crop
Mouth
Proventriculous
Ventriculous
Malphigian tubules
Rectum
C
Foregut
Midgut
Hindgut

Figure 6

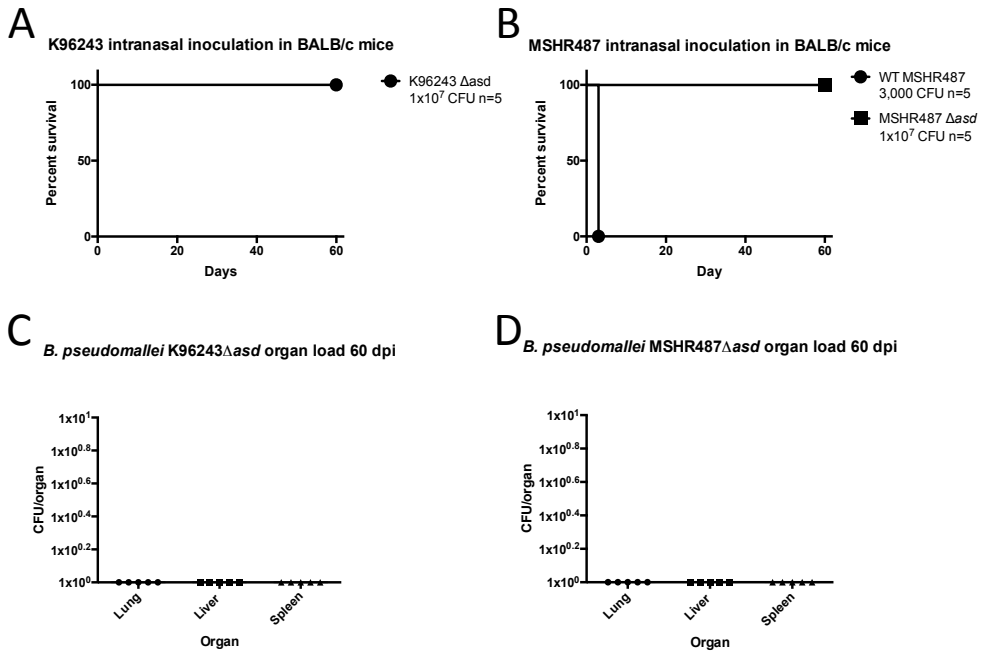
A
K96243 intranasal inoculation in BALB/c mice
Percent survival
Days
K96243 Δasd
1x10^7 CFU n=5
B
MSHR487 intranasal inoculation in BALB/c mice
Percent survival
Day
WT MSHR487
3,000 CFU n=5
MSHR487 Δasd
1x10^7 CFU n=5
C
B. pseudomallei K96243Δasd organ load 60 dpi
CFU/organ
Lung
Liver
Spleen
Organ
D
B. pseudomallei MSHR487Δasd organ load 60 dpi
CFU/organ
Lung
Liver
Spleen
Organ

Figure 7

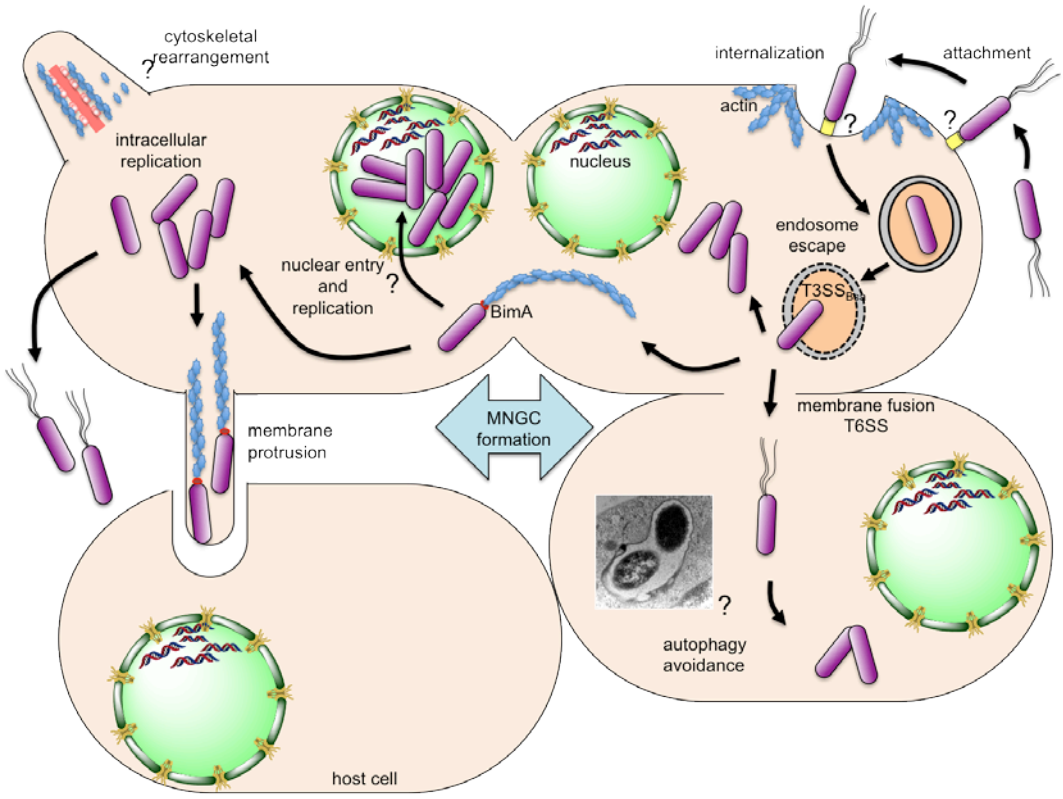
cytoskeletal rearrangement
?
intracellular replication
nuclear entry and replication
?
nucleus
BimA
internalization
attachment
actin
?
?
endosome escape
T3SS$_{BI}$
membrane fusion T6SS
MNGC formation
membrane protrusion
?
autophagy avoidance
host cell

Figure 8

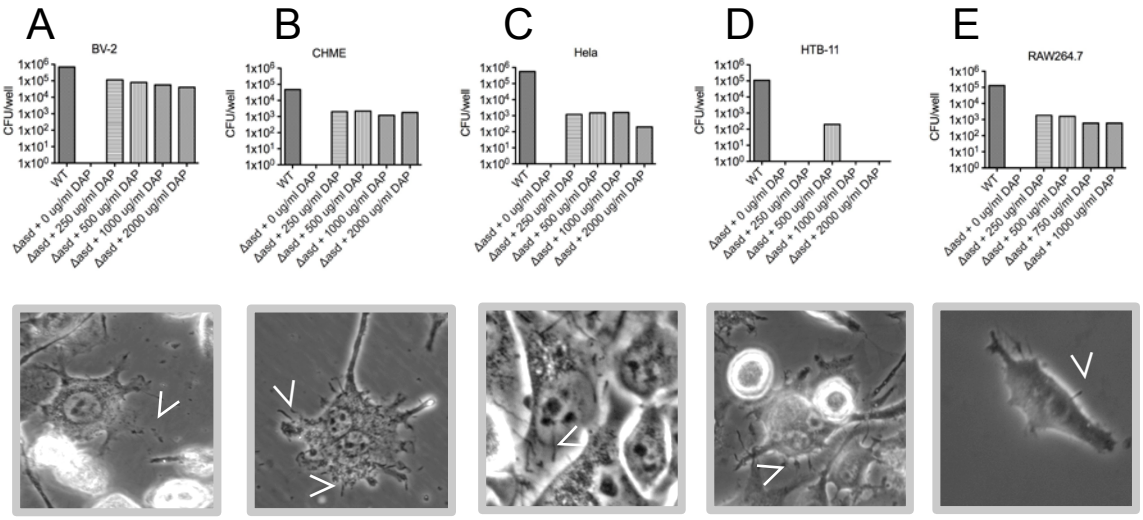
A
BV-2
B
CHME
C
Hela
D
HTB-11
E
RAW264.7
CFU/well
WT
Δasd + 0 ug/ml DAP
Δasd + 250 ug/ml DAP
Δasd + 500 ug/ml DAP
Δasd + 750 ug/ml DAP
Δasd + 1000 ug/ml DAP
Δasd + 2000 ug/ml DAP

Figure S1

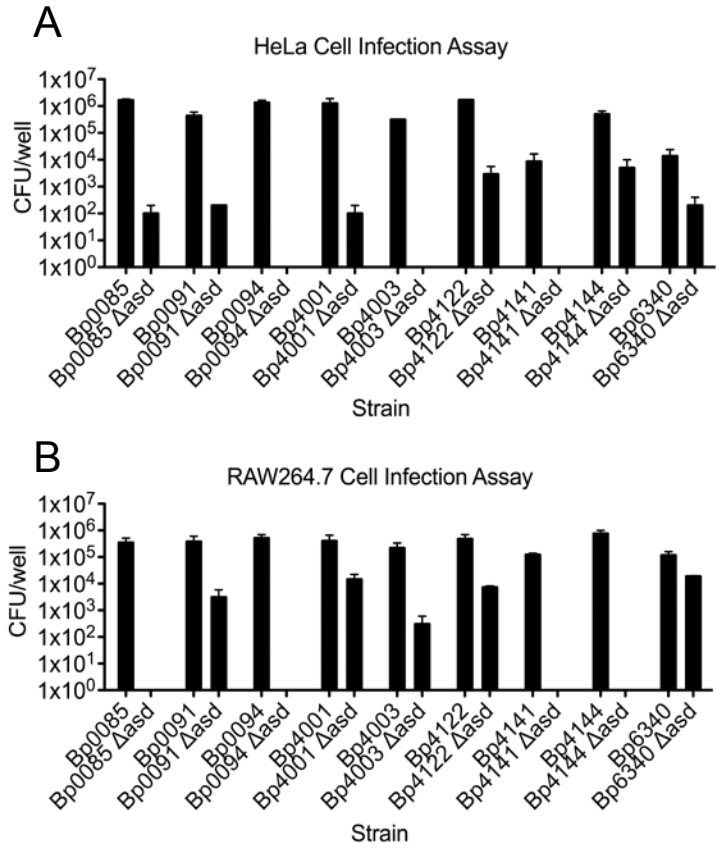
A
HeLa Cell Infection Assay
CFU/well
1x10^7
1x10^6
1x10^5
1x10^4
1x10^3
1x10^2
1x10^1
1x10^0
Bp0085
Bp0085 Δasd
Bp0091
Bp0091 Δasd
Bp0094
Bp0094 Δasd
Bp4001
Bp4001 Δasd
Bp4003
Bp4003 Δasd
Bp4122
Bp4122 Δasd
Bp4141
Bp4141 Δasd
Bp4144
Bp4144 Δasd
Bp6340
Bp6340 Δasd
Strain
B
RAW264.7 Cell Infection Assay
CFU/well
1x10^7
1x10^6
1x10^5
1x10^4
1x10^3
1x10^2
1x10^1
1x10^0
Bp0085
Bp0085 Δasd
Bp0091
Bp0091 Δasd
Bp0094
Bp0094 Δasd
Bp4001
Bp4001 Δasd
Bp4003
Bp4003 Δasd
Bp4122
Bp4122 Δasd
Bp4141
Bp4141 Δasd
Bp4144
Bp4144 Δasd
Bp6340
Bp6340 Δasd
Strain

Figure S2

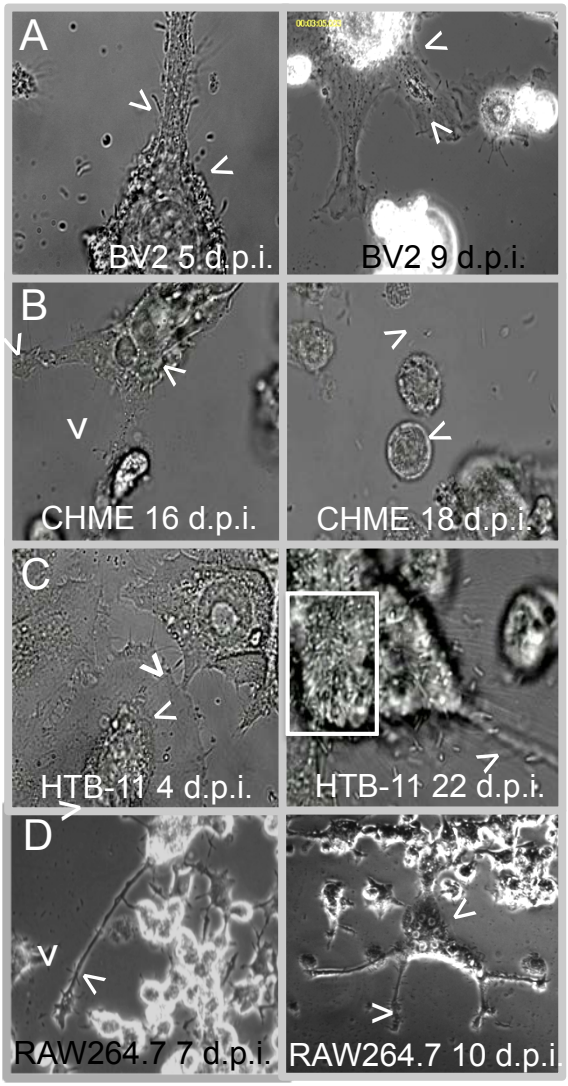
A
BV2 5 d.p.i.
BV2 9 d.p.i.
B
CHME 16 d.p.i.
CHME 18 d.p.i.
C
HTB-11 4 d.p.i.
HTB-11 22 d.p.i.
D
RAW264.7 7 d.p.i.
RAW264.7 10 d.p.i.

Figure S3

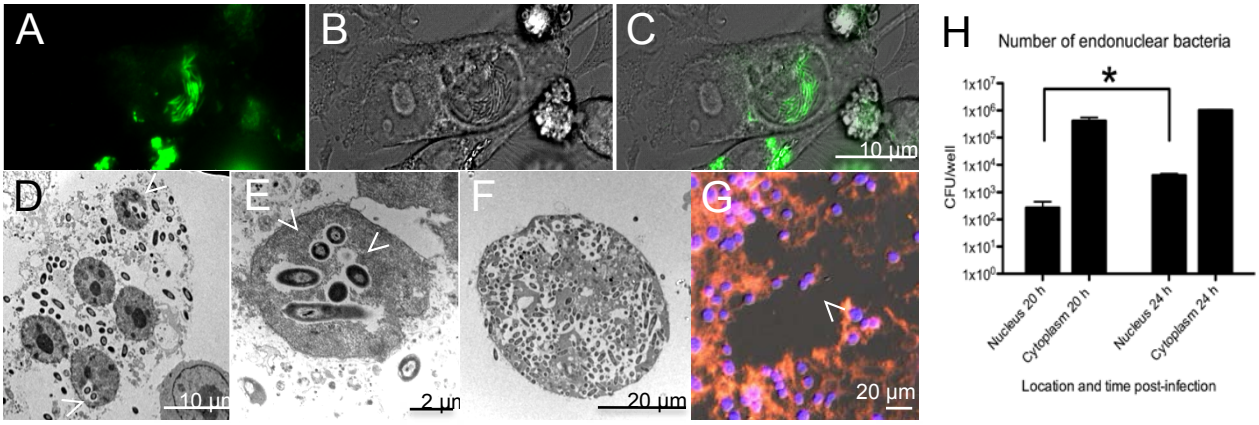
A
B
C
10 µm
D
E
F
G
10 µm
2 µm
20 µm
20 µm
H
Number of endonuclear bacteria
*
CFU/well
1x10^7
1x10^6
1x10^5
1x10^4
1x10^3
1x10^2
1x10^1
1x10^0
Nucleus 20 h
Cytoplasm 20 h
Nucleus 24 h
Cytoplasm 24 h
Location and time post-infection

Figure S4

5.8 REFERENCES

1. Cheng AC, Currie BJ (2005) Melioidosis: Epidemiology, Pathophysiology, and Management. Clin Microbiol Rev 18: 383-416.

2. Dance DAB (1991) Melioidosis: the Tip of the Iceberg? Clin Microbiol Rev 4: 52-60.

3. Wiersinga WJ, van der Poll T, White NJ, Day NP, Peacock SJ (2006) Melioidosis: insight into the pathogenicity of *Burkholderia pseudomallei*. Nat Rev Microbiol 4: 272-282.

4. (2002) Public Health Security and Bioterrorism Preparedness and Response Act 107th ed.

5. Norris MH, Kang Y, Lu D, Wilcox BA, Hoang TT (2009) Glyphosate resistance as a novel select-agent-compliant, non-antibiotic selectable-marker in chromosomal mutagenesis of the essential genes *asd* and *dapB* of *Burkholderia pseudomallei*. Appl Environ Microbiol 75: 6062-6075.

6. Norris MH, Propst KL, Kang Y, Dow SW, Schweizer HP, et al. (2011) The *Burkholderia pseudomallei* {delta} *asd* mutant exhibits attenuated intracellular infectivity and imparts protection against acute inhalation melioidosis in mice. Infection and Immunity 79: 4010-4018.

7. Richmond JY, and R.W. McKinney (2007) Biosafety in microbiological and biomedical laboratories. Atlanta, GA: Centers for Disease Control and Prevention.

8. Barrett AR, Kang, Y., Inamasu, K. S., Son, M. S., Vukovich, J. M., and Hoang, T. T. (2008) Genetics tools for allelic-replacement in *Burkholderia* species. Appl Environm Microbiol 74: 4498-4508.

9. Kang Y, Norris MH, Wilcox BA, Tuanyok A, Keim PS, et al. (2011) Knockout and pullout recombineering for naturally transformable *Burkholderia thailandensis* and *Burkholderia pseudomallei*. Nat Protocols 6: 1085-1104.

10. Norris MH, Kang Y, Wilcox B, Hoang TT (2010) Stable, site-specific fluorescent tagging constructs optimized for *Burkholderia* species. Appl Environ Microbiol 76: 7635-7640.

11. Biedler JL, Helson L, Spengler BA (1973) Morphology and Growth, Tumorigenicity, and Cytogenetics of Human Neuroblastoma Cells in Continuous Culture. Cancer Research 33: 2643-2652.

12. Seeger RC, Rayner SA, Banerjee A, Chung H, Laug WE, et al. (1977) Morphology, growth, chromosomal pattern, and fibrinolytic activity of two new human neuroblastoma cell lines. Cancer Research 37: 1364-1371.

13. Wu C, Lu Y (2010) High-titre retroviral vector system for efficient gene delivery into human and mouse cells of haematopoietic and lymphocytic lineages. Journal of General Virology 91: 1909-1918.

14. Janabi N, Peudenier S, Héron B, Ng KH, Tardieu M (1995) Establishment of human microglial cell lines after transfection of primary cultures of embryonic microglial cells with the SV40 large T antigen. Neuroscience Letters 195: 105-108.

15. Bocchini V, Mazzolla R, Barluzzi R, Blasi E, Sick P, et al. (1992) An immortalized cell line expresses properties of activated microglial cells. Journal of Neuroscience Research 31: 616-621.

16. Garcea RL, Schachat F, Epstein HF (1978) Coordinate synthesis of two myosins in wild-type and mutant nematode muscle during larval development. Cell 15: 421-428.

17. Law RJ, Hamlin JNR, Sivro A, McCorrister SJ, Cardama GA, et al. (2008) A functional phenylacetic acid catabolic pathway is required for full pathogenicity of *Burkholderia cenocepacia* in the *Caenorhabditis elegans* host model. Journal of Bacteriology 190: 7209-7218.

18. Ward S, Miwa J (1978) Characterization of temperature-sensitive, fertilization-defective mutants of the nematode *Caernohabditis elegans*. Genetics 88: 285-303.

19. A. Latifi MF, K. Tanaka, P. Williams, A. Lazdunski (1996) A hierarchical quorum-sensing cascade in *Pseudomonas aeruginosa* links the transcriptional activators LasR and RhlR (VsmR) to expression of the stationary-phase sigma factor RpoS. Molecular Microbiology 21: 1137-1146.

20. Jones AL, Beveridge TJ, Woods DE (1996) Intracellular survival of *Burkholderia pseudomallei*. J Bacteriol 64: 782-790.

21. Kespichayawattana W, Rattanachetkul S, Wanun T, Utaisincharoen P, Sirisinha S (2000) *Burkholderia pseudomallei* induces cell fusion and actin-associated membrane protrusion: a possible mechanism for cell-to-cell spreading. Infect Immun 68: 5377-5384.

22. French CT, Toesca IJ, Wu T-H, Teslaa T, Beaty SM, et al. (2011) Dissection of the *Burkholderia* intracellular life cycle using a photothermal nanoblade. Proceedings of the National Academy of Sciences 108: 12095-12100.

23. O'Quinn AL, Wiegand EM, Jeddeloh JA (2001) *Burkholderia pseudomallei* kills the nematode *Caenorhabditis elegans* using an endotoxin-mediated paralysis. Cellular Microbiology 3: 381-393.

24. Lee S-H, Ooi S-K, Mahadi NM, Tan M-W, Nathan S (2011) Complete killing of *Caenorhabditis elegans* by *Burkholderia pseudomallei* is dependent on prolonged direct association with the viable pathogen. PLoS ONE 6: e16707.

25. Jia K, Thomas C, Akbar M, Sun Q, Adams-Huet B, et al. (2009) Autophagy genes protect against *Salmonella typhimurium* infection and mediate insulin signaling-regulated

pathogen resistance. Proceedings of the National Academy of Sciences 106: 14564-14569.

26. Fay D, Bender A (2006) Genetic mapping and manipulation. In: Community TCeR, editor. WormBook.

27. Stiernagle T (February 11, 2006) Maintenance of *C. elegans*. In: Community TCeR, editor. WormBook: WormBook.

28. Choi K-H, Mima T, Casart Y, Rholl D, Kumar A, et al. (2008) Genetic tools for select-agent-compliant manipulation of *Burkholderia pseudomallei*. Appl Environ Microbiol 74: 1064-1075.

29. Shalom G, Shaw JG, Thomas MS (2007) *In vivo* expression technology identifies a type VI secretion system locus in *Burkholderia pseudomallei* that is induced upon invasion of macrophage. Microbiology 153: 2689-2699.

30. D'Cruze T, Gong L, Treerat P, Ramm G, Boyce JD, et al. (2011) Role for the *Burkholderia pseudomallei* type three secretion system cluster 1 *bpscN* gene in virulence. Infection and Immunity 79: 3659-3664.

31. Uehara A, Fujimoto Y, Kawasaki A, Kusumoto S, Fukase K, et al. (2006) Meso-diaminopimelic acid and meso-lanthionine, amino acids specific to bacterial peptidoglycans, activate human epithelial cells through NOD1. The Journal of Immunology 177: 1796-1804.

32. Heinzen RA, Grieshaber SS, Van Kirk LS, Devin CJ (1999) Dynamics of actin-based movement by *Rickettsia rickettsii* in Vero cells. Infect Immun 67: 4201-4207.

33. Dabiri GA, Sanger JM, Portnoy DA, Southwick FS (1990) *Listeria monocytogenes* moves rapidly through the host-cell cytoplasm by inducing directional actin assembly. Proceedings of the National Academy of Sciences 87: 6068-6072.

34. Price EP, Hornstra HM, Limmathurotsakul D, Max TL, Sarovich DS, et al. (2010) Within-host evolution of *Burkholderia pseudomallei* in four cases of acute melioidosis. PLoS Pathog 6: e1000725.

35. Lieberman TD, Michel J-B, Aingaran M, Potter-Bynoe G, Roux D, et al. (2011) Parallel bacterial evolution within multiple patients identifies candidate pathogenicity genes. Nat Genet 43: 1275-1280.

36. Kespichayawattana W, Intachote P, Utaisincharoen P, Sirisinha S (2004) Virulent *Burkholderia pseudomallei* is more efficient than avirulent *Burkholderia thailandensis* in invasion of and adherence to cultured human epithelial cells. Microbial Pathogenesis 36: 287-292.

37. Shin W, Boo SM, Fritz L (2003) Endonuclear bacteria in *Euglena hemichromata* (*Euglenophyceae*): a proposed pathway to endonucleobiosis. Phycologia 42: 198-203.

38. Ogata H, La Scola B, Audic Sp, Renesto P, Blanc G, et al. (2006) Genome sequence of *Rickettsia bellii* illuminates the role of amoebae in gene exchanges between intracellular pathogens. PLoS Genet 2: e76.

39. Lee S-H, Ooi S-K, Mahadi NM, Tan M-W, Nathan S (2011) Complete killing of *Caenorhabditis elegans* by *Burkholderia pseudomallei* is dependent on prolonged direct association with the viable pathogen. PLoS ONE 6: e16707.

40. Gan Y-H, Chua KL, Chua HH, Liu B, Hii CS, et al. (2002) Characterization of *Burkholderia pseudomallei* infection and identification of novel virulence factors using a *Caenorhabditis elegans* host system. Molecular Microbiology 44: 1185-1197.

41. Burtnick MN, Brett PJ, Harding SV, Ngugi SA, Ribot WJ, et al. (2011) The Cluster 1 Type VI Secretion System Is a Major Virulence Determinant in *Burkholderia pseudomallei*. Infection and Immunity 79: 1512-1525.

42. DeShazer D, Brett PJ, Woods DE (1998) The type II O-antigenic polysaccharide moiety of Burkholderia pseudomallei lipopolysaccharide is required for serum resistance and virulence. Mol Microbiol 30: 1081-1100.

43. Tuanyok A, Stone JK, Mayo M, Kaestli M, Gruendike J, et al. (2012) The genetic and molecular basis of O-antigenic diversity in *Burkholderia pseudomallei* lipopolysaccharide. PLoS Negl Trop Dis 6: e1453.

44. van Schaik EJ, Tom M, Woods DE (2009) *Burkholderia pseudomallei* isocitrate lyase is a persistence factor in pulmonary melioidosis: implications for the development of isocitrate lyase inhibitors as novel antimicrobials. Infect Immun 77: 4275-4283.

45. Goodyear A, Bielefeldt-Ohmann H, Schweizer H, Dow S (2012) Persistent gastric colonization with *Burkholderia pseudomallei* and dissemination from the gastrointestinal tract following mucosal inoculation of mice. PLoS ONE 7: e37324.

46. Lebreton A, Lakisic G, Job V, Fritsch L, Tham TN, et al. (2011) A bacterial protein targets the BAHD1 chromatin complex to stimulate type III interferon response. Science 331: 1319-1321.

47. Bierne H, Cossart P (2012) When bacteria target the nucleus: the emerging family of nucleomodulins. Cellular Microbiology 14: 622-633.

48. Deitsch KW, Driskill CL, Wellems TE (2001) Transformation of malaria parasites by the spontaneous uptake and expression of DNA from human erythrocytes. Nucleic Acids Research 29: 850-853.

49. Wahlby C, Kamentsky L, Liu ZH, Riklin-Raviv T, Conery AL, et al. (2012) An image analysis toolbox for high-throughput *C. elegans* assays. Nat Meth 9: 714-716.

50. Brenner S (1974) The genetics of *Caenorhabditis elegans*. Genetics 77: 71-94.

51. DeShazer D, Brett PJ, Carlyon R, Woods DE (1997) Mutagenesis of *Burkholderia pseudomallei* with Tn5-OT182: isolation of motility mutant and molecular characterization of the flagellin structural gene. J Bacteriol 179: 2116-2125.

Chapter 6. Utilization of Tn-seq to analyze the intramacrophagic virulome of *Burkholderia pseudomallei*

(To be submitted to PLoS Pathogens)

Norris, M.H.[2], Zarzycki-Siek, J.[1], Belcaid, M.[3], Marlenee, N.[4], Bowen, R.[4], Schweizer, H.[4] and Hoang, T.T[1,2].

[1]*Department of Microbiology,*

[2]*Department of Molecular Biosciences and Bioengineering,*

[3]*Bioinformatics core, John A. Burns School of Medicine, University of Hawaii at Manoa, Honolulu, HI 96822, USA*

[4]*Department of Microbiology, Immunology, and Pathology, Colorado State University, Fort Collins, CO 80523, USA*

6.1 ABSTRACT

The select-agent bacterium *Burkholderia pseudomallei* possesses a large repertoire of virulence factors that culminate in the infection known as melioidosis. The objective of the research is to identify unknown virulence genes that contribute to the cellular infectious process through a genome-wide screen. A comprehensive transposon mutant library was constructed from an engineered strain of *B. pseudomallei* and used to infect RAW264.7 murine macrophages. Tn-seq was used to obtain between 6 and 10 million reads per sample. HT-Seq python scripts were used to count the reads per gene, which were visualized using IGV (Integrative Genome Viewer 2.3) and analyzed using MeV (Multi-Experiment Viewer). Bacterial genes that had lower reads after serial passaging through the macrophages were considered putative virulence genes. 901 genes were identified as being 10-fold negatively selected against. 333 of those genes were 100-fold negatively selected against and 113 were 1,000-fold negatively selected against. Several loci already associated with virulence were identified, including genes of the T6SS-5, Bsa (*Burkholderia* secretion apparatus T3SS), flagella, and LPS biosynthesis; lending confidence that the data are reliable. DAVID gene ontology analysis of the gene list indicated enrichment for the term pathogenesis. Numerous loci encoding secondary metabolite biosynthetic genes and transcriptional regulators were also enriched for. Cytotoxicity assays were then used to screen 134 mutants for virulence levels. 22 mutants that showed decreased cytotoxicity towards macrophages were further characterized in intracellular replication, attachment, and invasion assays. 5 genes were complemented for data verification and neighboring genes were investigated. 20 mutants were assessed in the BALB/c mouse inhalation melioidosis model with 10 demonstrating various levels of attenuation. Tn-seq is a powerful tool that allowed the identification of previously unknown virulence factors that contribute to *B.*

pseudomallei cell infection. Refinement of the intramacrophagic virulome provides novel targets for therapeutics and increases our understanding of the arsenal that *B. pseudomallei* utilizes to overcome host defenses.

6.2 AUTHOR SUMMARY

When the Public Health Security and Bioterrorism Preparedness and Response Act was passed by the 107th US congress in 2002, research on treatment and prevention of illnesses caused by the newly termed select agent bacteria (such as *B. pseudomallei)* became a public health priority. Several major virulence factors have been identified but full understanding of *B. pseudomallei* cellular infection is still lacking in depth and detail. Here we use a genome wide screen and a relatively new method of Tn-seq to identify the intramacrophagic virulome and novel virulence genes of *B. pseudomallei*. Initial analysis showed a large enrichment in putative and hypothetical genes indicative of the dearth of knowledge of the intracellular pathogenesis of *B. pseudomallei.* We found several novel secondary metabolite, putative, and hypothetical genes that play a role during macrophage infection and cell-cell spread. Screening of mutants allowed identification of virulence factors that can be putatively assigned roles in attachment, invasion, intracellular replication, cell-cell spread as well as *in vivo* infection.

6.3 INTRODUCTION

The melioid bacillus, *Burkholderia pseudomallei (Bp)*, is typically found in soil and water environments between the latitudes of 20°N and 20°S and so to is melioidosis primarily a tropical disease [1]. In Thailand, very high levels of the bacterium are found in the pooled surface waters of rice paddies [9] coinciding with high disease and seroprositivity rates in rural rice farmers. Typically there is a regional hospital at great distance from the individuals home and by the time they arrive at the hospitals, the disease has progressed acutely leading to a high mortality rate of 40.5% [12]. 79% of individuals diagnosed as having melioidosis are farmers and nearly 70% of those are patients that have type 2 diabetes mellitus that is poorly controlled or undiagnosed [13]. Not only does the melioid bacillus pose a public health challenge in Northeastern Thailand but the US Centers for Disease Control have listed *Bp* as a Tier-1 select agent. Tier 1 organisms have the potential to pose a severe threat to US public health and safety and the US congress passed laws to develop vaccines and therapeutics for them, including *Bp* [20]. An important step in combating a disease, is understanding the fundamentals at the base. In this case, only by understanding the molecular pathogenesis of *Bp* will an effective vaccine come to fruition.

When *Bp* cells come into contact with host cells, a plethora of host modifications occur in response to bacterial infiltration and virulence factor expression leading to the diseased state. Within-host, *Bp* can infect most tissues and invades, then replicates inside the cytoplasm of many cell types [51,57-61]. To accomplish this feat *Bp* attaches to the host cell via an unknown mechanism, causing actin rearrangement and inducing bacterial phagocytosis [62]. Once, internalized *Bp* utilizes the *Burkholderia secretion apparatus* (Bsa, one of three genomically encoded type 3 secretion systems, T3SS) to secrete the effector BopE through the membrane of

the phagocytic vesicle [63,64]. BopE is a guanine-nucleotide-exchange factor that interacts with the Rho GTPase Cdc42 undermining the surrounding cytoskeletal framework, damaging the membrane and allowing vesicular escape before phagosomal degradation of *Bp* occurs [65,197]. Once inside the cytoplasm the well characterized *Bp*-intracellular motility protein A, BimA, polymerizes host-cell actin [69]. The polar actin "tail" allows intracellular movement and eventually leads to formation of bacteria containing membrane protrusions [70]. The membrane protrusions allow *Bp* to seek out uninfected cells and begin the cycle anew without transitioning into the extracellular milieu. Intracellular motility can quickly oscillate between actin-mediated movement and use of flagella, where *Bp* swims within the host-cell cytoplasm [71]. During the infectious process an infected cell may fuse with healthy neighboring host cells and is at least partially attributed to the main *Bp* type 6-secretion system (T6SS-5; nomenclature according to Shalom et. al.) [72,180]. The formation of multi-nucleated giant cells (MNGCs) has been observed *in vitro* and *in vivo* and is a major hallmark of *Bp* infection [70,73]. The bacteria replicate concurrently with the production of several known and unknown virulence factors causing death of the host-cell. However questions remain, how does *Bp* sense when to fuse, where to travel, what nutrients to use, how are mediators (e.g. autophagy) of innate immunity avoided, and what causes the observed cytoskeletal rearrangements? These questions are indicative of the knowledge gap present in fully understanding the molecular pathogenesis of *Bp.*

Mutating many of these virulence factors lead to attenuation in mouse models of infections but *in vitro* cell infection mutational studies indicate a delay of the cellular infectious events rather than abolishment [67,72,89]. *Bp* has nearly 6,000 genes and an open genome [90,91]. Many genes (approximately 35.5% in *Bp* strain K96243) are hypothetical or putative with no proven function [90]. It stands to reason that there are *Bp*-specific virulence factors

contributing to disease that remain to be discovered and that mutating these factors may produce a live-attenuated strain that is capable of protecting from inhalation melioidosis. Our data indicate this to be true. The development of a vaccine remains elusive, placing urgency on elucidating the functional contributions of hypothetical/putative genes to the molecular pathogenesis model. In total, we consider the effort of this work in identification of novel virulence factors to be of significance to the field.

Here, a genome wide screen and the relatively new method of Tn-seq [92] were used to identify the intramacrophagic virulome and novel virulence genes. Initial analysis showed a large enrichment in putative and hypothetical genes indicative of the dearth of knowledge of the intracellular pathogenesis of *Bp.* Cytotoxicity assays were used to characterize the virulence of 134 mutant *Bp* strains of the initial 901 putative virulence candidates identified. Intracellular replication assays were used to measure reduced replication inside RAW264.7 macrophages. Growth curves were carried out to make sure there were no *in vitro* growth defects accounting for reduced intracellular replication. Mutants showing no *in vitro* growth defect and reduced intracellular replication were submitted to invasion and attachment assays. Fluorescent microscopy was used to characterize cell fusion, actin polymerization, and plaque formation when compared to wildtype and a T6SS-5 mutant (*tssC*-5::T24) identified in the Tn-seq data. Two genes were chosen for mini-Tn*7* based complementation and verification in intracellular replication assays. Neighboring genes of these 2 were investigated in their cytotoxicity and intracellular replication characteristics. Several novel secondary metabolite, putative, and hypothetical genes that play a role during macrophage infection and cell-cell spread were identified and verified to be essential for full virulence of *Bp.* Twenty candidate mutants were used to challenge BALB/c mice in an intranasal infection model. Ten of those mutants

demonstrated some level of attenuation and have now been added to the arsenal that is the *Bp* intramacrophagic virulome.

6.4 RESULTS

Tn-seq analysis of the intramacrophagic virulome of *Bp*. To identify any and all genes of the 'intramacrophagic virulome' a saturating transposon library was created in *Bp* K96243 Δ*asd* strain [28] using a pBT20 transposon based on non-antibiotic complementation (Fig. 1). Briefly, the transposon mutant library was pooled and used to infect the murine macrophage cell-line, RAW264.7. The infection was allowed to proceed for 12 h, for a total of three passages. The genomic DNA from passaged and unpassaged pools were isolated and transposon/genome junctions identified by Tn-seq on the Illumina system [27]. Infection replicates at multiplicity of infections (MOIs) of 10:1 and 1:1 were carried out and data compared to the unpassaged pool. Genes with reads before but not after passaging were implicated as the 'intramacrophagic virulome'. Following analysis we found many genes in both replicates and grouped them into those ≥10, ≥100, or ≥1,000 times negatively selected against. Presumably, the higher the negative selection the more essential the genes are to the intracellular infectious process. A majority of genes were shared between replicates (Fig. 2A). 901 genes showing ≥10 negative selection were shared between both replicates. 333 of those genes (roughly one third) underwent ≥100 negative selection in both replicates and 113 genes ≥ 1,000 (Table S1). Each time the stringency of selection was increased 10 times, one third of the genes dropped out. The genes shared between replicates, located in the overlapping regions of the Venn diagrams (Fig. 2A), were further analyzed for functionality and a large amount were ascribed a hypothetical or putative function. When looking at the classification for all genes in the K96243 genome ~35.5% are hypothetical or putative. Among the genes with ≥10-times negative selection from the Tn-seq data that number increases to 51.3% and among genes with ≥1,000-times negative selection, hypothetical and putative genes comprise 76% of the group

(Fig. 2B). At higher stringency of selection there is an increasing majority of genes considered hypothetical or putative. When analyzed in the context of intracellular infection, it becomes clear that their remains a lack of knowledge surrounding *Bp* activity during host-cell infection.

Functional Analysis of Genes Identified from Tn-seq. Functionally annotated genes were clustered with DAVID [29] to compare functional enrichment in our data to levels in the *Bp* K96243 genome. Many known virulence factors were present in the gene lists as well as some metabolic processes that *Bp* conducts during host cell infection (Fig. 3A). The ≥100-fold selection showed the greatest enrichment in virulence associated terms including, "pathogenesis, LPS, flagellum and cilia" while increasing the stringency to ≥1,000-fold left "flagella and cilia" and metabolic processes. The processes "actin cytoskeletal rearrangement" and "activation of Rho GTPase activity" are known to be important for *Bp* cellular pathogenesis as described above. "Trehalose biosynthesis" is also known to be important for infection and is enriched 10 times in all groups beyond the number present in the K96243 genome. The "chemotaxis" functional group was enriched by 5 times and those genes may be responsible for *Bp* detection of chemical gradients in the cell. Functional ontology analysis was accompanied by looking at the individual genes of known virulence factors. If the screen was successful, many of the well-characterized virulence factors would have ≥10 times negative selection. Flagellar motor, hook, and filament genes as well as genes involved in flagella expression were identified (Fig. S1A). Genes involved in LPS biosynthesis (Fig. S1B) and structural genes of the T2SS, T3SS, T6SS, and twin arginine targeting systems also experienced ≥10 times negative selection (Fig. S1C). The well-characterized Bsa effectors BopA, BopE, and Cif_{Bp} were enriched between 10 and 100 times underscoring the relevance of the dataset to *Bp* pathogenesis. A quick perusal of read

saturation across samples and chromosomes gives an immediate indication of the rich data obtained by the method (Fig. 3B). The horizontal axis represents each of the *Bp* chromosome and samples with $\log_{10}$ reads as the vertical lines. Virulence loci are visible by looking at areas in the 10:1 and 1:1 that have less read saturation than the initial pool, represented in Figure 3B by emphasizing the known virulence locus of the T6SS-5 and Bsa. The virulence loci (areas of decreased read saturation) include two loci of branched amino acid transport and utilization, two genomic islands (GI7 and GI16), four unknown and two known (malleilactone and syringolin) secondary metabolite operons, two well characterized (T6SS-5 and Bsa) and three uncharacterized (BPSS0958-0963, BPSS1250-1265, and BPSS1614-1630) *Bp* secretion apparatuses (Fig. S2A chromosome 1 and Fig. S2B chromosome 2). Genes that received zero reads from either replicate after passage were analyzed and divided into groups based on the number of reads in the initial pool. Two flagella genes are located on the list. FliL is at the top of the list with several thousand reads from the initial pool compared to none after the passaging. The *Salmonella enterica* FliL mutant is impaired in swimming and completely deficient in swarming where the torsional stress causes rod breakage and ejection [30]. Other genes with over 1,000 reads are stress-induced morphogen *bolA*, histidine utilization gene *hutf*, and several housekeeping genes. Genes of known functional roles in pathogenensis (i.e., Bsa and T6SS) validate that this method can be used to identify other genes of unknown function in the *Bp* intramacrophagic virulome.

Characterization of Hypothetical and Putative Virulence Factor Candidates.

For this study the primary interest was in the hypothetical, putative, and uncharacterized genes and whether they could be described as virulence factors. All genes from the ≥100 and

≥1,000 list with hypothetical function annotations were chosen and combined with all genes with putative functions from the ≥1,000 list resulting in a 134 gene list of putative virulence factors for further characterization. 134 insertional mutants, representing the 134 genes, made in the *Bp* strain 1026b background were obtained for a high-throughput cytotoxicity screen in a modified aminoglycoside protection assay to measure damage to RAW264.7 macrophage monolayers (Table S2). The *tssC-5* gene (BP1026B_II1588), forming part of the contractile sheath along with *tssB-5* in the major T6SS-5 and confirmed with great detail in *P. aeruginosa* [31], was identified in the ≥100 list, and its insertional mutant was used as a negative control for this experiment along with wildtype 1026b. Figure 4A shows the data obtained from the cytotoxicity experiment carried out in triplicate for each mutant represented as a percentage of total monolayer lysis (refer to table S2 for identification of mutants). Many mutants exhibited lower cytotoxicity than wildtype at 24 hours post-infection (hpi) and 32 of them exhibited statistically significant lower levels of lactate dehydrogenase (LDH) release (Table 1). Growth curves on all 32 mutants were carried out to ensure the low cytotoxicity readings were not because of *in vitro* growth defects (Fig. 4B). Our experimental setup was designed to limit this effect but was essential before moving forward with characterization. Two mutants showed significantly different growth characteristics when compared to wildtype (Fig. 4B, orange line). Mutant 84 (Fig. 4B, blue line, BP1026B_I2891, oxidoreductase, FAD-binding protein) and mutant 96 (Fig. 4B, red line, BP1026B_I0173, addiction module antidote protein) had interesting growth characteristics but were excluded from further characterization. Mutant 60 (Fig. 4B, green line, BPS1026B_I1231, hypothetical protein) was slightly lower than wildtype but was left in the pool for further characterization.

Intracellular Replication Assays of 21 Putative Virulence Factors.

Modified aminoglycoside protection assays performed in triplicate were used to determine defects in intracellular replication of 21 mutants from the list while using internal positive (mutant 39, BP1026B_I1079) and negative (mutant 126, *tssC-5*) controls as determined from the cytotoxicity assay in comparison to wildtype. Average intracellular CFU as a percentage of wildtype was compared to average cytotoxicity as a percentage of wildtype at 24 hpi (Fig. 4C). For some of the mutants (mutants 21, 25, 27, 60, 78, 95) cytotoxicity and intracellular replication agree, suggesting a linkage between cell injury and replication for these virulence factors. Others (mutants 2, 4, 5, 7, 8, 16, 20, 108) show an inverse relationship between cytotoxicity and intracellular replication with low cytotoxicity levels and wildtype levels of intracellular replication. Only three of the 21 mutants (mutants 110, 113, 119) have higher cytotoxicity percentages than CFU percentages but both being lower than wildtype.

Additional time points of the aminoglycoside protection assays were carried out to look at the overall intracellular growth trend of all 21 mutants (Fig. 4D). Two strains had extremely different replication assay curves. Mutants 60 and 95 had no deficiencies in *in vitro* growth but showed a severe defect at 2, 12, and 24 hpi. Mutant 60 (BP1026B_I1231) encodes a hypothetical protein, which shows high similarity to the *E. coli* ZipA protein. In *E. coli* the ZipA protein is a membrane-anchored protein that recruits the Fts complex during cell division [32]. Mutant 95 (BP1026B_I0717) encodes the transmembrane cell division/chromosome segregation protein FtsK [33,34]. This mutant also showed no defect in *in vitro* growth but substantial defect in intracellular replication. Mutants 4 (BP1026B_I1575), 20 ((BP1026B_II1256), 25 (BP1026B_I2174), 108 (BP1026B_I1664), and 113 (BP1026B_II0522) were deficient in intracellular replication at 12 hpi compared to wildtype (Fig. 4D, red line and bar). Mutants 21

(BP1026B_I2818), 27 (BP1026B_I2220), and the two cell division mutants had replication levels comparable to or less than the *tssC-5* mutant (Fig. 4D, orange line and bar) at 12 hpi. The remaining mutants had less replication than wildtype but not significantly so. By 24 hours the two cell division mutants had the highest defect in replication compared to wildtype and 7 mutants (20, 21, 25, 27, 110, 113, 119) had significantly lower intracellular CFUs with the mean CFU, 2.42 x 10^5, being 48% of the wildtype and positive control levels. All 22 mutants were then submitted to an invasion assay to determine if the defect of these mutants was at the vacuolar escape stage of the intracellular infection. *Bp* were allowed to infect the cell monolayers for 1 h to allow internalized bacteria to escape the phagocytic vesicle into the host-cell cytoplasm. Following an hour of killing, the host cells were lysed and intracellular CFU were counted then divided by the amount used for the infection, resulting in the invasion efficiency (Fig. 5A). Those mutants that showed an invasion frequency significantly lower than the wildtype (mutants 2, 4, 5, 16, 20, 21, 25, 27, 60, 78, 80, 95, 109, 110) were submitted to an attachment assay to help define which stage of infection the mutants were deficient in (Fig. 5B). Both cell division mutants, FtsK and ZipA, were deficient in invasion but only the FtsK mutant was deficient in attachment.

At least some of the mutants were believed to have a deficiency in cell-cell spread. To understand the mutants' ability to spread from cell to cell, plaque assays were carried out for 14 of the putative virulence factor mutants and plaque diameters were measured and compared to both the *tssC-5* mutant, the internal positive control, and wildtype 1026b (Fig. 5C). Nine of the mutants produced significantly smaller plaques when compared to the wildtype but were not as small as the *tssC-5* mutant. These nine mutants are hypothesized to be deficient in cell-cell spread to some degree. Insertional mutants in genes BP1026B_I1969 (a LivH-like branched

chain amino acid permease) and BP1026B_II1463 (putative glutathione-S-transferase) produced plaques with a diameter slightly smaller than wildtype. Insertional mutants of seven genes (BP1026B_I1231, BP1026B_I1764, BP1026B_I2174, BP1026B_I2220, BP1026B_II1256, BP1026B_II1463 and BP1026B_II1694) formed plaques significantly smaller than wildtype but slightly larger than the *tssC-5* insertion mutant.

Microscopy and Cell Infection Characteristics of Select Putative Virulence Factors.

Plaque diameters were measured but plaque phenotype was investigated to note any differences to wildtype. Figure 6A shows representative plaque images from RAW264.7 macrophages infected with the indicated mutants for 24 h. Mutants of BP1026B_I1969 and BP1026B_II1463 were verified to create plaques phenotypically similar to wildtype but of smaller size. Mutants of BP1026B_I1764, BP1026B_I2174, BP1026B_I2220, and BP1026B_II1256 were unable to form plaques similar to the wildtype. The specified mutants appeared unable to cause cell fusion as efficiently as wildtype resulting in globular MNGCs that never fuse with neighboring uninfected cells. Plaques formed by these mutants resemble larger versions of MNGCs formed by the *tssC-5* mutant. Gene BP1026B_I1231 (*zipA*) created plaques but were neither circular nor as extensive as the plaques of wildtype. All 32 mutants that were analyzed in the growth curve experiment were used to infect RAW264.7 murine macrophages. The infected monolayers were fixed and the monolayers were stained as described in the materials and methods to visualize nuclei (blue), actin (green), cell membranes (red), and bright field for monolayers. Several mutants did not form plaques as well as the wildtype. Mutant 39 and the *tssC-5* were used as positive and negative controls for the data in addition to the uninfected and wildtype controls for plaque formation. The insertion mutants within the *ftsK,*

zipA, and antidote protein (mutant 96, BP1026B_I0173) had major decreases in MNGC formation and plaque formation. Insertions in *ftsK* and the antidote protein (mutant 96, BP1026B_I0173) greatly affected *in vitro* growth so an inability to infect was expected. However, the *zipA* (BP1026B_I1231) insertion mutant formed long strands of bacteria that are stuck at various cell division stages *in vitro* (Fig. 6B, left) similar in phenotype to an effective *Yersinia pestis* vaccine strain mutated in the *nlpD* gene [35]. The *Bp zipA* mutant showed decreased invasion efficiencies but was still able to infect RAW264.7 macrophages. Long strands of *Bp* are seen in the phase contrast image inside the MNGC and when overlaid with the fluorescence you can see red tendrils of infecting bacteria (Fig. 6B, right). Actin polymerization appears to have a slight defect most likely because of difficulty localizing to the poles, translating to a defect in cell-cell spread.

Other mutants did not have such an obvious bacterial phenotype but the infection characteristics were much different for some of the mutants tested compared to our controls. Several mutants demonstrated reduced plaque formation (Fig. 6C). Bacteria in red have spread to many cells but fusion and plaque formation appears to lag behind that of the wildtype infected monolayers.

Virulence Phenotype Summation.

A visual summation of all the virulence data is presented in a "mutant virulence phenotype" matrix or MVP matrix (Fig. 7). Each mutant was assigned a number based on the significance of difference to wildtype in the various assays then clustered on similar trends. Red tiles mean similarity to wildtype, the brighter the green the more lacking the phenotype of the mutant compared to wildtype. All mutants have lower cytotoxicity levels compared to wildtype

whether they are significant or not. Mutants were clustered into 7 groups based on performance in all the assays. Group 1 consists of only the BP1026B_II1256 mutant and performed consistently worse than wildtype in all the assays suggesting a deficiency in all aspects of infection. Group 2 includes BP1026B_II0927 (79), BP1026B_I1764 (8), and BP1026B_II1463 (7). These 3 genes behave the same as wildtype except for in the plaque formation category, where they form significantly smaller plaques indicative of a cell-cell spread deficiency. Group 3 genes have deficiencies after attachment including invasion, replication, and plaque formation. The *tssC-5* insertion mutant is part of this group that also includes BP1026B_I1231, BP1026B_I2220, and BP1026B_I2174. The outlier is the *ftsK* mutant, which was unable to progress through any of the infectious stages. The three mutants in Group 4 (BP1026B_I2818, BP1026B_II0522, and BP1026B_I3714) show no difference in plaque formation but show inabilities in invasion or replication. Group 5 mutants (BP1026B_II2523 and BP1026B_I1664) show behavior similar to wildtype in all assays except cytotoxicity and may represent genes that cause release of a cytotoxic compound. Eight group 6 mutants (BP1026B_I1747, BP1026B_I1969, BP1026B_I1522, BP1026B_I1575, BP1026B_II0034, BP1026B_II0207, BP1026B_II1508, and BP1026B_II1870) show no difference in intracellular replication or plaque formation but show deficiencies in the beginning stages of infection resulting in lower cytotoxicity. Group 7 includes wildtype 1026b and the internal positive control mutant, BP1026B_I1079, both with no deficiencies in any of the assays.

Analysis and Complementation of Two Virulence Candidates and Neighboring Genes.

The *Bp phoU* gene is BP1026B_I2174, and the *E. coli phoU* has been well characterized as a negative regulator of the phosphate regulon (knocking out results in constitutive expression of the pho regulon). *PhoU* lies at the center of the phosphate transport operon with phosphate permease subunit genes (BP1026B_I2175-BP1026B_I2178, *ptsB, A, C, S*) and phosphate sensing (BP1026B_I2172, *phoB*) and regulatory genes (BP1026B_I2173, *phoR*); (Fig. 8C). The *phoU* gene has been shown to mediate adherence of entero-pathogenic *E. coli* to epithelial cell cultures and the murine urinary tract [36,37] that upon mutation results in attenuation of septicemia-inducing *E. coli* in pigs [38]. The *Bp* phosphate regulon sensor protein, *phoR* (BP1026B_I2172), also underwent >1,000 times negative selection during the initial screen. However, the BP1026B_I2174 mutant was not defective in attachment to RAW264.7 cells. This may be because phosphate-limiting conditions do not predominate until *Bp* is in the phagocytic vesicle, therefore deregulation of virulence expression does not occur until the invasion stage.

The second gene is BP1026B_II1256. It is a hypothetical protein that is Sec secreted with an alpha-beta hydrolase fold. BP1026B_II1256 is predicted to be in an operon with a non-ribosomal peptide synthase (NRPS) (BP1026B_II1250) which underwent >10 times negative selection and an N-acylhomoserine lactone synthase (BP1026B_II1251) which underwent >1,000 times negative selection. These genes form a secondary metabolite biosynthetic cluster with several polyketide synthases (PKS) and the entire region was analyzed with antiSMASH [39]. The region from BP1026B_II1224 to BP1026B_II1284, was identified as a 95.312 kb secondary metabolite cluster with BP1026B_II1256 near the middle (Fig. S4A). The product is an NRPS-typeI PKS-homoserine lactone hybrid molecule with the predicted scaffold indicated in figure S4B. This region is conserved among many *Bp* strains (Fig. S4C) but a homologue of BP1026B_II1256 is conspicuously absent from *Burkholderia thailandensis* E264. Additionally, a

~15kb region containing secondary metabolite genes near a mobile element, BP1026B_II1278 through BP1026B_II1286, is 1.4 Mbp away on the *B. thailandensis* E264 chromosome II. The region contains transposase genes, hypothetical genes, and a T6SS Rhs element VgrG gene. Gene clusters as compared by antiSMASH and webACT show the missing gene and regions (Fig. S4C and S4D). Movement of the genes may result in changing of the core scaffold, tailoring reactions, or expression of the secondary metabolite. The regions are conserved between *Bp* strains 1026b and K96243 (data not shown).

Mini-Tn7-*gat* was used to complement the 2 insertion mutants [28]. Complementation was verified with an intracellular replication assay in RAW264.7 macrophages (Fig. 8A and B) with insets showing growth defects in the linear scale. Complemented strains had intracellular replication similar to the wildtype. Plaque assays also verified complementation with both mutants showing significant defects in comparison to the complemented strains and wildtype but not as low as the *tssC-5* mutant (Fig. 8C). Neighboring insertional mutants to these two target genes were used to infect RAW264.7 macrophages and their cytotoxicities as a percentage of total monolayers lysis were measured and compared to the cytotoxicity levels of the gene of interest, the *tssC-5* mutant, mutant 39, and wildtype (Fig. 8D and E). Mutants in genes *pstA* (BP1026B_I2176) and *phoR* (BP1026B_I2172), which neighbor BP1026B_I2174, were found to have cytotoxicity levels lower than wildtype, *phoR* had significantly lower levels. The NRPS/PKS containing BP1026B_II1256 is predicted to span 60 genes from BP1026B_II1224 to BP1026B_II1284. In this work we only looked at the immediate operon from BP1026B_II1245 to BP1026B_II1256 that are in the same operon as BP1026B_II1256 (Fig. 8E). Only our original target gene showed very low cytotoxicity levels. BP1026B_II1256 may be a tailoring gene that modifies a major functional portion of the NRP.

BALB/c attenuation study.

Twenty candidate virulence factors that showed decreased cytotoxicity were tested in the BALB/c intranasal melioidosis mouse model (Fig. 9A). 10 mutants had no attenuation *in vivo* (Fig. 9B). 8 mutants (BP1026B_I1522, BP1026B_I1664, BP1026B_I1764, BP1026B_I2174, BP1026B_II0207, BP1026B_II1256, BP1026B_II1463, and BP1026B_II1508) showed various levels of attenuation but only one mutant (BP1026B_I1231) was completely avirulent with all mice looking healthy and only one had low levels of bacteria in the lung at 60 dpi (Fig. 9I and J). Mice infected with 10 times the LD_{50} (4,500 CFU) of wildtype *Bp* 1026b succumb to the infection by day 3 (red line, all curves). Five mice were infected with each insertion mutant. From most attenuated to least attenuated: mutants of BP1026B_II1463, and BP1026B_II1508 had nearly all mice survive to 4 dpi (days post infection) with 60% survival the rest of the study (Fig. 9G). Two surviving mice from each had bacteria in the lungs and high levels of bacteria in the spleens (Fig. 9H). Splenic abscesses were observed in some survivors. Mutants of BP1026B_I1522, BP1026B_I1764, and BP1026B_I2174 had a 40% survival rate (Fig. 9D). There were no bacteria detected in surviving mice after infection with mutant BP1026B_I1522 but survivors from the other two groups had between 10 and 1,000 CFU in the lungs (Fig. 9E). Mutants of BP1026B_I1664, BP1026B_II0207, and BP1026B_II1256 had a 20% survival rate (Fig. 9C) and all surviving mice had bacteria in the lungs but not in the liver or spleen (Fig. 9D). Generally the higher bacterial load in the spleen the more pronounced the splenomegaly.

6.5 DISCUSSION.

Nutrient acquisition: A major component of understanding intracellular infection is identifying where *Bp* obtains nutrients for such robust growth. The branched chain amino acid transporter *livH* experienced almost 4,000 time negative selection. The *liv* ABC transporter is essential for maximal *Streptococcus pneumonia* infection in both pneumonic and septicemic models [40]. *Franicsella tularensis* has also been shown to utilize free amino acids derived from autophagic degradation of host-cell proteins as an energy source during intracellular infection [41]. The *livH Bp* mutatnt did not show a growth defect *in vitro* indicating branched chain amino acids are a nutrient source in the host cell. A cystine binding transport gene (BPSL1867, BP1026B_I1828) was selected for >3000 times in both replicates. Cystine is essentially two cysteine molecules covalently linked via a disulfide bond and is released upon degradation of host proteins. A histidine degradation gene (BPSL2339, BP1026B_I0987) was also identified. Genes involved in phosphate sensing (BPSL1365, BP1026B_I2172, *phoR*) and regulation of the phosphate regulon (BPSL1363, BP1026B_I2174, *phoU*) had very high levels of negative selection, whose effects on infection by *Bp* were characterized in this work. Taken together *Bp* transports and degrades amino acids while replicating intracellularly and requires the ability to respond to nutrient limitations present inside the host cell.

Regulators: Twelve regulatory genes were identified in the Tn-seq data with >1,000 times negative selection in both replicates. Several of the regulators have been characterized by our lab independently of this work and have been shown to be of importance in the inhalation BALB/c mouse infection model (in preparation).

Secretion systems: The Bsa (T3SS-3) effector genes *bopC, bopA,* and *bopE* were negatively selected for through the passage in addition to the Bsa sorting platform gene BPSS1538 (BP1026B_II1634, *bsaV*) and the secretion apparatus gene BPSS1543 (BP1026B_II1639, *bsaQ*). Interestingly, potential effector genes BPSS1386 (BP1026B_II1478, a hypothetical protein with a GTP binding domain and an actinin-type actin binding domain; effective T3 score of 0.76299 [42]) and BPSS1416 (BP1026B_II1508, a hypothetical protein 73% homologous at the amino acid level to the *Pseudomonas syringae* effector HopAN1) of the T3SS-1 apparatus were also identified as having >100 and >1,000-times negative selection respectively. Host actinin is regulated by phosphorylation to mediate association of F-actin bundles with cell adhesion points and between actin filaments [43]. The actin-binding domain of BPSS1386 would target the protein to the ends of actin bundles where the GTP binding domain would serve as a GTPase-Activating Protein (GAP) and terminate downstream adhesion or rearrangement events. The *P. syringae* HopAN1 protein has been observed to inhibit the innate immune response in plants [44] and may perform similar functions in *Bp*. BPSS1394 (BP1026B_II1486, *sctN*) and BPSS1407 (BP1026B_II1499, *sctD*), genes encoding basal body proteins of the T3SS-1 were identified in the Tn-seq data but barely made the >10-fold cutoff. In agreement with previous studies of apparatus knockouts, weak selection of the structural genes indicates they are not contributing greatly to pathogenesis. Strong selection of the effectors of T3SS-1 indicates that they play an important role and may be secreted via other secretion systems affecting pathogenesis.

Structural genes of the major T6SS-5 were identified with the *tssC-5* gene undergoing the highest negative selection. Gene *tssL-1* (BPSL3111, BP1026B_I0182), a *dotU/icmH* homologue, of the T6SS-1 had very high levels of negative selection in both replicates of the Tn-seq data but cytotoxicity levels did not show any difference from wildtype. Previously published data show

that Syrian hamsters vaccinated against components of T6SS-1 can be protected from infection and mutating this T6SS resulted in slight attenuation over the wildtype [20]. The *tssC-2* gene (mutant 40, BPSS0098, BP1026B_II0106) of the T6SS-2 showed a high level of negative selection and cytotoxicity levels lower but not significantly lower than wildtype. Two genes of the T6SS-3 (BPSS0173, BP1026B_II0194 and BPSS0175, BP1026B_I0174) underwent low levels of negative selection. The ATPase and *tagAB-4* genes of T6SS-4 were both negatively selected against with *tagAB-4* experiencing nearly 500 times negative selection. The protein contains pentapeptide repeat regions and a partial C-terminal PipB2 domain of the *Salmonella* secreted effector PipB2. PipB2 is secreted through both T3SSs of *Salmonella* and interacts with the host-cell kinesin-1 motor complex while in the bacteria containing vacuole to modulate vesicle trafficking [45,46].

Other known virulence factors: The Tn-seq data had many genes involved in capsular polysaccharide synthesis. Genes *wcbB*, *wcbD*, *wcbG* experienced >100 times negative selection while *wcbP*, *wcbS*, and *wcbT* experienced >10 times negative selection. The importance of the capsular polysaccharide to *Bp* replication within macrophages has bee previously reported [47]. A putative undecaprenyl phosphate N-acetylglucosaminyl transferase (BPSL2671, BP1026B_I0648) involved in LPS biosynthesis experienced very high levels of negative selection at >4,000 times negative selection in both replicates. A hypothetical protein involved in LPS biosynthesis (BPSL0537, BP1026B_I2958) experienced >100 times negative selection after passaging. A *Bp* LPS mutant has been shown to have the same replication levels inside RAW264.7 macrophages [48] which would explain why more genes involved in LPS synthesis were not identified with our screen. The YadA-like autotransporter adhesin, *bpaC* (BPSL1631, BP1026B_I1575) showed negative selection and our data agreed with the previous publications

that this protein effects attachment in *B. mallei* and *Bp* but has no impact on mouse survival [49,50].

Uncharacterized virulence factors: Secondary metabolite operons encode for a diverse array of molecules; from the siderophore malleobactin [51] to the proteasome inhibitor syringolin [52]. There are a predicted 16 clusters on the first chromosome and 24 clusters on the second chromosome spanning a total of ~1.3 Mb of DNA or ~18% of the genome. Dedicating such a large region of the genome to these clusters underscores the importance of the produced molecules to *Bp* survival in diverse environments. Several NRPS/PKS secondary metabolite operons were indicated as having importance during the infection (BPSL1710-1727/ BP1026B_I1663-1681, BPSL2214-2229/BP1026B_I1161-1176, BPSS0482-0489/BP1026B_II0536-0544, BPSS2023-BPSS2037/BP1026B_II2177-BP1026B_II2192). A few genes from several of the NRPS operons experienced >1,000 fold negative selection. One such secondary metabolite is investigated in this work.

Other uncharacterized genes that show a high amount of negative selection are GI7 and GI16, which include transporter, regulatory, and hemagluttinin genes with varying similarities to *Yersinia, Vibrio,* and *E. coli* genes. Genes in GI8, BPSL1660-1665/BP1026B_I1605-1610, encoding hemagluttinin, hemolysin, and toxin secretion genes with homology to *Vibrio* were also identified. An unidentified VgrG T6SS in the BPSS0958-0963/ BP1026B_II1049-1055 region made it on the list.

Melioidosis BALB/c mouse experiment

The previously unknown virulence factors screened in this study include genes annotated as hypothetical and putative whose role in infection remains unclear. Out of the initial 134-

unknown/hypothetical virulence factor mutants, the pool was narrowed down to 20 virulence factors from the various screens. Of the 20 screened in animal studies, 10 demonstrated some level of attenuation *in vivo*. These 10 genes produce virulence factors that directly affect the mammalian infection. One of the genes BP1026B_I2174 has high homology to *phoU* (as described above), a phosphate regulon transcriptional regulator, which has been shown to co-activate T3SS and T6SS proteins under phosphate limiting conditions in *Edwardsiella tarda* [53]. Bacteria were only found in the lungs of surviving mice so *phoU* may be important for chronic disease or dissemination. Gene BP1026B_II1508 shows 65%ID 75%H at the amino acid level to the *Pseudomonas syringae* HopAN1 T3SS effector (as described above). The exact function of the HopAN1 effector during plant infections is unknown but it reduces the hypersensitivity response (analogous to the animal innate immune response to PAMPs) to *P. syringae* in plants [54]. Previous works have shown that the T3SS-2 is only important for plant infections by deleting genes BPSS1386-1411 (according to the K96243 gene ID) [55]. In this work we targeted two effectors known as BPSS1386 and BPSS1416. The BPSS1386 (BP1026B_II1478) mutant was just as infectious as wildtype and killed all 5 mice by 3 dpi in agreement with the previous study. However, the BPSS1416 mutant (HopAN1; BP1026B_II1508), was attenuated with all mice surviving to 4 dpi and 60% surviving thereafter. However, high levels of bacteria were isolated form 2 out of 3 surviving mice indicating establishment of a chronic infection. Synthesis of the data indicates BP1026B_II1508 may be important during acute infection to avoid the host immune system. This *Bp* effector was not targeted previously and may be secreted via one of the other T3SS during host-cell infection.

The novel virulence candidate BP1026B_II1463 is a sigma class glutathione-S-transferase family protein. These proteins are essential in the scavenging of oxidative compounds

that can damage DNA and proteins that are a known component of innate immunity. During initial inflammation, activated macrophages and neutrophils release large amounts of reactive nitrogen intermediates (RNI) and reactive oxygen species (ROS). ROS has been shown to be important for controlling *Bp* intracellular replication in mouse monocytes and in C57Bl/6 mice [56,57]. RNI has been show to be unimportant in controlling bacterial replication in the resistant C57Bl/6 [57] but plays a very important role in controlling bacterial replication during early infection in the sensitive BALB/c mouse model [58]. Glutathione-S-transferases play pivotal roles in detoxification during oxidative stress [59] including to ROS and RNI. Without a way to prevent macrophage induced oxidative damage, many bacteria would be killed by DNA and protein damage resulting in the survival rates observed in BALB/c mice challenged with GST mutant *Bp*.

BP1026B_I1522 is a hypothetical protein with BLAST matches to a polyhydroxybutyrate (PHB) depolymerase. PHB depolymerase enzymes act on the biopolymer PHB. PHB is stored as a granule inside the cell and used as an alternative source of acetyl-CoA under conditions of oxygen and nutrient limitation [60]. PHB cycle enzymes of *Legionella pneumophila* have been shown to be important during bacterial infection [61]. Without the ability to metabolize PHB *L. pneumophila* was unable to replicate within U937 macrophages and amoebae. Enzymes of the PBH provide an alternative source of acetyl CoA to the glyoxylate shunt, the importance of which has been demonstrated in *Bp* infection models [62]. Recently, enzymes of the PHB have been implicated as drug targets for bacterial pathogens including *M. tuberculosis* [63,64]. Neither of the two surviving mice infected with the BP1026B_I1522 mutant had any detectable bacteria in the organs tested implying that PHB may be an important nutrient source during host

infection. The *Bp* PHB mutant is attenuated; consequently targeting these enzymes in *Bp* may be a viable co-treatment to the current regimen of therapy.

Gene BP1026B_I1764 encodes a metalloendopeptidase with an NlpD/M23 peptidase domain. Annotations from 1026b predict a start site that would produce a peptide with an extra 60 AA on the N-terminal of the protein compared to the K96243 annotation. All secretion signal predictions are very weak for the 1026b protein BP1026B_I1764 (Sec 0 and T3SS 0.08904) but the shorter K96243 input protein BPSL1806 gives a high probability that it is secreted by the T3SS (0.8084) [42]. All similar proteins only match to the ~200 C-terminal AA containing the Gly-Gly endopeptidase NlpD domain, with the 200 N-terminal AA belonging to the PRK06132 domain of unknown function. The *Bp nlpD* gene is encoded by BPSL1504 and is predicted to be Sec secreted with a very low T3SS prediction score. The NlpD product is believed to contribute to cell division and results in an inability to divide properly, similar to what was observed with the *zipA* mutant. Our microscopy indicates the BP1026B_I1764 insertion mutant divides the same as wildtype during host-cell infection (data not shown) so the target of the peptidase during host-cell infection is not *Bp* peptidoglycan. Mice surviving infection with the BP1026B_I1764 mutant have low levels of the bacteria in the lung indicating the gene may play a role in dissemination. The domain structure is similar to the well-characterized protease LasA of *P. aeruginosa* that affects many aspects of cell invasion and the T3SS [65] and may help unmask the protein's true function.

The least attenuated strains are the mutants of BP1026B_I1664, BP1026B_II0207, and BP1026B_II1256. The gene region of T6SS-4 (according to Burtnick et. al.)/T6SS-3 (according to Shalom et. al.) was found to have lower read density than the surrounding area. The last gene of the secretion system BP1026B_II0207 (BPSS0185) is a small gene known as T6SS associated

gene D-3 (*tagD-3*). No insertions were detected in the initial pool, but this mutant piqued our interest. I-TASSER analysis [66,67] used ten threading templates to predict the structure and function. All ten templates indicate the hypothetical protein of unknown function was a PAAR repeat protein homologous to T4 phage gp5 and other bacterial PAAR motif T6SS proteins. Recently, PAAR repeat proteins have been shown to sit atop the VgrG proteins at the tip of the T6SS needle, sharpening it and diversifying effector functions during injection [68]. The function of T6SS-4/3 in *Bp* infection is unknown but Syrian hamsters challenged with an *hcp4* mutant died just as wildtype [20]. In our study we used BALB/c mice, where 20% survival was observed, perhaps allowing for observation of nuanced virulence. Interestingly, this T6SS is only present in the select agents *B. pseudomallei* and *B. mallei* but absent in *B. thailandensis*.

BP1026B_I1664, and BP1026B_II1256 are genes in two different NRPS/PKS operons. The unmodified peptide scaffolds were predicted and are in the supplementary information (Fig. S4 and S5). The BP1026B_II1256 mutant had a low level of attenuation and, while one mouse survived, was not significantly different than wildtype. Mutant BP1026B_I1664 had a significant increase in time to death of infected mice compared to wildtype. The carbamoyl transferase activity of this gene likely tailors the NRP to its fully functional final form. A transporter in this gene cluster also experienced >1,000 fold negative selection and the mutant was subjected to the cytotoxicity screen but the results of this assay were not significantly different than wildtype, potentially highlighting the weakness of such an assay in identifying some virulence factors. However, this assay, although not perfect, was a good high throughput method for us to screen many mutants at once. Secondary metabolites have a wide range of mammalian cell modifying properties. The effect of these *Bp* secondary metabolites on the host-cell during infection will require further analysis. Of the 20% survival group each surviving mouse had low levels of

bacteria in only the lungs, indicative of minor roles in bacterial spread. Future investigations of this T6SS and secondary metabolites will help to determine roles in infection.

Taken together, this data has determined 10 novel virulence factors that contribute to RAW macrophage and murine melioidosis infection. They make up a diverse group of proteins, which collectively with other characterized virulence factors, allows *Bp* to infect the host efficiently. The arsenal that is the intramacrophagic virulome is fluid and future work will tackle the task of characterizing the function of these newly described factors.

6.6 MATERIALS and METHODS

Bacterial strains, media, and culture conditions. All manipulations of wildtype *B. pseudomallei* were conducted in CDC/USDA approved and registered BSL-3 facilities at the University of Hawaii at Manoa John A. Burns School of Medicine (JABSOM) and experiments with select agents were performed in accordance with the recommended BSL-3 practices [147]. *Escherichia coli* strain E2188 (Δ*dapA*::*pir* Δ*asd*::*mob*-Kan) was used for cloning and culturing of the R6K-*ori* based pBT20-asd_{Pa}-T7 plasmid. The strain was grown in 1xM9 minimal media with 20mM glucose (MG), 1mM lysine and 100 μg/ml diaminopimelic acid (DAP) with the plasmid maintained through complementation of methionine and threonine auxotrophy. Wildtype *B. pseudomallei* strains 1026b were cultured in LB while the K96243 Δ*asd* strain [80] was cultured in LB with 400 μg/ml diaminopimelic acid (LB+DAP400) or in minimal salts media containing 1 mM lysine, 1 mM, methionine, 1 mM threonine, and 400 μg/ml DAP (3AA+DAP). *B. pseudomallei* 1026b::T24 insertion mutants were kindly provided by Dr. Herbert Schweizer at Colorado State University. Antibiotics were not used for selection but LB + 1,000μg/ml kanamycin was used for purifying the 1026b::T24 insertion mutants. Growth on and preparation of DAP were carried out as previously described [148]. All bacterial growth was carried out at 37°C and shaken cultures were maintained at 225 rpm.

Molecular methods and reagents. Molecular methods and reagents were carried out as described previously [51,80,150,167]

Cell line and culture conditions. Murine macrophage cell line RAW264.7 was cultured in DMEM containing 4500 mg/l glucose with 4.0 mM L-glutamine. All cultures were

supplemented with 10% (v/v) heat-inactivated standard fetal bovine serum (FBS; HyClone) and antibiotic/antimycotic solution (100 U/ml penicillin, 100 μg/ml streptomycin, and 250 ng/ml amphotericin B; HyClone). Cells were maintained at 37°C and 5% CO_2 in a humidified incubator. RAW264.7 cell lines were maintained at 50-80% confluency and were passaged by scraping the cells from the flasks using a cell scraper. Cell lines were maintained in Corning™ flasks and plates with CellBIND™ surfaces. Cell concentrations were verified with the Scepter handheld automated cell counter (Millipore).

Transposon library creation in the *B. pseudomallei* K96243 Δ*asd* strain. Three mls each of *E. coli* strain E2188 harboring the pBT20-asd_{Pa}-T7 and the *B. pseudomallei* K96243 Δ*asd* strain were grown to log phase and the cells were harvested by centrifugation in a biosafety cabinet within the BSL3. The pellets were combined and gently resuspended by pipetting in 50 μl of LB. The mixture was spotted onto an LB plate containing 200 μg/ml of DAP and incubated for 12 h at 37°C. After 12 h, the conjugation mixture was scraped off the plate with a plastic inoculation loop and resuspended in 1x M9 salts buffer. The mixture was plated onto 3-150 mm petri dishes containing MG media without any additional amino acids. Without additional amino acids neither donor nor recipient can grow unless the K96243 Δ*asd* strain has the BT20-asd_{Pa}-T7 transposon inserted in the genome. Minimal media was used to remove a good portion of the biosynthetic/metabolic insertion mutants from the pool as virulence factors were the major target. There were approximately 20,000-30,000 colonies per plate. All colonies were scraped from the plates and pooled into 6 ml of MG and then 500 μl aliquots were frozen in glycerol at -80°C.

Passaging the K96243 transposon mutant pool through RAW264.7 macrophages. RAW264.7 macrophages were grown to near confluency in T75 cell culture flasks. The K96243 pool was grown to log phase in MG and diluted down to an MOI of 10:1 and 1:1. The different MOI dilutions were each used to infect a flask of RAW264.7 macrophages for 1 h. Bacteria were washed from the monolayer and DMEM containing 750 μg/ml amikacin and 750 μg/ml kanamycin was added. The infection was allowed to progress for 12 h before the DMEM media was removed and the monolayers were washed 3 times with pre-warmed PBS. The monolayers were incubated with 2 ml of 0.2% Triton X-100 in PBS and gentley rocked back and forth for 5 minutes to lyse the monolayers and liberate the intracellular *B. pseudomallei*. The 2 ml were harvested and 500 μl of each MOI were inoculated into 5 ml of MG broth and grown 12 h at 37°C with shaking. The respective cultures were diluted down to their respective MOIs (10:1 or 1:1) and used to infect another two T75 flasks of RAW264.7 macrophages in the same manner as above. This was repeated 3 times total. At the end of each passage the liberated bacteria were isolated and grown in MG broth then frozen at -80°C.

gDNA isolation and Tn-seq. 500 μl of the transposon library samples were inoculated into 4.5 ml of MG media and grown overnight. Genomic DNA (gDNA) of the passaged and unpassaged pools was isolated with the Promega Wizard Genomic DNA Purification Kit following the protocol for gram-negative bacteria. The kit protocol was checked for sample sterility prior to removal from the BSL3 laboratory. The samples were prepared by combining steps from the TUFTS University Core Facility protocol and as described previously [92]. 10 μg of gDNA samples (5-200 μl) were resuspended in shearing buffer (40% glycerol+10 mM Tris pH 8 + 1mM EDTA) to a total volume of 800 μl. The samples were nebulized separately for 4-5

minutes at 35 p.s.i. of N_2. 30 mg/ml of dextran sulfate in water was added to each sample to a final concentration of 0.2 μg/ml. Add $1/10^{th}$ the volume of 3M potassium acetate + 6M acetic acid and vortex. Precipitate with an equal volume of isopropanol at -80°C for 10 min. The samples were centrifuged and washed with 70% ethanol and the pellets were resuspended in 16 μl Qiagen EB buffer for quantification via Nanodrop. The sheared DNA was end repaired with the NEB Next End Repair Kit according to protocol then purified with the Qiagen QIAquick PCR Purification Kit according to protocol. Each sample was divided into 4 samples and 3' A-tailing was carried out with in-house Taq polymerase at 70°C for 20 min. Design of adapters was as previously described with modification for sequence specific to our transposon [92] while preparation of adapters and ligation was according to the TUFTS sequencing core recommendations. Samples were purified with the QIAquick PCR kit then digested with XbaI overnight at 37°C to separate the two genome-transposon junctions. The DNA samples were run on a 2% TAE gel and the DNA smears between 200 and 400 bp were excised and purified through the QIAquick Gel Extraction Kit according to protocol and eluted with 30 μl of EB buffer. Samples were at a concentration of between 27 ng/μl and 54 ng/μl of DNA in water. Circularization of adaptor ligated gDNA and exonuclease digestion were carried out as previously described using Ampligase heat stable ligase [92]. The transposon ends were amplified with PCR and eluted with the MinElute PCR Purification Kit in 10 μl EB. The molar amount of DNA was calculated and the three samples were multiplexed for Illumina sequencing at the TUFTS sequencing core.

Tn-seq data analysis. After demultiplexing, each sample received between 5 and 8 million reads. Reads were mapped with Bowtie [231] using the Galaxy suite [232-234]. The

SAM files were visualized with Integrative Genomics Viewer (IGV) [235]. Expression data was not being produced so to identify read differences between genes not operons, the HTSeq python script htseq-count was used to count reads per feature (gene) of each sample [236]. Reads of the passaged samples were compared to the unpassaged to determine fold negative selection. Heat maps were generated by importing read files into MeV [237]. Gene lists were manipulated by sorting with Excell into >10, >100, >1000 fold negative selection and 0 reads post-passage groups. Functional analyses of these groups were done by broadcasting groups of genes via Gaggle and Firegoose [238] to KEGG. Functional ontology enrichment was analyzed using Comparative GO [239] and DAVID [198]. Gene clusters with lower read densities after passaging were identified by visual analysis of the read maps in IGV. Prism 6 was used to create all graphs.

Cytotoxicity assay. The cytotoxicity assay was preformed as previously described [51]. *B. pseudomallei* strain 1026b::T24 insertion mutants were obtained from Colorado State University. RAW264.7 macrophages were inoculated in 96-well CellBIND plates then spun at 350 x g to assist cellular attachment. *B.p.* strains were grown overnight with LB in 96-deepwell plates sealed with a breathable microporous film. The next day the bacteria were serially diluted and used to infect the RAW264.7 macrophages in triplicate for each mutant at an MOI of 1:1 in 30 μl. After 1 h of infection unattached bacteria were washed off with 1xPBS followed by addition of DMEM containing 1,500 μg/ml of amikacin was added to kill any uninternalized bacteria. Initially cytotoxicity levels at 12, 24 and 48 hpi were measured but the ideal time point for measurement of lactate dehydrogenase (LDH) release was at 24 hpi. LDH released into the supernatant was measured at 24 hpi in triplicate for each mutant with the Promega CytoTox 96

Non-Radioactive Cytotoxicity Assay kit. A BioTek ELx808 plate reader was used to measure the absorbance at 490 nm after 30 min incubation at room temperature in the dark according to the protocol. The average cytotoxicity levels are presented with the standard error of the mean (SEM).

Growth curves of *B. pseudomallei* 1026b insertion mutants. Growth curves of the mutants were initiated by growing them overnight in 96-deepwell plates then diluting them 200 x into fresh LB. The 96-well plate was incubated at 37°C with shaking in the BioTek ELx808IU and measuring the O.D. 600 nm every 30 min for 48 h. Each growth curve was done in duplicate with the average and the SEM shown.

Intracellular replication assays of *B. pseudomallei* 1026b insertion mutants. Intracellular replication assays were carried out using a modified aminoglycoside protection assay as previously described [51,120] and as above. RAW264.7 macrophages were infected singly with wildtype *B. pseudomallei* and 21 insertion mutants with the *tssC-5*::T24 and BP1026B_I1079::T24 mutants as negative and positive controls, respectively. The monolayers were infected at an MOI of 1:1 for 1 h then washed and the medium was replaced with DMEM containing 1,500 μg/ml amikacin. At 2, 12, and 24 hpi monolayers were lysed with 0.2% Triton-X100 in PBS, lysates were diluted in PBS, plated onto LB, and incubated at 37°C for 48 h. Colonies were enumerated and bacterial numbers were determined. The experiment was carried out in triplicate and the numbers represent the average of three replicates with the error bars representing the SEM. The student t-test was used to determine the significance between replication of the wildtype and mutant strains. Calculating the average measurements from the

cytotoxicity assay and the intracellular assay and presenting it as a percentage of wildtype allowed comparison of the two assays.

Invasion assays. Invasion assays were initiated by diluting *B. pseudomallei* 1026b strains in PBS to an MOI of 1:1 in DMEM. The dilutions were plated on LB and colonies were counted 48 h later to accurately determine the number of CFU used to initiate the infections. The dilutions were used to infect the RAW264.7 macrophages in 96-well CellBIND plates at an MOI of 1:1. At 1 hpi the bacteria-containing medium was removed and the monolayers were washed twice with pre-warmed PBS and fresh DMEM containing 1,500 μg/ml amikacin was added to kill extracellular bacteria for another hour. At this point (2 hpi) the medium was removed and monolayers washed twice with pre-warmed PBS. Monolayers were lysed with 0.2% Triton-X100 in PBS, diluted, plated onto LB and incubated at 37°C for 48 h. Colonies were enumerated and invasion efficiency was determined by dividing the counted colonies by the total number of infecting bacteria. The experiment was carried out in triplicate and the numbers represent the average of all three replicates with the error bars representing the SEM. The student t-test was used to determine the significance between invasion efficiencies of the wildtype and insertional mutants.

Attachment assays. The attachment assay was carried out by diluting *B. pseudomallei* 1026b strains in PBS to an MOI of 1:1 in DMEM. The dilutions were plated on LB and colonies were counted 48 h later to accurately determine the number of CFU used to initiate the infection. The dilutions were used to infect the RAW264.7 macrophages in 96-well CellBIND plates at an MOI of 1:1. At 1 hpi the bacteria-containing medium was removed and the monolayers were

washed 3 times with pre-warmed PBS. Monolayers were lysed with 0.2% Triton-X100 in PBS, diluted, plated onto LB and incubated at 37°C for 48 h. Colonies were enumerated and attachment efficiency was determined by dividing the attached number by the initial number of infecting bacteria. The experiment was carried out in triplicate and the numbers represent the average of all three replicates with the error bars representing the SEM. The student t-test was used to determine the significance between attachment efficiencies of the wildtype and insertional mutants.

Plaque assays. *B. pseudomallei* 1026b strains were grown overnight and diluted and used to infect RAW264.7 monolayers at an MOI of 1:1 in 24-well CellBIND plates the same as the intracellular replication assay. After 1 h of infection the bacteria containing media was washed off the monolayers and further washed once more with PBS. 1.2% low-melt SeaPlaque agarose (Lonza) in DMEM was heated to 60°C cooled to ~37°C then amikacin was add to 1,500 μg/ml. 500 μl was used to overlay each monolayer and they were incubated for 24 h at 37°C in 5% CO_2. The monolayers were fixed with 4% paraformaldehyde (PFA) in PBS for 45 min and the agarose plugs were removed. Monolayers were then stained with a 1% crystal violet solution for ease of viewing. Plaques were viewed with a Zeiss AxioObserver D1 and the accompanying AxioVision 64 bit 4.9.1 software was used to measure plaque diameter. 10 to 20 plaques per well were measured for comparison. A multiple one-way ANNOVA tested significance against the wildtype plaque diameter. Numbers presented are the average with the SEM.

Complementation and plaque assay of 5 gene candidates with mini-Tn*7-kan*. The 5 genes, BP1026B_I2174 (mutant 25), BP1026B_I2220 (mutant 27), BP1026B_I2818 (mutant 21), BP1026B_II0034 (mutant 110) and BP1026B_II1256 (mutant 20), were amplified by PCR and cloned into mini-Tn*7-gat* [80]. The resultant plasmids were maintained in an *E. coli pir*$^+$ *mob*$^+$ strain and mated into the respective insertion mutants as previously described [118] then selected on MG+ 0.3% glyphosate media where Tn*7* insertion for each mutant was verified by PCR as previously described [80,113]. Plaque assays for the 5 mutants and the respective complemented strains was carried out as described above for the other plaque assays.

Differential interference contrast and fluorescence microscopy. Glass bottom 12-well plates were obtained from MatTek Corporation (Ashland, MA). The plates were sterile, uncoated, and contained bottoms of No. 1.5 covers lips. Glass coverslip bottoms were treated for four hours with 150 µg/ml poly-L-lysine in ddH_2O. The plates were washed twice with ddH_2O and allowed to air-dry within a biosafety cabinet overnight. Monolayers were seeded at nearly $3x10^8$ cells/well verified by the Scepter handheld automated cell counter. Cells were allowed to attach and grow for 24 h prior to initiating the infection. Cell lines were infected with an MOI of 1:1 bacteria and the rest of the infection was carried out as above for the plaque assay. After 24 h of infection the monolayers were fixed with 4% PFA for 45 min before removing the agarose overlay. Fixed monolayers were permeablized with 0.2% Triton X-100 in PBS for 5 minutes. Monolayers were washed with PBS then incubated with 1% BSA in PBS for 30 min to remove background. The actin was stained with AlexaFluor 488 phalloidin (Invitrogen) according to the manufacturers protocol. After washing, the cell membranes and nuclei were stained by mixing FM 4-64FX (a lipophilic styryl dye that dyes membranes red, Invitrogen) and ProLong Gold

antifade with DAPI (to stabilize dyes for long term storage and DAPI to dye nuclei blue, Invtirogen). Plates were sealed, protected from light, and stored at 4°C for up to 2 months. Images were captured with an AxioObserer D1 and accompanying Axiovision 4.9.1 software. Multi-color fluorescent images were captured with the multichannel fluorescence acquisition module of the Axiovision software. Images were deconvolved using the imageJ plugin Iterative Deconvolve 3D.

Animal studies. BALB/c mice between 4 and 6 weeks of age were purchased from Jackson Laboratories (Bar Harbor, ME). Animals were housed in micro-isolator cages under pathogen-free conditions. The Institutional Animal Care and Use Committee at Colorado State University approved all animal studies (CSU protocol 12-3586A). Every infection with *B. pseudomallei* was done using intranasal (i.n.) inoculation [82]. Animals were anesthetized with 100 mg/kg ketamine plus 10 mg/kg xylazine. A challenge dose of 4,500 CFU (10 times the LD_{50}) of the various *B. pseudomallei* were suspended in PBS and 20 µl was delivered i.n., alternating nostrils. For all *B. pseudomallei* survival studies, animals were monitored for disease symptoms twice daily and were euthanized according to pre-determined humane endpoints. Lungs, liver, and spleen were removed and plated to determine bacterial counts in surviving infected mice 60 d post-infection. Statistical differences in survival times were determined by Kaplan-Meier curves followed by the log-rank test. At 60 dpi all surviving animals were humanely sacrificed and the lungs, liver, and spleen were removed and homogenized in 1 ml saline. Aliquots were plated and observed for organ load CFU.

6.7 FIGURE LEGENDS

FIG 1. Tn-seq experimental setup. The *P. aeruginosa* PAO1 *asd* gene was cloned into the mariner transposon pBT20. It was mated into *B. pseudomallei* K96243 Δ*asd*. Only the *B.p.* that had the wildtype copy of the *asd* gene inserted in the genome would have a return of the wildtype phenotype and grow on minimal glucose media without DAP. All colonies were pooled and used to infect RAW264.7 murine macrophages for 12 h and a total of 3 passages. gDNA from the unpassaged and passaged pools was isolated and sequenced with Illumina sequencing. Data was analyzed using IGV. 134 insertion mutants of hypothetical and putative genes that demonstrated high levels of negative selection were obtained and used to infect RAW264.7 macrophages to verify importance of the genes during infection.

FIG 2. Genes shared between replicates and hypothetical enrichment. A, Venn diagrams of the genes shared between replicates. The number of genes present in only the MOI of 10:1 replicate (blue) and the number of genes present in only the MOI 1:1 replicates (red) are indicated and those shared are in the overlapping region. Each Venn diagram has an increasing negative stringency increasing from ≥10 to ≥1,000. A majority of genes are shared between the replicates. B, Pie charts indicating the percentage representation of hypothetical/putative genes in the K96243 genome, and genes shared between replicates of the ≥10 and the ≥1000 data sets. Hypothetical/putative genes undergo higher negative selection and are overrepresented amongst genes the more stringent the cutoff.

FIG 3. Gene functional enrichment of low read saturation regions and genes. A, Gene ontology enrichment of genes with known or predicted functions. The X-axis is the gene function. The Y-axis is the fold enrichment of the function in our data compared to that present in the genome. The genes in the ≥10 (blue bar), ≥100 (green bar), and ≥1,000 (red bar) are the same genes in the overlapping Venn diagrams of Figure 2A representing the genes shared between replicates. B, Visual comparison of the mapped reads from the unpassaged pool compared to the two passaged replicates in the IGV program. Highlighted as an example is the well-characterized region of *B.p.* chromosome two. This region contains the T6SS-5 and the T3SS-3 *Burkholderia* secretion apparatus (*Bsa*). Vertical grey bars represent mapped reads in log-scale. Lower read saturation is visible in this region of the passaged replicates (10:1 and 1:1; bottom two rows) compared to the unpassaged (POOL; top row) sample, reiterating the importance of this region to bacterial replication in host cells.

FIG 4. Cytotoxicity and intracellular replication screening of novel putative virulence factors. A, 134 gene candidates were tested for reduced cytotoxicity. The y-axis is the LDH released as a % of total possible LDH release. Vertical bars represent the average of 3 biological replicates with error bars representing the standard error of the mean (SEM); * means $p<0.05$ as determined by the student t-test. For comparison the red line indicates the average level of cytotoxicity attributed to infection by wildtype. B, Growth rates of the insertion mutants were carried out to make sure there were no *in vitro* growth defects by measuring the OD every 30 minutes for 48 h. Two mutants had growth defects and were not investigated further (blue and red line). The remaining mutants (green and black lines) were all similar to wildtype (orange line) indicating there were no other *in vitro* growth defects and that cytotoxicity readings were

not due to an inability to grow. Growth curves were done in duplicate and the average is shown with the SEM. C, Cytotoxicity of *Bp* insertion mutants with lower cytotoxicity than the wildtype was calculated as a % of wildtype (black bar) and compared to intracellular bacteria CFU of % of wildtype (grey bar) at 24 hpi to observe trends in the two measurements. D, Intracellular replication assays for the insertion mutants were carried out and presented in linear scale where the groups of mutants were significantly different at the 12 or 24 hpi time points. The 12 and 24 hpi time points are presented as bar graphs to allow for ease of comparison between wildtype (WT; red line and bar), the internal positive control insertion mutant BP1026B_I1079 (39; light blue line and bar), the internal negative control insertion mutant BP1026B_II1588 (*tssC-5*::T24, 126; orange line and bar) and the remaining insertion mutants. *=p<0.05, **=p<0.005, ***=p<0.0005, ****=p<0.00005 by the student t-test.

FIG 5. Virulence assays characterize the putative virulence factors. A, Invasion assays were carried out on all mutants that had intracellular replication deficiencies and compared to the *tssC-5*, BP1026B_I1079 insertion mutants, and wildtype. Numbers shown are the number of intracellular bacteria recovered after 2 h infection divided by the total number of bacteria used to initiate the infection. The average of three experiments and the SEM is shown. B, Attachment assays were carried out for all mutants that demonstrated a deficiency in the invasion assay and compared to the BP1026B_I1079 insertion mutants and wildtype. The numbers shown are the number of bacteria recovered after 1 h of attachment divided by the total number of bacteria used to initiate the infection. All numbers are the average of three replicate experiments with the SEM. C, Plaque assays were carried out on genes of interest and compared to the *tssC-5* and the

wildtype. At least 10 plaques were measured with the bars representing the average and the SEM. *=$p<0.05$, **=$p<0.005$, ***=$p<0.0005$, ****=$p<0.00005$ by the student t-test.

FIG 6. Plaque phenotypes of putative virulence factor mutants. A, Plaque phenotypes of the mutants most deficient in plaque formation from Fig. 5C were observed via DIC microscopy at 24 hpi after removing the agarose overlay. The mutants were compared to the internal negative control *tssC-5* and positive control BP1026B_I1079 mutants and wildtype. Carats indicate the MNGC/plaque formation in the representative images. For ease of viewing a light red border has been drawn around the regions of MNGC formation for clarity.

FIG 7. Mutant Virulence Phenotype "MVP" Matrix. A summation of all virulence assays of 23 mutants including the negative internal control *tssC-5* and positive internal control mutant 39 compared to wildtype 1026b. Columns represent the different assays and rows represent the different mutants. If a mutant behaved like wildtype in the assays the heat map tile is red. The more deficient in the assays than wildtype the more green the tile. The heat map was clustered using Pearson correlative hierarchical clustering to place mutants that behave similarly near each other. They are divided into 7 different groups based on there behaviors in the assays and more simply those that have deficiencies in the beginning and later stages of the cellular infection model.

FIG 8. Complementation of two novel virulence factors and contributions of neighboring genes. Intracellular replication assay of BP1026B_I2174 (A) and BP1026B_II1256 (B) mutants along with their Tn*7*-complemented strains compared to wildtype and the *tssC-5* mutant, measured in triplicate with the SEM shown. The x-axis is log scale internal CFU with y-axis as time post-infection. Insets show details in linear scale. C, Plaque assay of the same strains with at least ten plaques measured 24 hpi. Significance determined by one-way ANOVA compared to WT as control. **** =p<0.00005. D and E are LDH assays performed in triplicate presented as % total cytotoxicity of wildtype. Yellow bar is gene of interest, grey/black are neighboring genes as labeled on x-axis, orange is the negative control, blue is the positive control, and red is the wildtype control. *=p<0.05, **=p<0.005, ***=p<0.0005, ****=p<0.00005 by one-way ANOVA compared to WT as control.

FIG 9. BALB/c virulence mutant attenuation study. Twenty mutants from the original 134 were selected for attenuation studies in the BALB/c inhalation melioidosis model. Five mice were infected with 10x the LD_{50} or 4,500 CFU of each of the transposon mutants or wildtype 1026b and survival was observed. Mice infected with wildtype become moribund 3 dpi and the survival curve is red in all the figures in order of increasing attenuation. A, all survival curves. B, Survival curve of mutants that killed all mice. C, Survival curve of mutants with 20% survival. D, Survival curve of mutants with 40% survival. E, Survival curve of mutants with 60% survival. F, Survival curve of the mutant with 100% survival. All curves compared to wildtype (red line) using Log-rank (Mantel-Cox) test with *=p<0.05 and **=p<0.005. D,F,H, and J, Bacterial organ loads of each surviving mouse from the survival curves to the immediate left of each organ load graph.

Table 1. Genes showing greater than 10, 100, and 1,000 fold negative selection in both replicates compared to the unpassaged pool. Gene ID for these lists is I the K96243 gene ID. Functional annotation is shown for select genes in the >10 group and all genes in the >1,000 group. Genes involved in secondary metabolite biosynthesis, flagellar assembly, secretion, and regulation are indicated by the color, see legend.

Table 2. List of genes targeted in this study. A list of 134 insertion mutants targeted in this study. This table indicates the gene mutant number in this study (1-134), the K96243 and the 1026b gene IDs, the annotated function in each genome, additional data obtained through bioinformatics, and virulence data (where applicable).

FIG S1. Virulence factors identified in the Tn-seq data. KEGG figures of known virulence factors. A, Flagella. B, Lipopolysaccharide biosynthesis. C, Secretion systems. Boxes outlined in red are genes identified with >10 times negative selection.

FIG S2. Potential virulence loci identified in the Tn-seq data. For each column, mapped reads for each sample are on the left with each gene on the right and a heat map representation in the middle. These are regions of low read saturation in both the "10_1" and "1_1" passaged pools when compared to the unpassaged "POOL" sample. Black means 10 times more reads and yellow means greater than 100 ties more reads than blue for a given gene row. A summary of

functions for selected gene regions are below the heat maps. A, *Bp* chromosome I. B, Chromosome II.

FIG S3. Gene receiving 0 reads after passage. A, Genes that had 0 reads in both replciates after passaging (y-axis) and the number of reads received from the unpassaged pool (x-axis), red circles. B, Heat maps comparing the reads from the unpassaged pool (left) and the average reads from both passaged replicates.

FIG S4 and S5. anti-SMASH analysis of secondary metabolite operons. A, secondary metabolite clusters and predicted function of genes in the cluster. B, anti-SMASH predicted peptide scaffold without tailoring modifications by nearby genes resulting in potentially different "isotope" modifications. C, Cluster homology among the Burkholderia and conservation of genes by color. S4D, only webACT alignment of the 1026b region and the *B. thailandensis* E264 region showing absence of a BP1026B_II1256 homologue in the E264 genome. The deletion and relocation of BP1026B_II1278 through BP1026B_II1286 homologues in the E264 genome is also depicted in C.

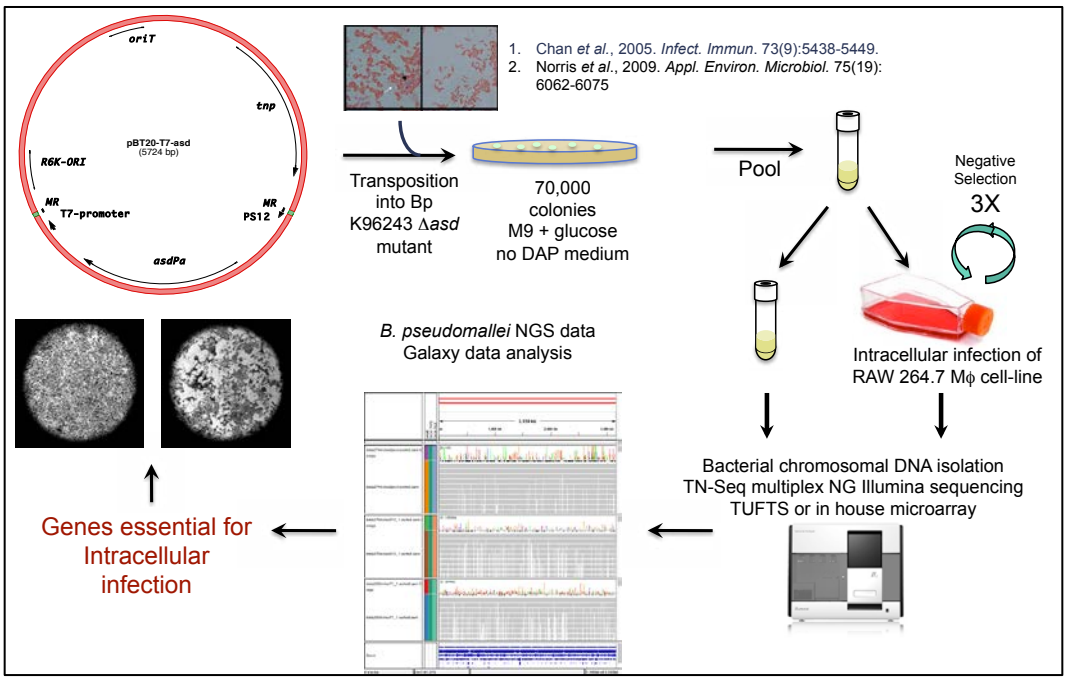

Figure 1

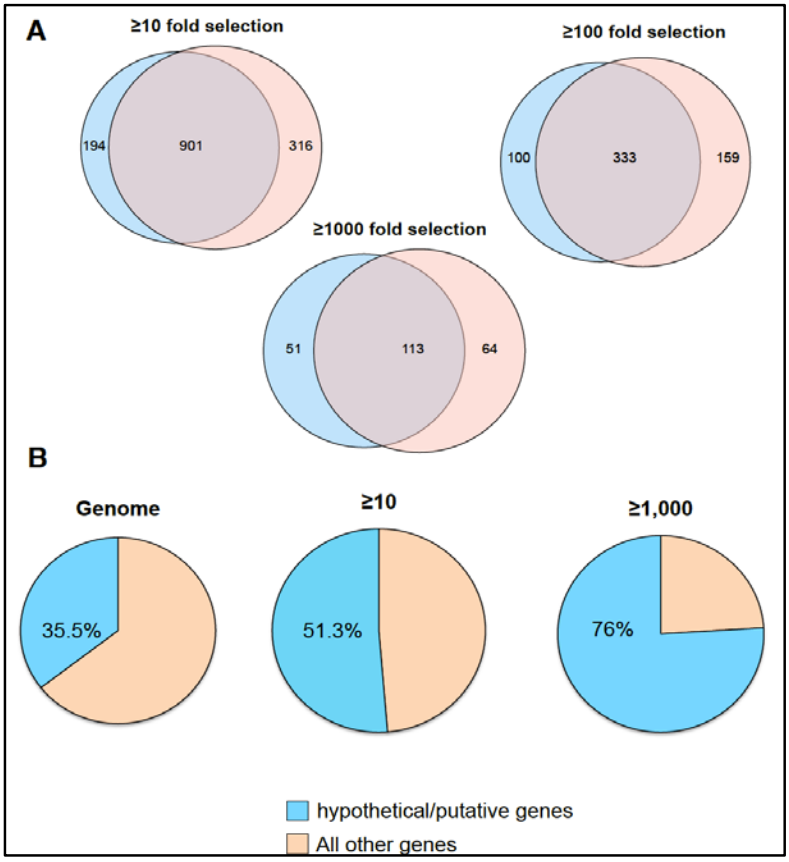

Figure 2

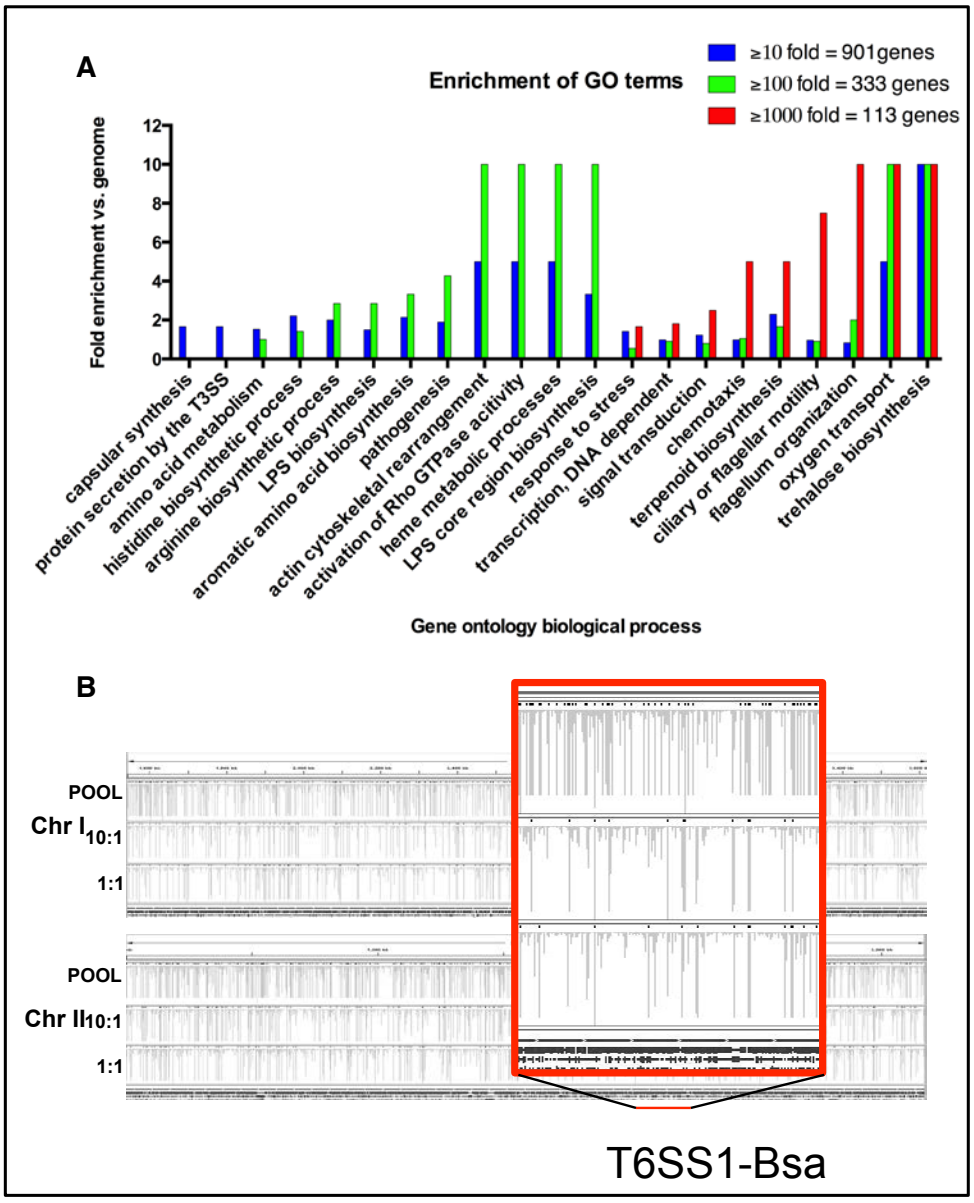
A
Enrichment of GO terms
≥10 fold = 901genes
≥100 fold = 333 genes
≥1000 fold = 113 genes
Fold enrichment vs. genome
0
2
4
6
8
10
12
capsular synthesis
protein secretion by the T3SS
amino acid metabolism
histidine biosynthetic process
arginine biosynthetic process
LPS biosynthesis
aromatic amino acid biosynthesis
pathogenesis
actin cytoskeletal rearrangement
activation of Rho GTPase acitivity
heme metabolic processes
LPS core region biosynthesis
response to stress
transcription, DNA dependent
signal transduction
chemotaxis
terpenoid biosynthesis
ciliary or flagellar motility
flagellum organization
oxygen transport
trehalose biosynthesis
Gene ontology biological process
B
POOL
Chr I 10:1
1:1
POOL
Chr II 10:1
1:1
T6SS1-Bsa

Figure 3

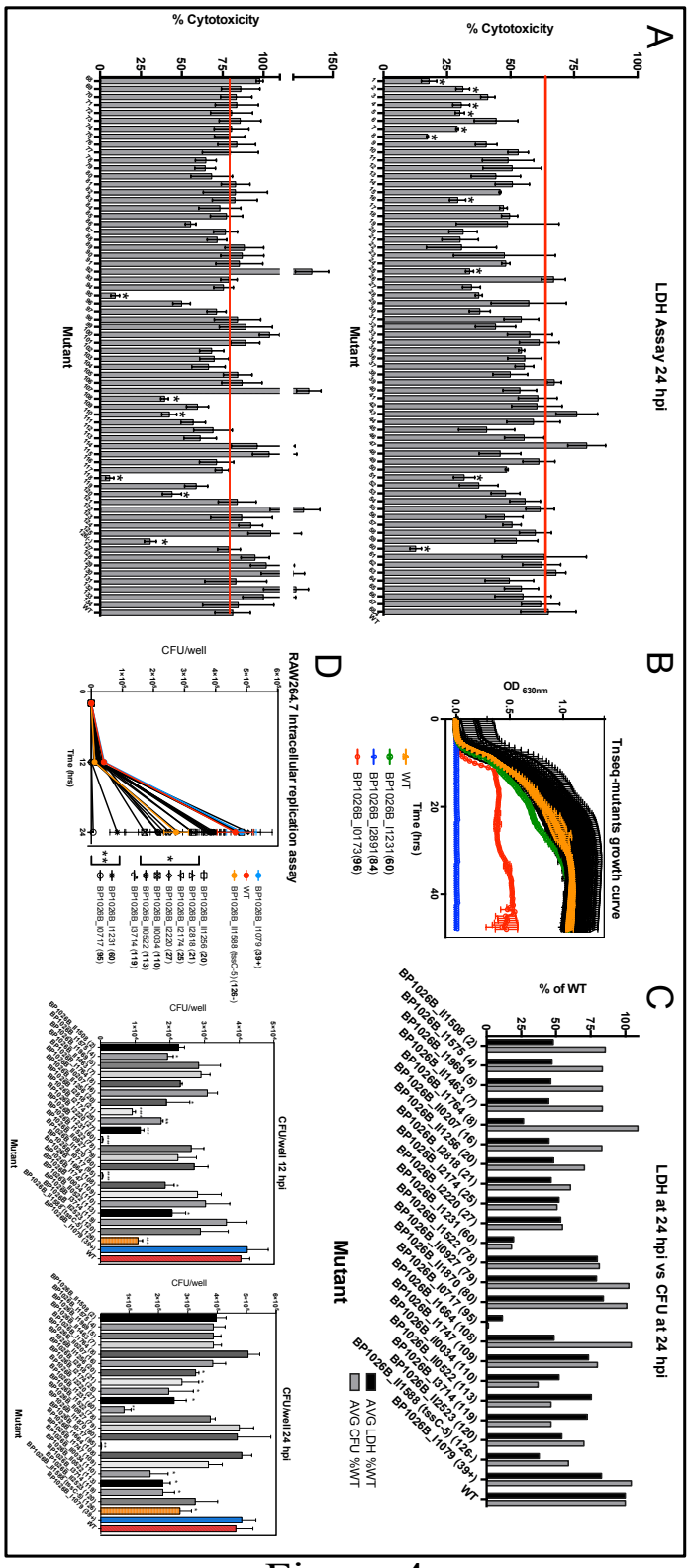
A
LDH Assay 24 hpi
% Cytotoxicity
Mutant
B
Tnseq-mutants growth curve
OD 630nm
Time (hrs)
WT
BP1026B_I1231(60)
BP1026B_I2891(84)
BP1026B_I0173(96)
C
LDH at 24 hpi vs CFU at 24 hpi
% of WT
Mutant
AVG LDH %WT
AVG CFU %WT
D
RAW264.7 Intracellular replication assay
CFU/well
Time (hrs)
CFU/well 12 hpi
CFU/well 24 hpi

Figure 4

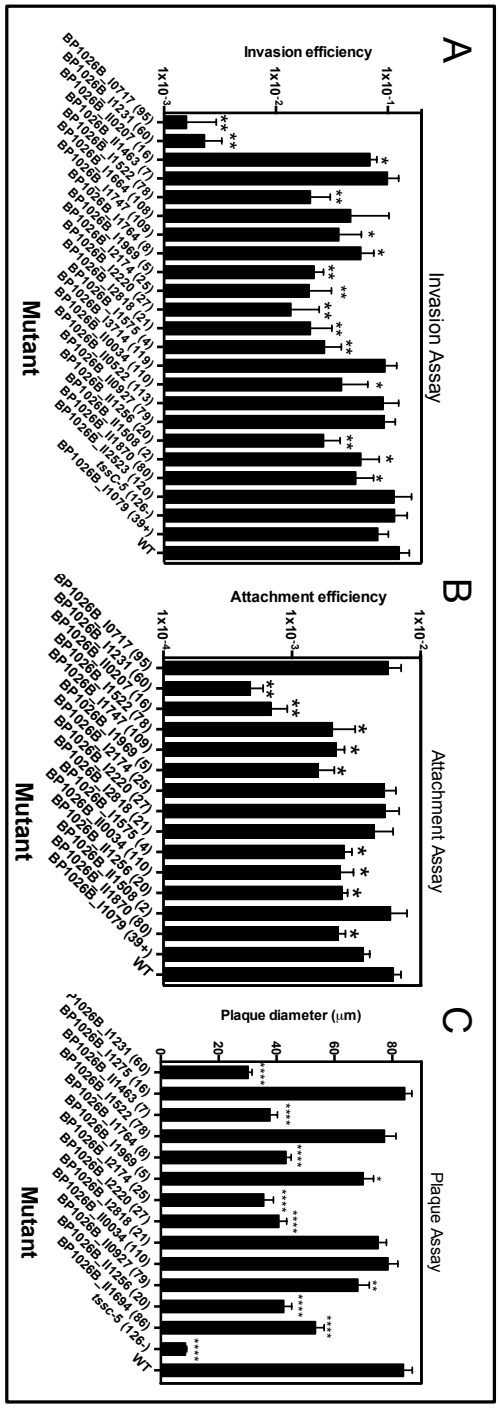
A
Invasion efficiency
1x10-3
1x10-2
1x10-1
Invasion Assay
Mutant
BP1026B_I0717 (95)
BP1026B_I1231 (60)
BP1026B_I0207 (16)
BP1026B_I1483 (7)
BP1026B_I1522 (78)
BP1026B_I1664 (108)
BP1026B_I1747 (109)
BP1026B_I1764 (8)
BP1026B_I1969 (5)
BP1026B_I2174 (25)
BP1026B_I2220 (27)
BP1026B_I2818 (21)
BP1026B_I3175 (4)
BP1026B_I0034 (110)
BP1026B_I0522 (113)
BP1026B_I0927 (79)
BP1026B_I1256 (20)
BP1026B_I1508 (2)
BP1026B_I1870 (60)
BP1026B_I2523 (60)
fssC-5 (126-)
BP1026B_I1079 (39+)
WT
B
Attachment efficiency
1x10-4
1x10-3
1x10-2
Attachment Assay
Mutant
BP1026B_I0717 (95)
BP1026B_I1231 (60)
BP1026B_I0207 (16)
BP1026B_I1522 (78)
BP1026B_I1747 (109)
BP1026B_I1969 (5)
BP1026B_I2174 (25)
BP1026B_I2220 (27)
BP1026B_I2818 (21)
BP1026B_I0034 (110)
BP1026B_I1575 (4)
BP1026B_I1256 (20)
BP1026B_I1508 (2)
BP1026B_I1870 (60)
BP1026B_I1079 (39+)
WT
C
Plaque diameter (μm)
0
20
40
60
80
Plaque Assay
Mutant
BP1026B_I1231 (60)
BP1026B_I1275 (16)
BP1026B_I1463 (7)
BP1026B_I1522 (78)
BP1026B_I1764 (8)
BP1026B_I1969 (5)
BP1026B_I2174 (25)
BP1026B_I2220 (27)
BP1026B_I2818 (21)
BP1026B_I0034 (110)
BP1026B_I0927 (79)
BP1026B_I1256 (20)
BP1026B_I1894 (86)
fssC-5 (126-)
WT

Figure 5

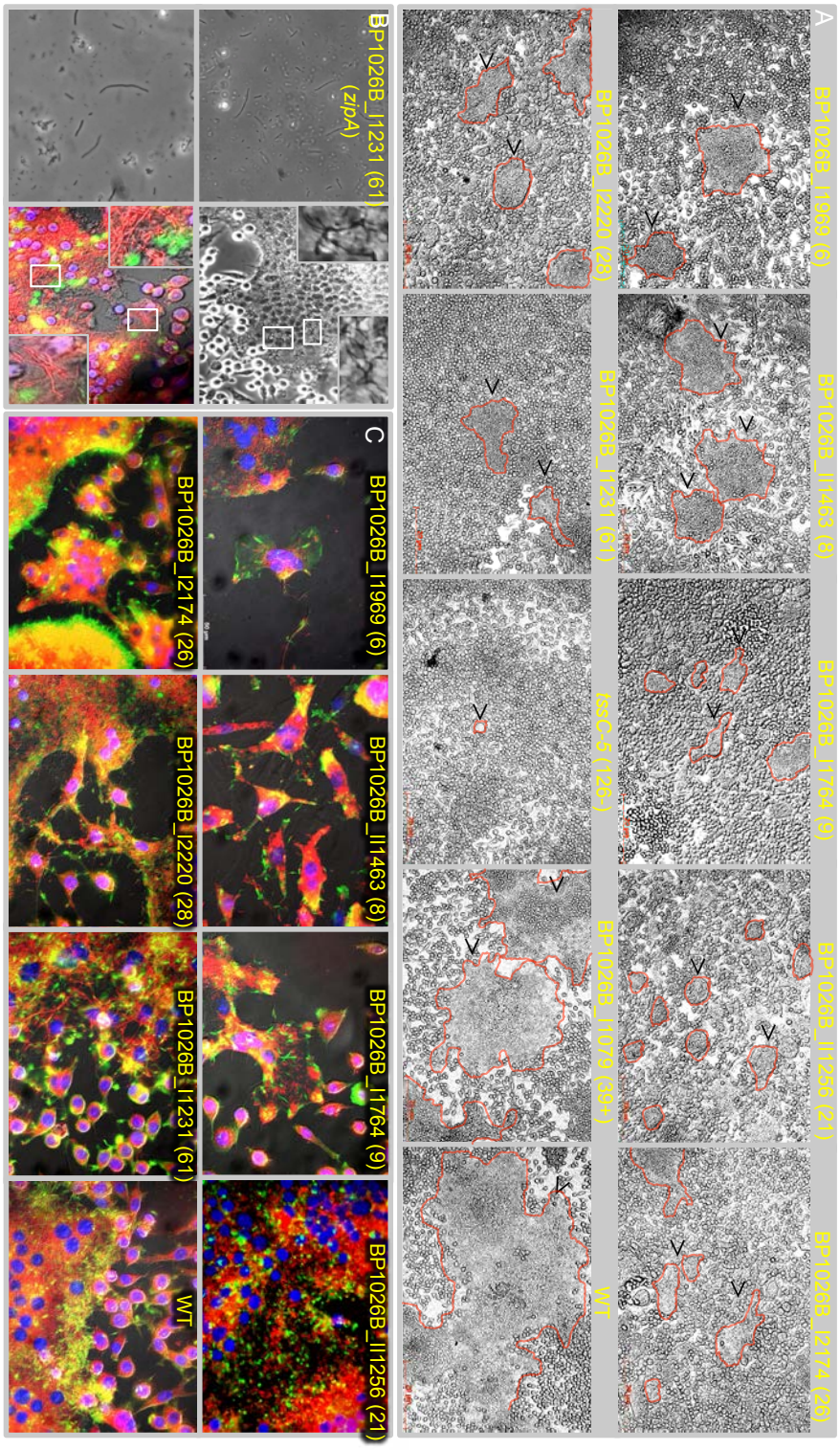
A
BP1026B_I1969 (6)
BP1026B_II1463 (8)
BP1026B_I1764 (9)
BP1026B_II1256 (21)
BP1026B_I2174 (26)
BP1026B_I2220 (28)
BP1026B_I1231 (61)
fsC-5 (126-)
BP1026B_I1079 (90+)
WT
BP1026B_I1231 (61)
(zipA)
C
BP1026B_I1969 (6)
BP1026B_II1463 (8)
BP1026B_I1764 (9)
BP1026B_II1256 (21)
BP1026B_I2174 (26)
BP1026B_I2220 (28)
BP1026B_I1231 (61)
WT

Figure 6

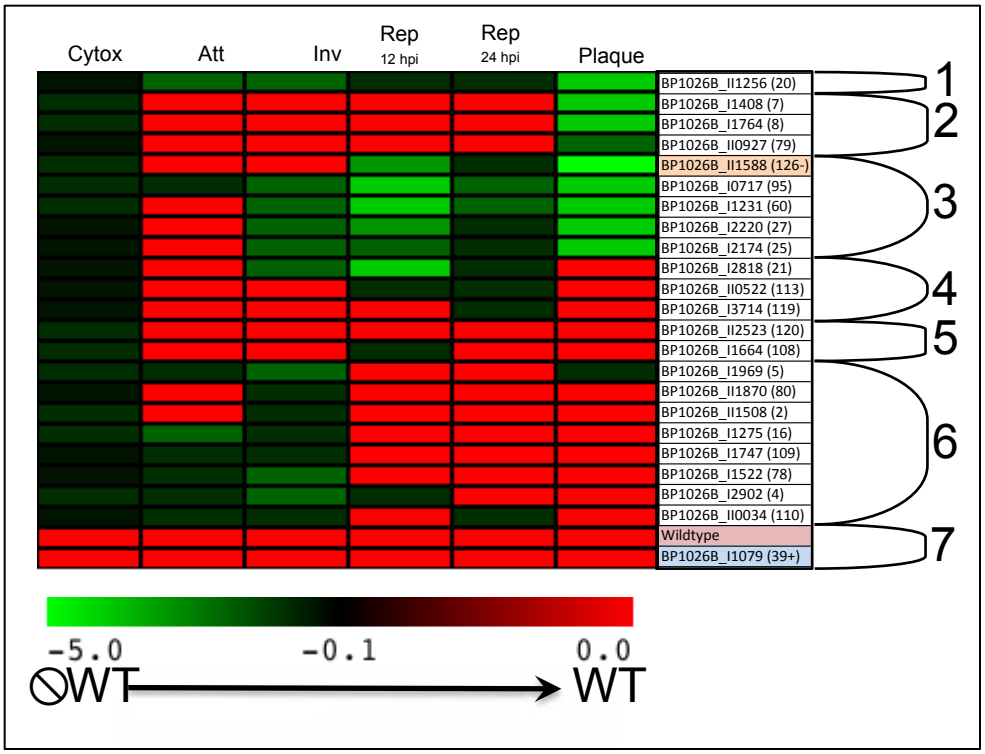

Figure 7

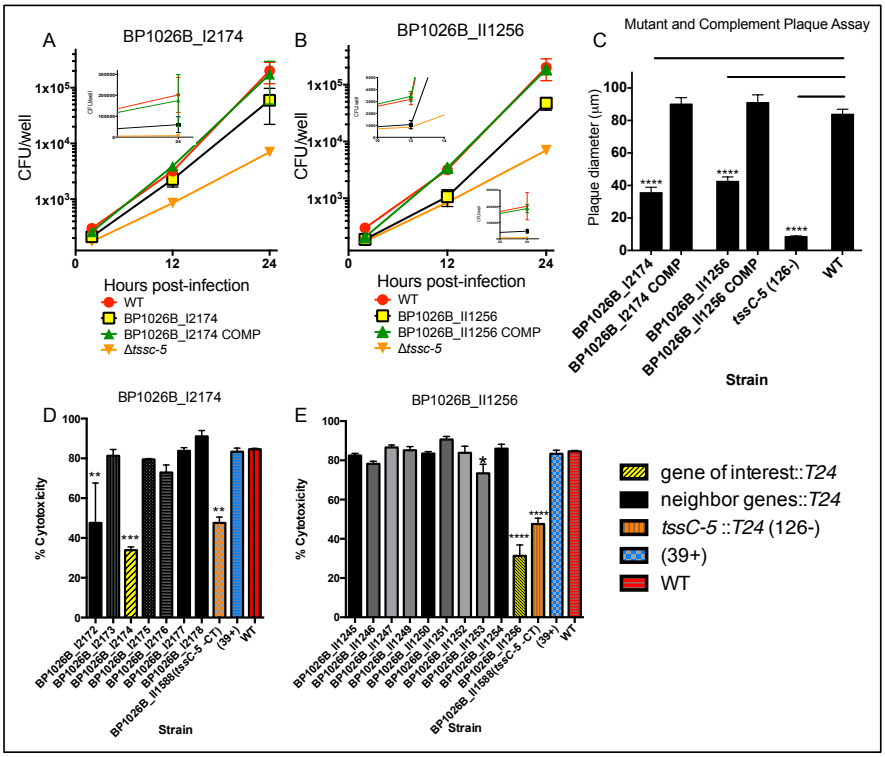

Figure 8

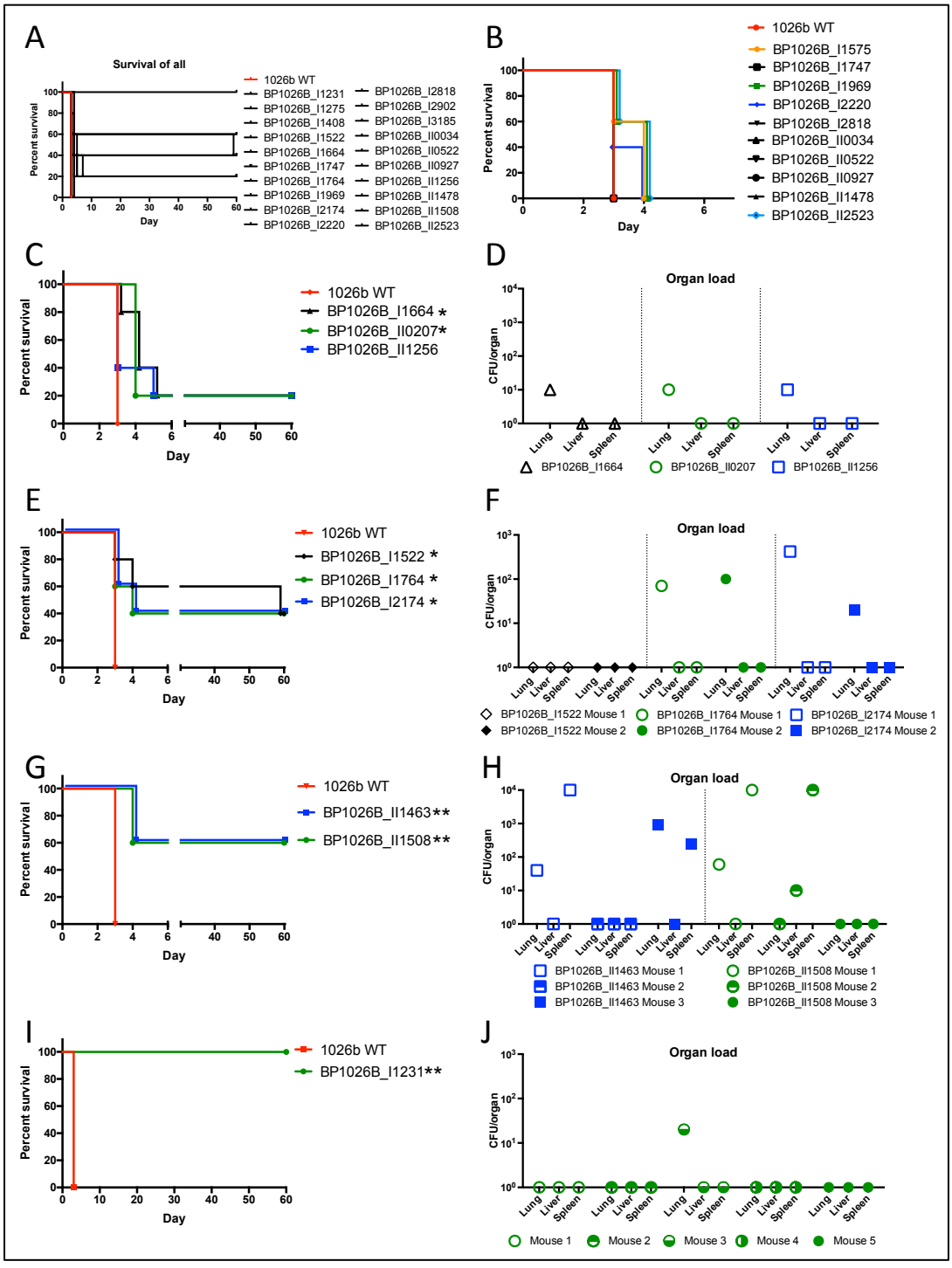
A
Survival of all
Percent survival
Day
1026b WT
BP1026B_I1231
BP1026B_I1275
BP1026B_I1408
BP1026B_I1522
BP1026B_I1664
BP1026B_I1747
BP1026B_I1764
BP1026B_I1969
BP1026B_I2174
BP1026B_I2220
BP1026B_I2818
BP1026B_I2902
BP1026B_I3185
BP1026B_II0034
BP1026B_II0522
BP1026B_II0927
BP1026B_II1256
BP1026B_II1478
BP1026B_II1508
BP1026B_II2523
B
Percent survival
Day
1026b WT
BP1026B_I1575
BP1026B_I1747
BP1026B_I1969
BP1026B_I2220
BP1026B_I2818
BP1026B_II0034
BP1026B_II0522
BP1026B_II0927
BP1026B_II1478
BP1026B_II2523
C
Percent survival
Day
1026b WT
BP1026B_I1664 *
BP1026B_II0207*
BP1026B_II1256
D
Organ load
CFU/organ
Lung
Liver
Spleen
BP1026B_I1664
BP1026B_II0207
BP1026B_II1256
E
Percent survival
Day
1026b WT
BP1026B_I1522 *
BP1026B_I1764 *
BP1026B_I2174 *
F
Organ load
CFU/organ
BP1026B_I1522 Mouse 1
BP1026B_I1522 Mouse 2
BP1026B_I1764 Mouse 1
BP1026B_I1764 Mouse 2
BP1026B_I2174 Mouse 1
BP1026B_I2174 Mouse 2
G
Percent survival
Day
1026b WT
BP1026B_II1463**
BP1026B_II1508**
H
Organ load
CFU/organ
BP1026B_II1463 Mouse 1
BP1026B_II1463 Mouse 2
BP1026B_II1463 Mouse 3
BP1026B_II1508 Mouse 1
BP1026B_II1508 Mouse 2
BP1026B_II1508 Mouse 3
I
Percent survival
Day
1026b WT
BP1026B_I1231**
J
Organ load
CFU/organ
Mouse 1
Mouse 2
Mouse 3
Mouse 4
Mouse 5

Figure 9

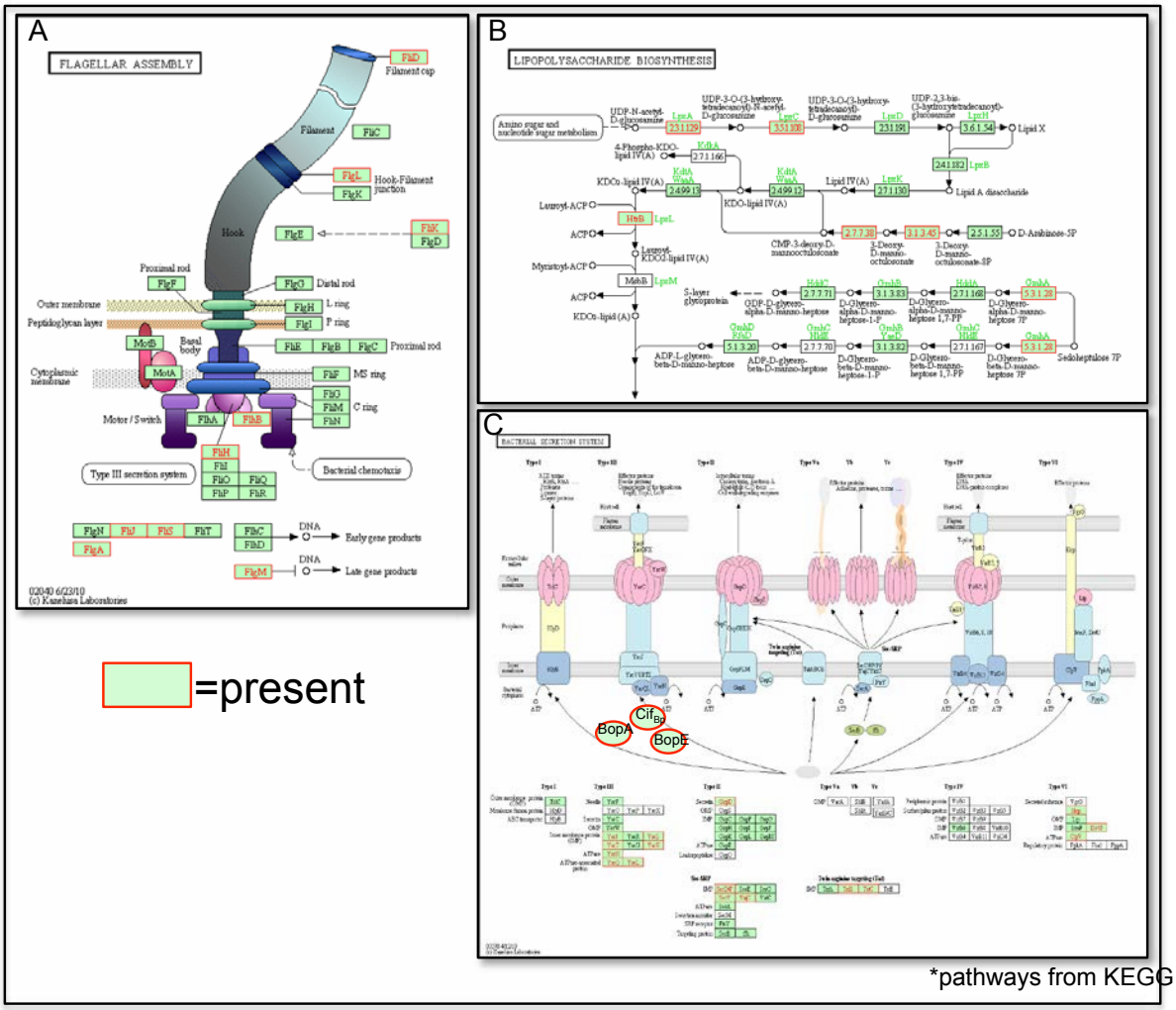
A
FLAGELLAR ASSEMBLY
Filament cap
Filament
Hook-Filament junction
Hook
Proximal rod
Distal rod
Outer membrane
L ring
Peptidoglycan layer
P ring
Basal body
Proximal rod
Cytoplasmic membrane
MS ring
C ring
Motor / Switch
Type III secretion system
Bacterial chemotaxis
DNA
Early gene products
DNA
Late gene products
02040 6/23/10
(c) Kanehisa Laboratories
=present
B
LIPOPOLYSACCHARIDE BIOSYNTHESIS
C
BopA
BopE
*pathways from KEGG

Figure S1

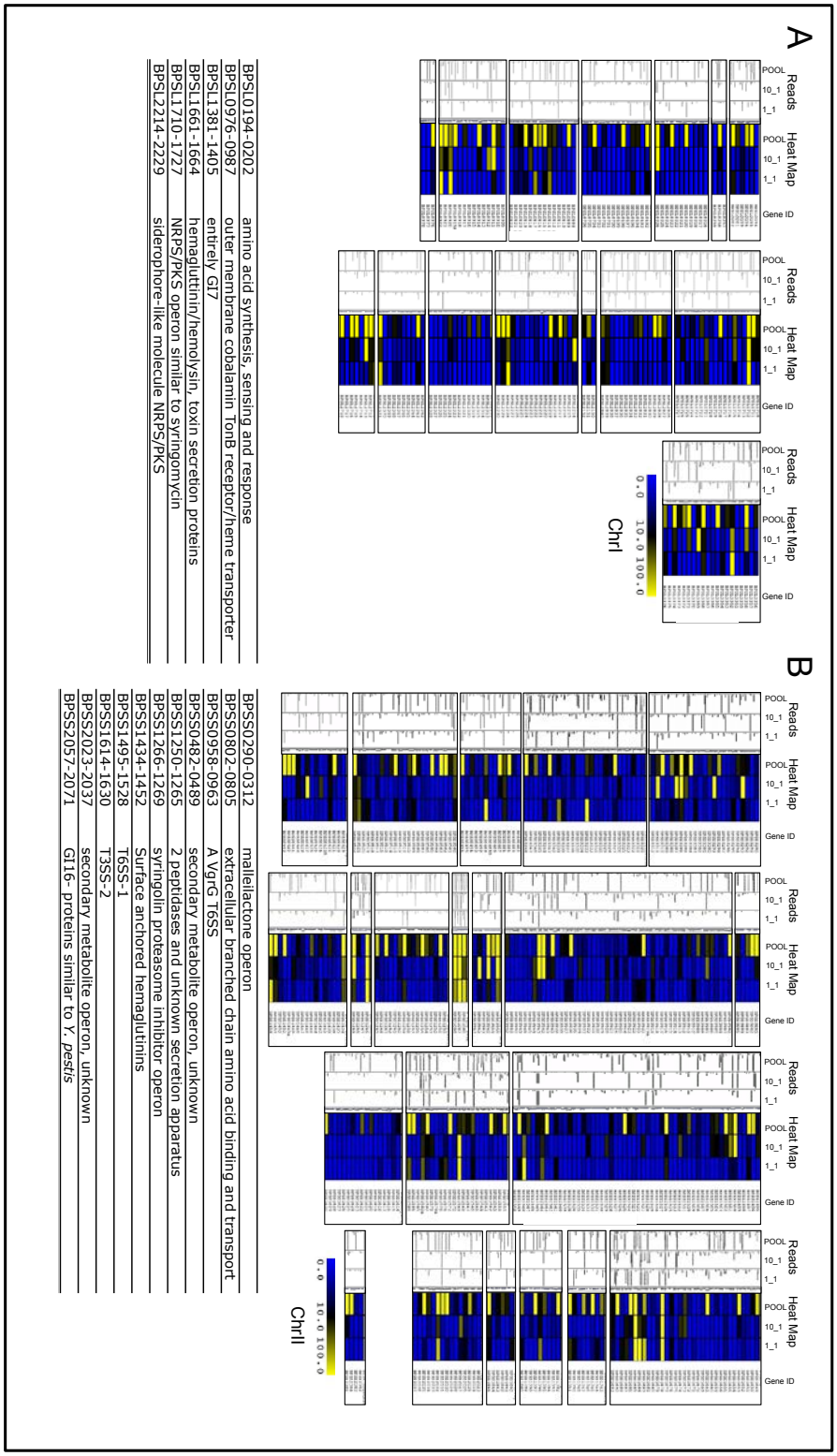

BPSL0194-0202	amino acid synthesis, sensing and response
BPSL0976-0987	outer membrane cobalamin TonB receptor/heme transporter
BPSL1381-1405	entirely GI7
BPSL1661-1664	hemagluttinin/hemolysin, toxin secretion proteins
BPSL1710-1727	NRPS/PKS operon similar to syringomycin
BPSL2214-2229	siderophore-like molecule NRPS/PKS

BPSS0290-0312	malleilactone operon
BPSS0802-0805	extracellular branched chain amino acid binding and transport
BPSS0958-0963	A VgrG T6SS
BPSS0482-0489	secondary metabolite operon, unknown
BPSS1250-1265	2 peptidases and unknown secretion apparatus
BPSS1266-1269	syringolin proteasome inhibitor operon
BPSS1434-1452	Surface anchored hemaglutinins
BPSS1495-1528	T6SS-1
BPSS1614-1630	T3SS-2
BPSS2023-2037	secondary metabolite operon, unknown
BPSS2057-2071	GI16- proteins similar to *Y. pestis*

Figure S2

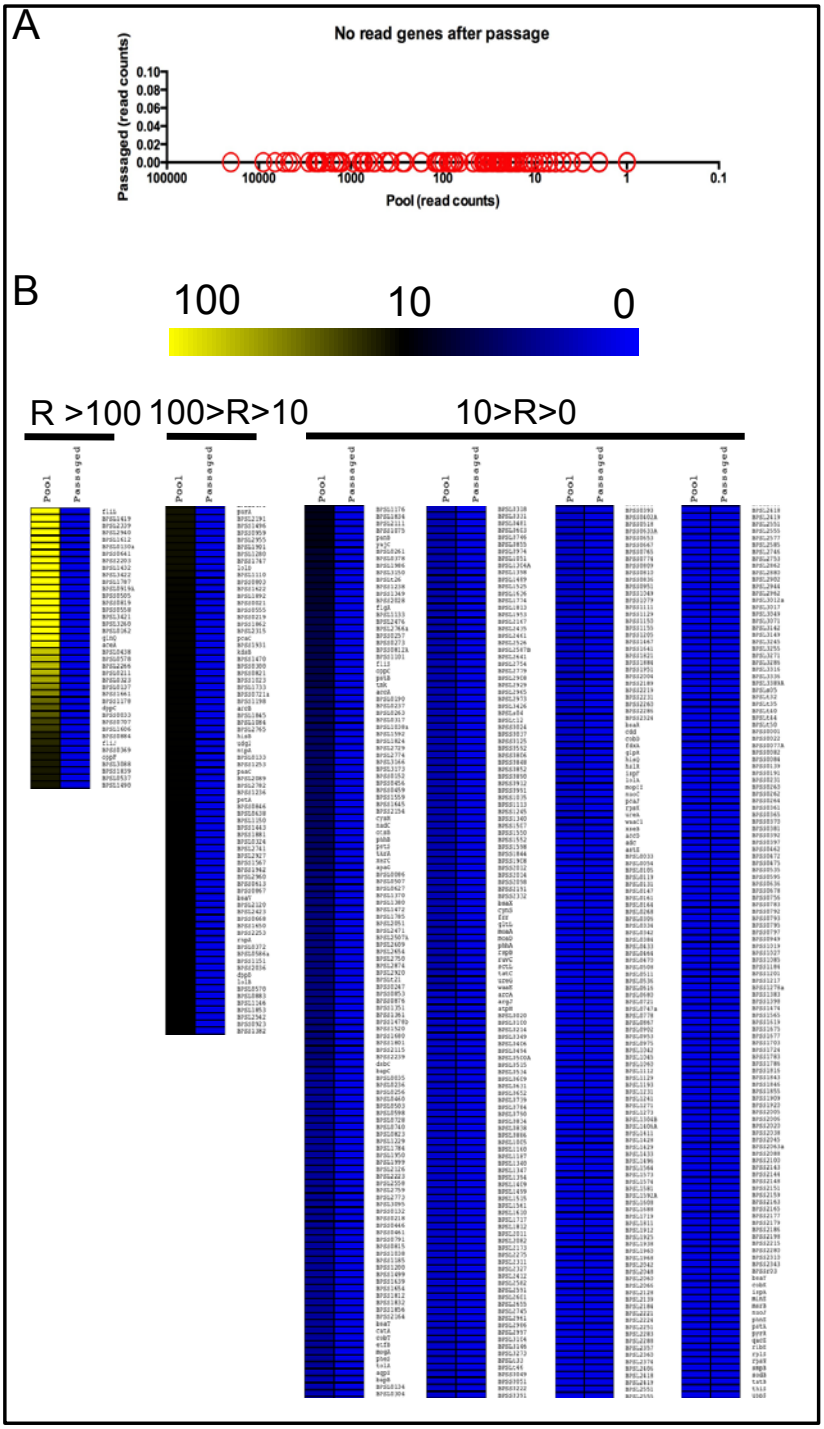
A
No read genes after passage
Passaged (read counts)
0.10
0.08
0.06
0.04
0.02
0.00
100000
10000
1000
100
10
1
0.1
Pool (read counts)
B
100
10
0
R >100
100>R>10
10>R>0
Pool
Passaged

Figure S3

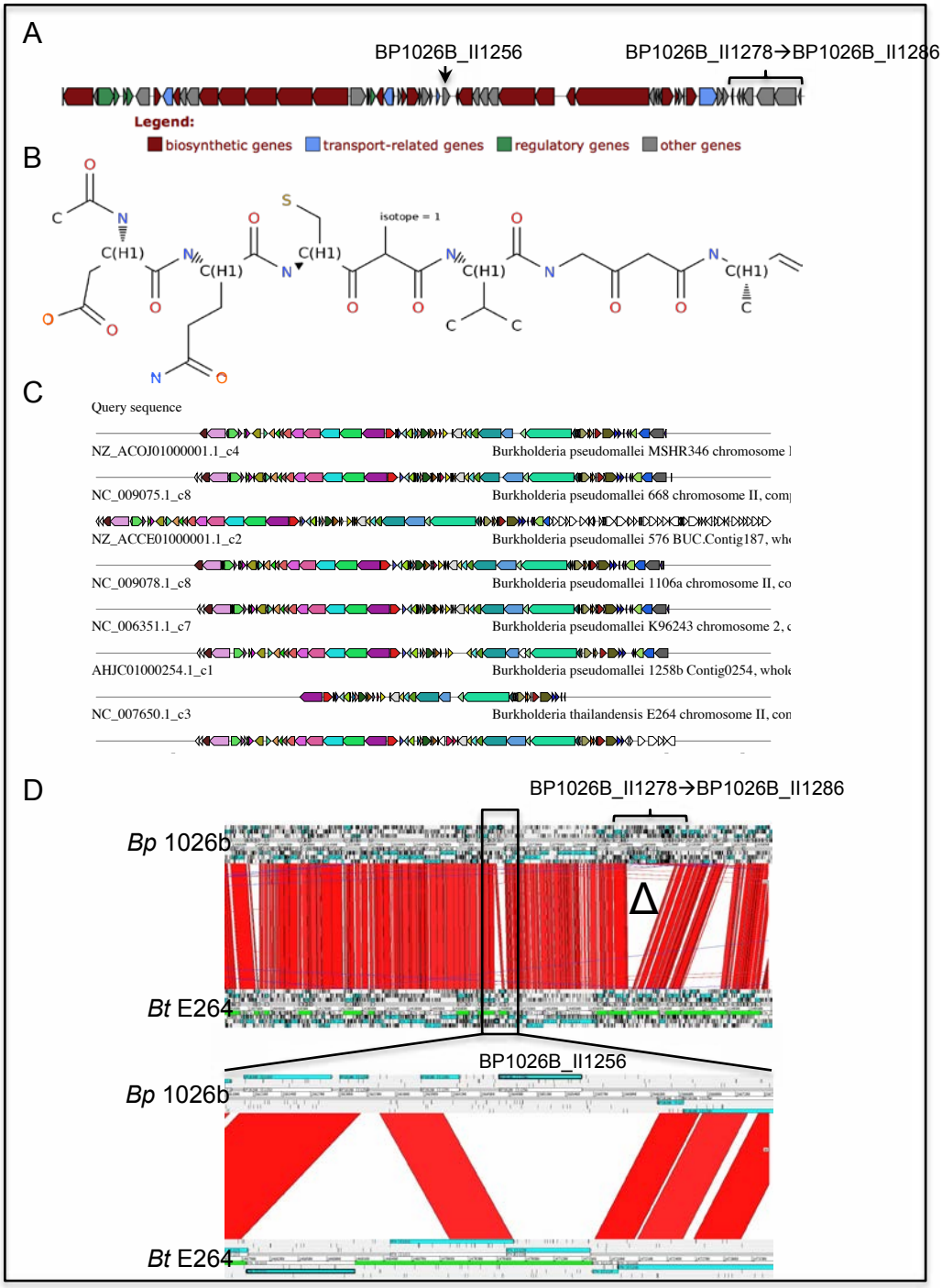
A
BP1026B_II1256
BP1026B_II1278→BP1026B_II1286
Legend:
biosynthetic genes
transport-related genes
regulatory genes
other genes
B
isotope = 1
C
Query sequence
NZ_ACOJ01000001.1_c4
Burkholderia pseudomallei MSHR346 chromosome
NC_009075.1_c8
Burkholderia pseudomallei 668 chromosome II, com
NZ_ACCE01000001.1_c2
Burkholderia pseudomallei 576 BUC.Contig187, wh
NC_009078.1_c8
Burkholderia pseudomallei 1106a chromosome II, co
NC_006351.1_c7
Burkholderia pseudomallei K96243 chromosome 2,
AHJC01000254.1_c1
Burkholderia pseudomallei 1258b Contig0254, whol
NC_007650.1_c3
Burkholderia thailandensis E264 chromosome II, con
D
BP1026B_II1278→BP1026B_II1286
Bp 1026b
Δ
Bt E264
BP1026B_II1256
Bp 1026b
Bt E264

Figure S4

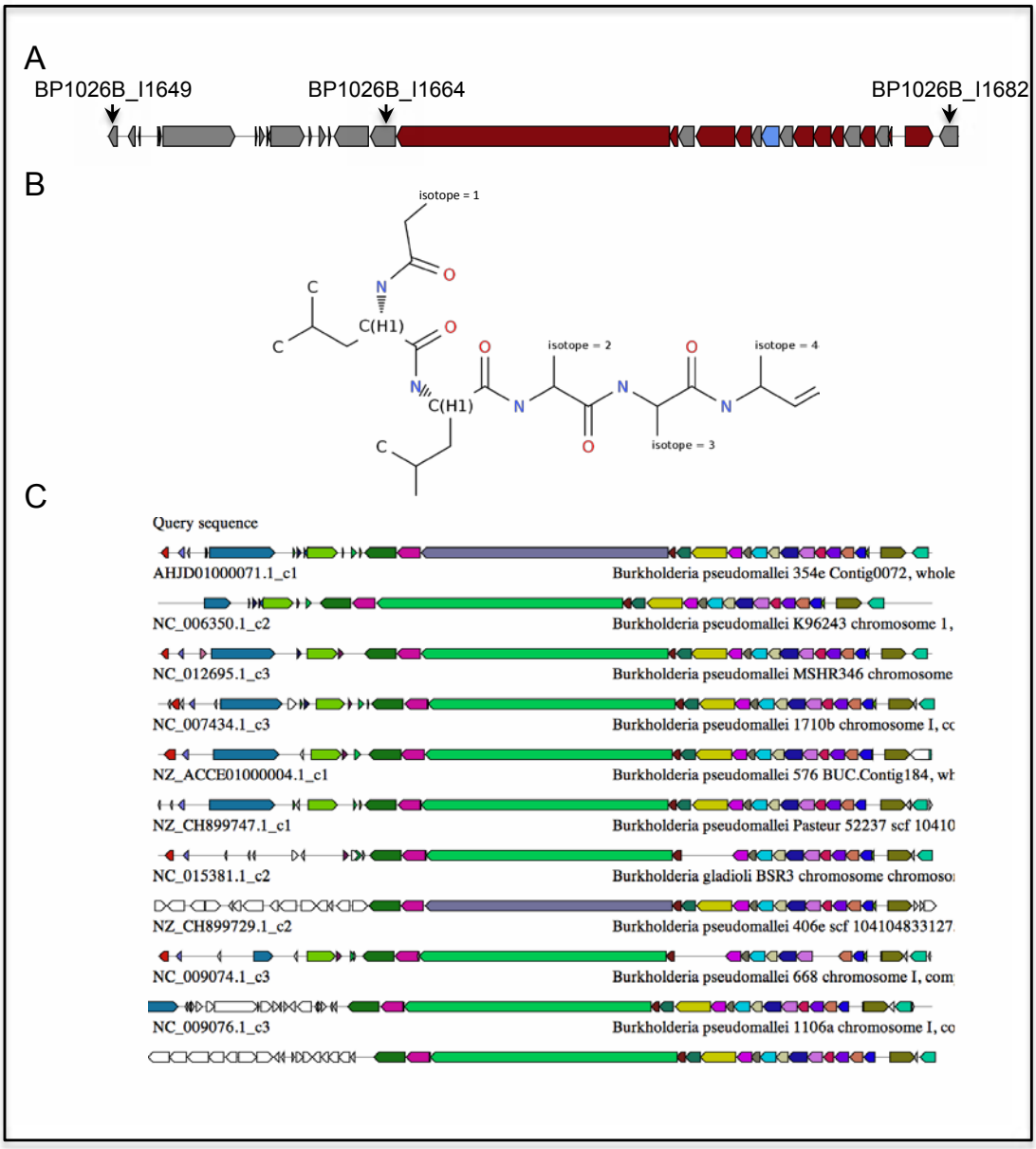
A
BP1026B_I1649
BP1026B_I1664
BP1026B_I1682
B
isotope = 1
isotope = 2
isotope = 3
isotope = 4
C
Query sequence
AHJD01000071.1_c1
Burkholderia pseudomallei 354e Contig0072, whole
NC_006350.1_c2
Burkholderia pseudomallei K96243 chromosome 1,
NC_012695.1_c3
Burkholderia pseudomallei MSHR346 chromosome
NC_007434.1_c3
Burkholderia pseudomallei 1710b chromosome I, cc
NZ_ACCE01000004.1_c1
Burkholderia pseudomallei 576 BUC.Contig184, wh
NZ_CH899747.1_c1
Burkholderia pseudomallei Pasteur 52237 scf 10410
NC_015381.1_c2
Burkholderia gladioli BSR3 chromosome chromoso
NZ_CH899729.1_c2
Burkholderia pseudomallei 406e scf 104104833127
NC_009074.1_c3
Burkholderia pseudomallei 668 chromosome I, com
NC_009076.1_c3
Burkholderia pseudomallei 1106a chromosome I, co

Figure S5

6.8 REFERENCES

1. Cheng AC, Currie BJ (2005) Melioidosis: Epidemiology, Pathophysiology, and Management. Clin Microbiol Rev 18: 383-416.
2. Finkelstein RA, Atthasampunna P, Chulasamaya M (2000) Pseudomonas (Burkholderia) pseudomallei in Thailand, 1964-1967: geographic distribution of the organism, attempts to identify cases of active infection, and presence of antibody in representative sera. The American Journal of Tropical Medicine and Hygiene 62: 232-239.
3. Limmathurotsakul D, Wongratanacheewin S, Teerawattanasook N, Wongsuvan G, Chaisuksant S, et al. (2010) Increasing incidence of human melioidosis in Northeast Thailand. The American Journal of Tropical Medicine and Hygiene 82: 1113-1117.
4. Tiyawisutsri R, Peacock SJ, Langa S, Limmathurotsakul D, Cheng AC, et al. (2005) Antibodies from patients with melioidosis recognize *Burkholderia mallei* but not *Burkholderia thailandensis* antigens in the indirect hemagglutination assay. Journal of Clinical Microbiology 43: 4872-4874.
5. (2002) Public Health Security and Bioterrorism Preparedness and Response Act 107th ed.
6. Ahmed K, Enciso HD, Masaki H, Tao M, Omori A, et al. (1999) Attachment of *Burkholderia pseudomallei* to pharyngeal epithelial cells: a highly pathogenic bacteria with low attachment ability. The American Journal of Tropical Medicine and Hygiene 60: 90-93.
7. Harley VS, Dance DA, Drasar BS, Tovey G (1998) Effects of *Burkholderia pseudomallei* and other *Burkholderia* species on eukaryotic cells in tissue culture. Microbios 96: 71-93.
8. Jones AL, Beveridge TJ, Woods DE (1996) Intracellular survival of *Burkholderia pseudomallei*. Infection and Immunity 64: 782-790.

9. Pruksachartvuthi S, Aswapokee N, Thankerngpol K (1990) Survival of *Pseudomonas pseudomallei* in human phagocytes. Journal of Medical Microbiology 31: 109-114.

10. Razak N, Ismail G (1982) Interaction of human polymorphonuclear leukocytes with *Pseudomonas pseudomallei*. The Journal of General and Applied Microbiology 28: 509-518.

11. Norris MH, Propst KL, Kang Y, Dow SW, Schweizer HP, et al. (2011) The *Burkholderia pseudomallei* {delta} *asd* mutant exhibits attenuated intracellular infectivity and imparts protection against acute inhalation melioidosis in mice. Infection and Immunity 79: 4010-4018.

12. Harley VS, Dance DA, Tovey G, McCrossan MV, Drasar BS (1998) An ultrastructural study of the phagocytosis of *Burkholderia pseudomallei*. Microbios 94: 35-45.

13. Warawa J, Woods DE (2005) Type III secretion system cluster 3 is required for maximal virulence of *Burkholderia pseudomallei* in hamster infection model. FEMS Microbiol Lett 242: 101-108.

14. Stevens MP, Wood MW, Taylor LA, Monaghan P, Hawes P, et al. (2002) An Inv/Mxi-Spa-like type III protein secretion system in *Burkholderia pseudomallei* modulates intracellular behavior of the pathogen. Mol Microbiol 46: 649-659.

15. Stevens MP, Friebel A, Taylor LA, Wood MW, Brown PJ, et al. (2003) A *Burkholderia pseudomallei* type III secreted protein, BopE, facilitates bacterial invasion of epithelial cells and exhibits guanine nucleotide exchange factor activity. J Bacteriol 185: 4992-4996.

16. Upadhyay A, Wu HL, Williams C, Field T, Galyov EE, et al. (2008) The guanine-nucleotide-exchange factor BopE from *Burkholderia pseudomallei* adopts a compact version of the

Salmonella SopE/SopE2 fold and undergoes a closed-to-open conformational change upon interaction with Cdc42. Biochem J 411: 485-493.

17. Stevens MP, Stevens JM, Jeng RL, Taylor LA, Wood MW, et al. (2005) Identification of a bacterial factor required for actin-based motility of *Burkholderia pseudomallei*. Mol Microbiol 56: 40-53.
18. Kespichayawattana W, Rattanachetkul S, Wanun T, Utaisincharoen P, Sirisinha S (2000) *Burkholderia pseudomallei* induces cell fusion and actin-associated membrane protrusion: a possible mechanism for cell-to-cell spreading. Infect Immun 68: 5377-5384.
19. French CT, Toesca IJ, Wu T-H, Teslaa T, Beaty SM, et al. (2011) Dissection of the *Burkholderia* intracellular life cycle using a photothermal nanoblade. Proceedings of the National Academy of Sciences 108: 12095-12100.
20. Burtnick MN, Brett PJ, Harding SV, Ngugi SA, Ribot WJ, et al. (2011) The Cluster 1 Type VI Secretion System Is a Major Virulence Determinant in *Burkholderia pseudomallei*. Infection and Immunity 79: 1512-1525.
21. Shalom G, Shaw JG, Thomas MS (2007) *In vivo* expression technology identifies a type VI secretion system locus in *Burkholderia pseudomallei* that is induced upon invasion of macrophage. Microbiology 153: 2689-2699.
22. Wong KT, Puthucheary SD, Vadivelu J (1995) The histopathology of human melioidosis. Histopathology 26: 51-55.
23. Stevens MP, Haque A, Atkins T, Hill J, Wood MW, et al. (2004) Attenuated virulence and protective efficacy of a *Burkholderia pseudomallei* bsa type III secretion mutant in murine models of melioidosis. Microbiology 150: 2669-2676.

24. Burtnick MN, Brett PJ, Nair V, Warawa JM, Woods DE, et al. (2008) *Burkholderia pseudomallei* type III secretion system mutants exhibit delayed vacuolar escape phenotypes in RAW 264.7 murine macrophages. Infect Immun 76: 2991-3000.

25. Holden MTG, Titball RW, Peacock SJ, Cerdeno-Tarraga AM, Atkins T, et al. (2004) Genomic plasticity of the causative agent of melioidosis, *Burkholderia pseudomallei*. Proc Natl Acad Sci USA 101: 14240-14245.

26. Tuanyok A, Leadem B, Auerbach R, Beckstrom-Sternberg S, Beckstrom-Sternberg J, et al. (2008) Genomic islands from five strains of *Burkholderia pseudomallei*. BMC Genomics 9: 566.

27. Gallagher LA, Shendure J, Manoil C (2011) Genome-Scale Identification of Resistance Functions in *Pseudomonas aeruginosa* Using Tn-seq. mBio 2.

28. Norris MH, Kang Y, Lu D, Wilcox BA, Hoang TT (2009) Glyphosate resistance as a novel select-agent-compliant, non-antibiotic selectable-marker in chromosomal mutagenesis of the essential genes *asd* and *dapB* of *Burkholderia pseudomallei*. Appl Environ Microbiol 75: 6062-6075.

29. Huang da W, Sherman BT, Lempicki RA (2009) Systematic and integrative analysis of large gene lists using DAVID bioinformatics resources. Nat Protoc 4: 44-57.

30. Attmannspacher U, Scharf BE, Harshey RM (2008) FliL is essential for swarming: motor rotation in absence of FliL fractures the flagellar rod in swarmer cells of *Salmonella enterica*. Mol Microbiol 68: 328-341.

31. Lossi NS, Manoli E, Forster A, Dajani R, Pape T, et al. (2013) The HsiB1C1 (TssB-TssC) complex of the *Pseudomonas aeruginosa* type VI secretion system forms a bacteriophage tail sheathlike structure. J Biol Chem 288: 7536-7548.

32. Hale CA, de Boer PAJ Direct Binding of FtsZ to ZipA, an Essential Component of the Septal Ring Structure That Mediates Cell Division in E. coli. Cell 88: 175-185.

33. Wang L, Lutkenhaus J (1998) FtsK is an essential cell division protein that is localized to the septum and induced as part of the SOS response. Mol Microbiol 29: 731-740.

34. Aussel L, Barre FX, Aroyo M, Stasiak A, Stasiak AZ, et al. (2002) FtsK Is a DNA motor protein that activates chromosome dimer resolution by switching the catalytic state of the XerC and XerD recombinases. Cell 108: 195-205.

35. Tidhar A, Flashner Y, Cohen S, Levi Y, Zauberman A, et al. (2009) The NlpD lipoprotein is a novel *Yersinia pestis* virulence factor essential for the development of plague. PLoS One 4: e7023.

36. Buckles EL, Wang X, Lockatell CV, Johnson DE, Donnenberg MS (2006) PhoU enhances the ability of extraintestinal pathogenic *Escherichia coli* strain CFT073 to colonize the murine urinary tract. Microbiology 152: 153-160.

37. Ferreira GM, Spira B (2008) The *pst* operon of enteropathogenic *Escherichia coli* enhances bacterial adherence to epithelial cells. Microbiology 154: 2025-2036.

38. Daigle F, Fairbrother JM, Harel J (1995) Identification of a mutation in the *pst-phoU* operon that reduces pathogenicity of an *Escherichia coli* strain causing septicemia in pigs. Infection and Immunity 63: 4924-4927.

39. Blin K, Medema MH, Kazempour D, Fischbach MA, Breitling R, et al. (2013) antiSMASH 2.0--a versatile platform for genome mining of secondary metabolite producers. Nucleic Acids Res 41: W204-212.

40. Basavanna S, Khandavilli S, Yuste J, Cohen JM, Hosie AHF, et al. (2009) Screening of *Streptococcus pneumoniae* ABC Transporter Mutants Demonstrates that LivJHMGF, a

Branched-Chain Amino Acid ABC Transporter, Is Necessary for Disease Pathogenesis. Infection and Immunity 77: 3412-3423.

41. Steele S, Brunton J, Ziehr B, Taft-Benz S, Moorman N, et al. (2013) *Francisella tularensis* harvests nutrients derived via ATG5-independent autophagy to support intracellular growth. PLoS Pathog 9: e1003562.

42. Sjoblom B, Salmazo A Fau - Djinovic-Carugo K, Djinovic-Carugo K Alpha-actinin structure and regulation.

43. Guo M, Tian F, Wamboldt Y, Alfano JR (2009) The majority of the type III effector inventory of *Pseudomonas syringae* pv. tomato DC3000 can suppress plant immunity. Mol Plant Microbe Interact 22: 1069-1080.

44. Baison-Olmo F, Cardenal-Munoz E, Ramos-Morales F (2012) PipB2 is a substrate of the *Salmonella* pathogenicity island 1-encoded type III secretion system. Biochem Biophys Res Commun 423: 240-246.

45. Henry T, Couillault C, Rockenfeller P, Boucrot E, Dumont A, et al. (2006) The *Salmonella* effector protein PipB2 is a linker for kinesin-1. Proc Natl Acad Sci U S A 103: 13497-13502.

46. Wikraiphat C, Charoensap J, Utaisincharoen P, Wongratanacheewin S, Taweechaisupapong S, et al. (2009) Comparative in vivo and in vitro analyses of putative virulence factors of *Burkholderia pseudomallei* using lipopolysaccharide, capsule and flagellin mutants. FEMS Immunol Med Microbiol 56: 253-259.

47. Arjcharoen S, Wikraiphat C, Pudla M, Limposuwan K, Woods DE, et al. (2007) Fate of a *Burkholderia pseudomallei* lipopolysaccharide mutant in the mouse macrophage cell line RAW 264.7: Possible role for the O-antigenic polysaccharide moiety of

lipopolysaccharide in internalization and intracellular survival. Infection and Immunity 75: 4298-4304.

48. Chakraborty S, Sivaraman J, Leung KY, Mok Y-K (2011) Two-component PhoB-PhoR Regulatory System and Ferric Uptake Regulator Sense Phosphate and Iron to Control Virulence Genes in Type III and VI Secretion Systems of *Edwardsiella tarda*. Journal of Biological Chemistry 286: 39417-39430.

49. Guo M, Tian F, Wamboldt Y, Alfano JR (2009) The majority of the type III effector inventory of *Pseudomonas syringae* pv. *tomato* DC3000 can suppress plant immunity. Mol Plant Microbe Interact 22: 1069-1080.

50. Lee Y, Chen Y, Ouyang X, Gan Y-H (2010) Identification of tomato plant as a novel host model for *Burkholderia pseudomallei*. BMC Microbiology 10: 28.

51. Trent MS, Ribeiro AA, Lin S, Cotter RJ, Raetz CRH (2001) An inner membrane enzyme in *Salmonella* and *Escherichia coli* that transfers 4-amino-4-deoxy-l-arabinose to lipid A: induction in polymyxin-resistant mutants and role of a novel lipid-linked donor. Journal of Biological Chemistry 276: 43122-43131.

52. Ganz T (2003) The role of antimicrobial peptides in innate immunity. Integrative and Comparative Biology 43: 300-304.

53. Wang X, Ribeiro AA, Guan Z, McGrath SC, Cotter RJ, et al. (2006) Structure and biosynthesis of free lipid A molecules that replace lipopolysaccharide in *Francisella tularensis* subsp. *novicida*. Biochemistry 45: 14427-14440.

54. Brett PJ, Burtnick MN, Snyder DS, Shannon JG, Azadi P, et al. (2007) *Burkholderia mallei* expresses a unique lipopolysaccharide mixture that is a potent activator of human Toll-like receptor 4 complexes. Mol Microbiol 63: 379-390.

55. Dawes EA (1988) Polyhydroxybutyrate: an intriguing biopolymer. Biosci Rep 8: 537-547.

56. Aurass P, Pless B, Rydzewski K, Holland G, Bannert N, et al. (2009) bdhA-patD operon as a virulence determinant, revealed by a novel large-scale approach for identification of *Legionella pneumophila* mutants defective for amoeba infection. Applied and Environmental Microbiology 75: 4506-4515.

57. van Schaik EJ, Tom M, Woods DE (2009) *Burkholderia pseudomallei* isocitrate lyase is a persistence factor in pulmonary melioidosis: implications for the development of isocitrate lyase inhibitors as novel antimicrobials. Infect Immun 77: 4275-4283.

58. Dunn MF, Ramírez-Trujillo JA, Hernández-Lucas I (2009) Major roles of isocitrate lyase and malate synthase in bacterial and fungal pathogenesis. Microbiology 155: 3166-3175.

59. Purohit HJ, Cheema S, Lal S, Raut CP, Kalia VC (2007) In Search of Drug Targets for *Mycobacterium tuberculosis*. Infect Disord Drug Targets 7: 245-250.

60. Cowell BA, Twining SS, Hobden JA, Kwong MS, Fleiszig SM (2003) Mutation of *lasA* and *lasB* reduces *Pseudomonas aeruginosa* invasion of epithelial cells. Microbiology 149: 2291-2299.

61. McGhee GC, Jones AL (2000) Complete nucleotide sequence of ubiquitous plasmid pEA29 from *Erwinia amylovora* strain Ea88: gene organization and intraspecies variation. Appl Environ Microbiol 66: 4897-4907.

62. Gotoh Y, Eguchi Y, Watanabe T, Okamoto S, Doi A, et al. (2010) Two-component signal transduction as potential drug targets in pathogenic bacteria. Current Opinion in Microbiology 13: 232-239.

63. Rajan SS, Yang X, Shuvalova L, Collart F, Anderson WF (2004) YfiT from *Bacillus subtilis* is a probable metal-dependent hydrolase with an unusual four-helix bundle topology. Biochemistry 43: 15472-15479.

64. Richmond JY, and R.W. McKinney (2007) Biosafety in microbiological and biomedical laboratories. Atlanta, GA: Centers for Disease Control and Prevention.

65. Barrett AR, Kang, Y., Inamasu, K. S., Son, M. S., Vukovich, J. M., and Hoang, T. T. (2008) Genetics tools for allelic-replacement in *Burkholderia* species. Appl Environm Microbiol 74: 4498-4508.

66. Kang Y, Norris MH, Wilcox BA, Tuanyok A, Keim PS, et al. (2011) Knockout and pullout recombineering for naturally transformable *Burkholderia thailandensis* and *Burkholderia pseudomallei*. Nat Protocols 6: 1085-1104.

67. Norris MH, Kang Y, Wilcox B, Hoang TT (2010) Stable, site-specific fluorescent tagging constructs optimized for *Burkholderia* species. Appl Environ Microbiol 76: 7635-7640.

68. Langmead B, Trapnell C, Pop M, Salzberg S (2009) Ultrafast and memory-efficient alignment of short DNA sequences to the human genome. Genome Biology 10: R25.

69. Blankenberg D, Kuster GV, Coraor N, Ananda G, Lazarus R, et al. (2001) Galaxy: A Web-Based Genome Analysis Tool for Experimentalists. Current Protocols in Molecular Biology: John Wiley & Sons, Inc.

70. Giardine B, Riemer C, Hardison RC, Burhans R, Elnitski L, et al. (2005) Galaxy: A platform for interactive large-scale genome analysis. Genome Research 15: 1451-1455.

71. Goecks J, Nekrutenko A, Taylor J, The Galaxy T (2010) Galaxy: a comprehensive approach for supporting accessible, reproducible, and transparent computational research in the life sciences. Genome Biology 11: R86.

72. Robinson JT, Thorvaldsdottir H, Winckler W, Guttman M, Lander ES, et al. (2011) Integrative genomics viewer. Nat Biotech 29: 24-26.

73. Anders S HTSeq: Analysing high-throughput sequencing data with Python.

74. Saeed AI, Bhagabati NK, Braisted JC, Liang W, Sharov V, et al. (2006) TM4 Microarray Software Suite. In: Alan K, Brian O, editors. Methods in Enzymology: Academic Press. pp. 134-193.

75. Shannon P, Reiss D, Bonneau R, Baliga N (2006) The Gaggle: An open-source software system for integrating bioinformatics software and data sources. BMC Bioinformatics 7: 176.

76. Fruzangohar M, Ebrahimie E, Ogunniyi AD, Mahdi LK, Paton JC, et al. (2013) Comparative GO: A Web Application for Comparative Gene Ontology and Gene Ontology-Based Gene Selection in Bacteria. PLoS ONE 8: e58759.

77. Jones AL, Beveridge TJ, Woods DE (1996) Intracellular survival of *Burkholderia pseudomallei*. J Bacteriol 64: 782-790.

78. Kang Y, Norris MH, Barrett AR, Wilcox BA, Hoang TT (2009) Engineering of tellurite-resistant genetic tools for single-copy chromosomal analysis of *Burkholderia* spp. and characterization of the *Burkholderia thailandensis betBA* operon. Appl Environ Microbiol 75: 4015-4027.

79. Choi K-H, Mima T, Casart Y, Rholl D, Kumar A, et al. (2008) Genetic tools for select-agent-compliant manipulation of *Burkholderia pseudomallei*. Appl Environ Microbiol 74: 1064-1075.

80. Propst KL, Mima T, Choi K-H, Dow SW, Schweizer HP (2010) A *Burkholderia pseudomallei* {Delta}*purM* mutant is avirulent in immunocompetent and immunodeficient animals: candidate strain for exclusion from select-agent lists. Infect Immun 78: 3136-3143.

Chapter 7. Identifying *Burkholderia pseudomallei* transcriptional regulators that contribute to virulence.

To be published in future works.

7.1 INTRODUCTION

Burkholderia pseudomallei (*Bp)* commands an arsenal of virulence factors that are put into use during host-cell infection. To organize and time the use of these virulence factors for full effect, a complex regulatory cascade must be fine tuned and maintained. Identifying the transcriptional regulators that are responsible for such fine-tuning would give insight to the virulence network of *Bp* and provide targets for novel therapeutic development.

Transcriptional regulation of virulence genes has been well studied in *Vibrio cholerae* as well as in *Pseudomonas aeruginosa.* In these pathogens external compounds and sensors are known to turn on a suite of transcriptional regulators that then mediate toxin, pili, flagella, phospholipases and proteases production among others. *V. cholerae* responds to temperature, osmolarity, bile, and pH to up regulate cholera toxin synthesis [1]. Indeed, studies have uncovered several regulons of virulence factors that control the ability of *V. cholerae* to attach and adhere to intestinal mucosa (ToxR regulon and the toxin coregulated pilus), but that all need to be coordinated for successful colonization. Secretion of mucinases, lipases, and proteases must also be coordinated to digest the mucous surrounding the membranes. The model pathogen, *P. aeruginosa*, is known to coordinate a complex and intricate web of regulation that allows the bacterium to infect a wide variety of hosts and survive in a wide variety of environments [2].

A few *Bp* transcriptional regulators have been investigated. The AraC-type regulator, HrpB, and its role in regulating the plant-pathogen like T3SS has been elucidated [3]. BsaN has been identified as a direct regulator of the T6SS-5, a major virulence factor [4] and BspR has been identified as a regulator of the major virulence factor T3SS [5]. These regulators are located proximal to these virulence factors and were obvious candidates for direct regulation of these two loci. Our goal was to identify additional regulators including global regulators that affect

virulence factor expression during host infection and aide in coordinating the process of host-cell infection (Fig. 1). Previous data generated in the lab by Dr. Yun Kang using single-cell transcriptomics [6] of the *Bp* transitome (in preparation) identified the global transcriptional profile of *Bp* as it transits through the host-cell during infection. Many genes were differentially regulated as *Bp* invaded host cells, replicated in the cytoplasm, and formed protrusions. Within this data set, 40 transcriptional regulators were identified that showed differential gene expression during host-cell infectious stages (Fig. 2). The targets of these regulators are unknown and we hypothesized that at least some of them would be contributing to the coordinated expression of virulence factors during infection.

In this work, I utilized lambda RED recombineering to produce knockout mutants of all 40 transcriptional regulators in the naturally competent BSL3 select agent *Bp* strain 1026b [7]. The 40 transcriptional knockout mutants were then tested for deficiencies in plaque formation within HEK293T cells, a human embryonic kidney cell line. The mutants that showed reduced ability to form plaques compared to wildtype were submitted to a growth curve to make sure the inability to form plaques was not due to an inability to grow *in vitro*. After demonstrating the mutants were important for monolayer plaque formation and not affected in *in vitro* growth they were complemented with ChIP-seq vectors to ensure functionality of the vector encoded transcriptional regulators. Six of the regulators were chosen for animal studies in BALB/c mice. Survival of the mice was observed over 60 days post-infection. Bacterial organ loads in the lung, liver, and spleen were determined in all surviving mice.

7.2 MATERIALS and METHODS

Bacterial strains, media, and culture conditions. All manipulations of *B. pseudomallei* were conducted in CDC/USDA approved and registered BSL3 facilities at the University of Hawaii at Manoa, and experiments with select agents were performed in accordance with the recommended BSL3 practices [8]. Derivatives of *Escherichia coli* strain EPMax10B (BioRad), E1345, E1354, E1869, and E1889 (Table 1) were routinely used for cloning or plasmid mobilization into *B. pseudomallei* as described previously [9,10]. Luria-Bertani (LB) medium (Difco) was used to culture *E. coli* strains. *B. pseudomallei* strains were cultured in LB or 1x M9 minimal medium supplemented with 20 mM glucose (MG). Antibiotics and non-antibiotic anitbacterials in solid media were utilized as follows: for *E. coli*, glyphosate (GS) 0.3% (w/v); for *B. pseudomallei*, GS 0.3% (w/v) was used. Growth of *E. coli* Δ*asd* strains and preparation of DAP were carried out as previously described [11]. Selection for *gat* genes in *E. coli* and *B. pseudomallei* strains was performed as previously described [10].

Generation of 40 regulatory mutants in *Bp* 1026b using lambda RED recombineering. The 40 *Bp* transcriptional regulatory genes were knocked out in strain 1026b using lambda RED recombineering as previously described [7] but with modifications as follows. For each gene, two primers whose 3' regions anneal to the upstream or downstream M13 regions surrounding the *FRT-gat-pheS* cassette and designed to contain 45 bp of homology to the upstream or downstream regions of the targeted gene, respectively, were used in the PCR to create an *FRT-gat-pheS* cassette bounded upstream by 45 bp homologous to the upstream region of the knock out target and downstream by 45 bp homologous to the downstream region of the knock out target (~2.3 kb). Primers were then used in amplification by PCR of the lambda

RED region from pKaKa1, to include the *beta, gam,* and *exo* genes to create a second DNA fragment (~3 kb). Strain 1026b was grown in 4 ml of M9 media + 20 mM glucose overnight to an O.D. of 1-1.4 then all 4 ml were pelleted by centrifugation at 14,000 g and all supernatant removed. 1 μg of each of the two DNA fragments was combined in a total volume of 5 μl and resuspended with the pelleted bacteria. The suspension was incubated at room temperature for 30 min then allowed to outgrow in 3-4 ml of the same media at 37°C with shaking for 2 h. The bacteria were then pelleted and plated on MG+0.3% GS. Colonies appeared 2-3 d later and were screened for correct insertion size using primers outside of the region used to create the knockout cassette.

HEK293T plaque assay using 40 *Bp* regulatory mutants. Plaque assays were carried out as previously described [12] but with some modifications. Briefly, 293T cells were seeded in CellBIND™ coated Corning™ 24-well plates with an ~ 16 mm diameter. The plates were incubated with a 1:40 dilution of phenol-red free BD Matrigel Matrix with reduced growth factors in PBS for 30 min prior to seeding. After a short period of drying within a bio-safety cabinet, cells were seeded at $7.5x10^4$ cells/well and allowed to attach overnight. In the morning the media was removed and the monolayers were washed twice with PBS. Overnight cultures of *Bp* regulatory mutants were resuspended in DMEM. The culture was diluted down in the same media to reach an MOI of 1:1. The suspension of bacteria was used to infect monolayers at an MOI of 1:1 all for 1 h. After 1 h, the bacteria-containing media was removed and the monolayers were gently washed twice with PBS to remove any extracellular bacteria. DMEM containing 1.2% low melt agarose, 750 μg/ml of amikacin, and 750 μg/ml of kanamycin was cooled to near solidity then used to overlay the 293T monolayers. At 24 hours post-infection (hpi), 400 μl of

DMEM with 0.1% (w/v) neutral red solution (Invitrogen) was added to the agarose overlay and incubated for 2 h to allow staining. Plaques were imaged on an Olympus IX82 inverted microscope and captured with QCapture Pro 7 software. At least 10 plaques per mutant were measured (where available) with the QCapture Pro 7 software.

Growth curves of plaque deficient mutants. Growth curves of the regulatory mutants were initiated by growing them overnight in 96-deepwell plates then diluting them 200 times into LB. The 96-well plate was incubated at 37°C with shaking in the BioTek ELx808IU and the O.D. 600 nm was measured every 30 min for 48 h. All growth curves were done in quadruplicate with the average and the SEM shown.

Complementation of the regulatory mutants of interest. Mutant strains had the chromosomally located *gat* resistance marker removed by Flp-*FRT* excision [13] and were verified by PCR and phenotypically as GS^S. The ChIP-seq vector pAM3GIQ-3xTY1 was constructed in our lab and is a GS^r plasmid that encodes *lacI* to repress the P_{lac} promoter in *Bp.* The *lac* promoter is induced by IPTG (removing repression by LacI) and drives expression of cloned genes. The multiple cloning site (MCS) is designed to allow N-terminal translational fusions to contain the ChIP-seq tag TY1 repeated three times (3xTY1). Genes BPSL0849, BPSL1938, BPSL2496, BPSS0012, BPSS1134, BPSS1569, BPSS1889, and BPSS2146 were cloned by NdeI and HindIII double digests as translational fusions with the 3xTY1 tag. Gene BPSS1471 was blunt end cloned as a translational fusion. The plasmids were then electroporated into their cognate GS^S mutant strains that had the chromosomally located *gat* resistance marker removed by Flp-*FRT* excision. Transformants were selected for on MG+0.3% GS plates and

verified by PCR. Complementation was verified by plaque assay as described above but by adding various amounts of IPTG in the agarose overlay for ideal induction of the cloned genes (0.5, 2.5, 5, and 10 mM IPTG). Plaques were measured in the same manner as above.

BALB/c acute inhalation melioidosis animal model and bacterial organ load determination study. Three tubes of each mutant to be tested were frozen at -80°C for 48 h. One tube was thawed and diluted to determine the CFU/ml of the remaining tubes. After determining the concentration and on the day of the challenge experiment, a second tube was thawed and diluted as required in PBS. Each group of five BALB/c male mice between 4 and 6 weeks of age were purchased from Jackson Laboratories (Bar Harbor, ME). Animals were housed in micro-isolator cages under pathogen-free conditions at ABSL3 in the JABSOM Bio-containment Facility (JBF). The Institutional Animal Care and Use Committee at the University of Hawaii at Manoa approved all the animal studies (Protocol # 10-1073-4). Animals were anesthetized with 100 mg/kg ketamine plus 10 mg/kg xylazine until unresponsive. The mice were inoculated with 10x the LD_{50}, or 4,500 CFU of each regulator mutant in 20 µl of PBS by pipette into the nose alternating nostrils, 5 mice per group. For all *Bp* survival studies, animals were monitored for disease symptoms twice daily and were euthanized according to pre-determined humane endpoints. Mice surviving 60 d were euthanized with CO_2 and the lungs, livers, and spleens were removed. Statistical differences in survival times were determined by Kaplan-Meier curves followed by the log-rank test. Each organ was separately resuspended in 5 ml PBS and homogenized in a Seward Stomacher® 80 Biomaster for 4 minutes. Aliquots were diluted and bacterial organ loads determined.

7.3 RESULTS and DISCUSSION

The mutants that were differentially regulated include domains from many families of regulators including GntR, AraC, Lrp, LysR, TetR, LuxR, PadR, DeoR, AcrR, MerR, RocR, and RpiR. Regulators within each domain have a wide range of gene targets with little besides protein domain organization gleaned from that information. These 40 regulators also demonstrated differential gene expression during transit through the host-cell infection, implying that they are induced or repressed in response to specific signals during the infection that direct them to up or down-regulate their target genes. Although all three data sets are from inside the host cell, the different intracellular niches are diverse enough to induce changes in transcriptional regulator profiles that account for the several thousand differentially expressed genes detected.

The regulatory mutants were made using co-incubation lambda RED recombineering. A few were unable to be made and deemed essential for growth. The 35 transcriptional mutants made in *Bp* 1026b and verified by PCR were tested in multiple plaque assays for deficiencies in plaque formation. Nine of the 35 regulator mutants had severe inabilities to create plaques on HEK293T monolayers (Fig. 3) and are indicated in figure 2 with red dots. The results were highly significant for these nine candidates with significance at $p<0.0001$ from the unpaired student t-test. The nine regulators encompass many of the transcriptional regulatory families: AcrR (BPSS1471), AraC (BPSS1889), DmlR (BPSS0012), Lrp (BPSL0849 and BPSL2496), LysR (BPSS2146), PadR (BPSS1134), TetR (BPSS1569), and putative regulator BPSL1938. Most of the regulators had marked up-regulation while *Bp* was in the vacuolar stage (BPSL1938, BPSS1889 and BPSS2146) or cytoplasm (BPSL0849 and BPSL2496). Two other regulators demonstrated significant down-regulation in either the vacuole (BPSL1569) or cytoplasm (BPSS1134). BPSS1471 showed up-regulation in the cytoplasm and during protrusion. These

nine regulators contribute to intricate regulation of virulence factors during infection at the predicted stages of infection; turning on genes essential for progression of the infection through the vacuole, cytoplasm, and protrusion stages eventually resulting in plaque formation.

Growth curves on the mutants of interest were done to make sure plaque-forming deficiencies were not due to an in ability to grow *in vitro*. Figure 4 shows the growth rates of the mutants compared to wildtype *Bp* 1026b in the rich media LB broth. Mutants in BPSL1938 and BPSL2496 showed considerable growth defects in *in vitro* growth indicating these two mutants have general growth defects not related to infection. The other mutants had growth rates similar to wildtype *Bp* 1026b. Mutants in BPSS1471 and BPSS2146 had a lag-phase a little longer than wildtype but eventually reached the same optical density. These two mutants plus the remaining regulatory mutants were hypothesized to have a defect in virulence regulation and not in *in vitro* growth.

After Flp-*FRT* excision of the *gat* cassette from the chromosome, the mutants were complemented with ChIP–seq vectors. ChIP-seq vectors were chosen so that we could identify the direct regulon of our newly identified virulence regulators in the future. For the purpose of this study, I looked at the ability of the complemented strains to form plaques on HEK293T cell monolayers in comparison to wildtype 1026b and their respective mutants (Fig. 5). Complemented BPSL1889 and BPSL2496 mutants were unable to form plaques as wildtype (WT). Inefficient complementation may be because we used an inducible promoter that causes constant transcription. Figure 2 shows that expression of the regulators fluctuates as the bacteria infect host-cells thus requiring subtle changes in expression to successfully form plaques. Attempts were made at varying the induction levels of IPTG for BPSL1889 and BPSL2496 in the media to no avail. These two vectors were also cloned with native promoters and some

degree of plaque formation was obtained. Complemented BPSL1569, BPSL1938, BPSS1134, BPSS1471, and BPSS2146 all created plaques on HEK293T monolayers similar to the wildtype and much higher than the mutant strains indicating complementation was successful. The complemented strains were saved and are undergoing the ChIP-seq protocol to identify the direct regulon of each virulence regulator.

Once initial characterization of the regulator mutant infection phenotypes was complete, the mutants were tested for attenuation in the inhalation melioidosis BALB/c mouse model. Verification of a role in pathogenesis needs to be done with an *in vivo* animal infection model. Groups of five mice were infected with each transcriptional regulator mutant (knockout mutants of BPSL0849, BPSL1569, BPSS0012, BPSS1134, BPSS1471, BPSS2146 and wildtype). The intranasal infection model where lethal inoculum is pipetted into the nares of anesthetized mice, simulating inhalation melioidosis, was used. Five groups had all mice survive the length of the 60-day experiment (Fig. 6A, 6C-F, column I). In our experience this timeframe is appropriate to allow for chronic infections deaths to occur. Wildtype *Bp* infected mice are succumb to the infection around 3-4 days whereas the BPSL0849, BPSS0012, BPSS1134, BPSS1471, BPSS2146 mutants infected mice survived the length of the study. BPSL1569 mutant infected mice began succumbing to chronic infection at ~40 dpi (Fig. 6B, I). Mice that survived the 60 days of the study were humanely euthanized and their lung, liver, and spleen removed and homogenized to determine bacterial organ load (Fig. 6A-F column II). Of all groups, only BPSL0849 mutant infect mice survived the length of the study and whose organs were sterile and free of *Bp* (Fig. 6A). Three of the five mice infected with the BPSS0012 mutant had bacteria in the lungs while the spleen and liver were clear, indicating that in the host the DmlR regulator BPSS0012 is responsible for regulating processes needed for dissemination beyond the lungs

(Fig. 6C). Mice infected with the BPSS1471 mutant also demonstrated similar survival and bacterial dissemination characteristics but only one mouse had *Bp* in the lungs, suggesting a role for BPSS1471 in survival of *Bp* in all tissues including the lungs (Fig. 6E). Three mice infected with the BPSL1569 mutant died of chronic infections and one that survived had very high levels of *Bp* in all the organs tested and gross splenic abnormality (Fig. 6B). The last mouse appeared to have no *Bp* in its organs. The regulator encoded by BPSL1569 is suggested to have an intermediate role in pathogenesis and may control bacterial behavior associated with acute infectious processes such as growth at primary infection sites. All mice infected with *Bp* mutant BPSS1134 survived the 60-day infection but there were very high levels of bacteria in the organs following homogenization and plating (Fig. 6D). Bacteria were found in the lungs of four mice, in the spleens of three, and in the liver of one. The BPSS1134 mutant was able to disseminate but was unable to cause acute disease. Mice infected with the last regulator mutant, BPSS2146, survived the length of the experiment and one mouse had bacteria in the lungs and spleen indicating an intermediate level of attenuation.

Taken together, I created 40 transcriptional regulator mutants. Through screening we narrowed down to nine regulators that were involved in plaque formation in cell-monolayers. Complementation of the regulator knockouts verified essentiality in the cell monolayer infection model while growth curves verified little effect on *in vitro* growth kinetics. BALB/c mouse infections showed attenuation of six regulators of interest. One regulator still infected mice with a mortal chronic infection while the remaining five presented with various levels of attenuation and inability to disseminate. Based on this work, we have identified six new virulence regulators that play a vital role in coordinating virulence factor expression. Ongoing projects include next generation illumina sequencing using the ChIP-seq vectors produced in this work. ChIP-seq will

allow us to identify the promoters that the regulators physically interact with, also known as the direct regulon. We are also working on RNA-seq experiments for each of the regulator mutants versus the wildtype *Bp*. After analyzing the data from both of these experiments we will know the direct and indirect regulon of each regulator and be able to round out a clearer picture of virulence regulation in *Bp*.

7.4 FIGURE LEGENDS:

FIG 1. Transcriptional regulators affect virulence processes in *Bp*. As *Bp* infects a host-cell a highly intricate and coordinated process occurs whereby the bacterial transcriptional regulators activate genes for phagosome escape, cytoplasmic replication, and cell-cell spread. Activation of virulence genes in a coordinated manner results in bacterial internalization A), invasion B), actin polymerization C), and membrane protrusion/spread D).

FIG 2. 40 transcriptional regulators differentially regulated inside host-cells. Each row lists a transcriptional regulator gene ID along with its putative function. The heat maps indicate the gene expression in the vacuole (V), cytoplasm (C), and during protrusion (P) in comparison to control bacteria grown in cell culture media. Replicates and average of those replicates are shown for each region of the cell where green indicates higher expression compared the control, red lower expression, black same as control, and grey not detected. Red dots highlight the transcriptional regulators of particular interest in this work.

FIG 3. HEK293T plaque assay of 40 transcriptional regulators. Plaque diameters were measured during monolayers infections of HEK293T cells. Plaque size on the Y-axis is the average diameter of 10 to 20 plaques with the standard error of the mean shown. Gene IDs are listed on the X-axis. Significant diameter differences were determined by the unpaired student t-test for each regulator compared to wildtype *Bp* 1026b. ****= $p<0.0001$.

FIG 4. Growth curve of *Bp* transcriptional regulator mutants. Starter cultures were diluted 100 times in LB broth. The optical density (OD) at 600 nm was read every 30 min for 48 h.

Black lines indicate wildtype *Bp*1026b and mutants that grew the same as wildtype. Red and green lines represent mutants that had a longer lag but final OD similar to wildtype. Blue and purple lines represent the two mutants that were unable to grow to the same OD as wildtype. Each line is the average of a quadruplicate experiment with standard error of the mean shown.

FIG 5. Plaque assay of complemented *Bp* transcriptional regulator mutants. Regulator mutants complemented with ChIP-seq vectors induced with IPTG. Plaque diameter in μm is shown on the Y-axis and strain ID is shown on the X-axis. 10-20 plaques were measured and the standard error of the mean is shown compared to wildtype.

FIG 6. *Bp* transcriptional regulators are attenuated in the inhalation melioidosis BALB/c mouse infection model. For all regulators, five mice were infected with 10x the LD_{50} and survival was monitored in I. In each survival curve mice infected with wildtype 1026b were used as control. For each regulator, bacterial organ loads were determined in the indicated organ for each surviving mouse in II. A) BPSL0849, B) BPSL1569, C) BPSS0012, D) BPSS1134, E) BPSS1471, and F) BPSS2146

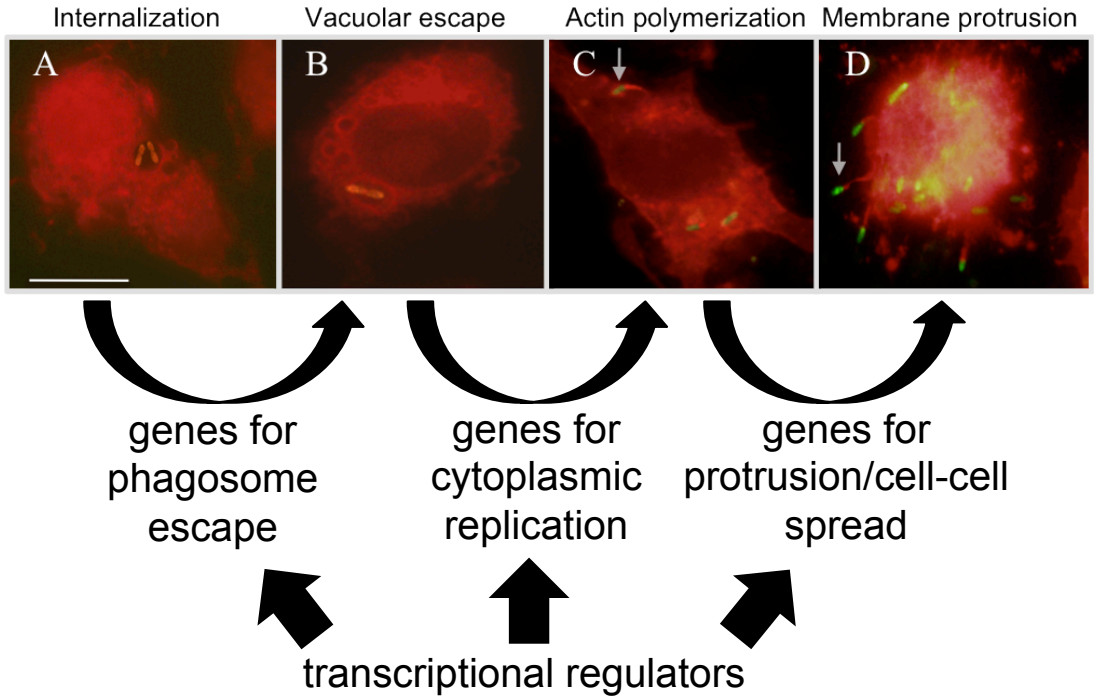
Internalization
Vacuolar escape
Actin polymerization
Membrane protrusion
A
B
C
D
genes for phagosome escape
genes for cytoplasmic replication
genes for protrusion/cell-cell spread
transcriptional regulators

Figure 1


-2.0
0.0
2
V1
V2
V3
V
C1
C2
C3
C
P1
P2
P3
Gene ID
Name/function
BPSS0765 GntR, Transcriptional regulators
BPSL0849 Lrp, Transcriptional regulators
BPSL1729 AraC family transcriptional regulator
BPSL2496 Lrp, leucine-responsive regulatory protein
BPSS0726 GntR family regulatory protein
BPSS0616 AraC family regulatory protein
BPSL1572 LysR family transcriptional regulator
BPSS1469 LysR family transcriptional regulator
BPSL2546 LysR, Transcriptional regulator
BPSS0008 TetR-family regulatory protein
BPSS0438 LysR-family transcriptional regulator
BPSS0041 LysR family transcriptional regulator
BPSS0912 transcription regulator AsnC
BPSS0505 AraC family transcription regulator
BPSS1483 TetR family transcriptional regulator
BPSS1586 LysR-family transcriptional regulator
BPSS1889 AraC-family transcriptional regulator
BPSL1938 putative transcriptional regulator
BPSL0939 DeoR family regulatory protein
PSS0956 RpiR, Transcriptional regulators
PSS1467 Transcriptional regulators
PSS2146 LysR family transcriptional regulator
PSL0647 TetR family regulatory protein
PSL1569 TetR family regulatory protein
PSS0312 LuxR family transcriptional regulator
PSL1105 TetR family regulatory protein
PSS1134 PadR-like family regulatory protein
PSL0067 PaaX, Phenylacetic acid-responsive transcriptional repressor
PSS2028 TetR-family transcriptional regulator
PSS0187 LysR-family transcriptional regulator
PSL2862 Predicted transcriptional regulators
PSL1494 MerR family transcriptional regulator
PSS0681 AraC family transcription regulator
PSL0838 DeoR, putative transcriptional regulator
PSS1471 AcrR, Transcriptional regulator
PSS2132 RocR, sigma-54 dependent transcriptional regulator
PSS2207 LysR-family transcriptional regulator

Figure 2

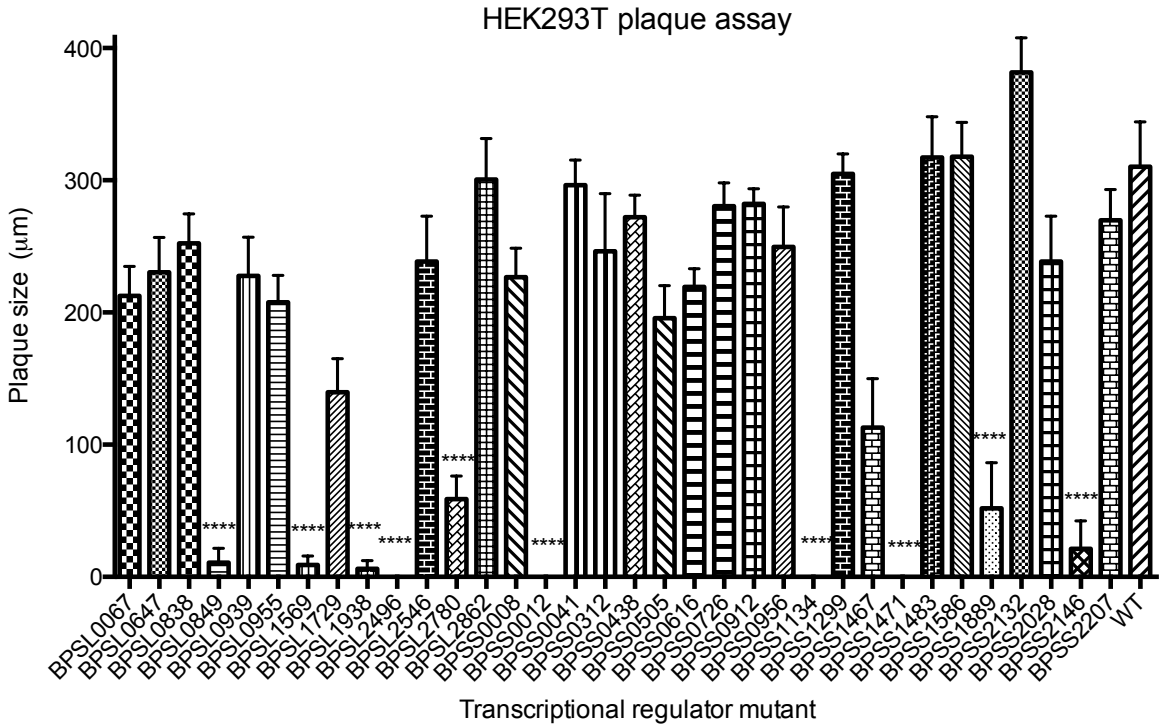

Figure 3

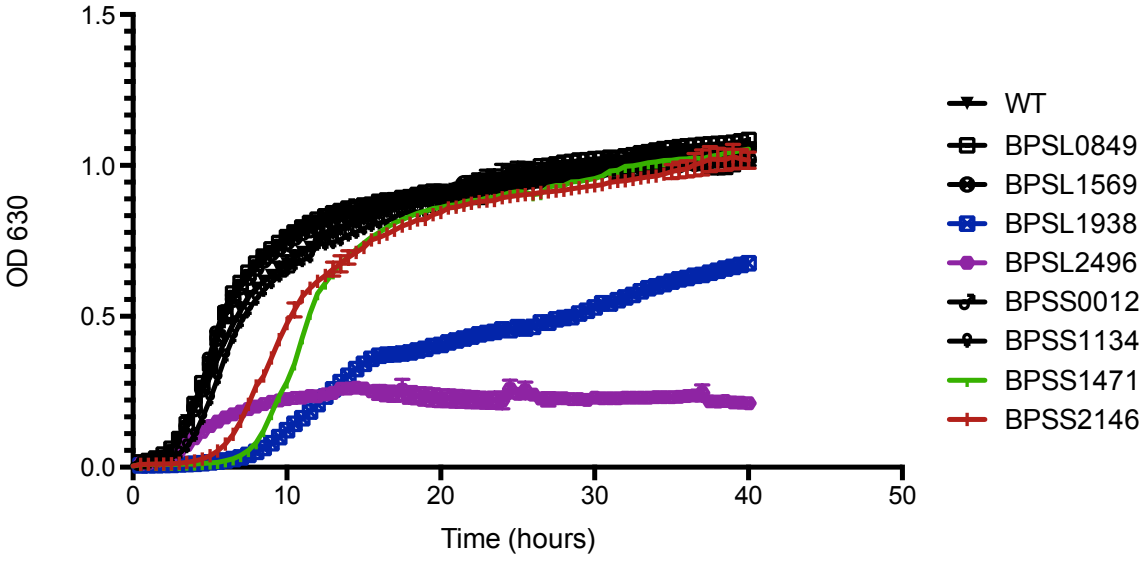

Figure 4

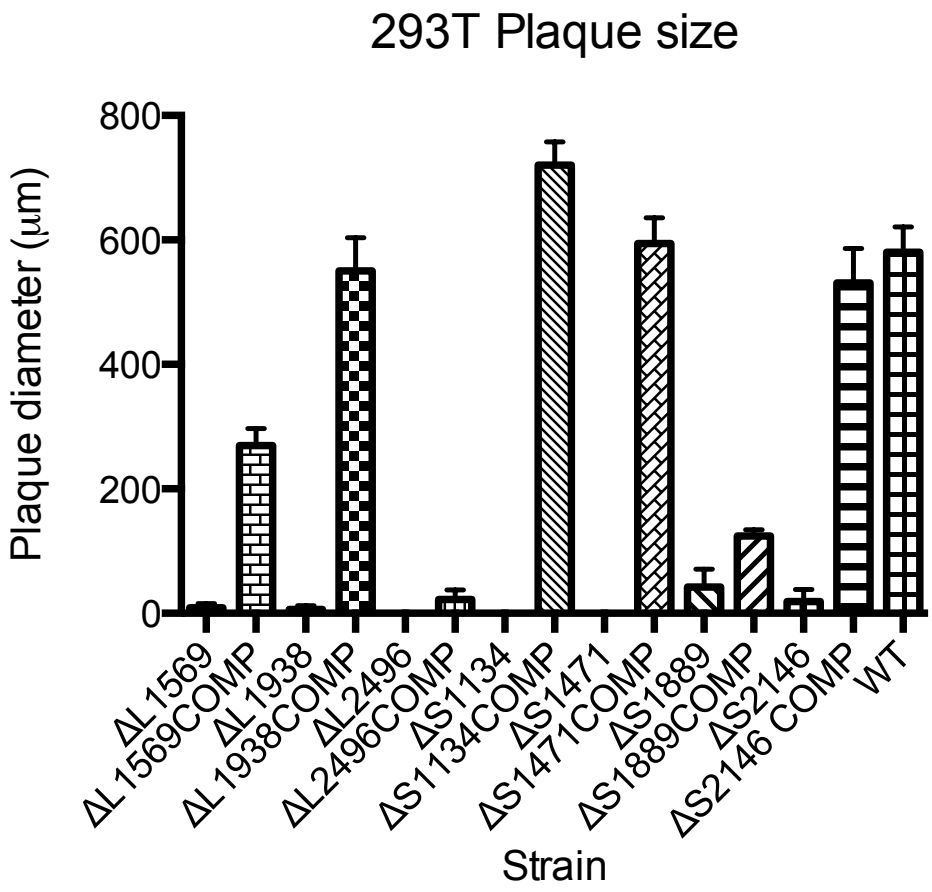
293T Plaque size
Plaque diameter (μm)
800
600
400
200
0
ΔL1569
ΔL1569COMP
ΔL1938
ΔL1938COMP
ΔL2496
ΔL2496COMP
ΔS1134
ΔS1134COMP
ΔS1471
ΔS1471COMP
ΔS1889
ΔS1889COMP
ΔS2146
ΔS2146 COMP
WT
Strain

Figure 5

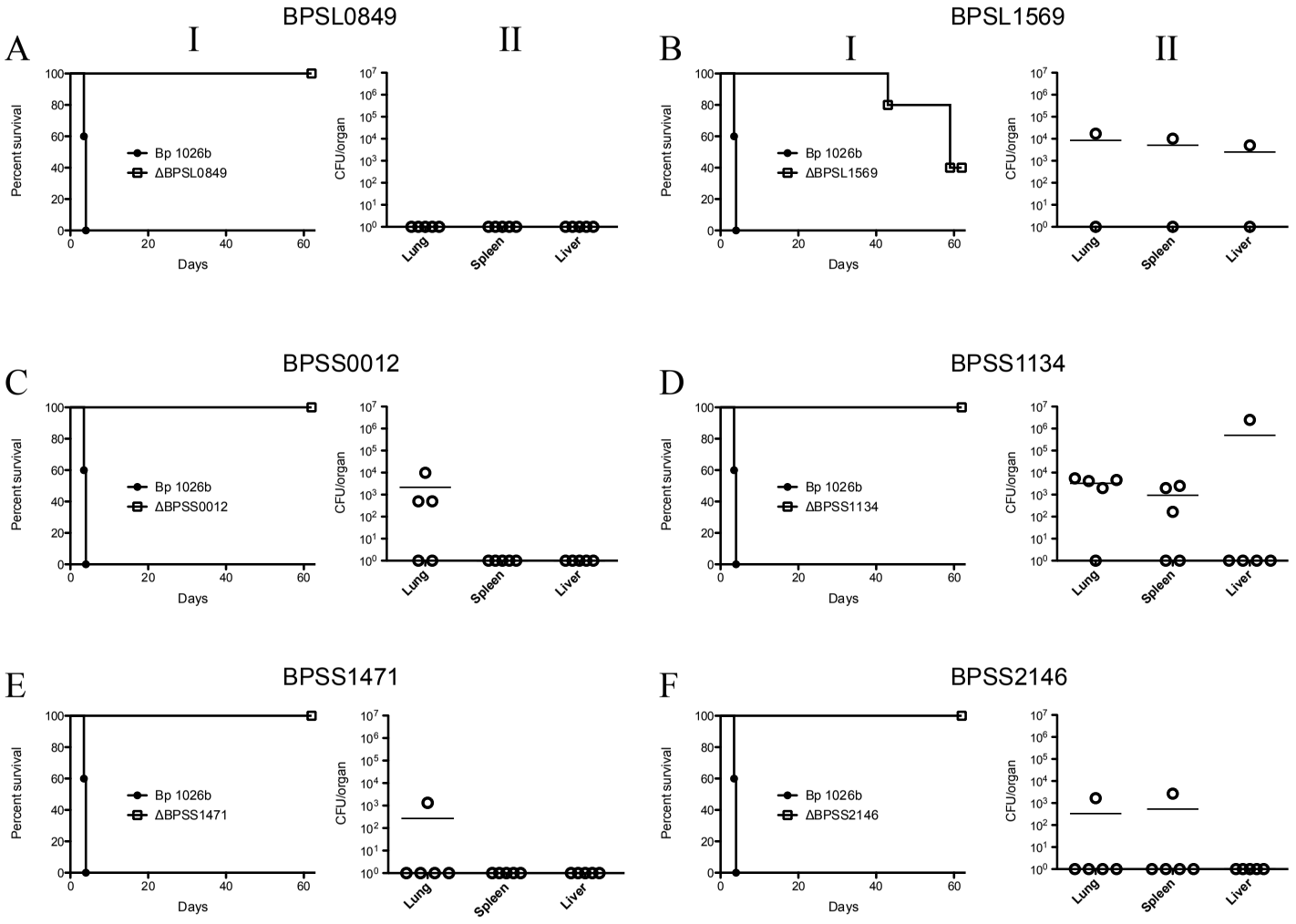
A
BPSL0849
I
II
Percent survival
Days
Bp 1026b
ΔBPSL0849
CFU/organ
Lung
Spleen
Liver
B
BPSL1569
ΔBPSL1569
C
BPSS0012
ΔBPSS0012
D
BPSS1134
ΔBPSS1134
E
BPSS1471
ΔBPSS1471
F
BPSS2146
ΔBPSS2146

Figure 6

7.5 REFERENCES

1. Peterson KM (2002) Expression of *Vibrio cholerae* virulence genes in response to environmental signals. Curr Issues Intest Microbiol 3: 29-38.

2. Balasubramanian D, Schneper L, Kumari H, Mathee K (2013) A dynamic and intricate regulatory network determines *Pseudomonas aeruginosa* virulence. Nucleic Acids Research 41: 1-20.

3. Lipscomb L, Schell MA (2011) Elucidation of the regulon and cis-acting regulatory element of HrpB, the AraC-type regulator of a plant pathogen-like type III secretion system in *Burkholderia pseudomallei*. J Bacteriol 193: 1991-2001.

4. Chen Y, Wong J, Sun GW, Liu Y, Tan GY, et al. (2011) Regulation of type VI secretion system during *Burkholderia pseudomallei* infection. Infect Immun 79: 3064-3073.

5. Sun GW, Chen Y Fau - Liu Y, Liu Y Fau - Tan G-YG, Tan Gy Fau - Ong C, Ong C Fau - Tan P, et al. Identification of a regulatory cascade controlling Type III Secretion System 3 gene expression in *Burkholderia pseudomallei*.

6. Kang Y, Norris MH, Zarzycki-Siek J, Nierman WC, Donachie SP, et al. (2011) Transcript amplification from single bacterium for transcriptome analysis. Genome Research 21: 925-935.

7. Kang Y, Norris MH, Wilcox BA, Tuanyok A, Keim PS, et al. (2011) Knockout and pullout recombineering for naturally transformable *Burkholderia thailandensis* and *Burkholderia pseudomallei*. Nat Protocols 6: 1085-1104.

8. Richmond JY, and R.W. McKinney (2007) Biosafety in microbiological and biomedical laboratories. Atlanta, GA: Centers for Disease Control and Prevention.

9. Kang Y, Norris MH, Barrett AR, Wilcox BA, Hoang TT (2009) Engineering of tellurite-resistant genetic tools for single-copy chromosomal analysis of *Burkholderia* spp. and characterization of the *Burkholderia thailandensis betBA* operon. Appl Environ Microbiol 75: 4015-4027.

10. Norris MH, Kang Y, Lu D, Wilcox BA, Hoang TT (2009) Glyphosate resistance as a novel select-agent-compliant, non-antibiotic selectable-marker in chromosomal mutagenesis of the essential genes *asd* and *dapB* of *Burkholderia pseudomallei*. Appl Environ Microbiol 75: 6062-6075.

11. Barrett AR, Kang, Y., Inamasu, K. S., Son, M. S., Vukovich, J. M., and Hoang, T. T. (2008) Genetics tools for allelic-replacement in *Burkholderia* species. Appl Environm Microbiol 74: 4498-4508.

12. Kespichayawattana W, Rattanachetkul S, Wanun T, Utaisincharoen P, Sirisinha S (2000) *Burkholderia pseudomallei* induces cell fusion and actin-associated membrane protrusion: a possible mechanism for cell-to-cell spreading. Infect Immun 68: 5377-5384.

13. Hoang TT, Karkhoff-Schweizer RR, Kutchma AJ, Schweizer HP (1998) A broad-host-range Flp-*FRT* recombination system for site-specific excision of chromosomally-located DNA sequences: application for isolation of unmarked *Pseudomonas aeruginosa* mutants. Gene 212: 77-86.

APPENDICES

Applied and Environmental Microbiology

Engineering of Tellurite-Resistant Genetic Tools for Single-Copy Chromosomal Analysis of *Burkholderia* spp. and Characterization of the *Burkholderia thailandensis betBA* Operon

Yun Kang, Michael H. Norris, Ashley R. Barrett, Bruce A. Wilcox and Tung T. Hoang

Appl. Environ. Microbiol. **2009, 75(12):4015. DOI: 10.1128/AEM.02733-08.**
Published Ahead of Print 17 April 2009.

Applied and Environmental Microbiology, June 2009, p. 4015–4027 Vol. 75, No. 12
0099-2240/09/$08.00+0 doi:10.1128/AEM.02733-08

Engineering of Tellurite-Resistant Genetic Tools for Single-Copy Chromosomal Analysis of *Burkholderia* spp. and Characterization of the *Burkholderia thailandensis betBA* Operon▽†

Yun Kang,[2] Michael H. Norris,[2] Ashley R. Barrett,[1] Bruce A. Wilcox,[3] and Tung T. Hoang[1,2]*

Department of Microbiology,[1] Department of Molecular Biosciences and Bioengineering,[2] and Department of Ecology and Health,[3] University of Hawaii at Manoa, Honolulu, Hawaii 96822

Received 30 November 2008/Accepted 7 April 2009

There are few appropriate single-copy genetic tools for most *Burkholderia* species, and the high level of antibiotic resistance in this genus further complicates the development of genetic tools. In addition, the utilization of resistance genes for clinically important antibiotics is prohibited for the bioterrorism agents *Burkholderia pseudomallei* and *Burkholderia mallei*, necessitating the development of additional nonantibiotic-based genetic tools. Three single-copy systems devoid of antibiotic selection based on two nonantibiotic selectable markers, tellurite resistance (Tel^r) and *Escherichia coli* aspartate-semialdehyde dehydrogenase (asd_{Ec}), were developed to facilitate genetic manipulation in *Burkholderia* species. These systems include one mariner transposon, a mini-Tn*7*-derived site-specific transposon, and six *FRT* reporter fusion vectors based on the *lacZ*, *gfp*, and *luxCDABE* reporter genes. Initially, we showed that the random mariner transposon pBT20-Δ*bla*-Tel^r-*FRT* efficiently transposed within *Burkholderia cenocepacia*, *Burkholderia thailandensis*, *B. pseudomallei*, and *B. mallei*. We then utilized the mini-Tn*7*-Tel^r-based transposon vector (mini-Tn*7*-Tel^r-*betBA*) and a transposase-containing helper plasmid (pTNS3-asd_{Ec}) to complement the *B. thailandensis* Δ*betBA* mutation. Next, one of the *FRT-lacZ* fusion vectors (pFRT1-*lacZ*-Tel^r) was integrated by Flp (encoded on a helper plasmid, pCD13SK-Flp-*oriT*-asd_{Ec}) to construct the *B. thailandensis* Δ*betBA*::*FRT-lacZ*-Tel^r reporter fusion strain. The *betBA* operon was shown to be induced in the presence of choline and under osmotic stress conditions by performing β-galactosidase assays on the *B. thailandensis* Δ*betBA*::*FRT-lacZ*-Tel^r fusion strain. Finally, we engineered *B. thailandensis* Δ*betBA*::*FRT-gfp*-Tel^r and Δ*betBA*::*FRT-lux*-Tel^r fusion strains by utilizing fusion vectors pFRT1-*gfp*-Tel^r and pFRT1-*lux*-Tel^r, respectively. The induction of the *betBA* operon by choline and osmotic stress was confirmed by performing fluorescent microscopy and bioluminescent imaging analyses.

The genus *Burkholderia*, consisting of more than 40 different species, occupies diverse ecological niches ranging from the soil rhizosphere to the human respiratory tract (39). Within this genus, members exhibit considerable genetic diversity and broad metabolic capabilities (26, 39), facilitating their adaptation to a variety of environmental conditions including nutrient limitation, the presence of antibiotics and toxic compounds, and pH fluctuations. Many *Burkholderia* species are known plant pathogens, including *Burkholderia caryophylli*, *B. plantarri*, and *B. glumae*, while others (e.g., *B. cepacia* complex) cause opportunistic infections (39). In addition, *Burkholderia pseudomallei* and *B. mallei* are primary pathogens for humans and animals and are listed as category B select agents in the United States.

To best exploit the genomic information available for several *Burkholderia* species, a wide array of tools is required for molecular genetic and pathogenesis studies of these bacteria. For *Burkholderia* species not classified as select agents, antibiotic-resistance-based tools could be used for genetic manipulation. However, the Centers for Disease Control and Prevention restricts the introduction of markers conferring resistance against clinically important antibiotics into the two select agents *B. mallei* and *B. pseudomallei*. At present, only gentamicin, kanamycin, and zeocin resistance markers are approved for limited use for *B. pseudomallei*, while only the kanamycin and zeocin resistance markers are approved for *B. mallei* (35). However, most wild-type strains of *B. mallei* and *B. pseudomallei* have high levels of resistance to all three antibiotics (7, 29, 36), and even at high concentrations, the selection is not tight, and spontaneous resistance still arises (10, 15, 32). Consequently, there is still a need to expand universal genetic tools based on nonantibiotic selectable markers, allowing broader applications in various *Burkholderia* species.

Several nonantibiotic selection schemes have been used in bacteria including, but not limited to, resistance to various compounds (e.g., arsenate; bialaphos or its degradation product, phosphinothricin; mercury; and tellurite [Tel]) and metabolic markers (e.g., lactose utilization and purine and amino acid biosynthesis). Potential drawbacks to using arsenate and mercury are high toxicity levels and narrow selective concentration ranges (4, 16). Bialaphos and its degradation product, phosphinothricin, have been shown to be ineffective for *Burkholderia* select agents, requiring concentrations greater than 1,000 μg/ml, whereas these bacteria have been shown to be

* Corresponding author. Mailing address: Department of Microbiology, University of Hawaii at Manoa, 2538 The Mall-Snyder 310, Honolulu, HI 96822. Phone: (808) 956-3522. Fax: (808) 956-5339. E-mail: tongh@hawaii.edu.

† Supplemental material for this article may be found at http://aem.asm.org/.

▽ Published ahead of print on 17 April 2009.

sensitive to Tel concentrations of less than 1 μg/ml (M. Frazier, K. Choi, A. Kumar, C. Lopez, R. R. Karkhoff-Schweizer, and H. P. Schweizer, presented at the American Society for Microbiology Biodefense and Emerging Diseases Research Meeting, Washington, DC, 2007). Therefore, the nonantibiotic selectable marker based on Tel resistance (Tel^r) could be useful for genetic manipulation in various *Burkholderia* species, particularly *B. mallei* and *B. pseudomallei*. The Tel^r marker, consisting of three genes (*kilA*, *telA*, and *telB*) (38), has been successfully employed as a nonantibiotic selectable marker originally in *Pseudomonas putida* (34), in several other gram-negative bacteria (25), and, more recently, in *B. thailandensis* (2). Additionally, the *asd* gene (a metabolic marker encoding aspartate-semialdehyde dehydrogenase for amino acid biosynthesis) has been used as a nonantibiotic selectable marker in Δ*asd* backgrounds (2, 30). Combining the Tel^r marker and the *asd* gene may expand the repertoire of genetic tools available for *Burkholderia* species.

Strategies and tools for the manipulation of genetic elements as a single copy on the chromosome have been developed, such as *Himar1*-based mariner transposons (22, 32), the mini-Tn*7* site-specific transposition system (1, 9), and *FRT-lacZ* fusion vectors (12, 37). The random *Himar1*-based mariner transposon plasmid pBT20 was successfully used for mutant library construction in *Pseudomonas aeruginosa* (6, 19, 22) and has also been proven useful for transposition in a broad range of gram-negative bacteria (20). Similarly, the *Himar1*-based transposons carrying the Km^r cassette were proven to be useful in *B. pseudomallei* (32). The second single-copy system based on the mini-Tn*7* site-specific transposon, when used in conjunction with the transposase-encoding helper plasmid, has broad applications for the introduction of single-copy chromosomal elements into gram-negative bacteria (9) and the select agent *B. mallei* (8). Lastly, after mutant construction with an *FRT*-flanked selectable marker and Flp excision, the introduction of an Flp-containing helper plasmid and an *FRT-lacZ* fusion vector allows for simple Flp-catalyzed recombination to the "*FRT* scar" at the target gene downstream of the native promoter, facilitating regulation studies without prior knowledge of the promoter sequence (12, 37). Nevertheless, there are disadvantages to these existing systems when used in *Burkholderia* species, particularly in the select agents *B. pseudomallei* and *B. mallei*, due to the antibiotic resistance markers used (e.g., gentamicin, kanamycin, ampicillin, and streptomycin) and the occurrence of spontaneously resistant mutants (10, 15, 32). Moreover, to our knowledge, no *FRT*-reporter fusion vectors based on reporter genes other than *lacZ* have been developed.

In this study, genetic tools using the Tel^r marker for selection were developed for single-copy analyses of chromosomally targeted genetic elements. These include a *Himar1*-based random mariner transposon plasmid and a mini-Tn*7* site-specific transposon vector. We also engineered *FRT*-reporter fusion vectors based on three common reporters, *lacZ*, *gfp*, and the *luxCDABE* operon, allowing for Flp-catalyzed recombination. These systems expand upon our previously published nonantibiotic selectable marker approach for allelic replacement (2) and will aid in routine genetic manipulations including transposon mutagenesis, complementation studies, and promoter regulation studies of *Burkholderia* species. Most importantly, all genetic tools presented here are completely devoid of antibiotic resistance selection and are in compliance with select-agent regulations. We utilized these tools to characterize the *B. thailandensis betBA* operon, encoding betaine aldehyde dehydrogenase (BetB) and choline dehydrogenase (BetA).

MATERIALS AND METHODS

Bacterial strains, media, and culturing conditions. All the strains and plasmids involved in this study are listed in Tables 1 and 2. *Escherichia coli* strain EPMax10B-*pir116* was routinely used as a cloning strain. *E. coli* strain DH5α-*pir* was used for the cloning of pBT20-Δ*bla*-Tel^r-*FRT*. *E. coli* strain E1345 was used to clone *E. coli asd* (asd_{Ec})-containing vectors. The *E. coli* conjugal and suicidal strain E1354 was routinely used for introducing plasmids into *Burkholderia* species through conjugation. An alternative *E. coli* conjugal donor, E463, was used for the conjugal transfer of transposon plasmid pBT20-Δ*bla*-Tel^r-*FRT*. Luria-Bertani (LB) medium (Difco) was used to culture all *E. coli*, *Burkholderia cenocepacia*, *B. pseudomallei*, and *B. mallei* strains. *B. thailandensis* wild-type strain E264 and its derivatives were cultured in LB medium or 1× M9 minimal medium supplemented with 20 mM glucose (MG). For the single-copy complementation study (see Fig. 3), *B. thailandensis* strains were grown in 1× M9 minimal medium plus 1% Brij 58 (Sigma) and 20 mM glucose or 30 mM choline chloride (Sigma). One percent Brij 58 was added to prevent bacterial clumping during growth. To study *betBA* regulation, *B. thailandensis* strains were grown in MG plus 1% Brij 58 along with different concentrations of choline chloride (see Fig. 5) or in no-salt LB medium (LS medium; Teknova) supplemented with different NaCl concentrations (see Fig. 6). Antibiotics and nonantibiotic bactericidal compounds were added to the media utilized for both selection and plasmid maintenance as follows: 110 μg/ml ampicillin (Ap), 25 μg/ml chloramphenicol (Cm), 15 μg/ml gentamicin (Gm), 35 μg/ml kanamycin (Km), 25 μg/ml, streptomycin (Sp), and 20 μg/ml potassium Tel (Teknova) for *E. coli*; 125 μg/ml Tel for *B. cenocepacia* strain K56-2 and *B. thailandensis*; 200 μg/ml Tel for *B. cenocepacia* strain J2315; and 25 μg/ml Tel for *B. pseudomallei* strains K96243 and 1026b and *B. mallei* strain ATCC 23344. For the growth of *E. coli* Δ*asd* strains E463, E1345, and E1354, without asd_{Ec}-containing plasmids, 100 μg/ml of diaminopimelic acid (Sigma) was supplied. All manipulations of *B. pseudomallei* and *B. mallei* were conducted in a CDC/USDA-approved and -registered biosafety level 3 facility at the University of Hawaii at Manoa. All experiments with these two select agents were performed with biosafety level 3 practices according to recommendations described previously (32a).

Molecular methods and reagents. All restriction enzymes, deoxynucleoside triphosphates, T4 DNA polymerase, T4 polynucleotide kinase, and T4 DNA ligase were purchased from New England Biolabs and used as recommended by the supplier. Plasmids and DNA gel bands were isolated using the Zyppy plasmid miniprep kit I and Zymoclean gel DNA recovery kit, respectively (Zymo Research Corporation). Competent cells were prepared as previously described (2). All other molecular techniques were conducted according to methods described previously by Sambrook and Russell (33). Oligonucleotide primers (Table 3) were synthesized by Integrated DNA Technology. *Pfu* polymerase was purchased from Stratagene. Generally, the various PCRs were performed by an initial denaturation step for 1 min at 94°C and 34 cycles of 45 s at 94°C, 30 s at 60°C, and 1 min kb^{-1} at 72°C, and a final step for 10 min at 72°C was included.

Conjugal transfer of vectors into *Burkholderia* species. *E. coli* strain E463 was used as the conjugal donor to introduce transposon plasmid pBT20-Δ*bla*-Tel^r-*FRT* into all *Burkholderia* species. Another *E. coli* conjugal strain, E1354, was used to introduce the mini-Tn*7* and *FRT-lacZ* vectors and their respective helper plasmids into *B. thailandensis* strains. Conjugation of non-select-agent *Burkholderia* species was carried out as follows. The donor and recipients were grown to log phase for conjugation. One milliliter of each culture was harvested separately by centrifugation at 9,000 × *g* for 1 min at room temperature and washed twice with 1 ml of LB medium. The cell pellets of the donor and recipients were then resuspended together in 30 μl of LB medium. The 30-μl cell suspension was spotted onto cellulose acetate filters (Satorius) on LB agar plates and incubated at 37°C for 8 h. Filters were then vortexed in 1 ml of 1× M9 minimal medium, and 100 μl of this cell suspension and 100 μl of 10× dilutions were plated onto LB or MG plates with appropriate concentrations of Tel. Conjugations into *B. pseudomallei* or *B. mallei* cells were performed directly on LB plates without filters. Bacteria were gently scraped off the LB plates with disposable inoculation loops and resuspended in 1× M9 medium, and plating was done similarly as described above. Plates were usually incubated for 2 to 3 days at 37°C until single Tel^r colonies were observed.

TABLE 1. Bacterial strains utilized in this study

Strain	Lab ID[a]	Relevant characteristic(s)	Source or reference
E. coli			
EPMax10B-*pir116*	E1249	F$^-$ λ$^-$ *mcrA* Δ(*mrr-hsdRMS-mcrBC*) ϕ80d*lacZ*ΔM15 Δ*lacX74 deoR recA1 endA1 araD139* Δ(*ara leu*)*7697 galU galK rpsL nupG* Tn-*pir116-FRT2*	Laboratory collection
DH5α-*pir*	E0175	Tc^r; F$^-$ λ$^-$ ϕ80d*lacZ*ΔM15 (*lacZYA-argF*)*U169 deoR recA1 endA1 hsdR17*(r_K^- m_K^+) *phoA supE44 thi-1 gyrA96 relA1 uidA::pir zdg-232*::Tn*10*	31
HPS1-*mob*-Δ*asd*-*pir*	E0463	Tc^r Km^r Cm^r; e14$^-$ (*mcrA*) *recA1 endA1 gyrA96 thi-1 hsdR17 supE44 relA1* Δ(*lac-proAB*) *rif zxx*::mini-Tn*5*-Lac4 (*lacI*$^{q+}$ *lacZ* M15) Δ*asd*::*FRT uidA*::*pir zdg-232*::Tn*10 recA*::*RP4-2* Tc::Mu Km^r	—[b]
EPMax10B-*pir116*-Δ*asd*::Gm^r	E1345	Gm^r; F$^-$ λ$^-$ *mcrA* Δ(*mrr-hsdRMS-mcrBC*) ϕ80d*lacZ*ΔM15 Δ*lacX74 deoR recA1 endA1 araD139* Δ(*ara leu*)*7697 galU galK rpsL nupG* Tn-*pir116-FRT2* Δ*asd*::Gm^r	—[b]
EPMax10B-*pir116*-Δ*asd*-*mob*-Km^r-Δ*trp*::Gm^r	E1354	Km^r Gm^r; F$^-$ λ$^-$ *mcrA* Δ(*mrr-hsdRMS-mcrBC*) ϕ80d*lacZ*ΔM15 Δ*lacX74 deoR recA1 endA1 araD139* Δ(*ara leu*)*7697 galU galK rpsL nupG* Tn-*pir116-FRT2* Δ*asd*::*FRT recA*::*RP4-2* Tc::Mu Km^r Δ*trp*::Gm^r	—[b]
DH5α-λ*attB*::pCD13SK-Flp	E0982	Sp^r; F$^-$ ϕ80d*lacZ*ΔM15 (*lacZYA-argF*)*U169 deoR recA1 endA1 hsdR17*(r_K^- m_K^+) *phoA supE44 thi-1 gyrA96 relA1* λ*attB*::pCD13SK-Flp	—[b]
B. thailandensis			
E264	E1298	Prototroph	5
E264-Δ*betBA*::*FRT*	E1671	*B. thailandensis* Δ*betBA*::*FRT* mutant	2
E264-Δ*betBA*::*FRT*/*attTn7*::Tel^r	E1709	Tel^r; *B. thailandensis* Δ*betBA*::*FRT* mutant with empty vector mini-Tn*7*-Tel^r integrated at the *att*Tn*7* site	This study
E264-Δ*betBA*::*FRT*/*attTn7*::Tel^r-*betBA*	E1711	Tel^r; *B. thailandensis* Δ*betBA*::*FRT* mutant with mini-Tn*7*-Tel^r-*betBA* integrated at the *att*Tn*7* site	This study
E264-Δ*betBA*::*FRT-lacZ*-Tel^r	E1731	Tel^r; *B. thailandensis* Δ*betBA*::*FRT* mutant with *FRT-lacZ*-Tel^r fusion	This study
E264-Δ*betBA*::*FRT-gfp*-Tel^r	E2045	Tel^r; *B. thailandensis* Δ*betBA*::*FRT* mutant with *FRT-gfp*-Tel^r fusion	This study
E264-Δ*betBA*::*FRT-lux*-Tel^r	E2047	Tel^r; *B. thailandensis* Δ*betBA*::*FRT* mutant with *FRT-lux*-Tel^r fusion	This study
E264-Δ*betBA*::*FRT-lacZ*-Tel^r/*attTn7*::*betBA*	E1849	Tel^r; E264-Δ*betBA*::*FRT*/*attTn7*::*betBA* with Δ*betBA-lacZ*-Tel^r fusion	This study
E264-Δ*betBA*::*FRT-gfp*-Tel^r/*attTn7*::*betBA*	E2046	Tel^r; E264-Δ*betBA*::*FRT*/*attTn7*::*betBA* with Δ*betBA-gfp*-Tel^r fusion	This study
E264-Δ*betBA*::*FRT-lux*-Tel^r/*attTn7*::*betBA*	E2048	Tel^r; E264-Δ*betBA*::*FRT*/*attTn7*::*betBA* with Δ*betBA-lux*-Tel^r fusion	This study
B. cenocepacia			
K56-2	E1554	Prototroph; cystic fibrosis isolate	P. Sokol
J2315	E1553	Prototroph	J. Goldberg
B. pseudomallei			
K96243	B0005	Prototroph; clinical isolate	18
1026b	B0003	Prototroph; clinical isolate	11
B. mallei ATCC 23344	B0001	Prototroph; clinical isolate	40

[a] For strains constructed in this study, please see the text for further details. Please use the laboratory identification (Lab ID) number to request strains.
[b] —, details on the engineering of these strains will be published elsewhere.

Construction and testing of pBT20-Δ*bla*-Tel^r-*FRT*. A new mariner transposon vector was constructed based on the Tel^r marker (Fig. 1). pwFRT-PC$_{S12}$-Tel^r was digested with SmaI, and the 3.2-kb PC$_{S12}$-Tel^r fragment was cloned into the pBT20-Δ*bla* backbone (~4.3 kb) following BsaI digestion and blunt ending. This replaced the Gm^r cassette with the Tel^r marker, resulting in transposon vector pBT20-Δ*bla*-Tel^r-*FRT*.

The transposition frequencies of pBT20-Δ*bla*-Tel^r-*FRT* were determined by conjugation into several different *Burkholderia* species and strains: *B. cenocepacia* strains K56-2 and J2315, *B. thailandensis* strain E264, *B. pseudomallei* strains K96243 and 1026b, and *B. mallei* strain ATCC 23344. Following conjugation as described above, the mating mixtures were diluted and plated onto LB plates and LB plates supplemented with the appropriate concentration of Tel. The transposition frequencies for individual conjugation experiments were calculated based on the ratio of the number of colonies counted that were grown on LB medium plus Tel to the number of colonies that were grown on LB medium. Three independent conjugation experiments were carried out to obtain the average transposition frequency and standard error of the mean for each strain. Similar control conjugation experiments, omitting the *E. coli* conjugal donor harboring pBT20-Δ*bla*-Tel^r-*FRT*, were performed on all recipient strains to ensure that no spontaneous mutants arose from Tel selection. For *B. thailandensis* and *B. cenocepacia*, 15 random Tel^r colonies were purified on LB plates with Tel and PCR screened using *telB*-specific oligonucleotides 834 and 854

TABLE 2. Bacterial plasmids utilized in this study

Plasmid	Lab ID[a]	Relevant properties	Reference or source
pBT20-Δ*bla*	E1029	Gm^r; mariner transposon plasmid	20
pwFRT-P$_{S12}$-Tel^r	E1584	Tel^r; P$_{S12}$-Tel^r cassette flanked by wild-type *FRT* sequences	2
pBT20-Δ*bla*-Tel^r-*FRT*	E1727	Tel^r; mariner transposon plasmid based on Tel^r	This study
pCD11-Gm^r-*pir116-oriT*	E1254	Cm^r Gm^r; conjugation vector	Laboratory collection
pUC18R6KT-mini-Tn*7*	E1190	Ap^r; Tn*7*-based broad-host-range transposon vector	9
mini-Tn*7*-Tel^r-*bla*	E1645	Ap^r Tel^r; Tel^r cassette cloned into pUC18R6K-mini-Tn*7*	This study
mini-Tn*7*-Tel^r	E1825	Tel^r; mini-Tn*7*-*bla*-Tel^r with *bla* gene deleted	This study
mini-Tn*7*-Tel^r-*betBA*	E1829	Tel^r; mini-Tn*7*-Tel^r with *betBA* operon cloned	This study
pTNS3	E1189	Ap^r; helper plasmid for Tn*7* transposition system	9
pTNS3-*asd*$_{Ec}$	E1831	pTNS3 with *bla* replaced by the *E. coli asd* gene	This study
pFRT1-*lacZ*	E0790	Gm^r; *FRT1-lacZ* fusion containing suicidal vector	37
pFRT1-*lacZ*-Tel^r	E1707	Tel^r; pFRT1-*lacZ* with Gm^r cassette replaced by Tel^r cassette	This study
pFRT2-*lacZ*	E0787	Gm^r; *FRT2-lacZ* fusion containing suicidal vector	37
pFRT2-*lacZ*-Tel^r	E1708	Tel^r; pFRT2-*lacZ* with Gm^r cassette replaced by Tel^r cassette	This study
pPS856-ΔXbas	E1044	Gm^r Ap^r; Gm^r cassette flanked by wild-type *FRT* sequences	—[b]
pPS747	E0042	Ap^r; *gfp*-containing vector	17
pAKlux2	E1863	Ap^r; *luxCDABE* bioluminescence operon-containing vector	21
pFRT1-Gm^r-*lacZ*-Tel^r	E2049	Gm^r Tel^r; pFRT1-*lacZ*-Tel^r with *FRT1* replaced by the *FRT1*-Gm^r-*FRT1* fragment	This study
pFRT2-Gm^r-*lacZ*-Tel^r	E2050	Gm^r Tel^r; pFRT1-*lacZ*-Tel^r with *FRT1* replaced by the *FRT2*-Gm^r-*FRT2* fragment	This study
pFRT1-*lacZ*-Tel^r-ΔBam	E2051	Tel^r; pFRT1-Gm^r-*lacZ*-Tel^r with Flp-excised *FRT1*-Gm^r	This study
pFRT2-*lacZ*-Tel^r-ΔBam	E2052	Tel^r; pFRT2-Gm^r-*lacZ*-Tel^r with Flp-excised *FRT2*-Gm^r	This study
pFRT1-*gfp*-Tel^r	E2053	Tel^r; pFRT1-*lacZ*-Tel^r-ΔBam with *gfp* replacing *lacZ*	This study
pFRT2-*gfp*-Tel^r	E2055	Tel^r; pFRT2-*lacZ*-Tel^r-ΔBam with *gfp* replacing *lacZ*	This study
pFRT1-*lux*-Tel^r	E2064	Tel^r; pFRT1-*lacZ*-Tel^r-ΔBam with *luxCDABE* replacing *lacZ*	This study
pFRT2-*lux*-Tel^r	E2066	Tel^r; pFRT2-*lacZ*-Tel^r-ΔBam with *luxCDABE* replacing *lacZ*	This study
pCD13SK-Flp-*oriT*	E0803	Sp^r; Flp-containing suicidal vector	37
pCD13SK-Flp-*oriT*-*asd*$_{Ec}$	E1827	pCD13SK-Flp-*oriT* with *asd*$_{Ec}$ replaced by the Sp^r cassette	This study
pFlpAB-5	E1662	Tp^r; broad-host-range Flp-containing vector	2

[a] For plasmids constructed in this study, please see the text for further details. Please use the laboratory identification (Lab ID) number when requesting plasmids.
[b] —, details on the engineering of this plasmid are to be published elsewhere.

(Table 3). For *B. pseudomallei* and *B. mallei*, five random Tel^r colonies were purified on LB plates with Tel and PCR screened using *kilA* oligonucleotides 831 and 1066, *telA* oligonucleotides 827 and 1067, and *telB* oligonucleotides 834 and 854 (Table 3). Southern hybridization analysis was also performed, as described previously (17), for the *B. pseudomallei* and *B. mallei* Tel^r colonies using a *telB*-specific probe after the digestion of chromosomal DNA with XhoI.

Construction of mini-Tn*7* site-specific transposon vectors and their helper plasmid. The mini-Tn*7*-Tel^r site-specific transposon, based on Tel^r, was constructed as described below. pwFRT-PC$_{S12}$-Tel^r was digested with SacI and blunt ended, and the PC$_{S12}$-Tel^r fragment (3.2 kb) was cloned into pUC18R6KT-mini-Tn*7* (EcoRV digested), resulting in mini-Tn*7*-Tel^r-*bla*. The R6Kγ*ori*-*oriT* region, amplified from pCD11-Gm^r-*pir116-oriT* using oligonucleotides 696 and 702, was ligated with the mini-Tn*7*-Tel^r-*bla* backbone (including the Tel^r cassette) following AflII and NarI digestion and blunt ending. This resulted in a mini-Tn*7*-Tel^r vector (Fig. 2A).

TABLE 3. Oligonucleotide primers utilized in this study

Primer (name)	Sequence[a]
89 (*asd*$_{Ec}$-up)	5′-CGGTTGAATTCTACTCCGGTGCGCAAATGGC-3′
91 (*asd*$_{Ec}$-down)	5′-TACTGAATTCCGCCAAAATGGCCTGCAATTA-3′
696 (*oriT*-ClaI-1)	5′-TGGGTATCGATTCCTTAAGGTATACTTT-3′
702 (*R6K*)	5′-TGTCAGCCGTTAAGTGTTCC-3′
713 (*lacZ*α)	5′-TGTTGGGAAGGGCGATC-3′
827 (*telA*-SmaI)	5′-GGGAACGACCCTGGCCGCGTGCA-3′
831 (*tel-kilA*)	5′-AGCTAAAATGGAAGAACAAA-3′
834 (*telB*-XhoI)	5′-CCTCCTCGAGCAGAAAGTCAAAAGCCTC-3′
854 (*telB*-down)	5′-TACCAGCAGGAATGGAAC-3′
861 (Bt-*betBA*-HindIII)	5′-CCCGCAAGCTTGCCGGCAA-3′
862 (Bt-*betBA*-KpnI)	5′-GACCGGTACCCGGCGGGCGGGGATAT-3′
874 (*glmS1*-DN)[b]	5′-GTTCGTCGTCCACTGGGATCA-3′
875 (*glmS2*-DN)[b]	5′-AGATCGGATGGAATTCGTGGAG-3′
876 (Tn*7*L)[b]	5′-ATTAGCTTACGACGCTACACCC-3′
885 (*gfp*-BspHI-down)	5′-CAGGTCATGACACCTCTCTTTATTTGTATAGTTC-3′
1030 (*lux*-rev)	5′-GGATTGCACTAAATCATC-3′
1066 (*kilA*-rev)	5′-TCGGCTTCGTCCAGCAAC-3′
1067 (*telA*-rev)	5′-GCATTGCGCTTCATCAGG-3′

[a] Restriction enzyme sites utilized in this study are underlined.
[b] Oligonucleotides were synthesized as previously described (9).

FIG. 1. Plasmid map of mariner transposon vector pBT20-Δ*bla*-Tel^r-*FRT* based on Tel^r. The Tel^r cassette, consisting of the *kilA*, *telA*, and *telB* genes, is flanked by two identical *FRT* sequences. A *B. cenocepacia* PC$_{S12}$ promoter was included upstream of the Tel^r cassette. Abbreviations: Ω, *tonB* transcriptional terminator; *FRT*, Flip recombination target; *oriT*, conjugal origin of transfer; MR, mariner repeats; PC$_{S12}$, *B. cenocepacia rpsL* promoter; R6Kγ*ori*, suicidal R6K origin of replication; *tnp*, mariner transposase gene.

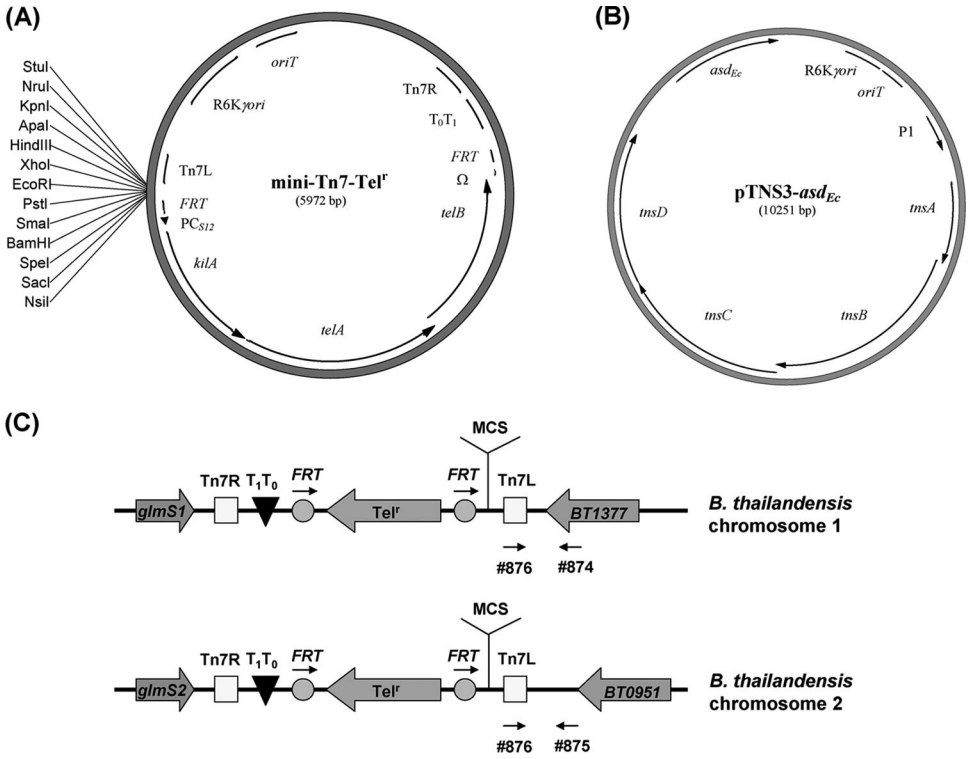

FIG. 2. The mini-Tn7-Tel^r integration vector and its pTNS3-*asd*$_{Ec}$ helper plasmid. (A) mini-Tn7-Tel^r, a Tn7-based suicidal vector with the Tel^r marker. (B) pTNS3-*asd*$_{Ec}$ suicidal helper plasmid encoding the transposase, which catalyzes Tn*7* transposition. (C) Chromosomally inserted mini-Tn7-Tel^r elements at two different *B. thailandensis att*Tn*7* sites as previously described (6). Oligonucleotides 874, 875, and 876, indicated by arrows, were used to screen for the location of transposition. *glmS1* and *glmS2* encode glucosamine-6-phosphate synthetases; MCS, multiple-cloning site; P1, P1 integron promoter; Tn7L, Tn*7* transposase left recognition sequence; Tn7R, Tn*7* transposase right recognition sequence; T_0T_1, transcriptional terminators; *tnsABCD*, Tn*7* transposases.

Helper plasmid pTNS3-*asd*$_{Ec}$ (Fig. 2B), containing the Tn*7* transposase genes, was also constructed based on *asd*$_{Ec}$. The *asd*$_{Ec}$ fragment was amplified from *E. coli* K-12 chromosomal DNA using oligonucleotides 89 and 91. The 2.5-kb PCR product was digested with EcoRI and PstI and blunt ended, and the 1.6-kb *asd*$_{Ec}$ gene was ligated into the pTNS3 backbone (digested with BglI and blunt ended), yielding pTNS3-*asd*$_{Ec}$.

Single-copy complementation of E264-Δ*betBA*::*FRT*. The mini-Tn7-Tel^r and the *betBA* operon fragment (amplified from E264 with oligonucleotides 861 and 862) were digested with HindIII and KpnI and ligated together, yielding mini-Tn7-Tel^r-*betBA*. The *B. thailandensis* E264-Δ*betBA*::*FRT* mutant was complemented using the constructed mini-Tn7-Tel^r-*betBA*. Two E1354 strains, each harboring either mini-Tn7-Tel^r-*betBA* or helper plasmid pTNS3-*asd*$_{Ec}$, were used to perform triparental matings with the *B. thailandensis* recipient E264-Δ*betBA*::*FRT*, creating the E264-Δ*betBA*::*FRT*/*attTn7*::Tel^r-*betBA* complemented strain. As a control, an empty mini-Tn7-Tel^r vector was conjugated into the E264-Δ*betBA*::*FRT* strain, resulting in E264-Δ*betBA*::*FRT*/*attTn7*::Tel^r. *B. thailandensis* transconjugants with the mini-Tn7 transposon inserted at the *att*Tn7 site were selected on LB plates with Tel and screened by PCR using oligonucleotides 874 and 876 or oligonucleotides 875 and 876 (Fig. 2C).

Characterization of growth of E264-Δ*betBA*::*FRT* and the complemented strain. Growth curve experiments were performed on three *B. thailandensis* strains: wild-type E264, the E264-Δ*betBA*::*FRT*/*attTn7*::Tel^r control, and the E264-Δ*betBA*::*FRT*/*attTn7*::Tel^r-*betBA* complement. These strains were grown overnight at 37°C in LB medium. Cultures grown overnight were washed twice with 1 volume of 1× M9 buffer and resuspended in an equal volume of the same buffer. Resuspended cultures were then diluted 100-fold into a solution containing fresh 1× M9 medium, 1% Brij 58, and 20 mM glucose or 30 mM choline chloride, and growth was initiated by shaking at 250 rpm and 37°C. At all time points, aliquots of each culture were taken, and optical densities were measured at 600 nm.

Construction of *FRT-lacZ*, *FRT-gfp*, and *FRT-lux* fusion vectors. An *flp*-carrying helper plasmid containing a nonantibiotic resistance marker was first created for the recombination of the various reporter fusion vectors. pCD13SK-Flp-*oriT* was digested with NdeI and SalI, blunt ended, and ligated with the above-mentioned 1.6-kb *asd*$_{Ec}$ fragment. The resulting helper plasmid, pCD13SK-Flp-*oriT*-*asd*$_{Ec}$ (see Fig. 4A), contains the *asd*$_{Ec}$ marker in place of the Sp^r cassette.

Two pFRT-*lacZ*-Tel^r vectors, pFRT1-*lacZ*-Tel^r and pFRT2-*lacZ*-Tel^r (Fig. 4B), were constructed in this study by replacing the Gm^r cassette with the Tel^r cassette. To create pFRT1-*lacZ*-Tel^r, pwFRT-PC$_{S12}$-Tel^r was digested with EcoRV and XhoI and blunt ended, and the resulting PC$_{S12}$-Tel^r fragment was cloned into pFRT1-*lacZ* (digested with BsrGI and SacII and blunt ended to remove the Gm^r cassette). Similarly, pFRT2-*lacZ*-Tel^r was constructed by cloning the PC$_{S12}$-Tel^r fragment into the pFRT2-*lacZ* backbone.

Four different fusion vectors were constructed based on the *gfp* reporter gene and the *luxCDABE* operon. In order to replace the *lacZ* gene with the promoterless *gfp* reporter gene or the *lux* operon, several cloning steps were carried out to eliminate one of the BamHI sites flanking the *FRT* sequence, leaving a unique BamHI site downstream of the *FRT* sequence. First, pPS856-ΔXbas was digested with SmaI to recover the *FRT*-Gm^r-*FRT* fragment, which was cloned into the pFRT1-*lacZ*-Tel^r backbone following digestion with the same enzyme. This cloning step resulted in the creation of pFRT1-Gm^r-*lacZ*-Tel^r (with the Gm^r cassette in the same orientation as the *lacZ* gene) and pFRT2-Gm^r-*lacZ*-Tel^r (with the Gm^r cassette in the opposite orientation of the *lacZ* gene). To Flp excise the Gm^r-*FRT* fragment, both pFRT1-Gm^r-*lacZ*-Tel^r and pFRT2-Gm^r-*lacZ*-Tel^r were introduced into Flp-containing strain DH5α-λ*attB*::pCD13SK-Flp. The resulting constructs, pFRT1-*lacZ*-Tel^r-ΔBam and pFRT2-*lacZ*-Tel^r-ΔBam, were digested with NdeI, blunt ended, and then digested with BamHI. These Tel^r cassette-containing vectors were ligated with the *gfp* gene from pPS747 (digested with HindIII, blunt ended, and then digested with BamHI), yielding pFRT1-*gfp*-Tel^r and pFRT2-*gfp*-Tel^r, respectively (Fig. 4C). Finally, pFRT1-*lacZ*-Tel^r-ΔBam and pFRT2-*lacZ*-Tel^r-ΔBam were digested with BamHI and NdeI and blunt ended, and the *luxCDABE* operon, obtained from pAKlux2 (Addgene plasmid 14080) following EcoRI digestion and blunt ending, was cloned to yield pFRT1-*lux*-Tel^r and pFRT2-*lux*-Tel^r (Fig. 4D).

Engineering of *B. thailandensis* E264-Δ*betBA*::*FRT* reporter fusion strains. To construct the E264-Δ*betBA*::*FRT-lacZ*-Tel^r reporter strain for the *betBA* promoter study, pFRT1-*lacZ*-Tel^r and the helper plasmid (pCD13SK-Flp-*oriT*-*asd*$_{Ec}$) were conjugated from E1354 into E264-Δ*betBA*::*FRT* in a triparental mating experiment. Colonies on MG plates with 125 μg/ml Tel were screened by PCR using oligonucleotides 713 and 861 to confirm the correct orientation of the *lacZ* gene relative to the *betBA* promoter region. This strain was then used in the choline induction study (see Fig. 5B and C).

The E264-Δ*betBA*::*FRT-lacZ*-Tel^r fusion strain was complemented by engineering the E264-Δ*betBA*::*FRT-lacZ*-Tel^r/*attTn7*::*betBA* strain in several steps (see Fig. 6A). First, the Tel^r cassette in strain E264-Δ*betBA*::*FRT*/*attTn7*::Tel^r-*betBA* (described above) was Flp excised using pFLP-AB5 according to a previously described procedure (2). The resulting strain, E264-Δ*betBA*::*FRT*/*attTn7*::*betBA*, was conjugated with two E1354 donor strains harboring either pFRT1-*lacZ*-Tel^r or pCD13SK-Flp-*oriT*-*asd*$_{Ec}$ in a triparental mating experiment. This triparental mating mixture was then plated onto MG plates with 125 μg/ml Tel to select for fusion strain E264-Δ*betBA*::*FRT-lacZ*-Tel^r/*attTn7*::*betBA*, harboring a *lacZ* reporter driven by the native *betBA* promoter. Colonies were screened by PCR using oligonucleotides 713 and 861 (Fig. 6A). Isolates with *lacZ* integrated at the *betBA* locus were purified once on LB medium and used in the osmotic regulation study (see Fig. 6B and C).

Fusion vector pFRT1-*gfp*-Tel^r was also integrated into the Δ*betBA*::*FRT* mutant and complemented strains as described above. The resulting fusion strains, E264-Δ*betBA*::*FRT-gfp*-Tel^r and E264-Δ*betBA*::*FRT-gfp*-Tel^r/*attTn7*::*betBA*, were screened by PCR using oligonucleotides 861 and 885 (Fig. 6A). Similarly, vector pFRT1-*lux*-Tel^r was used to construct fusion strains E264-Δ*betBA*::*FRT-lux*-Tel^r and E264-Δ*betBA*::*FRT-lux*-Tel^r/*attTn7*::*betBA*, which were screened by PCR using oligonucleotides 861 and 1030 (see Fig. 6A).

Choline and osmotic regulation studies of the *betBA* operon. β-Galactosidase activity of the integrated *betBA*::*FRT-lacZ*-Tel^r fusion was measured under various growth conditions. To study choline induction of the *betBA* operon, fusion strain E264-Δ*betBA*::*FRT-lacZ*-Tel^r was grown overnight in LB medium. Cultures grown overnight were washed twice with 1 volume of 1× M9 medium and resuspended in an equal volume of the same medium. Resuspended cultures were then diluted 100-fold into a solution containing fresh 1× M9 medium, 1% Brij 58, 20 mM glucose, and 0, 1, 2, 4, or 8 mM choline chloride. Growth curve experiments were performed on each culture by diluting sample aliquots twice in 4% Brij 58 and measuring the optical density at 600 nm (see Fig. 5B). Additional 1-ml cell culture aliquots were taken at each time point during the growth curve experiments to assay for β-galactosidase activity. These assays were done in triplicate and are displayed as average Miller units (28), with standard errors of the means (see Fig. 5C). *gfp* fusion strain E264-Δ*betBA*::*FRT-gfp*-Tel^r was grown in a solution containing 1× M9 medium, 1% Brij 58, and 20 mM glucose with or without 8 mM choline chloride to early stationary phase (~36 h), at which point wet mounts were prepared and examined under an Olympus BX51 fluorescent microscope to assay fluorescent activity in the presence or absence of choline (Fig. 5D). Fusion strain E264-Δ*betBA*::*FRT-lux*-Tel^r was grown in 1× M9 medium with 1% Brij 58 and 20 mM glucose with or without 8 mM choline chloride to early stationary phase, at which point 1 ml of each culture was centrifuged, and the cell pellet was resuspended with 20 μl of 1× M9 medium. The resuspended cells were then spotted onto an MG plate, and images were obtained immediately using a Bio-Rad biochemiluminescent imaging system.

To study the NaCl-mediated osmotic regulation of the *betBA* operon, we complemented the Δ*betBA* mutant because NaCl significantly affected the growth in the absence of the *betBA* operon. Growth curve experiments were conducted on the complemented fusion strain (E264-Δ*betBA*::*FRT-lacZ*-Tel^r/*attTn7*::*betBA*) and the wild-type strain (E264) by first growing cultures overnight in LS medium. Cultures grown overnight were washed with 1 volume of LS medium, resuspended in an equal volume of the same medium, and diluted 100-fold into fresh LS medium with 0, 0.3, and 0.4 M NaCl. Growth curve experiments were performed for each culture by taking optical density measurements at 600 nm (see Fig. 6B). Additional 1-ml cell culture aliquots of E264-Δ*betBA*::*FRT-lacZ*-Tel^r/*attTn7*::*betBA* were taken at each time point during the growth curve experiments to assay for β-galactosidase activity (Fig. 6C). Two other fusion strains, E264-Δ*betBA*::*FRT-gfp*-Tel^r/*attTn7*::*betBA* and E264-Δ*betBA*::*FRT-lux*-Tel^r/*attTn7*::*betBA*, were grown in LS medium with or without 0.3 M NaCl to late log phase (~30 h), at which time fluorescent microscopy and bioluminescence imaging analyses (see Fig. 6D and E) were performed as described above.

Nucleotide sequence accession numbers. All sequences of vectors presented in Fig. 1, 2, and 4 were submitted to the GenBank database. The accession numbers are as follows: EU626135 for pBT20-Δ*bla*-Tel^r-*FRT*, EU626136 for mini-Tn*7*-Tel^r, FJ797680 for pTNS3-*asd*$_{Ec}$, EU626138 for pCD13SK-Flp-*oriT*-*asd*$_{Ec}$, EU626139 for pFRT1-*lacZ*-Tel^r, EU626140 for pFRT2-*lacZ*-Tel^r, FJ455408 for pFRT1-*gfp*-Tel^r, FJ455409 for pFRT2-*gfp*-Tel^r, FJ455410 for pFRT1-*lux*-Tel^r, and FJ455411 for pFRT2-l*ux*-Tel^r.

TABLE 4. Transposition frequencies of pBT20-Δ*bla*-Tel^r-*FRT* in *Burkholderia* species

Species (strain)	Avg frequency of transposition ± SEM[a]
B. cenocepacia (K56-2)	$(1.22 \pm 0.21) \times 10^{-5}$
B. cenocepacia (J2315)	$(2.34 \pm 0.33) \times 10^{-6}$
B. thailandensis (E264)	$(4.29 \pm 0.42) \times 10^{-6}$
B. pseudomallei (K96243)	$(1.51 \pm 0.23) \times 10^{-5}$
B. pseudomallei (1026b)	$(1.07 \pm 0.10) \times 10^{-5}$
B. mallei (ATCC 23344)	$(2.08 \pm 0.16) \times 10^{-6}$

[a] All experiments were performed in triplicate, and averages are shown with the standard error of the mean.

RESULTS

Engineering and utilization of a random Tel^r transposon in *Burkholderia* species. A *Himar1*-based mariner transposon carrying a Km^r marker has been used successfully in *B. pseudomallei* although with some reported leakiness (32). To further develop and test a mariner transposon based on the alternative nonantibiotic Tel^r marker for a broader range of *Burkholderia* spp., we replaced the Gm^r marker on mariner transposon plasmid pBT20. pBT20, originally based on the Gm^r marker with a *bla* gene in its plasmid backbone, is not appropriate for selection in *Burkholderia* species due to their high level of Gm^r and may be inappropriate for use in the select-agent species *B. pseudomallei* and *B. mallei*. In this study, we constructed a mariner transposon, pBT20-Δ*bla*-Tel^r-*FRT*, based on the nonantibiotic Tel^r marker (Fig. 1) previously shown to be effective in *B. thailandensis* (2). We eliminated the *bla* gene from pBT20 and replaced the Gm^r cassette on the transposon with the Tel^r marker for selection in both *E. coli* and *Burkholderia*. To demonstrate the effectiveness of this transposon, we conjugated pBT20-Δ*bla*-Tel^r-*FRT* from a suicidal Δ*asd E. coli* strain into four different *Burkholderia* species: *B. cenocepacia* (two strains), *B. thailandensis*, *B. pseudomallei* (two strains), and *B. mallei*. For each species, three independent mating experiments were conducted, and the average transposition frequencies were determined and are shown in Table 4. We determined the effective Tel concentrations for the four *Burkholderia* species, and no spontaneous Tel^r mutants were detected when 10^9 CFU were plated alone on LB medium with Tel as controls (see Materials and Methods). On average, conjugation mixtures were resuspended in 1 ml of LB medium and diluted 10×, where 100-μl volumes were plated onto LB medium with Tel, yielding 50 to 200 colonies depending on the species. Fifteen random Tel^r colonies from *B. cenocepacia* (J2315 and K56-2) and *B. thailandensis* were screened by PCR using *telB*-specific oligonucleotides, and five random colonies from *B. pseudomallei* (K96243 and 1026b) and *B. mallei* were positively screened by PCR using *kilA*-, *telA*-, and *telB*-specific oligonucleotides (see Fig. S1A to S1F in the supplemental material). Southern blot analysis was also performed on the 15 Tel^r isolates of *B. pseudomallei* and *B. mallei* using a *telB*-specific probe (see Fig. S1G in the supplemental material). Single bands with different sizes were obtained in all isolates, suggesting random transposition into the *B. pseudomallei* and *B. mallei*

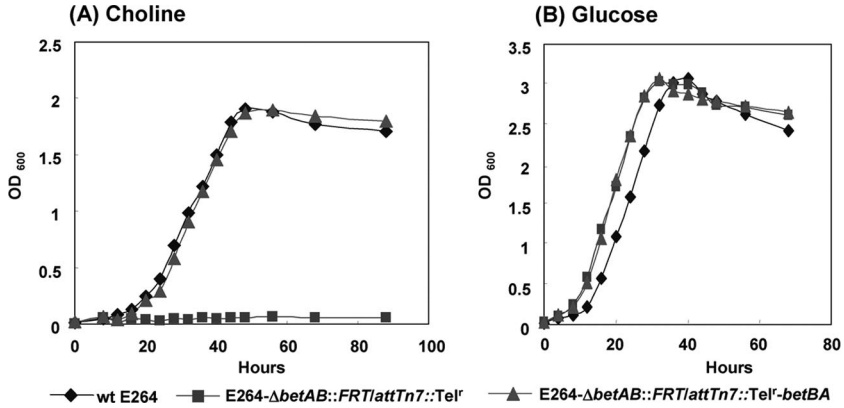

FIG. 3. Growth analyses of the *B. thailandensis* Δ*betBA* mutant and its complement on choline and glucose. Wild-type strain E264, the E264-Δ*betBA*::*FRT*/*attTn7*::Tel^r mutant, and the E264-Δ*betBA*::*FRT*/*attTn7*::Tel^r-*betBA* complement were grown in 1× M9 minimal medium supplemented with 30 mM choline (A) or 20 mM glucose (B). All three strains exhibited similar growth rates and overall cell densities when grown in glucose. The complemented strain, E264-Δ*betBA*::*FRT*/*attTn7*::Tel^r-*betBA*, displayed the same growth rate as the wild-type (wt) strain on choline. However, the *betBA* mutant strain containing the empty Tn*7* transposon control, E264-Δ*betBA*::*FRT*/*attTn7*::Tel^r, was not able to grow on choline as a sole carbon source. OD_{600}, optical density at 600 nm.

genomes (see Fig. S1G in the supplemental material). All *Burkholderia* species tested displayed similar transposition frequencies, ranging from $2.08 \times 10^{-6} \pm 0.16 \times 10^{-6}$ to $1.51 \times 10^{-5} \pm 0.23 \times 10^{-5}$ (Table 4), which are comparable to the frequencies obtained when using a Km^r-based transposon in *B. pseudomallei* (32). However, analyses of 5 to 15 Tel^r colonies showed that 100% of the Tel^r colonies contained the transposon, demonstrating the effectiveness of Tel^r selection (see Fig. S1 in the supplemental material). No spontaneous resistance was observed when 10^9 CFU were plated, indicating that the spontaneous resistance frequency is $<10^{-9}$. If required, the transposon insertion sites could easily be determined by sequencing the flanking region of the transposon using semirandom PCR methods as previously described (19, 24). The Tel^r cassette in our transposon, flanked by *FRT* sequences (17), could then be excised by Flp recombinase for subsequent recycling of the Tel^r cassette or integration of *FRT*-reporter fusions (below) at the transposed loci for immediate gene regulation studies.

Engineering and testing of the single-copy mini-Tn*7*-Tel^r site-specific transposon by complementing the *B. thailandensis* Δ*betBA* mutant. The mini-Tn*7* site-specific transposon and helper plasmid (carrying the Tn*7* transposase genes) were utilized in various species (1, 3, 8, 23). This system could be used for single-copy complementation studies, promoter-reporter fusion integration, and reporter gene (e.g., fluorescence and bioluminescence proteins) tagging in *Burkholderia* species (1, 3, 8, 23). However, all these systems contain antibiotic resistance markers for selection, requiring the need for reengineering with nonantibiotic selectable markers. In this study, we developed a mini-Tn*7*-Tel^r site-specific transposon and a helper plasmid for *Burkholderia* species based on two nonantibiotic selectable markers, the Tel^r cassette and the asd_{Ec} gene, respectively (Fig. 2A and B). This mini-Tn*7*-Tel^r vector contains a multiple-cloning site for conveniently cloning genes of interest for subsequent site-specific transposition, which is catalyzed by the transposase encoded on the pTNS3-asd_{Ec} helper plasmid. The location of the chromosomally inserted transposon could be determined by PCR with site-specific and transposon-specific oligonucleotides (9) (Fig. 2C). The *FRT*-flanked Tel^r cassette allows Flp-catalyzed excision of the Tel^r marker while maintaining the introduced gene of interest at the specific transposition site.

As a proof of concept, the mini-Tn*7*-Tel^r system was used to complement the *betBA* mutation in *B. thailandensis*. Previously, we engineered a *B. thailandensis* Δ*betBA* mutant that exhibits a growth defect when grown in choline as a sole carbon source (2). A wild-type copy of the *betBA* operon was cloned into the multiple-cloning site of mini-Tn*7*-Tel^r (Fig. 2A), resulting in the mini-Tn*7*-Tel^r-*betBA* vector. The helper plasmid pTNS3-asd_{Ec} and the mini-Tn*7*Tel^r-*betBA* vector were simultaneously conjugated by triparental mating into strain E264-Δ*betBA*::*FRT*. Site-specific transposition of the *betBA*-Tel^r complement was confirmed by PCR as previously described (9). In the majority of Tel^r isolates (8 out of 10 screened), the mini-Tn*7* transposon was inserted downstream of the *glmS2* gene on the second chromosome, while two transpositions occurred downstream of the *glmS1* gene on the first chromosome (9). None of the isolates displayed integration on both chromosomes (see Fig. S2 in the supplemental material).

To show the complementation of the Δ*betBA* mutant, the constructed strain E264-Δ*betBA*::*FRT*/*attTn7*::Tel^r-*betBA* was tested for its ability to grow on choline as a sole carbon source. As shown in Fig. 3A, this chromosomally integrated copy of the *betBA* operon recovered the growth ability of the Δ*betBA* mutant strain on choline as a sole carbon source, displaying a growth rate and an overall cell density comparable to those of wild-type strain E264. The transposition of the empty mini-Tn*7*-Tel^r control into the Δ*betBA* mutant yielded no complementation of the Δ*betBA* mutation, and it was unable to grow with choline as a sole carbon source (Fig. 3A). Growth curve studies for these three strains on glucose as a sole carbon source were also conducted (Fig. 3B) to show that the integrated mini-Tn*7* system did not alter any other growth phenotypes of mutant strain E264-Δ*betBA*::*FRT*.

Engineering of reporter gene constructs and regulation studies of the *betBA* operon. Recombination of the *FRT-lacZ* reporter fusion with the single chromosomally located "*FRT* scar"

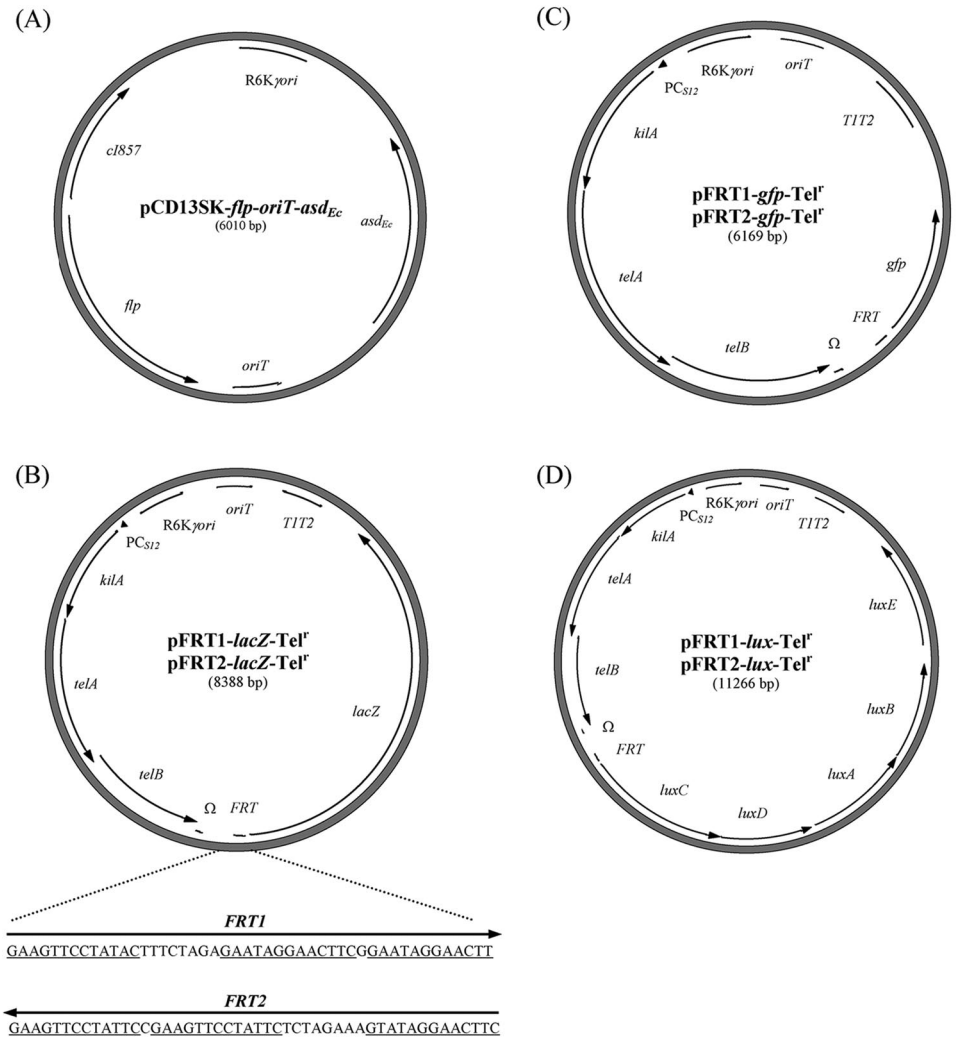

FIG. 4. Plasmid maps of the *FRT*-reporter fusion vectors and their helper plasmids. (A) pCD13SK-Flp-*oriT-asd*$_{Ec}$ is a *flp*-containing helper plasmid for the recombination of all *FRT*-reporter fusions. (B to D) Various fusion vectors were constructed based on the reporters *lacZ* (B), *gfp* (C), and the *luxCDABE* operon (D). With the exception of the *FRT* oriented relative to the reporter genes, all of the paired pFRT1-Tel^r and pFRT2-Tel^r vectors have the same sequence. Depending on the orientation of *FRT* on the chromosome, either pFRT1-Tel^r or pFRT2-Tel^r would be used to orient the promoterless reporter fusion in the same direction as the promoter of interest. Abbreviations: *cI857*, temperature-sensitive repressor; *gfp*, green fluorescent protein gene; *lacZ*, β-galactosidase gene; *luxCDABE*, genes encoding the bacterial bioluminescent operon; T_1T_2, transcriptional terminators.

aided by the Flp-encoding helper plasmid, following mutant construction with an *FRT*-flanked antibiotic resistance cassette and Flp excision, has facilitated regulation studies of target genes at their native chromosomal loci (12, 37). In our experience, when coupled with *FRT*-based resistant-marker approaches for chromosomal mutagenesis (e.g., allelic replacement or *FRT*-based transposon) (32), these fusion vectors were found to be simple and powerful tools for studying gene regulation without promoter mapping or prior knowledge of promoter sequence or location. The disadvantages of previously reported fusion vectors and helper plasmids (12, 37) are the use of antibiotic resistance markers (Ap^r, Cm^r, Gm^r, Km^r, and Sp^r) and the limitation of a single reporter gene (*lacZ*). Here, the Tel^r cassette replaced the Gm^r cassette in the previously reported vectors pFRT1-*lacZ* and pFRT2-*lacZ* (37), resulting in pFRT1-*lacZ*-Tel^r and pFRT2-*lacZ*-Tel^r (Fig. 4B). The difference between these two new vectors is the orientation of the *FRT* sequence relative to that of the reporter gene, accounting for the selection of the appropriate fusion vector relative to the orientation of the "*FRT* scar" on the chromosome, thus aligning the reporter gene in the same direction as the promoter. To provide more reporter gene options, four other fusion vectors (pFRT1-*gfp*-Tel^r, pFRT2-*gfp*-Tel^r, pFRT1-*lux*-Tel^r, and pFRT2-*lux*-Tel^r) were constructed based on the *gfp* and *lux* operon reporters (Fig. 4C and D). We constructed an Flp-encoding helper plasmid (pCD13SK-Flp-*oriT-asd*$_{Ec}$) based on the *asd*$_{Ec}$ nonantibiotic selectable marker for plasmid maintenance in *E. coli* Δ*asd* strains (e.g., E463 and E1354) (Table 1 and Fig. 4A).

The regulation mechanisms of the *betBA* operon have been widely studied in a variety of organisms such as *E. coli* (13), *Pseudomonas putida* (14), and *Sinorhizobium meliloti* (27). Extensive characterization of the *betBA* operon in *E. coli* (13) has shown that this operon is regulated by osmolarity, tempera-

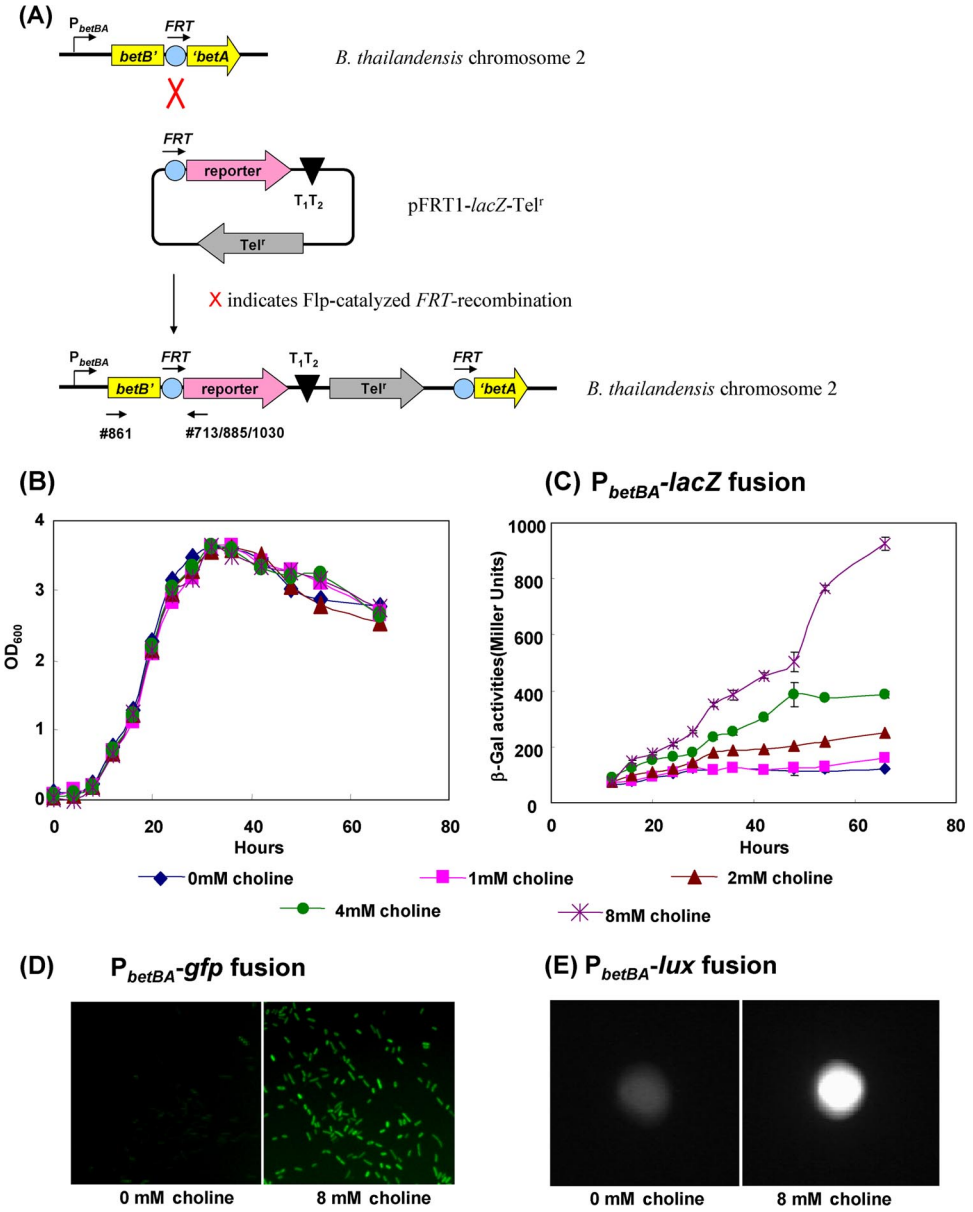

FIG. 5. Induction of the *betBA* operon by choline. (A) Flp-catalyzed recombination of the promoterless *FRT-lacZ* fusion into the *B. thailandensis* chromosome at the Δ*betBA*::*FRT* loci. Oligonucleotides 713 and 861 were used to screen for correct integration and are indicated by arrows. Oligonucleotides 885 and 1030 were used along with oligonucleotide 861 to screen *gfp* and *lux* reporters, respectively. (B) E264-Δ*betBA*::*FRT-lacZ* was grown in 1× M9 medium plus 20 mM glucose supplemented with 0, 1, 2, 4, or 8 mM choline. (C) β-Galactosidase assays were performed in triplicate for all of the growth cultures shown above (B) at various time points, indicating that *betBA* is inducible by choline. Two alternative fusion strains, E264-Δ*betBA*::*FRT-gfp*-Tel^r (D) and E264-Δ*betBA*::*FRT-lux*-Tel^r (E), were grown in MG medium or MG medium plus 8 mM choline. (D and E) The expressions of GFP (D) and bioluminescent proteins (E) were significantly induced in the presence of choline. Images in D are representative of multiple fields for the same samples. OD_{600}, optical density at 600 nm.

ture, oxygen, choline, and glycine betaine. However, little is known about the regulation of the *betBA* operon in *B. thailandensis*. As a proof of concept, we used one of the reporter fusion vectors to determine the regulatory mechanism of the *betBA* operon in *B. thailandensis* by choline and osmotic stress. *B. thailandensis* strain E264-Δ*betBA*::*FRT-lacZ*-Tel^r was engineered using fusion vector pFRT1-*lacZ*-Tel^r and helper plasmid pCD13SK-Flp-*oriT-asd*$_{Ec}$ (Fig. 4A and B and 5A). Flp-catalyzed recombination and the orientation of the *FRT-lacZ* fusion at the "*FRT* scar" within the chromosome of the Δ*betBA* mutant, a location at which the *lacZ* reporter gene is controlled by an unknown *betBA* promoter, were verified by PCR using oligonucleotides 713 and 861 (Fig. 5A). Choline induction of the *betBA* operon was studied by growing fusion strain E264-Δ*betBA*::*FRT-lacZ*-Tel^r in 1× M9 medium with glucose and supplemented with different concentrations of choline. These conditions resulted in similar growth rates and overall cell densities (Fig. 5B). β-Galactosidase assays were performed

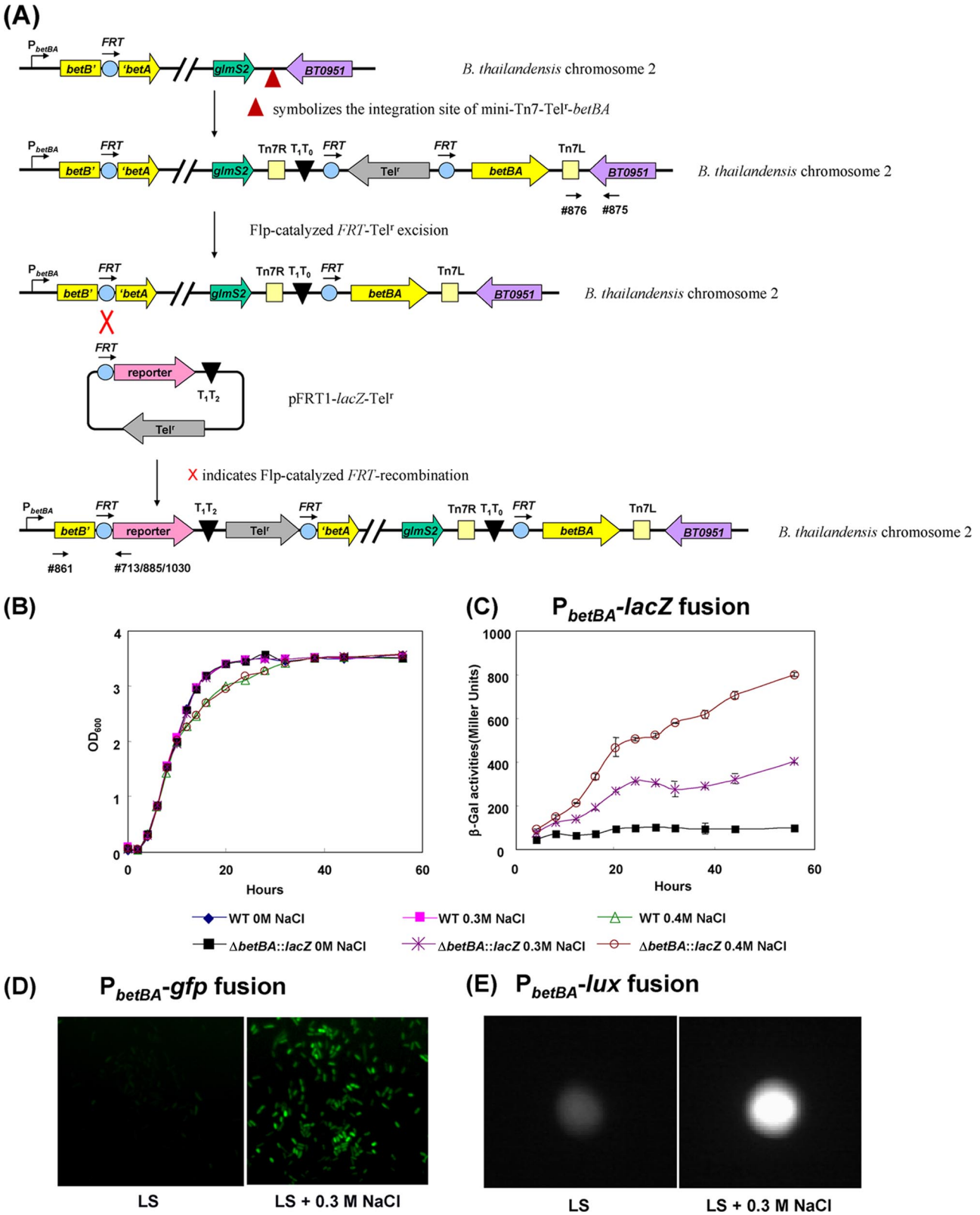

FIG. 6. Induction of the *betBA* operon by osmotic stress. (A) Strategy for constructing fusion strain E264-Δ*betBA*::*FRT-lacZ*-Tel^r/*attTn7*::*betBA*. Oligonucleotide 861 was used along with oligonucleotide 713, 885, or 1030 for screening, and they are indicated by arrows. Parallel diagonal lines indicate a large distance of separation on the chromosome. (B) The resulting strain, E264-Δ*betBA*::*FRT-lacZ*-Tel^r/*attTn7*::*betBA*, and wild-type (WT) strain E264 were grown in LS (0 M NaCl) medium supplemented with 0.3 and 0.4 M NaCl. Both the wild-type and fusion strains produced identical growth characteristics in LS medium and LS medium plus 0.3 M NaCl yet displayed slightly decreased levels of growth in 0.4 M NaCl after mid-log phase. (C) At

to compare the expression levels of the *betBA* operon in different choline concentrations (Fig. 5C). As choline concentrations increased, corresponding increases in β-galactosidase activities were observed, indicating that the *betBA* operon was responsive to choline. Utilizing two alternative gene fusion vectors (pFRT1-*gfp*-Tel^r and pFRT1-*lux*-Tel^r), fusion strains E264-Δ*betBA*::*FRT-gfp*-Tel^r and E264-Δ*betBA*::*FRT-lux*-Tel^r were also constructed. By comparing the fluorescent and luminescent intensities, the induction of the *betBA* operon by choline was observed using the *gfp* or *lux* reporter, respectively (Fig. 5D and E).

A previously reported study has shown that the *E. coli betBA* operon was involved in osmotic regulation and was induced by osmotic stress (13). Here, we demonstrated that osmotic stress (e.g., NaCl) induces the *B. thailandensis betBA* operon by utilizing the mini-Tn*7*-Tel^r-based system and the reporter fusion vectors described above. To compare the level of expression of the *betBA* operon in the presence of osmotic stress to that in the absence of osmotic stress, it was necessary to obtain the same growth rates and overall cell densities through complementation of the Δ*betBA* mutation (Fig. 6B). Consequently, fusion strain E264-Δ*betBA*::*FRT-lacZ*-Tel^r/*attTn7*::*betBA* was constructed in the E264-Δ*betBA*::*FRT*/*attTn7*::*betBA* background (Fig. 6A) because we found that the growth of the Δ*betBA* mutant was significantly affected by NaCl without complementing the Δ*betBA* mutation. The constructed strain, E264-Δ*betBA*::*FRT-lacZ*-Tel^r/*attTn7*::*betBA*, and wild-type strain E264 were grown in LS (0 M NaCl) medium supplemented with 0.3 and 0.4 M NaCl. These strains produced identical growth characteristics in LS medium and LS medium with 0.3 M NaCl, but both strains displayed slightly decreased growth rates in 0.4 M NaCl after the mid-log growth phase (Fig. 6B). The presence of 0.3 M NaCl significantly induced the *betBA* operon as determined by β-galactosidase assays (Fig. 6C). Despite the increased induction of the *betBA* operon in the presence of 0.4 M NaCl relative to that in the absence of NaCl, this comparison was unreliable due to differing growth rates. These data indicated that the *betBA* operon in *B. thailandensis* was induced by osmotic stress. Similarly, two fusion strains (E264-Δ*betBA*::*FRT-gfp*-Tel^r/*attTn7*::*betBA* and E264-Δ*betBA*::*FRT-lux*-Tel^r/*attTn7*::*betBA*) were constructed to show the induction of the *betBA* operon by observing the increased fluorescence and bioluminescence levels under conditions of osmotic stress (Fig. 6D and E).

DISCUSSION

In this study, the nonantibiotic Tel^r cassette was utilized to construct three genetic systems: a random mariner transposon, a mini-Tn*7* site-specific transposon vector, and six *FRT*-reporter fusion vectors based on three different reporters. A constitutive promoter, PC_{S12} (*B. cenocepacia rpsL* gene) (41), was included upstream of the Tel^r cassettes in all these tools to ensure the efficient expression of this resistance marker. First, the constructed *Himar1*-based random mariner transposon was successfully tested in four different *Burkholderia* spp.: *B. cenocepacia*, *B. thailandensis*, *B. pseudomallei*, and *B. mallei*. PCR screening with Tel-specific oligonucleotides revealed that 100% of Tel^r colonies harbored the Tel^r cassette. Next, the mini-Tn*7* system was utilized successfully to complement the Δ*betBA* mutant. Finally, three different *FRT*-reporter fusion vectors were used to study the regulation of the *B. thailandensis betBA* operon. Results showed that the *betBA* operon, which is essential for *B. thailandensis* choline degradation, was induced significantly by choline and osmotic stress (NaCl).

There are several advantages to including *FRT*-flanked resistance cassettes in random transposon mutagenesis and allelic replacement (2, 32). First, unmarked mutations can be obtained subsequent to allelic replacement or transposon mutagenesis by Flp excision of *FRT*-flanked resistance selection cassettes. The use of *FRT*-flanked resistance cassettes in allelic replacement allows for easier selection, resulting in higher mutation frequencies than that reported for a recently published approach to obtain unmarked mutations where there was a lack of positive selection for the second homologous recombination (15). Furthermore, the lack of positive selection requires laborious screening, and mutating essential genes may not be possible. In addition, the remaining "*FRT* scar" adds flexibility to subsequent fusion integrations, aiding in the construction of fusion strains for regulation studies of nonessential genes without prior knowledge of the identity and location of promoter sequences. For essential genes, mutant fusion strains can be complemented with the mini-Tn*7*-Tel^r system presented here, and gene regulation studies can be performed. Because single copies are more representative of the natural genetic regulation mechanism, as opposed to multicopy plasmids, single-copy tools could ameliorate the difficulties of complementation and promoter studies. The six *FRT*-reporter fusion vectors, based on three different reporters (*lacZ*, *gfp*, and the *luxCDABE* operon), add further flexibility and provide simplified visualization and quantification of gene expression during regulation studies. For example, by fusing the *gfp* reporter downstream of a target gene with pFRT-*gfp*-Tel^r vectors, it is possible to measure gene expression via detecting the bacterial green fluorescent protein (GFP) signal under different growth conditions or during eukaryotic cell infections. Similarly, by utilizing the pFRT-*lux*-Tel^r vectors, the regulation of target genes during animal model infections can be studied by measuring the bacterial bioluminescence intensity.

The genetic tools described in this paper will aid in elucidating the physiology, environmental behavior, and pathogenic mechanisms of *Burkholderia* species. Although the model or-

each time point, β-galactosidase assays were performed in triplicate on fusion strain E264-Δ*betBA*::*FRT-lacZ*-Tel^r/*attTn7*::*betBA* grown in LS medium with 0, 0.3, or 0.4 M NaCl. When the complemented fusion strain was grown under osmotically stressed conditions (0.3 and 0.4 M NaCl), the *betBA* operon was significantly induced, compared to conditions with no osmotic stress (no salt). (D and E) Two alternative fusion strains, E264-Δ*betBA*::*FRT-gfp*-Tel^r/*att*Tn*7*::*betBA* (D) and E264-Δ*betBA*::*FRT-lux*-Tel^r/*attTn7*::*betBA* (E), were grown in LS medium or LS medium plus 0.3 M NaCl. The expressions of GFP (D) and *luxCDABE* (E) were significantly induced in the presence of NaCl. Images in D are representative of multiple fields in the same sample. OD_{600}, optical density at 600 nm.

ganism *B. thailandensis* was utilized primarily to demonstrate the efficacy of these tools, Tel^r selection was successfully tested in the select agents *B. pseudomallei* and *B. mallei* by using the transposon pBT20-Δ*bla*-Tel^r-*FRT*. Thus, we believe that these tools could be particularly useful for various studies of *B. pseudomallei* and *B. mallei*. The alternative nonantibiotic asd_{Ec} selectable marker in helper plasmids pTNS3-asd_{Ec} and pCD13SK-Flp-*oriT*-asd_{Ec} may allow their use in other select-agent species. The genetic tools presented here could be further developed by substituting the Tel^r cassette with other nonantibiotic selectable markers. Finally, because these tools are completely devoid of any antibiotic resistance markers, they are in full compliance with CDC select-agent regulations.

ACKNOWLEDGMENTS

This work was supported by an NIH grant (R21-AI074608) to T.T.H. A graduate stipend to M.H.N. was supported by NSF IGERT award 0549514 to B.A.W. Salary support for A.R.B. was provided by grant P20RR018727 from the National Center for Research Resources, a component of the NIH.

The contents of the paper are solely the responsibility of the authors and do not necessarily represent the official views of the NCRR or the NIH.

We thank Herbert Schweizer (Colorado State University) for the gifts of pUC18R6KT-mini-Tn*7* and pTNS3 and Attila Karsi (Mississippi State University) for the gift of pAKlux2.

REFERENCES

1. **Bao, Y., D. P. Lies, H. Fud, and G. P. Roberts.** 1991. An improved Tn7-based system for the single-copy insertion of cloned genes into chromosomes of gram-negative bacteria. Gene **109:**167–168.
2. **Barrett, A. R., Y. Kang, K. S. Inamasu, M. S. Son, J. M. Vukovich, and T. T. Hoang.** 2008. Genetic tools for allelic replacement in *Burkholderia* species. Appl. Environ. Microbiol. **74:**4498–4508.
3. **Barry, G. F.** 1986. Permanent insertion of foreign genes into the chromosomes of soil bacteria. Nat. Biotechnol. **4:**446–449.
4. **Baulard, A., V. Escuyer, N. Haddad, L. Kremer, C. Locht, and P. Berche.** 1995. Mercury resistant as a selective marker for recombinant mycobacteria. Microbiology **141:**1045–1050.
5. **Brett, P. J., D. DeShazer, and D. E. Woods.** 1998. *Burkholderia thailandensis* sp. nov., description of *Burkholderia pseudomallei*-like species. Int. J. Syst. Bacteriol. **48:**317–320.
6. **Caiazza, N. C., R. M. Q. Shanks, and G. A. O'Toole.** 2005. Rhamnolipids modulate swarming motility patterns of *Pseudomonas aeruginosa*. J. Bacteriol. **187:**7351–7361.
7. **Chan, Y. Y., T. M. C. Tan, Y. M. Ong, and K. L. Chua.** 2004. BpeAB-OprB, a multidrug efflux pump in *Burkholderia pseudomallei*. Antimicrob. Agents Chemother. **48:**1128–1135.
8. **Choi, K. H., D. DeShazer, and H. P. Schweizer.** 2006. Mini-Tn7 insertion in bacteria with multiple *glmS*-linked *attTn7* sites: example *Burkholderia mallei* ATCC 23344. Nat. Protoc. **1:**162–169.
9. **Choi, K. H., J. B. Gaynor, K. G. White, C. Lopez, C. M. Bosio, R. R. Karkhoff-Schweizer, and H. P. Schweizer.** 2005. A Tn7-based broad-range bacterial cloning and expression system. Nat. Methods **2:**443–448.
10. **Choi, K. H., T. Mima, Y. Casart, D. Rholl, A. Kumar, I. R. Beacham, and H. P. Schweizer.** 2008. Genetic tools for select-agent-compliant manipulation of *Burkholderia pseudomallei*. Appl. Environ. Microbiol. **74:**1064–1075.
11. **DeShazer, D., P. J. Brett, R. Carlyon, and D. E. Woods.** 1997. Mutagenesis of *Burkholderia pseudomallei* with Tn*5*-OT182: isolation of motility mutants and molecular characterization of the flagellin structural gene. J. Bacteriol. **179:**2116–2125.
12. **Ellermeier, C. D., A. Janakiraman, and J. M. Slauch.** 2002. Construction of targeted single copy *lac* fusions using lambda Red and Flp-mediated site-specific recombination in bacteria. Gene **290:**153–161.
13. **Eshoo, M. W.** 1988. *lac* fusion analysis of the *bet* genes of *Escherichia coli*: regulation by osmolarity, temperature, oxygen, choline, and glycine betaine. J. Bacteriol. **170:**5208–5215.
14. **Galvão, T. C., V. de Lorenzo, and D. Cánovas.** 2006. Uncoupling of choline-O-sulphate utilization from osmoprotection in *Pseudomonas putida*. Mol. Microbiol. **62:**1643–1654.
15. **Hamad, M. A., S. L. Zajdowicz, R. K. Holmes, and M. I. Voskuil.** 2009. An allelic exchange system for compliant genetic manipulation of the select agents *Burkholderia pseudomallei* and *Burkholderia mallei*. Gene **430:**123–131.
16. **Herrero, M., V. De Lorenzo, and K. N. Timmis.** 1990. Transposon vectors containing non-antibiotic resistance selection markers for cloning and stable chromosomal insertion of foreign genes in gram-negative bacteria. J. Bacteriol. **172:**6557–6567.
17. **Hoang, T. T., R. R. Karkhoff-Schweizer, A. J. Kutchma, and H. P. Schweizer.** 1998. A broad-host-range Flp-*FRT* recombination system for site-specific excision of chromosomally-located DNA sequences: application for isolation of unmarked *Pseudomonas aeruginosa* mutants. Gene **212:**77–86.
18. **Holden, M. T., R. W. Titball, S. J. Peacock, A. M. Cerdeno-Tarraga, T. Atkins, L. C. Crossman, T. Pitt, C. Churcher, K. Mungall, S. D. Bentley, M. Sebaihia, N. R. Thomson, N. Bason, I. R. Beacham, K. Brooks, K. A. Brown, N. F. Brown, G. L. Challis, I. Cherevach, T. Chillingworth, A. Cronin, B. Crossett, P. Davis, D. DeShazer, T. Feltwell, A. Fraser, Z. Hance, H. Hauser, S. Holroyd, K. Jagels, K. E. Keith, M. Maddison, S. Moule, C. Price, M. A. Quail, E. Rabbinowitsch, K. Rutherford, M. Sanders, M. Simmonds, S. Songsivilai, K. Stevens, S. Tumapa, M. Vesaratchavest, S. Whitehead, C. Yeats, B. G. Barrell, P. C. Oyston, and J. Parkhill.** 2004. Genomic plasticity of the causative agent of melioidosis, *Burkholderia pseudomallei*. Proc. Natl. Acad. Sci. USA **101:**14240–14245.
19. **Kang, Y., D. T. Nguyen, M. S. Son, and T. T. Hoang.** 2008. The *Pseudomonas aeruginosa* PsrA responds to long-chain fatty acid signals to regulate the *fadBA5* beta-oxidation operon. Microbiology **154:**1584–1598.
20. **Kang, Y., M. S. Son, and T. T. Hoang.** 2007. One step engineering of T7-expression strains for protein production: increasing the host-range of the T7-expression system. Protein Expr. Purif. **55:**325–333.
21. **Karsi, A., and M. L. Lawrencea.** 2007. Broad host range fluorescence and bioluminescence expression vectors for gram-negative bacteria. Plasmid **57:**286–295.
22. **Kulasekara, H. D., I. Ventre, B. R. Kulasekara, A. Lazdunski, A. Filloux, and S. Lory.** 2005. A novel two-component system controls the expression of *Pseudomonas aeruginosa* fimbrial *cup* genes. Mol. Microbiol. **55:**368–380.
23. **Lambertsen, L., C. Sternberg, and S. Molin.** 2004. Mini-Tn7 transposons for site-specific tagging of bacteria with fluorescent proteins. Environ. Microbiol. **6:**726–732.
24. **Levano-Garcia, J., S. Verjovski-Almeida, and A. C. R. da Silva.** 2005. Mapping transposon insertion sites by touchdown PCR and hybrid degenerate primers. BioTechniques **38:**225–229.
25. **Lynch, M. D., and R. T. Gill.** 2006. Broad host range vectors for stable genomic library construction. Biotechnol. Bioeng. **94:**151–158.
26. **Mahenthiralingam, E., T. A. Urban, and J. B. Goldberg.** 2005. The multifarious, multireplicon Burkholderia cepacia complex. Nat. Rev. Microbiol. **3:**144–156.
27. **Mandon, K., M. Osterås, E. Boncompagni, J. C. Trinchant, G. Spennato, M. C. Poggi, and D. Le Rudulier.** 2003. The *Sinorhizobium meliloti* glycine betaine biosynthetic genes (*betlCBA*) are induced by choline and highly expressed in bacteroids. Mol. Plant-Microbe Interact. **16:**709–719.
28. **Miller, J. H.** 1992. A short course in bacterial genetics. Cold Spring Harbor Laboratory Press, Cold Spring Harbor, NY.
29. **Moore, R. A., D. DeShazer, S. Reckseidler, A. Weissman, and D. E. Woods.** 1999. Efflux-mediated aminoglycoside and macrolide resistance in *Burkholderia pseudomallei*. Antimicrob. Agents Chemother. **43:**465–470.
30. **Nakayama, K., M. S. Kelly, and R. Curtiss III.** 1988. Construction of an asd^+ expression-cloning vector: stable maintenance and high level expression of cloned genes in a *Salmonella* vaccine strain. Nat. Biotechnol. **6:**693–697.
31. **Platt, R., C. Drescher, S.-K. Park, and G. J. Phillips.** 2000. Genetic systems for reversible integration of DNA constructs and *lacZ* gene fusions into the *Escherichia coli* chromosome. Plasmid **43:**12–23.
32. **Rholl, D. A., L. A. Trunck, and H. P. Schweizer.** 2008. *Himar1* in vivo transposon mutagenesis of *Burkholderia pseudomallei*. Appl. Environ. Micrbiol. **74:**7529–7535.

32a. **Richmond, J. Y., and R. W. McKinney.** 2007. Biosafety in microbiological and biomedical laboratories, 5th ed. Centers for Disease Control and Prevention, Atlanta, GA.

33. **Sambrook, J., and D. W. Russell.** 2001. Molecular cloning: a laboratory manual, 3rd ed. Cold Spring Harbor Laboratory Press, Cold Spring Harbor, NY.
34. **Sanchez-Romero, J. M., R. Diaz-Orejas, and V. De Lorenzo.** 1998. Resistance to tellurite as a selection marker for genetic manipulations of *Pseudomonas* strains. Appl. Environ. Microbiol. **64:**4040–4046.
35. **Schweizer, H. P., and S. J. Peacock.** 2008. Antimicrobial drug-selection markers for *Burkholderia pseudomallei* and *B. mallei*. Emerg. Infect. Dis. **14:**1689–1692.
36. **Simpson, A. J., N. J. White, and V. Wuthiekanun.** 1999. Aminoglycoside and macrolide resistance in *Burkholderia pseudomallei*. Antimicrob. Agents Chemother. **43:**2332.
37. **Son, M. S., D. T. Nguyen, Y. Kang, and T. T. Hoang.** 2008. Engineering of

FRT-lacZ fusion constructs: induction of the *Pseudomonas aeruginosa fadAB1* operon by medium and long chain-length fatty acids. Plasmid **59:** 111–118.

38. **Taylor, D. E.** 1999. Bacterial tellurite resistance. Trends Microbiol. **7:**111–115.
39. **Vandamme, P., J. Govan, and J. LiPuma.** 2007. Diversity and role of *Burkholderia* spp., p. 1–28. *In* T. Coenye and P. Vandamme (ed.), Burkholderia: molecular microbiology and genomics. Horizon Scientific, Wymondham, United Kingdom.
40. **Yabuuchi, E., Y. Kosako, H. Oyaizu, I. Yano, H. Hotta, Y. Hashimoto, T. Ezaki, and M. Arakawa.** 1992. Proposal of *Burkholderia* gen. nov. and transfer of seven species of the genus *Pseudomonas* homology group II to the new genus, with the type species *Burkholderia cepacia* (Palleroni and Holmes 1981) comb. nov. Microbiol. Immunol. **36:**1251–1275.
41. **Yu, M., and J. S. H. Tsang.** 2006. Use of ribosomal promoters from *Burkholderia cenocepacia* and *Burkholderia cepacia* for improved expression of transporter protein in *Escherichia coli*. Protein Expr. Purif. **49:** 219–227.

OPEN ACCESS Freely available online

PLoS one

Multiple FadD Acyl-CoA Synthetases Contribute to Differential Fatty Acid Degradation and Virulence in *Pseudomonas aeruginosa*

Yun Kang[2], Jan Zarzycki-Siek[1], Chad B. Walton[3], Michael H. Norris[2], Tung T. Hoang[1,2]*

1 Department of Microbiology, University of Hawaii at Manoa, Honolulu, Hawaii, United States of America, **2** Department of Molecular Biosciences and Bioengineering, University of Hawaii at Manoa, Honolulu, Hawaii, United States of America, **3** Department of Medicine, University of Hawaii at Manoa, Honolulu, Hawaii, United States of America

Abstract

A close interconnection between nutrient metabolism and virulence factor expression contributes to the pathophysiology of *Pseudomonas aeruginosa* as a successful pathogen. *P. aeruginosa* fatty acid (FA) degradation is complicated with multiple acyl-CoA synthetase homologs (FadDs) expressed *in vivo* in lung tissue during cystic fibrosis infections. The promoters of two genetically linked *P. aeruginosa fadD* genes (*fadD1* and *fadD2*) were mapped and northern blot analysis indicated they could exist on two different transcripts. These FadDs contain ATP/AMP signature and FA-binding motifs highly homologous to those of the *Escherichia coli* FadD. Upon introduction into an *E. coli fadD*$^-$/*fadR*$^-$ double mutant, both *P. aeruginosa fadD*s functionally complemented the *E. coli fadD*$^-$/*fadR*$^-$ mutant, allowing degradation of different chain-length FAs. Chromosomal mutagenesis, growth analysis, induction studies, and determination of kinetic parameters suggested that FadD1 has a substrate preference for long-chain FAs while FadD2 prefers shorter-chain FAs. When compared to the wild type strain, the *fadD2* mutant exhibited decreased production of lipase, protease, rhamnolipid and phospholipase, and retardation of both swimming and swarming motilities. Interestingly, *fadD1* mutant showed only increased swarming motility. Growth analysis of the *fadD* mutants showed noticeable deficiencies in utilizing FAs and phosphatidylcholine (major components of lung surfactant) as the sole carbon source. This defect translated into decreased *in vivo* fitness of *P. aeruginosa* in a BALB/c mouse lung infection model, supporting the role of lipids as a significant nutrient source for this bacterium *in vivo*.

Citation: Kang Y, Zarzycki-Siek J, Walton CB, Norris MH, Hoang TT (2010) Multiple FadD Acyl-CoA Synthetases Contribute to Differential Fatty Acid Degradation and Virulence in *Pseudomonas aeruginosa*. PLoS ONE 5(10): e13557. doi:10.1371/journal.pone.0013557

Editor: Michael Otto, National Institutes of Health, United States of America

Received May 19, 2010; **Accepted** September 28, 2010; **Published** October 21, 2010

Funding: This project was supported by a National Institutes of Health (NIH) grant R21-AI073816 and in parts by NIH grant numbers G12RR003061 and P20RR01872 from the National Center for Research Resources (NCRR), a component of the NIH. The funders had no role in study design, data collection and analysis, decision to publish, or preparation of the manuscript.

Competing Interests: The authors have declared that no competing interests exist.

* E-mail: tongh@hawaii.edu

Introduction

To occupy a diverse range of ecological niches, *Pseudomonas aeruginosa* must evolve and maintain a wide array of metabolic pathways for nutrient uptake and utilization. This adaptive flexibility allows *P. aeruginosa*, a ubiquitous Gram-negative saprophyte, to occupy environmental niches in both soil and water and to transition into a potentially pathogenic lifestyle with humans, plants, animals, and other microbes [1–4]. This bacterium has been responsible for a myriad of infections including serious bacteremia and nosocomial pneumonia [5–8], and it has been shown to be the major cause of morbidity and mortality among cystic fibrosis (CF) patients aged 18–24 years [9,10]. *P. aeruginosa* thrives both environmentally and within a human host because of its extensive repertoire of virulence factors (e.g., LasA/LasB and alkaline proteases, phospholipases, lipases, exotoxin A, type III secretion exoenzymes S/T/U/Y, rhamnolipid, alginate biofilm, hydrogen cyanide synthesis, and others) and its capacity to metabolize 70–80 different organic substrates as sole carbon sources, notably different chain-length fatty acids (FA, C_4–C_{18}) [11]. Our previous work suggested that *P. aeruginosa* expresses phospholipases and lipases *in vivo* that degrades phosphatidylcholine (PC; Fig. 1A) as a nutrient source for bacterial replication in the lungs of CF patients [12]. In support of these results, Miller et al. [13] have shown that *P. aeruginosa* utilizes type IV pili to twitch towards phospholipids (i.e. phosphatidylethanolamine and PC) and long-chain FA (LCFAs).

Fatty acid degradation (Fad) in the model microbe, *Escherichia coli*, employs enzymes of the Fad pathway encoded by the *fad*-regulon [14,15]. *E. coli* possesses a single FadD, a 62-kDa fatty acyl-CoA synthetase (FACS or AMP-forming fatty acid:CoA ligase), encoded by the *fadD* gene [16,17]. The FadD protein possesses two highly conserved sequence elements corresponding to a proposed ATP/AMP signature motif [17,18], as well as a signature motif involved in FA substrate binding and specificity [19] (Fig. 1C). Following FadL-mediated importation of exogenous FAs through the outer membrane [20–22] and an unknown transportation process through the inner membrane, FadD appears to employ these two motifs to activate FAs in a two-step process [18,19]. In the first step of activation, an acyl bond between the α-phosphoryl group of an ATP and the carboxyl group of a FA is formed creating a fatty acyl-adenylate intermediate and releasing pyrophosphate. In the second step, the release of AMP occurs concomitantly during thioester bond

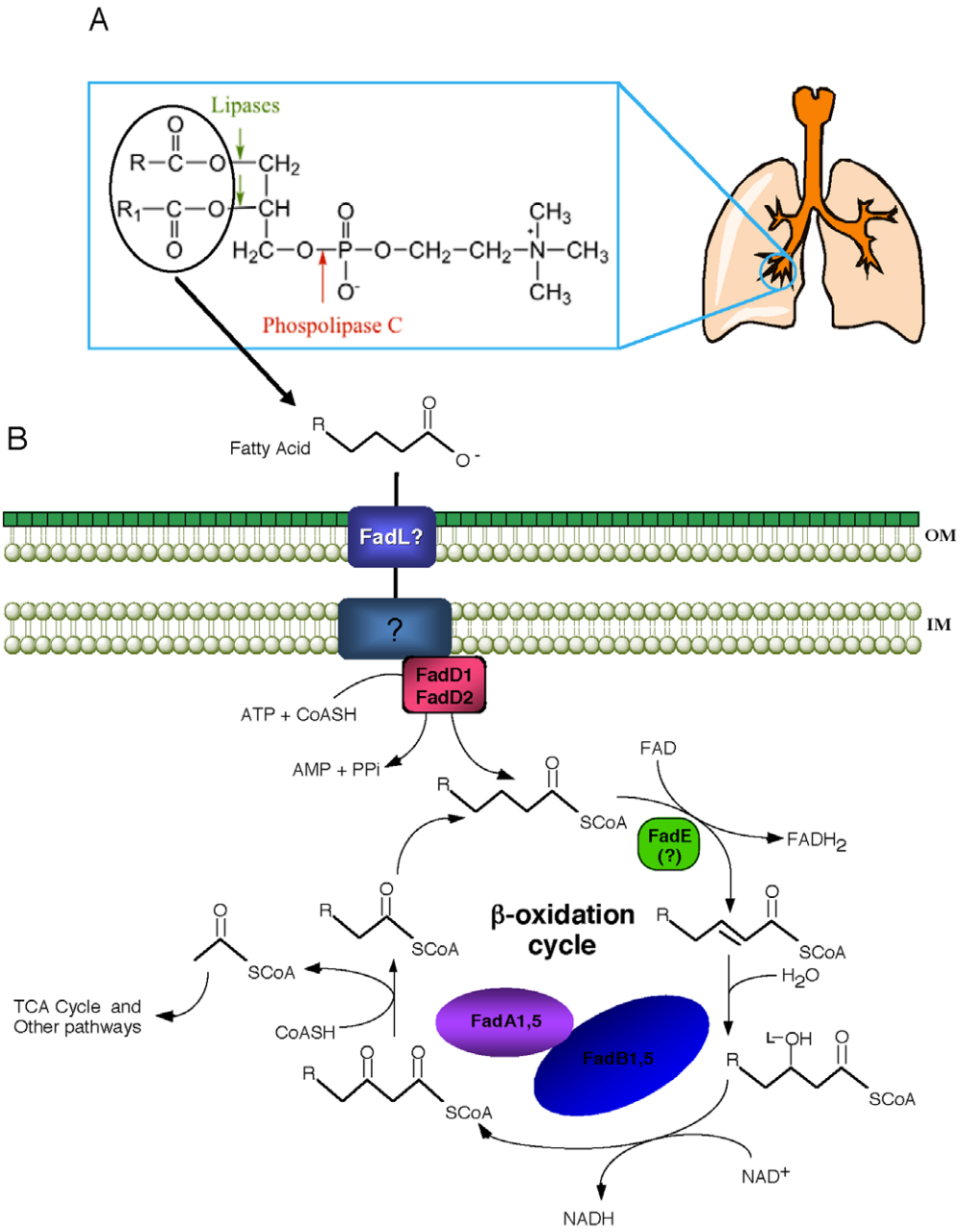

C

ATP/AMP Signature Motif | Fatty Acid Binding Motif

FadD1	214 YTGTGVTAKGA 225	357 GYGMTE 362	432 DGWLKTGDIA I I QEDGYMRIVDRKK 456
E. coli FadD	213 YTGTGVTAKGA 224	356 GYGLTE 361	431 NGWLHTGDIAVMDEEGFLRIVDRKK 455
FadD2	214 YTGTGVTSKGA 225	364 GYGLTE 369	441 EGWLKTGDIAV I DEDGFVRIVDRKK 465

Figure 1. The proposed FA degradation pathway in *P. aeruginosa* based on *E. coli* β-oxidation. (A) Phosphatidylcholine (PC) is the major component of lung surfactant. PC can be cleaved by *P. aeruginosa* phospholipase C and lipases producing free fatty acids that are degraded via the β-oxidation pathway by this bacterium. (B) FAs are transported through the outer membrane aided by an unidentified *P. aeruginosa* FadL [13,67]. In *E. coli*, FA may be transported through the inner membrane via an unknown mechanism coupled to a single peripheral membrane FadD protein [18]. However, *P. aeruginosa* contains at least two FadDs (FadD1 and FadD2). Although there are over a dozen potential FadE homologues in the *P. aeruginosa* genome, the specific enzyme(s) that catalyzes this reaction has not been identified. FadB catalyzes the next two steps followed by cleavage of the 3-keto-acyl-CoA by FadA. Two *fadBA* operons (*fadBA1* and *fadBA5*) have been identified in *P. aeruginosa* [29,30]. (C) Alignment of the *P. aeruginosa* FadD1 and FadD2 ATP/AMP-signature and FA-binding motifs with the FadD motifs of *E. coli* [18,19]. Abbreviation for Fad-proteins:

FadA, 3-ketoacyl-CoA thiolase; FadB, enoyl-CoA hydratase and 3-hydroxyacyl-CoA dehydrogenase; FadD, acyl-CoA synthetase; FadE, acyl-CoA dehydrogenase; FadL, outer membrane FA translocase.
doi:10.1371/journal.pone.0013557.g001

formation between the fatty acyl group and the sulfhydryl group of coenzyme A in the second step [23]. This FadD-catalyzed reaction produces fatty acyl-CoA, a molecule capable of degradation by the β-oxidation cycle or exerting transcriptional control on the *E. coli fad*-regulon by interacting with the FadR regulator to derepress *fad*-genes [24–27]. However, it seems currently that some *fad*-genes in *P. aeruginosa* are induced, not by fatty acyl-CoA, but by LCFAs [24–28]. While the biochemistry and physiology of FadD have been well characterized in *E. coli*, relatively little is known about FadD(s) in *P. aeruginosa*. The *P. aeruginosa* β-oxidation cycle in Fad has only been partially characterized with respect to FadBAs (Fig. 1B) [29,30]. Fad enzymes, including the broad substrate specificity of the FACS, have also been characterized in *Pseudomonas fragi* [31–33]. A study on *Pseudomonas putida* originally isolated and characterized one FACS with a broad substrate range [34]. Additional work further characterized the role of this *P. putida* enzyme and identified a second FACS, naming them FadD1 and FadD2, respectively [35,36]. In this dual FadD system, it was shown that FadD1 played a dominant role in FA metabolism while FadD2 was activated only when FadD1 was inactivated [36]. Comparison of the significantly larger size of the *Pseudomonas* genome relative to that of *E. coli*, such genetic redundancies are not unexpected. However, the importance of the redundancy and functions of these enzymes in Fad are uncertain.

Studies on other species have indicated a link between FACS, nutrient metabolism, and the expression of virulence factors [37–43]. In *Mycobacterium tuberculosis*, 36 *fadD* homologues were identified [39]. A null mutation in the *M. tuberculosis fadD28* gene showed significant replication restriction in mouse lungs, as a result of defects in cell-wall biosynthesis and the production of complex lipids [40]. In addition, *fadD33* in the *M. tuberculosis* H37Ra strain was shown to play a role in supporting growth in mouse livers [42]. Similar to these *Mycobacterium* studies, the use of random transposon mutagenesis has led to the isolation of a *fadD* mutant in *Salmonella enterica* serovar Typhimurium which was shown to reduce the expression of *hilA* (a proposed transcriptional activator of genes in the type III secretion system [38]) and invasion genes three- to five-fold [41]. A *Xanthomonas campestris fadD* homolog *rpfB* mutant has decreased production of protease, endoglucanase, and polygalacturonate lyase due to the inability to generate a diffusible extracellular factor containing a FA moiety [37]. A Tn5 insertion in the *fadD* gene of *Sinorhizobium meliloti* displayed an increased swarming phenotype compared to wild-type, resulting in an observed decrease in alfalfa root nodulation [43]. Many of these studies correlated *fadD* mutations with decreased virulence, but did not confirm or elucidate its enzymatic role in FA metabolism. We have previously shown that *P. aeruginosa* expresses *fadD1* and *fadD2* (PA3299 and PA3300) during lung infections in CF patients, suggesting the importance of Fad in lipid nutrient acquisition *in vivo* [12]. However, the role of *fadD* on virulence and growth of the bacteria *in vivo* has not been characterized.

Here, we characterized the FadD1 and FadD2 (PA3299 and PA3300) and the respective genes with relevance to their biochemistry and the effect on *P. aeruginosa* pathophysiology. The results of genetic analyses and biochemical characterization provided insight into reasons why redundancies in *fadD* are beneficial to this pathogen. Interestingly, *fadD* mutants displayed alterations in swimming and swarming motility and the production of lipases, phospholipases, rhamnolipids, and proteases. The *fadD* mutants with reduced ability to grow on phosphatidylcholine as a sole carbon source showed decreased fitness in a mouse lung infection model. These results provide the initial characterization of *P. aeruginosa fadD* genes and suggest a pathophysiological link between Fad and virulence.

Results

Comparison of two *fadD*s in *P. aeruginosa*

Our previous work showed that two *P. aeruginosa fadD*s (*fadD1* and *fadD2*) were expressed *in vivo* during lung infection in CF patients [12]. FadD1 (PA3299) and FadD2 (PA3300) are 72% similar (54% identical) and 72% similar (53% identical) to the *E. coli* FadD, respectively, while *P. aeruginosa* FadD1 and FadD2 are 76% similar (60% identical) to each other. In addition, *fadD*1 and *fadD*2 are adjacent genes, separated by 234-bp and a possible Rho-independent transcriptional terminator (Fig. 2C). Convincingly, the ATP/AMP signature and FA-binding motifs described for the *E. coli* FadD are highly conserved in both *P. aeruginosa* FadD1 and FadD2 (Fig. 1C). This preliminary analysis suggests that *fadD1* and *fadD2* are both involved in Fad.

To confirm that *fadD1* and *fadD2* are important for Fad, we complemented the *E. coli fadD*$^-$/*fadR*$^-$ strain (E2011) with these *P. aeruginosa* genes. This *E. coli* strain contains a mutation in the *fadR* gene (*fadR*$^-$), the main repressor of the *fad*-regulon in *E. coli*, allowing the constitutive expression of other *fad*-genes of the aerobic Fad-pathway [24–27]. Both *fadD1* and *fadD2* of *P. aeruginosa* were able to functionally complement the *E. coli fadD*$^-$ mutant (Table 1). The *E. coli* K12 wildtype strain was able to metabolize $C_{12:0}$ to $C_{18:1}^{\Delta 9}$ as expected, because long-chain acyl-CoA ($\geq C_{12:0}$) binds efficiently to FadR to induce the *fad*-regulon. Complementation of strain E2011 with the *E. coli fadD* gene (*fadD*$_{EC}$) on plasmid pET15b resulted in growth similar to that of *E. coli* K12 on $C_{12:0}$ to $C_{18:1}^{\Delta 9}$, as well as on $C_{10:0}$ because of the deregulated *fad*-regulon as previously observed [44]. Both *P. aeruginosa fadD*s were able to complement the *E. coli fadD*$^-$/*fadR*$^-$ strain to a similar level as the *fadD*$_{EC}$ complement (Table 1), suggesting that both FadD1 and FadD2 could activate LCFAs and medium-chain FAs (MCFAs). The various complements did not grow on short-chain FAs (SCFAs), suggesting that other *E. coli* Fad-enzymes may not support growth on SCFAs [45] and not necessarily that the *Pseudomonas* FadD proteins are incapable of producing short-chain fatty acyl-CoAs. The E2011 control strains, either with or without the pET15b empty vector, showed no growth on any FA (Table 1).

fadD2 and *fadD1* exist on two transcripts and are induced by FA of different lengths

To gain information on the regulatory regions of the *P. aeruginosa fadD*s, we mapped their transcriptional start sites to assign putative promoter sequences, and then determined transcription levels of each gene on various carbon sources (Figs. 2 and 3). Promoter mapping experiments indicated that each *fadD* had an independent transcriptional start site, suggesting that they were independently transcribed; however, northern blot analyses indicated that *fadD2* and *fadD1* can be co-transcribed on a single larger transcript or as smaller independent transcripts (Fig. 3A and 3B). Both *fadD2* and *fadD1* can exist as two different transcripts, suggesting some level of regulation by the predicted transcriptional terminator or attenuator sequence within the intergenic region (Fig. 2C). From

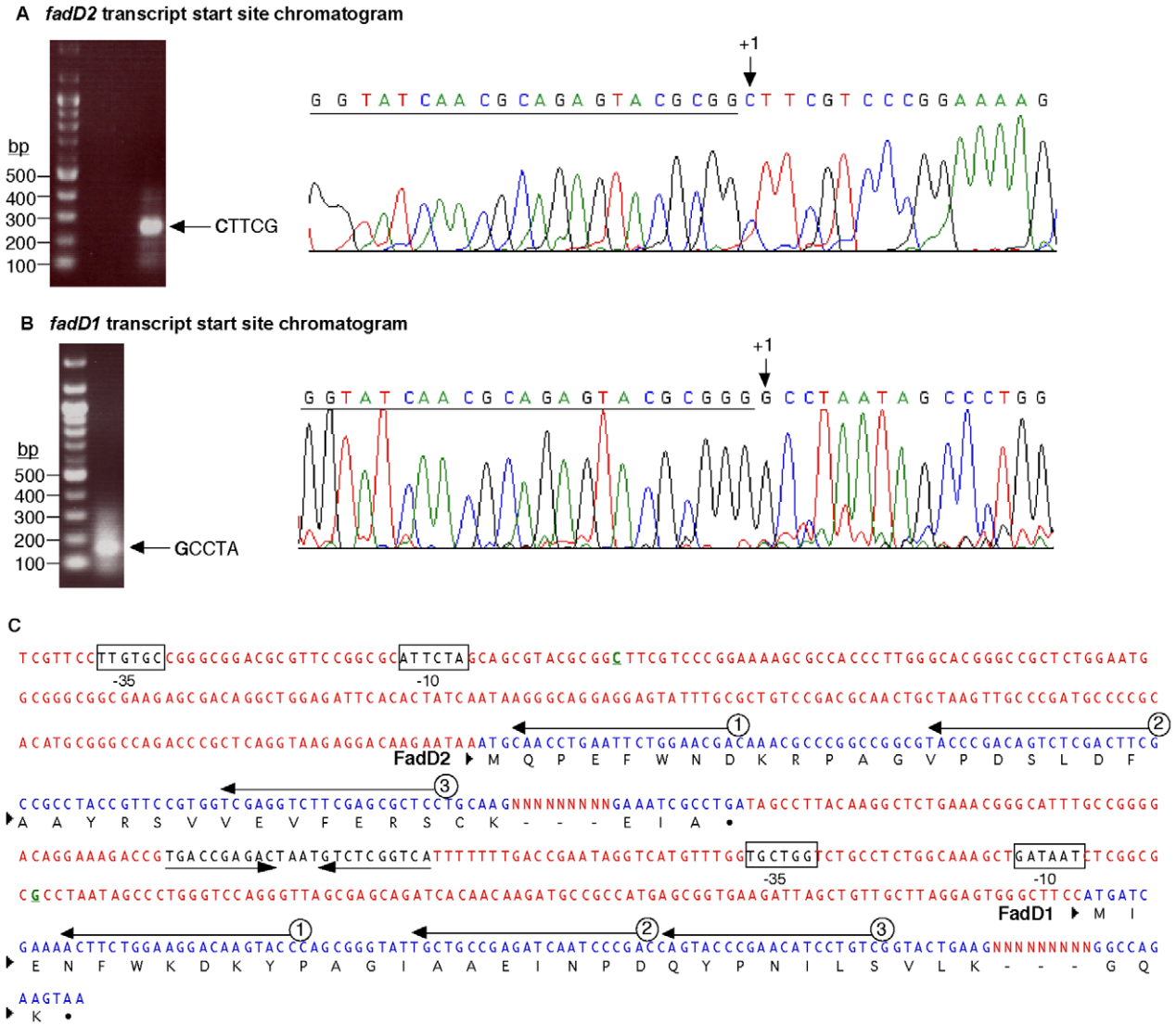

Figure 2. SMART mapping of the transcriptional start sites for *fadD2* and *fadD1*. (A) One SMART product was observed after PCR amplification of the cDNA with SMART and *fadD2* primers (oligonucleotides #798 and #373). Sequencing of the single band with a nested *fadD2* primer (oligonucleotide #374) displayed a reverse-complement sequence chromatogram, showing the *fadD2* transcriptional start site (indicated by +1 at the **C**TTCG sequence) and the underlined SMART primer sequence. (B) Likewise, the downstream *fadD1* transcriptional start site was mapped (at the **G** of the sequence **G**CCTA) by sequencing a single PCR product. (C) *fadD2* and *fadD1* coding sequences and the predicted −10 and −35 promoter regions are indicated (boxed). The intergenic region between *fadD2* and *fadD1* contains a potential transcriptional terminator or attenuator sequence (inverted arrows). For each gene, three black arrows indicate primers 1, 2 and 3 (#372/#375, #373/376, and #374/377) used for mapping *fadD2* and *fadD1*. Dashed lines indicate missing protein sequences and dots indicate stop codons.
doi:10.1371/journal.pone.0013557.g002

Table 1. Complementation of the *E. coli fadD* mutant with *P. aeruginosa fadD* homologues.

		Growth on different FAs and casamino acids[a]								
Strain	**Plasmid**	$C_{4:0}$	$C_{6:0}$	$C_{8:0}$	$C_{10:0}$	$C_{12:0}$	$C_{14:0}$	$C_{16:0}$	$C_{18:1}^{\Delta 9}$	**CAA**
K12 (wildtype)	none	-	-	-	-	+4	+5	+4	+5	+6
E2011 (*fadD*⁻ *fadR*⁻)	none	-	-	-	-	-	-	-	-	+6
E2011 (*fadD*⁻ *fadR*⁻)	pET15b	-	-	-	-	-	-	-	-	+6
E2011 (*fadD*⁻ *fadR*⁻)	pET15b-$fadD_{Ec}$	-	-	-	+2	+3	+3	+4	+4	+6
E2011 (*fadD*⁻ *fadR*⁻)	pET15b-*fadD1*	-	-	-	+2	+4	+4	+4	+4	+6
E2011 (*fadD*⁻ *fadR*⁻)	pET15b-*fadD2*	-	-	318	+2	+4	+3	+4	+4	+6

[a](-) denotes no growth on a patch; (+) denotes growth: (+1) is very little growth and (+6) is heavy growth after 3 days.
doi:10.1371/journal.pone.0013557.t001

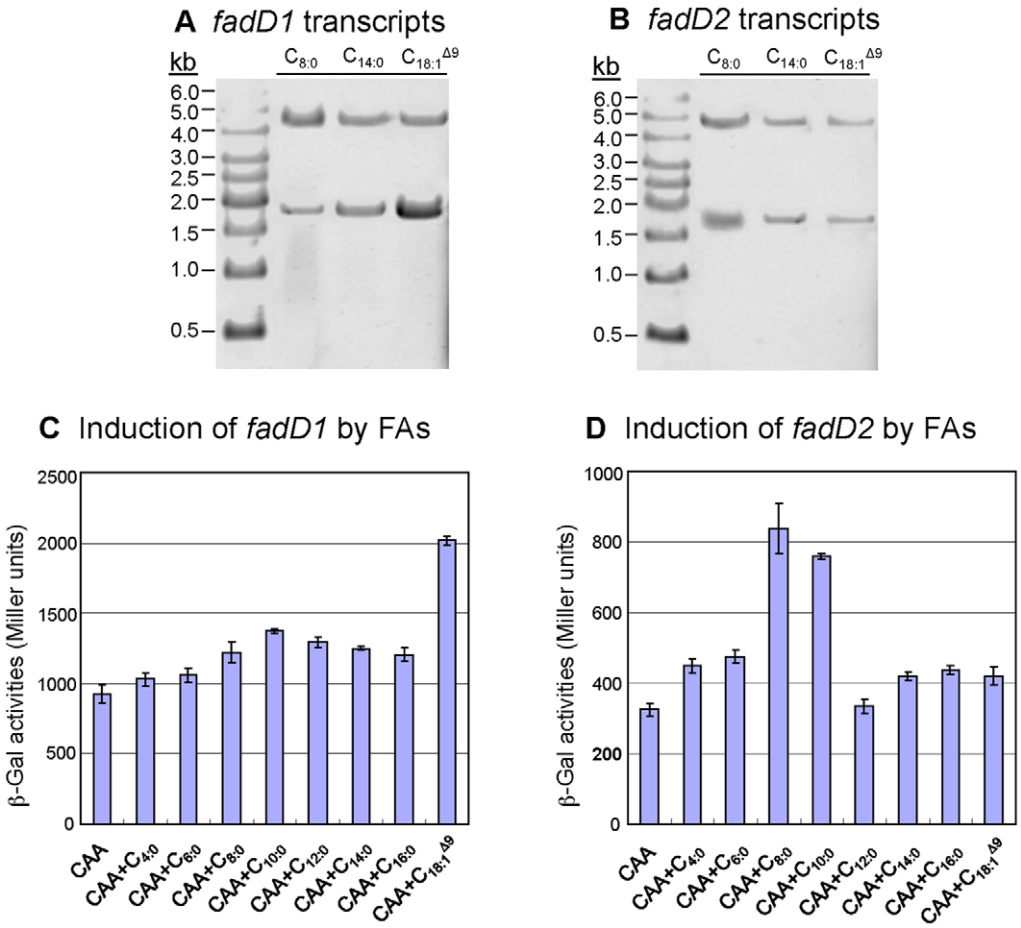

Figure 3. Transcriptional profile of *fadD1* and *fadD2* in various FAs. For a short- ($C_{8:0}$), medium- ($C_{10:0}$), and long-chain FA ($C_{18:1}^{\Delta 9}$), northern blot analysis indicated two possible transcripts for both *fadD* genes when probed with either *fadD1* (A) or *fadD2* (B). Gene-fusion studies of strains P518 (P_{fadD1}-*lacZ*) and P520 (P_{fadD2}-*lacZ*), grown to mid-log phase, showed differential expression of *fadD1* and *fadD2* in the presence of different FAs (C and D). (C) *fadD1* was up-regulated in the presence of the unsaturated LCFA ($C_{18:1}^{\Delta 9}$), while *fadD2* expression was significantly increased in the presence of shorter chain FAs ($C_{8:0}$, $C_{10:0}$) (D). For (C) and (D), all cultures had identical growth-rates and overall cell densities (data not shown).
doi:10.1371/journal.pone.0013557.g003

Figure 3, we hypothesize that the promoter upstream of *fadD2* drives the expression of both genes, and the intergenic terminator attenuates the larger *fadD1* transcript. The *fadD1* promoter immediately downstream of this regulatory element was induced by LCFA (e.g. $C_{18:1}^{\Delta 9}$), and initiated the expression of the smaller *fadD1* transcript (Fig. 2C, 3A and 3B). Presumably, when there was no termination of transcription from the *fadD2* promoter, *fadD2* and *fadD1* were transcribed together on the larger transcript of the same size observed on both blots (Fig. 3A and 3B). Based on the determination that these *fadD* genes could be independently transcribed or co-transcribed, it was necessary to determine which chain-length FA induced *fadD1* and *fadD2*. The observed levels of induction showed that *fadD1* was mainly induced by LCFA, particularly $C_{18:1}^{\Delta 9}$, while *fadD2* was specifically induced by short- to medium-chain FA (Fig. 3C and 3D). Both *fadD* genes showed some level of expression under all conditions tested, indicating low levels of constitutive expression.

fadD mutants showed reduced ability to grow on various FAs

To further confirm the involvement of each *fadD* in Fad, we generated single and double mutants for growth analysis on various FAs as sole carbon sources (Fig. 4). As previously observed for *fadBA* mutants [30], growth defects were exemplified by slower growth and lower overall final cell densities in various FA media, presumably, due to reduced rates of Fad and growth inhibiting intermediates. Both *fadD1* and *fadD2* single mutants had various levels of defects when grown on all FAs (Fig. 4). However, the *fadD1* mutant displayed a greater growth defect on all FAs than the single *fadD2* mutant, with the exception of $C_{8:0}$ and $C_{10:0}$ where FadD2 seems to be equally as important as FadD1 (Fig. 4D and 4E). The Δ*fadD2D1* mutant showed more dramatic growth defects on all FAs than the individual single mutants, indicating that both proteins were involved in the metabolism of all chain-length FAs tested. The lack of a complete defect in Fad of this double mutant suggests that other *fadDs* exist in *P. aeruginosa*. The complemented single and double mutants fully restored growth on all FAs (Fig. 4), while empty vector miniCTX2 controls did not complement growth on the FAs (data not shown). No apparent defects were observed for any mutant grown with casamino acids (CAA) as a sole carbon source (Fig. 4A). Based on the physiological data (Fig. 3 and 4), *fadD1* was found to be important for the metabolism of all FAs, particularly the unsaturated LCFA oleate, while *fadD2* was also important in Fad but more so for MCFA ($C_{8:0}$ and $C_{10:0}$) degradation.

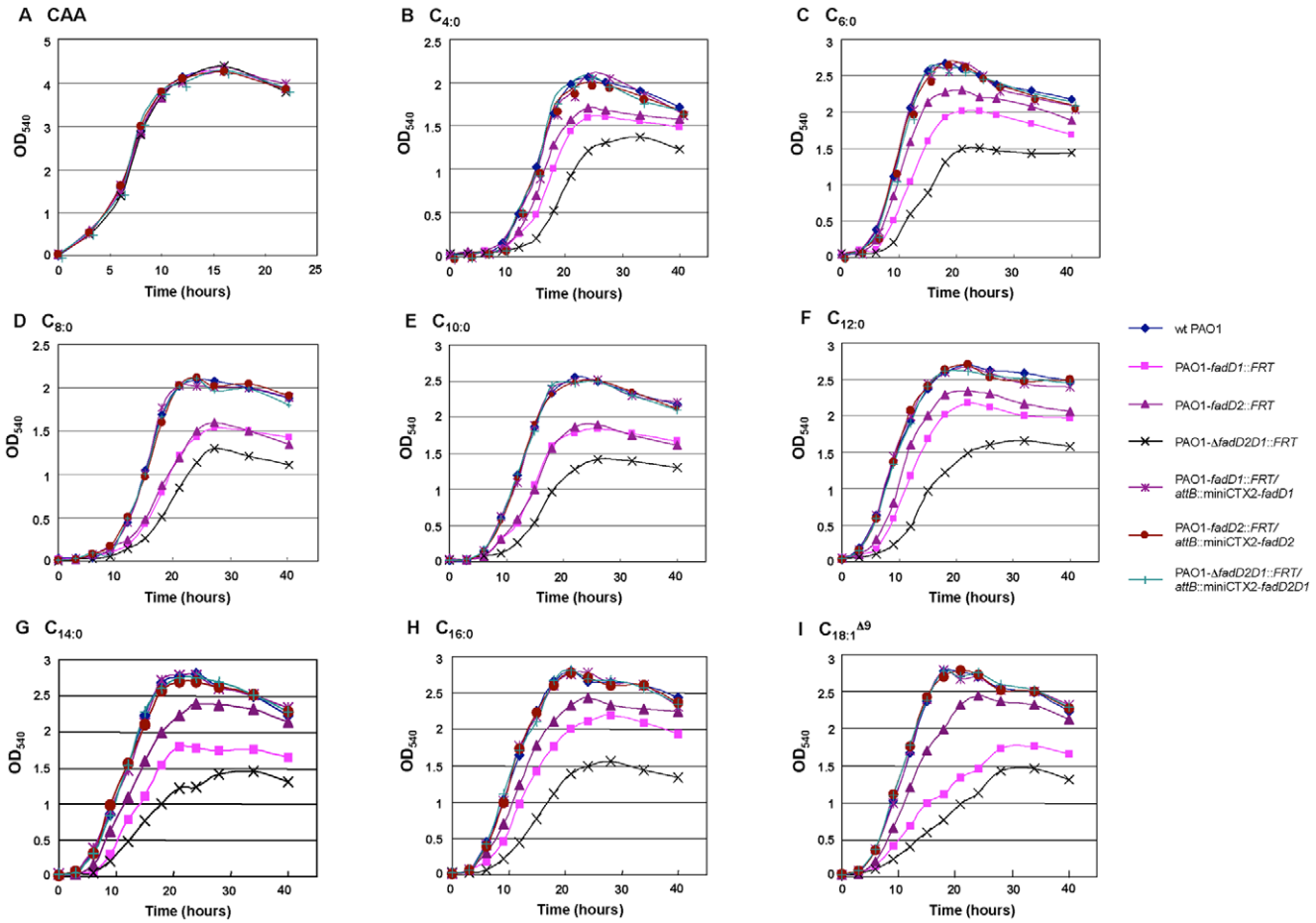

Figure 4. Growth analysis of *fadD* mutants using various FAs as sole carbon sources. Although *fadD* mutants showed various defects when grown with FAs of different chain-lengths (see top of graphs in B-I), no growth defects were observed for any of the mutants when grown with casamino acids (CAA) as a control (A). All three *P. aeruginosa* mutants were fully complemented by the respective missing gene(s) and grew as well as the wildtype PAO1 on all carbon sources. Not shown are the three control mutant strains (PAO1-*fadD1*::*FRT*/*attB*::miniCTX2, PAO1-*fadD2*::*FRT*/*attB*::miniCTX2, and PAO1-Δ*fadD2D1*::*FRT*/*attB*::miniCTX2) having the empty miniCTX2 integrated into their chromosomes, where all had similar growth characteristics to the non-complemented mutants.
doi:10.1371/journal.pone.0013557.g004

Kinetic properties of purified FadDs support differential FA chain-length preferences

To determine the substrate specificities of each FadD and further clarify the reason why *P. aeruginosa* possesses multiple *fadD* homologues, both FadD proteins were purified to near homogeneity from an *E. coli fadD*$^-$ strain to ensure that all acyl-CoA synthetase activities were derived only from purified recombinant FadD1 or FadD2 (Fig. 5A). FadD1 of *P. aeruginosa* coupled CoASH to LCFA better than to SCFA or MCFA, as exemplified by larger V_{max} and lower K_m values for $C_{18:1}{}^{\Delta 9}$ and $C_{16:0}$ than FAs of other chain-lengths (Fig. 5B and Table 2). The reverse was true for FadD2, where this enzyme had higher V_{max} and lower K_m for SCFA and MCFA than LCFA (Fig. 5C and Table 2). The catalytic efficiency (k_{cat}/K_m) of FadD1 was significantly higher for LCFA ($C_{18:1}{}^{\Delta 9}$, $C_{16:0}$, and $C_{14:0}$) than MCFA ($C_{12:0}$ to $C_{8:0}$) or SCFA ($C_{6:0}$ and $C_{4:0}$), while the catalytic efficiency of FadD2 was higher for MCFA and SCFA than LCFA (Table 2). The kinetic parameters for ATP and catalytic efficiency of both enzymes were comparable when ATP was limited in the reaction, with FadD1 being a slightly better catalytic enzyme for ATP than FadD2 (Table 2). Clearly, multiple FadDs in *P. aeruginosa*, with broad substrate conversion capabilities and overlapping chain-length preferences, afford this bacterium the ability to optimally metabolize FAs of various chain-lengths.

fadD mutants influence virulence behavior of *P. aeruginosa*

Based on work in other bacteria that showed an interconnection between *fadD* genes and expression of virulence factors [37–43], we sought to determine if a similar connection existed in *P. aeruginosa*. Increased swarming motility of *S. meliloti*, leading to altered virulence, was previously attributed to hyperflagellation observed by transmission electron microscopy (TEM) [43]. While no apparent differences in structure or numbers of flagella were observed for the *fadD* mutants compared to wildtype PAO1 using TEM in the current study (data not shown), we showed that *fadD* mutations could still significantly influence swarming and swimming motility in *P. aeruginosa* (Fig. 6). The *fadD2* mutant was severely defective in swimming and swarming motility relative to the wildtype PAO1 strain (Fig. 6). Although the *fadD1* single mutant showed no apparent difference in swimming motility, it displayed increased swarming migration compared to PAO1. Swarming was most pronounced in the Δ*fadD2D1* mutant. In the Δ*fadD2D1* mutant, it was very interesting to observe that the *fadD1*

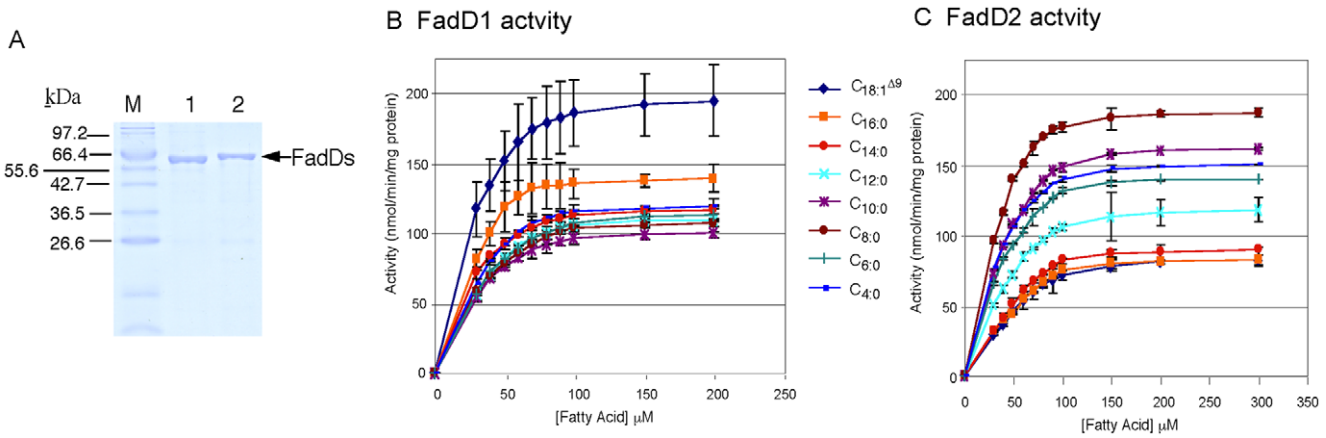

Figure 5. Purification and biochemical characterization of the two *P. aeruginosa* FadDs. (A) FadD1 (lane 1; MW = 61,655) and FadD2 (lane 2; MW = 61,737) were purified to near homogeneity from an *E. coli fadD*$^-$ strain to prevent potential contamination of *E. coli* FadD. FadD1 activities (B) were higher for LCFAs ($C_{18:1}^{\Delta 9}$>$C_{16:0}$), while FadD2 (C) had higher activities for shorter chain FAs ($C_{8:0}$>$C_{10:0}$>$C_{4:0}$>$C_{6:0}$).
doi:10.1371/journal.pone.0013557.g005

mutation suppressed the swarming and swimming defects of the *fadD2* mutation. Each complemented strain showed that swimming and swarming motility could be restored to wildtype levels, indicating no unforeseen secondary or polar mutations affected these behaviors.

The production of other virulence factors was also monitored for the *fadD* mutants. Interestingly, the *fadD2* mutant showed significantly decreased production of total hemolysins, proteases, lipases, and rhamnolipids (Fig. 7). No other mutant or complement showed noticeable decreases in the production of these virulence factors compared to the wildtype PAO1 strain. The supression of the *fadD2* mutation by the *fadD1* mutation, in the Δ*fadD2D1* mutant, reversed the reduction in virulence factor expression seen in the single *fadD1* mutation alone (Fig. 7). Similar suppression was observed in swimming and swarming motilities (Fig. 6). The altered virulence behaviors and suppression were not due to differences in growth-rates or overall final cell densities, as all seven strains (i.e. wildtype, mutants, and complements) grew identically in LB media prior to testing for these virulence traits (Fig. 7E). Mechanisms governing these differences remain to be elucidated.

Compromised ability of *fadD* mutants to degrade FA and PC leads to reduced *P. aeruginosa* fitness in mice

Since *fadD1* and *fadD2* are expressed *in vivo* during CF lung infections [12] and are potentially important for PC degradation (Fig. 1A), it was necessary to determine whether these mutants are deficient in growth on PC. Growth analysis on PC showed only slight decreases in the maximum cell density of the individual single *fadD* mutants, while the *fadD2* mutant exhibited a delayed log phase (Fig. 8A). The Δ*fadD2D1* mutant exhibited the greatest growth defect, while the single and double *fadD* complements restored growth to wildtype levels. Since PC is the major component (70%) of the essential lung surfactant [46] and is a potential nutrient source *in vivo* [12], it was important to assess whether the growth defects of these mutants on PC would result in decreased fitness *in vivo*.

Table 2. Kinetic properties of FadD1 and FadD2 with various substrates.

	FadD1 Kinetic Parameter[a]				FadD2 Kinetic Parameter[a]			
Substrate varied	V_{max}[b]	k_{cat}[c]	K_m[d]	k_{cat}/K_m[e]	V_{max}[b]	k_{cat}[c]	K_m[d]	k_{cat}/K_m[e]
ATP	213	0.219	10.6	20.7	182	0.187	10.9	17.2
$C_{4:0}$	137	0.141	27.4	5.1	167	0.172	33.3	5.2
$C_{6:0}$	133	0.137	26.7	5.1	159	0.164	31.8	5.2
$C_{8:0}$	125	0.128	25.0	5.1	204	0.210	20.4	10.3
$C_{10:0}$	116	0.119	23.3	5.1	182	0.187	36.4	5.1
$C_{12:0}$	130	0.134	26.0	5.1	137	0.141	41.1	3.4
$C_{14:0}$	130	0.134	13.0	10.3	109	0.112	43.5	2.6
$C_{16:0}$	154	0.158	15.4	10.3	99	0.102	49.5	2.1
$C_{18:1}^{\Delta 9}$	217	0.223	21.7	10.3	101	0.104	50.5	2.1

[a]Kinetic constants (V_{max} and K_m) determined using Hanes-Woolf plot.
[b]nmole of acyl-CoA formed/min/mg of protein.
[c]s^{-1}; determined using MW of FadD1 (61,655) and FadD2 (61,373).
[d]mM of ATP or FA.
[e]mM^{-1} s^{-1}; represents enzyme catalytic efficiency.
doi:10.1371/journal.pone.0013557.t002

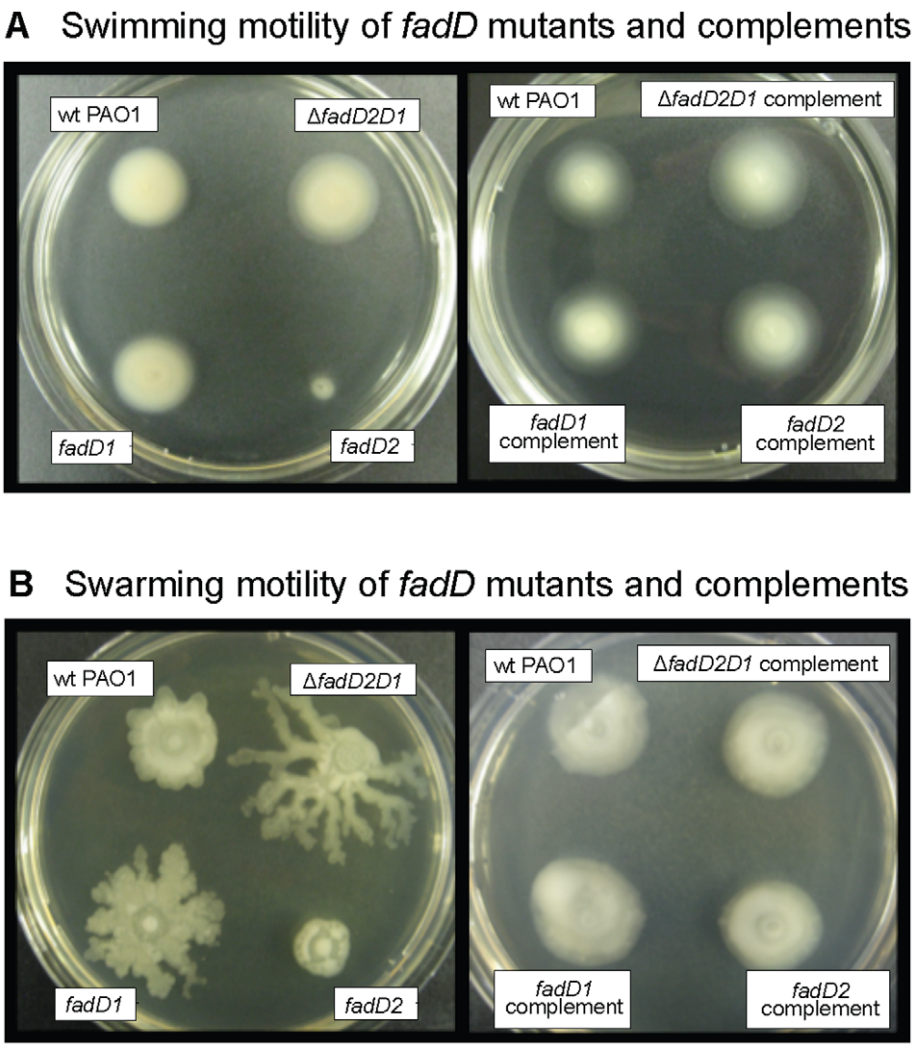

Figure 6. Altered swimming and swarming motility of *P. aeruginosa fadD* mutants. (A) Swimming motility of *fadD* mutants and their complements. (B) Swarming migration of *fadD* mutants and their complements. These figures are representative of multiple experiments. Strain designation is the same as shown in Table 3: wildtype PAO1, P007; *fadD1*⁻, P175; *fadD2*⁻, P547; Δ*fadD2D1*, P177; *fadD1*⁻ complement, P541; *fadD2*⁻ complement, P549; and Δ*fadD2D1* complement, P543.
doi:10.1371/journal.pone.0013557.g006

In vitro competition between the various *fadD* mutants and their complements were first tested to determine if the defect reduced their ability to utilize various sole carbon sources. Each mutant and complement pair was inoculated into seven growth media with different sole carbon sources including LB, CAA, glucose, PC, $C_{18:1}^{\Delta 9}$, choline, and glycerol, and bacterial CFU were determined after 24–48 h growth (Fig. 8B). As, expected, all three single or double *fadD* mutants were less competitive than their corresponding complements but only in media containing PC or $C_{18:1}^{\Delta 9}$ as sole carbon sources. Next, to evaluate the fitness of the *fadD* mutants within the lung environment, *in vivo* competition between the mutants and their complements was analyzed. Following intratrachael inoculation of equal ratios of each mutant and its complement pair into BALB/c mice (6×10^6 CFU/animal), bacterial CFU recovered from the lungs were determined 24 h and 48 h postinfection and the competitive index (CI) was calculated (Fig. 8C and 8D). The CI is defined as the ratio of mutant CFU relative to CFU of the respective complement [47]. In all of these competition experiments, with the exception of the *fadD2* mutant after 48 h, the average total CFU/mouse recovered was greater than the initial inoculum showing that these strains maintained the ability to replicate within the mouse lung. Although the *fadD1* single mutant showed decreased competitive fitness within the lung compared to the complement, the CI of the *fadD1* mutant remained relatively unchanged between the two time points analyzed. At 24 h postinfection, all of the mutants exhibited decreased competition levels relative to their respective complements and the *fadD2* and Δ*fadD2D1* mutant strains showed greater reduced fitness than the *fadD1* mutant. By allowing the infections to persist for 48 h, the reduced CI of the *fadD2* mutant showed a significantly higher defect in competitive fitness. By 48 h, the CI of the Δ*fadD2D1* mutant was half of that observed at 24 h. Clearly, the Δ*fadD2D1* mutant with significantly reduced ability to degrade PC (Fig. 8A), while showing no altered virulence factor secretion (Fig. 7), had its competitive fitness reduced by three-fold. This strongly suggests that the ability to degrade PC as a nutrient source allows *P. aeruginosa* to replicate within the lung environment.

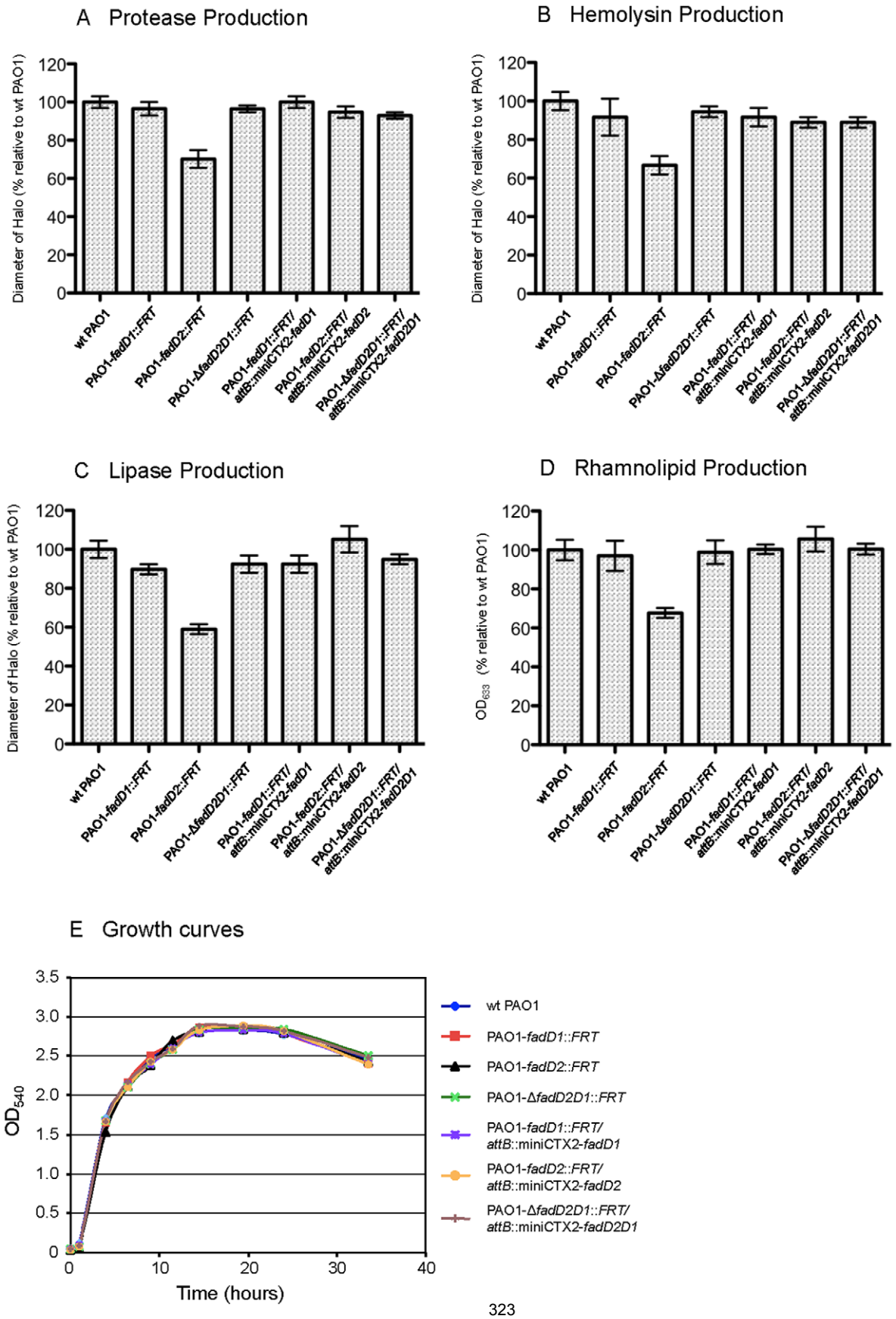
A Protease Production
Diameter of Halo (% relative to wt PAO1)
B Hemolysin Production
Diameter of Halo (% relative to wt PAO1)
C Lipase Production
Diameter of Halo (% relative to wt PAO1)
D Rhamnolipid Production
OD633 (% relative to wt PAO1)
wt PAO1
PAO1-fadD1::FRT
PAO1-fadD2::FRT
PAO1-ΔfadD2D1::FRT
PAO1-fadD1::FRT/ attB::miniCTX2-fadD1
PAO1-fadD2::FRT/ attB::miniCTX2-fadD2
PAO1-ΔfadD2D1::FRT/ attB::miniCTX2-fadD2D1
E Growth curves
OD540
Time (hours)
wt PAO1
PAO1-fadD1::FRT
PAO1-fadD2::FRT
PAO1-ΔfadD2D1::FRT
PAO1-fadD1::FRT/ attB::miniCTX2-fadD1
PAO1-fadD2::FRT/ attB::miniCTX2-fadD2
PAO1-ΔfadD2D1::FRT/ attB::miniCTX2-fadD2D1

Figure 7. Analysis of protease, hemolysin, lipase, and rhamnolipid production by *P. aeruginosa fadD* mutants. The *fadD2* mutant displayed significantly decreased production of proteases (A), hemolysins (B), lipases (C), and rhamnolipids (D), while no growth defects in LB were observed (E). These assays were conducted in triplicate and are expressed as a percentage of the mean value of the wildtype PAO1 ± s.e.m.
doi:10.1371/journal.pone.0013557.g007

Discussion

This study focused on characterizing two *P. aeruginosa* acyl-CoA synthetases (FadD1 and FadD2), which are expressed during lung infection in CF patients suggesting their importance in lipid degradation for bacterial replication [12]. The transcriptional profile and substrate preferences of FadD1 and FadD2 were determined to initially shed light onto why *P. aeruginosa* has this genetic redundancy. The *fadD1* and *fadD2* of *P. aeruginosa* were differentially regulated in response to the type of available FA (Fig. 3), suggesting that each FadD has a different FA substrate preference. While both *fadD1* and *fadD2* were controlled by their common and independent promoters, the expression of *fadD1* downstream could be partially attenuated by some FAs due to a putative intergenic Rho-independent transcriptional-terminator (Fig. 2). Based on the growth defects, both *fadD* genes are individually important for the degradation of all chain-length FAs tested. These results are further supported by the observation that the Δ*fadD2D1* mutant had the greatest growth defect on all chain-length FAs (Fig. 4). These growth defects may be due to a bottleneck in the conversion of exogenous FA to acyl-CoA created by the inactivation of two genes that facilitate this process. The complementation study in *E. coli* was initially inconclusive with respect to metabolism of SCFA and some MCFA substrates by *P. aeruginosa* FadDs (Table 1), as other *E. coli* Fad-proteins (e.g. FadE, FadA and FadB) do not allow the metabolism of shorter-chain FAs [45]. However, the kinetic parameters, especially the catalytic efficiencies (Table 2), provided more precise biochemical evidence for the differences in substrate preferences. By comparing the kinetic measurements of these enzymes, it appears that FadD1 preferred LCFA for degradation, while FadD2 was more suited to the degradation of SCFAs and MCFAs (Fig. 5 and Table 2). Together, the enzyme kinetics, gene-fusion, and growth analyses data all support the importance of FadD2 for degradation of SCFA and MCFA and FadD1 is more suited for LCFA degradation (Fig. 3, 4 and 5). Therefore, we can conclude that these proteins have different substrate preferences and are not functionally equivalent.

We showed here that mutations in *fadD* genes, important for FA β-oxidation in *P. aeruginosa*, also influenced two modes of motility and virulence factor expression. Our *fadD2* mutant had reduced swimming and swarming motilities and decreased virulence factor expression (proteases, phospholipases, rhamnolipids, and lipases), while the *fadD1* mutant and the Δ*fadD2D1* double mutant only showed an increased swarming phenotype. In the double mutant background, the presence of the *fadD1* mutation suppresses the phenotype of the *fadD2* mutation (Figs. 6 and 7). It will be interesting to determine the exact cause of the phenotypic suppression in future investigations. At this point, we speculate that the reduced swarming phenotype of the *fadD2* mutant is due to decreased production of rhamnolipids (Fig. 6 and 7), as rhamnolipids were previously shown to be necessary for *P. aeruginosa* swarming motility [48]. These phenotypic differences in virulence factor expression further support the observation that FadD1 and FadD2 are not functionally equivalent. Although we did not exhaust the large list of virulence determinants, nor were able to show the exact method by which FadD2 influences their expression, this characterization of several virulence factors links Fad and virulence factor expression in *P. aeruginosa*.

Additionally, the expression of genes *in vivo* that encode proteins with β-oxidative activity, along with several other PC degradation genes, strongly support the hypothesis that lipids within the lung may be important nutrient sources for *P. aeruginosa* [12] and serve as signals to control virulence factor expression [13]. Phospholipase- and lipase-derived components of PC (LCFA, glycerol, and phosphorylcholine) could individually serve as sole carbon sources (Fig. 1A) and provide nitrogen and phosphorous contributing to virulence [49,50]. Of these three PC components, the two LCFAs from each PC molecule yield the most carbon and energy. Therefore, the determination that both FadD1 and FadD2 were important for LCFA degradation was pivotal as PC, the major component of lung surfactant, is primarily composed of LCFA ($C_{16:0}$, 50–60%; $C_{14:0}$, $C_{16:1}$, $C_{18:1}$, and $C_{18:2}$ each at 10–20%) [46]. To that end, we analyzed the growth of these mutants on PC as a sole carbon source. The delayed log-phase of the *fadD2* mutant is likely due to the decreased expression of lipase and phospholipase, thereby reducing the cleavage rate of exogenous PC into its usable components and thus slowing growth. Since it was shown that the Δ*fadD1D2* mutant had no apparent deficiencies in lipase or phospholipase expression, yet exhibited the greatest decrease in growth on all FAs tested, we believe that its reduced growth on PC is attributed to a reduced ability to degrade FAs, as this double mutant degrades phosphorylcholine and glycerol as well as the complement. Since the *fadD* mutants fully retained the ability to degrade choline and glycerol and only had reduced levels of FA degradation, it was not surprising that the Δ*fadD1D2* double mutant could still degrade PC.

Because PC is a major lung surfactant common in all mammals, including mice [51], a mouse lung infection model [52] was utilized to analyze the competitive growth *in vivo* between the *P. aeruginosa fadD* mutants and their complements. Replication of the *fadD2* mutant was observed after 24 h, while all other strains showed an increase after 48 h, indicating all strains were able to replicate *in vivo*. This could be explained by the fact that our Δ*fadD1D2* double mutant still had significant ability to degrade PC and its components, and that *P. aeruginosa* expresses genes in the lung for both amino acid and PC degradation [12] and possibly DNA [53]. After 24 h and 48 h, all mutants showed lower *in vivo* fitness than their complements, which means that lipids are significant nutrient sources in the mouse lung. The CIs of the *fadD2* mutant were consistently lower than those of the *fadD1* mutant after both 24 h and 48 h, attributed to the *fadD2* mutant's decreased production of virulence factors. Although the Δ*fadD2D1* mutant only showed partial defect in PC degradation and no effect in virulence factor expression or the ability to grow with amino acids, this partial defect in PC degradation translated into significantly reduced *in vivo* lung fitness. This is further supported by the *in vitro* competition results where all single and double *fadD* mutants exhibited competition defect only on PC and $C_{18:1}^{\Delta 9}$. Therefore, the significantly lowered CI after 48 h for the double Δ*fadD2D1* mutant can only be due to a reduced ability to degrade PC as a nutrient source for replication in the mouse lung.

In this study, a pathophysiological link between the acquisition of lipid nutrients and virulence *in vivo* was established by i) characterizing these two *P. aeruginosa fadD* genes expressed during lung infection in CF patients, ii) determining that there may be some connection between *fad*-genes and the expression of certain virulence traits, and iii) showing that mutations in these genes

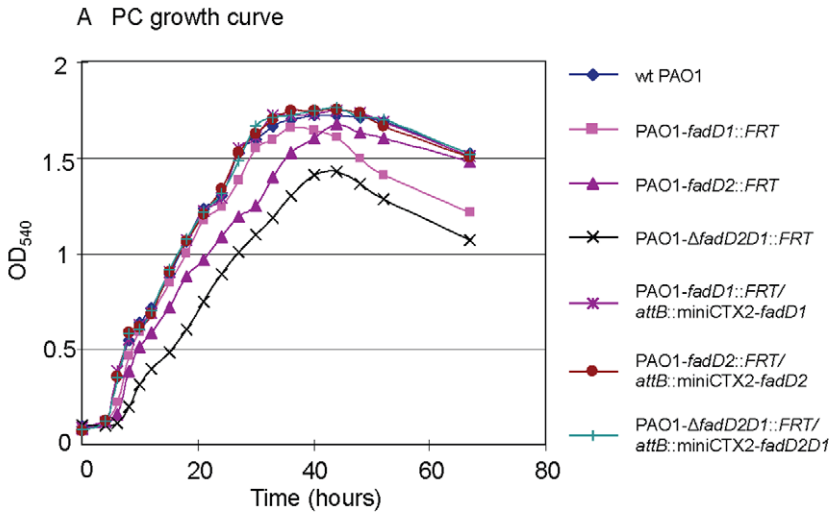
A PC growth curve
OD540
Time (hours)
wt PAO1
PAO1-fadD1::FRT
PAO1-fadD2::FRT
PAO1-ΔfadD2D1::FRT
PAO1-fadD1::FRT/ attB::miniCTX2-fadD1
PAO1-fadD2::FRT/ attB::miniCTX2-fadD2
PAO1-ΔfadD2D1::FRT/ attB::miniCTX2-fadD2D1

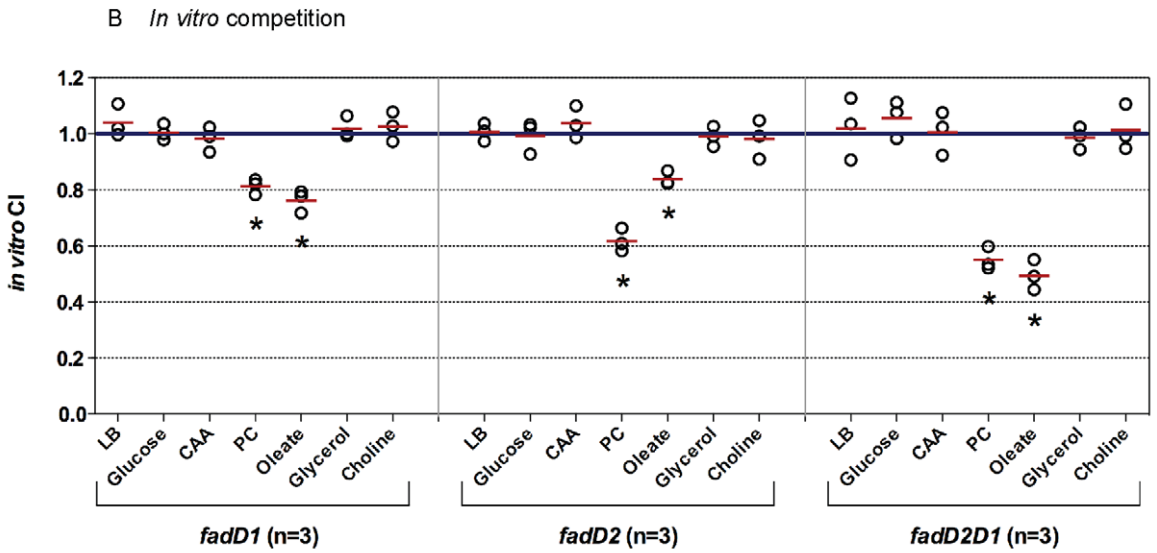
B In vitro competition
in vitro CI
LB
Glucose
CAA
PC
Oleate
Glycerol
Choline
fadD1 (n=3)
fadD2 (n=3)
fadD2D1 (n=3)

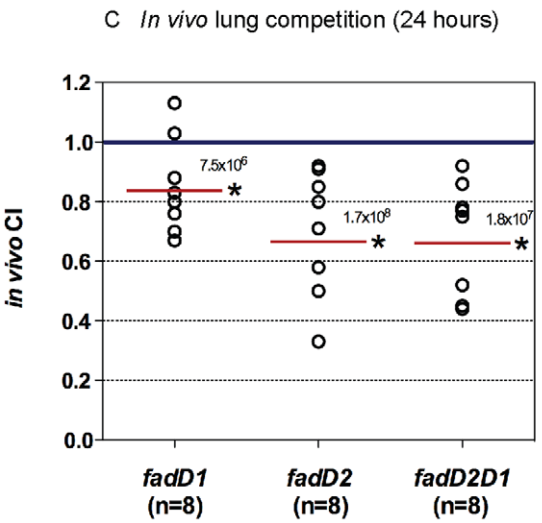
C In vivo lung competition (24 hours)
in vivo CI
7.5x10^6
1.7x10^8
1.8x10^7
fadD1 (n=8)
fadD2 (n=8)
fadD2D1 (n=8)

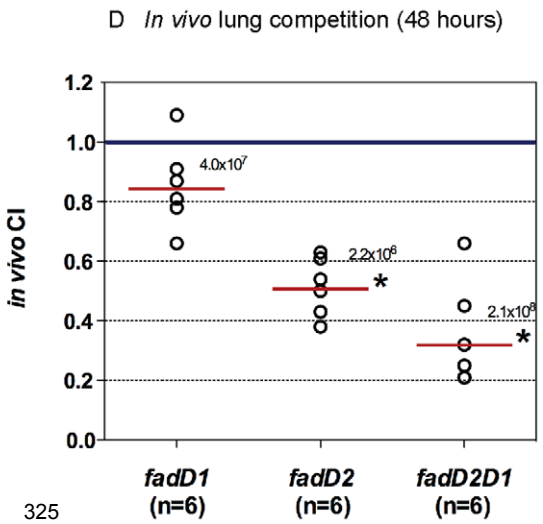
D In vivo lung competition (48 hours)
in vivo CI
4.0x10^7
2.2x10^6
2.1x10^8
fadD1 (n=6)
fadD2 (n=6)
fadD2D1 (n=6)

Figure 8. Growth analysis on phosphatidylcholine and competition studies. (A) The Δ*fadD2D1* mutant exhibited a growth defect when grown on PC as a sole carbon source, while the *fadD2* mutant had a delayed log phase compared to the wildtype PAO1 strain. The growth defects were fully recovered in complemented strains, as they had identical growth rates compared to the wildtype PAO1 strain. (B) *In vitro* competition studies of the various *fadD* mutants and their complemented strains in different growth media (*n* = the number of independent *in vitro* competition experiments performed with each carbon source). *In vivo* lung competition of the various *fadD* mutants and their complemented strains after 24 h (C) and 48 h (D). *n* equals the number of mice in each group that were inoculated with a total of 6×10^6 CFU/mouse. The solid red line indicates the geometric mean of the competitive indices (CI) in each competition group. CI<1 indicates the *fadD* mutant was less competitive than its complemented strain in various growth media (B) or within the lungs (C and D) (*, $P<0.05$ based on one sample *t* test) [47]. Numbers above the red line represent the average total recovered CFU/mouse for each competition group.
doi:10.1371/journal.pone.0013557.g008

correspond to a deficiency in the ability to replicate in mouse lungs. These data support results from a previous *in vivo* gene expression study showing that *P. aeruginosa* expresses *glp*-, *bet*-, and especially, *fad*-genes to degrade PC as one of the nutrient sources in the lungs [12]. We predict that *P. aeruginosa* mutants, completely blocked in PC utilization, will have significantly lower *in vivo* fitness, further supporting PC as a significant nutrient source for this important pathogen in mammalian lungs.

Materials and Methods

Ethics statement

All animal experiments were conducted in compliance with the NIH (National Institutes of Health) Guide for the Care and Use of Laboratory Animals and were approved by the University of Hawaii Institutional Animal Care and Use Committee (protocol No. 06-023-04).

Bacterial strains and growth media

Strains and plasmids used in this study are shown in Tables 3 and 4. *E. coli* EPMax10B was routinely used as a strain for cloning and was cultured in Luria-Bertani (LB) medium (Difco). *P. aeruginosa* strain PAO1 and derivatives were cultured on Pseudomonas Isolation Agar or Broth (PIA or PIB; Difco) or LB medium. PAO1-*fadD1*::*FRT*, PAO1-*fadD2*::*FRT*, PAO1-Δ*fadD2D1*::*FRT*, and their complements were cultured in 1x M9 minimal medium +1% Brij-58 (Sigma) +1% casamino acids (CAA) or 0.2% (w/v) of the individual FA, $C_{4:0}$ to $C_{16:0}$, or $C_{18:1}{}^{\Delta9}$ (Sigma; Fig. 4), and 1x M9 minimal medium +1% Brij-58 +0.2% phosphatidylcholine (PC, Sigma; Fig. 8A) for growth analyses. The fusion strains PAO1-*fadD1*::*FRT-lacZ/attB*::miniCTX2-*fadD1* and PAO1-*fadD2*::*FRT-lacZ/attB*::miniCTX2-*fadD2* were cultured in 1x M9 +1% Brij-58 +1% CAA±0.1% (w/v) $C_{4:0}$ to $C_{16:0}$, or $C_{18:1}{}^{\Delta9}$ for induction studies (Fig. 3C and 3D). For *in vitro* competition studies (Fig. 8B), each mutant/complement mixture of equal cell density was grown in seven different media, including LB, 1x M9 +20 mM glucose, 1x M9 +1% CAA, 1x M9 +1% Brij-58 +0.2% PC, 1x M9 +1% Brij-58 +0.2% $C_{18:1}{}^{\Delta9}$, 1x M9 +40 mM glycerol, and 1x M9 +30 mM choline. Stock solutions of all FAs were made as previously described [30]. Unless indicated otherwise, all liquid cultures were grown at 37°C with a shaking speed of 200 r.p.m.

General molecular methods

All molecular methods and their components were employed as previously described [54]. Oligonucleotides utilized in this study were ordered through Integrated DNA Technology (IDT, Table 5).

Complementation of *E. coli fadD* mutant

The *E. coli fadD*$^-$ *fadR*::Km^r mutant (E2011) was engineered by transferring the *fadR*::Km^r mutation from JWC285 into the K27 (*fadD*$^-$) strain via P1 transduction. The resulting double mutant strain was then used for the complementation study. To construct the *E. coli* complementation vectors, coding regions of *P. aeruginosa fadD1* and *fadD2* were amplified from PAO1 chromosomal DNA using oligos #341 +#342 and #339 + #340, respectively. PCR products were then digested with NdeI + BamHI and ligated individually into pET15b, digested with the same enzymes, yielding pET15b-*fadD1* and pET15b-*fadD2*. As a control for the complementation study, the *E. coli fadD* gene (*fadD*$_{Ec}$) was also amplified from strain K12 chromosomal DNA using oligos #1092 + #1093. The 1.8-kb PCR product was digested with AseI + BamHI, and ligated with pET15b digested with NdeI + BamHI, yielding pET15b-*fadD*$_{Ec}$. These three vectors, pET15b-*fadD1*, pET15b-*fadD2*, and pET15b-*fadD*$_{Ec}$, were introduced into *E. coli* strain E2011 for complementation. E2011, harboring each complementation vector, was patched on 1x M9 minimal medium + 1% Brij-58 +1% CAA or 0.2% various fatty acids, and growth was determined after 3 days incubation at 37°C (Table 1).

Construction of PAO1 *fadD* mutant and complementation strains

Three *fadD* mutant strains (PAO1-*fadD1*::*FRT*, PAO1-*fadD2*::*FRT*, and PAO1-Δ*fadD2D1*::*FRT*) were engineered, respectively, using three allelic-replacement plasmids (pEX18T-*fadD1*::Gm-*FRT*, pEX18T-*fadD2*::Gm-*FRT*, and pEX18T-Δ*fadD2D1*::Gm-*FRT*) as previously described [55]. These gene-replacement vectors were constructed by inserting the SmaI Gm^r-*FRT* cassette at the EcoRV site to inactivate *fadD1* gene, the SmaI site to inactivate *fadD2* gene, or at the deleted *fadD2D1* SmaI-EcoRV locus. These PAO1 *fadD* mutants were confirmed by PCR (data not shown).

These newly engineered mutant strains, PAO1-*fadD1*::*FRT*, PAO1-*fadD2*::*FRT*, and PAO1-Δ*fadD2D1*::*FRT*, were complemented using the relevant gene(s) on the miniCTX2 single copy integration vector as described previously [56]. The resulting strains, PAO1-*fadD1*::*FRT*/*attB*::miniCTX2-*fadD1*, PAO1-*fadD2*::*FRT*/*attB*::miniCTX2-*fadD2*, and PAO1-Δ*fadD2D1*::*FRT*/*attB*::miniCTX2-*fadD2D1*, were used in the growth curve experiments (Fig. 4 and 8A). Controls were also performed with the empty miniCTX2 integrated into each mutant strain.

Growth characterization of *fadD* mutant and complemented strains

The *fadD* mutants, their corresponding complemented strains, and the PAO1 wildtype strain were initially grown overnight in PIB medium. The overnight cultures were centrifuged and the cell pellets were washed twice with 1x M9 minimal media and resuspended with equal volumes of the same 1x M9 media. The cell resuspensions were then diluted 100-fold in 1x M9 +1% Brij-58 +1% CAA or 0.2% of the individual FAs ($C_{4:0}$ to $C_{16:0}$, or $C_{18:1}{}^{\Delta9}$; Fig. 4) or 0.2% PC (Fig. 8A), and growth was then initiated. At each time point, aliquots of individual cultures were diluted 4-fold in 4% Brij-58 (pre-incubated at 42°C) to clarify any insoluble FA and OD_{540} measurements were taken.

Table 3. Bacterial strains used in this study[a].

Strains	Lab ID[b]	Relevant properties	Reference
E. coli			
EPMax10B	E1231	F⁻ λ⁻ *mcrA* Δ*(mrr-hsdRMS-mcrBC)* φ*80dlacZ* Δ*M15* Δ*lacX74 deoR recA1 endA1 araD139* Δ*(ara, leu)7697 galU galK rpsL nupG*	BioRad
K12	E0577	Prototroph	ATCC #23740
K27	E0410	*fadD*⁻ (*oldD88*) mutant	[16]
K27-T7	E1063	Gm^r; K27 with T7 expression system *fadD*⁻ (*oldD88*) λ*attB*::T7(*pol-lysS*)-*lacI*^{q}-Gm^r	Lab strain
JWC285	E1560	Km^r; *fadA*::*Tn10 yfcYX*::*cat fadR*::Km^r	[44]
K27-*fadR*⁻	E2011	Km^r; *fadD*⁻ *fadR*::Km^r (transduced from strain JWC285 P1-lysate into strain K27)	This study
P. aeruginosa			
PAO1	P007	prototroph	[68]
PAO1-*fadD1*::*FRT*	P175	PAO1 with *fadD1* insertional mutation	This study
PAO1-*fadD2*::*FRT*	P547	PAO1 with *fadD2* insertional mutation	This study
PAO1- Δ*fadD2D1*::*FRT*	P177	PAO1 with *fadD2D1* deletional mutation	This study
PAO1-*fadD1*::*FRT*/ *attB*::miniCTX2-*fadD1*	P541	Tet^r; PAO1-*fadD1*::*FRT* complemented with miniCTX2-*fadD1*	This study
PAO1-*fadD2*::*FRT*/ *attB*::miniCTX2-*fadD2*	P549	Tet^r; PAO1-*fadD2*::*FRT* complemented with miniCTX2-*fadD2*	This study
PAO1-Δ*fadD2D1*::*FRT*/ *attB*::miniCTX2-*fadD2D1*	P543	Tet^r; PAO1-Δ*fadD2D1*::*FRT* complemented with miniCTX2-*fadD2D1*	This study
PAO1-*fadD1*::*FRT-lacZ*/ *attB*::miniCTX2-*fadD1*	P518	Tet^r, Gm^r; *fadD1* complement strain with *fadD1-FRT-lacZ* fusion	This study
PAO1-*fadD2*::*FRT-lacZ*/ *attB*::miniCTX2-*fadD2*	P520	Tet^r, Gm^r; *fadD2* complement strain with *fadD2-FRT-lacZ* fusion	This study
PAO1-*fadD1*::*FRT*/ *mucA*::pUC18	P663	Cb^r; *fadD1* mutant with pUC18 inserted in *mucA* gene	This study
PAO1-*fadD2*::*FRT*/ *mucA*::pUC18	P667	Cb^r; *fadD2* mutant with pUC18 inserted in *mucA* gene	This study
PAO1-Δ*fadD2D1*::*FRT*/ *mucA*::pUC18	P665	Cb^r; *fadD2D1* mutant with pUC18 inserted in *mucA* gene	This study
PAO1-*fadD1*::*FRT*/ *attB*::miniCTX2-*fadD1*/ *mucA*::pUC18	P657	Cb^r, Tet^r; *fadD1* mutant with pUC18 inserted in *mucA* gene	This study
PAO1-*fadD2*::*FRT*/ *attB*::miniCTX2-*fadD2*/ *mucA*::pUC18	P659	Cb^r, Tet^r; *fadD2* mutant with pUC18 inserted in *mucA* gene	This study
PAO1-Δ*fadD2D1*::*FRT*/ *attB*::miniCTX2-*fadD2D1*/ *mucA*::pUC18	P661	Cb^r, Tet^r; *fadD2D1* mutant with pUC18 inserted in *mucA* gene	This study

[a]For strains constructed in this study, please see text for further details.
[b]Please use lab ID for requesting strains.
doi:10.1371/journal.pone.0013557.t003

Construction of *fadD1-lacZ* and *fadD2-lacZ* fusion strains and induction by FAs

To take advantage of the native *fadD1*-promoter and create a transcriptional fusion of P_{fadD1}-*lacZ*, pFRT1-*lacZ* was integrated at the *FRT* locus in strain PAO1-*fadD1*::*FRT* as previously described [29]. The resulting fusion strain, PAO1-*fadD1*::*FRT-lacZ*, was PCR confirmed using oligos #341 + #713, which are specific for the *fadD1* and *lacZ* genes, respectively. Similarly, PAO1-*fadD2*::*FRT-lacZ* was constructed and PCR confirmed using oligos #377 + #501 (data not shown). Complementation vectors miniCTX2-*fadD1* and miniCTX2-*fadD2* were then integrated into these newly developed *lacZ*-fusion strains, to yield two complemented fusion strains, PAO1-*fadD1*::*FRT-lacZ*/*attB*::miniCTX2-*fadD1* and PAO1-*fadD2*::*FRT-lacZ*/*attB*::miniCTX2-*fadD2*, respectively.

β-Galactosidase activities were measured for these two complemented fusion strains under various growth conditions. Cells were first grown overnight in PIB medium, washed twice with one volume of 1x M9, and resuspended in an equal volume of the same medium. Cell resuspensions were then diluted 100-fold into fresh 1x M9 +1% Brij-58 +1% CAA±0.1% of the individual FAs ($C_{4:0}$ to $C_{16:0}$, or $C_{18:1}^{\Delta 9}$), and growth curve experiments were performed. Cell cultures were taken at mid-log phase (OD_{540}

Table 4. Plasmids used in this study[a].

Plasmids	Lab ID[b]	Relevant properties	Reference
pEX18T	E0055	Ap^r; gene replacement vector	[55]
pEX18T-*fadD2D1*	E0551	Ap^r; pEX18T with *fadD2D1*	This study
pEX18T-*fadD1*::Gm-*FRT*	E0635	Ap^r, Gm^r; Gm^r-*FRT*-cassette inserted into *fadD1*	This study
pEX18T-*fadD2*::Gm-*FRT*	E2163	Ap^r, Gm^r; Gm^r-*FRT*-cassette inserted into *fadD2*	This study
pEX18T-Δ*fadD2D1*::Gm-*FRT*	E0455	Ap^r, Gm^r; Gm^r-*FRT*-cassette inserted into *fadD2D1*	This study
pPS856	E0050	Ap^r, Gm^r; plasmid with Gm^r-*FRT*-cassette	[55]
pET15b	E0047	Ap^r; T7 expression vector	Novagen
pET15b-*fadD1*	E0753	Ap^r; pET15b with *fadD1*	This study
pET15b-*fadD2*	E0756	Ap^r; pET15b with *fadD2*	This study
pET15b-$fadD_{Ec}$	E2177	Ap^r; pET15b with *E. coli fadD*	This study
pET15b-*fadD2*::Gm-*FRT*	E2155	Ap^r, Gm^r; Gm^r-*FRT*-cassette inserted into *fadD2*	This study
miniCTX2	E0076	Tet^r; site-specific integration vector	[56]
miniCTX2-*fadD1*	E2157	Tet^r; miniCTX2 with cloned *fadD1*	This study
miniCTX2-*fadD2*	E2159	Tet^r; miniCTX2 with cloned *fadD2*	This study
miniCTX2-*fadD2D1*	E2143	Tet^r; miniCTX2 with cloned *fadD2D1*	This study
pUC18	E0135	Ap^r; cloning vector	[69]
pUC18-'*mucA*'	E1907	Ap^r; *mucA* internal region cloned into pUC18	This study
pUC19	E0014	Ap^r; cloning vector	[69]
pUC19-*fadD2D1*	E0545	Ap^r; pUC19 with cloned *fadD1* and *fadD2*	This study
pUC19-Δ*fadD2D1*::Gm-*FRT*	E0416	Ap^r, Gm^r; pUC19-*fadD2D1* with a Gm^r-*FRT*-cassette insertion	This study
pFRT1-*lacZ*-Gm	E0790	Gm^r; *FRT-lacZ* fusion vector	[29]
pCD13SK-*flp-oriT*	E0783	Sp^r; suicidal Flp-containing plasmid	[29]
pFLP2	E0067	Ap^r; Flp-containing plasmid	[55]

[a]For plasmids constructed in this study, please see text for further details.
[b]Please use lab ID for requesting plasmids.
doi:10.1371/journal.pone.0013557.t004

~2.0) and β-galactosidase assays were performed in triplicate and Miller Units (mean±s.e.m.) were determined [57] (Fig. 3).

FadD1 and FadD2 purification

Histidine-tagged FadD1 and FadD2 were expressed on the pET15b vector and purified using a Ni^+-NTA column (Qiagen, Valencia, CA) as described elsewhere [58]. The *E. coli* K27-T7 (*fadD*$^-$) strain was used for protein expression to prevent any possible *E. coli* FadD contamination in protein preparations (Fig. 5A).

Measurement of fatty acyl-CoA synthetase (FadD1 and FadD2) activity

Fatty acyl-CoA synthetase activity was monitored using Ellman's reagent, as previously described in several studies, to detect the amount of free thiol (i.e. CoASH used in the reaction) [23,59–61]. Reactions (450 µl total) were prepared with 20 µg of purified FadD1 (or FadD2) in a reaction buffer containing final concentrations of 150 mM Tris-HCl (pH 7.2), 10 mM $MgCl_2$, 2 mM EDTA, 0.1% Triton X-100, 5 mM ATP, 0.5 mM coenzyme A (CoASH), and an individual FA (30 to 300 µM) in thin-walled glass tubes. Briefly, to perform the reaction, each mixture was assembled containing all components above (excluding CoASH) and the 405 µl mixture was pre-incubated at 37°C for 3 min. The reaction was then initiated with the addition of 45 µl of CoASH (5 mM stock in 20 mM Tris-HCl, pH 6.7, diluted to a final concentration of 0.5 mM) that was pre-incubated at 37°C for 3 min, quickly mixed, and incubated at 37°C during the course of the reaction. Immediately after mixing, a time zero point was taken by removing 75 µl from the 450 µl reaction mix and adding it to 600 µl of 0.4 mM 5,5′-dithiobis(2-nitrobenzoic acid) (DTNB, dissolved in 0.1 M potassium phosphate at pH 8.0) and the A_{412} were measured. Subsequent 75 µl aliquots of the reaction were taken at 20-sec intervals and mixed with DTNB for additional measurements. Additionally, control experiments without FadD enzymes were performed exactly as above to show no change in absorbance at 412 nm and verify the stability of CoASH and DTNB under these conditions. Reactions with FadD were repeated to obtain triplicate data for each FA at each concentration. For each FA substrate, decreases in A_{412} values (loss of CoASH) over time were used to calculate the initial velocity (V_0) for each FA concentration (Fig. 5B and 5C). The maximum velocity (V_{max}) of the enzymes and affinity for the different substrates (Michaelis constant, K_m) were then determined using the Hanes-Woolf plot, rather than the Lineweaver-Burk plot, for increased accuracy [62]. To determine the V_{max} and K_m for the substrate ATP, the same procedure was followed, except that the concentration of $C_{18:1}^{\Delta 9}$ was constant (1 mM) and varying concentrations of ATP (0.05 to 2.5 mM) were used (Table 2).

Motility assays

Strains for swarming and swimming were grown overnight in LB medium. Cell pellets of 500 µl culture aliquots were washed twice with equivalent volumes of 1x M9 medium and resuspended

Table 5. Primers used in this study.

Number and Name	Sequence[a]
***fadD* cloning**	
302; *fadD*-up-Hind	5′-ATCGGAAGCTTCCGGGTGCTGCTGGCGGAT-3′
303; *fadD*-down	5′-TTCGTGGAGCTGCCGGCGCAAGC-3′
339; *fadD2*-NdeI	5′-CAAGAACATATGCAACCTGAATTCTGGAACG-3′
340; *fadD2*-BamHI	5′-CGGCAAGGATCCGTTTCAGAGCCTTGTAAGGCT-3′
341; *fadD1*-NdeI	5′-TGGGCTCATATGATCGAAAACTTCTGGAAGG-3′
342; *fadD1*-BamHI	5′-GGGGCGGATCCAGGCAACGGCGGACTTACTTC-3′
501; Gm-up-reverse	5′-CATACGCTACTTGCATTACAG-3′
713; *lacZα*	5′-TGTTGGGAAGGGCGATC-3′
1092; *EcfadD*-up-AseI	5′-AAGGATTAATAAGAAGGTTTGGCTTAAC-3′
1093; *EcfadD*-down-BamHI	5′-AACGGGATCCTCAGGCTTTATTGTC-3′
Promoter mapping	
372 – *fadD2*-race3[b]	5′-GAGCGCTCGAAGACCTCGA-3′
373 – *fadD2*-race2	5′-GAAGTCGAGACTGTCGGGTA-3′
374 – *fadD2*-race1	5′-TCGTTCCAGAATTCAGGTTG-3′
375 – *fadD1*-race3[b]	5′-ACAGGATGTTCGGGTACTG-3′
376 – *fadD1*-race2	5′-CGGGATTGATCTCGGCAGCA-3′
377 – *fadD1*-race1	5′-GTACTTGTCCTTCCAGAAGT-3′
797 – SMART-IIA[b]	5′-AAGCAGTGGTATCAACGCAGAGTACGCGGG-3′
798 – SMART-IIB	5′-AAGCAGTGGTATCAACGCAGAGT-3′
***mucA* cloning**	
937 – *mucA*-up	5′-GAAGCGGATGAACTCGAG-3′
938 – *mucA*-down	5′-ACTGACGGCGGATTGTTG-3′

[a]Restriction enzyme sites utilized in this study are underlined.
[b]Primers synthesized RNase free and HPLC purified.
doi:10.1371/journal.pone.0013557.t005

in equal volumes of the same medium. Swarming motility was assayed by spotting 5 µl of the resuspended cultures onto BM2-glucose swarm agar plates, made as described previously [63]. Swimming motility was assayed by pin-stabbing 0.3% LB agar plates with the overnight liquid cultures grown in LB. All inoculated plates were allowed to dry at room temperature for 10 min, incubated at 37°C for 16 to 18 h, and motility zones were compared (Fig. 6).

Protease, phospholipase, lipase, and rhamnolipid detection

Strains were grown in LB medium and cultures were used for OD_{540} measurements at various time points (Fig. 7E). For protease, phospholipase, and lipase assays, clarified supernatant was obtained at 24 h from 1 ml culture aliquots centrifuged (16,000× *g*) for 2 min at 4°C and filtered through 0.2 µm hydrophilic PVDF filters (Fisher Scientific). To quantify protease and phospholipase activities, 4-mm diameter holes were punched into 2% skim milk NB agar protease plates or blood agar phospholipase plates (PML Microbiological) and filled twice with 50 µl of each cell-free supernatant, respectively. Both the skim milk and blood agar plates were incubated at 37°C for 18 h before analyzing. Similarly, 50 µl of the same cell-free supernatants were applied five times into 4-mm holes in rhodamine B agar plates [64], and the plates were imaged using a UV transilluminator after incubation at 37°C for 3 days to visualize lipase activity. These plate-based assays were conducted in triplicate and the clearance zone diameters for skim milk and blood agar plates or the fluorescent halo diameters for the rhodamine B plates were measured and compared by percentage conversion relative to the wildtype PAO1 value and were expressed as an average ± s.e.m (Fig. 7A, 7B and 7C).

Rhamnolipid production was assessed using a previously published methylene blue complexation assay [65]. All strains were grown for 24 h in LB medium and 1.5 ml of clarified supernatant for rhamnolipid extraction was obtained from each culture by room temperature centrifugation (16,000× *g*). This assay was conducted in triplicate and average absorbance was compared by percentage conversion relative to the wildtype PAO1 value and was expressed as an average ± s.e.m (Fig. 7D).

Promoter mapping

The transcriptional start sites of the *fadD1* and *fadD2* genes were determined as previously described [30]. Briefly, PAO1 was grown in 1x M9 minimal media supplemented with 0.2% $C_{16:0}$ to mid-log phase. This FA was chosen prior to the gene induction studies and, in retrospect, it was as appropriate as any other FA to map the *fadD* promoters. Cells were harvested and total RNA was isolated to perform cDNA synthesis using a SMART-IIA primer (#797, Table 5) and the first gene-specific primer (#375 for *fadD1* and #372 for *fadD2*, Table 5). The cDNA was subsequently used as the template in PCR, using oligos #798 + #376 and #798 + #373 for *fadD1* and *fadD2*, respectively. Finally, the PCR product was sequenced using a second nested oligo #377 for *fadD1*, or #374 for *fadD2* (Fig. 2).

Northern blot analysis

Wildtype strain, PAO1, was grown in 1x M9 minimal medium supplemented with 0.2% $C_{8:0}$, $C_{14:0}$, or $C_{18:1}{}^{\Delta 9}$ as sole carbon sources. After reaching mid-log phase (OD_{540}~1.0), cells were harvested at 4°C and total RNA was isolated. Thirty µg of each RNA sample was used for northern analysis as described previously [66]. The *fadD1* and *fadD2* genes were PCR amplified from pET15b-*fadD1* and pET15b-*fadD2* using oligos #341 + #342, and #339 + #340, respectively, and used individually as probes (Fig. 3A and 3B).

In vitro and *in vivo* competition studies

Various *fadD* mutant strains (*fadD1*, *fadD2* and *fadD2D1* mutants) and their corresponding complemented strains were utilized for the *in vitro and in vivo* competition studies (Table 3). A *mucA* insertional mutation was introduced into all strains to overproduce alginate, as we used a mouse model to allow these mucoid strains to survive and replicate in the lung as described previously [52]. Briefly, a 450-bp internal region of the *mucA* gene was PCR amplified from PAO1 chromosomal DNA using oligos #973 and #974 and cloned into the PvuI site of pUC18. The resultant vector pUC18-'*mucA*' was electroporated into the various *fadD* mutant/complemented strains and the mucoid transformants were selected on PIA plates supplemented with 500 µg/ml carbenicillin (Cb500). One mucoid colony of each mutant/complemented strain was then inoculated separately in 3 ml of PIB + Cb500. After 24 h of incubation in a shaking incubator at 37°C, these cultures were diluted 100 times into 5 ml of fresh PIB + Cb500 and grown overnight. Three ml of each overnight culture was centrifuged (20,000× *g*) for 10 min at 4°C and clarified supernatants were collected. The cell density of each culture was calculated by plating 10-fold serial dilutions on LB plates. Each culture was then adjusted to 2×10^8 CFU/ml in its own clarified supernatant, obtained above. At this point, each diluted *fadD* mutant strain (*fadD1*, *fadD2* and *fadD2D1* mutants) and its

corresponding complemented strain were mixed at a 1:1 CFU ratio and the resulting mixtures (*fadD1*/complement, *fadD2*/complement, and *fadD2D1*/complement) were used for inoculation into various growth media (*in vitro* competition) or mouse lungs (*in vivo* competition).

For *in vitro* competition, each mutant/complement mixture of equal cell density was diluted 100x into various growth media with LB, glucose, CAA, PC, $C_{18:1}^{\Delta 9}$, glycerol, or choline as sole carbon sources. All cultures were grown at 37°C with shaking for 1–2 days until the total cell densities reached $\sim 1\times10^9$ CFU/ml. Bacteria were then quantified by plating dilutions onto LB plates with and without tetracycline to determine the total number of bacteria (growth with no tetracycline) and the number of complemented bacteria (growth with tetracycline). These numbers were used to determine the *in vitro* CI ($CFU_{mutant}/CFU_{complement}$ when grown in media) [47]. All experiments were performed in triplicate and statistical analysis was performed using Graphpad Prism 5.0 software (Fig. 8B).

Male BALB/c mice, 6–8 weeks old, were purchased from Charles River Laboratories and used in this *in vivo* competition study [52]. Before challenge, the mice were anesthetized by the intraperitoneal injection of 100 mg/kg ketamine and 10 mg/kg xylazine. Thirty µl of the mutant/complemented strain mixture (3×10^6 CFU of each) was inoculated intratracheally into BALB/c mice using the BioLITE Intubation System (Braintree Scientific). After 24 or 48 h, mice were humanely euthanized and lungs were harvested and homogenized. Bacteria were quantified by plating dilutions onto growth media with and without tetracycline to determine the total number of bacteria (growth with no tetracycline) and the number of complemented bacteria (growth with tetracycline). These numbers were used to determine the *in vivo* CI ($CFU_{mutant}/CFU_{complement}$ when grown in mouse lungs) [47]. A control condition was included using PAO1-*mucA*::pUC18/PAO1-*mucA*::pUC18-miniCTX2 to show that no competitive advantage or disadvantage was conferred by the presence of the Tet^r marker during in vivo growth (data not shown). Statistical analysis was performed using Graphpad Prism 5.0 software (Fig. 8C and 8D).

Acknowledgments

We thank previous Hoang lab members for their technical assistance in some experiments and critical reading of this manuscript. We are grateful to Dr. J. E. Cronan (University of Illinois) for the gift of JWC285. We wish to thank Drs. D. W. Taylor and R. Yanagihara for critical reading of this manuscript.

Author Contributions

Conceived and designed the experiments: YK CBW TTH. Performed the experiments: YK JZS MHN. Analyzed the data: YK TTH. Contributed reagents/materials/analysis tools: JZS CBW MHN. Wrote the paper: YK TTH.

References

1. Rahme LG, Stevens EJ, Wolfort SF, Shao J, Tompkins RG, et al. (1995) Common virulence factors for bacterial pathogenicity in plants and animals. Science 268: 1899–1902.
2. Abd H, Wretlind B, Saeed A, Idsund E, Hultenby K, et al. (2008) *Pseudomonas aeruginosa* utilizes its type III secretion system to kill the free-living amoeba *Acanthamoeba castellanii*. J Eukaryot Microbiol 55: 235–243.
3. Matz C, Moreno AM, Alhede M, Manefield M, Hauser AR, et al. (2008) *Pseudomonas aeruginosa* uses type III secretion secretion system to kill biofilm-associated ameobae. ISME J 2: 843–852.
4. Weir TL, Stull VJ, Badri D, Trunck LA, Schweizer HP, et al. (2008) Global gene expression profiles suggest an important role for nutrient acquisition in early pathogenesis in a plant model of *Pseudomonas aeruginosa* infection. Appl Environ Microbiol 74: 5784–5791.
5. Baltch AL, Griffin PE (1977) *Pseudomonas aeruginosa* bacteremia: clinical study of 75 patients. Am J Med Sci 274: 119–129.
6. Bowton DL (1999) Nosocomial pneumonia in the ICU-year 2000 and beyond. Chest 115: 28S–33S.
7. Lode H, Raffenberg M, Erbes R, Geerdes-Fenge H, Mauch H (2000) Nosocomial pneumonia: epidemiology, pathogenesis, diagnosis, treatment and prevention. Curr Opin Infect Dis 13: 377–384.
8. Richards MJ, Edwards JR, Culver DH, Gaynes RP (1999) Nosocomial infections in medical intensive care units in the United States. Crit Care Med 27: 887–892.
9. Doring G (1997) Cystic fibrosis respiratory infections: interactions between bacteria and host defense. Monaldi Arch Chest Dis 52: 363–366.
10. Greenberger PA (1997) Immunologic aspects of lung diseases and cystic fibrosis. J Am Med Assoc 278: 1924–1930.
11. Stanier RY, Palleroni NJ, Doudoroff M (1966) The aerobic pseudomonads: a taxonomic study. J Gen Microbiol 43: 159–271.
12. Son MS, Matthews WJJ, Kang Y, Nguyen DT, Hoang TT (2007) *In vivo* evidence of *Pseudomonas aeruginosa* nutrient acquisition and pathogenesis in the lungs of cystic fibrosis patients. Infect Immun 75: 5313–5324.
13. Miller RM, Tomaras AP, Barker AP, Voelker DR, Chan ED, et al. (2008) *Pseudomonas aeruginosa* twitching motility-mediated chemotaxis toward phospholipids and fatty acids: specificity and metabolic requirements. J Bacteriol 190: 4038–4049.
14. Black PN, DiRusso CC (1994) Molecular and biochemical analyses of fatty acid transport, metabolism, and gene regulation in *Escherichia coli*. Biochim Biophys Acta 1210: 123–145.
15. Clark DP, Cronan Jr. JE (1996) Two-carbon compounds and fatty acids as carbon sources. In: Neidhardt FC, Curtiss III R, Ingraham JL, Lin ECC, Brooks Low K, et al., *Escherichia coli* and *Salmonella*: cellular and molecular biology, 2nd ed. Washington, D.C.: American Society for Microbiology. pp 343–358.
16. Overath P, Pauli G, Schairer HU (1969) Fatty acid degradation in *Escherichia coli*: An inducible acyl-CoA synthase, the mapping of old-mutations, and the isolation of regulatory mutants. Eur J Biochem 7: 559–574.
17. Black PN, DiRusso CC, Metzger AK, Heimert TL (1992) Cloning, sequencing, and expression of the *fadD* gene of *Escherichia coli* encoding acyl coenzymeA synthase. J Biol Chem 267: 25513–25520.
18. Weimar JD, DiRusso CC, Delio R, Black PN (2002) Functional role of fatty acid acyl-coenzyme A synthetase in the transmembrane movement and activation of exogenous long-chain fatty acids. J Biol Chem 277: 29369–29376.
19. Black PN, Zhang Q, Weimar JD, DiRusso CC (1997) Mutational analysis of a fatty acyl-coenzyme A synthetase signature motif identifies seven amino acid residues that modulate fatty acid substrate specificity. J Biol Chem 272: 4896–4903.
20. Black PN (1988) The *fadL* gene product of *Escherichia coli* is an outer membrane protein required for uptake of long-chain fatty acids and involved in sensitivity to bacteriophage T2. J Bacteriol 170: 2850–2854.
21. Black PN (1991) Primary sequence of the *Escherichia coli fadL* gene encoding an outer membrane protein required for long-chain fatty acid transport. J Bacteriol 173: 435–442.
22. Kumar GB, Black PN (1993) Bacterial long-chain fatty acid transport. Identification of amino acid residues within the outer membrane protein FadL. J Biol Chem 268: 15469–15476.
23. Groot PHE, Scholte HR, Hulsmann WC (1976) Fatty acid activation: specificity, localization, and function. Adv Lipid Res 14: 75–126.
24. DiRusso CC, Heimert TL, Metzger AK (1992) Characterization of FadR, a global transcription regulator of fatty acid metabolism in *Escherichia coli*. J Biol Chem 267: 8685–8691.
25. Raman N, Black PN, DiRusso CC (1997) Characterization of the fatty acid-responsive transcriptional factor FadR. J Biol Chem 272: 30645–30650.
26. van Aalten DMF, DiRusso CC, Knudsen J (2001) The structural basis of coenzyme A-dependent regulation of the transcription factor FadR. EMBO J 20: 2041–2050.
27. Campbell JW, Cronan Jr. JE (2002) The enigmatic *Escherichia coli fadE* gene is *yafH*. J Bacteriol 184: 3759–3764.
28. Kazakov AE, Rodionov DA, Alm E, Arkin AP, Dubchak I, et al. (2009) Comparative genomics of regulation of fatty acid and branched-chain amino acid utilization in proteobacteria. J Bacteriol 191: 52–64.
29. Son MS, Nguyen DT, Kang Y, Hoang TT (2008) Engineering of *FRT-lacZ* constructs: induction of the *Pseudomonas aeruginosa fadBA1* operon by medium and long-chain fatty acids. Plasmid 59: 111–118.
30. Kang Y, Nguyen DT, Son MS, Hoang TT (2008) The *Pseudomonas aeruginosa* PsrA responds to long-chain fatty acid signals to regulate the *fadBA5* β-oxidation operon. Microbiology 154: 1584–1598.
31. Imamura S, Ueda S, Mizugaki M, Kawaguchi K (1990) Purification of the multienzyme complex for fatty acid oxidation from *Pseudomonas fragi* and reconstitution of the fatty acid oxidation system. J Biochem 107: 184–189.
32. Sato S, Hayashi M, Imamura S, Ozeki Y, Kawaguchi A (1992) Primary structure of the genes, *faoA* and *faoB*, from *Pseudomonas fragi* B-0771 which encode

the two subunits of the HDT multienzyme complex involved in fatty acid β-oxidation. J Biochem 111: 8–15.
33. Sato S, Imamura S, Ozeki Y, Hayashi M, Kawaguchi A (1992) Induction of enzymes involved in fatty acid β-oxidation in *Pseudomonas fragi* B-0771 cells grown in media supplemented with fatty acid. J Biochem 111: 16–19.
34. Fernandez-Valverde M, Reglero A, Martinez-Blanco H, Luengo JM (1993) Purification of *Pseudomonas putida* acyl coenzyme A ligase active with a range of aliphatic and aromatic substrates. Appl Environ Microbiol 59: 1149–1154.
35. Garcia B, Olivera ER, Minambres B, Fernandez-Valverde M, Canedo LM, et al. (1999) Novel biodegradable aromatic plastics from a bacterial source. J Biol Chem 274: 29228–29241.
36. Olivera ER, Carnicero D, Garcia B, Minambres B, Moreno MA, et al. (2001) Two different pathways are involved in the β-oxidation of *n*-alkanoic and *n*-phenylalkanoic acids in *Pseudomonas putida* U: genetic studies and biotechnological applications. Mol Microbiol 39: 863–874.
37. Barber CE, Tang JL, Feng JX, Pan MQ, Wilson TJG, et al. (1997) A novel regulatory system required for pathogenicity of *Xanthomonas campestris* is mediated by a small diffusible signal molecule. Mol Microbiol 24: 555–566.
38. Bajaj V, Lucas RL, Hwang C, Lee CA (1996) Co-ordinated regulation of *Salmonella typhimurium* invasion genes be environmental and regulatory factors is mediated by control of *hilA*. Mol Microbiol 22: 703–714.
39. Cole ST, Brosch R, Parkhill J, Garnier T, Churcher C, et al. (1998) Deciphering the biology of *Mycobacterium tuberculosis* from the complete genome sequence. Nature 393: 537–544.
40. Cox JS, Chen B, McNeil M, Jacob WR, Jr. (1999) Complex lipid determines tissue-specific replication of *Mycobacterium tuberculosis* in mice. Nature 402: 79–83.
41. Lucas RL, Lostroh CP, DiRusso CC, Spector MP, Wanner BL, et al. (2000) Multiple factors independently regulate *hilA* and invasion gene expression in *Salmonella enterica* serovar typhimurium. J Bacteriol 182: 1872–1882.
42. Rindi L, Fattorini L, Bonanni D, Iona E, Freer G, et al. (2002) Involvement of the *fadD33* gene in the growth of *Mycobacterium tuberculosis* in the liver of BALB/c mice. Microbiology 148: 3873–3880.
43. Soto MJ, Fernandez-Pascual M, Sanjuan J, Olivares J (2002) A *fadD* mutant to *Sinorhizobium meliloti* shows multicellular swarming migration and is impaired in nodulation efficiency on alfalfa roots. Mol Microbiol 43: 371–382.
44. Campbell JW, Morgan-Kiss RM, Cronan JE, Jr. (2003) A new *Escherichia coli* metabolic competency: growth on fatty acids by a novel anaerobic β-oxidation pathway. Mol Microbiol 47: 793–805.
45. Iram SH, Cronan JE (2006) The β-oxidation systems of *Escherichia coli* and *Salmonella enterica* are not functionally equivalent. J Bacteriol 188: 599–608.
46. Postle AD, Mander A, Reid KBM, Wang J-Y, Wright SM, et al. (1999) Deficient hydrophilic lung surfactant protein A and D with normal surfactant phospholipid molecular species in cystic fibrosis. Am J Respir Cell Mol Biol 20: 90–98.
47. Brickman TJ, Vanderpool CK, Armstrong SK (2006) Heme transport contributes to *in vivo* fitness of *Bordetella pertussis* during primary infection in mice. Infect Immun 74: 1741–1744.
48. Caiazza NC, Shanks RMQ, O'Toole GA (2005) Rhamnolipids modulate swarming motility patterns of *Pseudomonas aeruginosa*. J Bacteriol 187: 7351–7361.
49. Krieg DP, Bass JA, Mattingly SJ (1988) Phosphorylcholine stimulates capsule formation of phosphate-limited mucoid *Pseudomoas aeruginosa*. Infect Immun 56: 864–873.
50. Wargo MJ, Szwergold BS, Hogan DA (2008) Identification of two gene clusters and a transcriptional regulator required for *Pseudomonas aeruginosa* glycine betaine catabolism. J Bacteriol 190: 2690–2699.
51. Bernhard W, Hoffmann S, Dombrowsky H, Rau GA, Kamlage A, et al. (2001) Phosphatidylcholine molecular species in lung surfactant: composition in relation to respiratory rate and lung development. Am J Respir Cell Mol Biol 25: 725–731.
52. Hoffmann N, Rasmussen TB, Jensen PO, Stub C, Hentzer M, et al. (2005) Novel mouse model of chronic *Pseudomonas aeruginosa* lung infection mimicking cystic fibrosis. Infect Immun 73: 2504–2514.
53. Mulcahy H, Charron-Mazenod L, Lewenza S (2010) *Pseudomonas aeruginosa* produces an extracellular deoxyribonuclease that is required for utilization of DNA as a nutrient source. Environ Microbiol 12: 1621–1629.
54. Kang Y, Lunin VV, Skarina T, Savchenko A, Schurr MJ, et al. (2009) The long-chain fatty acid sensor, PsrA, modulates the expression of *rpoS* and the type III secretion *exsCEBA* operon in *Pseudomonas aeruginosa*. Mol Microbiol 73: 120–136.
55. Hoang TT, Karkhoff-Schweizer RR, Kutchma AJ, Schweizer HP (1998) A broad-host-range Flp-*FRT* recombination system for site-specific excision of chromosomally-located DNA sequences: application for isolation of unmarked *Pseudomonas aeruginosa* mutants. Gene 212: 77–86.
56. Hoang TT, Kutchma AJ, Becher A, Schweizer HP (2000) Integration-proficient plasmids for *Pseudomonas aeruginosa*: site-specific integration and use for engineering of reporter and expression strains. Plasmid 43: 59–72.
57. Miller JH (1992) A short course in bacterial genetics. Cold Spring Harbor, N.Y.: Cold Spring Harbor Laboratory Press. pp 72–74.
58. Hoang TT, Sullivan SA, Cusick KC, Schweizer PH (2002) *β*-Ketoacyl carrier protein reductase (FabG) activity of the fatty acid biosynthetic pathway is a determining factor of 3-oxo-homoserine lactone acyl chain lengths. Microbiology 148: 3849–3856.
59. Bar-Tana J, Rose G, Shapiro B (1971) The purification and properties of microsomal palmitoyl-coenzyme A synthase. Biochem J 122: 353–362.
60. Ichihara K, Shibasaki Y (1991) An enzyme-coupled assay for acyl-CoA synthase. J Lipid Res 32: 1709–1712.
61. Wehrmann A, Vliet AV, Opsomer C, Botterman J, Schulz A (1996) The similarities of *bar* and *pat* gene products make them equally applicable for plant engineering. Nat Biotechnol 14: 1274–1278.
62. Dowd JE, Riggs DS (1965) A comparison of estimates of Michaelis-Menten kinetics constant from various linear transformations. J Biol Chem 240: 863–869.
63. Overhage J, Lewenza S, Marr AK, Hancock RE (2007) Identification of genes involved in swarming motility using a *Pseudomonas aeruginosa* PAO1 mini-Tn5-*lux* mutant library. J Bacteriol 189: 2164–2169.
64. Kouker G, Jaeger K-E (1987) Specific and sensitive plate assay for bacterial lipases. Appl Environm Microbiol 53: 211–213.
65. Pinzon NM, Ju L-K (2009) Analysis of rhamnolipid biosurfactants by methylene blue complexation. Appl Microbiol Biotechnol 82: 975–981.
66. Hoang TT, Schweizer HP (1997) Fatty acid biosynthesis in *Pseudomonas aeruginosa*: Cloning and characterization of the *fabAB* operon encoding *β*-hydroxyacyl-acyl carrier protein dehydratase (*fabA*) and *β*-ketoacyl-acyl carrier protein synthase I (*fabB*). J Bacteriol 179: 5326–5332.
67. van den Berg B, Black PN, Clemons WM, Jr., Rapoport TA (2004) Crystal structure of the long-chain fatty acid transporter FadL. Science 304: 1506–1509.
68. Holloway BW, Römling U, Tümmler B (1994) Genomic mapping of *Pseudomonas aeruginosa* PAO. Microbiology 140: 2907–2929.
69. Yanisch-Perron C, Vieira J, Messing J (1985) Improved M13 cloning vectors and host strains: nucleotide sequences of the M13mp18 and pUC19 vectors. Gene 33: 103–119.

Transcript amplification from single bacterium for transcriptome analysis

Yun Kang, Michael H. Norris, Jan Zarzycki-Siek, et al.

Genome Res. published online May 2, 2011
Access the most recent version at doi:10.1101/gr.116103.110

Method

Transcript amplification from single bacterium for transcriptome analysis

Yun Kang,[1] Michael H. Norris,[2] Jan Zarzycki-Siek,[1] William C. Nierman,[3] Stuart P. Donachie,[1] and Tung T. Hoang[1,2,4]

[1]*Department of Microbiology, University of Hawaii at Manoa, Honolulu, Hawaii 96822, USA;* [2]*Department of Molecular Biosciences and Bioengineering, University of Hawaii at Manoa, Honolulu, Hawaii 96822, USA;* [3]*J. Craig Venter Institute, Rockville, Maryland 20850, USA*

Total transcript amplification (TTA) from single eukaryotic cells for transcriptome analysis is established, but TTA from a single prokaryotic cell presents additional challenges with much less starting material, the lack of poly(A)-tails, and the fact that the messages can be polycistronic. Here, we describe a novel method for single-bacterium TTA using a model organism, *Burkholderia thailandensis*, exposed to a subinhibitory concentration of the antibacterial agent, glyphosate. Utilizing a *B. thailandensis* microarray to assess the TTA method showed low fold-change bias (less than twofold difference and Pearson correlation coefficient $R \approx 0.87–0.89$) and drop-outs (4%–6% of 2842 detectable genes), compared with data obtained from the larger-scale nonamplified RNA samples. Further analysis of the microarray data suggests that *B. thailandensis*, when exposed to the aromatic amino acid biosynthesis inhibitor glyphosate, induces (or represses) genes to possibly recuperate and balance the intracellular amino acid pool. We validated our single-cell microarray data at the multi-cell and single-cell levels with *lacZ* and *gfp* reporter-gene fusions, respectively. Sanger sequencing of 192 clones generated from the TTA product of a single cell, with and without enrichment by elimination of rRNA and tRNA, detected only *B. thailandensis* sequences with no contamination. These data indicate that RNA-seq of TTA from a single cell is possible using this novel method.

[Supplemental material is available for this article. The microarray data from this study have been submitted to the NCBI Gene Expression Omnibus (http://www.ncbi.nlm.nih.gov/geo) under accession no. GSE23419. The sequencing data have been submitted to GenBank (http://www.ncbi.nlm.nih.gov/Genbank/) under accession nos. JG731867–JG732058.]

Innovative methods in single-cell technology are needed to enhance the investigations of *Bacteria* and *Archaea* genomic material, particularly if we are to develop deeper insights into the functional and metafunctional genomics of these "prokaryotes." Functional-genomics or transcriptomics of a single-cell can produce a wealth of information at resolutions that cannot be attained by analysis of multi-cell populations or communities. Such advances hinge on the development of innovative methods for single-cell isolation (Podar et al. 2009) and transcript amplification from a minute amount of starting material with low gene expression bias. Single eukaryotic cell mRNA amplification methods for transcriptome analysis, via microarray (Kurimoto et al. 2007; Scanlon et al. 2009) and mRNA sequencing (Tang et al. 2009), have recently been described. These existing methods of transcript amplification, pioneered for eukaryotic transcript amplification, involve multiple rounds of exponential (Kurimoto et al. 2006) and/or linear (Scanlon et al. 2009) amplification of cDNA. However, no study has described total transcript amplification (TTA) from a single bacterium, possibly due to the major challenges one may encounter when working with single-bacterium TTA. These challenges include (1) the low amount of RNA (~0.1–2 pg/prokaryotic cell vs. ~10–50 pg/eukaryotic cell); (2) the lack of poly(A)-tails for ease of tagging and mRNA amplification; and (3) the fact that the messages can be polycistronic, and full-length amplification is critical for detecting expression of all genes in an operon. Due to these characteristics of prokaryotic transcripts, our experience with TTA using existing linear and exponential amplification methods for single bacterial cells shows the methods are labor intensive and yield unusable data with extensive gene expression bias and low reproducibility. If these challenges could be resolved, one could envisage numerous applications that may provide a wealth of functional-genomic information that was not previously possible (Supplemental Fig. S1).

Here, we describe a novel method for TTA from a single prokaryotic cell. Using *Burkholderia thailandensis* as a model bacterium exposed to a subinhibitory concentration of the antibacterial agent glyphosate (GS) (Norris et al. 2009), we developed a novel method for TTA using φ29 polymerase multiple displacement amplification (MDA) of circularized cDNA. We used microarray to assess the reproducibility, level of gene expression bias, and gene presence that resulted from this novel method. This low bias and simple single-tube method is reproducible and is not labor intensive. The data yielded a less than twofold difference in fold-changes compared with the nonamplified samples. In a typical experiment, we could amplify and detect ~94%–96% of the detectable transcripts (2842 genes) from a single cell by microarray. Exposure to GS up- or down-regulates many genes, resulting from GS inhibition of aromatic amino acid biosynthesis, to possibly compensate for amino acid imbalance. From the microarray data obtained through TTA of single cells exposed to GS versus no GS, we randomly picked five up-regulated genes, three down-regulated genes, and two control genes that showed no fold-change to validate our microarray data by reporter-gene fusions. We propose

[4]**Corresponding author.**
E-mail tongh@hawaii.edu; fax (808) 956-5339.
Article published online before print. Article, supplemental material, and publication date are at http://www.genome.org/cgi/doi/10.1101/gr.116103.110. 333

that this novel method can be applied to RNA-seq and will stimulate various important prokaryotic research areas that require single-cell level transcriptome analysis (Supplemental Fig. S1).

Results

Single-cell isolation and amplification method

We utilized laser capture microdissection (Emmert-Buck et al. 1996) to isolate *B. thailandensis* single cells, followed by *B. thailandensis* microarray analysis to assess our single-cell TTA method. Although various single-cell isolation techniques have been described (Podar et al. 2009), we chose to use the Zeiss Laser Capture Microdissection (LCM) MicroBeam IV system (hereafter referred to as the Zeiss LCM) to isolate single *B. thailandensis* cells grown in 1× M9 minimal glucose media (MG) ± GS (Fig. 1). We have recently discovered that *B. thailandensis* is very sensitive to the herbicide GS (Norris et al. 2009) because bacteria, in the presence of GS, cannot synthesize aromatic amino acids (Fischer et al. 1986). At a subinhbitory GS concentration of 0.01% compared with no GS, there is no apparent difference in growth rate or final cell density, which renders GS exposure appropriate as a model for gene-expression analysis between these two growth conditions (Fig. 1B). Our approach (Fig. 1A) was to perform large-scale RNA preparation from each of the two cultures (nonamplified samples). Single cells were then isolated from both cultures (Fig. 1C–E) and subjected to our single-cell TTA method (amplified samples). Microarray experiments were then performed to obtain gene expression fold-change (between the two growth conditions, i.e., ± GS) for both the amplified and the nonamplified samples, which were then compared to assess the suitability of the TTA method (Fig. 1A). We expected that genes differentially expressed between the two conditions from the amplified RNA samples would correlate, with minimal fold-change bias, to data from the large-scale nonamplified RNA preparations from more than 10^9 bacteria.

We devised a novel method for single-cell TTA, using φ29 polymerase for MDA of circularized cDNA (Fig. 2). Full details of the method can be found in the Methods section. Briefly, single

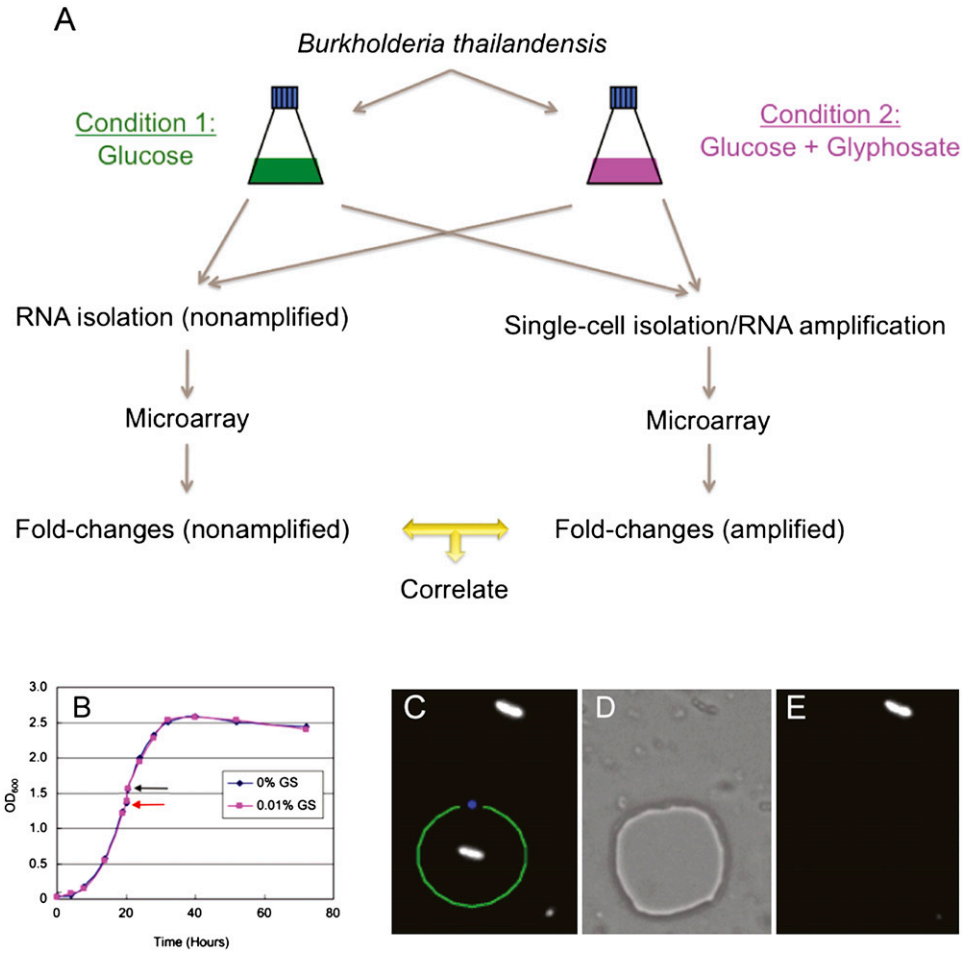

Figure 1. Single *B. thailandensis* cell isolation. (*A*) Experimental design for evaluating the single-cell transcript amplification method. *B. thailandensis* grown in two different conditions were used in large-scale (nonamplified) and single-cell level (amplified) microarray analysis. Fold-changes (between condition 1 and 2) of all genes detected from the nonamplified and amplified samples were then compared by correlation analysis. (*B*) Comparable growth curves of *B. thailandensis* in MG medium ± 0.01% GS (w/v) added at mid-log phase (red arrow) and harvested 30 min post-exposure (black arrow). (*C*) Fluorescent *B. thailandensis* cells were observed under 1000× magnification. The section of the membrane containing a single bacterium was drawn and cut by the focused laser (green line) and catapulted at a distance from the cell with unfocused low-intensity laser beam (blue spot), which aseptically catapulted and isolated the single cell into the lid of a 0.2-mL PCR tube containing the cell lysis buffer. (*D*) Bright-field mode showing the section of the membrane where the single bacterium had been. (*E*) Fluorescence mode confirming that the bacterium of interest has been transferred from the membrane slide to the PCR tube lid.

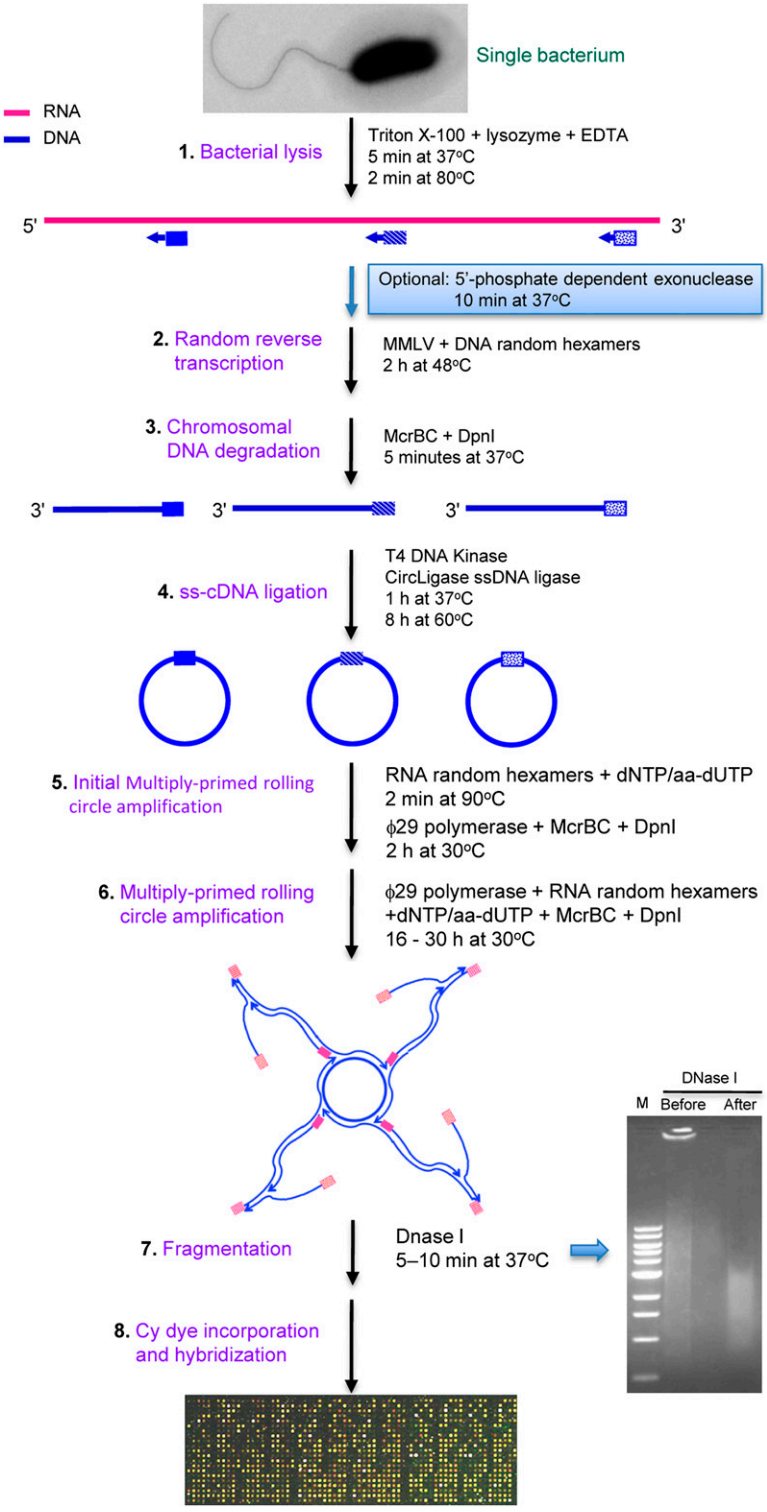

Figure 2. Single-bacterium total transcript amplification strategy. This strategy is developed based on multiply primed rolling circle amplification of circularized cDNA using φ29 DNA polymerase. Blue boxes indicate DNA random hexamers, and pink boxes indicate RNA thiophosphate-linked random hexamers. The purpose and components of each step are indicated (for further details, see text). Abbreviations are as follows: aa-dUTP indicates 5-(3-aminoallyl)-2′-deoxyuridine-5′-triphosphate; dNTP, deoxyribonucleotide triphosphate; DpnI, restriction endonuclease from *Diplococcus pneumoniae*; EDTA, ethylenediaminetetraacetic acid; φ29 polymerase, DNA polymerase from a *Bacillus subtilis* phage Phi29; M, 1 kb DNA marker from New England BioLabs; McrBC, *E. coli* homing endonuclease; MMLV, Moloney murine leukemia virus reverse transcriptase; and ss-cDNA, single-stranded cDNA.

B. thailandensis cells were isolated (Fig. 1C–E) and subjected to a lysis step with the nonionic detergent Triton X-100, EDTA, and lysozyme (Fig. 2). At this point, an optimal 5′-phosphate–dependent exonuclease step can be incorporated to remove rRNA and tRNA to enrich for mRNA, if the end product of the TTA method is to be used for deep sequencing (see Methods and below). Otherwise, cDNA synthesis was performed thereafter with DNA random hexamers and MMLV reverse transcriptase. McrBC and DpnI were added to remove bacterial chromosomal DNA and any potentially contaminating DNA, which are methylated and will be digested by these enzymes. The newly synthesized single-stranded (ss) cDNA (ss-cDNA) was 5′-end phosphorylated and ligated intramolecularly with CircLigase ssDNA ligase, which will not ligate ss-DNA <15 bp (e.g., excess random hexamers). The circularized ss-cDNA was then randomly primed with RNA hexamers and subjected to MDA with φ29 DNA polymerase. The use of thiophosphate-linked RNA random hexamers is critical to reduce falsely primed DNA by-product and primer dimers, while not interfering with the DNA synthesis (Takahashi et al. 2009). The thiophosphate-linked RNA random hexamers are also stable in the presence of φ29 DNA polymerase RNase activity (Lagunavicius et al. 2008). The φ29 DNA polymerase amplification was split into two steps (steps 5 and 6, Fig. 2), where the initial step was performed in a small total volume (~10 μL) to increase the template and substrate concentrations. The second MDA step was performed by adding another 90 μL of a φ29 DNA polymerase and substrate mixture to increase the cDNA yield. As a precaution, we included McrBC and DpnI endonucleases again to prevent amplification of potentially contaminating DNA during the MDA steps of circularized cDNA. The highly polymerized double-stranded (ds) cDNA (ds-cDNA), labeled with 5-(3-aminoallyl)-2′-deoxyuridine-5′-triphosphate (aa-dUTP), was fragmented to ~1–4 kb and incorporated with Cy dyes for microarray analysis (Fig. 2).

There are several advantages of this novel single-cell TTA method. In this study, the φ29 DNA polymerase provides rapid and efficient amplification from starting materials of a single cell with minimal fold-change bias (below). Several strategies were employed to eliminate template-independent amplification, including the use of thiophosphate-linked RNA random

hexamers as previously described (Takahashi et al. 2009), elimination of exogenous DNA contamination with endonucleases (McrBC and DpnI), and minimization of the reaction volume (10 μL for initial amplification and 100 μL total). All manipulations were performed from beginning to end in a single tube in a PCR chamber. In addition, this simple method is not labor intensive and requires very few manipulation steps, thereby reducing potential manipulation-derived contaminants. The typical yield of ds-cDNA from a single cell is ~25–30 μg, sufficient for microarray analysis (Fig. 3). If more ds-cDNA is required and further amplification is necessary for the technical microarray replicates below, additional φ29 DNA polymerase and substrate mixture can be added to the original amplification tube containing ~25–30 μg of ds-cDNA. This will increase ds-cDNA yield to ~75–90 μg.

Microarray analysis of genes expressed at the single-cell level

Our final TTA method amplifies and detects ~94%–96% of the total transcripts detectable by microarray (2842 genes), using from five cells down to the single-cell level. Although ~10 μg of labeled ss-cDNA is sufficient for nonamplified samples in a typical microarray experiment, our amplified product is ds-cDNA. Therefore, to optimize single-cell microarray experiments for our amplified samples, we initially performed TTA on groups of five *B. thailandensis* cells and used different amounts of the amplified cDNA for each microarray slide (Fig. 3). When 10–14 μg of amplified cDNA from TTA of the five cells was used, ~10.8% of the transcripts were not amplified to an amount detectable by microarray, while expression of these genes was detectable in the nonamplified samples (Fig. 3A). Increasing the amount of amplified cDNA used in microarray experiments to 20–25 μg reduced "drop-outs" to ~4.1% (Fig. 3B). Further increasing the amount of amplified cDNA used to 30–35 μg did not significantly reduce the percentage of genes that was missing from the amplified samples (~4.4%) (Fig. 3C). We next attempted amplification of total transcript from a single cell for microarray analysis, and the results were once again significantly improved at the higher concentration of cDNA used (Fig. 3E–G). To determine the reason for these missing genes (drop-outs) from the microarray data in the amplified samples, we examined their GC content, operon size, RNA secondary structure, or gene expression variation among the individual cells of the population (Supplementary Analysis). These analyses revealed these missing genes resulted from their low expression levels, which suggests the low abundance of their transcripts causes "drop-out" of these genes in the amplified samples (Fig. 3D,H). Although there were good Pearson correlations between the fold-change of the amplified and nonamplified samples in all these experiments (Fig. 3A–C, E–G), we recommend using 30 μg of amplified cDNA in a typical microarray experiment, as this amount of cDNA used yielded a minimal number of genes absent from the microarray data (~4%–5% drop-outs) (Fig. 3C,G).

Having optimized the amount of amplified cDNA (30 μg) to use in microarray experiments, we performed biological (Fig. 4A–C) and technical replicates (Fig. 4D) to obtain fold-change data from 2 pg of diluted total RNA to an actual single cell. Initially, microarray experiments were performed in triplicate using three independent amplifications of 2 pg of purified and diluted RNA. We correlated the fold-change of the amplified to nonamplified

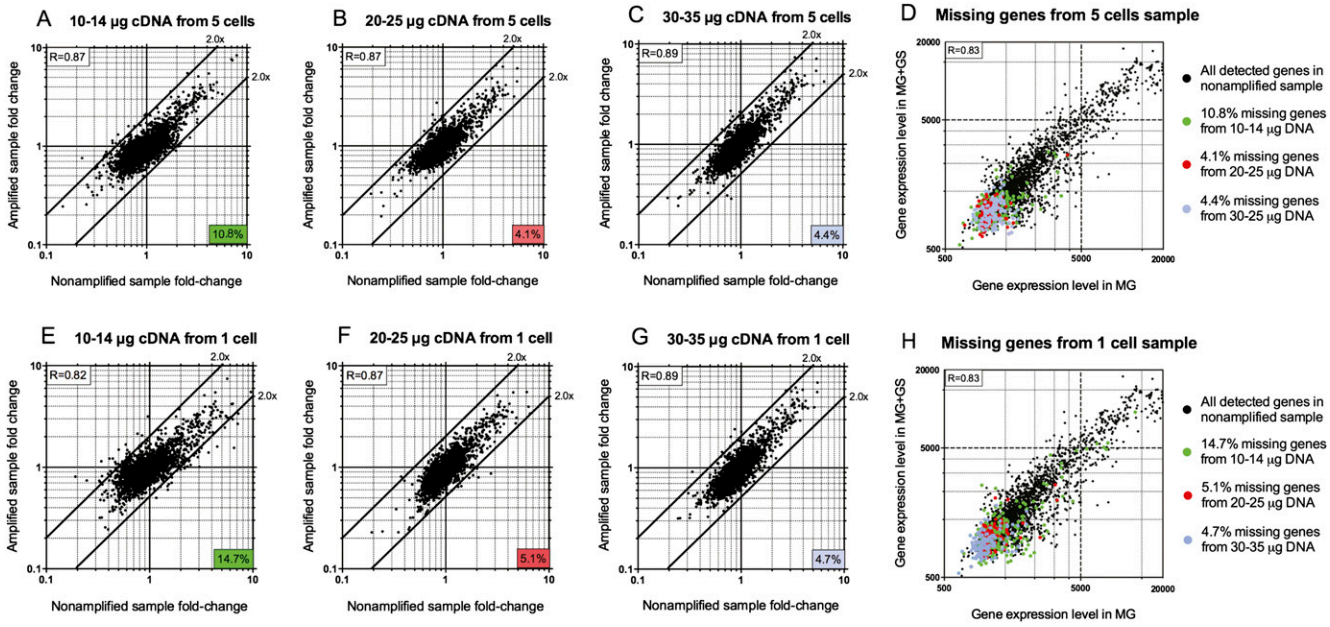

Figure 3. Fold-change scatter plots of expressed genes obtained from nonamplified versus amplified samples. 10–14 μg (*A*), 20–25 μg (*B*), or 30–35 μg (*C*) of DNA amplified from five-cell samples were hybridized to different slides, and the fold-changes of detected genes were plotted against those obtained from the nonamplified sample. The number located at the *right bottom* corner of each plot indicates the percentage of missing genes (drop-outs) from each amplified sample compared with the nonamplified sample (2842 genes total). (*D*) Gene expression levels from the nonamplified sample (black dots) were compared between two growth conditions (MG ± 0.01% GS). Expression levels of genes that were missing in the five-cell amplified samples are colored green (as a result of using 10–14 μg of cDNA), red (using 20–25 μg of cDNA), or purple (using 30–35 μg of cDNA), and are overlaid on the same graph in *D*. Similar comparisons were conducted with different amounts of cDNA amplified from one-cell samples: 10–14 μg (*E*), 20–25 μg (*F*), or 30–35 μg (*G*). Missing genes or drop-outs from each sample were color-coded similarly and overlaid with the total number of genes detected in the nonamplified samples (*H*). The *R* value in the *upper left* corner of each plot represents the Pearson correlation coefficient. All microarray experiments in this figure were conducted without the optional mRNA enrichment step.

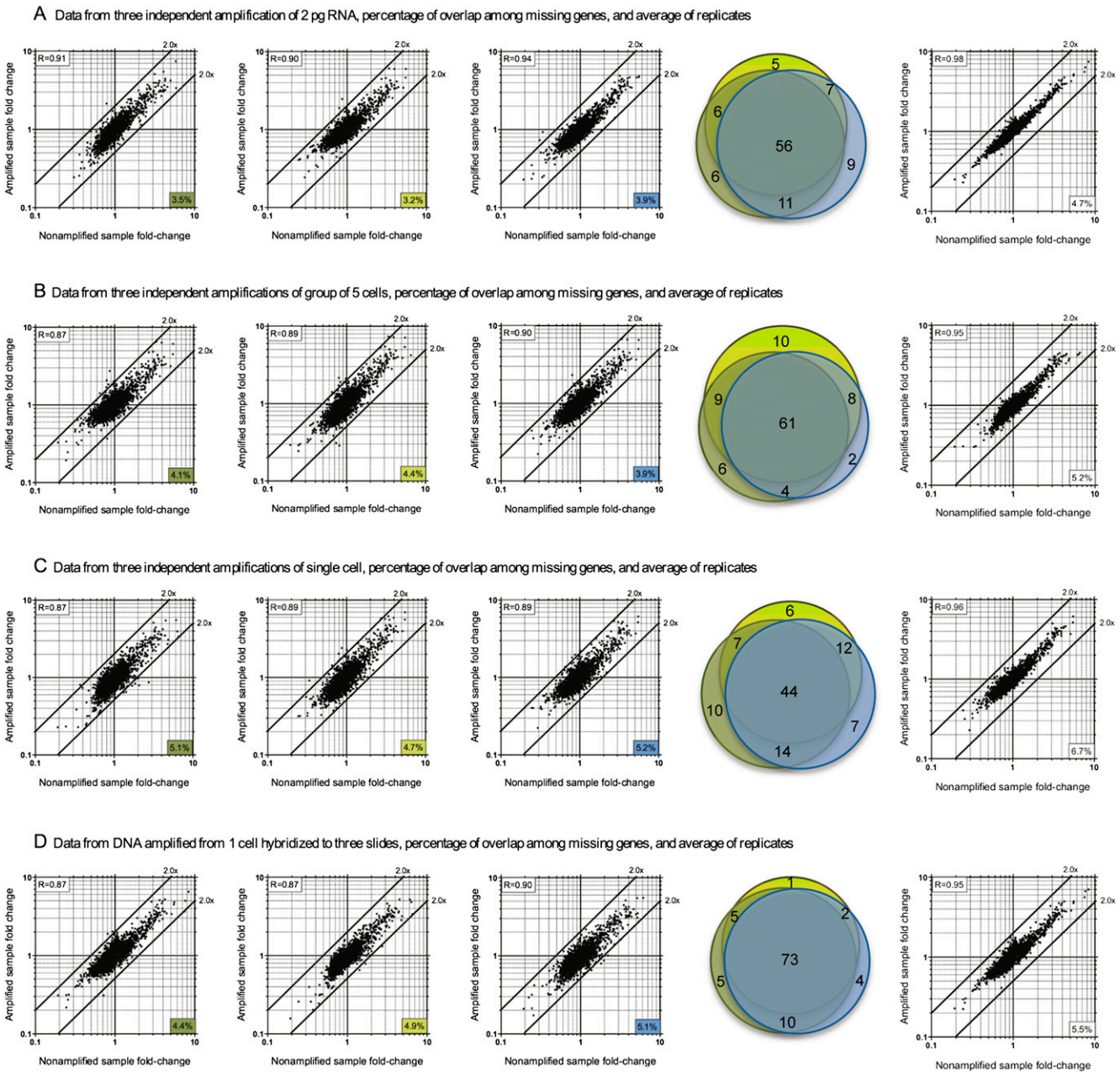

Figure 4. Microarray data fold-change comparison of nonamplified and amplified samples starting from 2 pg of diluted RNA (*A*), five cells (*B*), or one cell (*C*) as biological replicates; or a single cell hybridized to three different slides as technical replicates (*D*). The first three plots of each item are biological replicates (*A–C*) or technical replicates (*D*). The number in the *bottom right* corner of each plot indicates the percentage of genes that were missing in the amplified samples compared to the nonamplified samples. The Pearson correlation coefficient between the amplified and nonamplified fold-change data is shown at the *upper left* corner of each plot. The high correlation coefficient values ($P < 0.0001$) and the tight grouping of the dots within the twofold difference boundaries suggest a relatively low bias. The percentages of overlap among missing genes from each group are displayed as area-proportional Venn diagrams of three independent biological (*A–C*) or technical replicates (*D*). The color for each circle in the Venn diagram corresponds to the colored boxes in each scatter plot. The last plot of each item shows averaged data from the three biological (*A–C*) or technical replicates (*D*). All microarray experiments in this figure were performed without the optional mRNA enrichment step.

sample (Figs. 1A, 4A). Each amplified replicate produces ~3.2%–3.9% gene drop-outs, and the Venn diagram for the missing genes among these replicates indicated significant overlap among these low abundance transcripts (Fig. 4A). The averaged data from the triplicates showed excellent Pearson correlation of the fold-change to those of the nonamplified samples ($R = 0.98$) (Fig. 4A). A total of 4.7% drop-out genes in the averaged data indicated that we successfully amplified and detected ~95% of the total transcript expressed relative to the nonamplified sample when starting with 2 pg of purified total RNA. Similar results were observed for three groups of five cells (Fig. 4B). When microarray data were obtained from three individual single cells as biological replicates, comparable fold-change correlations and percentages of missing genes were observed (first three graphs of Fig. 4C). The averaged data

showed excellent correlations ($R = 0.96$), with 93.3% of the transcripts from single cells amplified and detected compared with the nonamplified sample (last graph of Fig. 4C). Technical replicates, where single-cell transcripts were amplified to sufficient level for three microarray slides, were relatively reproducible, confirming the consistency among different microarray experiments (Fig. 4D). An important point to note is that, in the averaged data, there was very little fold-change bias or skewing as a result of the amplification of transcripts from a single cell, and fold-change variations of all detectable genes were significantly less than a two-fold difference (i.e., all dots lie well within the 2× difference lines in Fig. 4). The averaged data set from three TTA replicates of a single cell (Fig. 4C) indicated that reliable data could be generated by using this TTA method, and >93% of the transcripts from a single cell could be amplified and detected in microarray experiments.

Correlation of the gene expression levels between amplified single cells versus nonamplified control and independent single cell amplifications was also analyzed (Supplemental Fig. S2). Expression levels from single cell amplified and nonamplified samples were poorly correlated (Supplemental Fig. S2A,B), indicating significant amplification bias, probably due to different amplification efficiencies among individual genes. However, correlations among transcripts amplified from independent single cells were significantly higher (Supplemental Fig. S2C,D), indicating more consistent amplification efficiencies for any particular gene in the two cells. Thus, any amplification bias of different genes due to differences in amplification efficiencies would "cancel out," when comparing gene expression levels in single cells of two conditions to obtain fold-change. Much like real-time RT-PCR comparison to obtain reliable gene expression fold-change, amplification efficiencies of a particular gene in two different conditions must be consistent, while amplification efficiency variations between different genes are acceptable. Thus, single cell gene expression profiling using the method described here should be performed and compared between single cells in two different conditions (e.g., GS and no GS). However, this method is not recommended for obtaining gene fold-changes by comparing between amplified and nonamplified samples.

GS-dependent gene expression by single-cell microarray analysis and validation via reporter gene fusions

With the averaged microarray data generated from the TTA of a single bacterium performed in technical triplicates (Fig. 4D), we assembled a list of genes that were induced or repressed in the presence of GS (Supplemental Tables S1, S2). We chose five genes up-regulated in the presence of GS, three genes down-regulated by GS, and two control genes with no fold-change (Supplemental Table S3) to perform reporter-gene fusions with *lacZ* and *gfp* for microarray data confirmation. The genes selected for microarray validation are involved in amino acid metabolism (Fig. 5A). After 2 and 4 h exposure to GS, increased green fluorescence signals and β-galactosidase activities indicated that the expression of the five genes up-regulated in our microarray data did increase as a result of GS (Fig. 5B,C). As indicated by the fluorescence signals and β-galactosidase activities, expression levels of the three genes down-regulated in the microarray data also decreased as a result of GS, while expression levels of the two control genes showed only insignificant changes (Fig. 5B,C). Overall, gene fusion experiments and the fold-change from the nonamplified sample microarray data showed strong agreement to the single-cell amplified samples microarray data (Fig. 5). Only a few genes in the single-cell data with a fold-change of two or more were less than two in the nonamplified data (potential false positives) (Supplemental Tables S1 and S2). However, the majority of the genes expressed comparably in the amplified and nonamplified samples, suggesting a strong and reliable correlation between the fold-change data generated from single cells and large-scale nonamplified samples (Fig. 4D; Supplemental Tables S1, S2).

Among the up-regulated genes in particular, three genes targeted for validation were responsible for aromatic amino acid (AAA) biosynthesis (BTH_I1295, BTH_I2909, and BTH_I3337) and two genes were responsible for shuffling benzoate and alanine to possibly replenish central pathway intermediates (BTH_I0506 and BTH_II0922) (Fig. 5A). Of the three genes down-regulated due to GS, two targeted genes convert pyruvate in the synthesis of other amino acids, potentially balancing other amino acid species (e.g., Met, Ile, and Val), and one gene was involved in conversion of TCA cycle intermediates (Fig. 5A). It seems that GS not only affects the EPSPS target (Fig. 5A) and reduces AAA synthesis but also has an overall influence on the amino acid pool. Reducing AAA signals a concurrent reduction in other amino acids (Met, Ile, Val, and Ala) to balance the cellular amino acid population.

Potential application to next-generation sequencing

We next evaluated if this TTA method can be used for transcriptome analysis by deep sequencing. RNA-seq methods for prokaryotes require mRNA enrichment to eliminate rRNA and tRNA, which can be upward of 90%–95% of the total RNA in the cell, to reduce the number of reads and costs. Additionally, transcriptome profiling by deep sequencing is less tolerant of potential contaminants or nonspecific amplification. Therefore, we analyzed our TTA products using real-time RT-PCR and Sanger sequencing to assess the potential use of this method for transcriptome analysis by deep sequencing. An mRNA enrichment step was added to our amplification method to amplify transcripts from single cells (Fig. 2). By real-time RT-PCR, we then analyzed amounts of rRNAs (23S and 16S) and a tRNA (Ala) relative to the mRNA amount of one gene (BTH_I2028) before and after enrichment in amplified single cell samples grown in MG medium (Fig. 6). The amounts of rRNAs and one tRNA species were significantly reduced after enrichment, relative to the mRNA transcript of BTH_I2028 (Fig. 6). A microarray analysis was then performed on the enriched or unenriched samples amplified from single cells grown in MG medium (same as the real-time experiment above) and MG + GS medium. Data from the enriched sample showed low fold-change bias resulting from the enrichment, with an optimized amount of 5′-phosphate–dependent exonuclease ($1\times = 1 \times 10^{-5}$ units of enzymes). However, a higher level of amplification bias was observed when more exonuclease ($10\times = 1 \times 10^{-4}$ units of enzymes) was used, possibly due to nonspecific digestion of mRNA (Fig. 6).

Single-cell cDNA libraries were constructed to analyze the purity of our enriched and amplified ds-cDNA to determine the potential for RNA-seq application (Supplemental Fig. S3). Sanger sequencing reads of 96 independent clones from each of the unenriched and enriched cDNA libraries were analyzed, and ~96% (188 out of 192) matched to *B. thailandensis* sequences (Supplemental Table S4). Approximately 4% did not match to any sequences in GenBank. This is typical in RNA-seq experiments, where ~5% of sequences cannot be assigned (i.e., no match) (Yoder-Himes et al. 2009). This demonstrated the effectiveness of the strategies to

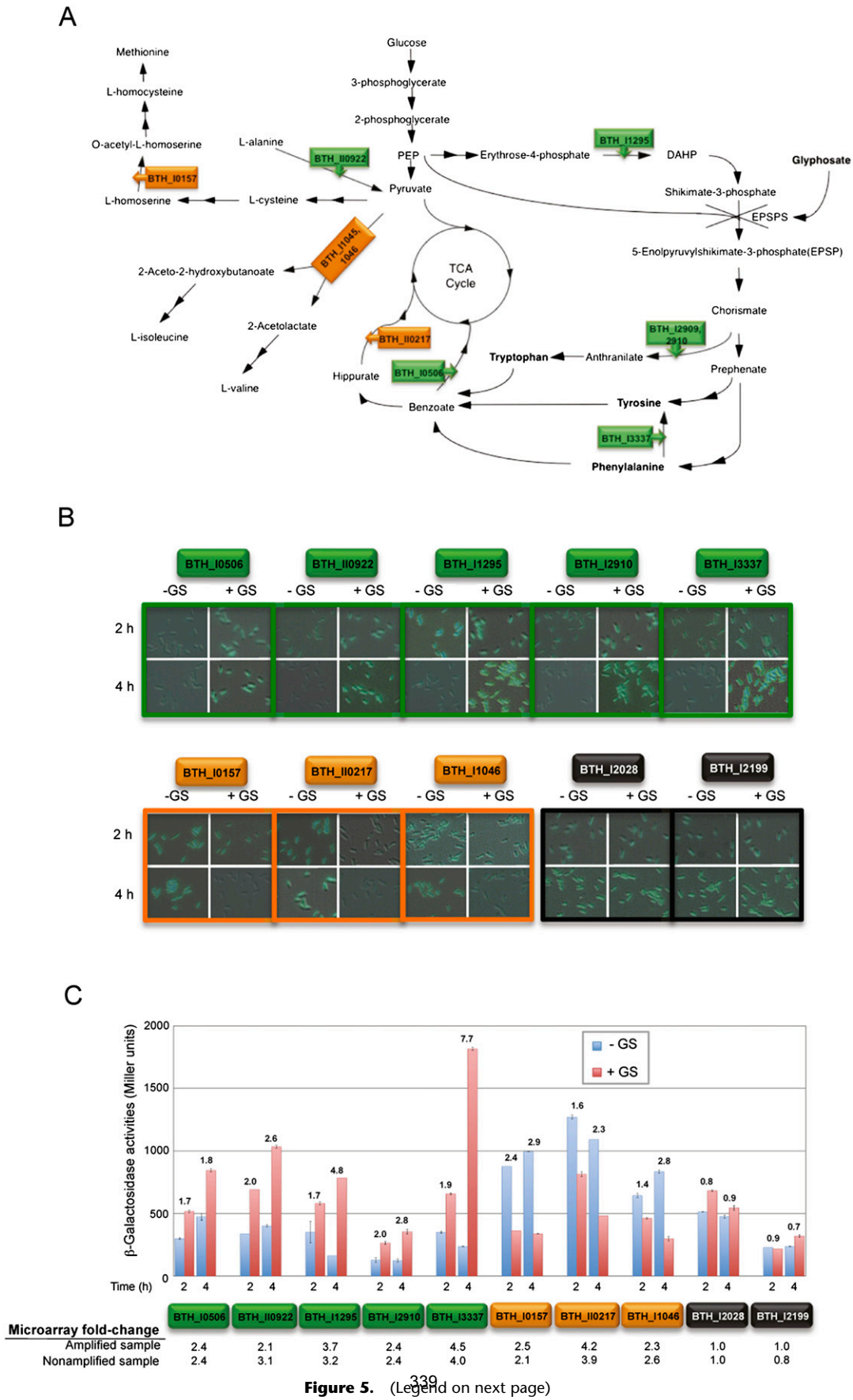

Figure 5. (Legend on next page)

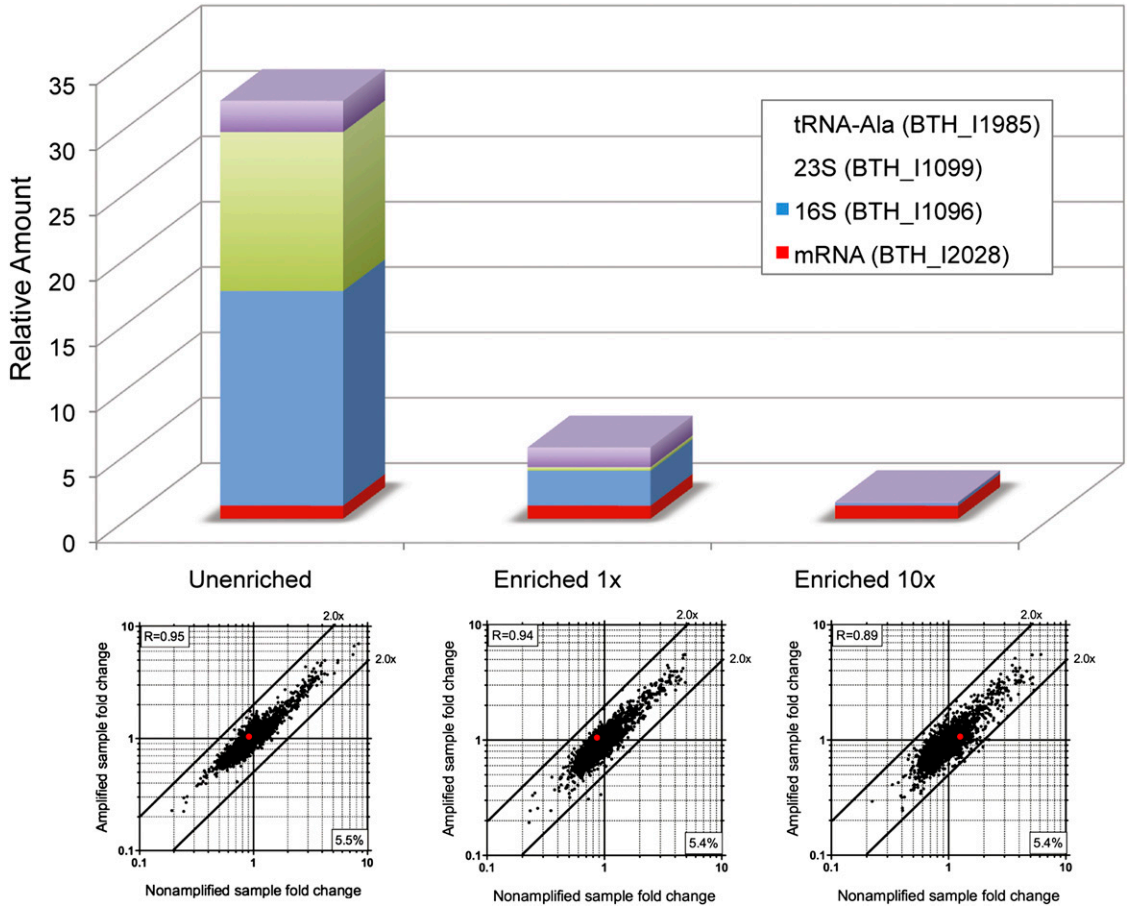

Figure 6. Evaluation of mRNA enrichment in amplified single cell samples. *Top* panel presents mRNA amount of a gene (BTH_I2028) relative to genes of 16S rRNA, 23S rRNA, and a tRNA-Ala detected by real-time RT-PCR. Unenriched represents amplified sample without the mRNA enrichment step. Enriched (1× or 10×) means treated with 1×10^{-5} U (as described in Methods) or 1×10^{-4} U of the Terminator 5′-Phosphate–Dependent Exonuclease, respectively. The relative transcriptional levels of rRNAs and tRNA are significantly higher than the BTH_I2028 gene (mRNA) in the unenriched sample but are greatly reduced in the enriched samples. Microarray analysis was performed for amplified samples (enriched and unenriched); fold-changes were compared to nonamplified samples as shown in the *bottom* plots. Fold-change correlation for the BTH_I2028 gene is indicated by the red dots. The number at the *bottom right* corner represents the percentage of transcripts that were missing in the single cell. Enrichment with 10× the amount of 5′-phosphate–dependent exonuclease resulted in a slightly higher fold-change bias as indicated by the Pearson correlation coefficient shown at the *upper left* corner for each plot.

eliminate template-independent amplification and exogenous DNA contamination. The significant reduction of rRNA sequences in the enriched sample was confirmed by both real-time RT-PCR and sequencing data, suggesting successful depletion of rRNAs in the enrichment step. Taken together, these results showed promise to apply our TTA method for transcriptome profiling by deep sequencing, which may allow detection of low abundance transcripts that were drop-outs in our less sensitive microarray analysis approach.

Discussion

There are currently no published methods for single prokaryotic cell TTA. However such a method is desperately needed if we are to expand multiple areas in prokaryote functional genomics (Supplemental Fig. S1). The model used in this study, *B. thailandensis* exposed to GS, was appropriate and sufficient for assessment of our TTA method because we could compare the transcriptomic fold-change data obtained from single cells to data obtained from the

Figure 5. Validation of microarray data via reporter-gene fusions. (*A*) Proposed amino acid metabolism pathways influenced by glyphosate (GS) in *B. thailandensis*. Two connecting arrows indicate two or more reaction steps. The target for GS is 5-enolpyruvylshikimate-3-phosphate synthase (EPSPS) (Fischer et al. 1986). In *A, B,* and *C,* green and orange boxes indicate genes induced and repressed, respectively, by GS. (*B,C*) *gfp* and *lacZ* reporters were fused to five GS-induced genes, three GS-repressed genes, and two GS-insensitive control genes (housekeeping gene controls in black boxes). (*B*) Cells were examined under 630× magnification at 2 and 4 h post-exposure to GS. Differential interference contrast (DIC) and green fluorescence images were merged, and the representative fields are shown. (*C*) At the same time points, β-galactosidase activities for these fusion strains were determined in triplicate, and the Miller units were plotted with the SEM. The numbers *above* the bars in the histogram in *C* indicate fold-induction or fold-repression differences by GS, as measured by β-galactosidase assays. For comparison, the microarray data fold-change of the corresponding genes from the amplified sample and the nonamplified sample are also displayed *below* the graph. As a general trend, these gene-fusion data agree with the microarray data at both 2 and 4 h post–GS-exposure.

larger-scale nonamplified RNA samples. Since there were excellent microarray data correlations of fold-change between the amplified and nonamplified samples in this study and the differences were significantly less than twofold when three replicates were averaged (Fig. 4), we are confident that the fold-changes generated from TTA of single cells between two different conditions are reliable (Supplemental Tables S1, S2). In summary, we have developed a single-tube TTA method that is simple, requiring very few steps. This method yielded reproducible data, low fold-change bias, and a high number of genes efficiently amplified from a single prokaryotic cell (94%–96% presence or low transcript drop-out as detectable by microarray).

We envisage that the method described will be used for transcriptome analysis by deep sequencing (Croucher et al. 2009; Passalacqua et al. 2009) of the amplified ds-cDNA, with an optional step to eliminate rRNAs and tRNAs for enrichment of mRNA (Figs. 2, 6). Deep sequencing may increase the dynamic range of detectable genes expressed to include low or highly expressed genes that may not be detectable or differentiated by microarray (Wang et al. 2009), and this may decrease or eliminate drop-outs. The limitation of this method is that antisense transcripts are not detectable, because the final product of our TTA method is ds-cDNA, and thus it is not strand specific (Vivancos et al. 2010). Our method yielded ds-cDNA, which could potentially be used in tiling arrays, possibly identifying untranslated regions and novel operons (Toledo-Arana et al. 2009). Hence, this method, beyond microarray, has the potential to detect global gene expression of a single cell, novel operons, and novel coding and noncoding regions (Sorek and Cossart 2010) in both cultured and noncultured prokaryotes (Supplemental Fig. S1).

Finally, we envisage that our method can be applied to single eukaryotic cell transcript amplification. This could be performed by substituting the DNA random hexamers to a poly(T) oligo during cDNA synthesis, and an mRNA enrichment step is not necessary. The remaining steps of the protocol are otherwise identical.

Methods

Bacterial strains, media, and culturing conditions

Escherichia coli EPMax10B-*lacI*^{q}-*pir* (Norris et al. 2010) was routinely used as a cloning strain. The *B. thailandensis* wild-type strain, E264 (Brett et al. 1998), and its derivatives were cultured in LB or 1× M9 minimal medium (Sambrook and Russell 2001) supplemented with 20 mM glucose (MG). For the *B. thailandensis* microarray and reporter-gene fusion studies (Fig. 5B,C), *B. thailandensis* wild-type strain E264 and derivatives were grown in MG medium + 1% (w/v) Brij-58 and exposed to a final concentration of 0.01% (w/v) GS. Brij-58 (1% w/v) was added to all cultures to prevent bacterial clumping during growth.

Molecular reagents

T4 polynucleotide kinase, dNTPs, MMLV (Moloney murine leukemia virus) reverse transcriptase, and endonucleases (McrBC and DpnI) were purchased from New England Biolabs. Ready-Lyse lysozyme, Terminator 5′-Phosphate–Dependent Exonuclease, CircLigase ssDNA ligase, and φ29 DNA polymerase were purchased from Epicentre Biotechnologies. Inorganic pyrophosphatase was purchased from Roche Applied Science. TRIzol reagent, RNaseOut reagent, RNase-free DNA random hexamers, and Live/Dead BacLight cell stain were purchased from Invitrogen. The RNeasy Mini Kit and RNAprotect reagent were purchased from Qiagen. DNA oligonucleotide primers and random RNA hexamers with five thiophosphate-linkages (6R5S) (Takahashi et al. 2009) were synthesized through Integrated DNA Technology (IDT). DNase I, aminoallyl-dUTP (aa-dUTP), and all the other chemicals used in this study were purchased from Sigma. Cy3 and Cy5 dyes were purchased from Amersham Biosciences.

Single bacterium level transcript preparation

Large-scale total RNA was extracted from *B. thailandensis* wild-type cells (Fig. 1A) using TRIzol reagent and purified with the RNeasy Mini Kit by following the manufacturer's total RNA cleanup protocol. Two picograms of RNA, representing the single bacterium level of RNA, was prepared by serially diluting the purified total RNA to a final concentration of 10 pg/μL in DEPC water containing 1 U/μL of RNaseOut. Then, 0.2 μL (2 pg) of the final dilution was directly added to 2 μL of the lysis buffer (100 mM Tris-Cl at pH 8.0, 200 mM KCl, 0.2 mM EDTA, 0.1% Triton X-100, 2 mM DTT, 0.04 U/μL RNaseOut, 2×10^{-7} U/μL Ready-Lyse lysozyme).

Single bacterium isolation

For single cell isolation, *B. thailandensis* cells were treated with RNAprotect reagent, and stained with Live/Dead BacLight fluorescent dyes. Stained cells were then smeared onto a PALM membrane Frameslide (Carl Zeiss), and observed under 1000× magnification on the Zeiss LCM system. Sections of membrane containing one or five fluorescent bacteria were cut by the focused laser and catapulted with unfocused low-intensity laser beam into 2 μL of the lysis buffer contained within a 0.2-mL PCR tube lid. The cDNA synthesis and amplification of the single cell total transcript were then performed as below.

Single bacterium transcript amplification

The *B. thailandensis* cells or diluted 2 pg total RNA was incubated in the lysis buffer for 5 min at 37°C, then heated for 2 min to 80°C. When necessary (e.g., RNA-seq is used rather than microarray), an optional mRNA enrichment step should be performed here. A 0.5 μL of the enrichment mixture (1×10^{-5} U Terminator 5′-Phosphate–Dependent Exonuclease and 5 nmol $MgCl_2$) is added and incubated for 10 min at 37°C. A 2 μL aliquot of RT mixture was then added, consisting of 4 U RNaseOut, dNTPs (0.25 nmol each), preheated DNA random hexamers (0.2 pg for one cell, 1 pg for five cells, or 2 pg for 2 pg diluted total RNA), 10 nmol $MgCl_2$, and 2 U MMLV. The reverse transcription was carried out for 2 h at 48°C. A 0.24 μL aliquot of endonucleases mixture (4 nmol GTP, 1 U McrBC, and 2 U DpnI) was then added to each tube, followed by incubation for 15 min at 37°C to degrade the chromosomal DNA. ss-DNA phosphorylation and ligation were accomplished by adding a 0.7 μL aliquot of the ss-DNA ligation mixture (0.25 nmol ATP, 12.5 nmol $MnCl_2$, 1 U T4 polynucleotide kinase, 10 U CircLigase ss-DNA Ligase) to each tube followed by incubation for 1 h at 37°C and then for 8 h at 60°C for ligation. The circularized ss-DNA (~5 μL) was then used as template in a two-step multiply primed rolling circle amplification (MPRCA) reaction as follows. First, a 25 mM dNTP/aa-dUTP stock was prepared following an established protocol, where a 1:2 dTTP:aa-dUTP ratio was used to efficiently label DNA with high GC% (http://pfgrc.jcvi.org/index.php/microarray/protocols.html). A 4.5 μL mixture (1× φ29 reaction buffer, 20 nmol DTT, 0.5 μL dNTPs/aa-dUTP stock, 15 pmol of RNA random hexamers 6R5S, and 4 nmol GTP) was then added, followed by heating for 2 min to 90°C then immediate cooling on ice. McrBC (2 U, 0.2 μL) was then added to each tube and incubated

for 5 min at 37°C. Fifty units of φ29 polymerase (0.5 μL) was added, followed by incubation for 2 h at 30°C to initiate the MPRCA reaction in a small total volume (~10 μL). After the initial MPRCA, a larger volume (90 μL) of the MPRCA mixture (1× φ29 reaction buffer, 360 nmol DTT, 4.5 μL dNTPs/aa-dUTP, 150 pmol RNA random hexamers, 100 U φ29 polymerase, 90 nmol GTP, 5 U McrBC, 10 U DpnI, and 20 U pyrophosphatase) was added, and the reaction was carried out for another 32 h at 30°C. After this step, the cDNA yield is typically 25–30 μg. For the higher yields (75–90 μg) required to perform microarray technical replicates, another 200 μL of the MPRCA mixture (1× φ29 reaction buffer, 800 nmol DTT, 10 μL dNTPs/aa-dUTP, 300 pmol RNA random hexamers, 200 U φ29 polymerase, 200 nmol GTP, 10 U McrBC, 20 U DpnI, and 40 U pyrophosphatase) was added to the reaction. The reaction mixture (300 μL total) was then aliquoted into three 0.2-mL PCR tubes and incubated for another 16 h at 30°C. After amplification, the reaction was stopped by heat-inactivation at 65°C for 10 min. The newly synthesized double-stranded cDNA was then randomly fragmented to 1–4 kb in length with DNase I and extracted with phenol/chloroform (1:1). Fragmented cDNA was precipitated with 0.1 volume of 3 M sodium acetate (pH 5.2) and 3 volumes of isopropanol and then incubated at −80°C for 1 h. The DNA pellet was then collected by centrifugation at 20,000*g* for 10 min, washed with 70% ethanol, and vacuum dried.

Two-color microarray and data analysis

For microarray analysis of the nonamplified samples, cDNA was synthesized from 10 μg of total RNA following established protocols (http://pfgrc.jcvi.org/index.php/microarray/protocols.html). Typically, 8–12 μg of nonamplified cDNA or 25–30 μg of amplified cDNA was used for each condition in microarray hybridization. Both the nonamplified and amplified cDNA were labeled with Cy3 (no-GS condition) and Cy5 (GS condition) dyes and then hybridized to the *B. thailandensis* 70-mer triplicate arrays (GEO accession number GPL7113) following the established protocols (http://pfgrc.jcvi.org/index.php/microarray/protocols.html). Microarray slides were scanned with a GenePix 4000B microarray scanner using GenePix Pro software 5.1. Individual TIFF images from each channel were processed with Spotfinder software 3.2.1 (available at http://www.tm4.org) to quantify the gene expression levels. Raw microarray data were processed and normalized by low intensity filtering, total intensity normalization, LOWESS normalization, standard deviation regularization, and in-slide replicate analysis using MIDAS software 2.21 (available at http://www.tm4.org). Finally, normalized gene expression data were used to generate data tables using MEV software 4.5.1 (available at http://www.tm4.org).

Fold-change data for all detected genes were obtained from triplicates of the nonamplified or amplified samples. GS-induced genes (fold-change ≥ 2, $P \leq 0.05$) are summarized in Supplemental Table S1, and GS-repressed genes (fold-change ≥ 2, $P \leq 0.05$) are summarized in Supplemental Table S2.

Scatter plots and Venn diagrams

GraphPad Prism 5 software was used generate all scatter plots and calculate the correlation coefficients in Figures 3, 4, and 6 and Supplemental Figure S2. The area-proportional Venn diagrams were drawn based on images generated using a free online software (http://bioinforx.com/free/bxarrays/venndiagram.php).

Gene assignment and pathway designation

Gene description assignment for some genes was assisted by reference to the *Burkholderia* Genome database (http://www.burkholderia.com). Genes involved in the GS pathway (Fig. 5A) were assigned according to the Kyoto Encyclopedia of Genes and Genomes (KEGG).

Microarray data validation via gene fusion studies

Eight genes predicted to be involved in the GS pathway (Fig. 5A) and two controls genes were chosen for validation of the microarray data. Two promoter-less reporter-genes, *gfp* and *lacZ*, were integrated downstream from each target gene via two-step λ red protein-mediated recombineering (data to be published elsewhere). Briefly, the *gfp-pheS-gat* fragment was amplified from pUCP28T-*gfp-pheS-gat* (laboratory plasmid) using oligos containing 40–45 bp homologous sequences to the downstream region of the target gene. The PCR product was then integrated downstream from the target gene after the stop codon to make a transcriptional fusion in the *B. thailandensis* chromosome via λ red protein-mediated recombineering. Positive integration was selected on 1× M9 minimal medium supplemented with 0.04% (w/v) GS and screened by PCR. Next, the second λ red protein-mediated recombineering was accomplished by introducing the *lacZ* fragment (with the 5′-end homologous to the downstream region of the *gfp* gene, and the 3′-end homologous to the downstream region of the *gat* gene) to replace the *pheS-gat* fragment. The final *gfp-lacZ* fusion strains were obtained via *pheS* counter-selection on cPhe-containing media, as previously described (Barrett et al. 2008), and confirmed by PCR using oligos which anneal to the target genes and the *lacZ* gene.

These newly engineered fusion strains were first grown in LB medium overnight. Cells were harvested by centrifugation, washed twice with 1× M9 minimal medium, and resuspended in the same medium. Resuspended cells were diluted 100× into MG medium + 1% (w/v) Brij, and two identical cultures of each fusion strain were grown to mid-log phase, at which point GS was added to one of the cultures to a final concentration of 0.01% (w/v). At 2 and 4 h post-exposure to GS, samples of both cultures (with and without GS) were taken for fluorescence microscopy and β-galactosidase assay. To immobilize bacteria for fluorescence microscopy, cells were mixed with warm (42°C) molten agarose to a final concentration of 0.1% (w/v) and were immediately mounted between glass slides and coverslips to solidify the agar. Fluorescence was observed under the 38HE filter set on a Zeiss Axio Observer D1 microscope, and images were recorded with an AxioCam MRc 5 camera. Differential interference contrast (DIC) and green fluorescence images were merged at the time of capture using Zeiss AxioVision software. Multiple images were captured for each sample, and representative fields are shown in Figure 5B. β-Galactosidase assay (Sambrook and Russell 2001) was performed in triplicate on these fusion strains, and average activities are shown in Figure 5C with SEM. For comparison of the fold-change data from the microarray and β-galactosidase assay, the GS-induced gene fold-changes were calculated as the gene expression levels in the presence of GS divided by those in the absence of GS; the GS-repressed or GS-insensitive gene fold-changes were calculated based on gene expression levels in the absences of GS, divided by gene expression levels in the presence of GS.

Microarray data accession number

Microarray data are available in the NCBI GEO repository under accession number GSE23419.

Real-time RT-PCR

Primers and probes for each target were designed using Integrated DNA Technologies Primer Quest software (http://www.idtdna.com) and are shown in Supplemental Table S5. Amplified ds-cDNA

from isolated single cells grown in MG medium were used as template for real-time RT-PCR, which was performed as previously described (Son et al. 2007). Real-time PCR was conducted in eight replicates for each target. To control for variations between runs, all PCRs were performed at the same time in one 96-well plate.

We followed the previously reported data analysis method (Peirson et al. 2003) to provide more accurate quantitative real-time PCR data. Real-time RT-PCR data were averaged over eight replicates for each target, and fold-changes were calculated using DART-PCR (Peirson et al. 2003). Accordingly, the average efficiencies of each target are within 4.1% differences (<5%) and permit accurate analysis. The expression level of mRNA BTH_I2028 was taken as 1 for each amplified sample tested, and the amounts of tRNA and rRNAs were normalized relative to this value.

cDNA library construction for sequencing

For construction of the single-cell cDNA library, aliquots of the same preparation of amplified ds-cDNA samples for real-time RT-PCR above were used. Amplified ds-DNA (10 μg) from unenriched or enriched (1×10^{-5} U exonuclease) samples were randomly fragmented with DNase I, blunt-ended with T4 DNA polymerase and 1 mM dNTPs, and ran on a 1% agarose gel. Fragments in two size ranges (0.1–1.5 kb and 1.5–4.0 kb) were extracted from the agarose gel and cloned into the SmaI site of pUC19 vector for library construction (Supplemental Fig. S3). Sanger sequencing reads of the inserts were generated at a local sequencing facility and identified using a homology search with the BLASTn algorithm (http://www.ncbi.nlm.nih.gov).

Competing interest statement

A provisional patent application (no. 61383699, submitted September 16, 2010) has been filed for the single bacterium TTA method described in this paper. T.T.H., Y.K., and M.H.N. are named as the inventors on this patent.

Acknowledgments

This project was supported by Award no. AI065359 from the National Institute of Allergy and Infectious Diseases and by the Center of Biomedical Research Excellence grant P20RR018727 from the National Center for Research Resources of the National Institutes of Health. The content is solely the responsibility of the authors and does not necessarily represent the official view of the funding agencies.

Authors' contributions: Y.K. performed the single-cell TTA, microarray analysis, real-time RT-PCR study, and cDNA library construction. M.H.N. performed the fluorescence microscopy experiments and contributed to data analysis. J.Z-S. contributed to data analysis. W.C.N. generated the *B. thailandensis* microarray slides, provided technical advice and performed critical reading of the manuscript. S.P.D. secured funding for the Carl Zeiss LCM system used in this study, assisted with the single cell isolation training, and critical editing of this manuscript. T.T.H. conceived of the method and supervised the experiments. T.T.H. and Y.K. wrote the manuscript.

References

Barrett AR, Kang Y, Inamasu KS, Son MS, Vukovich JM, Hoang TT. 2008. Genetic tools for allelic replacement in *Burkholderia* species. *Appl Environ Microbiol* **74:** 4498–4508.

Brett PJ, DeShazer D, Woods DE. 1998. *Burkholderia thailandensis* sp. nov., description of *Burkholderia pseudomallei*-like species. *Int J Syst Bacteriol* **48:** 317–320.

Croucher NJ, Fookes MC, Perkins TT, Turner DJ, Marguerat SB, Keane T, Quail MA, He M, Assefa S, Bahler J, et al. 2009. A simple method for directional transcriptome sequencing using Illumina technology. *Nucleic Acids Res* **37:** e148. doi: 10.1093/nar/gkp811.

Emmert-Buck MR, Bonner RF, Smith PD, Chuaqui RF, Zhuang Z, Goldstein SR, Weiss RA, Liotta LA. 1996. Laser capture microdissection. *Science* **274:** 998–1001.

Fischer R, Berry A, Gaines CG, Jensen RA. 1986. Comparative action of glyphosate as a trigger of energy drain in eubacteria. *J Bacteriol* **168:** 1147–1154.

Kurimoto K, Yabuta Y, Ohinata Y, Ono Y, Uno KD, Yamada RG, Ueda HR, Saitou M. 2006. An improved single-cell cDNA amplification method for efficient high-density oligonucleotide microarray analysis. *Nucleic Acids Res* **34:** e42. doi: 10.1093/nar/gkl1050.

Kurimoto K, Yabuta Y, Ohinata Y, Saitou M. 2007. Global single-cell cDNA amplification to provide a template for representative high-density oligonucleotide microarray analysis. *Nat Protoc* **2:** 739–752.

Lagunavicius A, Kiveryte Z, Zimbaite-Ruskuliene V, Radzvilavicius T, Janulaitis A. 2008. Duality of polynucleotide substrates for Phi29 DNA polymerase: 3′→5′ RNase activity of the enzyme. *RNA* **14:** 503–513.

Norris MH, Kang Y, Lu D, Wilcox BA, Hoang TT. 2009. Glyphosate resistance as a novel select-agent-compliant, non-antibiotic selectable marker in chromosomal mutagenesis of the essential genes *asd* and *dapB* of *Burkholderia pseudomallei*. *Appl Environ Microbiol* **75:** 6062–6075.

Norris MH, Kang Y, Wilcox B, Hoang TT. 2010. Stable site-specific fluorescent tagging constructs optimized for *Burkholderia* species. *Appl Environ Microbiol* **76:** 7635–7640.

Passalacqua KD, Varadarajan A, Ondov BD, Okou DT, Zwick ME, Bergman NH. 2009. Structure and complexity of a bacterial transcriptome. *J Bacteriol* **191:** 3203–3211.

Peirson SN, Butler JN, Foster RG. 2003. Experimental validation of novel and conventional approaches to quantitative real-time PCR data analysis. *Nucleic Acids Res* **31:** e73.

Podar M, Keller M, Hugenholtz P. 2009. Single cell whole genome amplification of uncultivated organisms. In *Uncultivated microorganisms* (ed. SS Epstein), Vol. 10, pp. 83–99. Springer-Verlag, Berlin/Heidelberg/New York.

Sambrook J, Russell DW. 2001. *Molecular cloning: A laboratory manual*. 2nd ed. Cold Spring Harbor Laboratory Press, Cold Spring Harbor, NY.

Scanlon MJ, Ohtsu K, Timmermans MC, Schnable PS. 2009. Laser microdissection-mediated isolation and in vitro transcriptional amplification of plant RNA. *Curr Protoc Mol Biol* **Chapter 25:** Unit25.A.3. doi: 10.1002/0471142727.mb25a03s87.

Son MS, Matthews WJJ, Kang Y, Nguyen DT, Hoang TT. 2007. In vivo evidence of *Pseudomonas aeruginosa* nutrient acquisition and pathogenesis in the lungs of cystic fibrosis patients. *Infect Immun* **75:** 5313–5324.

Sorek R, Cossart P. 2010. Prokaryotic transcriptomics: a new view on regulation, physiology and pathogenicity. *Nat Rev Genet* **11:** 9–16.

Takahashi H, Yamamoto K, Ohtani T, Sugiyama S. 2009. Cell-free cloning using multiply-primed rolling circle amplification with modified RNA primers. *Biotechniques* **47:** 609–615.

Tang F, Barbacioru C, Wang Y, Nordman E, Lee C, Xu N, Wang X, Bodeau J, Tuch BB, Siddiqui A, et al. 2009. mRNA-Seq whole-transcriptome analysis of a single cell. *Nat Methods* **6:** 377–382.

Toledo-Arana A, Dussurget O, Nikitas G, Sesto N, Guet-Revillet H, Balestrino D, Loh E, Gripenland J, Tiensuu T, Vaitkevicius K, et al. 2009. The *Listeria* transcriptional landscape from saprophytism to virulence. *Nature* **459:** 950–956.

Vivancos AP, Guell M, Dohm JC, Serrano L, Himmelbauer H. 2010. Strand-specific deep sequencing of the transcriptome. *Genome Res* **20:** 989–999.

Wang Z, Gerstein M, Snyder M. 2009. RNA-Seq: a revolutionary tool for transcriptomics. *Nat Rev Genet* **10:** 57–63.

Yoder-Himes DR, Chain PS, Zhu Y, Wurtzel O, Rubin EM, Tiedje JM, Sorek R. 2009. Mapping the *Burkholderia cenocepacia* niche response via high-throughput sequencing. *Proc Natl Acad Sci* **106:** 3976–3981.

Received October 1, 2010; accepted in revised form March 10, 2011.

Knockout and pullout recombineering for naturally transformable *Burkholderia thailandensis* and *Burkholderia pseudomallei*

Yun Kang[1], Michael H Norris[1], Bruce A Wilcox[2], Apichai Tuanyok[3], Paul S Keim[3,4] & Tung T Hoang[1,5]

[1]Department of Molecular Biosciences and Bioengineering, University of Hawaii at Manoa, Honolulu, Hawaii, USA. [2]Department of Ecology and Health, University of Hawaii at Manoa, Honolulu, Hawaii, USA. [3]Translational Genomics Research Institute, Flagstaff, Arizona, USA. [4]Northern Arizona University, Flagstaff, Arizona, USA. [5]Department of Microbiology, University of Hawaii at Manoa, Honolulu, Hawaii, USA. Correspondence should be addressed to T.T.H. (tongh@hawaii.edu).

Published online 7 July 2011; doi:10.1038/nprot.2011.346

Phage λ-Red proteins are powerful tools for pulling and knocking out chromosomal fragments but have been limited to the γ-proteobacteria. Procedures are described here to easily knock out (KO) and pull out (PO) chromosomal DNA fragments from naturally transformable *Burkholderia thailandensis* and *Burkholderia pseudomallei*. This system takes advantage of published compliant counterselectable and selectable markers (*sacB*, *pheS*, *gat* and the arabinose-utilization operon) and λ-Red mutant proteins. *pheS-gat* (KO) or *oriT-ColE1ori-gat-ori1600-rep* (PO) PCR fragments are generated with flanking 40- to 45-bp homologies to targeted regions incorporated on PCR primers. One-step recombination is achieved by incubation of the PCR product with cells expressing λ-Red proteins and subsequent selection on glyphosate-containing medium. This procedure takes ~10 d and is advantageous over previously published protocols: (i) smaller PCR products reduce primer numbers and amplification steps, (ii) PO fragments suitable for downstream manipulation in *Escherichia coli* are obtained and (iii) chromosomal KO increases flexibility for downstream processing.

INTRODUCTION

The ability to manipulate the bacterial chromosome for molecular genetics, pathogenesis and bacteria-host interaction studies is crucial for the discovery of novel vaccine, therapeutic and diagnostic targets. The Gam, Exo and Beta proteins of coliphage-λ aid in the RecA-independent homologous recombination process to pull out (PO) or knock out (KO) regions from bacterial chromosomes[1]. These λ-Red proteins facilitate high-frequency recombination between the chromosome and small homologous sequences (approximately 40–45 bp) flanking a selectable marker. However, PO and KO manipulation of the bacterial genome using the λ-Red system has been limited to the γ-proteobacteria class[2–5]. Therefore, protocols to expand the use of λ-Red recombineering beyond the γ-proteobacteria are needed, particularly for two closely related naturally transformable β-proteobacterial species: *Burkholderia thailandensis* and *Burkholderia pseudomallei*.

B. thailandensis is a relatively nonpathogenic bacterium often used as a model microbe to study various aspects of the potential bioterrorism agent *B. pseudomallei*. *B. pseudomallei* is the etiological agent of melioidosis, a globally emerging and often fatal infectious disease[6]. Work by Thongdee *et al.*[7] has demonstrated the KO of chromosomal fragments in both naturally transformable *Burkholderia* species, using PCR fragments generated by three-fragment overlap-extension PCR. The requirement for large homologous regions (800–1,000 bp) and overlapping PCR can be hampered by the size and G + C content of the target DNA. In addition, screening for KOs with primers annealing to chromosomal regions outside the 800–1,000 bp of homology can be difficult because of increased amplicon size. Because of these limitations and the lack of PO protocols, we developed protocols to extend the λ-Red recombineering potential in these two species. Here we present protocols for λ-Red recombineering to capture or delete, for example, large chromosomal DNA fragments from two β-proteobacteria species: *B. thailandensis* and *B. pseudomallei*.

Advantages and potential beyond the presented protocols

There are general advantages to this one-step λ-Red–facilitated PO/KO-recombineering protocol: (i) arabinose selection (*araBCDEFGHI*) of pKaKa2 (**Fig. 1**) works in *ara*$^-$ *Escherichia coli* and *B. pseudomallei* (**Table 1**); (ii) the *pheS-gat FRT* cassette, containing both selectable and counterselectable markers, is small and can be used throughout the *Burkholderia* genus[8,9]; (iii) the use of these non-antibiotic (counter)selectable markers is in compliance with US Centers for Disease Control (CDC) and National Institutes of Health (NIH) guidelines, and they provide efficient (counter)selection with high frequencies of positive recombinants; (iv) there is no requirement to maintain and/or cure a replicating plasmid encoding Flp for *FRT* cassette excision, and the *flp*-containing PCR product incubation protocol is simple and saves time; (v) it is more cost-effective because multiple fragment overlap-extension PCR[7] (which can be difficult for larger DNA fragments with high G + C content) is not required, thus reducing the number of oligos used; (vi) recombination aided by λ-Red proteins effectively reduces the length of homologous regions required (40–45 bp), whereas no recombination occurs without the induction of λ-Red proteins (i.e., DNA incubation alone); (vii) possible secondary chromosomal mutation(s) in the 800–1,000 bp of homology resulting from overlap-extension PCR are avoided in λ-Red recombineering, which requires only 40–45 bp of homology.

There are other advantages specific to λ-Red–mediated *in vivo* cloning (**Fig. 2**). PCR amplification of the insert, which can generate mutations in the fragment to be cloned, is not required. In addition, large PCR products can be difficult to amplify, especially from the high-G + C DNA of *Burkholderia* species. Using this protocol to PO large chromosomal fragments from *Burkholderia* spp. is much faster than, for example, *recA*-mediated recombination of a suicidal plasmid at

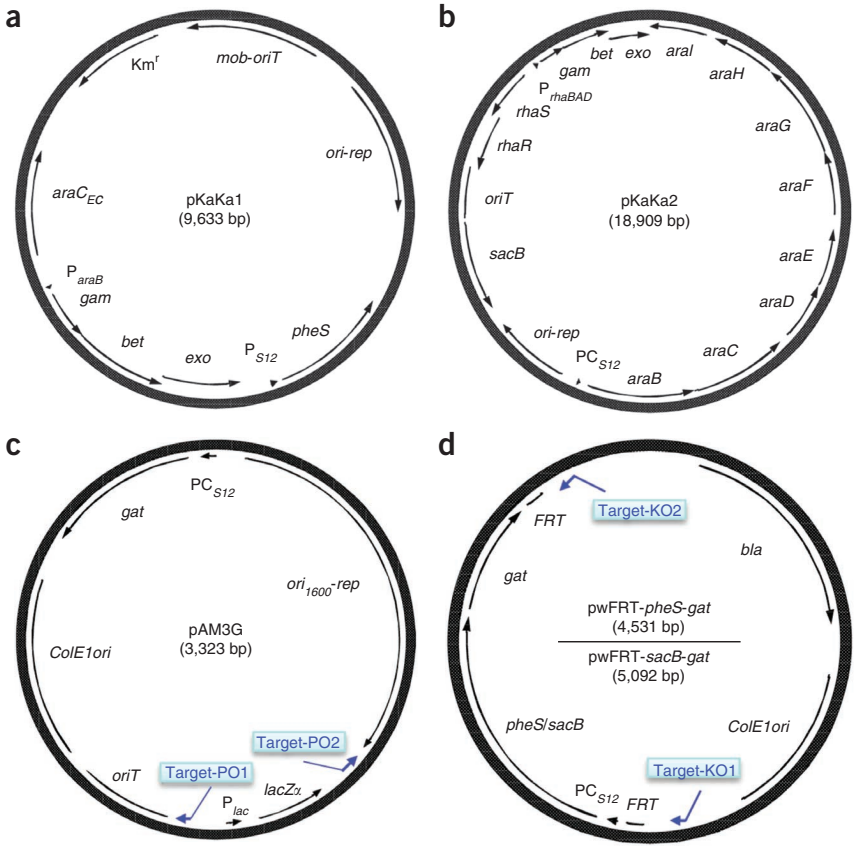

Figure 1 | Genetic constructs for KO and PO recombineering in *B. thailandensis* and *B. pseudomallei*. (**a**) Plasmid pKaKa1 contains λ-Red genes (*gam-bet-exo*)[17] driven by the arabinose-inducible promoter (P_{araB}). (**b**) Plasmid pKaKa2 is maintained in *ara*⁻ *E. coli* and *B. pseudomallei* strains by the *B. thailandensis* arabinose-utilization operon and growth on arabinose minimal medium, in which λ-Red genes are driven by the rhamnose-inducible promoter. (**c**) Broad-host-range (bhr) replicating plasmid used for PO recombineering (*in vivo* cloning). Target-PO1 and Target-PO2 indicate primers (blue arrows) with 40–45 bp homology to the targeted chromosomal region, used to obtain PCR products (*oriT-ColE1ori-gat-ori1600-rep*) to PO targeted sequences. (**d**) The *pheS-gat* and *sacB-gat FRT* cassettes used for KO recombineering experiments. Target-KO1 and Target-KO2 indicate primers (blue arrows), with 40–45 bp homology to chromosomal regions, used to amplify this cassette in KO experiments. Abbreviations: $araC_{Ec}$ of pKaKa1, activator of the arabinose-inducible promoter (P_{araB}) from *E. coli*; *araBCDEFGHI* of pKaKa2, *B. thailandensis* arabinose-utilization operon[10]; *bla*, encodes β-lactamase; ColE1-*ori*, ColE1 origin of replication obtained from high-copy-number pUC vectors[22]; *FRT*, yeast 2 μm plasmid Flp recombination target; *gat*, glyphosate (GS) acetyltransferase for GS resistance[9]; Km^r, kanamycin resistance, encoded by *nptII*[23]; *lacZα*, encodes LacZ α peptide; *mob-oriT*, RP4-dependent conjugal origin of transfer of *B. bronchiseptica* cryptic plasmid pBBR1 (ref. 16); ori_{1600}-*rep*, *Pseudomonas* and *Burkholderia* bhr origin of replication[24]; *ori-rep*, bhr replicon of *B. bronchiseptica* pBBR1 plasmid[16]; *oriT*, plasmid RP4 origin of transfer for conjugation; P_{araB}, arabinose-inducible promoter[3]; P_{lac}, *E. coli* lactose operon promoter; P_{rhaBAD}, rhamnose-inducible promoter[25]; P_{S12} and PC_{S12}, constitutive promoters of *B. pseudomallei* and *B. cenocepacia rpsL* genes[26]; *pheS*, engineered gene encoding a mutant version of the α-subunit of phenylalanyl tRNA synthase[8]; *rhaR* and *rhaS*, regulators of the rhamnose-inducible promoter[25]; *sacB*, encoding for a modified levansucrase counterselectable marker[14].

the region of interest followed by restriction fragmentation, ligation and cloning in *E. coli*[10]. The cloned junctions can be precise depending on primer design, and unique restriction sites can be added to the middle of the Target-PO oligos for easy downstream manipulation of *in vivo* cloned fragments. It can be envisioned that the PO protocol could generate clones of much larger or smaller fragments than the 11.6- to 31.5-kb fragments exemplified in this protocol.

Furthermore, the KO protocol could be extended to include other downstream applications. Insertional mutants may be created with the *pheS-gat FRT* cassette such that the counter-selectable markers could be used to counterselect and generate reporter-gene fusions, in-frame nonpolar deletions and chromosomal point mutations in these β-proteobacteria, *B. thailandensis* and *B. pseudomallei*, as previously described for other γ-proteobacteria species[1]. Overall, the ability to perform these types of genetic manipulations in these species using λ-Red recombineering significantly simplifies and reduces experimental labor, allowing high-throughput targeted chromosomal manipulation. For example, our laboratory has used this to KO over 200 targeted and confirmed mutations in 1 month through the efforts of two graduate students.

Limitations of the present protocol

The limitations of the current protocol are that (i) there is a requirement for minimal medium (typically 1× M9 glucose (MG)) supplemented with glyphosate (GS) or chlorinated phenylalanine (cPhe) during *gat* selection or *pheS* counterselection; (ii) when introduced into *E. coli* at high copy number, certain PO gene products may be toxic to the cell, potentially limiting the nature of downstream applications; and (iii) this protocol has been performed successfully in only the naturally transformable strains of *B. thailandensis* and *B. pseudomallei* (~50% of the strains tested in this study). We have not been able to extend its use to the non–naturally transformable *Burkholderia* strains (e.g., *B. pseudomallei* strain K96243 and *Burkholderia mallei* strain ATCC23344) because of potentially inefficient electrotransformation and/or restriction barriers against double-stranded DNA. Various published electroporation methods[11–13] were tested in non–naturally transformable strains (e.g., *B. pseudomallei* K96243 and *B. mallei* ATCC23344), but no colonies or recombinants were obtained. In these non–naturally transformable species and strains, mutation could be created with other established mutagenesis procedures as previously described[8,9,12,14]. However, λ-Red recombineering has a very broad host range (bhr), and we strongly believe that these

TABLE 1 | Bacterial strains and plasmids used in this study.

Strains and plasmids	Lab ID[a]	Accession number[b]	Relevant features and use	Reference
E. coli				
EPMax10B	E1231	—	F⁻ λ⁻ *mcrA* Δ*(mrr-hsdRMS-mcrBC)* ϕ*80dlacZ*Δ*M15* Δ*lacX74 deoR recA1 endA1 araD139* Δ*(ara, leu)7697 galU galK rpsL nupG*	Bio-Rad
EPMax10B-*lacI*^{q}/*pir*/*leu*$^{+}$	E1889	—	F⁻ λ⁻ *mcrA* Δ*(mrr-hsdRMS-mcrBC)* ϕ*80dlacZ*Δ*M15* Δ*lacX74 deoR recA1 galU galK rpsL nupG lacI*q-*FRT8 pir-FRT4*	—[c]
EPMax10B-*pir116*/Δ*asd*/*mob*-Km^{r}/Δ*trp*::Gm^{r}	E1354	—	Gm^{r}, Km^{r}; F⁻ λ⁻ *mcrA* Δ*(mrr-hsdRMS-mcrBC)* ϕ*80dlacZ*Δ*M15* Δ*lacX74 deoR recA1 endA1 araD139* Δ*(ara, leu)7697 galU galK rpsL nupG Tn-pir116-FRT2* Δ*asd*::*wFRT* Δ*trp*::Gm^{r}-*FRT5 mob*[*recA*::*RP4-2 Tc*::*Mu*-Km^{r}]	—[c]
MC4100-Δ*asd*::*FRT*/*mob*::*mFRT*	E1299	—	F⁻ (*argF*⁻ *lac*) *U169 araD139 rpsL150 relA1 thiA ptsF25 deoC1 flbB5301 rbsR* Δ*asd*::*FRT recA*::RP4-2Tc::Mu	
B. pseudomallei[d]				
1026b	B004	—	Wild-type strain; clinical melioidosis isolate	29
1026b-Δ*mba*::*pheS-gat*	B023	—	GS^{r}; 1026b with *pheS-gat-FRT* fragment replacing the *mba* cluster	This study
1026b-Δ*mba*::*FRT*	B025	—	1026b with *FRT*-sequence inserted into the *mba* cluster	This study
1026b-Δ*mba*	B027	—	1026b with *mba* cluster deleted	This study
Bp0085	B040	—	Wild-type strain; clinical strain from a sepsis case (fatal) in Thailand, 2006	This study
Bp0085-Δ*asd*::*pheS-gat*	B079	—	GS^{r}; Bp0085 with *pheS-gat-FRT* fragment replacing the *asd* gene	This study
Bp0091	B042	—	Wild-type strain; clinical strain from a sepsis case (fatal) in Thailand, 2006	This study
Bp0091-Δ*asd*::*pheS-gat*	B080	—	GS^{r}; Bp0091 with *pheS-gat-FRT* fragment replacing the *asd* gene	This study
Bp0094	B044	—	Wild-type strain; clinical strain from a sepsis case (fatal) in Thailand, 2006	This study
Bp0094-Δ*asd*::*pheS-gat*	B081	—	GS^{r}; Bp0094 with *pheS-gat-FRT* fragment replacing the *asd* gene	This study
Bp4001[e]	B054	—	Wild-type strain; environmental isolate from soil in Australia, 1997	This study
Bp4001-Δ*asd*::*pheS-gat*	B082	—	GS^{r}; Bp4001 with *pheS-gat-FRT* fragment replacing the *asd* gene	This study
Bp4003[e]	B058	—	Wild-type strain; clinical strain from a sepsis case (fatal) in Australia, 1999	This study
Bp4003-Δ*asd*::*pheS-gat*	B083	—	GS^{r}; Bp4003 with *pheS-gat-FRT* fragment replacing the *asd* gene	This study
Bp4122	B064	—	Wild-type strain; environmental isolate from soil in Australia, 2006	This study
Bp4122-Δ*asd*::*pheS-gat*	B084	—	GS^{r}; Bp4122 with *pheS-gat-FRT* fragment replacing the *asd* gene	This study
Bp4141[e]	B066	—	Wild-type strain; clinical isolate from a chronic case (survived) in Australia, 1991	This study
Bp4141-Δ*asd*::*pheS-gat*	B085	—	GS^{r}; Bp4141 with *pheS-gat-FRT* fragment replacing the *asd* gene	This study
Bp4144	B068	—	Wild-type strain; clinical isolate from a chronic case (survived) in Australia, 1995	This study
Bp4144-Δ*asd*::*pheS-gat*	B086	—	GS^{r}; Bp4144 with *pheS-gat-FRT* fragment replacing the *asd* gene	This study
Bp6340[e]	B078	—	Wild-type strain; clinical isolate from a chronic case (survived) in Australia, 2003	This study
Bp6340-Δ*asd*::*pheS-gat*	B087	—	GS^{r}; Bp6340 with *pheS-gat-FRT* fragment replacing the *asd* gene	This study

(continued)

TABLE 1 | Continued.

Strains and plasmids	Lab ID[a]	Accession number[b]	Relevant features and use	Reference
B. thailandensis				
E264	E1298	—	Prototroph; environmental isolate	30
Plasmids				
pAM3G	E1947	GU074522	GS^r; broad-host-range cloning vector based on GS resistance	This study
pwFRT-*pheS-gat*	E2336	GU074523	GS^r, Ap^r; *pheS-gat* fragment flanked by wild-type *FRT*s	This study
pwFRT-*gat-sacB*	E2456	GU450326	GS^r, Ap^r; *sacB-gat* fragment flanked by wild-type *FRT*s	This study
pKaKa1	E2273	GU074524	Km^r; broad-host-range λ-Red helper plasmid based on Km resistance	This study
pKaKa2	E2334	GU074525	Broad-host-range helper plasmid for λ-Red recombineering	This study
pCD13SK-Flp-*oriT-asd*$_{Ec}$	E1827	EU626138	Suicidal plasmid containing Flp	31

Ap^r, ampicillin resistant; F$^-$, F factor negative; Gm^r, gentamicin resistant; GS^r, glyphosate resistant; Km^r, kanamycin resistant.
[a]Please use Lab ID when requesting *E. coli* strains and plasmids. [b]GenBank accession number. [c]Details on the construction of these strains and plasmids will be published elsewhere. [d]Acquisition, possession and manipulation of these strains in the United States are limited to FBI-screened and cleared personnel, and experiments must be performed in a CDC/USDA-approved and registered BSL-3 select agent laboratory. [e]Multiple-contig shotgun assemblies from these strains are available on request.

tools will work in many other natural transformable strains. For example, we have extended the use of this technology successfully in nine other naturally transformable *B. pseudomallei* environmental and clinical strains (**Table 1**).

Experimental design

Genetic constructs for recombineering. This protocol takes advantage of our recently published *pheS* counterselectable and *gat*-selectable markers[8,9], along with the arabinose-utilization operon (*araBCDEFGHI*)[10] and the more established *sacB* counterselectable marker[14]. Two new bhr replicating plasmids containing λ-Red genes (*gam*, *bet* and *exo*) that are inducible with arabinose and rhamnose, pKaKa1 and pKaKa2, respectively, were engineered for this protocol (**Fig. 1a**,**b**). pKaKa1 is typically used for *B. thailandensis*, using the kanamycin-resistance selectable marker and the *pheS* gene as a counterselectable marker in the presence of cPhe, as described previously[8]. As kanamycin resistance has limited use in wild-type *B. pseudomallei* strains[15], the alternative *B. thailandensis* arabinose-utilization operon (*araBCDEFGHI*)[10] was used as a metabolic marker for selection of pKaKa2 in *B. pseudomallei*, whereas the *sacB* gene was chosen for counterselection, using sucrose. The pKaKa1 and pKaKa2 plasmids contain the *Bordetella bronchiseptica* bhr origin for replication in Gram-negative bacteria[16]. These plasmids can be electrotransformed into *B. thailandensis* and *B. pseudomallei* or conjugated from RP4-harboring *E. coli* (e.g., E1299, **Table 1**), in which they can eventually be cured using cPhe or sucrose after recombineering. The λ-Red proteins Gam, Redβ and Redα (encoded by *gam*, *bet* and *exo*) are

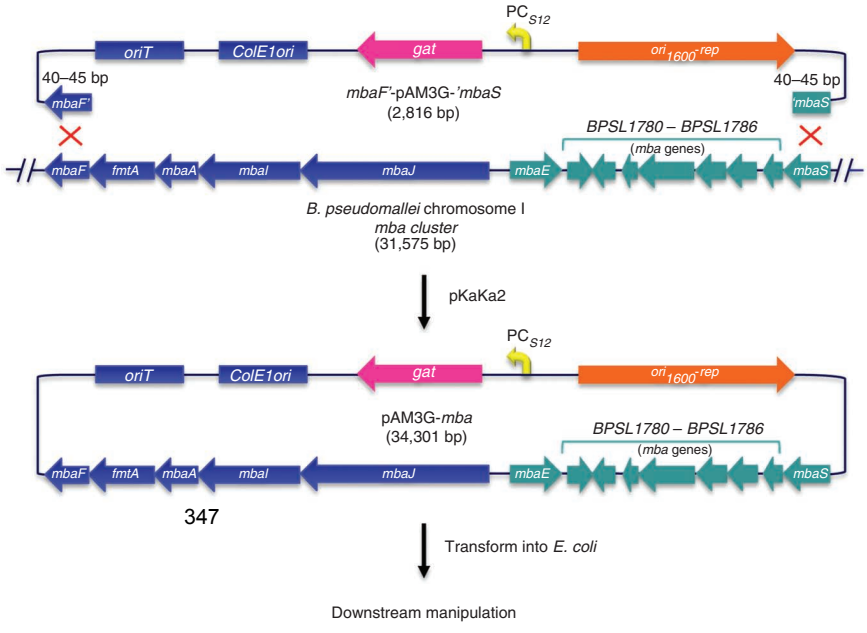

Figure 2 | Overview of an example of PO recombineering in *B. pseudomallei*. The 31.5-kb *mba* cluster was pulled out of the *B. pseudomallei* chromosome, using a PCR-amplified fragment of the pAM3G backbone (**Fig. 1c**), with correctly oriented 40- to 45-bp homologous sequences toward the *mbaF* and *mbaS* genes. Positive clones can be immediately obtained in one step by glyphosate-resistance selection. The pAM3G-*mba* bhr replicating plasmid could be screened (with the primers indicated by arrows) and isolated from glyphosate resistant *B. pseudomallei* colonies and transformed into *E. coli* for further characterization. Red crosses indicate λ-Red–mediated homologous recombination.

TABLE 2 | Oligonucleotides used in this study.

Number/name	Sequence[a]
#1178; araA-P01	5′-**CGCGCGGGAGATCTAC**GGGACGGCCCAATAGCTGCGCTCAGATTCCTTAAGGTATACTTT-3′
#1179; araI-P02	5′-**GAAGCGGGCTGCGCGAA**CGCCGGCGTGAAGCGCGGGCCGGACGGCCTCTAGGCCAGATCC-3′
#1227; araA-P03	5′-CGCGCGGGAGATCTAC-3′
#1228; araI-P04	5′-GAAGCGGGCTGCGCGAA-3′
#271; ori1600-rep-internal	5′-GGAAGATTTCAGATGCTGAG-3′
#1161; araI-rev	5′-TTCGTGTTCGGGATGAAG-3′
#1187; mbaF-P01	5′-**AAGAACGCGAGCTCGG**CGCCGAGCGCTTCGAGTTGATCGAGATTCCTTAAGGTATACTTT-3′
#1188; mbaS-P02	5′-**GCGGCACTTCGCTCGTC**CATCGTTGCCGGCCGCGCAACGAACGGCCTCTAGGCCAGATCC-3′
#1125; mbaF-P03	5′-AAGAACGCGAGCTCGG-3′
#1126; mbaS-P04	5′-GCGGCACTTCGCTCGT-3′
#1219; mbaF-K01	5′-**GCAGCGCCGCTTGCCG**CGCGCTTTGGGCTCGACGGGGGCGG*CAAGGCGATTAAGTTGGGTA*-3′
#1220; mbaS-K02	5′-**GCCTGCGGCGCGCAC**GCCGGGCGCGCGCGAGCACGGCGCGCTCGTATGTTGTGTGGAATTGTGA-3′
#1223; mbaF-K03	5′-GCAGCGCCGCTTGCCG-3′
#1224; mbaS-K04	5′-GCCTGCGGCGCGCAC-3′
#1229; mbaS-K05	5′-**GCCTGCGGCGCGCAC**GCCGGGCGCGCGCGAGCACGGCGCGCTCGT*TACCCAACTTAATCGCCTTG*-3′
#560; Plac-up	5′-GCCCAATACGCAAACCGCCTCTC-3′
#566; Flp-down	5′-TAAATGGATCCTTATATGCGTCTATTTATG-3′
#1221; mbaF-out	5′-GCCGCGCGTTCACCGAAG-3′
#1222; mbaS-out	5′-CTTCGAACGGGGCGTTTG-3′
#1189; mbaS-rev	5′-GACGAGCTTCACGAACAC-3′
#1484; asd-K01	5′-**TTCAGCACCAGCAACGCG**GGCGGCAAGGCGCCGTCGTTCGCGGATAACAATTTCACACAG-3′
#1485; asd-K02	5′-**CGCCACCCATCGCGAGCT**TGCGCAGGCGGCCGACCGGCACCGACGTTGTAAAACGACGGC-3′
#1486; asd-K03	5′-TTCAGCACCAGCAACGCG-3′
#1487; asd-K04	5′-CGCCACCCATCGCGAGCT-3′
#1488; asd-up	5′-ATCTGATCGAGCCGGTG-3′
#1489; asd-down	5′-GTAAATGCCGACAGGTAT-3′

[a]Underlined are homologous sequences to targets on the chromosome. **Boldface** sequences in the long oligos are identical to the shorter oligos used in the second PCR (Step 5 of the protocol). In *italics* are reverse complementary sequences of mbaF-K01 and mbaS-K05, where these primers are used to generate ~100 bp PCR product to create the unmarked mutation (Step 13A).

based on optimized expression of Gam and mutated versions of Redβ and Redα[17]. Upon induction of the λ-Red proteins, linear PCR products are naturally transformed into *B. thailandensis* or *B. pseudomallei* to generate POs or KOs. The relevant strains, plasmids and oligonucleotides used in this protocol are shown in **Tables 1** and **2**.

***In vivo* PO strategy.** The *in vivo* cloning or PO protocol involves the amplification of a PCR product from the engineered plasmid pAM3G, containing a GS-resistance selectable marker[9], a bhr origin of replication and an origin of transfer for conjugation (**Figs. 1c** and **2**). The PCR-amplified fragment (~2.8 kb), flanked by sequences homologous to the chromosomal PO region, is incubated with cells expressing the λ-Red proteins. As examples of the PO protocol, we will individually describe the *in vivo* cloning of the *B. thailandensis* arabinose-utilization operon (*araABCDEFGHI*, 11.6 kb)[10] and the *B. pseudomallei* siderophore malleobactin biosynthetic cluster (*mba*-cluster, 31.5 kb)[18] into the

TABLE 3 | Pullout recombineering efficiencies of the *ara* operon in *B. thailandensis*[a].

DNA amount	First PCR product[b] %	Second PCR product[c] %
2 μg	41 ± 9 (92)	245 ± 40 (89)
0.5 μg	3 ± 1 (92)	19 ± 3 (90)
0.1 μg	1 ± 1 (100)	4 ± 0.3 (93)

[a]Each experiment was performed in triplicate, and average number of GS-resistant colonies is shown with standard error of the mean. On average, 12 GS-resistant colonies were PCR screened for positive pullout and the percentage is shown in parentheses.
[b]The first PCR product, amplified with the non-PAGE purified long oligos, was directly used for PO.
[c]The second PCR product, amplified using shorter non-PAGE purified oligos and the first PCR product as template, was used for PO.

TABLE 4 | Pullout/knockout recombineering efficiencies of the *mba* cluster in *B. pseudomallei*[a].

DNA amount	Pullout %		Knockout %	
	Uninduced	Induced	Uninduced	Induced
2 μg	0	55 ± 11 (90)	0	45 ± 8 (92)
0.5 μg	ND	19 ± 5 (100)	ND	21 ± 7 (88)
0.1 μg	ND	3 ± 1 (100)	ND	5 ± 2 (92)

[a]Each experiment is performed in triplicate, and average number of GS-resistant colonies is shown with standard error of the mean. On average, 12 GS-resistant colonies were PCR screened for positive PO/KO and the percentage is shown in parentheses. ND, not determined.

pAM3G replicating plasmid backbone. The PO strategy for the *mba* cluster is depicted in **Figure 2**. Positive PO frequencies of GS-resistant colonies with *araABCDEFGHI* clones ranged from 88 to 93% in *B. thailandensis* (**Table 3**), whereas cloning frequencies for the *mba* cluster ranged from 90 to 100% in *B. pseudomallei* (**Table 4**).

Overview of KO strategy. The KO procedure uses a PCR-amplified *pheS-gat FRT* cassette flanked by 40–45 bp of sequence homologous to the targeted chromosomal regions (**Fig. 1d**). Upon introduction of the pKaKa2 plasmid and induction of the expression of λ-Red proteins, KOs can be achieved in one step by transformation of the PCR-amplified *pheS-gat* cassette and selection on GS. The helper plasmid pKaKa2 could be cured by counterselection with *sacB* on sucrose-containing medium (**Fig. 1b**). **Figure 3** depicts an example of chromosomal KO using pKaKa2 in *B. pseudomallei* at high frequencies (88–92%, **Table 4**). We foresee that for those laboratories approved to use kanamycin-resistance selection in *B. pseudomallei*, pKaKa1, in conjunction with the *sacB-gat* cassette, could be used to generate KO in *B. pseudomallei* (**Fig. 1a**,**d**). In this case, pKaKa1 could be cured by counterselection with *pheS* on cPhe-containing medium.

Recycling of useful markers. There are very few selectable or counterselectable markers for genetic manipulation in most bacteria, and the ability to reuse these precious markers in the same strain is essential. This protocol describes two strategies for recycling the *pheS-gat* or *sacB-gat FRT* cassettes (**Fig. 3**). A second round of λ-Red protein induction followed by incubation of cells with a short PCR fragment flanked by 40–45 bp homologous to the targeted region on the chromosome (**Fig. 3**) will generate an unmarked KO mutant in *B. thailandensis* or *B. pseudomallei*. This strategy can be achieved quickly because of the presence of pKaKa1 or pKaKa2 from the previous KO procedure. In an alternative strategy that does not require λ-Red proteins, the unmarked KO mutants can be generated by incubating cells with a PCR fragment containing *flp* (**Fig. 3**).

Overview of the protocol. This PO/KO protocol is summarized in **Figure 4**. Steps 1–12 demonstrate the generation of PO/KO in *B. pseudomallei* and *B. thailandensis* (left section). Following KO with the *pheS/sacB-gat FRT* cassette, unmarked mutations can be created with overlapping oligos (middle; Step 13A) or Flp-mediated excision (right; Step 13B). When desired, the helper plasmid can be cured by *pheS/sacB* counterselection (Step 14). The step-by-step protocol is described below.

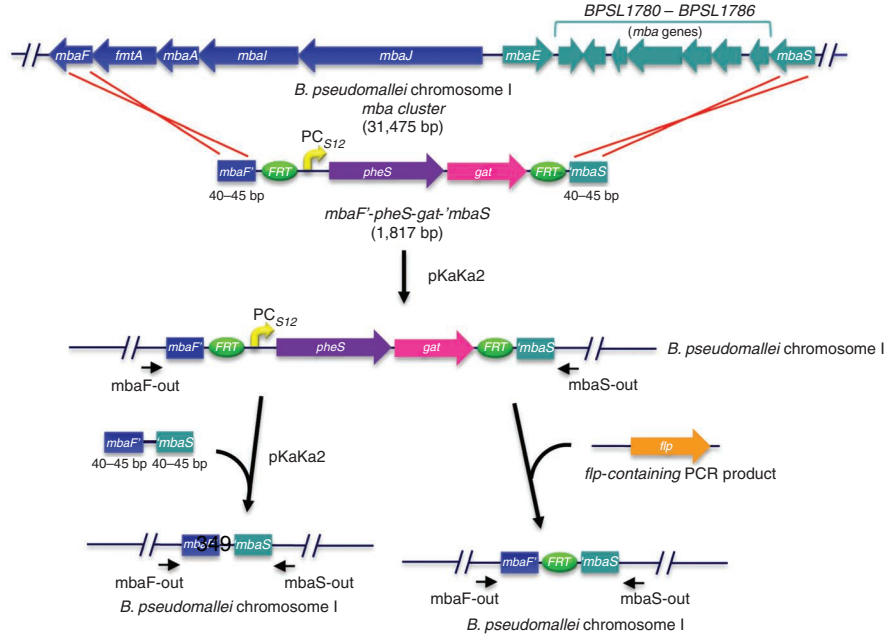

Figure 3 | KO recombineering strategy. The example shown here involves the amplification of the *pheS-gat* cassette with Target-KO primers (**Fig. 1d**) to generate a 1.8-kb PCR product containing 40–45 bp of homologous sequences to the end of *mbaF* and the beginning of *mbaS* genes. On uptake by the natural transformation system of *B. pseudomallei* and selection with GS, λ-Red proteins facilitate the one-step recombination of the PCR product to KO the 31.4-kb *mba* cluster on chromosome I. The resulting *B. pseudomallei*–marked mutant strain (Δ*mba*::*pheS-gat-FRT*), still containing pKaKa2, is reinduced to express λ-Red proteins a second time to create unmarked mutants. By transforming a smaller PCR fragment containing 40- to 45-bp homologies to *mbaF* and *mbaS* for recombination, unmarked mutants lacking *pheS-gat* can be easily selected by counterselection on cPhe-containing medium. Alternatively, the *pheS-gat-FRT* cassette can be easily removed by naturally transforming an *flp*-containing PCR fragment for transient expression. The black horizontal arrows indicate outside primers used to screen for mutants.

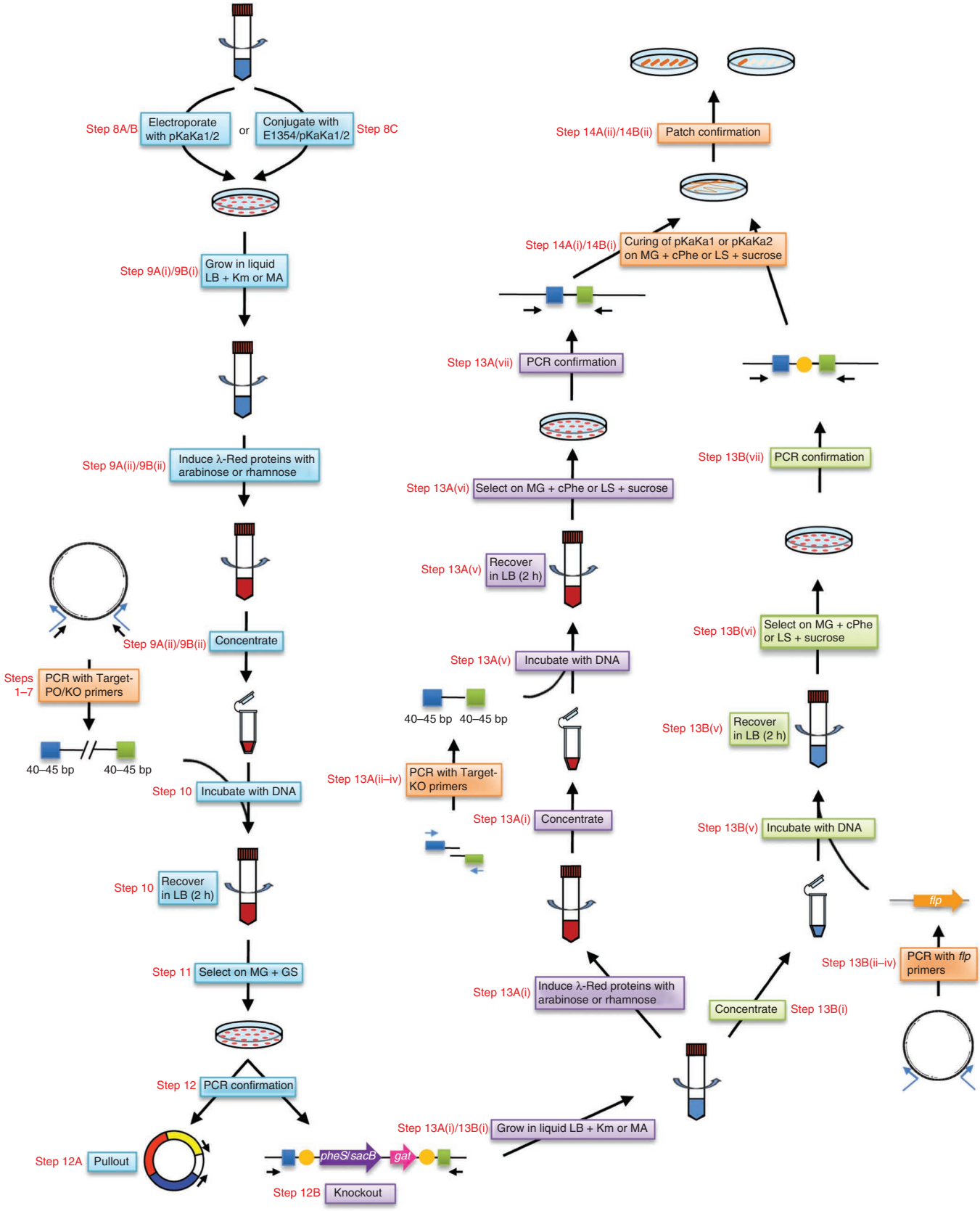

Figure 4 | λ-Red recombineering scheme for PO/KO in *B. thailandensis* and *B. pseudomallei*. Strategy for PO/KO recombineering is shown on the left (blue); the middle (purple) and right (green) sections present the strategies for creating unmarked mutants by λ-Red recombination or Flp-mediated excision, respectively. Detailed descriptions for each step are provided in the procedure. Numbers in red correspond to the steps in the protocol.

MATERIALS

REAGENTS

- Amino acids: 2,6-diaminopimelic acid (DAP; 100 mg ml^{-1} in 1 M NaOH, Acros Organics, cat. no. 235540010); L-leucine (Leu; 1 M; filter sterilized, Acros Organics, cat. no. 125121000); L-lysine (Lys; 1 M; filter sterilized, Acros Organics, cat. no. 303340050), L-methionine (Met; 1 M; filter sterilized, Acros Organics, cat. no. 166160250), L-threonine (Thr; 1 M; filter sterilized, Acros Organics, cat. no. 138930050) and (*S*)-tryptophan (Trp; 1 M; filter sterilized, Acros Organics, cat. no. 140591000)
- Bacterial strains
- *Burkholderia* strains (**Table 1**)
- *Burkholderia thailandensis* E264 (available from BEI Resources)
- *Burkholderia pseudomallei* 1026b, Bp0085, Bp0091, Bp0094, Bp4001, Bp4003, Bp4122, Bp4141, Bp4144 and Bp6340 **! CAUTION** Acquisition, possession and manipulation of *B. pseudomallei* strains in the United States are limited to FBI-screened and -cleared personnel, and experiments must be performed in CDC- and US Department of Agriculture (USDA)-approved and registered BSL-3 select agent facilities.
- *E. coli* strains (**Table 1**; available from T.T.H.)
- Plasmids (**Table 1**; available from T.T.H.)
- pKaKa1 or pKaKa2, replicating plasmids containing inducible λ-Red genes (**Fig. 1**)
- pAM3G, bhr plasmid encoding *gat* (GS acetyltransferase), source of PCR fragment for PO recombineering
- pwFRT-PC_{S12}-*pheS-gat* or pwFRT-PC_{S12}-*sacB-gat* plasmid DNA used as template for KO recombineering
- pCD13SK-Flp-*oriT-asd*$_{Ec}$ plasmid DNA used as a template to amplify *flp* gene–containing fragment
- Oligonucleotides (see **Table 2**; Integrated DNA Technologies)
- Target-PO1 (5′-N_{40}-GATTCCTTAAGGTATACTTT-3′); N_{40} refers to 40 bases of sequence homologous to your target gene. Underlined bases can be common to the target and also anneal to the PCR template to increase efficiency and reduce costs.
- Target-PO2 (5′-N_{40}-ACGGCCTCTAGGCCAGATCC-3′)
- Target-PO3 ($N_{16–20}$ identical to the 5′-end of Target-PO1)
- Target-PO4 ($N_{16–20}$ identical to the 5′-end of Target-PO2)
- Target-rev ($N_{16–20}$ anneals inside of the PO region; use with oligo ori1600-rep-internal to confirm PO by PCR)
- ori1600-rep-internal (5′-GGAAGATTTCAGATGCTGAG-3′; use with oligo Target-rev to confirm PO by PCR)
- Target-KO1 (5′-N_{40}-CAAGGCGATTAAGTTGGGTA-3′)
- Target-KO2 (5′-N_{40}-GCTCGTATGTTGTGTGGAATTGTGA-3′)
- Target-KO3 ($N_{16–20}$ identical to the 5′-end of Target-KO1)
- Target-KO4 ($N_{16–20}$ identical to the 5′-end of Target-KO2)
- Target-KO5 (5′-N_{40}-TACCCAACTTAATCGCCTTG-3′; this oligo has identical N_{40} as Target-KO2)
- Target-up-out ($N_{16–20}$ anneals outside of the homologous region; use with Target-down-out to confirm KO by PCR)
- Target-down-out ($N_{16–20}$ anneals outside of the homologous region; use with Target-up-out to confirm KO by PCR)
- Plac-up (5′-GCCCAATACGCAAACCGCCTCTC-3′)
- Flp-down (5′-TAAATGGATCCTTATATGCGTCTATTTATG-3′)
- DNA ladder (100 bp; range 100–1,500 bp, New England Biolabs, cat. no. N3231L)
- DNA ladder (1 kb; range 0.5–10 kb, New England Biolabs, cat. no. N3232L)
- dNTPs (2 mM; New England Biolabs, cat. no. N0447L)
- LB agar Lennox and LB broth Lennox (Teknova, cat. nos. L9330 and L9310)
- LS agar (LB agar without NaCl; Teknova, cat. no. L9200)
- Saccharides: L-arabinose (2 M; filter sterilized; MP Biomedicals, cat. no. 10076); L-rhamnose (10% (wt/vol) filter sterilized; Sigma-Aldrich, cat. no. R3875); D-glucose (1 M; filter sterilized; Sigma-Aldrich, cat. no. G7528); sucrose (1 M; filter sterilized; Tekanova, cat. no. S0002)
- DL-chlorinated phenylalanine (cPhe; Acros Organics, cat. no. 15728-0050)
- Enzyme *Pfu* polymerase (Stratagene, cat. no. 600153)
- $CaCl_2$ (1 M; autoclaved in water; Acros Organics, cat. no. 194635)
- $MgSO_4$ (1 M; autoclaved in water; Acros Organics, cat. no. 194699)
- M9 minimal salts (5×; Sigma-Aldrich, cat. no. M6030); alternative preparation[19]
- Agar (molecular biology grade; Teknova, cat. no. A777)
- Agarose (molecular grade; Research Products International, cat. no. A20065-100.0)
- TAE buffer (20×; Thermo Scientific Pierce Protein Research Products, cat. no. 28354); alternative preparation[19]
- Glyphosate: super-concentrated RoundUp (50% (vol/vol) GS from Home Depot or other farm or garden supply stores)
- Kanamycin sulfate salt (Sigma-Aldrich, cat. no. K4378)

EQUIPMENT, SUPPLIES AND FACILITIES

- Syringe filters (0.22-μm pore size; 25 mm diameters; Fisher Scientific, cat. no. 09-719E)
- Microcentrifuge tubes (1.5 ml; Corning, cat. no. 3621)
- Beveled pipette tips (1–200 μl; sterile; Fisher Scientific, cat. no. 02-707-450)
- Incubators (37 °C)
- Aerosol barrier plug tips (200 and 1,000 μl; sterile; Genesee Scientific, cat. nos. 24-412 and 24-430)
- Biosafety level three (BSL-3) laboratory (inspected and approved by CDC/USDA) and practices as recommended by the *Biosafety in Microbiological and Biomedical Laboratories*, 5th edition[20]. Although non-antibiotic markers and the kanamycin-resistance marker are described in this protocol, earlier approval for their use in *B. pseudomallei* must be sought with the CDC/USDA for work performed or funded by federal agencies within the United States.
- Culture tubes (14 ml, sterile disposable, snap cap; BD Falcon, cat. no. 352018)
- DNA purification kits: plasmids isolation kit (Zyppy Plasmid Miniprep Kit, Zymoresearch, cat. no. D4036); gel DNA recovery kit (Zymoclean Gel DNA Recovery Kit, Zymo Research, cat. no. D4001); DNA cleanup kit (Zymoclean DNA Clean & Concentrator Kit, Zymo Research, cat. no. D4003)
- Electroporation cuvettes (2 mm gap; Genesee Scientific, cat. no. 40-101)
- Electroporator (Bio-Rad Gene Pulser Xcell with pulse control module, cat. no. 165-2662)
- Falcon tubes (15 ml, conical, screw cap, sterile, disposable; BD Falcon, cat. no. 352097)
- Gradient cycler (Eppendorf Mastercyler gradient)
- Inoculation loop (Fisher Scientific, cat. no. 130753)
- Microcentrifuge (Eppendorf Mini-Spin Plus, cat. no. 5453-000.011)
- Petri dish (Fisher Scientific, cat. no. 08-757-12)
- Spectrophotometer (Eppendorf Biophotometer, cat. no. 6131 000.020)
- Vacuum concentrator (Thermal Scientific SpeedVac, cat. no. DNA120-115)

REAGENT SETUP

Agarose gels Agarose gels are prepared by adding molecular-grade agarose to 100 ml of 1× TAE buffer[19] to obtain desired concentrations. The mixture is then heated and allowed to cool in a gel mold. The agarose gels are prepared freshly before use.

Antibiotic stock and nutrient solution preparation Prepare stock solutions of D-glucose (1 M), kanamycin (35 mg ml^{-1}), L-arabinose (2 M), $CaCl_2$ (1 M), $MgSO_4$ (1 M) and L-rhamnose (10%, wt/vol). Dissolve all compounds in the appropriate amounts of double-distilled water (DDW). The arabinose, kanamycin, glucose and rhamnose solutions should be passed through 0.2-μm syringe filters in order to sterilize. M9 minimal salts solution (5×) is prepared by autoclaving the 5× salt mixture with the appropriate volume of DDW. The 1 M $CaCl_2$ and 1 M $MgSO_4$ can be autoclaved separately in order to sterilize them. Store the kanamycin stock solution at 4 °C. The sugar and salt solutions can be stored at room temperature (15–25 °C) for several months.

Liquid medium preparation Use LB broth Lennox to prepare rich media. To prepare 1 liter of MG medium, add 200 ml 5× M9 minimal salts solution, 20 ml of 1 M glucose, 500 μl of 1 M $MgSO_4$, 25 μl of $CaCl_2$ and 780 ml sterile DDW. Final concentrations are listed as follows: 1× M9 minimal salts, 20 mM glucose, 500 μM $MgSO_4$ and 25 μM $CaCl_2$. A volume of 1 liter of M9 arabinose (MA) medium is prepared by adding 200 ml 5× M9 minimal salts solution, 20 ml of 2 M arabinose, 500 μl of 1 M $MgSO_4$, 25 μl $CaCl_2$ and 780 ml sterile DDW. Final concentrations are listed as follows: 1× M9 minimal salts, 40 mM arabinose, 500 μM $MgSO_4$ and 25 μM $CaCl_2$. The liquid media can be prepared and stored at room temperature for several months.

Solid medium preparation All solid media could be prepared fresh or stored at 4 °C for several months. Use LB or LS agar to prepare rich plate media. One liter of MG or MA with agar is prepared by first mixing 15 g agar in 780 ml DDW and sterilizing. After autoclaving, add 200 ml 5× M9 minimal salts solution, 20 ml of 1 M glucose or 20 ml of 2 M arabinose. Let it cool to ~50 °C before adding 500 μl of 1 M $MgSO_4$ and 25 μl of $CaCl_2$.

The final concentrations are 1.5% (wt/vol) agar, 1× M9 minimal salts, 20 mM glucose or 40 mM arabinose, 500 μM $MgSO_4$ and 25 μM $CaCl_2$. Approximately 50 plates can be prepared from 1 liter of medium. When growing *B. pseudomallei asd*-specific mutant in minimal medium (**Table 1**), Met, Lys and Thr are added at a final concentration of 1 mM, and DAP was added at 200 μg ml^{-1}. Sucrose is added at a concentration of 15% (wt/vol). cPhe is added at a concentration of 0.1% (wt/vol), as previously described[8].

PROCEDURE

Preparing PO/KO DNA fragment ● TIMING 1 d

1| Design oligonucleotide primers such that the last 45 bases on the 5′ end are homologous to two corresponding regions on the chromosome for the PO/KO method, and order oligos prior to initiating the protocol. When designing the pair of PO or KO oligos, avoid having five consecutive matching base pairs between them within their 5′ ends to prevent intrafragment recombination[2]. All oligos do not require PAGE purification; however, the majority of the long oligos (60–65 bp) produced will be truncated or will have incorrect 5′ ends as the coupling or synthesis efficiency is not 100% (coupling efficiencies are available from oligo manufacturer), resulting in reduced recombineering efficiency (e.g., ~29% of the 60-bp oligos have truncated or incorrect ends when the coupling efficiency is 99%, or up to 95% will have truncated or incorrect ends if coupling efficiency is as low as 95%). To remedy this problem and increase recombineering efficiency at reduced cost, a two-step PCR approach is described below. The first PCR product is obtained using the long oligos, which is used as the template for subsequent amplification by shorter oligos (16–20 bp) annealing to the 5′ ends of the first PCR product. The shorter oligos required for the second PCR should have sequences identical to the 5′ end of the long oligos from the first PCR, which will thus repair them and yield more accurate 5′ ends (**Fig. 1** and **Table 2**).

2| Set up one PCR reaction using the long oligos and the following components in a thin-walled PCR tube.

Component	Amount (μl)	Final
ddH_2O	35.0	—
Pfu buffer (10×)	5.0	1×
dNTPs (2 mM)	5.0	0.2 mM
pAM3G or pwFRT-*pheS/sacB-gat* DNA (~20 ng μl^{-1})	1.0	~20 ng
Target-PO1 or Target-KO1 (30 μM)	1.0	30 pmol
Target-PO2 or Target-KO2 (30 μM)	1.0	30 pmol
Pfu polymerase (2.5 U μl^{-1})	2.0	5 U

▲ **CRITICAL STEP** It is essential to use *Pfu* polymerase or other polymerases that generate blunt ends in order to avoid the addition of unwanted bases (e.g., A at the 3′ end with *Taq*). The proofreading capability of *Pfu* polymerase will also significantly increase the fidelity of the PCR products.

3| Carry out the PCR as described below. Set the lid temperature to 98 °C to prevent condensation of the sample during the reaction.

Cycle number	Denaturation	Annealing	Extension	Termination
1	94 °C, 2 min			
2–34	94 °C, 30 s	58 °C, 30 s	72 °C, 3 min (pAM3G) or 2 min (pwFRT-*pheS/sacB-gat*)	
35			72 °C, 5 min	
36				4 °C, hold

■ **PAUSE POINT** PCR samples can be retained in the PCR machine or stored at 4 °C for a short period of time. For extended storage, it is recommended that the reaction be placed in a −20 °C freezer.

352

4| Visualize all PCR reactions by agarose gel electrophoresis using a 1.0% agarose gel submerged in TAE buffer (see REAGENT SETUP). Run alongside DNA ladder (e.g., 1 kb DNA ladder) for estimating PCR product size. If oligos are

designed as recommended, PCR products of ~2.7 kb (*oriT-ColE1ori-gat-ori1600-rep* from pAM3G template) or ~1.8 or 2.3 kb (*pheS/sacB-gat* from pwFRT-*pheS/sacB-gat* template) can be expected. Purify DNA from the gel with desired kit or protocol and quantify using a spectrophotometer at 260 nm. This first PCR product could be used directly for recombineering in *B. thailandensis*, with lower frequencies compared with the second PCR product (**Table 3**); however, the first PCR product should not be used directly for *B. pseudomallei* because of the lower frequencies obtained (**Table 4**).

PAUSE POINT If not used for transformation immediately, the DNA can be stored at 4 °C for a short period of time. For extended storage, it is recommended that the reaction be placed in a −20 °C freezer.

5| Set up the second PCR using the product from Step 4 as template. Typically, set up four PCR reactions to obtain sufficient amounts of DNA, using the shorter oligos as below. Multiply all of the following components by four and combine in a master mix. Pipette 50 µl of the master mix into four thin-walled PCR tubes.

Component	Amount (µl)	Final
ddH_2O	35.0	—
Pfu buffer (10×)	5.0	1×
dNTPs (2 mM)	5.0	0.2 mM
oriT-ColE1ori-gat-ori1600-rep or *pheS/sacB-gat* DNA (~20 ng μl^{-1})	1.0	~20 ng
Target-PO3 or Target-KO3 (30 µM)	1.0	30 pmol
Target-PO4 or Target-KO4 (30 µM)	1.0	30 pmol
Pfu polymerase (2.5 U μl^{-1})	2.0	5 U

▲ **CRITICAL STEP** It is essential to use *Pfu* polymerase or other polymerases that generate blunt ends in order to avoid the addition of unwanted bases. The proofreading capability of *Pfu* polymerase will significantly increase the fidelity of the PCR products.

6| Carry out the PCR as described below. Set the lid temperature to 98 °C to prevent condensation of the sample during the reaction.

Cycle number	Denaturation	Annealing	Extension	Termination
1	94 °C, 2 min			
2–34	94 °C, 30 s	58 °C, 30 s	72 °C, 3 min (pAM3G) or 2 min (pwFRT-*pheS/sacB-gat*)	
35			72 °C, 5 min	
36				4 °C, hold

PAUSE POINT PCR samples can be retained in the PCR machine or stored at 4 °C for a short period of time. For extended storage, it is recommended that the reaction be placed in a −20 °C freezer.

7| Visualize all PCR reactions by agarose gel electrophoresis, using a 1.0% agarose gel submerged in TAE buffer (see REAGENT SETUP). Run alongside DNA ladder (e.g., 1-kb DNA ladder) to estimate PCR product size. If oligonucleotides are designed as recommended, PCR products of ~2.7 kb (*oriT-ColE1ori-gat-ori1600-rep* fragment) or ~1.8 or 2.3 kb (*pheS/sacB-gat FRT* cassette) can be expected. Purify DNA from all bands produced with desired kit or protocol and quantify using a spectrophotometer at 260 nm.

Alternative strategy: If cost is not an issue, PAGE-purified long oligos could be ordered and the first PCR product could be used directly for recombineering without the need for a second PCR. The PCR with PAGE-purified long oligos should be set up exactly as the first PCR.

PAUSE POINT If not used for transformation immediately, the DNA can be stored at 4 °C for a short period of time. For extended storage, it is recommended that the reaction be placed in a −20 °C freezer.

? TROUBLESHOOTING

Introduction of pKaKa1 or pKaKa2 into *Burkholderia* species

8| The plasmids encoding λ-Red proteins are pKaKa1 (for *B. pseudomallei* and *B. thailandensis*) and pKaKa2 (for *B. pseudomallei*). One of these plasmids should be introduced into bacteria prior to PO/KO experiments, by electroporation or conjugation. Option A describes delivery of pKaKa1 by electroporation. pKaKa1 contains the kanamycin-resistance marker and selection is performed on LB + 500 μg ml^{-1} Km for *B. thailandensis* or on LB + 1,000 μg ml^{-1} Km for *B. pseudomallei*[21]. Delivery of pKaKa2 by electroporation or conjugation is described in options B and C, respectively. pKaKa2 confers arabinose-utilization ability to *B. pseudomallei* and is selected for on MA medium. The conjugation method (option C) is particularly useful for delivering plasmid into the select agent *B. pseudomallei*, as it reduces the risk of generating aerosols during electroporation. Although we only describe the mating protocol for pKaKa2 into *B. pseudomallei*, conjugation of pKaKa1 into *B. pseudomallei* could be done similarly. For KO in *B. pseudomallei*, the pKaKa1 helper plasmid should be used in conjunction with the *sacB-gat* fragment, whereas pKaKa2 should be used with *pheS-gat* fragment.

(A) Electroporation of pKaKa1 into *B. thailandensis* or *B. pseudomallei* ● **TIMING 4 d**

(i) Grow 5 ml of *B. thailandensis* or *B. pseudomallei* in LB broth from a single colony overnight at 37 °C in a shaking incubator set to 225 r.p.m. (This is the end of day 1.)

(ii) After the culture has reached a sufficient density (OD_{600} 0.8–1.5), spin down all 5 ml in a microcentrifuge at 10,000*g* for 1 min. Wash the cell pellet with 1 ml of cold, sterile ddH_2O. Repeat this four more times, adhering to the same centrifugation conditions.

! CAUTION Pipette and wash gently to minimize aerosolization of *B. pseudomallei* culture. Filtered pipette tips should be used for *B. pseudomallei* to avoid contamination of the pipette. Instead of using cold ddH_2O, 300 mM sucrose maintained at room temperature may be substituted when washing cells as previously described[15]. Comparable electroporation efficiencies can be obtained by using either method.

(iii) Remove all water from the washed pellet and resuspend the cell pellet with 40 μl of cold, sterile ddH_2O. Add 1 μl of purified pKaKa1 plasmid DNA (0.2–0.5 μg) to the competent cells and transfer the mixture into an electroporation cuvette. Place the eletroporation cuvette in the electroporator shock chamber and apply a shock of 2.5 kV, 25 μF and 200 Ω. Ensure an exponential decay of the applied shock and the absence of an arc.

? TROUBLESHOOTING

(iv) Immediately add 1 ml of rich broth medium (e.g., LB broth) to the cuvette and transfer to a round-bottom culture tube. Incubate the culture for 1 h at 37 °C with shaking at 225 r.p.m. in order to allow for kanamycin-resistance gene expression (**Fig. 1a**).

(v) Pipette 100 μl of the recovery mixture onto an LB + 500 μg ml^{-1} Km (*B. thailandensis*) or LB + 1,000 μg ml^{-1} Km (*B. pseudomallei*) plate while centrifuging the rest of the recovered culture at 16,000*g* for 1 min prior to plating. Remove all but 100 μl of medium, then spread the remaining culture on another LB + Km plate. Incubate both plates in a 37 °C incubator until colonies appear, ~2 d later.

(B) Electroporation of pKaKa2 into *B. pseudomallei* ● **TIMING 4 d**

(i) In a 15-ml Falcon tube, grow *B. pseudomallei* in 5 ml of LB broth overnight at 37 °C in a shaking incubator set to 225 r.p.m. (This is the end of day 1.)

(ii) After the culture has reached a sufficient density (OD_{600} 0.8–1.5), spin down all 5 ml in a minicentrifuge at 10,000*g* for 1 min. Wash the cell pellet with 1 ml of cold, sterile ddH_2O. Repeat this four more times adhering to the same centrifuge conditions. Alternatively, instead of using cold ddH_2O, 300 mM sucrose maintained at room temperature may be substituted when washing cells as previously described[15]. Comparable electroporation efficiencies can be obtained using either method.

(iii) Remove all water from the washed pellet and resuspend the cell pellet with 40 μl of cold, sterile ddH_2O. Add 1 μl of purified pKaKa2 plasmid (~0.2 μg) DNA to the competent cells and transfer the mixture to an electroporation cuvette. Place the eletroporation cuvette into the electroporator shock chamber and apply a shock of 2.5 kV, 25 μF and 200 Ω. Ensure an exponential decay of the applied shock and the absence of an arc.

? TROUBLESHOOTING

(iv) Immediately add 1 ml of rich broth medium (e.g., LB broth) to the cuvette and transfer to a 15-ml culture tube with a screw cap. Incubate the culture for 1 h at 37 °C with shaking at 225 r.p.m. for recovery.

(v) Transfer the recovery mixture into a 1.5-ml microcentrifuge tube and spin in a minicentrifuge at 10,000*g* for 1 min. Discard the supernatant, wash the cell pellet twice with 1 ml of 1× M9 buffer and resuspend the cell pellet in the same volume of 1× M9 buffer. Plate 100 μl of the resuspended cells onto an MA agar plate, while centrifuging the rest at 16,000*g* for 1 min. Remove all but 100 μl of buffer, then spread the remaining culture on another MA agar plate. Incubate both plates in a 37 °C incubator until colonies appear, ~2 d later.

(C) Conjugation of pKaKa2 into *B. pseudomallei* ● **TIMING 3 d**

(i) Grow a single colony of *B. pseudomallei* in 2 ml of LB broth, and grow the *E. coli* donor harboring pKaKa2 (E1354/pKaKa2) in 2 ml of MA, 1 mM Leu, 1 mM Lys, 1 mM Met, 1 mM Thr, 1 mM Trp and 100 μg ml^{-1} DAP, overnight at 37 °C in a shaking incubator set to 225 r.p.m. (This is the end of day 1.)

(ii) After both cultures have reached a sufficient density (OD_{600} 0.8–1.5), spin down 1 ml of each culture separately in a minicentrifuge at 10,000*g* for 1 min. Remove all medium from the *E. coli* donor and all but 40 µl LB from the *B. pseudomallei* tube, and resuspend both pellets in this 40 µl of LB. Spot this 40-µl mixture on the surface of a dried and prewarmed (37 °C) LB agar plate, and incubate at 37 °C for 4 h.

(iii) Gently scrape the cells off the plate with sterile inoculation loop and resuspend in 1 ml of 1× M9 in a 1.5-ml microcentrifuge tube; spin in a minicentrifuge at 10,000*g* for 1 min. Discard the supernatant, wash the cell pellet once more with 1 ml of 1× M9 buffer and resuspend the cell pellet in the same volume of 1× M9 buffer. Plate 100 µl of the resuspended cells onto an MA agar plate and incubate in a 37 °C incubator until colonies appear, ~2 d later.

Induction of λ-Red protein expression ● TIMING ~18 h

9| The λ-Red proteins encoded on pKaKa1 (Step 8A, and pKaKa2 (Step 8B) require different induction conditions, as detailed below. Option A describes the induction of the λ-Red proteins encoded on pKaKa1 with arabinose. Option B describes the induction of the λ-Red proteins encoded on pKaKa2 with rhamnose.

(A) Induction of the λ-Red proteins encoded on pKaKa1

(i) Grow the colonies of *B. thailandensis* or *B. pseudomallei* harboring pKaKa1 in 4 ml of LB broth containing 300 or 1,000 µg ml^{-1} Km, respectively.

(ii) When the culture grows to an OD_{600} of ~1.4 (*B. thailandensis*) or ~0.8 (*B. pseudomallei*), add arabinose to a final concentration of 10 mM to induce the λ-Red system on pKaKa1. After ~4 h of induction, harvest the culture by centrifugation. Concentrate the culture ~200 times by resuspending all cell pellets in 20 µl of LB broth. Proceed immediately to Step 10.
▲ **CRITICAL STEP** Induction at the proper OD is crucial for efficient recombineering. If the OD is too low, toxicity of λ-Red proteins can cause the cells to stop growing. If the OD is too high, cells tend to be 'unhealthy' after induction and recombineering efficiencies decrease.

(B) Induction of the λ-Red proteins encoded on pKaKa2

(i) Grow the colonies of *B. pseudomallei* harboring pKaKa2 in 4 ml of MA at 37 °C with shaking at 225 r.p.m.

(ii) When the culture grows to an OD_{600} of ~0.8, add rhamnose to a final concentration of 0.2% to induce the λ-Red system on pKaKa2. After ~4 h of induction, harvest the culture by centrifugation. Concentrate the culture ~200 times by resuspending all cell pellets in a 20-µl volume of LB broth. Proceed immediately to Step 10.
▲ **CRITICAL STEP** Induction at the proper OD is crucial for efficient recombineering. If the OD is too low, toxicity of λ-Red proteins can cause the cells to stop growing. If the OD is too high, cells tend to be 'unhealthy' after induction and recombineering efficiencies decrease.

DNA incubation ● TIMING ~4 d

10| Add 0.5–2.0 µg of the PO/KO DNA obtained in Step 7 of the protocol, depending on the desired frequency (**Tables 3** and **4**), to a 20-µl aliquot of induced and concentrated cells from Step 9A or 9B. Incubate the cultures for 30 min at room temperature without shaking. After 30 min, add 2 ml of LB and incubate at 37 °C with shaking at 225 r.p.m. for 1 h.
▲ **CRITICAL STEP** The DNA sample should be added to the concentrated cells in a small volume (≤10 µl), as close contact between the cells and DNA is critical for efficient DNA uptake. If the volume of the DNA sample exceeds 10 µl, dry it down in a vacuum concentrator.

11| Pipette the recovery mix into a 1.5-ml microcentrifuge tube and centrifuge at 16,000*g* for 1 min. Wash the pellet twice with 1 ml of 1× M9. Remove 800 µl of the 1× M9 and resuspend the cell pellet in the remainder of the M9. Pipette and spread 50 and 150 µl of the recovery mix onto two different MG plates containing 0.04% GS for *B. thailandensis* or 0.3% GS for various strains of *B. pseudomallei* (with the exception of strain Bp0091, for which 0.1% GS was used). Colonies should be visible in ~3 d.

PCR screening for successful PO/KO

12| The screening for correct clones for PO (A) or KO (B) is done differently, as detailed below.

(A) PO screen in *B. thailandensis* and *B. pseudomallei* ● TIMING ~3 d

(i) Single colonies, containing the PO fragment as a replicating plasmid, should appear with a frequency similar to those shown in **Table 3** or **4** (typically, when 0.5–2 µg PO DNA was used, 20–200 colonies should be expected for *B. thailandensis* or 20–60 colonies for *B. pseudomallei*). To verify a positive PO, a Target-rev gene-specific oligonucleotide (e.g., araI-rev or mbaS-rev) and a pAM3G-specific oligonucleotide (e.g., ori1600-rep-internal) should be used for PCR verification (**Table 2** and **Fig. 5**). PCR verification should be set up exactly as described above in Steps 2 and 3 with extension time ~1 min kb^{-1}.
? TROUBLESHOOTING

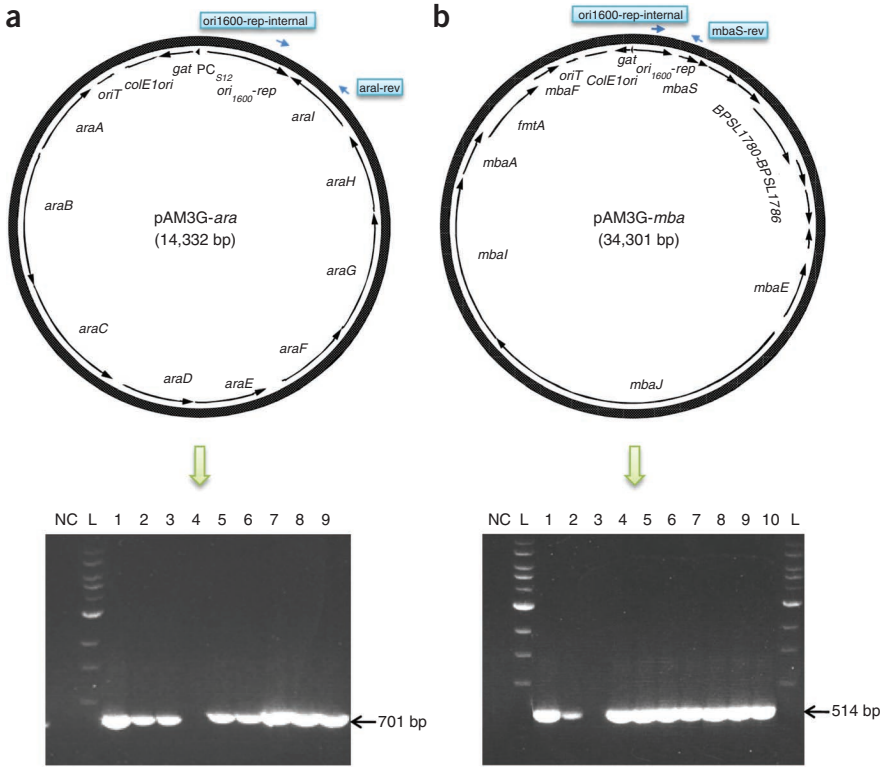

Figure 5 | PCR confirmation for pullout and knockout in *B. thailandensis* and *B. pseudomallei*. (**a**) As an example, the arabinose-utilization operon was pulled out from the *B. thailandensis* chromosome using the pAM3G backbone with 45-bp homologous sequences to the *araA* and *araI* genes. The genetic map of the resulting plasmid is shown with the oligos in blue used for PCR screening. Using these oligos, ten independent POs were screened by PCR. As indicated by the arrow, a PCR product with the correct size was obtained in 89% (eight out of nine) of the GS-resistant colonies. Abbreviations: NC, negative control using wild-type *B. thailandensis* as template; L, 1-kb DNA ladder from New England Biolabs. (**b**) Similarly, the *mba* cluster was pulled out from the *B. pseudomallei* strain 1026b chromosome, and the genetic map of the resulting plasmid, pAM3G-*mba*, was shown with the oligos in blue used for PCR screening. Using these oligos, 10 independent POs were screened by PCR. As indicated by the arrow, PCR products with the correct size were obtained in 90% (nine out of ten) of the GS-resistant colonies.

(ii) Once a successful PO of the desired fragment is verified, inoculate the positive colonies into liquid MG + 0.01% GS (*B. thailandensis*) or MG + 0.1% GS (*B. pseudomallei*). Isolate the plasmid with a plasmid isolation kit and electrotransform into an *E. coli* cloning strain (e.g., EPMax-10B or E1889 in **Table 1**) for maintenance and downstream manipulation. Electrotransformation of *E. coli* is described elsewhere[8]. Alternatively, instead of purifying plasmids from liquid culture, pipette 100 µl of the culture into a 1.5-ml microcentrifuge tube and boil the tube for 8 min. Centrifuge the tube at 16,000*g* for 1 min to spin down the cell debris. Electroporate 5 µl of the boiled supernatant into an electrocompetent *E. coli* cloning strain (e.g., EPMax-10B or E1889 in **Table 1**) for further downstream applications.

? TROUBLESHOOTING

(B) KO screen in *B. pseudomallei* ● TIMING ~5 h

(i) Single colonies, with the *pheS/sacB-gat* fragment recombined into the chromosome deleting the target gene, should appear with a similar frequency as shown in **Tables 4** and **5** (typically, when 0.5–2 µg KO DNA is used, 20–50 colonies should be expected). To verify a successful KO, a set of Target-up-out and Target-down-out oligos annealing to chromosomal regions outside the targeted KO primers are used (e.g., mbaF-out and mbaS-out, **Table 2**). PCR verification should be set up exactly as described above in Steps 2 and 3 with extension time ~1 min kb^{-1}.

? TROUBLESHOOTING

(ii) After verification of the KO, it is critical to purify the positive colonies once before growth for storage. To purify, transfer positive colonies onto an MG + GS plate and streak out for single colonies.

Recycling of the *pheS/sacB-gat* markers for KO in *B. pseudomallei* ● TIMING 3 d

13| If desired, the *pheS/sacB-gat* fragment can be removed from the mutant obtained in Step 12 by two different strategies. Option A describes replacement of the *pheS-gat* or *sacB-gat* cassette by a small PCR fragment homologous to the target gene,

Table 5 | Knockout recombineering efficiencies of the essential *asd* gene in various naturally transformable clinical and environmental *B. pseudomallei* isolates[a].

λ-Red	1026b	Bp0085	Bp0091	Bp0094	Bp4001	Bp4003	Bp4122	Bp4141	Bp4144	Bp6340
Uninduced	0	0	0	0	0	0	0	0	0	0
Induced	144 (100%)	22 (76%)	34 (88%)	15 (80%)	13 (69%)	26 (85%)	89 (53%)	52 (82%)	64 (62%)	23 (87%)

[a]Two micrograms of DNA (*pheS-gat* cassette flanked by *asd* homologous regions) was used for each incubation. Mutants were selected on MG + GS plates supplemented with 1 mM each of Met, Thr and Lys and 200 µg ml^{-1} DAP specific for this mutation. GS was used for *gat* selection at final concentration of 0.3% (wt/vol) in all strains, with the exception of 0.1% GS used for Bp0091. Twenty GS-resistant colonies were tested phenotypically and by PCR confirmation with external chromosomal primers, and the frequencies of true mutants are shown in parentheses.

by λ-Red recombination, generating a markerless mutant. Option B describes Flp-mediated excision of the *pheS-gat* or *sacB-gat* fragment, generating an unmarked mutant with a single *FRT* scar remaining in the target gene.

(A) Replacement of the *pheS-gat* or *sacB-gat* cassette with overlapping oligos

(i) Typically, set up two PCR reactions to obtain sufficient amounts of DNA, using the overlapping primers. Multiply all of the following components by two and combine in a master mix. Pipette 50 μl of the master mix into two thin-walled PCR tubes.

Component	Amount (μl)	Final
ddH_2O	30.0	—
Pfu buffer (10×)	5.0	1×
dNTPs (2 mM)	5.0	0.2 mM
[a]Target-K01 (1 μM)	1.0	1 pmol
[a]Target-K05 (1 μM)	1.0	1 pmol
Target-K03 (30 μM)	3.0	30 pmol
Target-K04 (30 μM)	3.0	30 pmol
Pfu polymerase (2.5 U μl^{-1})	2.0	5 U

[a]Target-K01 and Target-K05 anneal to each other and serve as template.

▲ **CRITICAL STEP** It is essential to use *Pfu* polymerase or other polymerases that generate blunt ends in order to avoid the addition of unwanted bases. The proofreading capability of *Pfu* polymerase will significantly increase the fidelity of the PCR products.

(ii) Carry out the PCR as described below. Set the lid temperature to 98 °C to prevent condensation of the sample during the reaction.

Cycle number	Denaturation	Annealing	Extension	Termination
1	94 °C, 2 min			
2–34	94 °C, 30 s	58 °C, 30 s	72 °C, 30 s	
35			72 °C, 5 min	
36				4 °C, hold

■ **PAUSE POINT** At this time, the DNA can be stored at 4 °C for a short period of time. For extended storage, it is recommended that the reaction be placed in a −20 °C freezer.

(iii) Visualize PCR reactions by agarose gel electrophoresis, using a 2.0% agarose gel submerged in TAE buffer (see REAGENT SETUP). Run alongside DNA ladder (e.g., 100-bp DNA ladder) to estimate PCR product size. A single PCR product of ~100 bp should be observed. Recover and purify DNA from the gel with desired kit or protocol and quantitate using a spectrophotometer.

■ **PAUSE POINT** The DNA can be stored at 4 °C for a short period of time. For extended storage, it is recommended that the reaction be placed in a −20 °C freezer.

(iv) Inoculate the purified colony obtained in Step 12B(ii) into 4 ml of MA broth (*B. pseudomallei* with pKaKa2 and the *pheS-gat* cassette) or 4 ml of LB + 1000 μg ml^{-1} Km broth (*B. pseudomallei* with pKaKa1 and the *sacB-gat* cassette) and incubate at 37 °C with shaking at 225 r.p.m. When the culture grows to an OD_{600} of ~0.8, add rhamnose to a final concentration of 0.2% (*B. pseudomallei* with pKaKa2 and the *pheS-gat* cassette) or arabinose to a final concentration of 10 mM (*B. pseudomallei* with pKaKa1 and the *sacB-gat* cassette) in order to induce the λ-Red system. After 4 h of induction, harvest all 4 ml of culture by centrifuging at 16,000*g* for 1 min. Discard the supernatant and resuspend the cell pellet in 20 μl of LB. Incubate the resuspended cells with DNA obtained in Step 13A(iii) below immediately.

▲ **CRITICAL STEP** Induction at the proper OD is crucial for efficient recombineering. If the OD is too low, toxicity of λ-Red proteins can cause the cells to stop growing. If the OD is too high, cells tend to be 'unhealthy' after induction and recombineering efficiencies decrease.

(v) Add 0.5–1.0 µg of PCR DNA (~10 µl) obtained in Step 13A(iv) to the 20 µl of resuspended cells from Step 13A(i). Incubate the mixture for 30 min at room temperature without shaking. After 30 min, add 2 ml of LB and incubate at 37 °C with shaking at 225 r.p.m. for 2 h.
▲ **CRITICAL STEP** A small volume of the DNA sample (≤10 µl) should be added to the concentrated cells, as close contact between the cells and DNA is critical for efficient uptake of DNA. If the volume of the DNA sample exceeds 10 µl, dry it down in a vacuum concentrator.

(vi) Aliquot the recovery mix into two 1.5-ml microcentrifuge tubes and centrifuge at 16,000*g* for 1 min. Combine the pellet and wash it twice with 1 ml of 1× M9. Remove 800 µl of the 1× M9 and resuspend the cell pellet in the remainder of the 1× M9. Spread 50 and 150 µl of the cell suspension onto two MG plates containing 0.1% cPhe (*B. pseudomallei* with pKaKa2 and the *pheS-gat* cassette) or two LS + 15% sucrose plates (*B. pseudomallei* with pKaKa1 and the *sacB-gat* cassette; see REAGENT SETUP). Colonies should be visible in ~2 d.

(vii) To verify successful recombination and loss of the *pheS-gat* or *sacB-gat* fragment, colonies can be patched onto MG ± 0.3% GS plates to confirm GS sensitivity. The same set of oligonucleotides used in Step 12B(i) (Target-up-out and Target-down-out), which anneal outside the homologous regions, should be used for PCR verification. PCR verification should be set up exactly as described in Steps 2 and 3 with extension time ~1 min kb^{-1}.
? TROUBLESHOOTING

(B) Flp-mediated excision of the *pheS-gat* or *sacB-gat* fragment

(i) Typically, set up four PCR reactions to obtain sufficient amounts of DNA. Multiply all of the following components by four and combine in a master mix. Pipette 50 µl of the master mix into four thin-walled PCR tubes.

Component	Amount (µl)	Final
ddH_2O	35.0	—
Pfu buffer (10×)	5.0	1×
dNTPs (2 mM)	5.0	0.2 mM
pCD13SK-Flp-*oriT*-asd_{Ec} (~20 ng μl^{-1})	1.0	~20 ng
Plac-up (30 µM)	1.0	30 pmol
Flp-down (30 µM)	1.0	30 pmol
Pfu polymerase (2.5 U μl^{-1})	2.0	5 U

▲ **CRITICAL STEP** It is essential to use *Pfu* polymerase or other polymerases that generate blunt ends in order to avoid the addition of unwanted bases. The proofreading capability of *Pfu* polymerase will significantly increase the fidelity of the PCR products.

(ii) Carry out the PCR explained as below:
Set the lid temperature to 98 °C to prevent condensation of the sample during the reaction.

Cycle number	Denaturation	Annealing	Extension	Termination
1	94 °C, 2 min			
2–34	94 °C, 30 s	58 °C, 30 s	72 °C, 3 min	
35			72 °C, 5 min	
36				4 °C, hold

■ **PAUSE POINT** At this time, the DNA can be stored at 4 °C for a short period of time. For extended storage, it is recommended that the reaction be placed in a −20 °C freezer.

(iii) Visualize PCR reactions by agarose gel electrophoresis, using a 1.0% agarose gel submerged in TAE buffer (see REAGENT SETUP). Run alongside DNA ladder (e.g., 1-kb DNA ladder) to estimate PCR product size. A single PCR product of ~2.6 kb should be observed. Recover and purify DNA from the gel with desired kit or protocol and quantitate using a spectrophotometer.
■ **PAUSE POINT** The DNA can be stored at 4 °C for a short period of time. For extended storage, it is recommended that the reaction be placed in a −20 °C freezer.

(iv) Inoculate the purified colony obtained in Step 12B(ii) into 2 ml of LB and incubate at 37 °C with shaking at 225 r.p.m. Once the OD_{600} reaches 0.8–1.5, harvest the cells by centrifuging at 16,000*g* for 1 min. Discard the supernatant and resuspend the cell pellet in 20 µl of LB. Incubate the resuspended cells with DNA obtained in Step 13B(iii) below immediately.

(v) Add 0.5–1.0 µg of PCR DNA (~10 µl) obtained in Step 13B(iv) to the 20 µl of resuspended cells from Step 13B(i). Incubate the mixture for 30 min at room temperature without shaking. After 30 min, add 2 ml of LB and incubate at 37 °C with shaking at 225 r.p.m. for 2 h.
▲ CRITICAL STEP A small volume of the DNA sample (≤10 µl) should be added to the concentrated cells, as close contact between the cells and DNA is critical for efficient uptake of DNA. If the volume of the DNA sample exceeds 10 µl, dry it down in a vacuum concentrator.

(vi) Aliquot the recovery mix into two 1.5-ml microcentrifuge tubes and centrifuge at 16,000*g* for 1 min. Wash the pellet twice with 1 ml of 1× M9. Remove 800 µl of the 1× M9 and resuspend the cell pellet in the remainder of the 1× M9. Spread 50 and 150 µl of the cell suspension onto two MG plates containing 0.1% cPhe (*B. pseudomallei* with pKaKa2 and the *pheS-gat* cassette) or two LS + 15% sucrose plates (*B. pseudomallei* with pKaKa1 and the *sacB-gat* cassette). Colonies should be visible in ~2 d.

(vii) To verify successful *FRT* recombination and loss of the *pheS-gat* or *sacB-gat* fragment, colonies can be patched onto MG ± 0.3% GS plates to confirm GS sensitivity. The same set of oligonucleotides as in Step 12B(i) (Target-up-out and Target-down-out), which anneal outside of the homologous regions, should be used for PCR verification. PCR verification should be set up exactly as described in Steps 2 and 3 with extension time ~1 min kb^{-1}.
? TROUBLESHOOTING

Curing of pKaKa1 or pKaKa2 ● TIMING ~5 d

14| The pKaKa1 or pKaKa2 helper plasmid can be cured from *B. thailandensis* or *B. pseudomallei* in one step if required. Option A describes the curing of pKaKa1 by *pheS* counterselection and is achieved on cPhe-containing medium. Option B describes the curing of pKaKa2 by *sacB* counterselection and is achieved on sucrose-containing medium.

(A) Curing of pKaKa1 via *pheS* counterselection

(i) Pick 1–2 isolates of *B. thailandensis* or *B. pseudomallei* harboring pKaKa1 using a sterile inoculation loop and streak the cells out on MG + 0.1% cPhe plates. Incubate the plates at 37 °C for 1–2 d until single colonies appear.

(ii) To confirm the loss of pKaKa1 plasmid, patch 10–20 single colonies from MG + cPhe plate onto LB + 500 µg ml^{-1} Km (*B. thailandensis*) or 500 µg ml^{-1} Km (*B. pseudomallei*) plate and incubate at 37 °C. Be sure to include *B. thailandensis* or *B. pseudomallei* harboring pKaKa1 and wild-type *B. thailandensis* or *B. pseudomallei* on the plate as positive and negative controls, respectively.

(B) Curing of pKaKa2 by *sacB* counterselection

(i) Pick 1–2 isolates of *B. pseudomallei* harboring pKaKa2 using a sterile inoculation loop and streak the cells out on LS + 15% sucrose plates. Incubate the plates at 37 °C for 1–2 d until single colonies appear.

(ii) To confirm the loss of pKaKa2 plasmid, patch 10–20 single colonies from LS + sucrose plate onto MA plate and incubate at 37 °C. Be sure to include *B. pseudomallei* harboring pKaKa2 and wild-type *B. pseudomallei* on the plate as positive and negative controls, respectively.

? TROUBLESHOOTING

Troubleshooting advice can be found in **Table 6**.

TABLE 6 | Troubleshooting table.

Step	Problem	Possible reason	Possible solution
7	No second PCR product or high level of non-specific products is obtained	High-GC fragment causes inefficient denaturation and non-specific annealing.	Try a gradient PCR with annealing temperature range 50–70 °C, include 5–10% DMSO in the PCR reaction to aid amplification of high-GC fragments
		Majority of the long primers are truncated (not PAGE purified) in this batch, resulting in first PCR products with truncated ends	Inform primer synthesis company and resynthesize the non–PAGE purified long primers free of charge (from IDT and so on), and retry the PCR
		Poor design of primers	Redesign the primers so that their GC% is 50–60% with no significant primer-dimer and hairpin structure formation, and the amplicons are as small as possible

(continued)

Table 6 | Troubleshooting table (continued).

Step	Problem	Possible reasons	Possible solutions
8A(iii) and 8B(iii)	Arcing is observed when applying electopulse	Inefficient washing results in high-salt concentration, or too much DNA is used	Perform additional washes to the cell pellet, and/or use reduced amount of DNA (e.g., 0.5–1 μg instead of 2 μg)
12A(i) and 12B(i); 13A(vii) and 13B(vii)	No PCR product or high level of non-specific products is obtained	High-GC fragment causes inefficient denaturation and non-specific annealing	Try a gradient PCR with annealing temperature range 50–70 °C, include 5–10% DMSO in the PCR reaction to aid amplification of high-GC fragments
		Poor design of primers	Redesign the primers so that their GC% is 50–60% with no significant primer-dimer and hairpin structure formation, and the amplicons are as small as possible
		The clones do not contain the desired KO or PO fragments	Retry the recombineering
12A(ii)	No colonies are obtained	Size of the PO fragments and toxicity of their gene products may be an issue	Use a fragment containing a low-copy-number origin for PO (e.g., pBBR-based origin)

● TIMING

Steps 1–7, Preparing KO/PO DNA: 1 d
Step 8, Introduction of pKaKa1 or pKaKa2: 3–4 d
Step 9, Induction: 18 h
Steps 10 and 11, DNA incubation: 4 d
Step 12, PCR screening: 1–3 d
Step 13, Recycling of markers: 3 d
Step 14, Curing of pKaKa1 or pKaKa2: 5 d

ANTICIPATED RESULTS

PO recombineering efficiency of chromosomal fragments from *B. thailandensis*

Using the protocol provided will typically produce 40–200 colonies depending on the amount of DNA and type of PCR product used (**Table 3**). As an example, the *B. thailandensis ara* operon was pulled out of the chromosome with a PCR fragment containing a bhr origin of replication. Successful removal of the *ara* operon was verified using an *ara*-specific primer and a plasmid-origin-specific primer (**Fig. 5a**). A high percentage (~90%) of the colonies contained the pulled-out fragment (**Table 3** and **Fig. 5a**). Such a percentage should be common as these numbers were obtained from experiments that were done in triplicate, and bacteria that do not contain *gat* should not grow on medium containing GS.

PO recombineering in *B. pseudomallei*

Using the helper plasmid pKaKa2 (constructed with the *ara* operon pulled out from *B. thailandensis*), the efficiencies of PO recombineering in *B. pseudomallei* are shown in **Table 4**; these are relatively lower than those of PO in *B. thailandensis* (**Table 3**). Introduction of pKaKa2 into *B. pseudomallei* can be achieved through electroporation or conjugation. High efficiency can be expected from both methods. Selection and maintenance of pKaKa2 in *B. pseudomallei* is simple and tight, as cells without the plasmid will not be able to metabolize arabinose as a nutrient source. A higher concentration of GS (0.3% instead of 0.04% for *B. thailandensis*) should be used for selection of the PO plasmid. Successful PO of chromosomal fragments should be confirmed by PCR using two oligos, of which one anneals to the plasmid backbone and the other to the PO fragment (e.g., *mba* cluster in **Fig. 5b**). High frequencies (90–100%) of successful PO can be expected (**Fig. 5b** and **Table 4**). No GS-resistant colonies were observed when the λ-Red system was not induced, indicating that *recA*-mediated recombination did not recombine 40–45 bp of homology at any detectable frequencies (**Table 4**).

KO recombineering in *B. pseudomallei* strains

360

We first demonstrated the KO recombineering in *B. pseudomallei* by knocking out the *mba* cluster in strain 1026b. The efficiencies of KO recombineering in the *B. pseudomallei mba* cluster are shown in **Table 4**: 20–50 colonies are usually

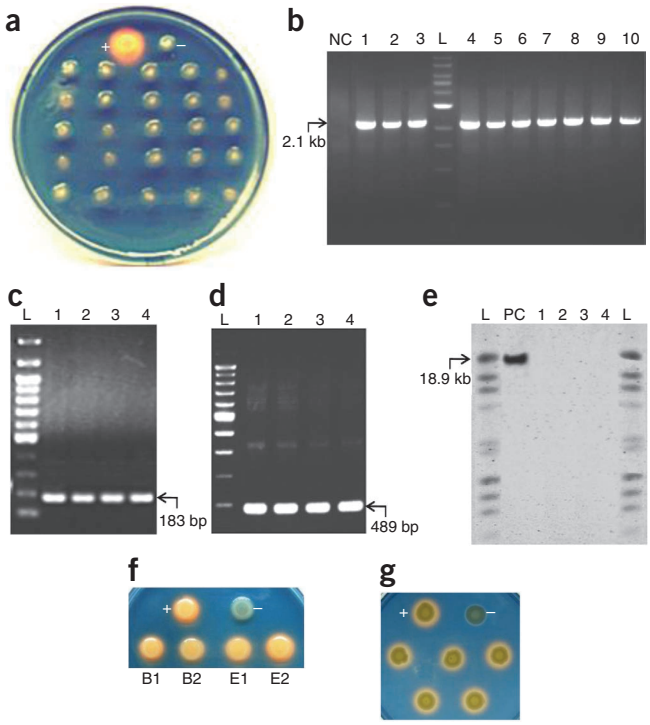

Figure 6 | Phenotypic and PCR confirmation for the *mba*-cluster knockouts in the *B. pseudomallei*. As an example, the *B. pseudomallei* strain 1026b *mba* cluster was knocked out, using the *pheS-gat* fragment with 45-bp homologous sequences to the *mbaF* and *mbaS* genes. A total of 25 independent knockout mutants were spotted onto a CAS (chrome azurol S) plate[27], along with the wild-type 1026b strain (+) and the enterobactin-negative *E. coli* mutant (−, JW0586-1 (ref. 28)) as the positive and negative control, respectively. As the *mba* cluster is involved in malleobactin synthesis and secretion, knockout mutants display the malleobactin-negative phenotype as an absence of orange halo. The knockout frequency is 100% in these 25 isolates. (**b**) Oligos annealing outside the homologous region were used to screen ten isolates from **a** for successful KOs (oligos mbaF-out and mbaS-out as in **Fig. 3**). A total of 100% (ten out of ten) of the GS-resistant colonies were shown to have the *pheS-gat* fragment inserted into the *mba* cluster, as indicated by the arrow. NC indicates negative control using wild-type 1026b as the PCR template. L indicates the 1-kb DNA ladder from New England Biolabs. (**c**,**d**) Following the second λ-Red–mediated recombination with overlapping oligos (**c**) or Flp-mediated excision (**d**), unmarked mutations were generated. PCR confirmation was done for both methods, using the same outside oligos as in **b**, yielding smaller PCR products lacking *pheS-gat* as indicated by arrows in **c** and **d**. In both **c** and **d**, L indicates the 100-bp DNA ladder from New England Biolabs. (**e**) After mutant construction, the pKaKa2 helper plasmid was cured from the 1026b-Δ*mba*::*pheS-gat* by *sacB* counterselection on sucrose-containing medium. Total nucleic acids were purified from strain 1026b-Δ*mba*::*pheS-gat*/pKaKa2 (lane 1) and four isolates of cured strain 1026b-Δ*mba*::*pheS-gat* without pKaKa2 (lanes 2–5) for Southern hybridization analysis, using the entire pKaKa2 plasmid as a probe. As indicated by arrow, the helper plasmid pKaKa2 exists only in strain 1026b-Δ*mba*::*pheS-gat*/pKaKa2, whereas the entire pKaKa2 sequence is completely lost in 1026b-Δ*mba*::*pheS-gat* after curing. L, prebiotinylated DNA ladder from New England Biolabs (mixture of HindIII-digested λ DNA and HaeIII-digested ϕ×174 DNA). (**f**) To demonstrate the integrity of the PO fragment, boiling preps of two 1026b/pAM3G-*mba* isolates were electroporated directly into 1026b-*mba*::*FRT* mutant for the complementation study (B1 and B2). In addition, the same boiling preps of 1026b/pAM3G-*mba* were transformed into an *E. coli* restriction-minus strain; plasmids were then reisolated from *E. coli* and reintroduced to complement the 1026b-*mba*::*FRT* mutant (E1 and E2). These four complemented strains were spotted on a CAS plate along with positive (+, wild-type 1026b) and negative (−, 1026b-*mba*::*FRT*) controls, and all four isolates regained the ability to produce malleobactin. (**g**) Boiling preps from five different isolates of 1026b/pAM3G-*mba* were electroporated into *E. coli* JW0586-1 strain, and the resulted strains were spotted onto CAS plates with positive (+, *E. coli* K-12 strain) and negative (−, *E. coli* JW0586-1 strain) controls. As shown, the *B. pseudomallei* 1026b *mba* operon complemented the enterobactin-deficient phenotype of *E. coli* JW0586-1 strain.

obtained when 0.5–2 μg KO DNA fragment is used. Independent GS-resistant isolates were screened by phenotypic and PCR confirmation (**Fig. 6a**,**b**), showing 100% frequency of successful KO. Generally, high frequencies (90–100%) are expected for the successful KO of chromosomal fragments when the *gat* marker is used for selection (**Fig. 6a**,**b**). Two options, via a second λ-Red–mediated recombination or Flp-catalyzed excision, were provided for the removal of the *pheS-gat* or *sacB-gat FRT* cassette from the mutant chromosomes. The λ-Red–mediated recombination results in a clean deletion of the chromosome fragment, whereas the Flp-catalyzed (λ-Red independent) excision leaves a single '*FRT*-scar' inside the targeted fragment. Alternatively, instead of *flp*-containing PCR product incubation, we have expressed Flp transiently by conjugating the suicidal vector, pCD13SK-Flp-*oriT*-asd_{Ec}, from *E. coli* Δ*asd* strain (E1354 in **Table 1**) and immediately counterselected the conjugation mix on cPhe- or sucrose-containing medium, yielding GS-sensitive clones. Use of the *pheS-gat* or *sacB-gat FRT* cassette for KO makes the creation of unmarked mutations easy, as little to no resistance to cPhe or sucrose was observed. As an example, the removal of the *pheS-gat* cassette was close to 100% efficient (**Fig. 6c**,**d** with the *mba* cluster as an example). The confirmation of unmarked mutations is simple, as the PCR products amplified using outside primers are small (approximately 200–500 bp; **Fig. 6c**,**d**). After introduction of the pKaKa2 plasmid, unmarked mutant could be obtained in ~10 d. pKaKa2 could be easily cured or maintained for the subsequent manipulation, such as creating multiple mutations in the same strain or introducing reporter-gene fusions. If required, the curing of pKaKa2 on sucrose medium could be confirmed by the inability to grow on arabinose as a sole carbon source. The curing efficiency was observed to be close to 100% (**Fig. 6**). If pKaKa1 in conjunction with the *sacB-gat* fragment was used for *B. pseudomallei* KO, then the efficiencies for KO and curing of helper plasmid pKaKa1 are expected to be similar to those when pKaKa2 and *pheS-gat* are used. Since the first submission of this protocol, we have used this system to PO and KO genes in both species with relative ease.

To demonstrate and extend the use of λ-Red recombineering in other naturally transformable *B. pseudomallei* strains, we tested 20 additional *B. pseudomallei* strains and found that 9 were naturally transformable (**Table 1**). We chose these nine strains encompassing clinical and environmental isolates (**Table 1**). The *pheS-gat* cassette was used to successfully KO the *asd* gene in these nine *B. pseudomallei* strains, and results are shown in **Table 5** and **Figure 7**. The frequencies

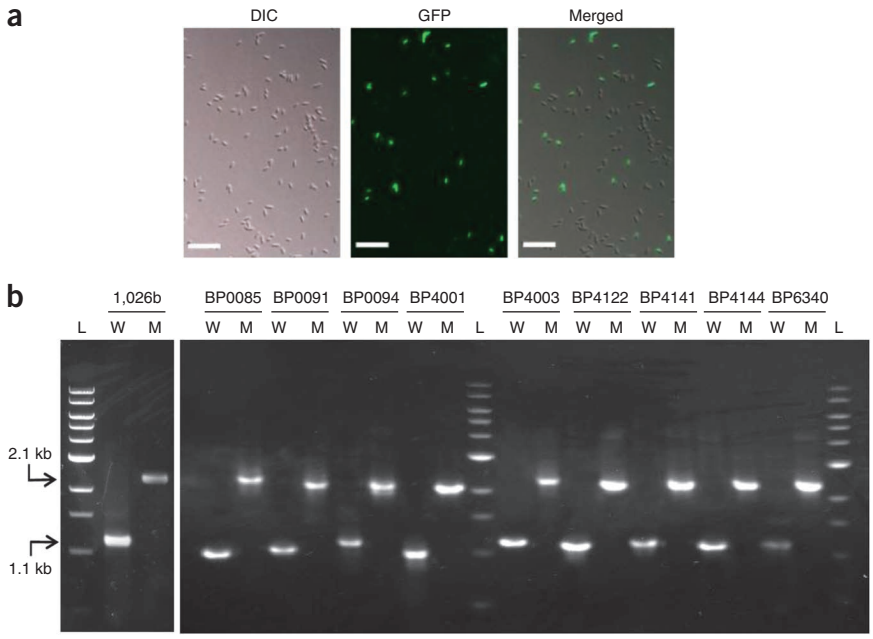

Figure 7 | KO recombineering in different *B. pseudomallei* strains. (**a**) Various clinical and environmental isolates of *B. pseudomallei* were incubated with *gfp*-containing PCR product to confirm their natural competency. After DNA incubation and a 45-min recovery in LB, transient expression of GFP was observed for all nine naturally transformable strains (**Table 1**); representative images are shown for one of these strains. The other 11 *B. pseudomallei* strains tested did not yield fluorescent bacteria and presumably are not naturally competent (data not shown). DIC, differential interference contrasts. White scale bars equal 10 µm in length. (**b**) Successful KO of the *asd* gene in 1026b strain and the nine newly identified naturally transformable *B. pseudomallei* strains were confirmed by PCR with oligos annealing outside the *asd* gene on the chromosome, and one isolate from each strain is shown. W, wild type; M, mutant; L, 1-kb DNA ladder from New England Biolabs. The ~2.1-kb PCR products obtained in all mutant strains are results of *pheS-gat* insertion in the *asd* region indicated by the ~1.1-kb PCR fragment in the corresponding wild-type strains.

of true mutants were high (>50%, **Table 5**), even for KO of the essential *asd* gene[9], and screening two colonies should yield mutants using this system.

ACKNOWLEDGMENTS The project described was supported by Award Number AI065359 from the US National Institute of Allergy and Infectious Diseases and in part by the Center of Biomedical Research Excellence grant P20RR018727 from the National Center for Research Resources (both components of the NIH). We are grateful to H.P. Schweizer for the generous gift of constructs containing a modified *sacB* gene and the rhamnose-inducible promoter.

AUTHOR CONTRIBUTIONS Y.K. created the constructs and performed the experiments in *B. pseudomallei*. M.H.N. performed the experiments in *B. thailandensis*. B.A.W. provided guidance for M.H.N. in this project. A.T. and P.S.K. isolated and sequenced the *B. pseudomallei* clinical and environmental isolates on **Table 1**. T.T.H. designed and supervised the experiments. Y.K., M.H.N. and T.T.H. wrote this manuscript.

COMPETING FINANCIAL INTERESTS The authors declare no competing financial interests.

Published online at http://www.natureprotocols.com/.
Reprints and permissions information is available online at http://npg.nature.com/reprintsandpermissions/.

1. Sawitzke, J.A. *et al.* Recombineering: *in vivo* genetic engineering in *E. coli*, *S. enterica*, and beyond. *Meth. Enzymol.* **421**, 171–199 (2007).
2. Zhang, Y., Muyrers, J.P.P., Testa, G. & Stewart, A.F. DNA cloning by homologous recombination in *Escherichia coli*. *Nat. Biotechnol.* **18**, 1314–1317 (2000).
3. Datsenko, K.A. & Wanner, B.L. One-step inactivation of chromosomal genes in *Escherichia coli* K-12 using PCR products. *Proc. Natl. Acad. Sci. USA* **97**, 6640–6645 (2000).
4. Sun, W., Wang, S. & Curtiss, R. III. Highly efficient methods for introducing successive multiple scarless gene deletions and markerless gene insertions into the *Yersinia pestis* chromosome. *Appl. Environ. Microbiol.* **74**, 4241–4245 (2008).
5. Lesic, B. & Rahme, L.G. Use of the lambda Red recombinase system to rapidly generate mutants in *Pseudomonas aeruginosa*. *BMC Mol. Biol.* **9**, 20 (2008).
6. Wiersinga, W.J., van der Poll, T., White, N.J., Day, N.P. & Peacock, S.J. Melioidosis: insight into the pathogenicity of *Burkholderia pseudomallei*. *Nat. Rev. Microbiol.* **4**, 272–282 (2006).
7. Thongdee, M. *et al.* Targeted mutagenesis of *Burkholderia pseudomallei* and *Burkholderia thailandensis* through natural transformation of PCR fragments. *Appl. Environ. Microbiol.* **74**, 2985–2989 (2008).
8. Barrett, A.R. *et al.* Genetic tools for allelic replacement in *Burkholderia* species. *Appl. Environ. Microbiol.* **74**, 4498–4508 (2008).
9. Norris, M.H., Kang, Y., Lu, D., Wilcox, B.A. & Hoang, T.T. Glyphosate resistance as a novel select-agent-compliant, non-antibiotic selectable marker in chromosomal mutagenesis of the essential genes *asd* and *dapB* of *Burkholderia pseudomallei*. *Appl. Environ. Microbiol.* **75**, 6062–6075 (2009).
10. Moore, R.A. *et al.* Contribution of gene loss to the pathogenic evolution of *Burkholderia pseudomallei* and *Burkholderia mallei*. *Infect. Immun.* **72**, 4172–4187 (2004).
11. Chandler, J.R. *et al.* Mutational analysis of *Burkholderia thailandensis* quorum sensing and self-aggregation. *J. Bacteriol.* **191**, 5901–5909 (2009).
12. Choi, K.-H., Kumar, A. & Schweizer, H.P. A 10-min method for preparation of highly electrocompetent *Pseudomonas aeruginosa* cells: application for the DNA fragment transfer between chromosomes and plasmid transformation. *J. Microbiol. Meth.* **64**, 391–397 (2006).
13. Mack, K. & Titball, R.W. Transformation of *Burkholderia pseudomallei* by electroporation. *Anal. Biochem.* **242**, 73–76 (1996).
14. Lopez, C.M., Rholl, D.A., Trunck, L.A. & Schweizer, H.P. Versatile dual-technology system for markerless allele replacement in *Burkholderia pseudomallei*. *Appl. Environ. Microbiol.* **75**, 6496–6503 (2009).
15. Choi, K.H. *et al.* Genetic tools for select-agent-compliant manipulation of *Burkholderia pseudomallei*. *Appl. Environ. Microbiol.* **74**, 1064–1075 (2008).
16. Antoine, R. & Locht, C. Isolation and molecular characterization of a novel broad-host-range plasmid from *Bordetella bronchiseptica* with sequence similarities to plasmids from Gram-positive organisms. *Mol. Microbiol.* **6**, 1785–1799 (1991).
17. Nakayama, M. & Ohara, O. Improvement of recombination efficiency by mutation of Red proteins. *BioTechniques* **38**, 917–924 (2005).
18. Alice, A.F., Lopez, C.S., Lowe, C.A., Ledesma, M.A. & Crosa, J.H. Genetic and transcriptional analysis of the siderophore malleobactin biosynthesis and transport genes in the human pathogen *Burkholderia pseudomallei* K96243. *J. Bacteriol.* **188**, 1551–1566 (2006).
19. Sambrook, J. & Russell, D.W. *Molecular Cloning: A Laboratory Manual* 2nd edn, (Cold Spring Harbor Laboratory Press, Cold Spring Harbor, New York, USA, 2001).

20. Wilson, D.E. & Chosewood, L.C. *Biosafety in Microbiological and Biomedical Laboratories (BMBL)* 5th edn. (Centers for Disease Control and Prevention, Atlanta, Georgia, USA, 2007).
21. Rholl, D.A., Trunck, L.A. & Schweizer, H.P. *Himar1 in vivo* transposon mutagenesis of *Burkholderia pseudomallei*. *Appl. Environ. Microbiol.* **74**, 7529–7535 (2008).
22. Yanisch-Perron, C., Vieira, J. & Messing, J. Improved M13 cloning vectors and host strains: nucleotide sequences of the M13mp18 and pUC19 vectors. *Gene* **33**, 103–119 (1985).
23. Kovach, M.E. *et al.* Four new derivatives of the broad-host-range cloning vector pBBR1MCS, carrying different antibiotic-resistance cassettes. *Gene* **166**, 175–176 (1995).
24. Schweizer, H.P., Klassen, T.R. & Hoang, T. Improved methods for gene analysis and expression in *Pseudomonas*. In *Molecular Biology of Pseudomonads.* (eds. Nakazawa, T., Furukawa, K., Haas, D. & Silver, S.) 229–237 (American Society for Microbiology, Washington, D.C., USA, 1996).
25. Cardona, S.T. & Valvano, M.A. An expression vector containing a rhamnose-inducible promoter provides tightly regulated gene expression in *Burkholderia cenocepacia*. *Plasmid* **54**, 219–228 (2005).
26. Yu, M. & Tsang, J.S.H. Use of ribosomal promoters from *Burkholderia cenocepacia* and *Burkholderia cepacia* for improved expression of transporter protein in *Escherichia coli*. *Protein Expr. Purif.* **49**, 219–227 (2006).
27. Schwyn, B. & Neilands, J.B. Universal chemical assay for the detection and determination of siderophores. *Anal. Biochem.* **160**, 47–56 (1987).
28. Baba, T. *et al.* Construction of *Escherichia coli* K-12 in-frame, single-gene knockout mutants: the Keio collection. *Mol. Syst. Biol.* **2**, 2006.0008 (2006).
29. DeShazer, D., Brett, P.J., Carlyon, R. & Woods, D.E. Mutagenesis of *Burkholderia pseudomallei* with Tn5-OT182: isolation of motility mutant and molecular characterization of the flagellin structural gene. *J. Bacteriol.* **179**, 2116–2125 (1997).
30. Brett, P.J., DeShazer, D. & Woods, D.E. *Burkholderia thailandensis* sp. nov., description of *Burkholderia pseudomallei*-like species. *Int. J. Syst. Bacteriol.* **48**, 317–320 (1998).
31. Kang, Y., Norris, M.H., Barrett, A.R., Wilcox, B.A. & Hoang, T.T. Engineering of tellurite-resistant genetic tools for single-copy chromosomal analysis of *Burkholderia* spp. and characterization of the *B. thailandensis betBA*-operon. *Appl. Environ. Microbiol.* **75**, 4015–4027 (2009).

OPEN ACCESS Freely available online

PLOS ONE

Elucidating the *Pseudomonas aeruginosa* Fatty Acid Degradation Pathway: Identification of Additional Fatty Acyl-CoA Synthetase Homologues

Jan Zarzycki-Siek[1], Michael H. Norris[2], Yun Kang[1], Zhenxin Sun[1], Andrew P. Bluhm[1], Ian A. McMillan[2], Tung T. Hoang[1,2]*

1 Department of Microbiology, University of Hawaii at Manoa, Honolulu, Hawaii, United States of America, **2** Department of Molecular Bioscience and Bioengineering, University of Hawaii at Manoa, Honolulu, Hawaii, United States of America

Abstract

The fatty acid (FA) degradation pathway of *Pseudomonas aeruginosa*, an opportunistic pathogen, was recently shown to be involved in nutrient acquisition during BALB/c mouse lung infection model. The source of FA in the lung is believed to be phosphatidylcholine, the major component of lung surfactant. Previous research indicated that *P. aeruginosa* has more than two fatty acyl-CoA synthetase genes (*fadD*; PA3299 and PA3300), which are responsible for activation of FAs using ATP and coenzyme A. Through a bioinformatics approach, 11 candidate genes were identified by their homology to the *Escherichia coli* FadD in the present study. Four new homologues of *fadD* (PA1617, PA2893, PA3860, and PA3924) were functionally confirmed by their ability to complement the *E. coli fadD* mutant on FA-containing media. Growth phenotypes of 17 combinatorial *fadD* mutants on different FAs, as sole carbon sources, indicated that the four new *fadD* homologues are involved in FA degradation, bringing the total number of *P. aeruginosa fadD* genes to six. Of the four new homologues, *fadD4* (PA1617) contributed the most to the degradation of different chain length FAs. Growth patterns of various *fadD* mutants on plant-based perfumery substances, citronellic and geranic acids, as sole carbon and energy sources indicated that *fadD4* is also involved in the degradation of these plant-derived compounds. A decrease in fitness of the sextuple *fadD* mutant, relative to the Δ*fadD1D2* mutant, was only observed during BALB/c mouse lung infection at 24 h.

Citation: Zarzycki-Siek J, Norris MH, Kang Y, Sun Z, Bluhm AP, et al. (2013) Elucidating the *Pseudomonas aeruginosa* Fatty Acid Degradation Pathway: Identification of Additional Fatty Acyl-CoA Synthetase Homologues. PLoS ONE 8(5): e64554. doi:10.1371/journal.pone.0064554

Editor: Mikael Skurnik, University of Helsinki, Finland

Received January 16, 2013; **Accepted** April 16, 2013; **Published** May 29, 2013

Funding: Funding for this research was provided by grant number P20GM103516 from the National Institute of General Medical Sciences of the National Institutes of Health. The study design and content are solely the responsibility of the authors and do not represent the official views of the National Institutes of Health. The funders had no role in study design, data collection and analysis, decision to publish, or preparation of the manuscript.

Competing Interests: The authors have declared that no competing interests exist.

* E-mail: tongh@hawaii.edu

Introduction

Pseudomonas aeruginosa is an important human pathogen [1], [2] responsible for myriad of infections of the human body [3–11]. This ubiquitous bacterium is also a leading cause of mortality and morbidity in patients with cystic fibrosis (CF) [1], [2].

Phosphatidylcholine (PC), the major component of lung surfactant [12], was suggested as a potential nutrient source for pathogenesis during *P. aeruginosa* infection of the CF lung [13]. The major carbon source within the PC molecule comes from the two highly reduced long-chain fatty acids (LCFA). Many fatty acid degradation (β-oxidation) genes are expressed by *P. aeruginosa* during CF lung infection (e.g. *fadD1*: PA3299, *fadD2*: PA3300, *fadA5*: PA3013, and *fadB5*: PA3014) [13] and mutants defective in the fatty acid (FA) degradation pathway were reported to have decreased fitness during mouse lung infection [14]. A link between FA degradation genes and virulence was also observed [14] and *P. aeruginosa* can chemotax towards FA [15]. Furthermore, FA was shown to modulate type three-secretion system expression in this bacterium [16].

Despite the connection between virulence and FA degradation during infections, not all genes involved in *P. aeruginosa* FA degradation are characterized (Fig. 1A). In contrast, genes needed by *Escherichia coli* for aerobic β-oxidation (*fadL*, *fadD*, *fadE*, and *fadBA* [17–20]), anaerobic FA degradation (*fadK* and *fadIJ* [21]), and auxiliary genes (*fadH* [22] and *fadM* [23]) are well characterized. For an exogenous FA to be degraded by this pathway, it must first be transported by the membrane transporter (FadL) into the cell [24]. FA is then activated with the use of adenosine triphosphate (ATP) and coenzyme A (CoASH) by FadD (fatty acyl-CoA synthetase, FACS) [19], [25]. The activated FA molecule can then proceed through the β-oxidation pathway (Fig. 1A). In *E. coli*, genes encoding enzymes needed for β-oxidation (*fadL, fadD, fadE, and fadBA*) are repressed in the absence of FAs by the transcriptional regulator FadR. Acyl-CoA of chain length $\geq C_{12:0}$ can bind to FadR to induce FA degradation [18], [26], [27] resulting in growth on FA ($> C_{10:0}$). Cyclic AMP and receptor protein complex levels [28], presence of oxygen [29], and osmotic pressure [30] also affect expression of FA degradation genes in *E. coli*. However, the existence of a central regulator, such as *fadR*, is unknown in *P. aeruginosa*, and only a few *fad*-genes have been found to be regulated by a FA sensor, PsrA [31].

P. aeruginosa exhibits greater metabolic capabilities for FA degradation than *E. coli* by growing aerobically on short, medium, and long-chain FAs as sole carbon and energy sources [31]. With a

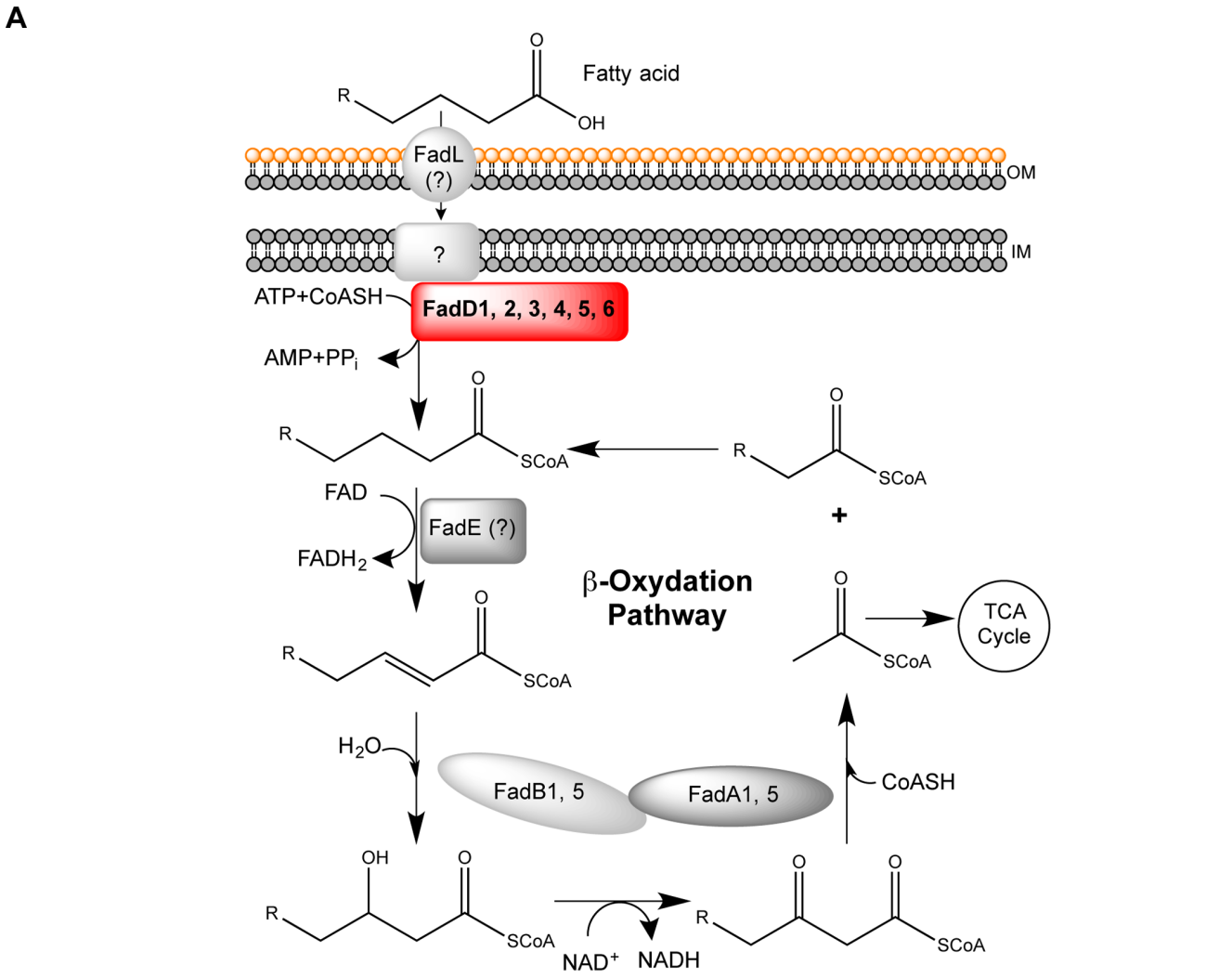

Figure 1. *P. aeruginosa* fatty acid degradation pathway (FA degradation). (A) *P. aeruginosa* FA degradation model was based on the *E. coli* β-oxidation pathway. Known *P. aeruginosa* FA degradation enzyme homologues are indicated by numbers: FadD1 (PA3299), FadD2 (PA3300), FadD3 (PA3860), FadD4 (PA1617), FadD5 (PA2893), FadD6 (PA3924), FadAB1 (PA1736–PA1737), and FadBA5 (PA3013–PA3014). Abbreviations: FadA, 3-ketoacyl-CoA thiolase; FadB, *cis*-Δ^3-*trans*-Δ^2-enoyl-CoA isomerase, enoyl-CoA hydratase, 3-hydroxyacyl-CoA epimerase, and 3-hydroxyacyl-CoA dehydrogenase; FadD, fatty acyl-CoA synthetase; FadE, acyl-CoA dehydrogenase; FadL, outer membrane long-chain fatty acid translocase; OM, outer membrane; IN, inner membrane. (B) Alignment of FadD homologues motifs with *E. coli* FadD motifs. Amino acids with similar properties are assigned the same colors using CLC Sequence Viewer 6 software (www.clcbio.com).
doi:10.1371/journal.pone.0064554.g001

genome of 6.3 Mb, *P. aeruginosa* could potentially have more FA degradation genes than *E. coli* [32], suggesting possible redundancies and a higher level of complexity in this pathway. Three potential *fadL*s have been investigated thus far in *P. aeruginosa* and their exact role in FA transport still remains unclear [15]. Two *fadBA* operon homologues (*fadAB1* and *fadBA5*) have been studied so far. The *fadAB1* (PA1736 and PA1737) operon was shown to be strongly induced by medium-chain fatty acids (MCFA, $C_{10:0}$ and $C_{12:0}$) and, to a lesser extent, LCFA ($C_{14:0}$–$C_{18:1}^{\Delta 9}$) [33]. The *fadBA5* (PA3014 and PA3013) operon was determined to be

involved in LCFA metabolism and to be induced by LCFA, especially oleate ($C_{18:1}^{\Delta 9}$) [31]. We have recently identified two FACS homologues of *P. aeruginosa*, *fadD1* (PA3299) and *fadD2* (PA3300) [14]. The FadD1 and FadD2 of *P. aeruginosa* were determined to have broad specificity for FA of different chain lengths. FadD1 has preference for LCFA whereas FadD2 has higher activities for shorter chain FAs. *fadD1*, *fadD2,* and *fadD2D1* mutants showed growth defects when grown on minimal media with different length FAs as sole carbon sources. *fadD1* was determined to be induced by LCFA and to be more important for growth on LCFA while *fadD2* was important for growth on short-chain fatty acids (SCFA) and was induced by MCFA. The double mutant *fadD2D1* displayed an impaired ability to grow on PC as a sole carbon source. This growth defect translated into decreased *in vivo* fitness during mouse lung infection, indicating that FadD1 and FadD2 may mediate *P. aeruginosa* replication in the CF lung [14]. However, the double mutant *fadD2D1* was still able to grow on FA, suggesting the involvement of other *fadD* homologues in FA degradation [14].

We surveyed the *P. aeruginosa* genome for additional *fadD* homologues to gain more insight into the degradation of FAs in this bacterium. Four new *fadD* homologues PA1617, PA2893, PA3860, and PA3924 were identified out of 11 potential candidates. Through genetic analyses, their contribution to FA degradation was assessed. The final four candidates were determined to be FACS homologues, but PA1617 (*fadD4*) was found to be the major contributor to FA degradation. Involvement of the newly discovered *fadD4* in catabolism of plant-derived acyclic terpenes suggests that the function of multiple FACS in *P. aeruginosa* is the degradation of compounds closely related to FAs. Growth defect on PC and decreased fitness in mouse lung of the sextuple *fadD* mutant supports the role of FA as a nutrient *in vivo*.

Results

Identification of *P. aeruginosa* Fatty acyl-CoA Synthetase Homologues

To identify *fadD* homologues of *P. aeruginosa*, *E. coli* FadD amino acid sequence was compared to *P. aeruginosa* PAO1 ORFs via BLAST [34]. The amino acid sequence of genes obtained in the search were further analyzed for the presence of ATP/AMP [19], [35–37] and fatty acid binding motifs [38]. Genes that encode eleven proteins containing amino acid sequences with high degree of similarity to the motifs found in *E. coli* FadD (Fig. S1) were chosen for complementation tests. Identity and similarity of the proteins range from 22% to 31% and from 37% to 52%, respectively (Table S1). When cloned into a high copy number pUC19 vector, only genes encoding PA3860, PA1617, PA2893, and PA3924 were found to complement the *E. coli* $fadD^{-}/fadR^{-}$ (E2011) strain on minimal medium containing oleate ($C_{18:1}^{\Delta 9}$) and decanoate ($C_{10:0}$) (Table S1) and were designated *fadD3*, *fadD4*, *fadD5*, and *fadD6*, respectively. Their ATP/AMP and FA binding motifs show high degree of similarity to those of *E. coli* FadD (Fig. 1B).

All four *P. aeruginosa fadD* genes (*fadD3*, *fadD4*, *fadD5,* and *fadD6*) were tested further for their ability to support growth of *E. coli* $fadD^{-}/fadR^{-}$ (E2011) on various FAs as a single copy on the *E. coli* chromosome. The *E. coli* $fadD^{-}/fadR^{-}$ double mutant was used to ensure that FadR does not inhibit expression of other *E. coli* β-oxidation enzymes. Mini-Tn7 based complementation vectors were constructed and integrated into the E2011 chromosome at the *att*Tn7 site and resulting strains were tested for growth on FAs (Table 1). As expected, wildtype *E. coli* control strain K-12 showed growth on longer FAs ($C_{12:0}$–$C_{18:1}^{\Delta 9}$) but not on the MCFA, $C_{10:0}$, or SCFAs ($C_{4:0}$–$C_{8:0}$). The E2011 and the integrated empty-vector control strain were not able to growth on any of the FAs. E2011 complemented with *E. coli fadD* ($fadD_{Ec}$) grew on $C_{12:0}$–$C_{18:1}^{\Delta 9}$ comparably to K-12. *P. aeruginosa fadD3*, *fadD4*, *fadD5*, and *fadD6* genes individually allowed E2011 to grow on $C_{14:0}$–$C_{18:1}^{\Delta 9}$ to similar levels as K-12. *fadD3* and *fadD6* complemented E2011 to a lesser degree than *fadD4* and *fadD5* on $C_{12:0}$, and four *fadD* genes supported minimal growth of E2011 on $C_{10:0}$ to the same level as $fadD_{Ec}$. E2011 complemented with $fadD_{Ec}$, *fadD3*, *fadD4*, *fadD5*, or *fadD6* did not grow on $C_{4:0}$–$C_{8:0}$, which was in agreement with previous observations that other *E. coli* FA degradation enzymes do not support metabolism of shorter FAs [39].

Contribution of *fadD3*, *fadD4*, *fadD5*, and *fadD6* to FA Degradation

To determine the role of the *fadD* homologues (*fadD3*, *fadD4*, *fadD5*, and *fadD6*) in *P. aeruginosa* FA degradation, strains with various combinations of *fadD* mutations were created. To prevent potential masking of phenotypes by *fadD1* and *fadD2*, 15 mutants were constructed in the *P. aeruginosa* PAO1 *ΔfadD1D2* background. Four triple, seven quadruple, four quintuple mutants and one sextuple mutant (Table 2) were tested for growth on $C_{4:0}$–$C_{18:1}^{\Delta 9}$ along with wildtype PAO1 and the Δ*fadD1D2* mutant.

As expected, all 17 mutant strains grew the same as PAO1 on glucose at 24 h and 96 h (Tables 3 and 4). On $C_{4:0}$, growth of all mutants was the same as PAO1 indicating that none of the *fadD* homologues contribute to the degradation of this FA or the differences were too small to be detected via plate-based growth assays. Throughout the study, the Δ*fadD3D4D5D6* strain had the same growth as PAO1 on $C_{6:0}$–$C_{18:1}^{\Delta 9}$ indicating that FadD1 and FadD2 are most likely providing a majority of FACS activity in *P. aeruginosa* (Tables 3 and 4). No difference in growth was observed between Δ*fadD1D2* strain and Δ*fadD1D2D3*, Δ*fadD1D2D5*, Δ*fadD1D2D6*, Δ*fadD1D2D5D6*, Δ*fadD1D2D3D5*, Δ*fadD1D2D5D6,* or Δ*fadD1D2D3D6* on $C_{6:0}$–$C_{18:1}^{\Delta 9}$. There was significantly less growth for Δ*fadD1D2D4* on $C_{6:0}$–$C_{18:1}^{\Delta 9}$ at 24 h in comparison to Δ*fadD1D2,* suggesting that *fadD4* is important for degradation of all FAs from $C_{6:0}$ to $C_{18:1}^{\Delta 9}$.

Addition of *fadD3*, *fadD5*, or *fadD6* mutation to Δ*fadD1D2D4* strain in a quadruple mutant combination resulted in larger deficiencies in growth on FAs in comparison to the triple Δ*fadD1D2D4* mutant (Tables 3 and 4), indicating that *fadD3*, *fadD5*, and *fadD6* also take part in FA degradation and suggesting the dominance of FadD4 over these homologues. The Δ*fadD1D2D3D4*, Δ*fadD1D2D4D5*, and Δ*fadD1D2D4D6* strains showed no growth on $C_{6:0}$ and $C_{8:0}$, even after four days, in contrast to the Δ*fadD1D2D4* mutant (Table 4), indicating that *fadD3*, *fadD5*, and *fadD6* are involved in the degradation of these FAs.

All quintuple mutants exhibited some level of growth on several FAs after 96 h (Table 4), whereas no growth was present for the sextuplet mutant combination (Δ*fadD1D2D3D4D5D6*), indicating that all four new *fadD* homologues contribute to FA degradation and that only six aerobic FACS genes are likely present in *P. aeruginosa*. Quintuple mutants with both *fadD4* and *fadD5* mutations (Δ*fadD1D2D3D4D5* and Δ*fadD1D2D4D5D6*) were most deficient in FA degradation (Table 3). Growth patterns of the four quintuple mutants after 96 h (Table 4) suggest that *fadD4*, besides *fadD1* and *fadD2*, is much more important for FA degradation than *fadD3*, *fadD5*, and *fadD6* combined, and *fadD5* contributes to FA degradation more than *fadD3* and *fadD6*. Furthermore, by comparing the phenotypes of double, triple, and quadruple mutants at two time points (Tables 3 and 4) a hierarchy of contributions of *fadD* homologues to the degradation of different

Table 1. Single copy complementation of the *E.coli fadD* mutant with *P. aeruginosa fadD* homologues.

	Growth on different carbon sources								
Strain	$C_{4:0}$	$C_{6:0}$	$C_{8:0}$	$C_{10:0}$	$C_{12:0}$	$C_{14:0}$	$C_{16:0}$	$C_{18:1}^{\Delta 9}$	**Glu**
K12	–	–	–	–	+4	+5	+5	+5	+6
E2011 (*fadD*$^-$/*fadR*$^-$)	–	–	–	–	–	–	–	–	+6
E2011/*att*Tn7::miniTn7-Gm^r	–	–	–	–	–	–	–	–	+6
E2011/*att*Tn7::*fadD*$_{Ec}$	–	–	–	+1	+5	+5	+5	+5	+6
E2011/*att*Tn7::*fadD3*	–	–	–	+1	+3	+5	+5	+5	+6
E2011/*att*Tn7::*fadD4*	–	–	–	+1	+5	+5	+5	+5	+6
E2011/*att*Tn7::*fadD5*	–	–	–	+1	+5	+5	+5	+5	+6
E2011/*att*Tn7::*fadD6*	–	–	–	+1	+2	+5	+5	+5	+6

Strains were grown on 1x M9 medium +1% (w/v) Brij-58 supplemented with 0.2% (w/v) fatty acids or 20 mM glucose (Glu) +0.25 mM IPTG for three days at 37°C.
– indicates no growth on a patch and+denotes growth.
+1 is very little growth whereas +6 is very heavy growth comparable to K12 on glucose at day 3.
doi:10.1371/journal.pone.0064554.t001

chain-length FAs can be assigned as follows: i) FadD4 degrades $C_{6:0}$–$C_{18:1}^{\Delta 9}$ (Δ*fadD1D2D4* versus Δ*fadD1D2* in Table 3); ii) FadD5 degrades $C_{6:0}$–$C_{14:0}$ (Δ*fadD1D2D4D5* versus Δ*fadD1D2D4* in Tables 3 and 4); iii) FadD3 degrades $C_{6:0}$-$C_{12:0}$ (Δ*fadD1D2D3D4* versus Δ*fadD1D2D4* in Tables 3 and 4); and iv) FadD6 degrades $C_{6:0}$–$C_{12:0}$ (Δ*fadD1D2D4D6* versus Δ*fadD1D2D4* in Tables 3 and 4).

fadD1 and *fadD2* in Comparison to *fadD3*, *fadD4*, *fadD5*, and *fadD6*

The growth phenotypes of various combinatory mutants on FAs indicated that out of the newly discovered FACS genes (*fadD3*, *fadD4*, *fadD5*, and *fadD6*) *fadD4* is most important for FA degradation (Tables 3 and 4), in addition to *fadD1* and *fadD2* [14]. To investigate further the contribution of *fadD4* to FA degradation in comparison to *fadD1* and *fadD2*, growth curve experiments were performed on SCFA, MCFA, and LCFAs with Δ*fadD1D2D4*, Δ*fadD3D4D5D6*, Δ*fadD1D2D3D5D6*, and Δ*fadD1D2D4D3D5D6* mutants along with PAO1 and Δ*fadD1D2* strains (Fig. 2). The growth experiments on FAs were conducted up to 30 h, which was sufficient to distinguish differences in growth patterns between various strains. The growth rates calculated from growth curves in Fig. 2 are presented in Table S3. The Δ*fadD1D2* mutant strain had impaired growth in comparison to PAO1 on FAs (Fig. 2B–2E). The phenotype of Δ*fadD1D2D3D5D6* in $C_{6:0}$–$C_{18:1}^{\Delta 9}$ (Fig. 2B–2E) was characterized by lower final optical density (OD) and/or longer lag phase than Δ*fadD1D2*, indicating that *fadD3*, *fadD5*, and *fadD6* also contribute to FA degradation. In comparison to Δ*fadD1D2* and Δ*fadD1D2D3D5D6*, Δ*fadD1D2D4* exhibited very small amounts of growth, and no increase in turbidity was observed for Δ*fadD1D2D3D4D5D6* on FAs (Fig. 2B–2E). The Δ*fadD3D4D5D6* mutant had almost identical growth in comparison to PAO1 in $C_{6:0}$ and $C_{18:1}^{\Delta 9}$ (Fig. 2B and 2E). In $C_{10:0}$ and $C_{14:0}$ Δ*fadD3D4D5D6* showed a similar final OD as PAO1 but longer lag phase (Fig. 2C and 2D). These data indicate that, although the activity of FadD4 is masked by the dominance of FadD1 and FadD2, the FadD4 plays a significant role in the degradation of FAs in *P. aeruginosa*.

Role of *fadD* Homologues in the Utilization of Plant-derived Acyclic Terpenes

One of the *P. aeruginosa fadD* homologues, *fadD5* (PA2893; *atuH*), was proposed to be part of the acyclic terpenes utilization (ATU) pathway and to contribute to degradation of citronellol and geraniol (perfumery compounds found in plants) by activating citonellic acid (CA) and geranic acid (GA) through addition of CoASH [40]. However, mutation of PA2893 alone did not abolish growth on acyclic terpenes possibly suggesting the involvement of other homologue(s) [40]. To determine the role of *fadD5* and other *fadD* homologues in degradation of acyclic terpenes as plant-derived nutrient sources, we grew PAO1 along with 17 combinatory *fadD* mutants in 1x M9 minimal media +1% (w/v) Brij-58 with 0.1% (w/v) of CA or GA (Fig. 3). All strains had similar OD measurements after one day of growth on glucose (Fig. 3A). After 24 h, all nine strains with the *fadD4* mutation (triple, quadruple, quintuple, and sextuple combinations) had significantly lower OD for both compounds in comparison to PAO1 (20% or less) (Fig. 3C and 3E). All other mutants had comparable growth to PAO1 in CA and GA (82%–96% and 88%–115%, respectively). None of the strains with *fadD4* mutations had higher OD in CA or GA at day six, than at day one, and the remainder of the mutants grew the same as PAO1 (Fig. S2). Since only strains with *fadD4* mutations exhibited growth defects in CA and GA, involvement of FadD4 in degradation of these compounds was further investigated using the single *fadD4* mutant (Fig. 3D and 3F). Single copy complementation returned growth of the Δ*fadD4* mutant to PAO1 levels indicating that *fadD4* is responsible for the majority of CA and GA degradation.

fadD3, *fadD4*, *fadD5*, and *fadD6* and Virulence in *P. aeruginosa*

A link between *fadDs* and production of virulence factors was previously observed in *P. aeruginosa* [14]. To determine if newly discovered homologues modulate virulence, single unmarked mutants Δ*fadD3*, Δ*fadD4*, Δ*fadD5*, Δ*fadD6*, along with Δ*fadD1D2D3D4D5D6* strain and its complement were tested for production of proteases, lipases, phospholipases, and rhamnolipids. No difference in production of these virulence determinates was observed between PAO1 and all strains tested (data not shown).

Table 2. Strains utilized in this study.

Strain	Lab ID	Relevant Properties	Source/reference
E. coli			
K-12	E0577	Prototroph	ATCC #23740
E. coli fadD^{-}/*fadR*$^{-}$	E2011	Km^r; *fadD*$^{-}$ (*oldD88*) *fadR*::Km^r	[14]
E2011/*att*Tn7::miniTn7-Gm^r	E2665	Gm^r, Km^r; E2011 with miniTn7-Gm^r vector inserted at *att*Tn7 site	This study
E2011/*att*Tn7::*fadD3*	E2666	Gm^r, Km^r; E2011 with *fadD3* inserted at *att*Tn7 site	This study
E2011/*att*Tn7::*fadD4*	E2667	Gm^r, Km^r; E2011 with *fadD4* inserted at *att*Tn7 site	This study
E2011/*att*Tn7::*fadD5*	E2799	Gm^r, Km^r; E2011 with *fadD5* inserted at *att*Tn7 site	This study
E2011/*att*Tn7::*fadD6*	E2798	Gm^r, Km^r; E2011 with *fadD6* inserted at *att*Tn7 site	This study
E2011/*att*Tn7::*fadD*$_{Ec}$	E2385	Gm^r, Km^r; E2011 with *fadD*$_{Ec}$ inserted at *att*Tn7 site	This study
P. aeruginosa			
PAO1	P007	Prototroph	[59]
Δ*fadD4*	P691	PAO1-*fadD4*::*FRT*	This study
Δ*fadD4*/*attB*::*fadD4*	P1041	Tc^r; PAO1-*fadD4*::*FRT*/*attB*::miniCTX2-*fadD4*	This study
Δ*fadD1D2*	P177	PAO1-Δ*fadD2D1*::*FRT*	[14]
Δ*fadD1D2D3*	P678	PAO1-Δ*fadD2D1*::*FRT*/Δ*fadD3*::*FRT*	This study
Δ*fadD1D2D4*	P696	PAO1-Δ*fadD2D1*::*FRT*/*fadD4*::*mFRT*	This study
Δ*fadD1D2D5*	P246	PAO1-Δ*fadD2D1*::*FRT*/*fadD5*::*FRT*	This study
Δ*fadD1D2D6*	P969	PAO1-Δ*fadD2D1*::*FRT*/*fadD6*::*FRT*	This study
Δ*fadD1D2D3D4*	P698	PAO1-Δ*fadD2D1*::*FRT*/Δ*fadD3*::*FRT*/*fadD4*::*mFRT*	This study
Δ*fadD1D2D3D5*	P768	PAO1-Δ*fadD2D1*::*FRT*/Δ*fadD3*::*FRT*/*fadD5*::*FRT*	This study
Δ*fadD1D2D3D6*	P769	PAO1-Δ*fadD2D1*::*FRT*/Δ*fadD3*::*FRT*/*fadD6*::*FRT*	This study
Δ*fadD1D2D4D5*	P770	PAO1-Δ*fadD2D1*::*FRT*/*fadD4*::*FRT*/*fadD5*::*FRT*	This study
Δ*fadD1D2D4D6*	P771	PAO1-Δ*fadD2D1*::*FRT*/*fadD4*::*mFRT*/*fadD6*::*FRT*	This study
Δ*fadD1D2D5D6*	P722	PAO1-Δ*fadD2D1*::*FRT*/*fadD5*::*FRT*/*fadD6*::*FRT*	This study
Δ*fadD3D4D5D6*	P781	PAO1-Δ*fadD3*::*FRT*/*fadD4*::*mFRT*/*fadD5*::*FRT*/*fadD6*::*FRT*	This study
Δ*fadD1D2D3D4D5*	P772	PAO1-Δ*fadD2D1*::*FRT*/Δ*fadD3*::*FRT*/*fadD4*::*mFRT*/*fadD5*::*FRT*	This study
Δ*fadD1D2D3D4D6*	P773	PAO1-Δ*fadD2D1*::*FRT*/Δ*fadD3*::*FRT*/*fadD4*::*mFRT*/*fadD6*::*FRT*	This study
Δ*fadD1D2D3D5D6*	P726	PAO1-Δ*fadD2D1*::*FRT*/Δ*fadD3*::*FRT*/*fadD5*::*FRT*/*fadD6*::*FRT*	This study
Δ*fadD1D2D4D5D6*	P766	PAO1-Δ*fadD2D1*::*FRT*/Δ*fadD3*::*FRT*/*fadD5*::*FRT*/*fadD6*::*FRT*	This study
Δ*fadD1D2D3D4D5D6*	P767	PAO1-Δ*fadD2D1*::*FRT*/Δ*fadD3*::*FRT*/*fadD4*::*mFRT*/*fadD5*::*FRT*/*fadD6*::*FRT*	This study
Δ*fadD1D2D3D4D5D6*/*mucA*$^{-}$	P973	Cb^r; P767/*mucA*::pUC18	This study
Δ*fadD1D2D3D4D5D6*/complement	P1021	Gm^r, Tc^r; P767/*attB*::miniCTX2-*fadD2D1D4*/*attTn7*::miniTn7-*fadD3-fadD5-fadD6*	This study
Δ*fadD1D2D3D4D5D6*/complement/*mucA*$^{-}$	P1028	Cb^r, Gm^r, Tc^r; P767/*attB*::miniCTX2-*fadD2D1D4*/*att*Tn7::miniTn7-*fadD3-fadD5-fadD6*/*mucA*::pUC18	This study

Abbreviations:
Cb^r; carbenicilin resistance; *Ec*, *E. coli*; *fadD*, gene encoding fatty acyl-CoA synthetase; Flp, *Sacchaomyces cerevisiae* recombinase; *FRT*, Flp recognition target; Gm^r, gentamicin resistance; Km^r, kanamycin resistance; *mucA*, anti-sigma factor, repressor of alginate biosynthesis in *P. aeruginosa*; *Pa*, *P. aeruginosa*; *pheS*, gene encoding a mutated α-subunit of phenylalanyl tRNA synthase; Tc^r, tetracycline resistance.
doi:10.1371/journal.pone.0064554.t002

Involvement of New *fadD* Homologues in PC Degradation and *in vivo* Growth

Our previous study indicated that the Δ*fadD1D2* mutant had a decreased ability to degrade PC and was less fit in BALB/c mice lungs [14]. We hypothesized that the sextuple *fadD* mutant, which does not grow on FAs, would exhibit impaired growth on PC and have significantly decreased *in vivo* fitness. We first investigated the role of the four newly discovered FACS in PC degradation (Fig. 4A). Before death phase, Δ*fadD1D2* exhibited slower growth rate and lower final turbidity than PAO1. Δ*fadD1D2D4* had a longer lag phase in comparison to Δ*fadD1D2* before reaching a similar OD, implying that *fadD4* contributes to degradation of PC. The Δ*fadD1D2D3D4D5D6* mutant further exhibited a significant growth defect on PC. The large differences in growth rate and final OD between the sextuple mutant and Δ*fadD1D2D4* suggest that not only *fadD4* but also *fadD3*, *fadD5*, and *fadD6* are required for growth on PC, which contains a mixture of FA chain lengths.

When *in vitro* competition studies were conducted on the sextuple *fadD* mutant and its competitor the complemented sextuple *fadD* mutant, mutation of all six FACS genes did not affect fitness when the bacteria were grown in rich Luria Bertani (LB) medium, and minimal medium supplemented with casamino acids, glucose, glycerol, and choline (Fig. 4B). In contrast, the *in vitro* competitive index (CI) in oleate ($C_{18:1}^{\Delta 9}$) and PC were low (~0.15 and ~0.3, respectively) indicating that Δ*fadD1D2D3D4D5D6* has a growth disadvantage on these carbon

Table 3. Growth of various *P. aeruginisa fadD* mutants on FAs after 24 h.

	Growth on different carbon sources								
Strain	$C_{4:0}$	$C_{6:0}$	$C_{8:0}$	$C_{10:0}$	$C_{12:0}$	$C_{14:0}$	$C_{16:0}$	$C_{18:1}^{\Delta 9}$	**Glu**
PAO1	+2	+3	+4	+4	+3	+3	+3	+3	+4
Δ*fadD1D2*	+2	+2	+3	+3	+2	+3	+2	+3	+4
Δ*fadD1D2D3*	+2	+2	+3	+3	+2	+3	+2	+3	+4
Δ*fadD1D2D4*	+2	–	–	+1	+1	+1	+1	+1	+4
Δ*fadD1D2D5*	+2	+2	+3	+3	+2	+3	+2	+3	+4
Δ*fadD1D2D6*	+2	+2	+3	+3	+2	+3	+2	+3	+4
Δ*fadD1D2D3D4*	+2	–	–	–	–	+1	+1	+1	+4
Δ*fadD1D2D3D5*	+2	+2	+3	+3	+2	+3	+2	+3	+4
Δ*fadD1D2D3D6*	+2	+2	+3	+3	+2	+3	+2	+3	+4
Δ*fadD1D2D4D5*	+2	–	–	–	–	–	–	+1	+4
Δ*fadD1D2D4D6*	+2	–	–	–	–	+1	+1	+1	+4
Δ*fadD1D2D5D6*	+2	+2	+3	+3	+2	+3	+2	+3	+4
Δ*fadD3D4D5D6*	+2	+3	+4	+4	+3	+3	+3	+3	+4
Δ*fadD1D2D3D4D5*	+2	–	–	–	–	–	–	–	+4
Δ*fadD1D2D3D4D6*	+2	–	–	–	–	+1	+1	+1	+4
Δ*fadD1D2D3D5D6*	+2	+2	+1	+3	+1	+3	+1	+3	+4
Δ*fadD1D2D4D5D6*	+2	–	–	–	–	–	–	–	+4
Δ*fadD1D2D3D4D5D6*	+2	–	–	–	–	–	–	–	+4

Strains were grown on 1x M9 medium +1% (w/v) Brij-58 supplemented with 0.2% (w/v) fatty acids or 20 mM glucose (Glu).
– indicates no growth on a patch and+denotes growth:
+1 is very little growth.
+4 is a heavy growth comparable to PAO1 on glucose at 24 h.
+6 is a very heavy growth comparable to PAO1 on glucose at 96 h.
doi:10.1371/journal.pone.0064554.t003

sources. The *in vivo* competition study showed that the sextuple *fadD* mutant was out numbered by its complement (Fig. 4C). An almost 10-fold increase in CFU per lung above inoculum (6×10^6) was observed for both time points indicating bacterial replication *in vivo*. At 24 h, the amount of the sextuple *fadD* mutant was half of its complement, which is lower than the reported CI for the Δ*fadD1D2* mutant at 24 h [14]. Even at 48 h the CI was significantly lower than 1, indicating that deletion of *fadD* genes decreases *in vivo* fitness of sextuple *fadD* mutant.

Discussion

Previous research on *fadD1* and *fadD2* indicated that more than two FACS genes are present in *P. aeruginosa* [14]. In this study, we focused on identification of additional *fadD* homologues. Four genes, *fadD3*, *fadD4*, *fadD5*, and *fadD6* (PA3860, PA1617, PA2893, and PA3924, respectively) were found to encode FACS (Tables S1 and 1). Each of these genes contributes at a varying degree to FA degradation (Tables 3 and 4). Surprisingly, none of the new *fadD*s were involved in degradation of butyrate ($C_{4:0}$; Table 3). It is possible that other unidentified genes with acyl-CoA synthetase functions are responsible for growth on $C_{4:0}$. Butyrate could also be processed through the acetoacetate degradation pathway (*ato*), an alternative pathway for degradation of SCFA [41]. This could be possible since two homologues of both of *E. coli* acetoacetyl-CoA transferase complex proteins, AtoA and AtoD, are present in *P. aeruginosa*: PA2000 (identity 45% and similarity 62%), PA0227 (identity 28% and similarity 62%), PA1999 (identity 40% and similarity 64%), and PA5445 (identity 33% and similarity 55%), respectively.

Growth studies with various mutants using FAs as sole carbon and energy sources indicated that FACS homologues are not of equal physiological significance and that there are disparities in importance and FA preference between them. *fadD1* and *fadD2*, along with *fadD4*, are responsible for almost all FA degradation and dominate over other homologues. When *fadD1* and *fadD2* are inactivated, the majority of growth on SCFAs, MCFAs and LCFAs is due to *fadD4* (Tables 3 and 4, Fig. 2). In comparison, *fadD3*, *fadD5*, and *fadD6* have small contributions to overall growth on FAs and their individual involvement can be only observed when *fadD1*, *fadD2* and *fadD4* are absent (Table 4). This is not unprecedented, since *Pseudomonas putida* FadD2 is only active when FadD1 is not present [42]. It could be possible that gene(s) ruled out by screening in *E. coli* for growth on LCFA (Table S1), might be involved in SCFA and/or MCFA degradation. However, lack of growth for the sextuple *fadD* mutant on $C_{6:0}$–$C_{18:1}^{\Delta 9}$ (Table 4) strongly indicates that *P. aeruginosa* has a total of six aerobic FACS genes.

P. aeruginosa is commonly found in soil, water, and on plant surfaces [43–45] and it is known to degrade over 70 different organic substances such as aromatic compounds, organic acids (e.g. isovalerate), alcohols, and acyclic terpenes (e.g., citronellol and geraniol) [44]. Sources of nutrients for pseudomonads on plant surfaces have not been determined. Citronellol and geraniol (perfumery compounds and possible bacterial nutrient sources found in plants) are degraded through the acyclic terpene utilization (ATU) pathway, β-oxidation pathway, and leucine/isovalerate utilization pathway [40,46]. The *fadD5* (PA2893 or *atuH*) was proposed to be part of ATU and to be involved in activation of the CA and GA intermediates of the

Table 4. Growth of various *P. aeruginosa fadD* mutants on FAs after 96 h.

	Growth on different carbon sources								
Strain	$C_{4:0}$	$C_{6:0}$	$C_{8:0}$	$C_{10:0}$	$C_{12:0}$	$C_{14:0}$	$C_{16:0}$	$C_{18:1}^{\Delta 9}$	**Glu**
PAO1	+4	+6	+6	+6	+6	+6	+6	+6	+6
Δ*fadD1D2*	+4	+4	+4	+4	+4	+4	+4	+4	+6
Δ*fadD1D2D3*	+4	+4	+4	+4	+4	+4	+4	+4	+6
Δ*fadD1D2D4*	+4	+2	+1	+4	+4	+4	+4	+4	+6
Δ*fadD1D2D5*	+4	+4	+4	+4	+4	+4	+4	+4	+6
Δ*fadD1D2D6*	+4	+4	+4	+4	+4	+4	+4	+4	+6
Δ*fadD1D2D3D4*	+4	–	–	+2	+2	+4	+4	+4	+6
Δ*fadD1D2D3D5*	+4	+4	+4	+4	+4	+4	+4	+4	+6
Δ*fadD1D2D3D6*	+4	+4	+4	+4	+4	+4	+4	+4	+6
Δ*fadD1D2D4D5*	+4	–	–	+1	+3	+3	+4	+4	+6
Δ*fadD1D2D4D6*	+4	–	–	+4	+4	+4	+4	+4	+6
Δ*fadD1D2D5D6*	+4	+4	+4	+4	+4	+4	+4	+4	+6
Δ*fadD3D4D5D6*	+4	+6	+6	+6	+6	+6	+6	+6	+6
Δ*fadD1D2D3D4D5*	+4	–	–	–	–	–	+3	+3	+6
Δ*fadD1D2D3D4D6*	+4	–	–	+2	+2	+4	+4	+4	+6
Δ*fadD1D2D3D5D6*	+4	+4	+4	+4	+4	+4	+4	+4	+6
Δ*fadD1D2D4D5D6*	+4	–	–	+1	+3	+1	–	+1	+6
Δ*fadD1D2D3D4D5D6*	+4	–	–	–	–	–	–	–	+6

Strains were grown on 1x M9 medium +1% (w/v) Brij-58 supplemented with 0.2% (w/v) fatty acids or 20 mM glucose (Glu).
– indicates no growth on a patch and+denotes growth:
+1 is very little growth.
+4 is a heavy growth comparable to PAO1 on glucose at 24 h.
+6 is a very heavy growth comparable to PAO1 on glucose at 96 h.
doi:10.1371/journal.pone.0064554.t004

pathway. However, *fadD5* was confirmed experimentally not to be part of ATU, and other homologues were thought to be also involved and to 'mask' the phenotype [40]. We investigated the possible role of *fadD* homologues in the degradation of acyclic terpenes, and we reasoned that combination of various *fadD* mutations would allow involvement of FACS homologues in ATU to be assessed. Surprisingly, *fadD5* along with *fadD1*, *fadD2*, *fadD3*, and *fadD6* had minimal if any contributions to the degradation of CA and GA (Fig. 3). Interestingly, *fadD5* is located right next to genes known to be involved in ATU and seems to be the last gene in *atuABCDEFGH* cluster [40]. On the other hand, *fadD4* is not only involved in ATU but it is almost solely responsible for degradation of these compounds as can be observed from growth phenotypes of the single *fadD4* mutant and its complement (Fig. 3D and 3F). Notably, homologues of *fadD4* with high similarity are present in *Pseudomonas fluorescens* (e.g., Pfl01_4205 in Pf0-1, 72% identity and 84% similarity), *Pseudomonas protegens* (e.g., PFL_1744 in strain Pf-5, 71% identity and 82% similarity), and *Pseudomonas mendocina* (e.g., MDS_2302 in strain NK-01, 75% identity and 87% similarity) and some strains of these pseudomonads are known to degrade acyclic terpenes [40], [47].

The ability of *P. aeruginosa* to degrade lipids and FAs, especially the main component of lung surfactant PC, has been linked to replication of this opportunistic pathogen during infection of CF patients' lungs [13]. Previously, we determined that Δ*fadD1*, Δ*fadD2*, and double Δ*fadD1D2* mutants have decreased fitness in BALB/c mice due to their deficiencies in degradation of FAs and PC [14]. We hypothesized that *P. aeruginosa* strains with greater defects in utilization of FAs and PC *in vitro* will have larger disadvantages during *in vivo* growth. Δ*fadD1D2D3D4D5D6* mutant exhibited the most significant growth defect in FAs and PC (Fig. 2, 4A and 4B), and similar level of virulence factors (i.e. proteases, hemolysins, lipases) production was observed between sextuple *fadD* mutant, its complement, and PAO1 (data not shown). The Δ*fadD1D2D3D4D5D6* mutant had some decrease of *in vivo* fitness in comparison to the Δ*fadD1D2* at 24 h (Fig. 4C and [14]); but at 48 h, Δ*fadD1D2D3D4D5D6* mutant was not less fit in mice lungs than Δ*fadD1D2* mutant. This latter result was surprising, as the impaired ability to utilize PC did not result in a more dramatic phenotype *in vivo* at 48 h (Fig. 4C). There are several possibilities, which could account for this unexpected phenotype. The sextuple mutant could utilize *in vivo* other constituents of PC such as choline and glycerol later in the infection. Additionally, pulmonary surfactants are composed of 10% proteins [48] and amino acids were suggested to be used by *P. aeruginosa* during lung infection [49] and could serve as an alternative nutrient source for sextuple *fadD* mutant. Other FACS genes (i.e. anaerobic which we could not identify because of limitations of our aerobic *in vitro* screening method) could be important for *in vivo* growth.

In summary, we have identified four additional FACS homologues of *P. aeruginosa* and determined their involvement in degradation of different FAs. The dual catabolic function of *fadD4* (PA1617) for FAs and acyclic terpenes exemplifies the interconnection of metabolic pathways and multiple roles that FACS homologues play in this ubiquitous bacterium. Our *in vivo* data show that nutrient acquisition during lung infection is a complicated process, involving alterative pathways that require

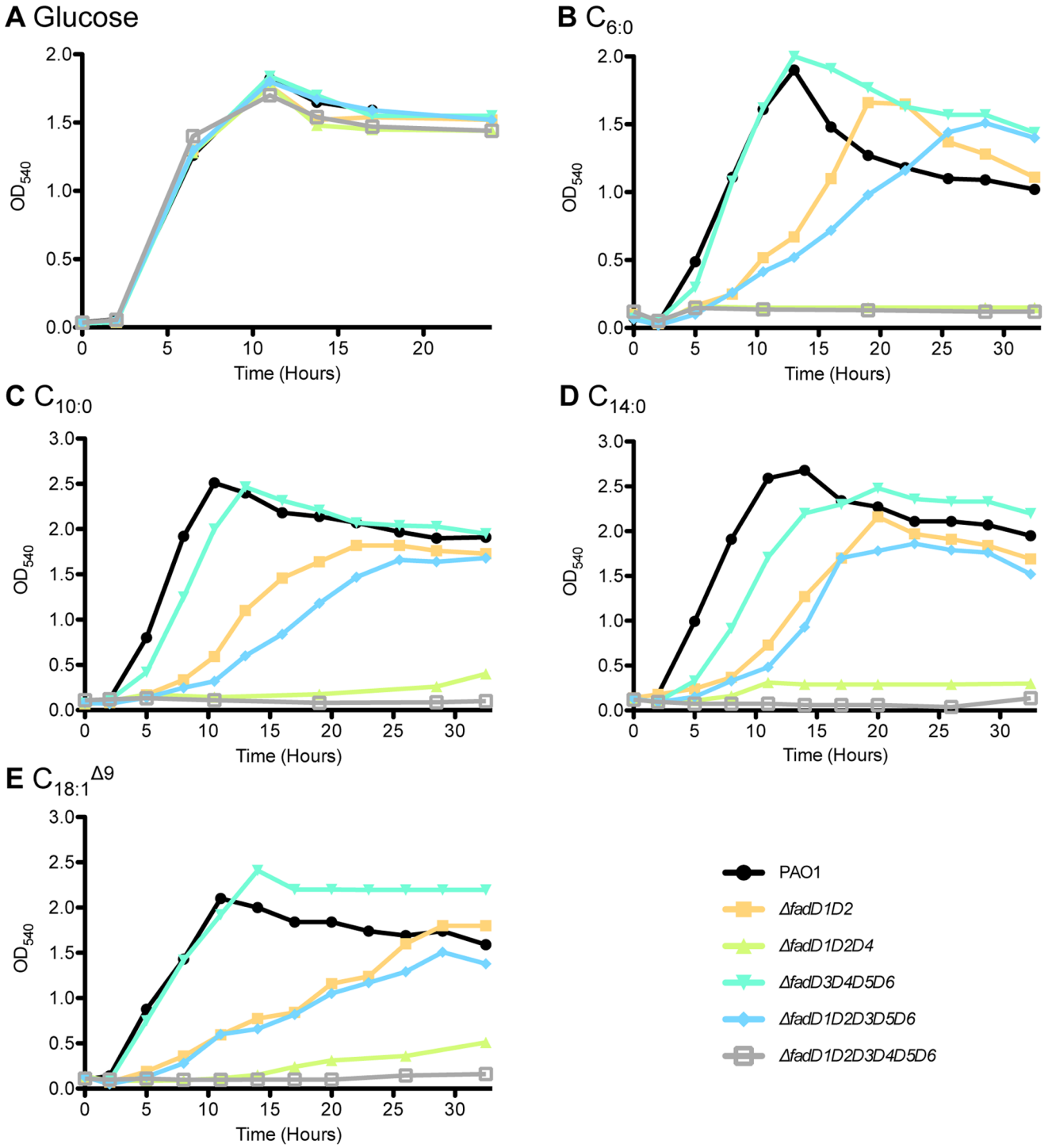

Figure 2. *fadD* mutants and growth on FAs. Various strains were grown on glucose (A), $C_{6:0}$ (B), $C_{10:0}$ (C), $C_{14:0}$ (D), and $C_{18:1}^{\Delta 9}$ (E) to investigate further the role of *fadD4* in FA degradation in comparison to rest of homologues. These growth curves demonstrate the hierarchical dominance of *fadD1*, *fadD2* and *fadD4* over other *fadD*s. Growth experiments were performed twice and representative curves are shown.
doi:10.1371/journal.pone.0064554.g002

further investigation. Knowledge of all *fadD* genes needed for FA degradation significantly increases our understanding of the FA degradation pathway and its importance for *in vivo* replication of *P. aeruginosa*.

Materials and Methods

Ethics Statement

All animal experiments were approved by University of Hawaii at Manoa Institutional Animal Care and Use Committee (protocol no. 06-023-6) and were conducted in compliance with the NIH

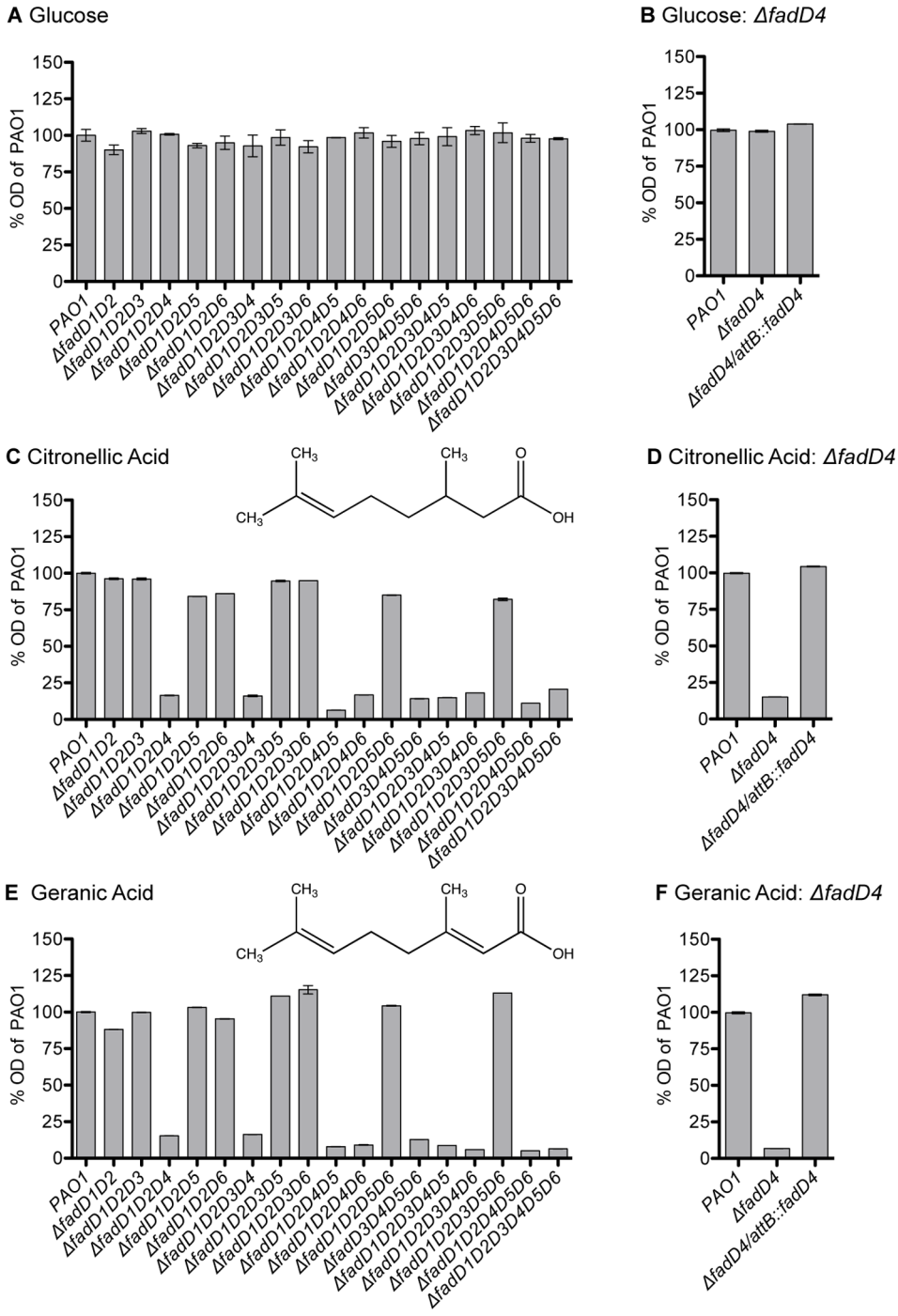

Figure 3. Growth phenotypes of various *fadD* homologues mutants on acyclic terpenes. Strains were grown in liquid 1x M9 medium +1% (w/v) Brij-58 supplemented with 20 mM glucose, 0.1% (w/v) of citronellic acid, or 0.1% (w/v) geranic acid at 30°C. Optical densities (ODs) of cultures were measured and compared to PAO1 at day one (A, C, and E). Growth of Δ*fadD4* mutant and Δ*fadD4*/*attB*::*fadD4* complement strain in different carbon source were compared to PAO1 and ODs from day six are presented (B, D, and F). Results shown are from representative experiments that were performed twice by measuring triplicate cultures.
doi:10.1371/journal.pone.0064554.g003

(National Institutes of Health) Guide for the Care and Use of Laboratory Animals.

Bacterial Strains and Growth Media

Strains and plasmids utilized in this study are listed in Tables 2, S2, and 5, respectively. All *P. aeruginosa* mutants constructed and utilized in this study are derived from strain PAO1. *E. coli* E1869 strain (Table S2) was routinely used for cloning and *E. coli* Δ*asd* or Δ*dapA* strains (E464, E1353, and E2072, Table S2) were used for mobilization of plasmids as described previously [50]. *E. coli* and *P. aeruginosa* strains were cultured in rich and minimal media as

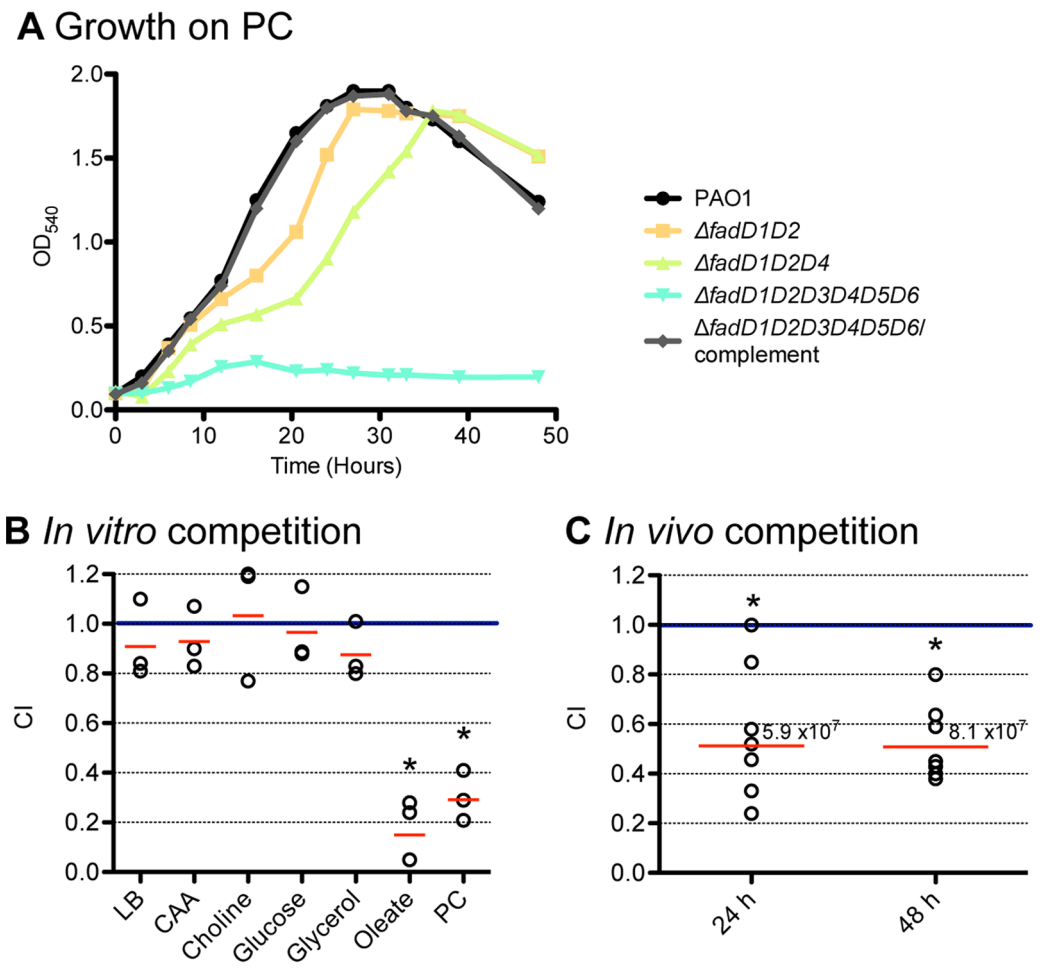

Figure 4. Growth characteristics on PC and competition studies of *fadD* sextuple mutant. (A) PAO1 and several mutant strains were individually grown on PC. Growth curves were performed twice and representative results are shown. (B) *In vitro* competition between Δ*fadD1D2D3D4D5D6* and its competitor, Δ*fadD1D2D3D4D5D6*/complement (P1021), in different growth media after 24 h. (C) *In vivo* competition between Δ*fadD1D2D3D4D5D6*/*mucA*$^-$ (P973) and its competitor, Δ*fadD1D2D3D4D5D6*/complement/*mucA*$^-$ (P1028), in BALB/c mice lungs. Seven mice for each time point were inoculated with 6 x10^6 CFU/mouse. The geometric mean of competitive indices (CI) from each group is marked by red line. Mutant strain is less competitive than complement when CI<1. Total average lung CFU recovered form mice in each group are indicated above red line. * P<0.05 based on one sample *t* test.
doi:10.1371/journal.pone.0064554.g004

described by Kang *et al.* [14] unless indicated otherwise. Fatty acids stocks were prepared as previously described [31].

General Molecular Techniques

Molecular techniques were performed as previously described [50]. Oligonucleotides (Table 6) were synthesized through Integrated DNA Technologies.

Identification of *P. aeruginosa* Fatty acyl-CoA Synthetase Homologues

Potential *P. aeruginosa fadD* homologues were identified through BLAST [34] utilizing *E. coli* FadD sequence and alignment of *E. coli* FadD ATP/AMP [19], [35–37] and fatty acid binding motifs [38] with the FadD motifs of *P. aeruginosa fadD* homologues. Prediction of function of genes was obtained from Pseudomonas Genome Database (www.pseudomonas.com) [51]. PA2557, PA3860, and PA4198 were PCR amplified and cloned into pUC19 as BamHI fragments. The *fadD* homologues PA1617, PA1997, PA2555, PA3568, PA2893, and PA3924, were PCR amplified and cloned into pUC19 as HindIII/EcoRI, BamHI/SmaI, HindIII/KpnI, HindIII/SalI, and XbaI/BamHI fragments, respectively. For functional complementation testing, pUC19 vectors containing PAO1 *fadD* homologues were transformed into *E. coli fadD*$^-$/*fadR*$^-$ strain (E2011) and the resulting transformants were patched onto 1x M9+1% (w/v) Brij-58+ ampicillin 100 μg/ml supplemented with 20 mM glucose, 0.2% (w/v) oleate ($C_{18:1}^{\Delta 9}$), or decanoate ($C_{10:0}$).

Single Copy Complementation of the E. coli *fadD*$^-$/*fadR*$^-$ Mutant

To construct *fadD3*, *fadD5*, and *fadD6* single copy complementation vectors, first *fadD3*, *fadD5*, and *fadD6* PCR product were cloned into pET15b as NdeI/BamHI fragments. Next, the *fadD3*-His_6, *fadD5*-His_6, and *fadD6*-His_6 BamHI/XbaI fragments were sub-cloned into miniTn7-Gm^r yielding miniTn7-*fadD3*, miniTn7-*fadD5* and miniTn7-*fadD6*. To construct the miniTn7-*fadD4*, first, the PCR product of *fadD4* was cloned into pET28a as NdeI/EcoRI fragment. The *fadD4*-His_6 fragment, obtained by EcoRI digest, blunt-ending, and XbaI digest, was sub-cloned into miniTn7-Gm^r digested with the BamHI, blunt-ended and digested

Table 5. Plasmids used in this study.

Plasmid	Lab ID	Relevant Properties	Source/reference
miniCTX2	E0076	Tc^r; *P. aeruginosa* site specific integration vector	[58]
miniCTX2-*fadD2D1*	E2143	Tc^r; *fadD2D1* cloned into miniCTX2	[14]
miniCTX2- *fadD2D1D4*	E2811	Tc^r; *fadD4* gene cloned into miniCTX2-*fadD2D1*	This study
miniCTX2-*fadD4*	E2589	Tc^r; *fadD4* gene cloned into miniCTX2	This study
miniTn7-Gm^r	E2643	Ap^r, Gm^r; pUC18R6Kmini-Tn7 [52] with *FRT8*-Gm^r cassette and *lac* promoter cloned	Laboratory collection
miniTn7-*fadD3*	E2645	Ap^r, Gm^r; *fadD3* cloned into miniTn7-Gm^r	This study
miniTn7-*fadD4*	E2647	Ap^r, Gm^r; *fadD4* cloned into miniTn7-Gm^r	This study
miniTn7-*fadD5*	E2793	Ap^r, Gm^r; *fadD5* cloned into miniTn7-Gm^r	This study
miniTn7-*fadD6*	E2794	Ap^r, Gm^r; *fadD6* cloned into miniTn7-Gm^r	This study
miniTn7-$fadD_{Ec}$	E2378	Ap^r, Gm^r; *E. coli fadD* cloned into miniTn7-Gm^r	This study
miniTn7-PA3860	E2377	Ap^r, Gm^r; *fadD3* with native *rbs* cloned into miniTn7-Gm^r	This study
miniTn7-PA3924	E2854	Ap^r, Gm^r; *fadD6* with native *rbs* cloned into miniTn7-Gm^r	This study
miniTn7-*fadD3-fadD5-fadD6*	E2860	Ap^r, Gm^r; *fadD3, fadD5,* and *fadD6* with native *rbs* cloned into miniTn7-Gm^r	This study
pCD13SK-*flp-oriT*	E0783	Sp^r; suicidal Flp-expressing plasmid	[33]
pET15b	E0047	Ap^r; T7 expression vector	Novagen
pET15b-*fadD3*	E2658	Ap^r; pET15b with *fadD3* gene	This study
pET15b-*fadD5*	E1127	Ap^r; pET15b with *fadD5* gene	This study
pET15b-*fadD6*	E2790	Ap^r; pET15b with *fadD6* gene	This study
pET28a	E0158	Km^r; T7 expression vector	Novagen
pET28a-*fadD4*	E2644	Km^r; pET28a with *fadD4* gene	This study
pEX18T	E0055	Ap^r; gene replacement vector	[53]
pEX18T-*fadD3*-Gm^r -$pheS_{Pa}$	E2438	Ap^r, Gm^r; Gm^r-$pheS_{Pa}$-*FRT* cassette inserted into *fadD3*	This study
pEX18T-*fadD4*-Gm^r -$pheS_{Pa}$	E2506	Ap^r, Gm^r; Gm^r-$pheS_{Pa}$-*mFRT* cassette inserted into *fadD4*	This study
pEX18T-*fadD5*-Gm^r	E0828	Ap^r, Gm^r; Gm^r-*FRT* cassette inserted into *fadD5*	This study
pEX18T-*fadD6*-Gm^r	E1476	Ap^r, Gm^r; Gm^r-*FRT* cassette inserted into *fadD6*	This study
pFLP2	E0067	Ap^r; broad-host range Flp expressing plasmid	[53]
pmFRT-Gm^r-$pheS_{Pa}$	E2382	Ap^r, Gm^r; plasmid with Gm^r-$pheS_{Pa}$-*mFRT* cassette	Laboratory collection
pPS856	E0050	Ap^r, Gm^r; plasmid with Gm^r-*FRT* cassette	[53]
pTNS2	E1189	Ap^r; helper plasmid for Tn7 transposition system	[52]
pUC18-'*mucA*'	E1907	Ap^r; pUC18 with internal fragment of *mucA* cloned	[14]
pUC19	E0014	Ap^r; cloning vector	[60]
pUC19-PA1617	E2472	Ap^r; PAO1 PA1617 gene cloned into pUC19	This study
pUC19-PA3860	E2356	Ap^r; PAO1 PA3860 gene cloned into pUC19	This study
pwFRT-Gm^r-$pheS_{Pa}$	E2380	Ap^r, Gm^r; plasmid with Gm^r -$pheS_{Pa}$-*FRT* cassette	Laboratory collection

Abbreviations:
Ap^r, ampicillin resistance; *lac*, *E. coli* lactose operon; *rbs*, ribosomal binding site; Sp^r, streptomycin resistance.
doi:10.1371/journal.pone.0064554.t005

with XbaI. To construct miniTn7-$fadD_{Ec}$, the $fadD_{Ec}$ PCR product was cloned as BamHI/blunt-end fragment into miniTn7-Gm^r digested with XbaI, blunt ended and digested BamHI.

Various miniTn7 vectors were integrated into E2011 using pTNS2 [52]. For the complementation study, two colonies of K-12, E2011, E2011/*att*Tn7::miniTn7-Gm^r, E2011/*att*Tn7::$fadD_{Ec}$, E2011/*att*Tn7::*fadD3*, E2011/*att*Tn7::*fadD4*, E2011/*att*Tn7::*fadD5*, and E2011/*att*Tn7::*fadD6* were patched onto 1x M9 medium +1% (w/v) Brij-58+0.25 mM isopropyl β-D-1-thiogalactopyranoside (IPTG) supplemented with 0.2% (w/v) FAs or 20 mM glucose. Plates were incubated for three days at 37°C and bacterial growth was scored from +1 to +6. Very little growth was marked as +1 and very heavy growth on a patch comparable to K12 on glucose at day three was marked as +6.

Construction of Mutant Strains of PAO1

The *fadD3*, *fadD4*, *fadD5*, and *fadD6* gene replacement vectors were obtained as follows. pEX18T-*fadD3*-Gm^r-$pheS_{Pa}$ was constructed by digesting pUC19-PA3860 with MscI and SgrAI, blunt-ending, and ligating it with Gm^r-$pheS_{Pa}$-*FRT* cassette that was SmaI excised from pwFRT-Gm^r-$pheS_{Pa}$. The PA3860-Gm^r-$pheS_{Pa}$ fragment was excised from the resulting vector using BamHI and cloned into pEX18T. Similarly, pEX18T-*fadD4*-Gm^r-$pheS_{Pa}$ was obtained by first sub-cloning *fadD4* gene as a HindIII/EcoRI fragment from pUC19-PA1617 into pEX18T, and *fadD4* was deactivated at the XhoI site by inserting the Gm^r-$pheS_{Pa}$-*mFRT* cassette SalI excised from pmFRT-Gm^r-$pheS_{Pa}$. pEX18T-*fadD5*-Gm^r was constructed by cloning *fadD5* PCR product (oligos #437 and #438) as BamHI/blunt-end fragment into pEX18T that was

Table 6. Oligonucleotides primers utilized in this study.

Primer number and name	Sequence[a]
438; PA2893-BamHI[b, c]	5′-CAGTAGGATCCCACGGTGCTCAGAAGCGGT-3′
512; PA3924-BamHI[b, c]	5′-TGCTTGGGATCCGGGCGTTTCGGCGGTGTA-3′
1093; EcfadD-down-BamHI[b]	5′-AACGGGATCCTCAGGCTTTATTGTC-3′
1109; PA3924-NdeI[b]	5′-GTGTACGCCATATGCTGAATACCC-3′
1151; PA1221 BamHI-up[d]	5′-ACCGTGGATCCATTCTCATCGCTTTTCTCTC-3′
1152; PA1221 BamHI-down[d]	5′-AGCGCGTTTTCGTCGGCGAAGGATCCGACT-3′
1153; PA2557 BamHI-up[d]	5′-TGGGCGGATCCGCCTCTTGCGTTTACCTT-3′
1154; PA2557 BamHI-down[d]	5′-GAAAGCGAAGCTGCCACTCTTCAGGATCCGCGA GT-3′
1155; PA3860 BamHI-up[d]	5′-GAACGGGATCCAGTGTAAAGCATGTTGCCAG-3′
1156; PA3860 BamHI-down[b, d]	5′- CTGGAGGAAATCCACGACATCGGATCCTGGCT G-3′
1157; PA4198 BamHI-up[d]	5′-CCAGAGGATCCAGCCGTTTTCGACGCAGT-3′
1158; PA4198 BamHI-down[d]	5′-CGAACACGTCGTTGAGCAGGATCCGCATG-3′
1218; fadDEc-HindIII-up[b]	5′-TCATAAGCTTGGGGTTGCGATGAC-3′
1251; fadD3-NdeI[b]	5′-AACCCATATGAATCCGTCCCCATCG-3′
1252; PA3568-Up-HindIII[d]	5′-ACTCCAAGCTTCACTCACTGCTTCATC-3′
1253; PA3568-Down-SalI[d]	5′-GGCTGGTCGACGAAGGCGTGTTGAA-3′
1254; PA1997-Up-BamHI[d]	5′-CCTGTGGATCCAGCAGATGCAGGA-3′
1255; PA1997-Down-SmaI[d]	5′-CTGAAGATGGCATTGTCG-3′
1256; PA0996-Up-BamHI[d]	5′-CTTCTTGCTTGGTTGCC-3′
1257; PA0996-Down-BamHI[d]	5′-CCAGCGGATCCTCCAGACACACATAGGA-3′
1258; PA2555-Up-HindIII[d]	5′-GCGTGAAGCTTCCGGCTACTCCATACA-3′
1259; PA2555-Down-KpnI[d]	5′-CCGCCGGTACCCAGGAACACTCGATTT-3′
1260; PA1617-Up-HindIII[d]	5′-CTAGGAAGCTTCTGGCGCAACGACTACAA-3′
1261; PA1617-Down-EcoRI[b, c, d]	5′-GTTCAGTTGCTCCAGGTC-3′
1441; PA1614-HindIII[c]	5′-GAAGCTTCATGACAGAGCAGCAAC-3′
1444; PA1617-NdeI[b]	5′-ATGCCATATGGTCACTGCAAATCGTCT-3′
2109; PA2893-up[c, d]	5′-GGCTATTTGCCGAAGTGC-3′
2110; PA3924-up[c, d]	5′-CGGATTCTATCTTGTGACC-3′

[a]Restriction enzyme sequences are underlined.
[b]Single copy complementation in *E. coli*.
[c]Single copy complementation in *P. aeruginosa*.
[d]*fadD* homologues cloning.
doi:10.1371/journal.pone.0064554.t006

digested with BamHI and SmaI, and *fadD5* was deactivated at the blunt-ended XhoI site by inserting the Gm^r-*FRT* cassette SmaI excised from pPS856. To construct pEX18T-*fadD6*-Gm^r, *fadD6* PCR product (oligos #1093 and #512) was cloned as BamHI/blunt-end fragment into pEX18T that was digested with BamHI and SmaI, and *fadD6* was deactivated at the blunt-ended KpnI site by inserting the Gm^r-*FRT* SmaI excised cassette from pPS856.

pEX18T-*fadD3*-Gm^r-*pheS$_{Pa}$*, pEX18T-*fadD4*-Gm^r-*pheS$_{Pa}$*, pEX18T-*fadD5*-Gm^r, and pEX18T-*fadD6*-Gm^r gene replacement vectors were utilized as previously described [53] to obtain several mutant strains (P239, P243, P416, P677, P678, P685, P696, P698, P691, P722 P726, and P767). Unmarked mutations of *fadD* genes in various strains were obtained utilizing pFLP2 [53] or in one step via Flp mediated excision of Gm^r-*pheS$_{Pa}$-FRT* cassettes utilizing mutated version of *P. aeruginosa pheS* gene [54] and chlorinated phenylalanine (cPhe) counter-selection by transiently expressing *flp* on the non-replicative plasmid, pCD13SK-*flp-oriT*, as described previously [55]. Mutations transfer from strains P685, P239, P416 into PAO1, P678, P696, P698, and P722 were done as previously described [56], followed by Flp mediated excision of Gm^r-*FRT* or Gm^r-*pheS$_{Pa}$-FRT* cassette, to obtain unmarked mutant strains P766, P768, P769, P770, P771, P772, P773, P969, and P972. Strain Δ*fadD3D4D5D6* (P781) was constructed in the PAO1-Δ*fadD3*::*FRT* background by subsequent transfer of mutation from strains P685, P239, and P416 followed by Flp mediated excision of Gm^r-*FRT* or Gm^r-*pheS$_{Pa}$-FRT* cassette. Presence or absence of mutations of *fadD2D1*, *fadD3*, *fadD4*, *fadD5*, and *fadD6* in all mutant strains were confirmed by PCR (data not shown).

Growth Phenotypes of Multiple *fadD* Mutants on Fatty Acids

To assess involvement of *P. aeruginosa fadD* homologues in FAs degradation, various strains (PAO1, double, triple, quadruple, quintuple, and sextuple *fadD* mutants) were purified on LB. After 24 h incubation at 37°C, two colonies of each strain were patched onto 1x M9 solid medium +1% (w/v) Brij-58 supplemented with 0.2% (w/v) FAs or 20 mM glucose. Plates were incubated at 37°C for four days. Growth of each strain was scored from +1 (little growth) to +6 (very heavy growth comparable to PAO1 on glucose at 96 h).

Growth Curves Experiments

To further characterize various *fadD* mutants of *P. aeruginosa*, growth curve studies were performed using FAs as sole carbon source as described previously [14]. Doubling time of various strains in log-phase (Table S3) was calculated as follow: doubling time = $[0.301(t_2\text{-}t_1)]/(\log OD_2\text{-}\log OD_1)$ [57].

Growth of *fadD* Mutants on Acyclic Terpenes

The Δ*fadD4*/*attB*::*fadD4* strain was constructed using a single copy complementation vector miniCTX2-*fadD4*, which was obtained by cloning the *fadD4* PCR product (oligos #1443 and #1261) as HindIII and EcoRI fragment into miniCTX2 and integrated into Δ*fadD4* mutant chromosome as described previously [58]. Stocks of citronellic (Sigma) and geranic acid (Sigma) (3% (w/v)) were prepared by neutralizing the compounds with equal molar sodium hydroxide and dissolving in 1% (w/v) Brij-58. PAO1 and various *fadD* mutants were grown overnight (14–16 h), starter culture were prepared as described by Kang *et al.* [14] and inoculated at 200-fold dilution into 1x M9 minimal medium +1% (w/v) Brij-58 supplemented with 0.1% (w/v) of citronellic acid, 0.1% (w/v) geranic acid or 20 mM glucose. Triplicate cultures were shaken at 30°C and optical densities were measured at day one and day six.

Virulence Factors Production

Lipase, protease, phospholipase, and rhamnolipd productions by *fadD* mutants were tested as previously described [14].

In vitro and *in vivo* Competition Studies

For *in vitro* and *in vivo* in competition studies, the Δ*fadD1D2D3D4D5D6* strain was complemented with *fadD2D1* and *fadD4* cloned into miniCTX2 and *fadD3*, *fadD5*, and *fadD6* cloned into miniTn7-Gm^r. MiniCTX2-*fadD2D1D4* complementation vector, was constructed by cloning *fadD4* gene PCR product (oligos #1443 and #1261) as HindIII/blunt-end fragment into miniCTX2-*fadD2D1* digested with XhoI, blunt-ended and digested with HindIII. To construct miniTn7-*fadD3-fadD5-fadD6* vector, first *fadD3* was sub-cloned as BamHI fragment from pUC19-PA3890 into miniTn7-Gm^r, resulting in miniTn7-PA3860. The *fadD6* was amplified with oligos #512 and #2210 and cloned as a BamHI/XbaI fragment into miniTn7-Gm^r, resulting in miniTn7-PA3924. The *fadD5* was amplified with oligos #438 and #2109 and digested with BamHI, blunt-ended, and digested with XbaI. To construct the final vector, the miniTn7-PA3924 was digested with XbaI, blunt-ended and digested with NdeI and the 2.5 kb fragment (containing *fadD6*) was cloned simultaneously along with *fadD5* fragment into miniTn7-PA3860 digested with NdeI and SpeI. Integration of these plasmids into the *P. aeruginosa* chromosomes was performed as previously described ([58] and [52]).

The *in vitro* competition between Δ*fadD1D2D3D4D5D6* and its complement (strain P1021) on LB, or casamino acids (CAA), choline, glucose, glycerol, oleate ($C_{18:1}^{\Delta 9}$) or PC was performed as described previously [14].

The *in vivo* competition study was performed as previously described [14]. Briefly, *mucA* was inactivated in the PAO1-Δ*fadD1D2D3D4D5D6* and its complement strains utilizing pUC18-'*mucA*'. Equal amounts of alginate overproducing sextuple mutant and its complement were resuspended in their own supernatants and mixed. Fourteen BALB/c mice were inoculated intratracheally with 6 $x10^6$ colony forming units (CFU) of mixture of mutant (strain P973) and complement (strain P1028) as described previously [14]. At each time point (24 h and 48 h) seven mice were humanly euthanized, lungs were homogenized in 0.85% (w/v) saline and serial dilutions were plated on LB and LB+tetracycline 100 μg/ml to determine the total CFU and the complemented strain CFU. The competitive index (CI) was calculated as described [14].

Supporting Information

Figure S1 Alignment of motifs of potential fatty acyl-CoA synthetase homologues. Amino acids with similar properties are assigned the same colors using CLC Sequence Viewer 6 software (www.clcbio.com).
(TIF)

Figure S2 Growth phenotypes of various *fadD* homologues mutants on acyclic terpenes at day six. Strains were grown in liquid 1x M9 medium +1% (w/v) Brij-58 supplemented with 0.1% (w/v) of citronellic acid or 0.1% (w/v) geranic acid at 30°C. Optical densities (ODs) of cultures were measured and compared to PAO1.
(TIF)

Table S1 Potential FadD homologues of *P. aeruginosa* identified through BLAST and tested for complementation in *E. coli* $fadD^-/fadR^-$ (E2011).
(DOC)

Table S2 Additional strains utilized in this study.
(DOC)

Table S3 Doubling time in minutes (min) of various strains in log-phase were calculated from growth curves in Fig. 2.
(DOCX)

Acknowledgments

We thank Patrick Videau for cloning and screening four of the eleven potential *fadD* homologues. We also wish to thank Mike Son and Geraldine Cadaline for their assistant in creation of three mutant strains. We are grateful to Chad B. Walton for his assistance with the animal study.

Author Contributions

Conceived and designed the experiments: JZS MHN YK TTH. Performed the experiments: JZS MHN. Analyzed the data: JZS MHN YK TTH. Contributed reagents/materials/analysis tools: JZS MHN YK ZS APB IM. Wrote the paper: JZS TTH. Edited manuscript: JZS MHN YK ZS APB IM.

References

1. Wilson R, Dowling RB (1998) *Pseudomonas aeruginosa* and other related species. Thorax 53: 213–219.
2. Driscoll J, Brody SL, Kollef MH (2007) The epidemiology, pathogenesis and treatemnt of *Pseudomonas aeruginosa* infection. Drugs 67: 351–368.
3. Smith RP (1994) Skin and soft tissue infections due to *Pseudomonas aeruginosa*. In: Baltch AL, Smith RP, editors. *Pseudomonas aeruginosa*: infections and treatment. New York: Marcel Dekker. 327–369.
4. Baltch AL, Griffin PE (1977) *Pseudomonas aeruginosa* bacteremia: clinical study of 75 patients. Am J Med Sci 274: 119–129.
5. Scheetz MH, Hoffman M, Bolon MK, Schulert G, Estrellado W, et al. (2009) Morbidity associated with *Pseudomonas aeruginosa* bloodstream infections. Diagn Microbiol Infect Dis 64: 311–319.
6. Fleiszig SMJ, Zaidl TS, Pier GB (1995) *Pseudomonas aeruginosa* invasion of and multiplication within corneal epithelial cells *in vitro*. Infect Immun 63: 4072–4077.
7. Pruitt Jr BA, McManus AT, Kim SH, Goodwin CW (1998) Burn wound infections: current status. World J Surg 22: 135–145.

8. Richards MJ, Edwards JR, Culver DH, Gaynes RP (1999) Nosocomial infections in medical intensive care units in the United States. Crit Care Med 27: 887–892.
9. Lepow ML (1994) *Pseudomonas aeruginosa* colonization and infection of the gastrointestinal tract. In: Baltch AL, Smith RP, editors. *Pseudomonas aeruginosa*: infections and treatment. New York: Marcel Dekker. 421–491.
10. Roos KL, Scheld WM (1994) *Pseudomonas aeruginosa* infections of the central nervous system. In: Baltch AL, Smith RP, editors. *Pseudomonas aeruginosa*: infections and treatment. New York: Marcel Dekker. 257–291.
11. Willcox MDP (2007) *Pseudomonas aeruginosa* infection and inflammation during contactlens wear: a review. Optom Vis Sci 84: 273–278.
12. Bernhard W, Hoffmann S, Dombrowsky H, Rau GA, Kamlage A, et al. (2001) Phosphatidylcholine molecular species in lung surfactant: composition in relation to respiratory rate and lung development. Am J Respir Cell Mol Biol 25: 725–731.
13. Son MS, Matthews Jr WJ, Kang Y, Nguyen DT, Hoang TT (2007) *In vivo* evidence of *Pseudomonas aeruginosa* nutrient acquisition and pathogenesis in the lungs of cystic fibrosis patients. Infect Immun 75: 5313–5324.
14. Kang Y, Zarzycki-Siek J, Walton CB, Norris MH, Videau P, et al. (2010) Multiple FadD acyl-CoA synthases contribute to differential fatty acid degradation and virulence expression in *Pseudomonas aeruginosa*. PLoS One 5: e13557.
15. Miller RM, Tomaras AP, Barker AP, Voelker DR, Chan ED, et al. (2008) *Pseudomonas aeruginosa* twitching motility-mediated chemotaxis towards phospholipids and fatty acids: specificity and metabolic requirements. J Bacteriol 190: 4038–4049.
16. Kang Y, Lunin VV, Skarina T, Savchenko A, Schurr MJ, et al. (2009) The long-chain fatty acid sensor, PsrA, modulates the expression of *rpoS* and the type III secretion *exsCEBA* operon in *Pseudomonas aeruginosa*. Mol Microbiol 73: 120–136.
17. Pramanik A, Pawar S, Antonian E, Schulz H (1979) Five different enzymatic acitivities are associated with the multienzyme complex of fatty acid oxidation in *Escherichia coli*. J Bacteriol 137: 469–473.
18. Campbell JW, Cronan JE Jr (2002) The enigmatic *Escherichia coli fadE* gene is *yafH*. J Bacteriol 184: 3759–3764.
19. Black PN, DiRusso CC, Metzger AK, Heimert TL (1992) Cloning, sequencing, and expression of the *fadD* gene of *Escherichia coli* encoding acyl coenzyme A synthase. J Biol Chem 267: 25513–25520.
20. Black PN, DiRusso CC (1994) Molecular and biochemical analyses of fatty acid transport, metabolism, and gene regulation in *Escherichia coli*. Biochim Biophys Acta 1210: 123–145.
21. Campbell JW, Morgan-Kiss RM, Cronan JE Jr (2003) A new *Escherichia coli* metabolic competency: growth on fatty acids by a novel anaerobic β-oxidation pathway. Mol Microbiol 47: 793–805.
22. Nie L, Ren Y, Schulz H (2008) Identification and characterization of *Escherichia coli* thioesterase III that functions in fatty acid β-oxidation. Biochemistry 47: 7744–7751.
23. Feng Y, Cronan JE (2009) A new member of the *Escherichia coli fad* regulon: transcriptional regulation of *fadM* (*ybaW*). J Bacteriol 191: 6320–6328.
24. Black PN (1988) The *fadL* gene product of *Escherichia coli* is an outer membrane protein required for uptake of long-chain fatty acids and involved in sensitivity to bacteriophage T2. J Bacteriol 170: 2850–2854.
25. Groot PHE, Scholte HR, Hulsmann WC (1976) Fatty acid activation: specificity, localization, and function. Adv Lipid Res 14: 75–126.
26. Cronan JE Jr, Satyanarayana S (1998) FadR, transcriptional co-ordination of metabolic expediency. Mol Microbiol 29: 937–943.
27. DiRusso CC, Heimert TL, Metzger AK (1992) Characterization of FadR, a global transcription regulator of fatty acid metabolism in *Escherichia coli*. J Biol Chem 267: 8685–8691.
28. Pauli G, Ehring R, Overath P (1974) Fatty acid degradation in *Escherichia coli*: requirement of cyclic adenosine monophosphate and cyclic adenosine monophosphate receptor protein for enzyme synthesis. J Bacteriol 117: 1178–1183.
29. Cho BK, Knight EM, Palsson BO (2006) Transcriptional regulation of the *fad* regulon genes of *Escherichia coli* by ArcA. Microbiology 152: 2207–2219.
30. Higashitani A, Nishimura Y, Hara H, Aiba H, Mizuno T, et al. (1993) Osmoregulation of the fatty acid receptor gene *fadL* in *Escherichia coli*. Mol Gen Genet 240: 339–347.
31. Kang Y, Nguyen DT, Son MS, Hoang TT (2008) The P*seudomonas aeruginosa* PsrA responds to long-chain fatty acid signals to regulate the *fadBA5* β-oxidation operon. Microbiology 154: 1584–1598.
32. Stover CK, Pham XQ, Erwin AL, Mizoguchi SD, Warrener P, et al. (2000) Complete genome sequence of *Pseudomonas aeruginosa* PA01, an opportunistic pathogen. Nature 406: 959–964.
33. Son MS, Nguyen DT, Kang Y, Hoang TT (2008) Engineering of *FRT-lacZ* fusion constructs: induction of the *Pseudomonas aeruginosa fadAB1* operon by medium and long chain-length fatty acids. Plasmid 59: 111–118.
34. Altschul SF, Madden TL, Schaffer AA, Zhang J, Zhang Z, et al. (1997) Gapped BLAST and PSI-BLAST: a new generation of protein database search programs. Nucleic Acids Res 25: 3389–3402.
35. Fulda M, Heinz E, Wolter FP (1994) The *fadD* gene of *Escherichia coli* K-12 is located close to *rnd* at 39.6 min of the chromosomal map and is a new member of the AMP-binding protein family. Mol Gen Genet 242: 241–249.
36. Weimar JD, DiRusso CC, Delio R, Black PN (2002) Functional role of fatty acid acyl-coenzyme A synthetase in the transmembrane movement and activation of exogenous long-chain fatty acids. J Biol Chem 277: 29369–29376.
37. Kameda K, Suzuki LK, Imai Y (1985) Further purification, characterization and salt activation of acyl-CoA synthetase from *Escherichia coli*. Biochim Biophys Acta 840: 29–36.
38. Black PN, Zhang Q, Weimar JD, DiRusso CC (1997) Mutational analysis of a fatty acyl-coenzyme A synthetase signature motif identifies seven amino acid residues that modulate fatty acid substrate specificity. J Biol Chem 272: 4896–4903.
39. Iram SH, Cronan JE (2006) The β-oxidation systems of *Escherichia coli* and *Salmonella enterica* are not functionally equivalent J Bacteriol 188: 599–608.
40. Förster-Fromme K, Höschle B, Mack C, Bott M, Armbruster W, et al. (2006) Identification of genes andproteins necessary for catabolism ofacyclic terpenes and leucine/isovalerate in *Pseudomonas aeruginosa*. Appl Environ Microbiol 72: 4819–4828.
41. Jenkins LS, Nunn WD (1987) Genetic and molecular characterization of the genes involved in short-chain fatty acid degradation in *Escherichia coli*: the *ato* system. J Bacteriol 169: 42–52.
42. García B, Olivera ER, Miñambres B, Fernández-Valverde M, Cañedo LM, et al. (1999) Novel biodegradable aromatic plastics from a bacterial source. Genetic and biochemical studies on a route of the phenylacetyl-CoA catabolon. J Biol Chem 274: 29228–29241.
43. Doggett RG (1979) *Pseudomonas aeruginosa*: Clinical Manifestations of infection and Current Therapy. New York: Academic Press Inc.
44. Stanier RY, Palleroni NJ, Doudoroff M (1966) The aerobic *Pseudomonads*: a taxonomic study. J Gen Microbiol 43: 159–271.
45. Cruickshank R, Duguid JP, Marmion BP, Awain RHA (1975) Medical microbiology. New York: Churchill Livingstone.
46. Höschle B, Gnau V, Jendrossek D (2005) Methylcrotonyl-CoA and geranyl-CoA carboxylases are involved in leucine/isovalerate utilization (Liu) and acyclic terpene utilization (Atu), and are encoded by *liuB/liuD* and *atuC/atuF*, in *Pseudomonas aeruginosa*. Microbiology 151: 3649–3656.
47. Cantwell SG, Lau EP, Watt DS, Fall RR (1978) Biodegradation of acyclic isoprenoids by Pseudomonas species. J Bacteriol 135: 324–333.
48. Bernhard W, Wang J-Y, Tschernig T, Tummler B, Hedrich HJ, et al. (1997) Lung surfactant in a cystic fibrosis animal model: increased alveolar phospholipid pool size without altered composition and surface tension function in *cftr*$^{m1HGU/m1HGU}$ mice. Thorax 52: 723–730.
49. Palmer KL, Mashburn LM, Singh PK, Whiteley M (2005) Cystic fibrosis sputum supports growth and cues key aspects of *Pseudomonas aeruginosa* physiology. J Bacteriol 187: 5267–5277.
50. Kang Y, Norris MH, Barrett AR, Wilcox BA, Hoang TT (2009) Engineering of tellurite-resistant genetic tools for single-copy chromosomal analysis of *Burkholderia* spp. and characterization of the *Burkholderia thailandensis betBA* operon. Appl and Environ Microbiol 75: 4015–4027.
51. Winsor GL, Van Rossum T, Lo R, Khaira B, Whiteside MD, et al. (2009) Pseudomonas Genome Database: facilitating user-friendly, comprehensive comparisons of microbial genomes. Nucleic Acids Res 37: D483–488.
52. Choi K-H, Gaynor JB, White KG, Lopez C, Bosio CM, et al. (2005) A Tn7-based broad-range bacterial cloning and expression system. Nat Methods 2: 443–448.
53. Hoang TT, Karkhoff-Schweizer RR, Kutchma AJ, Schweizer HP (1998) A broad-host-range Flp-*FRT* recombination system for site-specific excision of chromosomally-located DNA sequences: application for isolation of unmarked *Pseudomonas aeruginosa* mutants. Gene 212: 77–86.
54. Barrett AR, Kang Y, Inamasu KS, Son MS, Vukovich JM, et al. (2008) Genetic tools for allelic replacement in *Burkholderia* species. Appl Environ Microbiol 74: 4498–4508.
55. Kang Y, Norris MH, Wilcox BA, Tuanyok A, Keim PS, et al. (2011) Knockout and pullout recombineering for naturally transformable *Burkholderia thailandensis* and *Burkholderia pseudomallei*. Nat Protoc 6: 1085–1104.
56. Choi K-H, Kumar A, Schweizer HP (2006) A 10-min method for preparation of highly electrocompetent *Pseudomonas aeruginosa* cells: application for the DNA fragment transfer between chromosomes and plasmid transformation. J Microbiol Meth 64: 391–397.
57. White D (2007). Growth and cell division. In: White D editor. The physiology and biochemistry of prokaryotes. New York Oxford: Oxford University Press. 71–72.
58. Hoang TT, Kutchma AJ, Becher A, Schweizer HP (2000) Integration-proficient plasmids for *Pseudomonas aeruginosa*: site-specific integration and use for engineering of reporter and expression strains. Plasmid 43: 59–72.
59. Holloway BW (1955) Genetic recombination in *Pseudomonas aeruginosa*. J Gen Microbiol 13: 572–581.
60. Messing J (1983) New M13 vectors for cloning. Methods Enzymol 101: 20–78.

OPEN ACCESS Freely available online

PLOS ONE

Blocking Phosphatidylcholine Utilization in *Pseudomonas aeruginosa*, via Mutagenesis of Fatty Acid, Glycerol and Choline Degradation Pathways, Confirms the Importance of This Nutrient Source *In Vivo*

Zhenxin Sun[1☯], Yun Kang[1☯], Michael H. Norris[2], Ryan M. Troyer[4], Mike S. Son[3], Herbert P. Schweizer[4], Steven W. Dow[4], Tung T. Hoang[1,2]*

1 Department of Microbiology, University of Hawaii at Manoa, Honolulu, Hawaii, United States of America, **2** Department of Molecular Biosciences and Bioengineering, University of Hawaii at Manoa, Honolulu, Hawaii, United States of America, **3** Department of Biological Sciences, Plymouth State University, Plymouth, New Hampshire, United States of America, **4** Department of Microbiology, Immunology, and Pathology, Colorado State University, Fort Collins, Colorado, United States of America

Abstract

Pseudomonas aeruginosa can grow to very high-cell-density (HCD) during infection of the cystic fibrosis (CF) lung. Phosphatidylcholine (PC), the major component of lung surfactant, has been hypothesized to support HCD growth of *P. aeruginosa in vivo*. The phosphorylcholine headgroup, a glycerol molecule, and two long-chain fatty acids (FAs) are released by enzymatic cleavage of PC by bacterial phospholipase C and lipases. Three different bacterial pathways, the choline, glycerol, and fatty acid degradation pathways, are then involved in the degradation of these PC components. Here, we identified five potential FA degradation (Fad) related *fadBA*-operons (*fadBA1-5*, each encoding 3-hydroxyacyl-CoA dehydrogenase and acyl-CoA thiolase). Through mutagenesis and growth analyses, we showed that three (*fadBA145*) of the five *fadBA*-operons are dominant in medium-chain and long-chain Fad. The triple *fadBA145* mutant also showed reduced ability to degrade PC *in vitro*. We have previously shown that by partially blocking Fad, via mutagenesis of *fadBA5* and *fadD*s, we could significantly reduce the ability of *P. aeruginosa* to replicate on FA and PC *in vitro*, as well as in the mouse lung. However, no studies have assessed the ability of mutants, defective in choline and/or glycerol degradation in conjunction with Fad, to grow on PC or *in vivo*. Hence, we constructed additional mutants (Δ*fadBA145*Δ*glpD*, Δ*fadBA145*Δ*betAB*, and Δ*fadBA145*Δ*betAB*Δ*glpD*) significantly defective in the ability to degrade FA, choline, and glycerol and, therefore, PC. The analysis of these mutants in the BALB/c mouse lung infection model showed significant inability to utilize PC *in vitro*, resulted in decreased replication fitness and competitiveness *in vivo* compared to the complement strain, although there was little to no variation in typical virulence factor production (e.g., hemolysin, lipase, and protease levels). This further supports the hypothesis that lung surfactant PC serves as an important nutrient for *P. aeruginosa* during CF lung infection.

Citation: Sun Z, Kang Y, Norris MH, Troyer RM, Son MS, et al. (2014) Blocking Phosphatidylcholine Utilization in *Pseudomonas aeruginosa*, via Mutagenesis of Fatty Acid, Glycerol and Choline Degradation Pathways, Confirms the Importance of This Nutrient Source *In Vivo*. PLoS ONE 9(7): e103778. doi:10.1371/journal.pone.0103778

Editor: Hendrik W. van Veen, University of Cambridge, United Kingdom

Received March 24, 2014; **Accepted** July 2, 2014; **Published** July 28, 2014

Data Availability: The authors confirm that all data underlying the findings are fully available without restriction. All relevant data are within the paper and its Supporting Information files.

Funding: Funding for this research was provided by grant number P20GM103516 from the National Institute of General Medical Sciences of the National Institutes of Health. The study design and content are solely the responsibility of the authors and do not represent the official views of the National Institutes of Health. The funders had no role in study design, data collection and analysis, decision to publish, or preparation of the manuscript.

Competing Interests: The authors have declared that no competing interests exist.

* Email: tongh@hawaii.edu

☯ These authors contributed equally to this work.

Introduction

Pseudomonas aeruginosa is widespread in nature, inhabiting soil, water, plants and animals. In hospitals, it can be found in sinks, respirators, humidifiers and occasionally on the hands of medical personnel [1,2]. The ubiquitous nature of this bacterium has allowed it to adapt to a broad range of hosts in which it can cause diseases. The role of *P. aeruginosa* as an opportunistic human pathogen is of particular concern, especially because it is a frequent cause of nosocomial infections such as pneumonia, urinary tract infections, and bacteremia [1,3,4]. *P. aeruginosa* infection in the respiratory tract of cystic fibrosis (CF) patients causes a rapid deterioration in lung function and thus patient survival [5,6]. The pathogenicity of *P. aeruginosa* infection in CF patients has been extensively studied in terms of biofilm production [7–9] and quorum sensing (QS) controlled virulence [10–12]. However, little effort has been placed towards the contribution of *P. aeruginosa* nutrient acquisition aids high-cell-density (HCD) replication during lung infection.

Previous studies have shown that *P. aeruginosa* can undergo HCD replication in the lung of CF patients reaching $>10^9$ CFU/ml [13–15]. HCD replication is highly energy demanding,

requiring efficient nutrient acquisition and metabolism. However, evidence showed that the nutrients in the lung environment are lipids and amino acids derived from proteins or polypeptides [16–18], to allow *P. aeruginosa* HCD growth and maintenance *in vivo*. An *in vitro* study revealed that *P. aeruginosa* has directional twitching motility toward phosphatidylethanolamine (PE) and phosphatidylcholine (PC) [19]. Mammalian lungs are naturally coated by indispensible lung surfactant, which is composed of approximately 10% protein and 90% lipids, with about 80% of the lung surfactant lipids being phosphatidylcholine (PC) [20–22]. Thus, PC, the most abundant lipid in lung surfactant may provide significant nutrient for HCD bacterial growth *in vivo*. In accordance with this hypothesis, our initial studies suggest that PC is a major nutrient source of *P. aeruginosa* during lung infection and supports HCD replication [15,17,18].

Our previous *in vivo* CF sputa study showed that *P. aeruginosa* produced phospholipase C (heat-labile hemolysin) and lipases that could cleave exogenous PC into three components: a phosphorylcholine headgroup, glycerol and two long-chain fatty acids (LCFAs) [15] (Fig. 1A). These three components can be further metabolized by the choline (bet), glycerol (glp), and fatty acid degradation (Fad) pathways (Fig. 1B), respectively. Choline and glycerol metabolism by *P. aeruginosa* are well characterized [23–27]. However, LCFA degradation by *P. aeruginosa* and the genes involved in this process remain to be fully elucidated. Our previous *in vivo* CF sputa study also detected the expression of *P. aeruginosa* genes involved in each pathway for metabolizing all three PC components [15]. The *betAB*-operon was induced and *glpD* and *glpK* genes were constitutively expressed *in vivo* [15]. Among genes for Fad (Fig. 1B), the expression of *fadBA1* was detected when *P. aeruginosa* was grown on PC *in vitro,* and *fadBA5* and *fadA4* were induced and constitutively expressed in CF sputa [15], suggesting the involvement of *fadBA145* in LCFA degradation. We have also shown the reduced ability of the *fadD* mutants to utilize FAs as nutrients led to their decreased fitness during mouse lung infection [17,18]. However, further evidence is needed to support the hypothesis that all three components of lung surfactant PC (phosphorylcholine, glycerol and FA) serve as nutrient sources for *P. aeruginosa* during *in vivo* lung infection.

In this study, up to five potential *fadBA*-operons (encoding 3-hydroxyacyl-CoA dehydrogenase and acyl-CoA thiolase) were identified, and three of them *fadBA1* (PA1737, PA1736), *fadBA4* (PA4786, PA4785) *and fadBA5* (PA3014, PA3013) were shown to be significantly involved in medium- and long-chain Fad. Coupling of the *fadBA145* mutations with mutations in choline and/or glycerol degradation were investigated to determine the importance of these pathways to degrade PC *in vitro* and *in vivo*. Competition studies were initiated to analyze the competitive fitness of these mutants relative to strains with intact pathways.

Results and Discussion

P. aeruginosa has five *fadBA*-operons potentially involved in fatty acid degradation

The well-established aerobic fatty acid degradation (Fad) pathway in *E. coli* was used as a model to characterize *P. aeruginosa* Fad. *E. coli* possesses only a single copy of each *fad* gene for aerobic Fad [28,29], and the cyclic degradation of fatty acids by two carbons per cycle is primarily catalyzed by an acyl-CoA dehydrogenase coded by *fadE*, and the products of the *fadBA*-operon, 3-hydroxyacyl-CoA dehydrogenase and acyl-CoA thiolase, respectively. Up to five potential *fadBA*-operons were identified in *P. aeruginosa* by BLAST analysis of the *E.coli fadBA* sequence against the *P. aeruginosa* genome, including *fadBA1* (PA1737, PA1736), *fadBA2* (PA3590, PA3589), *fadBA3* (PA2554, PA2553), *fadBA4* (PA4786, PA4785), and *fadBA5* (PA3014, PA3013) (Fig. S1). Of these five FadBAs, FadBA5 showed the greatest homology to the *E.coli* FadBA with FadB5 having 72% similar (54% identical) and FadA5 having 76% similar (61% identical) to the *E.coli* FadBA, respectively [30,31].

Considering the larger size of the *P. aeruginosa* genome (6.29 Mb) [32] and its wide range of environmental niches and metabolic capabilities, it is not surprising that *P. aeruginosa* has up to five *fadBA*-operon homologues. Therefore, it is important next to narrow down which of these five operons are important in Fad, using a mutagenesis approach.

P. aeruginosa fadBA145-operons are important for degrading PC and medium- and long-chain fatty acids

Our previous work showed that the Δ*fadBA5* mutant has a reduced ability to utilize LCFA as a sole carbon source, but this Δ*fadBA5* mutant can still grow on LCFAs as a carbon source, indicating the existence of other potential *fadBA*-operons in *P. aeruginosa* for LCFA degradation [31]. Further supporting this idea, the *fadBA1*-operon was shown to be induced by medium-chain fatty acids (MCFAs) and to a lesser extent by LCFAs [33]. The *fadBA5*-operon plays the most significant role in LCFA degradation, because neither the single Δ*fadBA1* mutant, nor the single Δ*fadBA4* mutant, showed much defects in their ability to utilize MCFA and LCFA as sole carbon sources (Fig. S2). It is possible that the FadBA1 and/or other FadBA(s) might have overlapping functions with FadBA5 in the metabolism of different chain length FAs, but these activities are masked by the more dominant FadBA5. Evidence for the involvement of other FadBAs is lacking, and needs to be addressed.

Because it is too overwhelming to test all possible double, triple, and quadruple *fadBA*-mutant combinations and the complicated dominance of *fadBA5*, we demonstrated the involvement of each *fadBA*-operon by testing different triple mutant combinations. In this study, we generated several triple mutants (Δ*fadBA125*, Δ*fadBA135*, Δ*fadBA145*, Δ*fadBA235*, Δ*fadBA245*, Δ*fadBA345*) and a quintuple mutant Δ*fadBA1-5* (Table 1) for growth analysis on MCFA and LCFAs as sole carbon sources, to further characterize the function of these *fadBA*-operons. The growth defects were previously defined by the slower growth rate and lower overall final cell densities compared to wildtype strain PAO1, which suggest a reduced ability to metabolize these FAs, presumably due to the accumulation of growth inhibiting intermediates [17,31]. Significant growth defects were observed for any combinations of triple mutants in which both the *fadBA5*- and *fadBA1*-operons were deleted (i.e., Δ*fadBA125,* Δ*fadBA135* and Δ*fadBA145* mutants), revealing the importance of *fadBA1* and *fadBA5* contributing to growth on MCFA and LCFAs (Fig. 2A–D). Although the level of defects is different for each type of FA used, the trend is consistent for these mutants in all FAs (Fig. 2A–D). Only the Δ*fadBA145* triple mutant showed the same growth defect as the Δ*fadBA1-5* quintuple mutant on all fatty acids tested, suggesting the importance of all three *fadBA1*, *fadBA4*, and *fadBA5* operons and the minor role of *fadBA2* and *fadBA3*-operons in metabolizing MCFA and LCFAs. The importance of *fadBA4* was further confirmed by the fact that the Δ*fadBA245* and Δ*fadBA345* triple mutants showed an additional growth defect on all FAs compared to the Δ*fadBA235* mutant (Fig. 2A–D). However, the *fadBA4*-operon displays less of an involvement in metabolizing all FAs tested compared to both *fadBA1* and *fadBA5*-operons (i.e., comparing Δ*fadBA245* to Δ*fadBA125* or Δ*fadBA345* to Δ*fadBA135*). Knowing that only *fadBA1*, *fadBA4*, and *fadBA5* are important for degrading

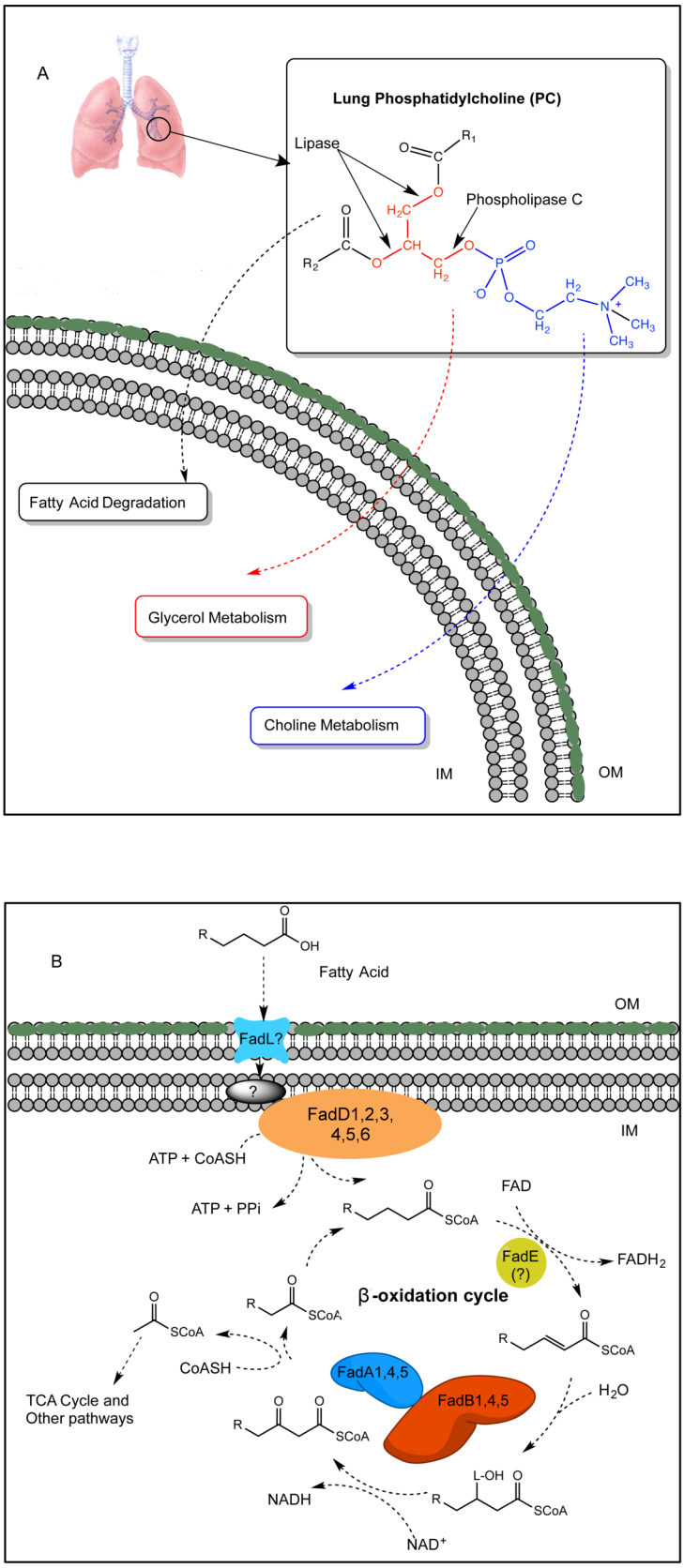

Figure 1. Phosphatidylcholine (PC) degradation pathways in *Pseudomonas aeruginosa*. (A) PC is the main component of lung surfactant and can be cleaved by phospholipase C and lipases, producing free fatty acids, glycerol, and phosphorylcholine. Three different pathways then further metabolize each component: the *bet* pathway for choline head group metabolism, the *glp* pathway for glycerol metabolism, and the *β*-

oxidation pathway for the degradation of the FAs. (B) The proposed *P. aeruginosa* FA β-oxidation pathway. Abbreviations: FadA, 3-ketoacyl-CoA thiolase; FadB, *cis*-Δ^3-*trans*-Δ^2-enoyl-CoA isomerase, enoyl-CoA hydratase, 3-hydroxyacyl-CoA epimerase, and 3-hydroxyacyl-CoA dehydrogenase; FadD, fatty acyl-CoA synthetase; FadE, acyl-CoA dehydrogenase; FadL, outer membrane long-chain fatty acid translocase; OM, out membrane; IN, inner membrane.

doi:10.1371/journal.pone.0103778.g001

MCFA and LCFA of PC, we continued with further experiments from this point forward in our study by using the Δ*fadBA145* mutant background, rather than the Δ*fadBA1-5* quintuple mutant.

We next tested the Δ*fadBA145* mutant for its ability to grow on PC. The Δ*fadBA145* triple mutant displayed a reduced growth rate and lower final cell density as compared to wildtype PAO1 when grown with PC as a sole carbon source (Fig. 3A). There was no growth defect observed for this mutant when grown in control LB medium (Fig. 3B). The Δ*fadBA145* mutant strain is competitively less fit than the complement in the *in vitro* competition study when grown in PC or FA ($C_{18:1}^{\Delta 9}$) (Fig. 4A panel i). No competitive defect was observed when the Δ*fadBA145* mutant was grown on LB, glucose, casamino acids (CAA), glycerol or choline controls (Fig. 4A panel i). We concluded that the reduced growth of the Δ*fadBA145* mutant strain on PC observed in figure 3A is due to a decreased ability to degrade LCFAs of PC and not glycerol or choline. All the evidence we have here strongly suggests the involvement of the three *fadBA1,4,5*-operons in Fad and PC degradation. We complemented Δ*fadBA145* mutant strain by integrating miniCTX2-*fadBA5* (i.e., the dominant *fadBA* operon as explained above) as a single copy into the Δ*fadBA145* mutant background (Table 1). The complemented strain was fully restored to wildtype growth on PC (Fig. 3A) and FAs (not shown). Hence, all complementation experiments in this study for any Δ*fadBA145* mutant background were performed with only the dominant *fadBA5*-operon.

Mutants blocked in FA, glycerol, and choline degradation displayed dramatically reduced ability to utilize PC *in vitro*

The enzymatic activity of phospholipase C on PC releases the phosphorylcholine headgroup and the diacylglycerol (DAG) molecule (Fig. 1A). The phosphorylcholine headgroup is first transported across the cell membrane and dephosphorylated by a phosphatase [23,34,35] to yield choline, which has previously been shown to be sufficient for *P. aeruginosa* to grow on as a sole carbon, nitrogen, and energy source [36]. *P. aeruginosa* BetAB (encoding choline dehydrogenase and a glycine betaine aldehyde dehydrogenase) catalyzes the conversion of choline to glycine betaine [23]. Glycine betaine is successively demethylated to form dimethylglycine (DMG), sarcosine (monomethylglcine), and finally glycine [24,37]. The DAG molecule is cleaved by the *P. aeruginosa* lipase, liberating a glycerol molecule and two LCFAs. Glycerol metabolism has been well characterized in *P. aeruginosa*. The operon primarily consists of *glpD* (a *sn*-glycerol-3-phosphate dehydrogenase [38]), *glpF* (a membrane-associated glycerol diffusion facilitator [27,39]), *glpK* (a glycerol kinase [27,39]), *glpM* (a membrane protein affecting alginate synthesis [26]), and *glpR* (a regulator of the *glp* operon [25]).

Since our previous data showed that *betAB* and *glpD* were expressed *in vivo* [15], they may potentially be involved in PC degradation during lung infection. However, before we could address the *in vivo* aspect of PC degradation, further experiments are needed to characterize *P. aeruginosa* PC degradation *in vitro*. We engineered double pathway mutants Δ*fadBA145*Δ*betAB* (blocked in FA and choline degradation) and Δ*fadBA145*Δ*glpD* (blocked in FA and glycerol degradation) and a triple pathway mutant Δ*fadBA145*Δ*betAB*Δ*glpD* (blocked in FA, choline, and glycerol degradation) (Table 1), to further determine whether these mutants are deficient in growth on PC. As expected, all three mutants experienced various growth defects with decreased cell density and delayed log-phase when grown on PC (Fig. 3A). The triple pathway mutant Δ*fadBA145*Δ*betAB*Δ*glpD* exhibited the most significant reduced ability to utilize PC, reaching to only about one-third of the wildtype final cell density. We complemented these mutants (i.e., Δ*fadBA145*Δ*betAB*, Δ*fadBA145*Δ*glpD*, and Δ*fadBA145*Δ*betAB*Δ*glpD*) by integrating the respective miniCTX2-*fadBA5/betAB*, miniCTX2-*fadBA5/glpD* or miniCTX2-*fadBA5/betAB/glpD* as a single copy on the *P. aeruginosa* chromosome and the complemented strains fully recovered these mutants' ability to grow on PC as compared to wildtype PAO1 (Fig. 3A). No mutants or complement showed any growth defects on control LB medium (Fig. 3B).

We performed an *in vitro* competition study between pathway mutants (Δ*fadBA145*Δ*betAB,* Δ*fadBA145*Δ*glpD,* Δ*fadBA145*Δ*betAB*Δ*glpD*) and their complements to exam whether the mutation reduced their ability to metabolize various carbon sources. As expected, all the pathway mutants were less competitive than their respective complements in media containing PC and other sole carbon sources involved in the respective pathways (Fig. 4A panels ii-iv). For example, the Δ*fadBA145*Δ*betAB* mutant was less competitive than its complement when grown using PC, FA, or choline, as sole carbon source (Fig. 4A panel ii), which is not the case in other control media (e.g., LB, glucose, CAA or glycerol). Likewise, the Δ*fadBA145*Δ*glpD* mutant was less competitive than its complement only if PC, FA, or glycerol was used as sole carbon source (Fig. 4A panel iii). The triple pathway mutant was almost completely outcompeted by its complemented strain with the competitive indices (CI) dramatically reduced to ~0.1 when growing in the media containing PC, choline, glycerol, or oleate FA (Fig. 4A panel iv). Overall, these *in vitro* data showed that we have three mutants (Δ*fadBA145*Δ*betAB,* Δ*fadBA145*Δ*glpD,* Δ*fadBA145*Δ*betAB*Δ*glpD*) and their complement that could be used to assess the utilization of PC *in vivo*, through competitive index experiments within the mouse lung.

Blocking FA, glycerol, and choline degradation significantly reduces replication fitness of *P. aeruginosa in vivo*

Since PC is the major component of lung surfactant in mammals, including mice [21], a mouse lung infection model [40] was utilized for our *in vivo* competition study to evaluate the fitness of the PC degradation pathway mutants within the lung environment. The mucoid, exopolysaccharide alginate-overproducing phenotype is a distinguishing feature of *P. aeruginosa* isolated from CF patients [40,41]. An alginate-overproducing strain carrying a *mucA* insertional mutation, which allows the mucoid strain to survive and replicate in the lung, has been successfully used in BALB/c mouse model to establish the connection between nutrient acquisition and *in vivo* lung fitness for *P. aeruginosa* [17]. Therefore, we constructed various *mucA*$^-$ alginate-overproducing strains, such as Δ*fadBA145-mucA*$^-$, Δ*fadBA145*Δ*glpD-mucA*$^-$, Δ*fadBA145*Δ*betAB-mucA*$^-$, Δ*fadBA145*Δ*betAB*Δ*glpD-mucA*$^-$ and their complemented strains for

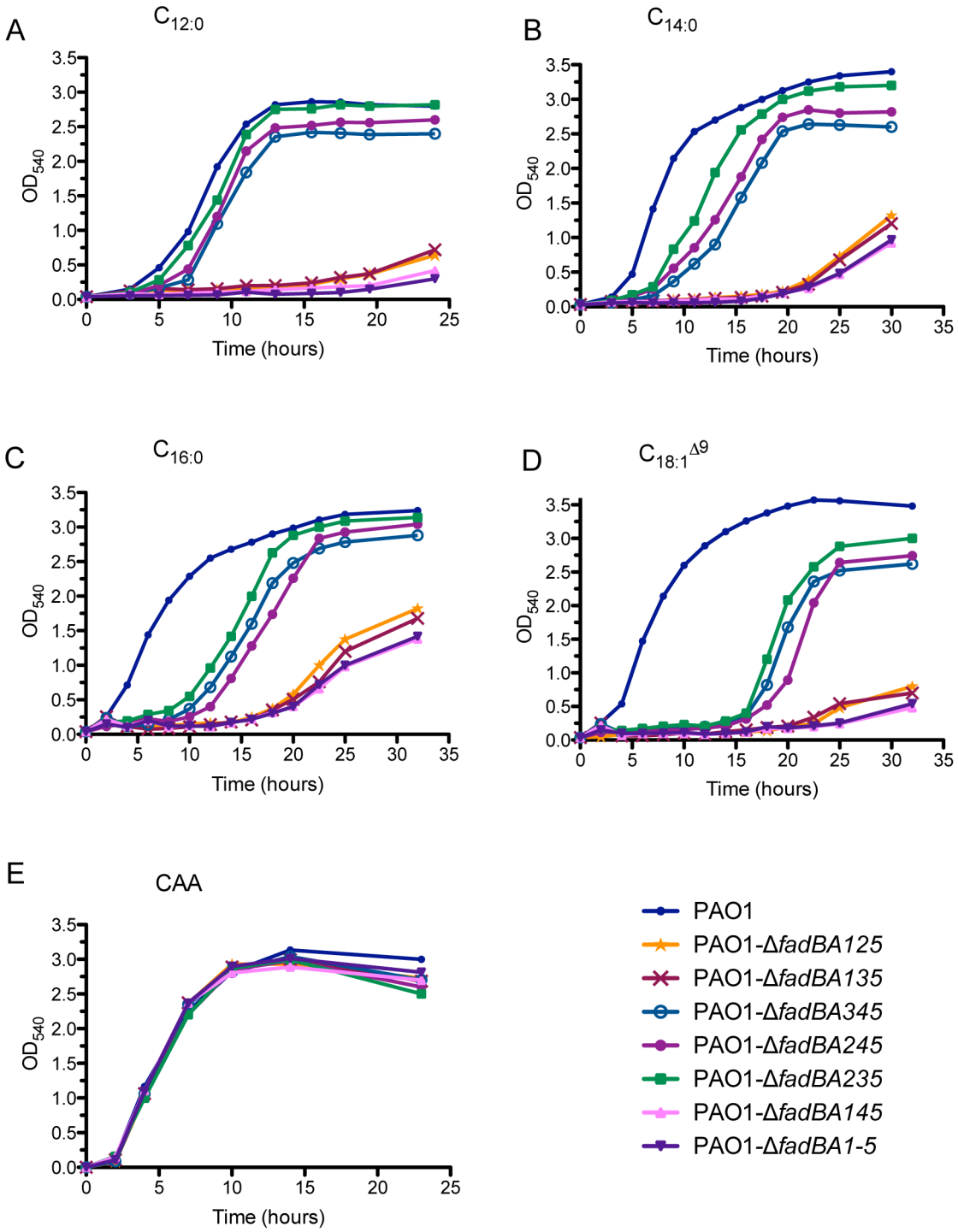

Figure 2. Growth analysis of different *fadBA* mutant combinations on medium ($C_{12:0}$) and long chain-length fatty acid ($C_{14:0}$, $C_{16:0}$ and $C_{18:1}^{\Delta 9}$). Along with the wildtype PAO1 strain, mutants were grown in 1×M9 minimal medium supplemented with 0.4% different test FAs (A to D) or 1% control casamino acids (CAA, E) as sole carbon sources. Although *fadBA* mutants showed various defects when grown with FAs of different chain-lengths, no growth defects were observed for any of the mutants when grown with CAA as a control.
doi:10.1371/journal.pone.0103778.g002

this study. Prior to the animal study, the phenotypes of all *mucA* strains were confirmed by patching on minimal media plates with FA, choline, or glycerol as sole carbon sources along with all appropriate controls (all *mucA* wild-type strains and complemented strains). As expected, the *mucA* mutation did not affect the metabolism of any of these carbon sources (Fig. S3). As previously described [17,40], BALB/c mice were inoculated via intratracheal intubation with equal ratios of each mutant and its complement pair (6×10^6 CFU/animal). At 24 h post-infection, bacterial CFU recovered from the lungs were determined, followed by CI calculations. For all the strains, the average total CFU per mouse lung recovered at 24 hours post-infection was greater than the

Table 1. Bacterial strains used in this study[a].

Strain	Lab ID[b]	Genotype/Description	Reference
E.coli			
EP-Max10B	E1231	F$^-$ λ$^-$ *mcrA* Δ(*mrr-hsdRMS-mcrBC*) φ80d*lacZ* Δ*M15* Δ*lacX74 deoR recA1 endA1 araD139* Δ(*ara, leu*)7697 *galU galKrpsL nupG*	BioRad
SM10	E006	*thi thr leu tonA lacY supE recA*::RP4-2Tc::Mu Km^r	[48]
P. aeruginosa			
PAO1	P007	Prototroph	[49]
PAO1- *mucA*$^-$	P447	Cb^r, PAO1 with pUC18 inserted in *mucA* gene	This study
Δ*fadBA125*	P122	Gm^r, PAO1-Δ*fadBA1*::*FRT,* Δ*fadBA2*::*FRT,* Δ*fadBA5*::Gm	This study
Δ*fadBA135*	P124	Gm^r, PAO1-Δ*fadBA1*::*FRT,* Δ*fadBA3*::*FRT,* Δ*fadBA5*::Gm	This study
Δ*fadBA145*	P319	Gm^r, PAO1-Δ*fadBA1*::*FRT,* Δ*fadBA4*::*FRT,* Δ*fadBA5*::Gm	This study
Δ*fadBA235*	P317	Gm^r, PAO1-Δ*fadBA2*::*FRT,* Δ*fadBA3*::*FRT,* Δ*fadBA5*::Gm	This study
Δ*fadBA245*	P130	Gm^r, PAO1-Δ*fadBA2*::*FRT,* Δ*fadBA3*::*FRT,* Δ*fadBA5*::Gm	This study
Δ*fadBA345*	P126	Gm^r, PAO1-Δ*fadBA3*::*FRT,* Δ*fadBA4*::*FRT,* Δ*fadBA5*::Gm	This study
Δ*fadBA1-5*	P102	Gm^r, PAO1-Δ*fadBA1*::*FRT,* Δ*fadBA2*::*FRT,* Δ*fadBA3*::*FRT,* Δ*fadBA4*::*FRT,* Δ*fadBA5*::Gm	This study
Δ*fadBA145* Δ*glpD*	P539	Gm^r, PAO1-Δ*fadBA1*::*FRT,* Δ*fadBA4*::*FRT,* Δ*fadBA5*::*FRT,* Δ*glpD*::Gm-*FRT1*	This study
Δ*fadBA145* Δ*betAB*	P555	Gm^r, PAO1-Δ*fadBA1*::*FRT,* Δ*fadBA4*::*FRT,* Δ*fadBA5*::*FRT,* Δ*betAB*::Gm-*FRT3*	This study
Δ*fadBA145* Δ*betAB* Δ*glpD*	P561	Gm^r, PAO1-Δ*fadBA1*::*FRT,* Δ*fadBA4*::*FRT,* Δ*fadBA5*::*FRT,* Δ*betAB*::*FRT3,* Δ*glpD*::Gm-*FRT1*	This study
Δ*fadBA145*/complement	P965	Gm^r, Tet^r; Δ*fadBA145* complemented with miniCTX2-*fadBA5*	This study
Δ*fadBA145* Δ*glpD*/complement	P1015	Gm^r, Tet^r; Δ*fadBA145* Δ*glpD* complemented with miniCTX2-*fadBA5/glpD*	This study
Δ*fadBA145* Δ*betAB*/complement	P1017	Gm^r, Tet^r; Δ*fadBA145* Δ*betAB* complemented with miniCTX2-*fadBA5/betAB*	This study
Δ*fadBA145* Δ*betAB* Δ*glpD*/complement	P1019	Gm^r, Tet^r; Δ*fadBA145* Δ*betAB* Δ*glpD* complemented with miniCTX2-*fadBA5/betAB/glpD*	This study
Δ*fadBA145-mucA*$^-$	P576	Gm^r, Cb^r; Δ*fadBA145* with pUC18 inserted in *mucA* gene	This study
Δ*fadBA145* Δ*glpD-mucA*$^-$	P570	Gm^r, Cb^r; Δ*fadBA145* Δ*glpD* with pUC18 inserted in *mucA* gene	This study
Δ*fadBA145* Δ*betAB-mucA*$^-$	P572	Gm^r, Cb^r; Δ*fadBA145* Δ*betAB* with pUC18 inserted in *mucA* gene	This study
Δ*fadBA145* Δ*betAB* Δ*glpD-mucA*$^-$	P574	Gm^r, Cb^r; Δ*fadBA145* Δ*betAB* Δ*glpD* with pUC18 inserted in *mucA* gene	This study
Δ*fadBA145-mucA*$^-$/complement	P584	Gm^r, Cb^r, Tet^r; Δ*fadBA145-mucA*$^-$ complemented with miniCTX2-*fadBA5*	This study
Δ*fadBA145* Δ*glpD-mucA*$^-$/complement	P578	Gm^r, Cb^r, Tet^r; Δ*fadBA145* Δ*glpD-mucA*$^-$ complemented with miniCTX2-*fadBA5/glpD*	This study
Δ*fadBA145* Δ*betAB-mucA*$^-$/complement	P580	Gm^r, Cb^r, Tet^r; Δ*fadBA145* Δ*betAB-mucA*$^-$ complemented with miniCTX2-*fadBA5/betAB*	This study
Δ*fadBA145* Δ*betAB* Δ*glpD-mucA*$^-$/complement	P582	Gm^r, Cb^r, Tet^r; Δ*fadBA145* Δ*betAB* Δ*glpD-mucA*$^-$ complemented with miniCTX2-*fadBA5/betAB/glpD*	This study

[a]For strains constructed in this study, please see text for further details.
[b]Please use Lab ID for requesting strains.
doi:10.1371/journal.pone.0103778.t001

initial inoculum (Fig. 4B), indicating that all these *P. aeruginosa* strains maintained the ability to replicate within the mouse lung. The Δ*fadBA145* mutant still replicated significantly *in vivo* compared to its complement. Surprisingly, the Δ*fadBA145* CI is quite high compared to other FAD mutants (i.e., *fadD* mutants) we have previously published where CI is approximately 0.5 [17,18]. The Δ*fadBA145*Δ*betAB*, Δ*fadBA145*Δ*glpD in vivo* CI is lower than the Δ*fadBA145* when compared to their respective complements (Fig. 4B), showing the importance of glycerol and choline degradation as potential nutrient sources *in vivo*. Most significantly, the mean CI value for the triple pathway mutant (i.e., Δ*fadBA145*Δ*betAB*Δ*glpD*) showed that the triple pathway mutant had a significantly reduced ability to survive and multiply in the lungs of mice compared to its complement.

We monitored all strains tested *in vivo* for different virulence expression, including proteases, rhamnolipid, hemolysins and lipases (Fig. S4). With similar level of these common secreted virulence factors observed between strains (Fig. S2), the low CI is most likely due to its inability to metabolize PC and the three components of PC (LCFAs, glycerol, and phosphorylcholine) as a nutrient source, rather than resulting from altered virulence expression. Overall, the altered ability for the pathway mutants to metabolize PC as nutrient *in vitro* was clearly mirrored by their competitive fitness within the lung.

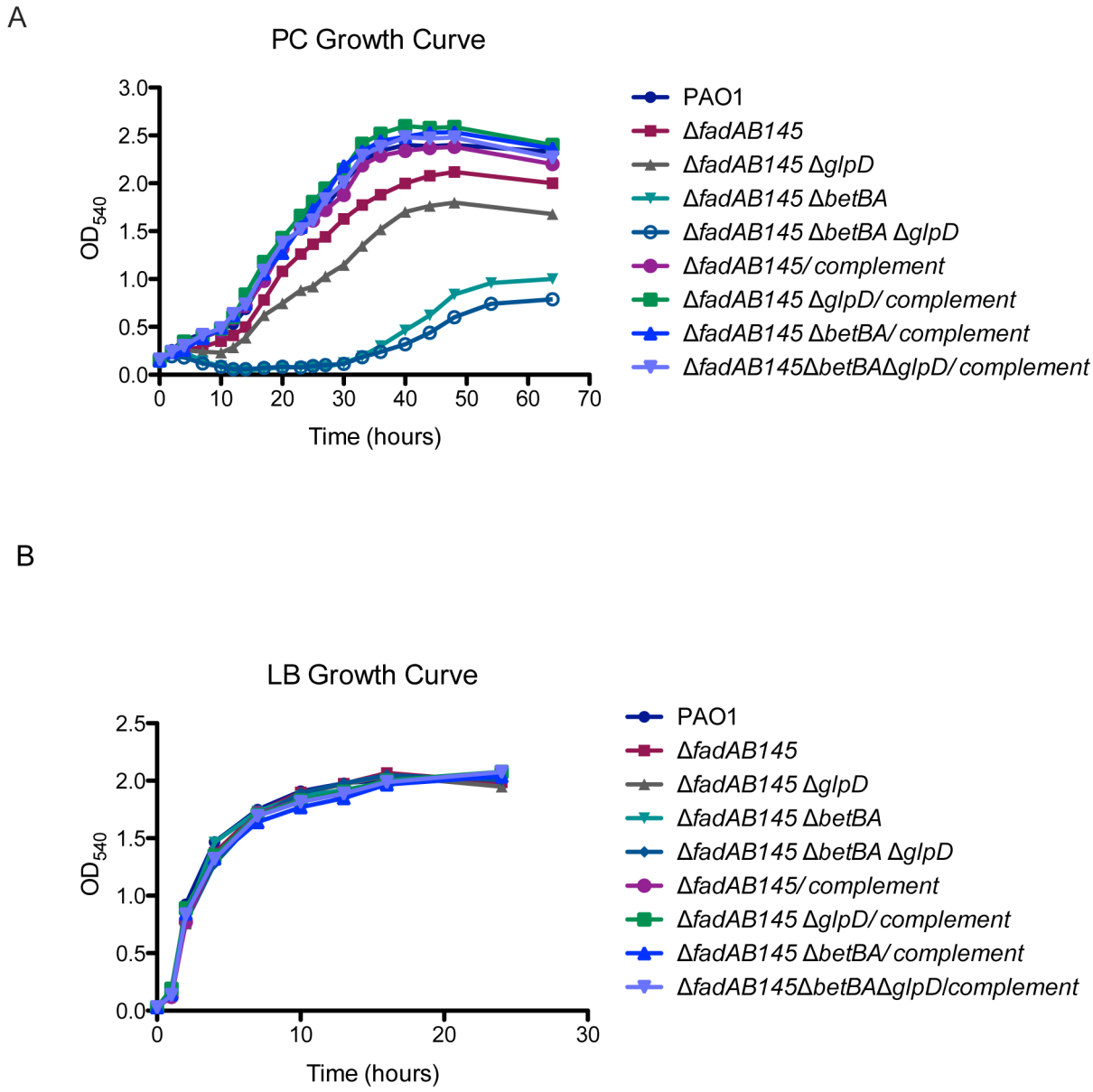

Figure 3. Growth analysis on phosphatidylcholine. (A) Some mutants exhibited growth defects on PC as a sole carbon source. The growth defects were fully recovered in complemented strains, as they had identical growth rates compared to the wildtype PAO1 strain. (B) No growth defects in control LB medium were observed.
doi:10.1371/journal.pone.0103778.g003

In summary, *P. aeruginosa* possesses an impressive repertoire of virulence factors, and the expression of most of these only occurs during the HCD replication and their timely expression is regulated by QS [42], which occurs at HCD. *P. aeruginosa* requires large amount of readily available energy to reach and maintain HCD and produce the high-energy dependent virulence structure like biofilm. Thus, exploration of the nutrient sources supporting such an energy intensive processes is of importance, especially for chronic *P. aeruginosa* lung infections in CF patients. In addition, the identification of the genes and pathways for *P. aeruginosa* HCD replication in CF lungs provides fundamental knowledge for possibly developing new therapeutic strategies targeting bacterial nutrient metabolism in the lung, thereby preventing bacterial HCD. The expression of genes involved in *P. aeruginosa* PC degradation within the lungs of CF patients has been previously demonstrated [15]. Our study focused on providing further evidence to determine whether PC serves as a significant nutrient source during *P. aeruginosa* lung infection. In order to decipher the role of PC *in vivo*, we first characterized PC degradation pathways *in vitro*. Of the three components released by the enzymatic cleavage of PC by bacterial phospholipase C and lipases (phosphorylcholine, LCFAs, and glycerol), LCFAs are highly reduced and yield the most carbon and energy. In our study, five potential *fadBA*-operons were investigated and three of them (i.e., *fadBA1,4,5*-operons) proved to be significantly involved in Fad. The *in vitro* growth analysis of different pathway mutants (Δ*fadBA145*, Δ*fadBA145*Δ*betAB*, Δ*fadBA145*Δ*glpD*, Δ*fadBA145*Δ*betAB*Δ*glpD*) on PC provided direct evidence to support that *P. aeruginosa* utilizes the FA, glycerol and choline degradation pathways to degrade individual components of PC

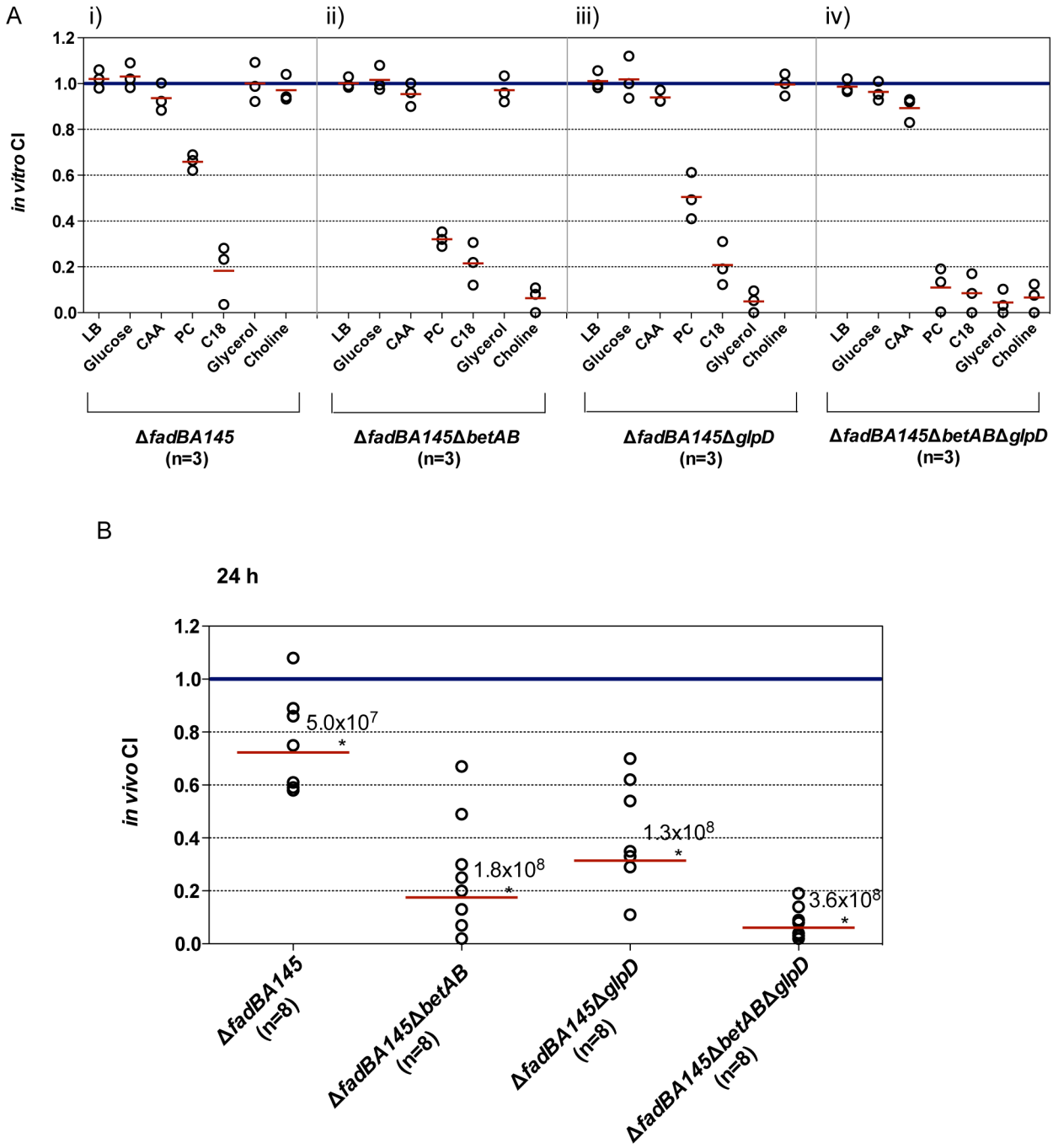

Figure 4. Competition studies of pathway mutants. (A) *In vitro* competition studies of the various mutants and their complemented strains in different growth media (n equals the number of independent *in vitro* competition experiments performed with each carbon source). (B) *In vivo* lung competition of the various mutants and their complemented strains after 24 h, where n equals the number of mice in each group that were inoculated with a total of 6×10^6 CFU/mouse. The solid red line indicates the geometric mean of the competitive indices (CI) in each competition group. CI<1 indicates the mutant was less competitive than its complemented strain in various growth media (A) or within the lungs (B). Numbers above the red line represent the average total recovered CFU/mouse for each competition group.
doi:10.1371/journal.pone.0103778.g004

in vitro. Our *in vivo* competition study was performed utilizing a mouse lung infection model [40] to evaluate the fitness of the pathway mutants within the lung environment. The triple pathway mutant Δ*fadBA145*Δ*betAB*Δ*glpD* exhibited the greatest growth defect on relevant carbon sources *in vitro* and was outcompeted by its complement *in vivo*. Since no altered expression of virulence factors was observed for all the pathway mutants and their complement pairs compared to wildtype PAO1, it is highly likely that the decreased ability to utilize PC resulted in lower replication fitness in the lung environment. This study strongly supports the hypothesis that *P. aeruginosa* utilizes lung surfactant PC as one of the nutrient sources for chronic lung infection.

Materials and Methods

Ethic Statement

All animal experiments were performed in compliance with the NIH (National Institutes of Health) Guide for the Care and Use of Laboratory Animals and were approved by the University of Hawaii Institutional Animal Care and Use Committee (protocol no. 06-023-04).

Bacterial strains and growth conditions

Bacterial strains and plasmids utilized in this study are listed in Table 1 and 2. *E. coli* EP-Max10B was used as cloning strains and cultured in Luria-Bertani (LB) medium (Difco). *Pseudomonas* Isolation Agar or Broth (PIA or PIB; Difco) or LB medium were used to culture *P. aeruginosa* strain PAO1 and derivatives. All fatty acids (FAs) stocks were made as previously described [17]. Strains for growth analyses were cultured in 1× M9 minimal medium +0.2% (w/v) Brij-58 (Sigma) +1% (w/v) casamino acids (CAA) or 0.4% (w/v) of the individual FA, $C_{12:0}$ to $C_{16:0}$, or $C_{18:1}{}^{\Delta 9}$ (Sigma; Fig. 2) and 1× M9 minimal medium +0.2% (w/v) Brij-58 (Sigma) +0.4% (w/v) phosphatidylcholine (PC, Sigma; Fig. 3A), at 37°C with a shaking speed of 200 r.p.m. Since most of FAs hydrolyzed from *in vivo* PC are $C_{16:0}$ (50–60%), with ~10–20% of each of $C_{14:0}$, $C_{16:1}$, $C_{18:1}{}^{\Delta 9}$, and $C_{18:2}$ constituting the rest [43], the growth analysis was performed in 1×M9 minimal medium supplied with each of $C_{12:0}$ (medium-chain fatty acid), $C_{14:0}$, $C_{16:0}$, and $C_{18:1}{}^{\Delta 9}$ (LCFAs) as a sole carbon source. Accordingly, the PC we used in these *in vitro* experiments contains mostly LCFAs, approximately 33% $C_{16:0}$, 13% $C_{18:0}$, 31% $C_{18:1}{}^{\Delta 9}$, and 15% $C_{18:2}$. The *in vitro* competition studies (Fig. 4A) were performed under the growth condition mentioned above as previously described [17].

General molecular methods

Oligonuceotides were synthesized through Integrated DNA Technology and are listed in Table 3. All molecular methods and their components utilized were employed as previously described [44].

Construction of mutants and complementation strains

All mutants were constructed as described previously [45]. Briefly, the *fadBA* (*fadBA1*, *fadBA2*, *fadBA3*, *fadBA4*, *fadBA5*) operons, *betAB* operon, and *glpD* gene were amplified by PCR using respective upstream and downstream primer pair listed in Table 3. The PCR products were purified from the gel, digested with appropriate restriction enzymes, and cloned into the gene replacement vector pEX18T, digested with the same restriction enzymes, to yield each of the pEX18T-target gene constructs. After deletions were made on plasmid in each of the *fadBA*-operons, the *glpD* gene, and the *betAB*-operon through restriction digestion (*fadBA1*: *Pst*I, *Bam*HI; *fadBA2*: *Stu*I, *Bam*HI; *fadBA3*: *Not*I, *Sma*I; *fadBA4*: *Eco*RV; *fadBA5*: *Sph*I, *Pst*I) and blunt-ended (except for *glpD*, which was blunt-ended using *SmaI*), the 1.1 kb *FRT*-Gm^R-*FRT* cassette obtained from pPS856 digested with *Sma*I was inserted into each gene. These newly constructed pEX18T vectors were transformed into *E.coli* SM10 or ER2566-mob, and conjugated into PAO1 to engineer the unmarked mutations as previously described [45]. To obtain all triple mutants, we invested an enormous amount of work to first create all single and double mutants with the proper confirmed Flp/*FRT*-excision of the gentamycin antibiotic resistance cassette to recycle this resistance marker for subsequent mutagenesis (data not shown).

The single copy integration vector, miniCTX2, was used to engineer the complemented strains for each triple-pathway mutant

Table 2. Plasmids used in this study[a].

Plasmids	Lab ID[b]	Relevant properties	Reference
pFlp2	E0067	Ap^r, *sacB*$^+$; Flp-containing plasmid	[45]
pPS856	E0050	Ap^r; Gm^r; plasmid with Gm^r-*FRT*-cassette	[45]
pUC18	E0135	Ap^r; cloning vector	[50]
pUC18-'*mucA*'	E1907	Ap^r; *mucA* internal region cloned into pUC18	This study
pUC19	E0014	Ap^r; cloning vector with P_{lac}	[50]
pUC19-*glpD*	E1843	Ap^r; pUC19 with *glpD* gene cloned in downstream of P_{lac}	This study
pEX18T	E0055	Ap^r, *oriT*$^+$, *sacB*$^+$; gene replacement vector	[45]
pEX18TΔ*fadBA1*::Gm	E0202	Ap^r, Gm^r; pEX18T with *ΔfadBA1 operon with* Gm^r-*FRT*-cassette insertion	This study
pEX18TΔ*fadBA2*::Gm	E0224	Ap^r, Gm^r; pEX18T with *ΔfadBA2 operon with* Gm^r-*FRT*-cassette insertion	This study
pEX18TΔ*fadBA3*::Gm	E0225	Ap^r, Gm^r; pEX18T with *ΔfadBA3 operon with* Gm^r-*FRT*-cassette insertion	This study
pEX18TΔ*fadBA4*::Gm	E0226	Ap^r, Gm^r; pEX18T with *ΔfadBA4 operon with* Gm^r-*FRT*-cassette insertion	This study
pEX18TΔ*fadBA5*::Gm	E0461	Ap^r, Gm^r; pEX18T with *ΔfadBA5 operon with* Gm^r-*FRT*-cassette insertion	This study
pEX18TΔ*glpD*::Gm	E1066	Ap^r, Gm^r; pEX18T with *ΔglpD operon with* Gm^r-*FRT*-cassette insertion	This study
pEX18TΔ*betAB*::Gm	E1070	Ap^r, Gm^r; pEX18T with *ΔbetAB operon with* Gm^r-*FRT*-cassette insertion	This study
miniCTX2	E0076	Tet^r; site-specific integration vector	[46]
miniCTX2-*fadBA5*	E1765	Tet^r; miniCTX2 with cloned *fadBA5*	This study
miniCTX2-*fadBA5/glpD*	E2035	Tet^r; miniCTX2 with cloned *fadBA5/glpD*	This study
miniCTX2-*fadBA5/betAB*	E1953	Tet^r; miniCTX2 with cloned *fadBA5/betAB*	This study
miniCTX2-*fadBA5/betAB/glpD*	E1992	Tet^r; miniCTX2 with cloned *fadBA5/betAB/glpD*	This study

[a]For plasmids constructed in this study, please see text for further details.
[b]Please use Lab ID for requesting plasmids.
doi:10.1371/journal.pone.0103778.t002

386

Table 3. Primers used in this study.

Primer number and name	Sequence[a]
186; *fadBA1*-upstream	5′-CGAAAGCTTGCATGGTGCTATCTTCC-3′
187; *fadBA1*-downstream	5′-GCGGAATTCGCCCTACCCGTGGCG-3′
218; *fadBA2*-upstream	5′-CGGTGAAGCTTTCGCGCACC-3′
219; *fadBA2*-downstream	5′-GGGGAATTCGGTGTCTCATCGGCAGCGC-3′
220; *fadBA3*-upstream	5′-GCGAAGCTTATTCAGCAGGAGAAAACGACG-3′
221; *fadBA3*-downstream	5′-TGCGGAATTCGACGGATAGTCGCCGCTAC-3′
211; *fadBA4*-upstream	5′-CGTAAGCTTGCCGGGGAGTCAGGGGC-3′
212; *fadBA4*-downstream	5′-CCCGAATTCGCACGGCACCGCCCAAG-3′
272; *fadBA5*-HindIII	5′-AGTTCAAGCTTCCATAATAGC-3′
273; *fadBA5*-EcoRI	5′-CCCGGAATTCCCCCTTCGAGAACGCTTAG-3′
518; *glpK*-BamHI	5′-AGCTGAAGTGGATCCTCGACAA-3′
519; *glpKD*-SacI	5′-CTGGCGAGCTCAGGCCGCATGCACCCG-3′
522; *betA*-SacI	5′-CAACGAGCTCGGCGATATCTACGGCGG-3′
523; *betB*-HindIII	5′-GCCAAAGCTTCCAGGACAAGAACGGCT3′
888; Xho-*fadB5*	5′-CCTGCGCAGAGGGCCTCGAGGAGGGC-3′
889; *fadB5*-Bam	5′-GGGCACGAGGATCCCCGGCTTTCCCC-3′
895; Spe-*betB*	5′-CGGATTCAGACTAGTACCTGCTCG-3′
896; Hind-*glpD*	5′-GCCTGGTGAAGCTTCGGGCTGGTC-3′
927; SacI-P_{lac}-*glpD*	5′-CGCTCGCCGGAGCTCGAACGACCGAGC-3′

[a]Restriction enzyme sites utilized in this study are underlined.

doi:10.1371/journal.pone.0103778.t003

as previously described [46]. Briefly, *fadBA5* and *betAB* were PCR amplified with primers 888/889 and 522/895, respectively. The miniCTX2-*fadBA5* was derived by inserting *fadBA5* fragment into miniCTX2, both digested with *Xho*I and *Bam*HI. The *betAB* gene was sub-cloned in using *Sac*I and *Spe*I, yielding miniCTX2-*fadBA5-betAB*. *glpD* was first cloned into pUC19 by digesting the PCR product with *Hind*III and *Sac*I, which was amplified using primers 896/519. P_{lac}-*glpD* fragment was amplified using primers 519/927 from pUC19-*glpD* and cloned into miniCTX2-*fadBA5* and miniCTX2-*fadBA5-betAB* to yield miniCTX2-*fadBA5-glpD* and miniCTX2-*fadBA5-betAB-glpD,* respectively.

The newly engineered mutant strains Δ*fadBA145*, Δ*fadBA145*Δ*glpD*, Δ*fadBA145*Δ*betAB*, and Δ*fadBA145*Δ*betAB*Δ*glpD*, were complemented using the relevant gene(s) on the miniCTX2 single copy integration vector as preciously described [46]. The resulting strains Δ*fadBA145*/complement, Δ*fadBA145*Δ*glpD*/complement, Δ*fadBA145*Δ*betAB*/complement, Δ*fadBA145*Δ*betAB*Δ*glpD*/complement were used in the growth curve experiment (Table 1 and Fig. 3A).

Growth characterization of mutants and complementation strains

Growth curve analyses have been described previously [17]. Briefly, all strains utilized were initially grown overnight in *Pseudomonas* Isolation Broth (PIB). The overnight cultures were centrifuged and the cell pellets were washed twice with 1×M9 minimal medium, and then a 1:50 dilution was made into 25 ml of the respective media (described above) for different growth curves. To clarify any insoluble FA, individual cultures were diluted 4-fold in 4% Brij-58, pre-incubated at 42°C for 2 minutes, prior to taking OD_{540} measurement at each time point (Fig. 2 and 3). To obtain the growth curves in Figure S2, all of the strains were grown overnight at 37°C in LB broth. The overnight cultures were centrifuged and the cell pellets were washed twice with 1×M9 minimal medium, and then a 1:400 dilution was made into respective media (described above) for different growth curves. 125 µl aliquots of the diluted cultures were transferred to a sterile, polystyrene 96-well assay plate (Falcon *Microtest flat bottom* plate, catalog no. *35–1172*; Becton-Dickinson Labware). Growth was recorded using an ELx808 Absorbance Microplate Reader (BioTek Instruments, Winooski, VT) under the following conditions: temperature37°C, and shaking at a low speed. The plate was read at 630 nm every 30 min for 40 h. All of the data was transferred and plotted using Prism.

Virulence factors detection

Strains used for virulence factors detection were grown in LB medium. At each time point, aliquots of individual culture were used for OD_{540} measurement (Fig. 3B). The detection of proteases, hemolysins, lipases, and rhamnolipid was performed as described elsewhere [17]. All assays were conducted in triplicate, and the data were analyzed as previously described [17].

Growth Phenotype Confirmation of Mucoid and Non-mucoid Strains

To confirm that mutations in *mucA* do not have additional effects on nutrient metabolism of the pathway mutant strains, all of the pathway mutants and complement strains were purified on LB plate or LB plate supplemented with 250 µl/ml carbenicillin (Cb250) for *mucA*$^-$ strains. After 24 h incubation at 37°C, single colony of each strain was patched on 1× M9 solid medium +1% (w/v) Brij-58 supplemented with 0.2% (w/v) $C_{18:1}^{\Delta 9}$, 40 mM glycerol or 30 mM choline as sole carbon source. They were also patched on LB plate, which served as a control. The growth pattern was observed after 24–36 h incubation at 37°C (Fig. S3).

In vitro and *in vivo* competition studies

In vitro and *in vivo* competition studies were performed as previously described [17]. Briefly, seven growth media with different carbon sources, including Luria-Bertani (LB) medium, casamino acids (CAA), glucose, PC, $C_{18:1}^{\Delta 9}$, choline, and glycerol, were used in this study. The bacterial CFU were determined after inoculation into each of the medium for 24–48 h. The CI was calculated as the CFU ratio of mutant/wildtype recovered at each time point divided by the CFU ratio of mutant/wildtype in the input inoculum [47]. The smaller the CI value, the more the significant reduction in fitness of the mutant.

Various alginate-overproducing strains, Δ*fadBA145-mucA*$^-$, Δ*fadBA145*Δ*glpD-mucA*$^-$, Δ*fadBA145*Δ*betAB-mucA*$^-$, Δ*fadBA145*Δ*betAB*Δ*glpD-mucA*$^-$ and the complement strains for each mutant utilized in this study are listed in Table 1. The use of the *mucA*$^-$ mutation is essential in this animal model as previously described [40].

Supporting Information

Figure S1 Five potential *fadBA*-operon homologues of *P. aeruginosa*. (A) Genes of operons (GenBank accession numbers in parentheses) are shown in light purple with percent of identity and similarity to the *E. coli* FadBA. *fadBA1* is 3.363 kb; *fadBA2* is 2.760 kb; *fadBA3* is 2.346 kb; *fadBA4* is 2.887 kb; and *fadBA5* is 3.353 kb, (B) Alignment of *P. aeruginosa* FadAs and FadBs with *E.* coli FadA and FadB motifs. Amino acids with similar properties are assigned the same colors using CLC Sequence Viewer 6.
(TIF)

Figure S2 Growth analysis of different single *fadBA* mutants on medium ($C_{12:0}$) and long chain-length fatty acid ($C_{14:0}$, $C_{16:0}$ and $C_{18:1}^{\Delta 9}$). Along with the wildtype PAO1 strain, mutants Δ*fadBA1*, Δ*fadBA2*, Δ*fadBA3*, Δ*fadBA4* and Δ*fadBA5* were grown in 1×M9 minimal medium supplemented with 0.05% different test FAs (A to D) and 1% Brij-58 or LB broth as a control (E). Only the Δ*fadBA5* mutant showed various defects when grown with FAs of different chain-lengths, no significant growth defects were observed for the rest of single *fadBA* mutants. All of the mutants grew to the same level as wildtype when grown in LB.
(TIF)

Figure S3 Growth Phenotype Confirmation of Mucoid and Non-mucoid Strains. Along with the wildtype PAO1 and PAO1-*mucA*$^-$ strains, all of the pathway mutants and their corresponding complement strains were patched on 1× M9 solid medium +1% (w/v) Brij-58 supplemented with 0.2% (w/v) $C_{18:1}^{\Delta 9}$ (B), 40 mM glycerol (C), or 30 mM choline (D). (A) Growth on LB was performed as a control. Alginate over-producing strains show a light sheen surface indicated by white arrow in panel A. Similar growth defects were shown between mucoid and non-mucoid strains on different plates. A detailed plate layout is shown in panel E with strains identification of Table 1 in parentheses.
(TIF)

Figure S4 Analyses of proteases, hemolysins, lipases, and rhamnolipid productions by *P. aeruginosa* various pathway mutant. No mutants displayed significant ($P \leq 0.05$, based on student *t*-test) decrease in productions of proteases (A), rhamnolipid (B), hemolysins (C), and lipases (D).
(TIF)

Acknowledgments

We would like to thank previous (Asha S. Nayar, and Joon Kim) and current (Jan Zarzycki-Siek) lab members for their assistance in some mutagenesis experiments, as well as current lab members (Andrew Bluhm and Ian McMillan) for their critical reading of this manuscript.

Author Contributions

Conceived and designed the experiments: ZS YK MHN RMT HPS SWD TTH. Performed the experiments: ZS YK MHN RMT MSS. Analyzed the data: ZS YK MHN TTH. Contributed reagents/materials/analysis tools: TTH HPS SWD YK MHN RMT. Contributed to the writing of the manuscript: ZS TTH.

References

1. Wilson R, Dowling RB (1998) *Pseudomonas aeruginosa* and other related species. Thorax 53: 213–219.
2. Driscoll J, Brody SL, Kollef MH (2007) The epidemiology, pathogenesis and treatemnt of *Pseudomonas aeruginosa* infection. Drugs 67: 351–368.
3. Richards MJ, Edwards JR, Culver DH, Gaynes RP (1999) Nosocomial infections in medical intensive care units in the United States. Crit Care Med 27: 887–892.
4. Lode H, Raffenberg M, Erbes R, Geerdes-Fenge H, Mauch H (2000) Nosocomial pneumonia: epidemiology, pathogenesis, diagnosis, treatment and prevention. Curr Opin Infect Dis 13: 377–384.
5. Pompilio A, Crocetta V, Scocchi M, Pomponio S, Di Vincenzo V, et al. (2012) Potential novel therapeutic strategies in cystic fibrosis: antimicrobial and anti-biofilm activity of natural and designed alpha-helical peptides against *Staphylococcus aureus*, *Pseudomonas aeruginosa*, and *Stenotrophomonas maltophilia*. BMC Microbiol 12: 145.
6. Emerson J, Rosenfeld M, McNamara S, Ramsey B, Gibson RL (2002) *Pseudomonas aeruginosa* and other predictors of mortality and morbidity in young children with cystic fibrosis. Pediatr Pulmonol 34: 91–100.
7. Wagner VE, Iglewski BH (2008) *P. aeruginosa* biofilms in CF infection. Clin Rev Allergy Immunol 35: 124–134.
8. Fricks-Lima J, Hendrickson CM, Allgaier M, Zhuo H, Wiener-Kronish JP, et al. (2011) Differences in biofilm formation and antimicrobial resistance of *Pseudomonas aeruginosa* isolated from airways of mechanically ventilated patients and cystic fibrosis patients. Int J Antimicrob Agents 37: 309–315.
9. Coban AY, Ciftci A, Onuk EE, Erturan Z, Tanriverdi Cayci Y, et al. (2009) Investigation of biofilm formation and relationship with genotype and antibiotic susceptibility of *Pseudomonas aeruginosa* strains isolated from patients with cystic fibrosis. Mikrobiyol Bul 43: 563–573.
10. Pesci EC, Iglewski BH (1997) The chain of command in *Pseudomonas* quorum sensing. Trends Microbiol 5: 132–134.
11. Bjarnsholt T, Jensen PO, Jakobsen TH, Phipps R, Nielsen AK, et al. (2010) Quorum sensing and virulence of *Pseudomonas aeruginosa* during lung infection of cystic fibrosis patients. PLoS One 5: e10115.
12. Smith RS, Iglewski BH (2003) *P. aeruginosa* quorum-sensing systems and virulence. Curr Opin Microbiol 6: 56–60.
13. Singh PK, Schaefer AL, Parsek MR, Moninger TO, Welsh MJ, et al. (2000) Quorum-sensing signals indicate that cystic fibrosis lungs are infected with bacterial biofilms. Nature 407: 762–764.
14. Storey DG, Ujack EE, Rabin HR (1992) Population transcript accumulation of *Pseudomonas aeruginosa* exotoxin A and elastase in sputa from patients with cystic fibrosis. Infect Immun 60: 4687–4694.
15. Son MS, Matthews Jr WJ, Kang Y, Nguyen DT, Hoang TT (2007) *In vivo* evidence of *Pseudomonas aeruginosa* nutrient acquisition and pathogenesis in the lungs of cystic fibrosis patients. Infection and immunity 75: 5313–5324.
16. Palmer KL, Mashburn LM, Singh PK, Whiteley M (2005) Cystic fibrosis sputum supports growth and cues key aspects of *Pseudomonas aeruginosa* physiology. J Bacteriol 187: 5267–5277.
17. Kang Y, Zarzycki-Siek J, Walton CB, Norris MH, Hoang TT (2010) Multiple FadD acyl-CoA synthetases contribute to differential fatty acid degradation and virulence in *Pseudomonas aeruginosa*. PLoS One 5: e13557.
18. Zarzycki-Siek J, Norris MH, Kang Y, Sun Z, Bluhm AP, et al. (2013) Elucidating the *Pseudomonas aeruginosa* Fatty Acid Degradation Pathway: Identification of Additional Fatty Acyl-CoA Synthetase Homologues. PLoS One 8: e64554.
19. Miller RM, Tomaras AP, Barker AP, Voelker DR, Chan ED, et al. (2008) *Pseudomonas aeruginosa* twitching motility-mediated chemotaxis towards phospholipids and fatty acids: specificity and metabolic requirements. Journal of Bacteriology 190: 4038–4049.
20. Bernhard W, Wang J-Y, Tschernig T, Tummler B, Hedrich HJ, et al. (1997) Lung surfactant in a cystic fibrosis animal model: increased alveolar phospholipid pool size without altered composition and surface tension function in *cftr*$^{m1HGU/m1HGU}$ mice. Thorax 52: 723–730.
21. Bernhard W, Hoffmann S, Dombrowsky H, Rau GA, Kamlage A, et al. (2001) Phosphatidylcholine molecular species in lung surfactant: composition in relation

to respiratory rate and lung development. Am J Respir Cell Mol Biol 25: 725–731.
22. Hite RD (2002) Surfactant deficiency in adults. Clin Pulm Med 9: 39–45.
23. Velasco-Garcia R, Mujica-Jimenez C, Mendoza-Hernandez G, Munoz-Clares RA (1999) Rapid purification and properties of betaine aldehyde dehydrogenase from *Pseudomonas aeruginosa*. J Bacteriol 181: 1292–1300.
24. Wargo MJ, Szwergold BS, Hogan DA (2008) Identification of two gene clusters and a transcriptional regulator required for *Pseudomonas aeruginosa* glycine betaine catabolism. J Bacteriol 190: 2690–2699.
25. Schweizer HP, Po C (1996) Regulation of glycerol metabolism in *Pseudomonas aeruginosa*: characterization of the *glpR* repressor gene. J Bacteriol 178: 5215–5221.
26. Schweizer HP, Po C, Bacic MK (1995) Identification of *Pseudomonas aeruginosa* GlpM, whose gene product is required for efficient alginate biosynthesis from various carbon sources. JBacteriol 177: 4801–4804.
27. Schweizer HP, Po C, Jump R (1997) Structure and gene-polypeptide relationships of the region encoding glycerol diffusion facilitator (*glpF*) and glycerol kinase (*glpK*) of *Pseudomonas aeruginosa*. Microbiology 143: 1287–1297.
28. Clark D (1981) Regulation of fatty acid degradation in *Escherichia coli*: anaylsis by operon fusion. J Bacteriol 148: 521–526.
29. Pramanik A, Pawar S, Antonian E, Schulz H (1979) Five different enzymatic acitivities are associated with the multienzyme complex of fatty acid oxidation in *Escherichia coli*. J Bacteriol 137: 469–473.
30. Campbell JW, Cronan Jr JE (2002) The enigmatic *Escherichia coli fadE* gene is *yafH*. J Bacteriol 184: 3759–3764.
31. Kang Y, Nguyen DT, Son MS, Hoang TT (2008) The *Pseudomonas aeruginosa* PsrA responds to long-chain fatty acid signals to regulate the *fadBA5* β-oxidation operon. Microbiology 154: 1584–1598.
32. Stover CK, Pham XQ, Erwin AL, Mizoguchi SD, Warrener P, et al. (2000) Complete genome sequence of *Pseudomonas aeruginosa* PA01, an opportunistic pathogen. Nature 406: 959–964.
33. Son MS, Nguyen DT, Kang Y, Hoang TT (2008) Engineering of *FRT-lacZ* fusion constructs: induction of the *Pseudomonas aeruginosa fadAB1* operon by medium and long chain-length fatty acids. Plasmid 59: 111–118.
34. Beassoni PR, Otero LH, Massimelli MJ, Lisa AT, Domenech CE (2006) Critical active-site residues identified by site-directed mutagenesis in *Pseudomonas aeruginosa* phosphorylcholine phosphatase, a new member of the haloacid dehalogenases hydrolase superfamily. Curr Microbiol 53: 534–539.
35. Massimelli ML, Beassoni PR, Forrellad MA, Barra JL, Garrido MN, et al. (2005) Identification, cloning, and expression of *Pseudomonas aeruginosa* phosphorylcholine phosphatase gene. Curr Microbiol 50: 251–256.
36. Nagasawa T KY, Tani Y, Ogata K. (1976) Purification and characterization of betaine aldehyde dehydrogenase from *Pseudomonas aeruginosa* A-16. Agric Biol Chem 40: 1743–1749.
37. Wargo MJ, Ho TC, Gross MJ, Whittaker LA, Hogan DA (2009) GbdR regulates *Pseudomonas aeruginosa plcH* and *pchP* transcription in response to choline catabolites. Infect Immun 77: 1103–1111.
38. Schweizer HP, Po C (1994) Cloning and nucleotide sequence of the *glpD* gene encoding *sn*-glycerol-3-phosphate dehydrogenase from *Pseudomonas aeruginosa*. J Bacteriol 176: 2184–2193.
39. Weissenborn DL, Larson TJ (1992) Structure and regulation of the *glpFK* operon encoding glycerol diffusion facilitator and glycerol kinase of *Escherichia coli* K-12. JBiolChem 267: 6122–6131.
40. Hoffmann N, Rasmussen TB, Jensen PO, Stub C, Hentzer M, et al. (2005) Novel mouse model of chronic *Pseudomonas aeruginosa* lung infection mimicking cystic fibrosis. Infect Immun 73: 2504–2514.
41. Boucher JC, Yu H, Mudd MH, Deretic V (1997) Mucoid *Pseudomonas aeruginosa* in cystic fibrosis: characterization of muc mutations in clinical isolates and analysis of clearance in a mouse model of respiratory infection. Infect Immun 65: 3838–3846.
42. Darch SE, West SA, Winzer K, Diggle SP (2012) Density-dependent fitness benefits in quorum-sensing bacterial populations. Proc Natl Acad Sci U S A 109: 8259–8263.
43. Postle AD, Mander A, Reid KBM, Wang J-Y, Wright SM, et al. (1999) Deficient hydrophilic lung surfactant protein A and D with normal surfactant phospholipid molecular species in cystic fibrosis. Am J Respir Cell Mol Biol 20: 90–98.
44. Kang Y, Norris MH, Barrett AR, Wilcox BA, Hoang TT (2009) Engineering of tellurite-resistant genetic tools for single-copy chromosomal analysis of *Burkholderia* spp. and characterization of the *Burkholderia thailandensis betBA* operon. Applied and Environmental Microbiology 75: 4015–4027.
45. Hoang TT, Karkhoff-Schweizer RR, Kutchma AJ, Schweizer HP (1998) A broad-host-range Flp-*FRT* recombination system for site-specific excision of chromosomally-located DNA sequences: application for isolation of unmarked *Pseudomonas aeruginosa* mutants. Gene 212: 77–86.
46. Hoang TT, Kutchma AJ, Becher A, Schweizer HP (2000) Integration-proficient plasmids for *Pseudomonas aeruginosa*: site-specific integration and use for engineering of reporter and expression strains. Plasmid 43: 59–72.
47. Brickman TJ, Vanderpool CK, Armstrong SK (2006) Heme transport contributes to *in vivo* fitness of *Bordetella pertussis* during primary infection in mice. Infect Immun 74: 1741–1744.
48. Simon R, Priefer U, Puehler A (1983) A broad-host-range mobilization system for *in vivo* genetic engineering: transposon mutagenesis in gram negative bacteria. Bio/Technology 1: 784–791.
49. Holloway BW, Roemling U, Tuemmler B (1994) Genomic mapping of *Pseudomonas aeruginosa* PAO. Microbiol 140: 2907–2929.
50. Yanisch-Perron C, Vieira J, Messing J (1985) Improved M13 cloning vectors and host strains: nucleotide sequences of the M13 mp18 and pUC19 vectors. Gene 33: 103–119.